

Tailor-Made Helicity in Polyaromatic Systems

Inauguraldissertation

zur

Erlangung der Würde eines Doktors der Philosophie

vorgelegt der

Philosophisch-Naturwissenschaftlichen Fakultät

der Universität Basel

von

Michel Rickhaus

aus Gündlischwand (BE), Schweiz

Basel 2016

Originaldokument gespeichert auf dem

Dokumentenserver der Universität Basel edoc.unibas.ch

Genehmigt von der Philosophisch-Naturwissenschaftlichen Fakultät auf
Antrag von

Prof. Dr. Marcel Mayor

Prof. Dr. Thomas Ward

Basel, den 15.09.2015

Prof. Dr. Jörg Schibler (Dekan)

Dem Steuerzahler ... und der Kunst

*Selig sind die geistig Armen,
denn sie stecken nie die Nase
in den Brunnenschacht des Lebens
voll gefährlich gift'ger Gase.*

*Trinken oben aus dem Becken
fromm mit Ochs und Schaf zugleich.
Und dereinst, wenn sie sich strecken,
erben sie das Himmelreich.*

Christian Morgenstern (1871 - 1914)

Acknowledgements

It has been a long journey, and it would not have started without one person: **Professor Marcel Mayor**, the stern father of Evelyne. I continue to feel honored and grateful for being a member of your team. Marcel, thank you not only, but also, for the almost unlimited liberty and resources you provided on good faith before any of us could be sure to ever fulfill what we were supposed to achieve. For your sense of aesthetics. For forcing me to look closer, to be relentless in understanding and achieving things on my own. And for that beautiful 27" display.

It is a privilege that **Professor Thomas Ward** committed himself to co-refereeing this thesis.

I am profoundly honored for having **THE Professor Larry T. Scott** as external examiner. Thank you for showing me and an entire generation of chemists the way. You will never be replaced.

I owe debts of gratitude to **Ina** for continuing to show me what courage means. The strength of this thesis is very much an honor to you. Any errors are entirely my own. And to you, **Markus**, for being the force of nature that you are.

My deepest thanks to my fellow researchers, many of which have become friends over these years. **Sylvie, Lukas, Almu, Michal, Mario, Vicky, Yves, Kevin, Lollo, Jürgen, Nicolas**. I believe there is no other resource like you anywhere. To all **members of the Mayor group**, past, present and beyond. So many thanks to you for your trust, advice and companionship.

Lukas, thank you for showing me all the space where our worlds overlapped. You will endure in my perception of music. There is much to learn from a dinosaur like you. **Sylvie**, you stand as an example for any scientist. You have evolved into something so much more dear to me than a dance in the rain. Grumpy **Almu**-who-is-never-grumpy, your unconditional friendship means the world to me. You are what Spain should be all about. **Michal**, my deep heartfelt thanks for spending more than a little time on our manuscripts and asking all the right questions. I bow before someone as talented and dear to me as you. Thank you, **Prince**, for allowing me to spend time with your helices.

Thank you, my spirited young researchers who took over the project. I am grateful, **Rajesh** and **Linda**, to leave Evelyne and her daughters in most capable hands. A deep bow of respect to **Olli**, for being both, the smartest and politest student I have ever come across. You will always have a place in a real lab.

PD Daniel Häussinger, Kaspar and **Heiko** for going above and beyond their NMR duties, anytime, anyday. And to you, **Markus Neuburger**, for turning my sad little lumps into things of beauty.

This thesis would not exist without the faith and hard work of all the people in the department. Special thanks to you, **Andreas Koller, Markus Hauri, Beatrice Erismann, Brigitte Hohwald, Heinz Nadig, Marina Mambelli-Johnson, Markus Ast, Andreas Sohler**, and the unique **Roy Lips**. Thank you for being patient while we grew up.

To my family, who are never far. Without you, this would never have had a chance to grow. To my **Damaris**, for filling my scientist heart with music. You are the light at the end of all my tunnels.

And finally,
to **Evelyne**, who appeared five years ago and changed everything.

It Started with a Ladder ...and a Name

This thesis was, and still is, the translation of a conceptual idea that took root years before its realization. As with many ideas that eventually get transcribed into actual molecular systems, it needed two things: a molecular design – and a name. For both existed a myriad of possibilities. But how to find a working title that reflects the topological beauty and simple elegance of the molecule? And how to address the general, underlying concept of a ladder with mismatched rails as an organic synthetic chemist? Eventually both were found: a molecular design involving six interlinked phenyl rings. And a name. Evelyne.

The thesis is grouped around that concept chronologically, starting with the initial conceptual publication in *Angewandte Chemie* and the detailed synthetic aspects in the *European Journal of Organic Chemistry*. Besides the resolution of the synthetic maze, the structure as obtained by X-Ray diffraction analysis as well as the dynamic behavior is described therein. The ensuing publication from *Chemistry – A European Journal* expands on the concept, finding ways to fine-tune the shape of the helical structures by targeted changes in the structure.¹ In a way, describing Evelyn's daughters. Schwefelyn. And Selenyn. The supplementary information provided in the manuscripts have been added for the reader's convenience at the very end, also chronologically ordered.²

Preceding these three manuscripts, the reader will find a review entitled “*Strain Induced Helical Chirality in Polyaromatic Systems*” which has been published in *Chemical Society Reviews*.¹ This tutorial article explains the rise of helical shapes due to steric interactions with carefully selected examples. It gives a clear systematic overview over the different concepts used to induce helical chirality in small organic molecules – including the one realized in this thesis. It connects the thesis' topic with the wider world of polyaromatic systems that become chiral due to steric interactions.

The last publication included arises from a wonderful collaboration with the group of Prof. Dr. Willem Klopper at the Karlsruhe Institute of Technology, Germany. The excellent theoretical work by Angela Bihlmeier and experimental work by Jürgen Rotzler on the atropisomerization of alkyl bridged biphenyls was complemented by kinetic circular dichroism studies.

Michel Rickhaus
Basel, September 2015
Amended for print: Basel, March 2016

¹ The publications were originally included in the state of evolved drafts. They have been published in the meantime and consequently been integrated as such in the print edition.

² Extended Versions only.

Table of Contents

1-7 Overview of the Thesis

9-23 Strain-Induced Helical Chirality in Polyaromatic Systems

Chemical Society Reviews, 2016, 45, 1542–1556.

M. Rickhaus, M. Mayor, M. Juriček

DOI: 10.1039/c5cs00620a

25 About the Project

27-31 Inducing Axial Chirality in a “Geländer” Oligomer by Length Mismatch of the Oligomer Strands

Angewandte Chemie International Edition, 2014, 53, 14587–14591.

M. Rickhaus, L. M. Bannwart, M. Neuburger, H. Gsellinger, K. Zimmermann, D. Häussinger, M. Mayor,

DOI: 10.1002/anie.201408424

33-48 Through the Maze: Cross-Coupling Pathways to a Helical Hexaphenyl “Geländer” Molecule

European Journal of Organic Chemistry, 2015, 4, 786–801.

M. Rickhaus, L. M. Bannwart, O. Unke, H. Gsellinger, D. Häussinger, M. Mayor,

DOI: 10.1002/ejoc.201403322

51-62 Tuning Helical Chirality in Polycyclic Ladder Systems

Chemistry – A European Journal, 2015, 21, 18156–18167.

M. Rickhaus, O. T. Unke, R. Mannancherry, L. Bannwart, M. Neuburger, D. Häussinger, M. Mayor

DOI: 10.1002/chem.201503202

65-73 Activation Enthalpies and Entropies of the Atropisomerization of Substituted Butyl-Bridged Biphenyls

Physical Chemistry Chemical Physics, 2015, 17, 11165–11173.

A. Bihlmeier, J. Rotzler, M. Rickhaus, M. Mayor, W. Klopper,

DOI: 10.1039/c4cp06009a

75 Conclusion and Outlook

77-121 Supporting Information for *Angewandte Chemie*

123-160 Supporting Information for *European Journal of Organic Chemistry*

161-192 Supporting Information for *Chemistry – A European Journal*

195-196 Curriculum Vitae

Overview of the Thesis

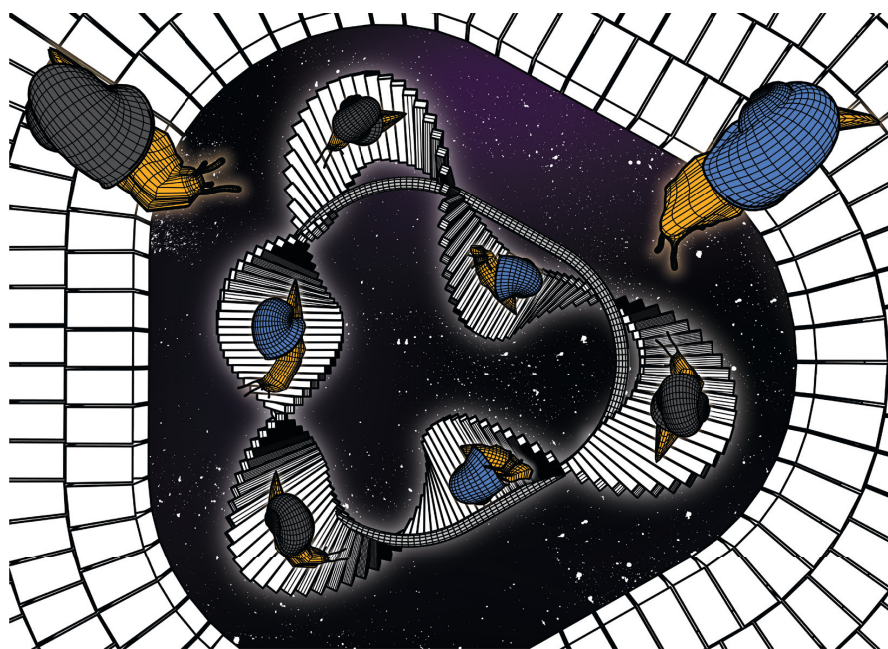
Helical molecules are not only esthetically appealing due to their structural beauty, they also display unique physical properties as a result of their chirality. This statement preludes the first publication that arose from this thesis. And indeed, both were found eventually; solid state structures with striking helical conformations as much as surprising racemization dynamics. The collected investigations and experimental data was presented to the scientific community in a communication and two full papers, along with a more specialized publication and a review. The following pages intend to reveal the *leitmotif* that ties together all publications and act as guide as not to be lost in the mesmerizing world of helical chirality.

I. Strain-Induced Helical Chirality in Polyaromatic Systems (2016, Review, Chemical Society Reviews)

Helicity is a complex phenomena and scientists have discovered and developed a vast number of concepts and ideas to induce and stabilize helical arrangements. DNA¹ and helicenes³⁻⁴ are excellent examples to demonstrate how different the designs and involved systems can be. One finds its helical nature based on the carefully arranged interactions of hydrogen bonds, or due to steric

interactions at the edge of the molecule. Important to our work were concepts towards helical systems that contain aromatic rings, as most of our designs contain aromatic structures. Turning to literature revealed that while some reviews⁵⁻⁹ exist that describe helical polyaromatic systems, they are grouped around one set of molecules (helicenes, twistacenes and the like) rather than giving a systematic overview of underlying concepts. Literature elaborating on the connection between the different model systems are to our knowledge not available. A possible reason is that many of these classes grew from investigations that were more or less independent of each other and only eventually got consolidated into one class or the other. But a classification based on topology rather than parent structures is what allows to find missing links and create a complete picture. And indeed, connections between the different topologies of the systems can be found and are summarized in the review "*Strain-Induced Helical Chirality in Polyaromatic Systems*" (2016) which foregoes this thesis. A general assessment of the existing structures revealed several classes: the helicenes^{1-3,10-12}, twistacenes^{4,13-17} and equitorennes¹⁸, bridged biphenyls¹⁹⁻²¹ and tolanes²² and their higher oligomers²³⁻²⁴, *ortho*-phenylenes²⁵⁻²⁸, as well as structures forming twisted loops²⁹⁻³¹, propellers³²⁻³³ and contorted sheets³⁴. Due to their structural diversity it is not

immediately obvious how they relate to each other except that all of them adopt helical conformations. We realized that all of them can be thought of as molecular ribbons that are twisted around a stereogenic axis. Three independent boundary cases exist: I) The axis is located outside of the ribbon causing the structures to adopt structures that resemble a helical staircase. This type is most likely the best described example due to their renowned representative, the helicenes. Other examples include *ortho*-phenylenes and naphthylenes³⁵⁻³⁶. II) the stereogenic axis dissects the molecular ribbon. Twistacenes and equitorennes are typical representatives of that class. III) The molecular axis is located at the edge of the ribbon. The edge which is



Cover for *Chemical Society Reviews* showing three types of a helically twisted ribbon. The stereogenic axis (ring) is either identical to the main axis of the ribbon, or at the edge of the ribbon, or does not have an intersection with the ribbon (left, bottom, right, respectively).

not part of the axis then describes a bannister of a helical staircase. Bridged biphenyls and derived structures are prominent members of that type. Other structures like propellers or contorted sheets contain usually multiple type I-III elements which makes them complex analogues rather than entirely new classes. It was this careful analysis that emphasized the need for true bannister model systems. While there are numerous examples of type I and II structures known that show extended stability of their adopted helix and well-studied physical and chiroptical properties, there did not exist an actual bannister model system beyond bridged biphenyls. It was this unexplored space that ultimately lead us to design and access type III bannister systems.

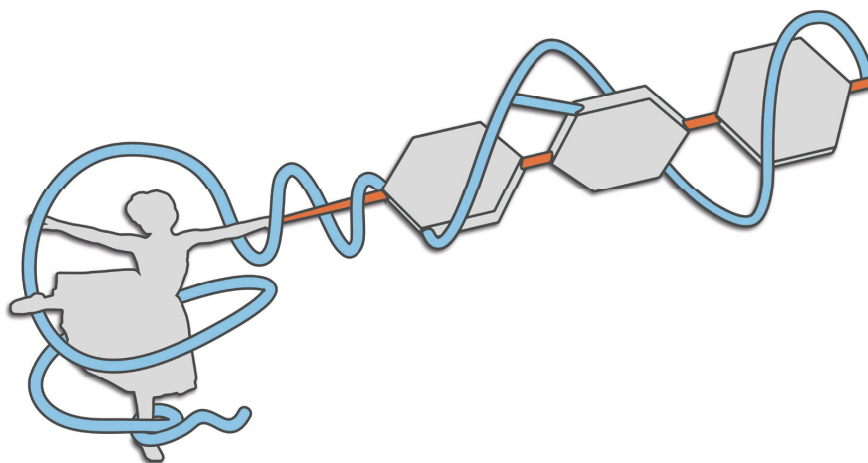
II. Inducing Axial Chirality in a “Geländer” Oligomer by Length Mismatch of the Oligomer Strands (2014, Communication, *Angewandte Chemie, International Edition*)

The simplest form of a type III structure is the bridged biphenyl³⁷⁻⁴³. The backbone (black) consists of two phenyl units which are directly connected over an aryl-aryl bond. Simultaneously, it also serves as the axis along which the twist occurs. The 2 and 2' positions serve as bridgeheads for an alkyl bridge (other bridge types are also known but less common) that span the two aryl rings. This bridge can be considered as the other edge (blue) of the molecular ribbon and adopts a helical conformation around the backbone. Depending on the length of the bridge, the torsion of the backbone is increased or decreased accordingly. Expanding on the concept, Vögtle developed the corresponding terphenylic structures, which were duped bannister oligomer. Analogue to the bridged biphenyls, an alkyl linker bridges two directly connected aryl units, resulting in a total of two bridges. While the introduction of a second bridge and an additional ring in the backbone allowed to enhance the chiroptical properties of the molecule, it suffered from a major drawback. Depending on the configuration of the two bridges, the structure possesses an inversion center and

as a consequence becomes achiral (the phenomena is known as *meso* formation). The nature of the issue lies in the missing communication between the bridges. As each bridge can adopt their relative configuration independent of the other, the sense of twist is not always continuous and results in partial retardation of the optical activity. Despite that drawback, these bannister systems have shown highly promising optical features, solubility and stabilities.

Another point that makes them highly appealing from a material standpoint is that in principle the bridge could be used as a chromophore, as per turn the bridge is longer than the corresponding segment on the backbone. This allows to use a conjugated system as bridge that profits from decreased strain and increased length compared to the backbone. So far the optical properties of the bannister oligomer arises exclusively from the backbone, where conjugation is interrupted from ring to ring due to their relative spatial arrangement. Deviation from an alkyl bridge to a OPV (oligo-phenylene-vinylene) for instance should enhance the optical properties and at the same the decreased flexibility of the bridge would lead to decreased rotation around the aryl-aryl bond(s) of the backbone.

From that onset we developed a new concept that addresses the missing communication of the bridge and allows to use an extended and possibly conjugated bridge.



TOC Graphic for *Angewandte Chemie* showing a molecular dance ribbon: Similar to a dance ribbon pirouetting around its handling stick, an elongated second oligomer (blue) is wrapped around the oligophenyl backbone (orange/gray), thereby inducing chirality, in a new type of “Geländer” structure.

Our manuscript which was published 2014 in *Angewandte Chemie* entitled “Inducing Axial Chirality in a “Geländer” Oligomer by Length Mismatch of the Oligomer Strands” is the cornerstone of this thesis. Within it, a new general concept for the induction of helicity is presented. To

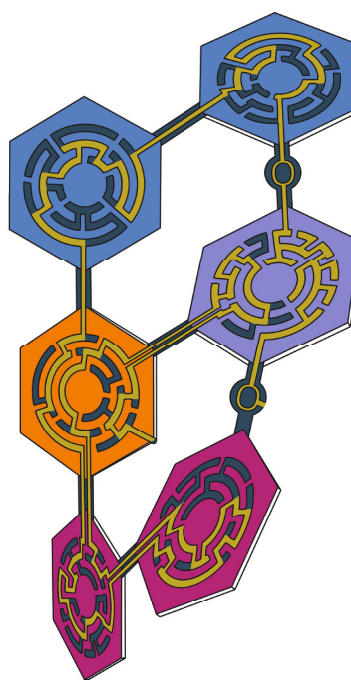
demonstrate the viability of the concept, the shortest oligomeric derivative of a polyaromatic ladder system was synthetically accessed and investigated in detail. That initial “Geländer” (or bannister) oligomer bases in principle on interlinking two oligomer strands of different length (i.e. the backbone and the bridge). If the two oligomer chains are interlinked with rigid linkers in a parallel fashion, a ladder-type structure is obtained. Both oligomers need to have a similar spacing between adjoining bridgeheads. Now, if the periodicity of one oligomer is increased with respect to the other, the two oligomeric chains are forced to compensate the mismatch in length. If the subunits are rigid enough, the discrepancy in length can only be overcome by wrapping the longer oligomer around the shorter. Each subunit relays the handedness of the helix and ensuring continuous helicity. Such a concept addresses all reasons for the formation of the *meso* structure: There is no possibility for the system to adopt a conformation with a point of inversion, and the helicity is now communicated across the entire structure.

The manuscript presents our translation of the concept into a polyaromatic structure featuring a terphenylic backbone and an extended benzyldiether as bridge. The stiffness and the structural integrity of the *paraxylylene* relay of the longer oligomer ensures the exclusive formation of two enantiomers as ground-state conformers. The structure still displays the spirit of Vögtle’s design with a terphenyl backbone, but instead of solely interlinking both biphenyl subunits with independent bridging structures, the entire oligo(*para*-benzyl ether) structure is wrapped around the terphenyl backbone. The result is a structure that resembles a dance ribbon pirouetting around its handling stick. The new “Geländer” oligomer was assembled in a sequence of functional-group transformations and cross-coupling steps. The synthetic work was assisted in part by Linda Bannwart and the sometimes meandering pathways were published independently. The final cyclizations were based on nucleophilic substitution reactions, and the resulting structure was fully characterized, including X-ray diffraction analysis. A team of NMR (Heiko Gsellinger, Kaspar Zimmerman and PD Dr. Daniel Häussinger) and X-Ray specialists (Dr. Markus Neuburger) made the full characterization possible. The isolation of pure enantiomers by HPLC on a chiral stationary phase enabled the racemization process to be studied by circular

dichroism spectroscopy. For that the decay of the Cotton band was observed over time and allowed to determine the rate constant from which the barrier was calculated. To our surprise, the structure showed racemization halftimes in the range of hours. The results were more than encouraging and turned out to be but the starting point of an entire story on type III bannister systems.

III. Through the Maze: Cross-Coupling Pathways to a Helical Hexaphenyl “Geländer” Molecule (2015, Full Paper, *European Journal of Organic Chemistry*)

While the *Angewandte* publication introduced the concept and displays the synthetic highlights of the initial structure, a lot of the synthetic legwork was required to finally obtain a reliable pathway. While presenting a detailed report of



TOC Graphic for *Eur. J. Org. Chem.*: The synthesis of a helical, interlinked Geländer (bannister)-type hexaphenyl oligomer is symbolized in the graphical abstract as a maze, which is representation of both, the often convoluted synthetic possibilities as well as the successful resolution of the maze to reach the target structure.

the synthesis simply goes beyond the scope of a communication, we felt that the gathered information was nevertheless important and should be made available to the scientific community. It was therefore decided to publish the retrosynthetic analysis and all synthetic details in a separate communication in the *European Journal of Organic Chemistry* (2015). The title of the publication “*Through the Maze: Cross-Coupling Pathways to a Helical Hexaphenyl “Geländer” Molecule*” emphasizes how challenging the assembly eventually

turned out to be (see also Fig. 3). Besides the two master students (Linda Bannwart and Oliver Unke) who turned out to be invaluable for exploring many of the synthetic roads, the complex nature of the NMR spectra required

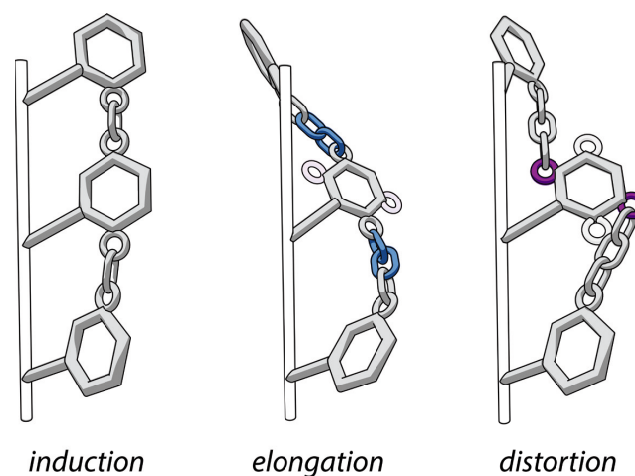
the dedicated work of Heiko Gsellinger and PD Dr. Daniel Häussinger to resolve the structures.

This publication highlights in particular cross-coupling strategies and explored synthetic pathways, and aims to serve as an Ariadne's thread for the synthesis of precisely functionalized, polyaromatic systems. Although a vast number of publications deal with the development and application of undoubtedly very complex aryl-aryl couplings, only a minority of these go beyond the synthesis of (hetero-)biaryls. The target structure presented here provided an excellent opportunity to contribute to the exploration of cross couplings for the construction of complex polyaromatic systems. The target structure requires the precise connection of often very demanding (both electronically and sterically) subunits. Especially the employment of Suzuki–Miyaura protocols⁴⁴⁻⁴⁵ was key for the targeted connection of polyaromatic fragments and ultimately to obtain the desired oligomeric structure. Further emphasis was put on the discussion of the encountered isomerizations as much as strategies to obtain functionalized intermediates with multiorthogonal moieties. Persistence was required to close the benzyl ether bannister and to isolate the target structure. In spite of numerous obstacles, the “Geländer” oligomer was assembled in an overall yield of 8%. Pure enantiomers were finally obtained by HPLC on a chiral stationary phase. The finished manuscript turned out to be the longest of the entire thesis, further emphasizing how much of the synthetic details often have to be abridged in short communications.

IV. Tuning Helical Chirality in Polycyclic Ladder Systems (2015, Full Paper, *Chemistry – A European Journal*)

While the initial hexaphenyl diether allowed to demonstrate the viability of the concept, the low yield of the final cyclization and the unexpected fast racemization of the structure left room for further investigations. Of particular interest was whether and how the racemization barrier could be influenced. The main motivation was to identify structural features that are especially important to the uniformity and stability of the helix. Those key features could then be integrated into the design of longer derivatives that show prolonged stability towards

racemization and possibly serve as an important step towards new functional materials.



TOC Graphic for *Chem. Eur. J.* depicting the evolution of a twisted ladder: A ladder oligomer adopts a helical conformation due to the size mismatch of the rails. Upon elongation of the chain-length between neighboring rings, the system responds by an increased twist. Changing the substitution pattern of the relay results in the distortion of the helix.

To that end, we strived to perform precise alterations on the structure to study the impact on the secondary structure and the dynamics of the system. We reasoned that especially the *paraxylene* relay would be sensitive towards changes, as it ensures the uniformity of the helix. The third publication – “Tuning Helical Chirality in Polycyclic Ladder Systems” which was accepted by *Chemistry – A European Journal* (2015) – presents two important ideas: a) the exchange of the heteroatom to sulfur and selenium. The assembly of a nonspecific tetrabrominated precursor allowed to efficiently introduce other chalcogens as heteroatoms at the last stage of the synthesis. The significantly larger and softer sulfur and selenium allowed fine-tuning of the helical structures. b) The change of the substitution pattern of the relay. Inversion of the relay's substitution pattern should cause a distortion of the structure, while maintaining the directionality of the helix. Master students Oliver Unke and Rajesh Mannancherry both spent considerable amount of time working on some of the synthetic steps, while (as before) Dr. Markus Neuburger performed the challenging X-Ray diffraction analyses and Pd. Dr. Daniel Häussinger recorded and interpreted the detailed high-resolution NMR experiments.

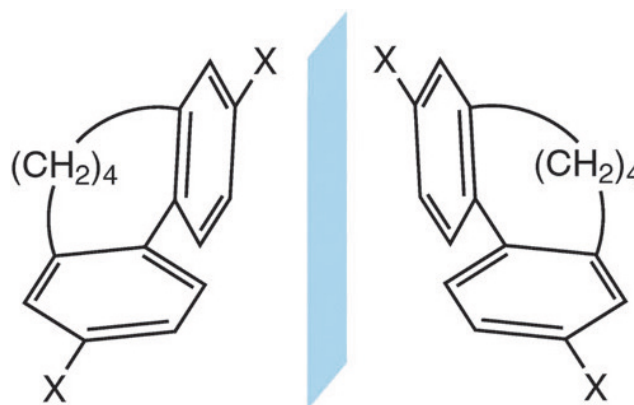
It was discovered that elongation of the bridge alters the torsion of the backbone while changes in ring size lead to

distortion of the helix. Including a minimal amount of borylations and a regioselective halogenation mediated by a neighboring boronic ester⁴⁶⁻⁴⁷, the publication presents a new efficient synthetic route to a modular precursor. This precursor allowed the successful integration of either two sulfur or selenium atoms and two consecutive macrocyclizations *in situ*. Two constitutional isomers with an inverted substitution pattern on the relay were observed and isolated as well. The total of eight structures – two constitutional isomers with the corresponding enantiomeric pair for each heteroatom – were accessed in high yields and separated into the individual isomers. Each structure was unambiguously identified by extensive NMR spectroscopy, High Resolution-MS and ECD spectroscopy. *In silico* ECD-calculations allowed assigning the absolute stereochemistry of each enantiomer and project the helical arrangement. For two of the four structural isomers the secondary structure was confirmed by X-Ray diffraction (one uniform and one distorted helix). In the case of the thioether an increased torsion was found while decreased torsion was observed for the selenoether. VT-NMR demonstrated that the bridge of the distorted helix derivatives is flexible and can undergo small structural changes on the NMR timescale. Precise values for the racemization barrier were obtained by dynamic ECD and allowed to relate the racemization to the spatial arrangement of the structures. Two trends were observed: The length of the heteroatomic bonds and the size of the heteronucleus are compensating each other in the case of sulfur. The much larger selenium reduces the racemization barrier to a reduced torsion angle *and* a softer nucleus in the case of the uniform helix. The distorted helices do not respond to the change in heteroatom. The obtained insights what governs the dynamics of the system and the shape of the helix are essential for designing helical type III bannister oligomers that are stable towards racemization.

V. Activation Enthalpies and Entropies of the Atropisomerization of Substituted Butyl-Bridged Biphenyls (2015, Full Paper, Physical Chemistry Chemical Physics)

Besides working on extended bannister systems and the achievements presented herein, the initial biphenyl model system has by far not revealed all its secrets. Especially the racemization process is still not satisfactorily clarified.

While for instance the influence of *para*-substitution on the butyl bridged biphenyls can be correlated to their racemization barrier, the detailed thermodynamic parameters remain ambiguous.⁴⁸ To obtain clear insight it is crucial to elucidate all factors that could lead to stable conformers. In turn all related systems are likely to profit from the gained knowledge, including our extended bannister systems.



TOC Graphic for *Phys. Chem. Chem. Phys.* showing the two possible atropisomers of a series of butyl bridged biphenyls.

In a combined effort by our experimental group and our computational collaborators in Karlsruhe (Prof. Dr. Willem Klopper, KIT), the influence of electron donating and withdrawing groups on the racemization barrier of butyl-bridged *para*-disubstituted biphenyls was studied and their enthalpic and entropic contributions compared. The resulting manuscript “Activation Enthalpies and Entropies of the Atropisomerization of Substituted Butyl-Bridged Biphenyls” was published by *Physical Chemistry Chemical Physics* (2015) and includes extensive computational and experimental data. Angela Bihlmeier performed the DFT calculations and analysis while Jürgen Rotzler accessed the required compounds and measured the dynamic HPLC traces. The author of this thesis recorded the dynamic CD measurements and calculated the thermodynamic parameters. The pathway for the racemization process including transition state structures was established using density functional theory (DFT) calculations. The derived Gibbs free activation energies are in accordance to the ones determined by temperature dependent high performance liquid chromatography (TD-HPLC) measurements⁴⁹⁻⁵⁰ on a chiral stationary phase. Only small changes were observed when exchanging the substituents but surprisingly large discrepancies were found for the contributions of enthalpy and entropy. The

impasse between experiment and computational predictions were resolved by using a complementary method: Thermodynamic data derived from solution based dynamic circular dichroism (CD) measurements support the quantum chemical calculations over the HPLC measurements. The careful analysis of the data and their acquisition led to the conclusion that HPLC relies heavily on the modelling of the elution profiles to obtain rate constants. Furthermore, data for the Eyring plot can only be measured in a relatively small temperature window. Extrapolation of that data may lead to large errors in the enthalpic and entropic contributions. The error in the overall Gibbs free activation energy remains small however. It was concluded that while dynamic HPLC represents a valuable tool to access the racemization parameters, it is less suited for detailed thermodynamic investigations. Of more importance was the comparison with the previously studied propyl-bridged biphenyls.⁵¹ Increasing the bridge length (i.e. going from propyl to butyl) is shown to have a larger effect on the inversion barrier than the different substituents in para position. Moreover, the obtained structure of the transition state showed that modification on the bridge rather than the biphenyl itself will have the largest impact on the atropisomerization. Especially this information is important when thinking about strategies how to stabilize our bannister oligomers.

Future Prospects

This thesis establishes a set of unprecedented bannister (or Geländer) systems based upon a mismatched ladder concept. The series of bannister oligomers allowed to investigate all aspects from their shape to their dynamics in detail. Structural changes like variation of the length of the bridge and distortion of the relay allowed to confirm that the structures exclusively adopt helices in all cases. These systems are case studies that have a large potential to become functional materials. Two main objectives are

especially significant and need to be addressed, namely a) the stability of the helix⁵² and b) the poor luminescence. The insight gained in this thesis allows to design systems that potentially resolve both. Stability of the helix is mainly a function of the bridge, as our investigations with the bannister chalcogen series and the butyl bridged biphenyls confirmed. It is therefore advisable to shorten the bridge by extrusion of the heteroatom or to increase the overall torsion by elongating the oligomer. Especially sulfur is a very promising candidate, as it was identified as having the largest impact on the torsion while showing superior synthetic accessibility. Furthermore, the sulfur bannisters showed prolonged stability towards oxygen and water. It is an ideal candidate to initiate multiple macrocyclization from a brominated precursor containing four or more biphenyls (instead of three) and would very likely allow the extensive purifications and investigations required. Even more promising: in many related systems, oxidation of sulfur was possible and allowed the subsequent extrusion using heat and base.⁵³⁻⁵⁶ Not only would that lead to a tighter wrapping of the oligomer as the bridge now contains an atom less. It potentially also addresses the second objective (b). Elimination of the sulfur leads eventually to the formation of two double bonds which likely are to some degree conjugated with the phenyl rings of the bridge. If the double bonds are arranged favorably, communication of the now isolated π -systems of the bridge may become possible, which in turn leads to enhanced optical properties. The double bond would also stiffen the bridge further, which will have an impact on the racemization barrier. Other possibilities to introduce double bonds include the use of Wittig sequences and/or Schiff base formation.

Overall, the detailed investigations and the deep knowledge acquired during our research allowed us to share our expertise with the wider scientific community. Bannister oligomers keep showing many promises both fundamentally and as candidates for functional materials and we do not expect the well to run dry anytime soon.

References

- 1 J. D. Watson and F. H. C. Crick, *Nature*, **1953**, *171*, 737–738.
- 2 M. Gingras, *Chem. Soc. Rev.*, **2013**, *42*, 968–1006.
- 3 M. Gingras, G. Félix and R. Peresutti, *Chem. Soc. Rev.*, **2013**, *42*, 1007–1050.
- 4 M. Gingras, *Chem. Soc. Rev.*, **2013**, *42*, 1051–1095.
- 5 R. A. Pascal Jr., *Chem. Rev.*, **2006**, *106*, 4809–4819.
- 6 C. Schmuck, *Angew. Chem. Int. Ed.*, **2003**, *42*, 2448–2452.
- 7 A. Rajca, S. Rajca, M. Pink and M. Miyasaka, *Synlett*, **2007**, *2007*, 1799–1822.
- 8 D. Wu, H. Ge, S. H. Liu and J. Yin, *RSC Adv.*, **2013**, *3*, 22727–22738.
- 9 M. Ball, Y. Zhong, Y. Wu, C. Schenck, F. Ng, M. Steigerwald, S. Xiao and C. Nuckolls, *Acc. Chem. Res.*, **2015**, *48*, 267–276.
- 10 F. L. Hirshfeld, S. Sandler and G. M. J. Schmidt, *J. Chem. Soc.*, **1963**, 2108–2125.
- 11 K. Mori, T. Murase and M. Fujita, *Angew. Chem. Int. Ed.*, **2015**, *54*, 6847–6851.
- 12 R. H. Martin and M. J. Marchant, *Tetrahedron*, **1974**, *30*, 347–349.
- 13 J. H. Brady, A. D. Redhouse and B. J. Wakefield, *J. Chem. Res. M*, **1982**, *137*, 1541–1554.
- 14 X. Qiao, M. A. Padula, D. M. Ho, N. J. Vogelaar, C. E. Schutt and R. A. Pascal, *J. Am. Chem. Soc.*, **1996**, *118*, 741–745.
- 15 J. Lu, D. M. Ho, N. J. Vogelaar, C. M. Kraml and R. A. Pascal, *J. Am. Chem. Soc.*, **2004**, *126*, 11168–11169.
- 16 J. Xiao, H. M. Duong, Y. Liu, W. Shi, L. Ji, G. Li, S. Li, X.-W. Liu, J. Ma, F. Wudl and Q. Zhang, *Angew. Chem. Int. Ed.*, **2012**, *51*, 6094–6098.
- 17 F. H. Herstein, *Acta Crystallogr., Sect. B*, **1979**, *35*, 1661–1670.
- 18 K. Yamamoto, N. Oyamada, S. Xia, Y. Kobayashi, M. Yamaguchi, H. Maeda, H. Nishihara, T. Uchimarui and E. Kwon, *J. Am. Chem. Soc.*, **2013**, *135*, 16526.
- 19 H. Schaefer, *J. Am. Chem. Soc.*, **1962**, *84*, 1449–1455.
- 20 D. Vonlanthen, A. Rudnev, A. Mishchenko, A. Käslin, J. Rotzler, M. Neuburger, T. Wandlowski and M. Mayor, *Chem. – Eur. J.*, **2011**, *17*, 7236–7250.
- 21 L. Eshdat, E. Shabtai, S. A. Saleh, T. Sternfeld, M. Saito, Y. Okamoto and M. Rabinovitz, *J. Org. Chem.*, **1999**, *64*, 3532–3537.
- 22 S. Menning, M. Krämer, B. A. Coombs, F. Rominger, A. Beeby, A. Dreuw and U. H. F. Bunz, *J. Am. Chem. Soc.*, **2013**, *135*, 2160–2163.
- 23 B. Kiupel, C. Niederalt, M. Nieger, S. Grimme and F. Vögtle, *Angew. Chem. Int. Ed.*, **1998**, *37*, 3031–3034.
- 24 M. Modjewski, S. Lindeman and R. Rathore, *Org. Lett.*, **2009**, *11*, 4656–4659.
- 25 C. S. Hartley and J. He, *J. Org. Chem.*, **2010**, *75*, 8627–8636.
- 26 S. M. Mathew, J. T. Engle, C. J. Ziegler and C. S. Hartley, *J. Am. Chem. Soc.*, **2013**, *35*, 6714–6722.
- 27 E. Ohta, H. Sato, S. Ando, A. Kosaka, T. Fukushima, D. Hashizume, M. Yamasaki, K. Hasegawa, M. Muraoka, H. Ushiyama, K. Yamashita and T. Aida, *Nat. Chem.*, **2011**, *3*, 68–73.
- 28 S. Ando, E. Ohta, A. Kosaka, D. Hashizume, H. Koshino, T. Fukushima and T. Aida, *J. Am. Chem. Soc.*, **2012**, *134*, 11084–11087.
- 29 Waka Nakanishi, Taisuke Matsuno, Junji Ichikawa and Hiroyuki Isobe, *Angew. Chem. Int. Ed.*, **2011**, *50*, 6048–6051. *Chem. Int. Ed.*, **2002**, *41*, 1, 171–173.
- 30 De Lie An, Takehiko Nakano, Akihiro Orita, and Junzo Otera, *Angew.*
- 31 Youichi Sakamoto and Toshiyasu Suzuki, *J. Am. Chem. Soc.*, **2013**, *135*, 14074–14077.
- 32 L. Barnett, D. M. Ho, K. K. Baldrige and R. A. Pascal, *J. Am. Chem. Soc.*, **1999**, *121*, 727–733.
- 33 S. Nobusue, Y. Mukai, Y. Fukumoto, R. Umeda, K. Tahara, M. Sonoda and Y. Tobe, *Chem. – Eur. J.*, **2012**, *18*, 12814–12824.
- 34 J. Luo, X. Xu, R. Mao and Q. Miao, *J. Am. Chem. Soc.*, **2012**, *134*, 13796–13803.
- 35 T. Motomura, H. Nakamura, M. Suginome, M. Murakami and Y. Ito, *Bull. Chem. Soc. Jpn.*, **2005**, *78*, 142–146.
- 36 C. Sparr et al., **2015**, *Angew. Chem. Int. Ed.* ASAP.
- 37 K. Ohkata, R. L. Paquette and L. A. Paquette, *J. Am. Chem. Soc.*, **1979**, *101*, 6687–6693.
- 38 K. Müllen, W. Heinz, F.-G. Klärner, W. R. Roth, I. Kindermann, O. Adamczak, M. Wette and J. Lex, *Chem. Ber.*, **1990**, *123*, 2349–2371.
- 39 L. Venkataraman, J. E. Klare, C. Nuckolls, M. S. Hybertsen and M. L. Steigerwald, *Nature*, **2006**, *442*, 904–907.
- 40 D. Vonlanthen, A. Mishchenko, M. Elbing, M. Neuburger, T. Wandlowski and M. Mayor, *Angew. Chem. Int. Ed.*, **2009**, *48*, 8886–8890.
- 41 J. Rotzler, H. Gsellinger, A. Bihlmeier, M. Gantenbein, D. Vonlanthen, D. Häussinger, W. Klopfer and M. Mayor, *Org. Biomol. Chem.*, **2012**, *11*, 110–118.
- 42 D. P. Iwaniuk, K. W. Bentley and C. Wolf, *Chirality*, **2012**, *24*, 584–589.
- 43 S. Menning, M. Krämer, B. A. Coombs, F. Rominger, A. Beeby, A. Dreuw and U. H. F. Bunz, *J. Am. Chem. Soc.*, **2013**, *135*, 2160–2163.
- 44 N. Miyaura, K. Yamada and A. Suzuki, *Tetrahedron Lett.*, **1979**, *36*, 3437–3440.
- 45 L. Xue and Z. Lin, *Chem. Soc. Rev.*, **2010**, *39*, 1692–1705.
- 46 F. Mo, J. M. Yan, D. Qiu, F. Li, Y. Zhang and J. Wang, *Angew. Chem. Int. Ed.*, **2010**, *49*, 2028–2032.
- 47 D. Qiu, F. Mo, Z. Zheng, Y. Zhang and J. Wang, *Org. Lett.*, **2010**, *12*, 5474–5477.
- 48 J. Rotzler, H. Gsellinger, M. Neuburger, D. Vonlanthen, D. Häussinger and M. Mayor, *Org. Biomol. Chem.*, **2011**, *9*, 86.
- 49 O. Trapp, *Anal. Chem.*, **2006**, *78*, 189.
- 50 O. Trapp, *Chirality*, **2006**, *18*, 489.
- 51 J. Rotzler, H. Gsellinger, A. Bihlmeier, M. Gantenbein, D. Vonlanthen, D. Häussinger, W. Klopfer and M. Mayor, *Org. Biomol. Chem.*, **2013**, *11*, 110.
- 52 G. Bringmann, A. J. Price Mortimer, P. A. Keller, M. J. Gresser, J. Garner and M. Breuning, *Angew. Chem., Int. Ed.*, **2005**, *44*, 5384.
- 53 Wolfgang Bieber and Fritz Vögtle, *Chem. Ber.*, **1978**, *111*, *4*, 1653–1654.
- 54 J. Kleinschroth and H. Hopf, *Angew. Chem. Int. Ed.*, **1982**, *21*, 469–480.
- 55 V. Boekelheide and Richard A. Hollins, *J. Am. Chem. Soc.*, **1973**, *95*, 10, 3201–3208.
- 56 T. Otsubo, Y. Aso, Fumio Ogura, S. Misumi, A. Kawamoto and J. Tanaka, *Bull. Chem. Soc. Jpn.*, **1989**, *62*, *1*, 164–170.



Cite this: DOI: 10.1039/c5cs00620a

Strain-induced helical chirality in polyaromatic systems

Michel Rickhaus,^a Marcel Mayor^{*abc} and Michal Juriček^a

Helicity in a molecule arises when the molecule contains a stereogenic axis instead of a stereogenic centre. In a molecule that is not inherently helically chiral, helicity can be induced by designing the molecule such that an unfavourable steric interaction, or strain, is present in its planar conformation. The release of this strain forces the molecule to adopt a helical twist against the cost of the torsional strain induced in the backbone, an interplay of forces, which must be balanced in favour of the helical conformation over the planar one. In this tutorial review, design principles that govern this process are analysed and the selected examples are categorised into three main (I, II and III) and two related (IV and V) classes, simply by their relation to one of the three types of helically twisted ribbons or two types of helically twisted cyclic ribbons, respectively. The presented examples were selected such that they illustrate their category in the best possible way, as well as based on availability of their solid-state structures and racemisation energy barriers. Finally, the relationship between the structure and properties is discussed, highlighting the cases in which induced helicity gave rise to unprecedented phenomena.

Received 10th August 2015

DOI: 10.1039/c5cs00620a

www.rsc.org/chemsocrev

Key learning points

- (1) Chirality can arise without stereogenic centres.
- (2) Strain introduced into a sufficiently rigid backbone can induce helical chirality.
- (3) Linked or fused aromatic rings are ideally suited to relay helicity within a structure.
- (4) Strained helical molecules often show surprisingly low racemisation barriers and are more flexible than is generally believed.
- (5) Helicity induced in a π -conjugated system often leads to an unusual electronic structure and unexpected properties.

1. Introduction

Since its elucidation in 1953, the double-helix structure of DNA has fostered the role that chirality plays¹ in living systems, namely, providing function with complexity. Helical chirality, in particular, governs² formation of many supramolecular assemblies composed of chiral or even achiral molecular building blocks in both biological and artificial systems. The helical secondary structure often defines the function of complex assemblies beyond a single stereogenic centre and translates chirality from the molecular level to the nanometer scale. Understanding how complexity arises from simple building blocks and the role of chirality in this process is the key to the design of functional systems.

Helical chirality is a property of chiral systems³ that do not contain stereogenic centres, that is, asymmetric units where four non-equivalent points represent the vertices of a tetrahedron. In a helical stereogenic unit, four points that can be identical are placed in a three-dimensional space such that the system is not superimposable on its mirror image. This type of chirality is also known as axial chirality because of the presence of a stereogenic axis instead of a centre. In molecules that are not inherently helically chiral, helicity can be induced. Flexible molecules, such as DNA, can be folded into a helical conformation by specific directional non-covalent interactions, for example, hydrogen bonding. In rigid molecules, helical conformations can arise if unfavourable steric interactions, or strain, are present in their non-helical conformations, which is the driving force towards formation of the energetically favoured helical conformations. This second type of helical chirality, here referred to as strain-induced, is the subject of this tutorial review.

The helical conformation is induced⁴ by minimising the steric interactions present in the planar conformation against the energy cost of the torsional strain, or deformation, induced upon twisting the molecule. The main requirement for a molecule to

^a Department of Chemistry, University of Basel, St. Johannis-Ring 19, 4056 Basel, Switzerland. E-mail: marcel.mayor@unibas.ch

^b Institute for Nanotechnology (INT), Karlsruhe Institute of Technology (KIT), P. O. Box 3640, 76021 Karlsruhe, Germany

^c Lehn Institute of Functional Materials (LIFM), Sun Yat-Sen University, Guangzhou, P. R. China

adopt a helical conformation is therefore the right balance of the two forces, the first one being the driving force. As a consequence, it is necessary that the molecule is both rigid and flexible at the same time. Fused or linked polyaromatic systems are ideally suited to serve this purpose because their core is sufficiently rigid. In parallel, the induced deformation is typically spread over a large number of bonds, which makes the core relatively flexible. Conceptually different types of strain-induced polyaromatic helices have been reported in the literature. These numerous significant achievements notwithstanding, there is still intellectual space left for designing conceptually new helical systems, which are induced by strain and which adopt well-defined geometries. Understanding how helicity arises and how it is translated into properties in these systems is crucial for understanding the interplay between chirality and function.

It is important to note that numerous examples are known in the literature, many of which could not be included in this review because of space restrictions. As most of these have recently been reviewed exhaustively, we focused on the qualitative rather than quantitative analysis and classification of the selected examples. Previous reviews on helically chiral strained polyaromatic compounds include four recent, extensive reviews on $[n]$ helicenes⁵⁻⁷ and twistacenes⁸ and one other review⁹ highlighting specific examples. Each review, however, deals mostly with one class of helical molecules and focuses on different synthetic approaches, including stereoselective synthesis, to these targets. A general concept bringing all the structural motifs together in a systematic way has been missing in the literature and is addressed in this conceptual review. The strain-induced helical architectures are organised by means that they adopt a helical conformation, and their structural design and its consequences are discussed. Because of the vast number of examples, the presented structures were selected thoroughly, such that they illustrate the differences between various types of strain-induced helical systems as clearly and simply as possible. To qualitatively assess the amount

of induced strain, structural and dynamic parameters are discussed in detail. Therefore, compounds, whose solid-state structures as well as the Gibbs free energy barriers (ΔG^\ddagger) of racemisation are available, were selected preferentially. In the case of less recent examples, the ΔG^\ddagger values were estimated from the activation energies (E_a) of racemisation and the corresponding A values, using the Arrhenius and Eyring equations. In addition, we have tried to include as many recent significant examples as possible, which have not been reviewed before.

Fig. 1 illustrates three limiting cases of twisting a ribbon with edges highlighted in black and blue for clarity. Depending on the position of the stereogenic axis, three types, namely, I, II and III, can be recognised. A type I helical ribbon coils around an axis, which does not have an intersection with the ribbon, leading to a structure reminiscent of a staircase. As a result, the blue and black edges do not have the same length, the blue edge being consistently the longer one in this review (except for the case of equal lengths of the two edges). Molecular analogues are known as *helicenes* (Section 2), the most archetypal examples of helical polyaromatic systems. The steric interaction between overlapping or partially overlapping rings forces helicenes to adopt a helical conformation against the energy cost of the torsional strain induced in the helicene backbone.

Type II features a stereogenic axis that is identical to the main axis of the untwisted, planar ribbon. When the ribbon is twisted around this axis, both edges have the same length and are pirouetting around the axis similarly to the strands of double-helix DNA. The closest molecular analogues of type II ribbon are known as *twistacenes* (Section 3). Unfavourable steric interactions are achieved by introducing steric crowdedness around the periphery. The energy benefit of minimising these steric interactions is optimised against the energy cost of distorting the π -system from planarity.

In type III, the stereogenic axis and the black edge of a ribbon, instead of the main axis of its planar form, are identical.



Michel Rickhaus (left), Marcel Mayor (middle) and Michal Juriček (right)

Michal Juriček received his MSc from Comenius University in Bratislava before he pursued his PhD at Radboud University Nijmegen with Professor Alan E. Rowan. In 2011, he joined the group of Professor J. Fraser Stoddart at Northwestern University as a postdoctoral fellow. He currently leads an independent research group at the University of Basel, where he investigates polycyclic hydrocarbons with delocalised spin densities.

Michel Rickhaus obtained his MSc (2011) and PhD (2015) from the University of Basel under the supervision of Professor Marcel Mayor. His research interests involve the development of new concepts for inducing twists and strain in aromatic materials. Under the supervision of Professor Lawrence T. Scott at Boston College, he worked as a visiting scholar on planarisation of curved aromatic systems.

Marcel Mayor received his PhD in 1995 supervised by Professor Rolf Scheffold and Professor Lorenz Walder. After working with Professor Jean-Marie Lehn at the University Louis Pasteur in Strasbourg and at the Collège de France in Paris, he founded his own research group at the Karlsruhe Institute of Technology in 1998. On defending his habilitation in 2002, he became Professor of Chemistry at the University of Basel in 2004. His current research interests are supramolecular chemistry, molecular electronics, nanoscale architectures, functional materials and hybrid materials.

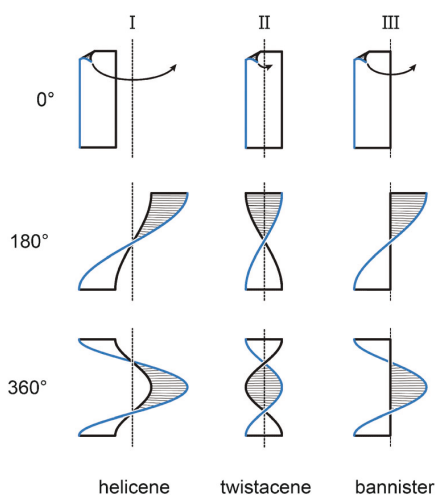


Fig. 1 Three types of helically twisted ribbons. The stereogenic axis is placed such that it (I) does not have an intersection with the ribbon (helicene-type), (II) is identical to the main axis of the ribbon (twistacene-type) or (III) is identical to the black edge of the ribbon (bannister-type). In type II, the blue and black edges have the same length, while in types I and III, the blue edge is longer than the black one. Twists of 180 and 360° are shown.

Twisting the ribbon around the stereogenic axis leads to a system, in which the blue edge is longer than the black one and coils around the black edge, similarly to the case of a *bannister* (Section 4). Known molecular analogues of type III system have a rigid oligo(*para*-phenylene) backbone (black edge) and a bannister-like flexible part (blue edge), encircling a “hollow” ribbon. Ring strain in the bannister systems induces the helically twisted conformation against the torsional strain generated in the oligo(*para*-phenylene) backbone, which is energetically less costly.

Section 5 of this review focuses on helical systems in which a “circular ribbon” (ribbon where both ends are “fused” together) is twisted around one or three axes to provide more complex helically twisted systems, namely, figure-of-eight (type IV) and propeller (type V) helices, respectively. In Section 6, the properties emerging from the helical nature of these systems are discussed.

2. Helicenes

Helicenes^{5–7} and truncated helicenes are the first structural type of strain-induced helical architectures shown in Fig. 1, in which both edges of a ribbon, one shorter (black) and one longer (blue), coil around an axis that does not have an intersection with the ribbon. In other words, the edges coil around circular cylinders that have a common axis but different diameters. The structure of an $[n]$ helicene (Fig. 2a) comprises *ortho*-fused benzene rings (n is the number of rings), which represent the body of the ribbon. In truncated $[n]$ helicenes, some rings are omitted (Fig. 2, top) such that the black edge remains intact, while the blue edge is interrupted. The number of turns

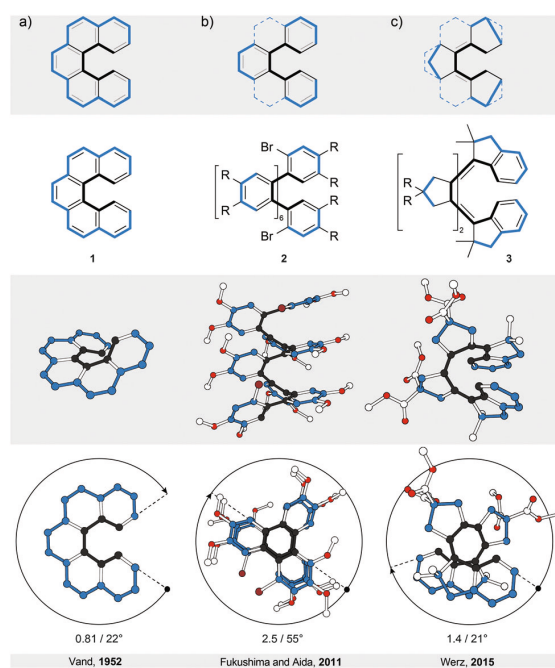


Fig. 2 Helicenes and truncated helicenes: structural formulae of **1–3** (top), and perspective (middle) and top (bottom) views of their corresponding solid-state structures (XRD). The truncation process is illustrated using the backbone of the parent [5]helicene (a) with a continuous annulation. Partial truncation of $[n]$ helicenes leads to *ortho*- $[m]$ phenylenes (b), and full truncation and embedding of five-membered rings leads to all-*s-cis* all-*Z* polyenes (c). The overall number of turns/average torsion-angle value per phenanthrene (a) or biphenyl (b and c) subunit are shown. The edges are highlighted in black and blue for clarity. In **2**, R = OMe; in **3**, R = COOMe.

(Fig. 2, bottom) in $[n]$ helicenes and truncated $[n]$ helicenes can be estimated using the formula $n/6$. According to this formula, [6]helicene shows approximately one and [12]helicene approximately two turns.

2.1. $[n]$ Helicenes

In a two-dimensional drawing of an $[n]$ helicene, some benzene rings overlap with one another and therefore suffer from steric interaction. The number of overlapping rings depends on the number of fused rings (n). When $n \leq 6$, the terminal benzene rings only partially overlap¹⁰ with each other (Fig. 2a). When $n > 6$, every k fused ring ($k > 6$) overlaps with the $(k - 6)$ ring and the steric interaction between these rings causes repulsion (Fig. 3a). To minimise the steric interaction, the structure undergoes a helical twist and the final thermodynamically most favoured conformation results from the optimisation of the energy cost of the induced torsional strain against the energy benefit of the minimised steric interaction. The induced torsional strain is best visible by looking at distortions in the bay region (black) of the phenanthrene subunits of $[n]$ helicenes. While in phenanthrene (the shortest $[n]$ helicene) the bay-region torsion-angle value is close to 0°, in $[n]$ helicenes with $n > 3$, the average bay-region torsion-angle values vary from 19° in [4]helicene⁵ to

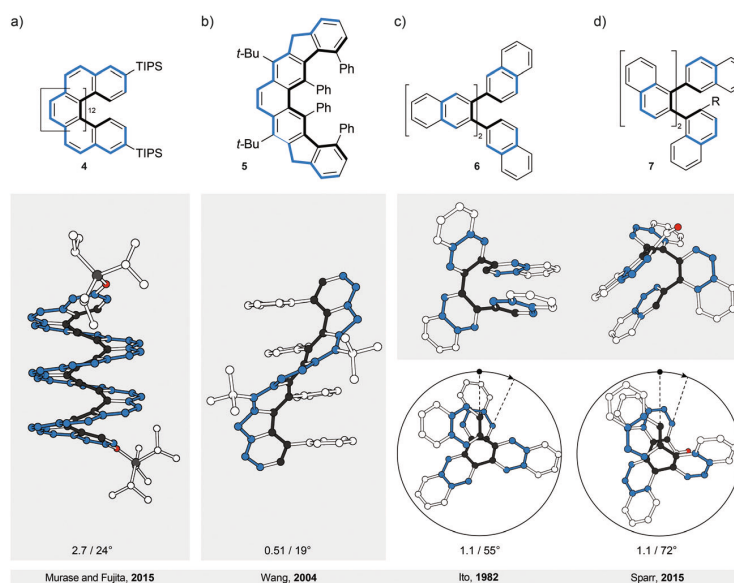


Fig. 3 Helicenes and *ortho*-naphthylenes: structural formulae of **4–7** (top), and perspective (middle) and top (bottom right) views of their corresponding solid-state structures (XRD). The overall number of turns/average torsion-angle value per phenanthrene (a), phenanthrene/fluorene (b) or binaphthyl (c and d) subunit are shown. The edges are highlighted in black and blue for clarity. In **7**, R = CHO.

24° in [16]helicene¹¹ (**4**), the longest [*n*]helicene (Fig. 3a) made to date. (Note: the average torsion-angle value is calculated from the torsion-angle values of all possible phenanthrene subunits in an [*n*]helicene.) The roughly constant values of the torsion angles across the series of [*n*]helicenes are the result of the close contact between the rings positioned above each other, with an average distance of ~ 3.5 Å (the π - π stacking distance), by which [*n*]helicenes gain additional stabilisation. [*n*]Helicene can be thus viewed as a tension spring.

Although the values of torsion angles are approximately uniform, the racemisation ΔG^\ddagger values of [*n*]helicenes increase⁶ with increasing *n* ($n/\Delta G^\ddagger$ (kcal mol⁻¹) at 300 K: 5/24.1, 6/35.6, 7/41.7, 8/42.4 and 9/43.5). In [*n*]helicenes with *n* > 6, in which at least two rings are fully overlapped, a plateau is reached and the energy barrier values of [7]- and higher [*n*]helicenes are very similar. This observation indicates that [*n*]helicenes are “much more flexible than is generally believed” as pointed out¹² by Martin and Mislow. It has been shown¹² that the racemisation of [*n*]helicenes most likely occurs through a conformational pathway, rather than an internal double Diels–Alder reaction, because the necessary molecular deformations are spread over a large number of bonds. Substituents introduced in the bay region of the terminal rings increase⁶ the energy barrier of racemisation in [*n*]helicenes, as they induce an additional steric interaction, reflected by an increased average “bay-region” angle.

A unique example of an [*n*]helicene is compound **5**¹³ (Fig. 3b), in which five- and six-membered rings are fused together in an alternating *ortho/meta* fashion. As a result of this topology, a less curved structure, compared to all-*ortho*-fused helicenes, is obtained. To induce a helical conformation in this system, four phenyl substituents were introduced at the inside (black edge)

and two *tert*-butyl substituents at the outside (blue edge) peripheries, respectively, to cause sufficient unfavourable steric interaction. The structure adopts a helical conformation, which is reminiscent of a spiral staircase, in which the four phenyl groups represent four parallel steps. Compared to all-*ortho*-fused helicenes, the *ortho/meta*-fused helical “spring” makes a full turn over a longer distance. It can therefore be categorised as a helicene that is, in part, twistacene-like. The structure is further stabilised by π - π stacking interactions between the parallel phenyl rings, which rotate around the single aryl–aryl bond with energy-barrier values between 12.6 kcal mol⁻¹ at 283 K and 14.3 kcal mol⁻¹ at 298 K. The energy barrier of racemisation was not determined for this compound, but it is expected to be stable against racemisation at room temperature.

2.2. Truncated [*n*]helicenes

Truncation of every second ring in [*n*]helicene with *n* \geq 5 (Fig. 2b) leads to an *ortho*-[*m*]phenylene structure ($m = (n + 1)/2$ for an *ortho*-[*m*]phenylene made by truncation of [*n*]helicene). Similarly to [*n*]helicenes, *ortho*-[*m*]phenylenes¹⁴ also adopt a helically twisted conformation to minimise the steric interaction between each pair of alternating phenylene rings. In contrast to [*n*]helicenes, however, *ortho*-[*m*]phenylenes do not contain phenanthrene but biphenylene subunits, which makes them more flexible as conformational changes involve rotation of phenylene rings around single aryl–aryl bonds. Because of their flexibility, *ortho*-[*m*]phenylenes adopt¹⁴ multiple helical conformations in solution. In the most stable helical conformation (“closed” helix) of *ortho*-[*m*]phenylenes, the phenylene rings are oriented with respect to each other such that every phenylene ring interacts through an offset π - π stacking¹⁵ with

every third phenylene ring, forming a well-defined helical architecture with small disorder at the ends. The steric interaction is minimised against torsional strain induced in each biphenylene subunit. For illustration, the average biphenylene torsion-angle value in *ortho*-[8]phenylene **2**¹⁶ is 55°, which is higher than the value (~45°) of the optimum biphenyl torsion angle. The induction of the torsional strain in biphenyl, however, is less energy-costly compared with phenanthrene, and *ortho*-[*m*]phenylenes are thus less strained than [*n*]helicenes.

The lack of strain and higher flexibility of *ortho*-[*m*]phenylenes are also reflected in the lower values of their racemisation ΔG^\ddagger when compared with [*n*]helicenes. The shortest *ortho*-[*m*]phenylene that could be partially resolved¹⁷ into its enantiomers by chiral-stationary-phase HPLC was *ortho*-[10]phenylene. Helical inversion of *ortho*-[16]phenylene and *ortho*-[24]phenylene is sufficiently slow and both compounds could be fully resolved, which allowed determination¹⁷ of their racemisation ΔG^\ddagger values at 298 K (23.4 and 23.9 kcal mol⁻¹, respectively). The longest reported *ortho*-phenylene contains¹⁶ 48 phenylene units, however, its racemisation barrier was not reported. An *ortho*-[8]phenylene derivative of **2** (with an NO₂ group instead of each Br atom) was successfully resolved¹⁶ into its enantiomers by crystallisation. Its racemisation ΔG^\ddagger value at 283 K was determined to be 20.4 kcal mol⁻¹, indicating fast helical inversion (half-life of 352 s) in solution. Interestingly, this compound adopts¹⁶ a tighter helical conformation (shorter π - π stacking distance between phenylene rings) upon oxidation, which dramatically changes its racemisation barrier at 283 K to 23.9 kcal mol⁻¹ (half-life of 44 h), a value similar to those of longer neutral analogues. The racemisation barrier can be increased by replacing the phenylene subunits with the naphthalene ones (Fig. 3c and d). Because of the increased steric interaction, naphthalene-1,2-diyl system **7**¹⁸ does not undergo racemisation even at elevated temperatures (the racemisation ΔG^\ddagger value of a related trimer at 453 K is 36.8 kcal mol⁻¹). Topologically, while in extended systems **6**¹⁹ a full offset overlap between the naphthalene moieties is expected based on the solid-state structure, in extended systems **7**, only partial offset overlap between the naphthalene moieties should take place. An extension of *ortho*-[*m*]phenylenes are oligo(*ortho*-phenylacetylenes),²⁰ which in some cases adopt a helical conformation in the solid state. In these systems, the helical conformation is not induced by strain and is usually one of many possible conformations that are in equilibrium in solution. Because oligo(*ortho*-phenylacetylenes) can be therefore categorised as foldamers,²¹ they do not fit into the category of strain-induced helices and are not discussed in more detail.

Truncation of all rings in an [*n*]helicene leads to a polyene structure (Fig. 2c). To induce a helical conformation in such a polyene system, five-membered aliphatic rings were annulated at the site of the single bonds. In this way, the polyene system was forced to adopt an all-*s-cis* all-*Z* arrangement. Milde reported²² the first example of such a polyene (**3**, truncated [9]helicene), which is coiled into a helical conformation with an average bay-region torsion angle of 21°. Double bonds connecting the five-membered rings induce rigidity in the system, which is, similar to [*n*]helicenes, more strained than *ortho*-[*m*]phenylenes. In fact, the racemisation

ΔG^\ddagger value of **3** was determined to be 28.1 kcal mol⁻¹ at 383 K. For a comparison, the racemisation ΔG^\ddagger value of non-truncated [9]helicene is 51.5 kcal mol⁻¹ at 383 K, which makes [*n*]helicenes more stable against racemisation than truncated [*n*]helicenes.

3. Twistacenes

The most intuitive deformation of a planar ribbon is the twist along its main molecular axis (Fig. 1, middle). Both edges of the resulting helically twisted ribbon have the same length and this degree of symmetry simplifies the synthesis of the molecular analogues. Acenes, polyaromatic hydrocarbons comprising linearly (or *meta*-) fused benzene rings, are ideally suited for induction of such a helical twist. They have well-defined chemically addressable rims, which allow substituents or annulated rings to be held in close proximity to each other. The steric crowdedness around the periphery forces an acene to adopt a helical conformation, which is energetically more favoured than the planar one. Such twisted acenes are known⁸ as *twistacenes*. Steric crowdedness can be achieved (Fig. 4) by the use of bulky substituents, such as phenyl groups, at all (a, crowded twistacenes)²³ or selected (b, equatorenes)²⁴ positions, by benzannulation (c, π -extended twistacenes),²⁵ or by embedding an acene into a bicyclic system (d, bicyclic twistacenes).²⁶ In the latter case, two pairs of opposing peripheral carbon atoms are bridged, one pair above and one below the acene plane. In this constitution, the carbon atoms are pulled out of the plane, each pair in the opposing relative direction, inducing helicity. Cases, where bulky substituents in combination with benzannulated rings are employed to induce helical twist, have also been described.²⁷ In this section, representative examples of all four types and their combinations are discussed.

To assess qualitatively the amount of induced torsional strain in a twistacene, the average torsion-angle values per benzene ring are compared, instead of the overall end-to-end torsion-angle values. Notably, twistacenes are less sensitive to light, heat, oxygen, dimerisation or polymerisation compared with planar acenes. They, however, retain⁸ the electronic and spectroscopic properties of the parent acenes, presumably because the twist is relatively small and continuous across the entire “ribbon”.

3.1. Crowded twistacenes

In perbrominated naphthalene **8**²³ (Fig. 4a), every hydrogen atom is substituted by a bromine atom. The shortest distance between the neighbouring bromine atoms at the 1-/4- and 8-/5-positions in planar **8** is ~2.5 Å, while the average distance between the neighbouring bromine atoms in helically twisted **8** is ~3.3 Å. Since the sum of the van der Waals radii of two bromine atoms is ~3.8 Å, a significant amount of strain energy is released upon twisting **8**. Indeed, X-ray diffraction analysis of the solid-state structure of **8** revealed an end-to-end twist of 31° (or ~15° per benzene ring), which was attributed solely to the effect of minimising steric interactions between the substituents. The steric effect is clearly visible when the end-to-end twist of **8** is compared with that (24°) of octachloronaphthalene,⁸ as chlorine

Tutorial Review

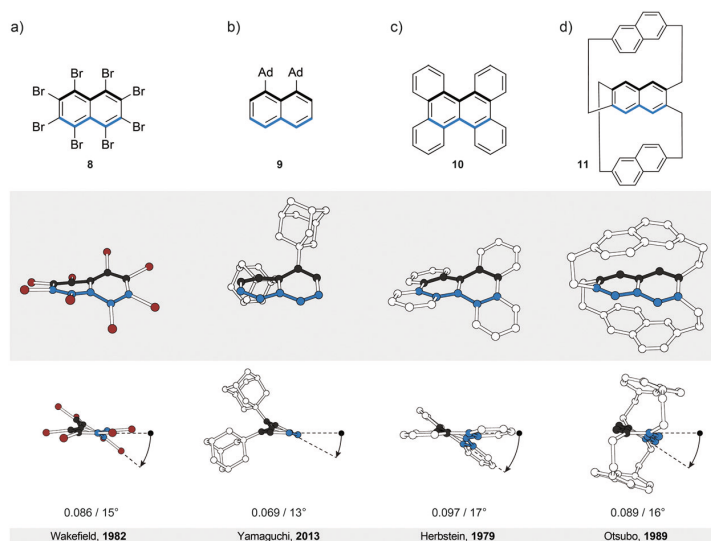


Fig. 4 Twistacenes: structural formulae of **8–11** (top), and perspective (middle) and side (bottom) views of their corresponding solid-state structures (XRD). A continuous helical twist of naphthalene around its main molecular axis was achieved by (a) substitution at all peripheral positions, (b) substitution at the positions on one side only, (c) benzannulation and (d) embedding naphthalene unit into a bicyclic system. The overall number of turns/average torsion-angle value per benzene ring are shown. The edges are highlighted in black and blue for clarity.

(radius 175 pm) is less bulky than bromine (radius 190 pm). When the bromine atoms in **1** were replaced by phenyl substituents to afford octaphenylnaphthalene,⁸ it was found that the naphthalene unit in this compound is almost perfectly planar in the solid state. The calculations performed on octaphenylnaphthalene and comparison with other analogues suggest⁸ that such planarisation should not be favoured,

indicating that crystal-packing forces overcompensated the induced steric strain in this case. Solution studies, if possible, are therefore an important addition to the solid-state analysis of the induced helical twist.

The perphenylated anthracene **12**²⁸ (Fig. 5a), an extended analogue of octaphenylnaphthalene, shows a 63° twist (or ~21° per benzene ring) in the solid-state structure. Notably, its

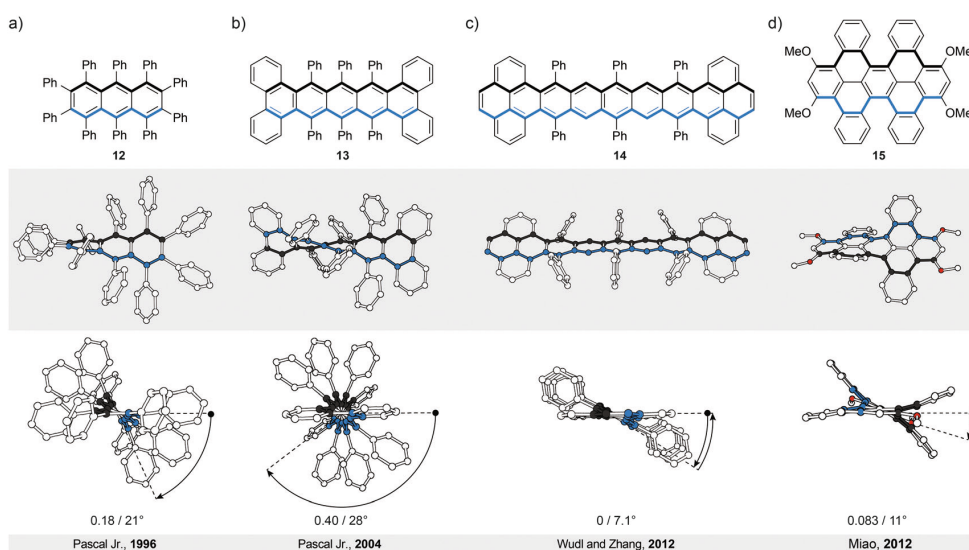


Fig. 5 Longer twistacenes: structural formulae of **12–15** (top), and side (middle) and top (bottom) views of their corresponding solid-state structures (XRD). (a) Fully substituted anthracene derivative, (b) pentacene with both bulky substituents and π -extended benzannulated ends, (c) the first example of a nonatwistacene, which adopts an achiral *meso* conformation and (d) naphthalene-based bicyclic cyclophane. The overall number of turns/average torsion-angle value per benzene ring are shown. The edges are highlighted in black and blue for clarity.

View Article Online

Chem Soc Rev

Tutorial Review

^{13}C NMR spectrum in solution features only 16 signals instead of the expected 22 for the D_2 symmetric structure, indicating that **12** is relatively flexible to yield a time-averaged D_{2h} or D_2 symmetry. The obtained spectroscopic data revealed a fine vibrational structure similar to anthracene, which suggests that distortions of up to 21° per benzene ring do not significantly affect the π -conjugation in acenes.

Twistacene **13** shows²⁷ an astonishing end-to-end torsion-angle value of 144° ($\sim 28^\circ$ per benzene ring) in the solid state (Fig. 5b), the largest induced twist to date. As a consequence, **13** is highly soluble in common organic solvents and air-stable at room temperature in the dark. It is also one of the few twistacenes that undergo a relatively slow racemisation (half-life ~ 9 h, $\Delta G^\ddagger = 23.8$ kcal mol $^{-1}$, 298 K), which allowed separation of its enantiomers. For a comparison, most of its analogues, which afforded enantiomerically pure crystals, undergo⁸ a much faster racemisation in solution. Racemisation of twistacenes occurs⁸ over several nonplanar intermediates with lower energy transition states, compared with a hypothetical planar transition state, which is the main reason for fast racemisation of most twistacenes.

The importance of sufficient steric crowdedness around the periphery for inducing the helical twist in acenes is demonstrated²⁹ best in the case of nonatwistacene **14**. In **14**, the periphery is decorated (Fig. 5c) with bulky substituents and benzannulated rings, however, four crucial positions around the centre of the acene are unsubstituted. The steric strain at each end (between phenyl and annulated benzene rings) induces a helical twist, with positive (at one end) and negative (at the other end) helicities. Because of the four missing substituents, the helical twist at one end does not propagate to the other end; rather it changes helicity in the centre of the acene. This conformation is energetically more favoured than that with a continuous twist because it results in a decreased average torsion-angle value of $\sim 7.1^\circ$ per benzene ring ($\sim 28^\circ$ in **13**) and consequently less induced strain. The central benzene ring has no twist (0° torsion angle), while the third-to-last benzene rings experience the largest twist (14° torsion angle). Such a disrupted-helix conformation has a plane of symmetry and represents an achiral *meso* form. A continuous crowdedness around the periphery is therefore of central importance for inducing helicity in acenes by strain. In contrast to the planar nonacene, which is extremely unstable and has never been isolated as a solid material, twistacene **14** is stable in air for more than five days. The increased stability is presumably the consequence of steric bulk and extended π -conjugation at the ends (pyrene subunits), which proved to increase the stability under oxygen and light exposure in shorter twistacenes. The twist, which typically does not affect significantly the electronic structure, might contribute to stability, but due to steric factors, as well. An example of an extended type II system is compound **15**,³⁰ in which dibenzo[*cd,lm*]perylene is employed instead of an acene as the “ribbon” (Fig. 5d). The helical conformation is induced by annulation of four benzene rings, which are part of two [5]helicene subunits that display the same helicity within the structure. The induced torsional twist of 11° is lower compared to most of the twistacenes, presumably as a result of the fact that

the induced strain is spread over a larger number of bonds in dibenzo[*cd,lm*]perylene compared with an acene of the same length. The second possible isomer is the *anti*-conformer (not shown), which is chiral despite the fact that the [5]helicene subunits show opposite helicities. Theoretical calculations predict similar energies for both stereoisomers and, indeed, heating of one or the other conformer leads to a mixture of both. Substitution of the methoxy groups in **15** for the hexyloxy groups allowed determination³⁰ of the conformer-interconversion barriers of the corresponding derivative (27.7 kcal mol $^{-1}$ for the twisted-to-*anti* and 28.7 kcal mol $^{-1}$ for the *anti*-to-twisted processes at 383 K) by ^1H NMR spectroscopy. These values, in principle, also correspond to the racemisation-barrier values for both conformers.

3.2. Equatorednes

A recently described type of longitudinally twisted acenes that is closely related to twistacenes are the equatorednes. Similarly to twistacenes, the torsional twist in equatorednes is caused by steric strain at the periphery, however, only on one side, resulting in a lower symmetry compared to twistacenes. Equatoredne **9**²⁴ (Fig. 4b) bearing two adamantyl (Ad) groups at the 1- and 8-positions shows an end-to-end twist of almost 25° ($\sim 13^\circ$ per benzene ring). Notably, the blue edge in **9** shows no deviation from planarity, as the twist affects solely the black (substituted) edge. Such dissymmetry is also present if the unsubstituted part of the acene (blue edge) is annulated, which distorts only the substituted part of the conjugated system from planarity. Remarkably, equatorednes do not racemise at room temperature, as the racemisation energy barriers have typically higher values than those of twistacenes. For example, the racemisation ΔG^\ddagger value of **9** was determined to be 26 kcal mol $^{-1}$ at 343 K. Benzannulation of the unsubstituted part of the acene core further increases this barrier. As the induced twist is higher in twistacenes than in equatorednes, the increase of the energy-barrier values in the case of equatorednes can be attributed to the substituent rather than the twist effect, as the equatoredne substituents are usually much bulkier than those of twistacenes (adamantly *versus* phenyl). Compared with the planar parent acenes, the emission maxima of equatoredne analogues are typically red-shifted²⁴ due to the decrease of the energy of the HOMO while maintaining the LUMO energy level.

3.3. π -Extended twistacenes

Benzannulation of an acene leads to structures with an interesting diversity of twists, when looking at their solid-state structures. Strictly speaking, they no longer belong to the category of acenes but are an entirely new class of polycyclic aromatic hydrocarbons (PAHs). They are related to acenes in the sense that they adopt a twisted-ribbon conformation similar to twistacenes. The torsional twist is caused by the steric interaction between the annulated rings. One selected example is given here but many more exist in the literature, often not being recognised as chiral molecules. Tetrabenzonaphthalene **10**²⁵ (Fig. 4c) demonstrates the principle of introducing steric strain by benzannulation, which induces a helical end-to-end twist of 35° ($\sim 17^\circ$ per benzene ring) in **10**. For a comparison, the

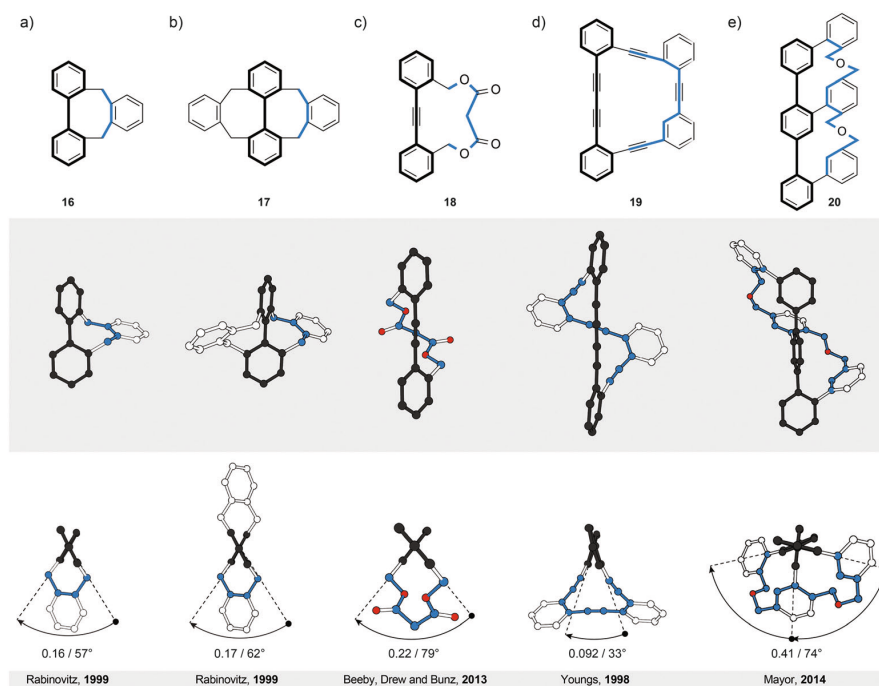


Fig. 6 Bannisters: structural formulae of **16–20** (top), and side (middle) and top (bottom) views of their corresponding solid-state structures (XRD). Singly (a) and doubly (b) bridged biphenyl, singly bridged diphenylacetylene (tolane, c) and bis(diphenylacetylene) (d) with an extended molecular axis compared with biphenyl, and singly bridged terphenyl (e) featuring one continuous bridge, which is connected to each ring of the backbone. The overall number of turns/average torsion-angle value per biphenyl subunit are shown. The edges are highlighted in black and blue for clarity.

value of this end-to-end twist is very close to that (31°) of crowded twistacene **8** (Fig. 4a).

3.4. Bicyclic twistacenes

A conceptually different approach to induce a helical twist in acenes is by crosswire-like bridging of two pairs of opposing edge positions. One bridge, if short enough, distorts an acene into a boat-like conformation. With two bridges of such length, the acene is distorted into a helically twisted conformation (Fig. 4d) if one bridge connects the two ends above and one below the plane of the acene. Tanaka *et al.* demonstrated²⁶ this concept in a naphthalene-based “triple-decker” bicyclic cyclophane **11** (Fig. 4d). The resulting end-to-end twist of the central naphthalene unit in **11** is 32° ($\sim 16^\circ$ per benzene ring), and is caused solely by the bicyclic strain without the contribution of steric bulk.

4. Bannisters

Similarly to helicenes and twistacenes described in Sections 2 and 3, respectively, the bannister-like structures also display a continuous helical twist along the stereogenic axis. The difference between the twistacene and bannister ribbon types is that in twistacenes, the stereogenic axis is identical to the main axis of the ribbon, while in bannisters, the stereogenic axis and the black edge of the ribbon are identical (Fig. 1, right). From a

different perspective, a bannister system can be viewed as one half of the twistacene system, in which the axis becomes the black edge. In this constitution, the blue edge resembles a bannister of a staircase rather than the steps, as it is longer and coils around the shorter black edge (the axis), which remains linear. The structures of the known molecular bannister analogues consist (Fig. 6) of an oligo(*para*-phenylene)^{31–34} (a, b and e) or a phenylene–acetylene^{35,36} (c and d) backbone, representing the black edge, and a linker bridging the terminal phenylene rings (blue edge), forming a macrocycle encircling a “hollow” ribbon. The energy barrier for the relative rotation of the individual phenylene rings in an unbridged oligo(*para*-phenylene) is relatively low and the rings are “free” to rotate around the single aryl–aryl bonds under ambient conditions. The macrocyclic strain of the hypothetically planar bannister oligomers forces the linker to coil around the oligo(*para*-phenylene) backbone in a helical fashion, inducing torsional strain in each biphenylene subunit. The general rule³³ to follow while designing bannister structures is to interlink two phenylene rings with a bridge that is longer than the distance between the two rings.

4.1. Bridged biphenyls

The smallest known bannister structures are bridged biphenyls⁴² (Fig. 6a, b and 7). The axially chiral *ortho*-substituted biphenyls do not fall into this category because their chirality is not merely induced by steric interactions between the substituents.

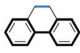
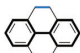
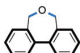
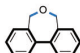
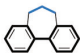
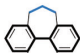
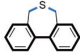
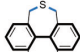
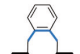
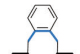
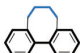
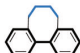
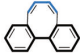
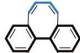
<i>n</i>	No.	Structure	$\theta / ^\circ$ ^a	$\Delta G^\ddagger / \text{kcal mol}^{-1}$	<i>T</i> / K	No.	Structure	$\theta / ^\circ$ ^a	$\Delta G^\ddagger / \text{kcal mol}^{-1}$	<i>T</i> / K
2	21		21 ^a	–	–	27		18 ^c	–	–
3	22		44 ^{ab}	10.6 ^a	189	28		44 ^d	26.1 ^{de}	378
3	23		49 ^{ef}	12.5 ^f	262	29		49 ^g	30.4 ^g	367
3	24		57 ^{ah}	19.8 ^a	315	30		57 ^{af}	42.5 ^{ag}	488
4	16		60 ⁱ	20.1 ⁱ	412	17		62 ⁱ	49.6 ⁱ	596
4	25		64 ^h	23.0 ^h	293	31		64 ^h	>48.2 ^h	673
4	26		64 ^h	29.6 ^h	360	32		68 ^h	>46.2 ^h	596

Fig. 7 Correlation between the values of the biphenyl torsion angles (θ), Gibbs free energy barriers (ΔG^\ddagger) of racemisation and the lengths (*n*) of the bridges (highlighted in blue) in singly (**16** and **21–26**) and doubly (**17** and **27–32**) bridged biphenyls. ^a Calculated value. ^b XRD Value, ref. 37. ^c XRD Value, ref. 38. ^d Ref. 39; the torsion-angle values were calculated only for singly bridged biphenyls. ^e 43° from XRD of a 4,4'-dibromo-derivative, ref. 40. ^f Ref. 41. ^g Estimated from the E_a and $\log A$ values by using Eyring and Arrhenius equations; $\Delta G^\ddagger = \Delta H^\ddagger - T\Delta S^\ddagger$, where $\Delta H^\ddagger = E_a - RT$ and $\Delta S^\ddagger = R(\ln A - 1 - \ln(k_B T/h))$; for **22** and **24**, the $\log A$ values of **28** and **30**, respectively, were used. ^h Ref. 42. ⁱ 45° (**23**) and 59° (**25**) from XRD of 4,4'-dicyano-derivatives, ref. 43. ^j Ref. 43. ^k 58° from XRD, ref. 44. ^l Ref. 32; 58° (**16**) and 57° (**17**) from XRD.

An additional criterion for *ortho*-substituted biphenyls to be axially chiral is that the two *ortho*-substituents of each phenyl ring are not equivalent. For example, the doubly bridged biphenyl **17**³² (Fig. 6b) bearing four equivalent *ortho*-substituents is C_2 -symmetric (62° torsional twist) and therefore chiral, while its unbridged analogue 2,2',6,6'-tetramethyl-1,1'-biphenyl is not because it has a plane of symmetry ($\sim 90^\circ$ torsional twist⁴³). Unsubstituted biphenyl⁴² itself has $\sim 45^\circ$ torsional twist in the lowest-energy conformation, which defines its chirality as a geometrical object. The energy barrier of rotation around the aryl–aryl bond in biphenyl is, however, relatively low and fast rotation under ambient conditions does not allow differentiation between the two enantiomers.

A series of singly and doubly *ortho,ortho'*-bridged biphenyls in Fig. 7 demonstrate the dependence of the induced torsional twist (θ) in a biphenyl on the length (*n*, the number of bridging atoms) and the number (one *versus* two) of its bridges, as well as the effect of the twist and the number of bridges on the racemisation barrier ΔG^\ddagger . The torsional twist is induced by minimising strain that is present in the ring formed by the bridge and the backbone in an untwisted, planar biphenyl. When the length (*n*) of the X_n -bridge exceeds one atom, the

coplanar phenyl units, as in the case of C_1 -bridged biphenyl (fluorene), adopt a helically twisted conformation by rotation around the single aryl–aryl bond. For both singly and doubly bridged biphenyls, the biphenyl torsion-angle values increase with increasing *n*, varying (Fig. 7) from 21° (C_2 -bridged **21**³⁷) to 64° (C_4 -bridged **25** and **26**⁴²) in the singly bridged series and from 18° (C_2 -bridged **27**³⁸) to 68° (C_4 -bridged **32**⁴²) in the doubly bridged series. The torsion angles of the singly and doubly bridged biphenyls featuring the same bridge types have similar values with differences of $< 4^\circ$, in accord with expectations for such C_2 symmetric systems. Fig. 7 further illustrates that the racemisation ΔG^\ddagger values increase with increasing torsion-angle values in each series. Although this trend cannot be generalised to all bridged biphenyls, it can be applied to systems, such as **22–24** and **28–30**, in which deformations induced during racemisation are equal in number and in kind. In these systems, the three-atom bridges comprise either an oxygen, a carbon or a sulphur atom in the middle, and the size of the central atom defines³⁹ the torsional twist and the racemisation barrier. It is also of interest to note that although the torsion-angle values of the singly and doubly bridged biphenyls featuring the same bridge are similar, the racemisation-barrier values of

Tutorial Review

the doubly bridged biphenyls are 2.1–2.5 times higher than those of the corresponding singly bridged biphenyls. An additional (second) bridge thus helps “locking” the helical conformation in the bannister-type biphenyls, which makes all doubly bridged biphenyls with $n > 2$ stable against racemisation under ambient conditions. The doubly bridged biphenyls can be viewed as “double-bannister”, or double-helix, systems, in which each bridge coils around the stereogenic axis similarly to the coiling of the two edges in twistacenes. Increasing the rigidity of the bridge(s)⁴² in the case of **26** and **32** also leads to a significant increase of the racemisation-barrier values, when compared to flexible systems **25** and **31**, although all four compounds display similar values of torsional twists.

4.2. Extended bannisters

Introduction of one and two acetylene linkers in between the two rings of a bridged biphenyl leads to elongated bannister systems **18**³⁵ and **19**,³⁶ respectively (Fig. 6c and d). The ease of induction of the torsional twist in such systems leads to an astonishing 79° twist in the case of **18**. The energy barrier of racemisation for this compound was not reported. Considering the flexibility of the system, however, the barrier is expected to be relatively low. In the case of **19**, the rigidity of the bridge accounts for the relatively low torsional twist (33°) and, presumably, for a higher energy barrier of racemisation compared to **18**, as evidenced by obvious deformations induced in the bridge (Fig. 6d).

The successful induction of helical chirality in bridged biphenyls encouraged the design and realisation of extended analogues, namely, terphenyls, with the backbone extended for an additional phenylene ring compared to biphenyls. Vögtle and co-workers pioneered³¹ the work in this field and synthesised the first doubly bridged terphenyl **33** (Fig. 8), using the same $-\text{CH}_2\text{SCH}_2-$ bridge as in biphenyls **24** and **30**. Because the bridges in **33** link one terminal ring each to the central ring, the bridges do not display a continuous helical twist around the backbone but around an axis that is parallel to the backbone (Fig. 8, left). From this view, **33** represents a type I helix rather than type III (Fig. 1), despite the fact that Vögtle introduced³¹ the term *bannister* (German *Geländer*) for this system. From a “bannister perspective”, **33** can be viewed as two bannister subunits linked together, each being able to undergo helicity inversion independently of one another.

As a result of two stereogenic units being present in **33**, two diastereomers of **33** exist, a pair of enantiomers (*P,P* and *M,M*) with a helical conformation (Fig. 8, left) and an achiral (*P,M*)-*meso*-form (Fig. 8, right) that is more stable than the chiral conformers. All three stereoisomers are in equilibrium with each other in solution, as confirmed by ¹H NMR spectroscopy. The fact that the two bannister subunits in **33** are independent of each other is evidenced³¹ by the torsion angles (57° on average) and the energy barrier of racemisation (>23 kcal mol⁻¹ at 298 K) for **33**, values that are similar to those of singly bridged **24** (57°, 19.8 kcal mol⁻¹ at 315 K), rather than doubly bridged **30** (57°, 42.5 kcal mol⁻¹ at 488 K). Rathore and co-workers later extended³³ this system to a quadruply bridged pentaphenyl analogue. No crystal structure has been

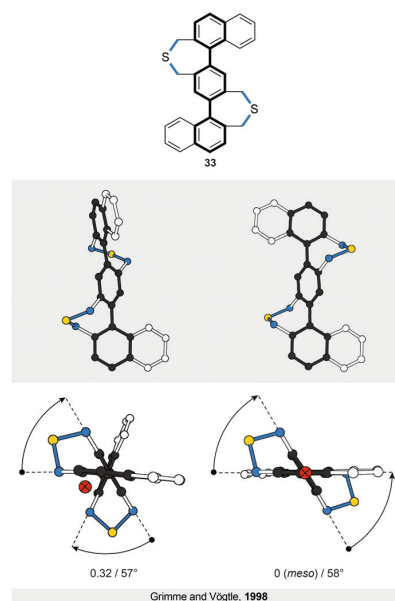


Fig. 8 Structural formula of **33** (top), and side (middle) and top (bottom) views of the solid-state structures (XRD) of its two diastereomers, a chiral (left, *P*)-enantiomer shown) and an achiral (right, *P,M*)-*meso*-form one. The two diastereomers exist because both bannister subunits can adopt either (*P*) or (*M*) helicities independently of each other. The overall number of turns/average torsion-angle value per biphenyl subunit are shown. The edges are highlighted in black and blue for clarity. The crossed red-filled ring indicates the stereogenic axis.

reported for this compound but, in principle, eight different diastereomers are possible with four stereogenic units.

A true bannister oligomer **20** with a continuous helical twist around the terphenyl backbone (Fig. 6e) has been recently reported^{33,34} by Mayor and co-workers, who presented a new concept that is related to Vögtle’s and Rathore’s idea of bannister oligomers. Instead of using two independent bridges as in **33**, only one continuous bridge attached to each ring of the backbone in a ladder-like fashion was employed in **20**. Similarly to other bannister oligomers, a helically twisted conformation is induced in **20** by strain that is present because the bridge and the terphenyl backbone do not have equal lengths. The new feature in this design is that the bridge is connected to each ring of the backbone with a linker (a phenyl ring), which acts as a relay. Once one end of the molecule adopts a helical conformation, the relay unit translates the helical twist onto the next segment, inducing a continuous twist of the bridge around the backbone that is collinear with the stereogenic axis. In this design, only (*P*) and (*M*) helical conformers, and not the *meso*-conformer, exist. Indeed, the X-ray crystallography, NMR spectroscopy and dynamic CD measurements confirmed the exclusive formation of two enantiomeric species, which presumably racemise *via* a uniform “dance-ribbon-like” pathway, with the racemisation ΔG^\ddagger value (~ 23.8 kcal mol⁻¹ at 298 K) similar to that of **33**. Compound **20** is to date the longest bannister oligomer that does not have a *meso*-form. Its stability against

racemisation could be further increased by either increasing the rigidity of the bridge or employing the “double-bannister” strategy, as in the case of doubly bridged biphenyls.

5. Figure-of-eights and propellers

This section covers polyaromatic structures that can be represented by a cyclic ribbon helically twisted around one or three axes (Fig. 9), which results in the figure-of-eight (type IV) or propeller-like (type V) helical architectures, respectively. Typically, these helices feature several structural elements that induce a helical twist continuously and with a high degree of symmetry. They illustrate how a variety of possibilities can arise by combining the right pieces and inspire the design of more complex and extended strain-induced helical polyaromatics.

5.1. Figure-of-eights

The first type (IV) of helically twisted cyclic ribbons is represented by molecules, in which aromatic rings are fused to form a circle, such as [8]circulene⁴⁵ (**34**, Fig. 10a).

Because of the strain within the inner eight-membered ring (black), **34** adopts a saddle-like conformation that displays a negative curvature. Based on DFT calculations, this conformation is achiral and has a D_{2d} symmetry, which is in accord with NMR observations. The helically twisted S_4 symmetric conformation observed in the solid state (Fig. 10a) is therefore most likely the result of the packing forces. This conformation is approximately $1.8 \text{ kcal mol}^{-1}$ higher in energy than the D_{2d} conformation according to DFT. The average torsion-angle value of the helically twisted S_4 conformation, calculated from the dihedral angles between the opposing carbon-carbon bonds of the inner eight-membered ring, is 49° .

Truncation (and extension) of [8]circulene leads to phenanthrene- (Fig. 10b) and [4]helicene-based (Fig. 10c) cyclic structures **35**⁴⁶ and **36**,⁴⁷ respectively. In these structures, two [n]helicene subunits are linked together to form a cycle twisted around one axis, a shape reminiscent of a figure-of-eight. The twist is induced either (1) by the strain present in the

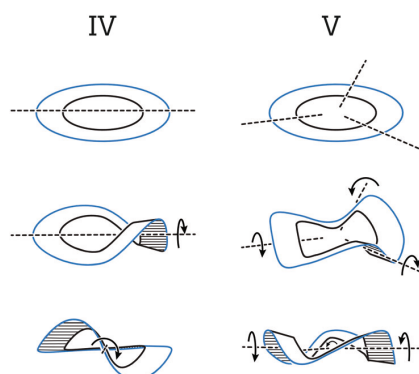


Fig. 9 Cyclic ribbon helically twisted around one (type IV) and three (type V) axes to afford figure-of-eight and propeller helices, respectively.

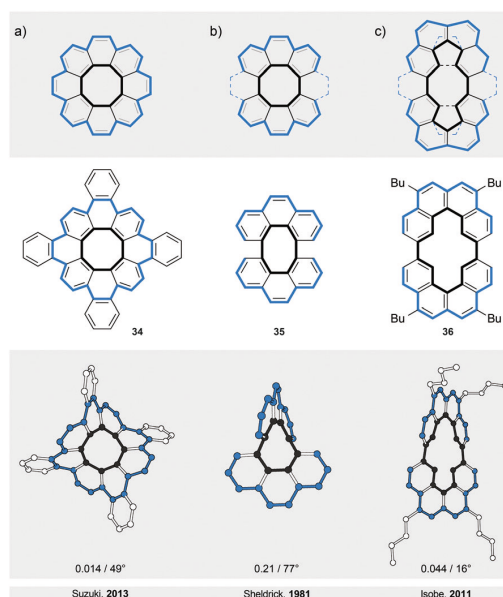


Fig. 10 Figure-of-eights: structural formulae of **34–36** (top), and perspective (bottom) views of their corresponding solid-state structures (XRD). (a) Tetrabenzo[8]circulene with a helically twisted conformation. (b and c) Cyclic bis[n]helicenes related to [8]circulene with well-defined helical twists. The overall number of turns/average torsion-angle value between opposing carbon-carbon bonds of the inner eight-membered ring (**34**) or between opposing carbon-carbon bonds linking the [n]helicene subunits (**35** and **36**) are shown. The edges are highlighted in black and blue for clarity.

eight-membered ring in the case of **35** or (2) by the steric interactions within the [4]helicene and biphenyl subunits in the case of **36**. In **35** and **36**, both helically twisted subunits show the same helicity as the overall structure, which has a helical twist of 77° and 16° , respectively. The racemisation ΔG^\ddagger values have not been determined for any of these structures, but a ΔG^\ddagger value of $10.1 \text{ kcal mol}^{-1}$ has been estimated for **36** by theoretical calculations. Structures **35** and **36** are unique in the sense that they represent⁴⁷ the illusory molecular expression of the “Penrose stairs”.

5.2. Propellers

Compounds **37**⁴⁸ and **38**⁴⁹ represent (Fig. 11) the second type (V) of helically twisted cyclic ribbons. They are reminiscent of a propeller because of their blade-shaped subunits. Compound **37**, also known as *cloverphene* (from “clover-like starphene”), is one of the first reported propellers and one of the smallest possible propellers derived from benzene. It adopts a D_3 symmetric helical conformation, in which three blades (blue-edged biphenyl subunits) are twisted out of the central-benzene-ring plane (black) by 30° on average per blade, as a result of the steric interaction between the blades. The structure of **37** also features three [5]helicene subunits, which share three rings each with one another. The average torsional twist of the [5]helicene subunits is 25° , a value slightly higher than that

Tutorial Review

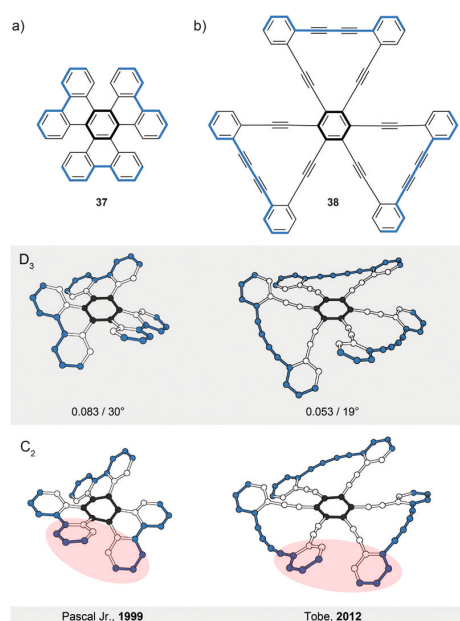


Fig. 11 Propellers: structural formulae of **37** and **38** (top), and perspective views of their D_3 (XRD, middle) and C_2 (model, bottom) conformations. The D_3 and C_2 conformations are twisted in an “up-down-up-down-up-down” and “up-down-up-up-down-down” fashions, respectively. The overall number of turns/average torsion-angle value per blade are shown for D_3 conformations. The edges are highlighted in black and blue for clarity. The red-filled circles highlight the parts of the C_2 conformations, where the packing sequence of the blades differs from that of the corresponding D_3 conformations.

of parent [5]helicene (Fig. 2a). In addition to the propeller D_3 conformation (Fig. 11a, middle), **37** can, in principle, also adopt a chiral C_2 symmetric conformation (Fig. 11a, bottom). While in the D_3 conformation the blades are twisted in an “up-down-up-down-up-down” fashion, the C_2 conformation displays an “up-down-up-up-down-down” packing sequence of the blades. Consequently, the central benzene ring is almost planar (shallow chair conformation) in the first case, while it is significantly distorted in the latter case (twisted boat conformation). According to DFT calculations, the D_3 conformation of **37** is lower in energy than the C_2 conformation by $5.0 \text{ kcal mol}^{-1}$, which is in agreement⁴⁸ with the fact that only single crystals of D_3 -**37** could be obtained. The racemisation barrier of D_3 -**37** was not determined but it likely has a magnitude similar to that of [5]helicene. The racemisation process of D_3 -**37** occurs presumably *via* the C_2 intermediate.

The D_3 propeller conformation is sometimes less stable than the C_2 conformation, for example, in the case of perchloro- or perfluorotriphenylene.⁴⁸ Pascal Jr. and co-workers carried out an extensive investigation of the D_3/C_2 dichotomy and found a simple rule-of-thumb⁴⁸ for the prediction of conformation in overcrowded D_{3h} polycyclic aromatics (D_{3h} is the symmetry of these structures when drawn flat on a paper): “if the central ring is expected to be aromatic (possessing shorter, benzene-like bonds), then a D_3 conformation should be preferred, but if the central ring is nonaromatic (possessing some very long

“single” bonds and great bond alteration), then a C_2 conformation will be observed.” In other words, if the central ring is more resistant to deformation, the twist occurs on the blades. If the blades are more resistant towards deformation, the core benzene ring is distorted. From these observations, the D_3/C_2 dichotomy seems to be mainly an electronic effect.

The second example of a D_3 symmetric helical propeller is compound **38**,⁴⁹ an ethynylene-extended analogue of **37**. The two outer benzene rings of each blade in **38** are linked by a diethynylene unit, which pushes these rings towards the rings of the neighbouring blades. The steric interaction between the neighbouring outer benzene rings forces the blades to twist by 19° on average with respect to the central benzene ring. In solution, **38** shows a rapid D_3/C_2 interconversion relative to the NMR timescale. Upon additional benzannulation of the blades, the barrier of the D_3/C_2 interconversion for the corresponding derivative was determined⁴⁹ to be $\sim 25 \text{ kcal mol}^{-1}$ at 220 K.

6. Properties arising from helicity

The overviewed concepts to induce helical chirality have merit in its own way. They, however, often provide us with structures that show unique properties or behaviour, some of which are discussed in this section. In particular, helical chirality in polyaromatic systems holds a promise to enhance optical and chiroptical properties, among others. Many of these promises have been met over the years, underlining the importance of design principles for making new strain-induced helices.

An induced helical twist can have a strong impact on the electronic structure of a π -conjugated system. For helicenes, this phenomenon is illustrated by a biradicaloid cethrene (**39**, Fig. 12), a dibenzo-annulated [5]helicene derivative. It has been shown⁵⁰ that the helical twist in **39** results in a significantly decreased singlet-triplet gap ($5.6 \text{ kcal mol}^{-1}$), when compared to that ($8.9 \text{ kcal mol}^{-1}$) of its planar analogue heptazethrene. Upon twisting hypothetically planar **39**, an antibonding and a bonding interaction within the HOMO and the LUMO, respectively, appear between the carbon atoms highlighted by red-filled circles (Fig. 12). In the triplet state, the HOMO and the LUMO contain one electron each, and the bonding and antibonding interactions roughly cancel out. In the singlet state, the two electrons are predominantly paired in the HOMO and singlet **39** suffers from the antibonding interaction more than triplet **39**, which results in the stabilisation of the triplet relative to singlet state and the decrease of the singlet-triplet gap. The interactions within the frontier MOs are visible also from the torsion-angle values of the [5]helicene subunit in the optimised geometries. While the average torsion-angle value in triplet **39** is 22° , singlet **39** features an increased torsion of 24° .

As mentioned briefly in Section 2.2, an NO_2 analogue of *ortho*-[8]phenylene **2** was successfully resolved¹⁶ into its enantiomers by crystallisation. Although its helical inversion in solution is fast, one-electron oxidation dramatically changes the half-life of inversion from 352 s to 44 h as it triggers compression of the helix by shortening the average π - π stacking distance between

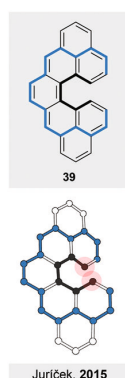


Fig. 12 Structural formula of **39** (top), a dibenzo-annulated [5]helicene, and the perspective view (bottom) of the optimised geometry of its singlet ground state. The edges are highlighted in black and blue for clarity.

the phenylene rings from 3.26 to 3.22 Å. The phenomenon of a helix compression in *ortho*-[*m*]phenylenes was also observed upon photoexcitation. Hartley *et al.* studied¹⁴ a series of *ortho*-[*m*]phenylenes with *m* ranging from 4 to 8 and found that the effective conjugation length (ECL) in this series is ~4 and ~5, as determined by experiments and calculations, respectively. The ECL value 4 means that the UV/Vis absorption maximum shifts bathochromically with the increasing length up to *m* = 4 and then remains approximately constant for oligomers with *m* > 4. This observation does not come as a surprise, as the biphenyl torsional twist makes the π -conjugation less effective compared to planar systems.

Interestingly, the emission maximum shifts hypsochromically with an increasing length for all members of this series as a result of a helix compression, which occurs¹⁴ on one end only in oligomers with *m* > 5 (Fig. 13). In the excited state, biphenyls typically adopt a planar quinoidal structure, but in *ortho*-[*m*]phenylenes, planarisation of the biphenyl units is not possible because of strain. As a result, the biphenyl torsion-angle values decrease upon photoexcitation to approximately 20–30° (quinoid-like structure), but are not zero. Furthermore, this compression occurs on one end only in oligomers with *m* > 5. Because longer oligomers are less able to accommodate

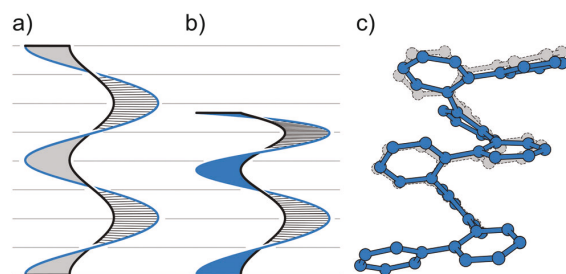


Fig. 13 Illustration of ground (a) and excited (b) states of *ortho*-[8]phenylene (c). In the excited state (blue in c), *ortho*-[8]phenylene adopts a helical conformation that is compressed on one end, in contrast to its ground state (gray in c) with no compression.

the excited-state planarisation, stability of the excited state decreases as the length of *ortho*-[*m*]phenylenes increases, which is the reason for the observed hypsochromic shift in the emission spectra. The emission behaviour of *ortho*-[*m*]phenylenes thus directly reflects the relationship between their conformational behaviour and their electronic structure.

The induced twist in twistacenes increases their stability. Because the twist does not significantly alter the electronic properties of the parent acene, this approach allows the preparation of longer acenes, which are otherwise not accessible or unstable. The elongation of acenes decreases the HOMO–LUMO gap and this feature makes longer acenes suitable candidates for constructing semiconductors. The access to stable longer acenes is therefore desired. Zhang *et al.* have recently synthesised and characterised²⁹ the longest stable acene, namely, nonacene derivative **14** (Fig. 5c). As mentioned in Section 3.1, nonacene **14** features an average 7° twist per benzene unit, but as it is not sufficiently crowded, it contains a plane of symmetry and is not chiral. The HOMO–LUMO energy gap in **14** was determined to be 1.7 eV by UV/Vis spectroscopy and cyclic voltammetry, which is a value in between those of hexacene (1.84 eV) and heptacene (1.36 eV). Although **14** does not display a continuous helical twist along the backbone, it is a proof-of-principle example, which demonstrates that an induced helical twist should allow for the preparation of even longer acenes that are not accessible by other methods.

Bannister compound **18** (Fig. 6c) demonstrates³⁵ how an induced helical twist can, quite unexpectedly, affect the absorption and emission behaviour. In contrast to biphenyl, an unsubstituted tolane (diphenylacetylene) has a flat energy profile of rotation around the alkyne unit, with an energy barrier of less than 1 kcal mol^{−1}. Similarly to biphenyl, however, the twisted conformation of tolane can be enforced by increasing steric bulk at the phenyl rings or by linking them. The linking approach is particularly appealing because it allows the tolane unit to adopt a planar conformation, which is more stable than the twisted one in the excited state. Compared with an unsubstituted tolane, a tolane with a fixed planar conformation displays a red-shifted absorption, while a tolane with a fixed twisted conformation shows a blue-shifted absorption. Bunz and co-workers have recently described³⁵ a malonate-bridged tolane **18** that exhibits an almost 80° twist in the solid state, a torsion which was later confirmed in solution. What makes this structure unique is its unexpected long-lived (4 s) phosphorescence at low temperature (77 K), which is most likely the result of the large twist that stabilises the triplet state. While the ground state of **18** is twisted, the system planarises upon excitation to the singlet S₁ state and at elevated temperature (298 K) fluoresces at a maximum wavelength similar to those of planar tolanes. At low temperature (77 K) in a glassy matrix, however, the twisted excited state conformation is fixed and instead of fluorescence, an inter-system crossing to the twisted triplet T₁ state, which enables phosphorescence, occurs. Presumably, this feature is possible if a large twist (>70°) is induced in a tolane, which has not yet been achieved by steric bulk.

7. Conclusion

Helical architectures have inspired artists, designers, engineers and scientists alike for centuries, because in helices, chirality is expressed in a highly symmetric fashion that appeals naturally to the eye. It is fascinating to realise that helical structures featuring an axis of symmetry look simpler than most of other chiral structures, and more beautiful than most of other achiral structures. It is not just their visage, however, that captured the attention of chemists. Helicity often gives rise to unprecedented properties, which would not exist without the helical twist. Polyaromatic systems, in particular, are ever-sought targets to induce helical chirality. Helical twisting of a π -conjugated backbone can often quite dramatically alter the electronic properties, or even lead to new unexpected features, as shown in the preceding section. Understanding the principles that govern the induction of helical chirality and its impact on the electronic structure is therefore of crucial importance. We hope that the classification concepts and principles to induce helicity that are presented in this review will inspire the design and synthesis of new “complex yet simple” helical structures. As many helices known from the literature are not configurationally stable at room temperature, structures with increased values of racemisation energy barriers would certainly represent an invaluable advancement in this field.

Available CCDC numbers

1 (1137287), 2 (773552), 3 (1020999), 4 (1051159), 6 (267858), 7 (1405203), 8 (1110604), 9 (947431), 10 (1268345), 11 (1192755), 12 (1314918), 13 (252291), 14 (857476), 15 (913485), 16 (1210912), 17 (1210914), 18 (918377), 19 (1170129), 20 (995567), 21 (1157531), 24 (726382), 27 (670511), 33 (101385), 34 (949624), 35 (1104816), 36 (806565), 37 (114449), 38 (872771).

Acknowledgements

The Swiss National Science Foundation (SNF, M. J./PZ00P2_148043; SNF, M. M./200020_159730) and the Novartis University of Basel Excellence Scholarship for Life Sciences (M. J.) are kindly acknowledged for their financial support.

References

- G. H. Wagniere, *On Chirality and the Universal Asymmetry: Reflections on Image and Mirror Image*, VHCA and Wiley-VCH, Zürich, 2007.
- Y. Wang, J. Xu, Y. Wang and H. Chen, *Chem. Soc. Rev.*, 2013, **42**, 2930–2962.
- K. Mislow, Molecular Chirality, in *Topics in Stereochemistry*, ed. S. E. Denmark, John Wiley & Sons, Inc., Hoboken, 1999, pp. 1–82.
- H. Förster and F. Vögtle, *Angew. Chem., Int. Ed. Engl.*, 1977, **16**, 429–441.
- M. Gingras, *Chem. Soc. Rev.*, 2013, **42**, 968–1006 and references cited therein.
- M. Gingras, G. Félix and R. Peresutti, *Chem. Soc. Rev.*, 2013, **42**, 1007–1050 and references cited therein.
- M. Gingras, *Chem. Soc. Rev.*, 2013, **42**, 1051–1095 and references cited therein.
- R. A. Pascal Jr., *Chem. Rev.*, 2006, **106**, 4809–4819 and references cited therein.
- C. Schmuck, *Angew. Chem., Int. Ed.*, 2003, **42**, 2448–2452.
- A. O. McIntosh, J. M. Robertson and V. Vand, *Nature*, 1952, **169**, 322–323.
- K. Mori, T. Murase and M. Fujita, *Angew. Chem., Int. Ed.*, 2015, **54**, 6847–6851.
- R. H. Martin and M. J. Marchant, *Tetrahedron*, 1974, **30**, 347–349 and ref. 9 cited therein.
- W. Dai, J. L. Petersen and K. K. Wang, *Org. Lett.*, 2004, **6**, 4355–4357.
- C. S. Hartley, *J. Org. Chem.*, 2011, **76**, 9188–9191 and ref. 5–7 cited therein.
- S. M. Mathew, J. T. Engle, C. J. Ziegler and C. S. Hartley, *J. Am. Chem. Soc.*, 2013, **135**, 6714–6722.
- E. Ohta, H. Sato, S. Ando, A. Kosaka, T. Fukushima, D. Hashizume, M. Yamasaki, K. Hasegawa, A. Muraoka, H. Ushiyama, K. Yamashita and T. Aida, *Nat. Chem.*, 2011, **3**, 68–73.
- S. Ando, E. Ohta, A. Kosaka, D. Hashizume, H. Koshino, T. Fukushima and T. Aida, *J. Am. Chem. Soc.*, 2012, **134**, 11084–11087.
- D. Lotter, M. Neuburger, M. Rickhaus, D. Häussinger and C. Sparr, *Angew. Chem., Int. Ed.*, 2015, DOI: 10.1002/anie.201510259.
- T. Motomura, H. Nakamura, M. Sugimoto, M. Murakami and Y. Ito, *Bull. Chem. Soc. Jpn.*, 2005, **78**, 142–146.
- R. H. Grubbs and D. Kratz, *Chem. Ber.*, 1993, **126**, 149–157.
- Foldamers: Structure, Properties and Applications*, ed. S. Hecht and I. Huc, Wiley-VCH, Weinheim, 2007.
- B. Milde, M. Leibelng, M. Pawliczek, J. Grunenberg, P. G. Jones and D. B. Werz, *Angew. Chem., Int. Ed.*, 2015, **54**, 1331–1335.
- J. H. Brady, A. D. Redhouse and B. J. Wakefield, *J. Chem. Res.*, 1982, **137**, 1541–1554.
- K. Yamamoto, N. Oyamada, S. Xia, Y. Kobayashi, M. Yamaguchi, H. Maeda, H. Nishihara, T. Uchimarui and E. Kwon, *J. Am. Chem. Soc.*, 2013, **135**, 16526–16532.
- F. H. Herbstein, *Acta Crystallogr.*, 1979, **B35**, 1661–1670.
- T. Otsubo, Y. Aso, F. Ogura, S. Misumi, A. Kawamoto and J. Tanaka, *Bull. Chem. Soc. Jpn.*, 1989, **62**, 164–170.
- J. Lu, D. M. Ho, N. J. Vogelaar, C. M. Kraml and R. A. Pascal Jr., *J. Am. Chem. Soc.*, 2004, **126**, 11168–11169.
- X. Qiao, M. A. Padula, D. M. Ho, N. J. Vogelaar, C. E. Schutt and R. A. Pascal Jr., *J. Am. Chem. Soc.*, 1996, **118**, 741–745.
- J. Xiao, H. M. Duong, Y. Liu, W. Shi, L. Ji, G. Li, S. Li, X.-W. Liu, J. Ma, F. Wudl and Q. Zhang, *Angew. Chem., Int. Ed.*, 2012, **51**, 6094–6098.
- J. Luo, X. Xu, R. Mao and Q. Miao, *J. Am. Chem. Soc.*, 2012, **134**, 13796–13803.
- B. Kiupel, C. Niederal, M. Nieger, S. Grimme and F. Vögtle, *Angew. Chem., Int. Ed.*, 1998, **37**, 3031–3034.

[View Article Online](#)

Chem Soc Rev

Tutorial Review

- 32 L. Eshdat, E. Shabtai, S. A. Saleh, T. Sternfeld, M. Saito, Y. Okamoto and M. Rabinovitz, *J. Org. Chem.*, 1999, **64**, 3532–3537.
- 33 M. Rickhaus, L. M. Bannwart, M. Neuburger, H. Gsellinger, K. Zimmermann, D. Häussinger and M. Mayor, *Angew. Chem., Int. Ed.*, 2014, **53**, 14587–14591 and ref. 4 cited therein.
- 34 M. Rickhaus, O. T. Unke, R. Mannancherry, L. M. Bannwart, M. Neuburger, D. Häussinger and M. Mayor, *Chem. – Eur. J.*, 2015, **21**, 18156–18167.
- 35 S. Menning, M. Krämer, B. A. Coombs, F. Rominger, A. Beeby, A. Dreuw and U. H. F. Bunz, *J. Am. Chem. Soc.*, 2013, **135**, 2160–2163.
- 36 K. P. Baldwin, R. S. Simons, D. A. Scheiman, R. Lattimer, C. A. Tessier and W. J. Youngs, *J. Chem. Crystallogr.*, 1998, **28**, 353–360.
- 37 R. Cosmo, T. W. Hambley and S. Sternhell, *J. Org. Chem.*, 1987, **52**, 3119–3123.
- 38 H. Dang, T. Maris, J.-H. Yi, F. Rosei, A. Nanci and J. D. Wuest, *Langmuir*, 2007, **23**, 11980–11985.
- 39 K. Mislaw, M. A. W. Glass, H. B. Hopps, E. Simon and G. H. Wahl, *J. Am. Chem. Soc.*, 1963, **86**, 1710–1733.
- 40 H.-Q. Zhang, B. Li, G.-D. Yang and Y.-G. Ma, *Acta Crystallogr.*, 2008, **E64**, o1304.
- 41 R. J. Kurland, M. B. Rubin and W. B. Wise, *J. Chem. Phys.*, 1964, **40**, 2426–2427.
- 42 K. Müllen, W. Heinz, F.-G. Klärner, W. R. Roth, I. Kindermann, O. Adamczak, M. Wezze and J. Lex, *Chem. Ber.*, 1990, **123**, 2349–2371.
- 43 J. Rotzler, H. Gsellinger, A. Bihlmeier, M. Gantenbein, D. Vonlanthen, D. Häussinger, W. Klopper and M. Mayor, *Org. Biomol. Chem.*, 2013, **11**, 110–118 and ref. 4 cited therein.
- 44 N. Yoshinari and T. Konno, *Acta Crystallogr.*, 2009, **E65**, o774.
- 45 Y. Sakamoto and T. Suzuki, *J. Am. Chem. Soc.*, 2013, **135**, 14074–14077.
- 46 H. Irngartinger, W. R. K. Reibel and G. M. Sheldrick, *Acta Crystallogr.*, 1981, **B37**, 1768–1771.
- 47 W. Nakanishi, T. Matsuno, J. Ichikawa and H. Isobe, *Angew. Chem., Int. Ed.*, 2011, **50**, 6048–6051.
- 48 L. Barnett, D. M. Ho, K. K. Baldrige and R. A. Pascal Jr., *J. Am. Chem. Soc.*, 1999, **121**, 727–733.
- 49 S. Nobusue, Y. Mukai, Y. Fukumoto, R. Umeda, K. Tahara, M. Sonoda and Y. Tobe, *Chem. – Eur. J.*, 2012, **18**, 12814–12824.
- 50 P. Ravat, T. Šolomek, M. Rickhaus, D. Häussinger, M. Neuburger, M. Baumgarten and M. Juriček, *Angew. Chem., Int. Ed.*, 2015, DOI: 10.1002/anie.201507961.

About the Project

As outlined in the preceding review, helical chirality is a promising structural feature for polyaromatic systems. Three types of twist have been presented: (I) The rotating axis is not part of the molecule, but coincides with the longest molecular axis. (II) The axis of rotation is identical to the longest molecular axis. The third class (III), where the axis is located at the edge of the molecule, neither being part of the molecule nor being outside, was addressed conceptually only in a few examples to date. While there exists a large class of molecules (the rotationally hindered biphenyls and naphthyls) that are important from fundamental research to asymmetric catalysis, they are seldom recognized as being a member of type III. Recently, recognize these bannister type geometries have gained interest as an interesting new subclass with unique characteristics. These systems showed especially chiroptical features that compete well with type I or II systems, which are considered to be one of the chiral benchmark classes in polyaromaticity. Due to their internal symmetry, the bannister oligomers known to date all adopt besides their *M* and *P* helices also the achiral *meso* form (Figure 1a). In these systems, *meso* translates to an inversion of the helix at

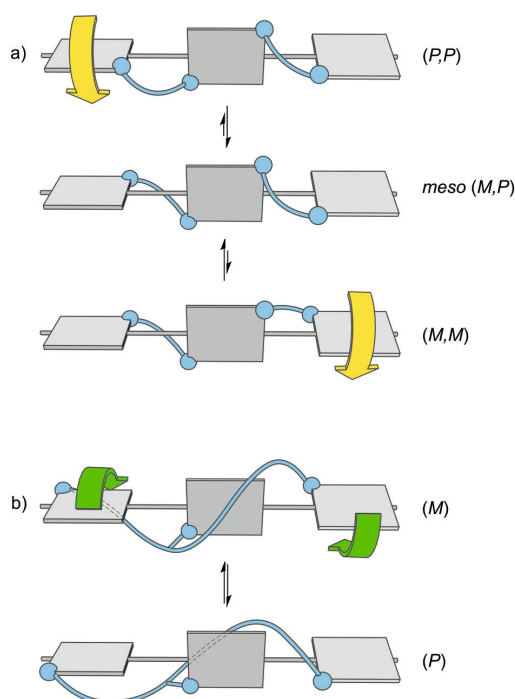


Figure 1: Illustrated racemization behavior of bannister systems. a) Independent inversion of the bridge configuration of a classical bannister oligomer. b) Behavior of a system with a continuous bridge preventing the occurrence of a *meso* form. Inversion at one end results in inversion of the entire helix.

the center of the molecule. One consequence is that obtained crystals often show variable optical activity while the chiral information is eroded in solution over time, due to fast racemization and degradation into the *meso* form. If the bridges are sufficiently independent of each other, the distribution of conformers is statistical, resulting in 25% of each helix (*M,M* and *P,P*) as well as 50% of the *meso* form (*M,P* and *P,M* which are identical).

The goal of this thesis was to develop a new set of bannister (Geländer in German) models to achieve uniform helical structures, without the possibility of losing the chiroptical activity. To that end, it required more than improving the existing systems – to obtain uniform helices it needed a new concept (Figure 1b), especially addressing the concern of communicating the sense of twist across the entire structure. A relayed handedness would prevent formation of an inversion center and thus an achiral *meso* form.

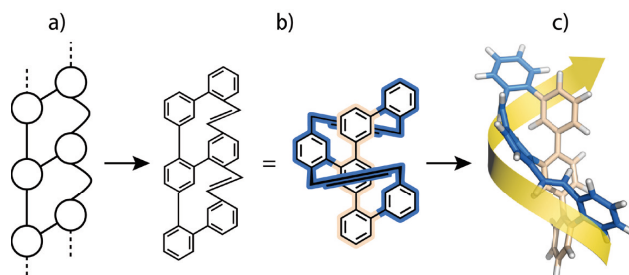


Figure 2: Schematic overview of the project. a) A cross-linked infinite polymer with extension of the right rail. b) Molecular transcription of concept into a hexaphenyl analogue. c) Calculated structure displaying the proposed helical topology.

The concept, which found its realization over the course of this thesis, is in its most basic terms a special type of ladder (Figure 2). Upon extending one rail with respect to the other and maintaining the position of the bridgeheads, the system responds by wrapping the longer rail around the shorter. A stiff relay located in the extended rail relays the twist onto the next segment of the ladder. In principle this concept is applicable to structures beyond the scope of a synthetic organic chemist. As proof of concept a hexaphenyl system was developed, consisting of three interlinked biphenyls that form the rugs of the ladder. The left rail is shorter with the phenyls directly linked via aryl-aryl bonds. The right side (the longer rail), is extended by two heteroalkyl bridges, which should, and did, translate into the expected helical conformation. The detailed concept, the structural conformation, the spectroscopic, chiroptic and dynamic properties of the initial system and beyond, are described in the ensuing manuscripts.

VIP Helical Structures Very Important Paper

DOI: 10.1002/anie.201408424

Inducing Axial Chirality in a “Geländer” Oligomer by Length Mismatch of the Oligomer Strands**

Michel Rickhaus, Linda Maria Bannwart, Markus Neuburger, Heiko Gsellinger, Kaspar Zimmermann, Daniel Häussinger, and Marcel Mayor*

Dedicated to Professor Fritz Vögtle on the occasion of his 75th birthday

Abstract: Helical molecules are not only esthetically appealing due to their structural beauty, they also display unique physical properties as a result of their chirality. We describe herein a new approach to “Geländer” oligomers by interlinking two oligomer strands of different length. To compensate for the dimensional mismatch, the longer oligo(benzyl ether) oligomer wraps around the oligophenyl backbone. The new “Geländer” oligomer **1** was assembled in a sequence of functional-group transformations and cross-coupling steps followed by final cyclizations based on nucleophilic substitution reactions, and was fully characterized, including X-ray diffraction analysis. The isolation of pure enantiomers enabled the racemization process to be studied by circular dichroism spectroscopy.

At the end of the 1990s, Vögtle and co-workers described an entirely new class of chiral polyaromatic compounds.^[1] In contrast to the well-established helicenes^[2] (Figure 1 b), which resemble the steps of a helical staircase (Figure 1 a, yellow), these “Geländer”-type oligomers^[3] (Figure 1 c) combine a *p*-phenylene backbone, as the principal axis, with (hetero)alkyl chains that bridge the phenyl rings. The resulting twist between adjacent phenyl rings gives a chiral structure that resembles the helical bannister of a staircase (Figure 1 a, blue).

Despite the different conceptual approach, Vögtle’s “Geländer”-type oligomers showed chiroptical properties comparable to helicenes, namely, intense Cotton effects and high degrees of optical rotation. In contrast to helicenes, the “Geländer”-type oligomers show a high tendency to racemize. Vögtle and co-workers improved the enantiomeric stability by incorporating bulky substituents (R in Figure 1 e) into the oligomeric backbone, which raised the racemization

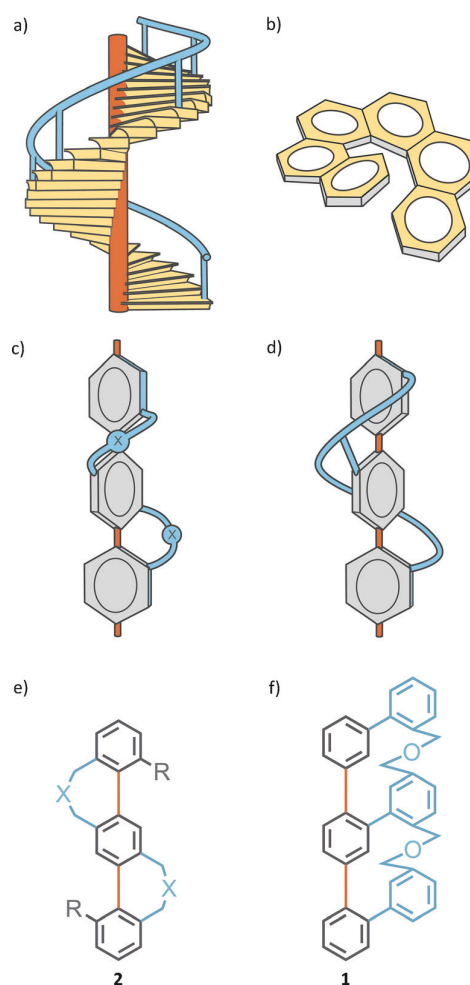


Figure 1. Schematic representations of different types of helical structures (only one enantiomer is shown). a) Helical staircase with a central propagation axis (orange), steps (yellow), and a bannister (blue). b) [6]Helicene. c) “Geländer” oligomer described by Vögtle and co-workers, in which two bridges interlink the central *p*-phenylene unit with the two end phenyl groups. e) Structural formula of the “Geländer” oligomer in (c), with X=S or C(CO₂Me)₂; R=H or Me. d) Schematic representation and f) structural formula of the new “Geländer” oligomer **1** described, in which a second elongated oligomer (blue) ensnares all three rings.

[*] M. Rickhaus, L. M. Bannwart, Dr. M. Neuburger, H. Gsellinger, K. Zimmermann, Dr. D. Häussinger, Prof. Dr. M. Mayor
Department of Chemistry, University of Basel
St. Johanns-Ring 19, 4056 Basel (Switzerland)
E-mail: marcel.mayor@unibas.ch
Prof. Dr. M. Mayor
Institute for Nanotechnology (INT)
Karlsruhe Institute of Technology (KIT)
P. O. Box 3640, 76021 Karlsruhe (Germany)

[**] We acknowledge Prof. Dr. Willem Klopper for fruitful discussions and financial support by the Swiss National Science Foundation (SNF).

Supporting information for this article is available on the WWW under <http://dx.doi.org/10.1002/anie.201408424>.

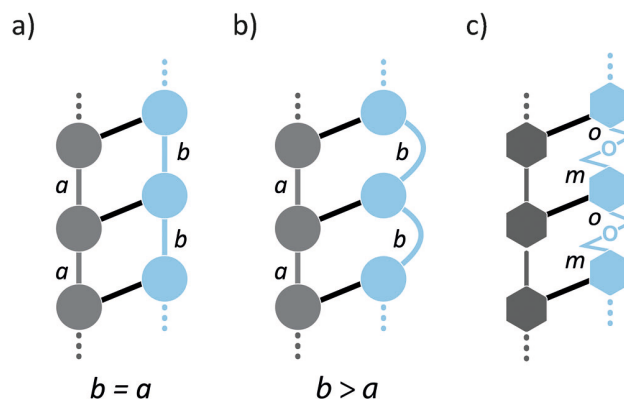
barrier ΔG^\ddagger above 22 kcal mol⁻¹. Inspired by these results, Rathore and co-workers^[4] mounted bulky substituents onto the bridging structures. Their synthetic strategy even allowed quadruply bridged pentaphenylenes to be accessed. The racemization barriers in these systems, however, were significantly lower ($\Delta G^\ddagger \approx 12$ kcal mol⁻¹). Although racemization processes in bridged biphenyl systems have been studied extensively,^[5] investigations on higher oligomeric systems are rare. Enantiomerically pure samples of “Geländer” oligomers not only racemize quickly, but they are even more likely to adopt an achiral *meso* conformation. To display a *meso* form, the structure needs an internal element of symmetry (a point of inversion in the case of “Geländer” oligomers). The synthetic strategies used to access all “Geländer” oligomers result in structures with high degrees of symmetry, which allow the adoption of *meso* forms. Even more importantly, the conformation of one bridge does not necessarily relate to the other—the “helical information” is not relayed across the structure. It ultimately allows each bridge to independently adopt either an *M* or a *P* conformation. The actual chirality of the molecule becomes, in principle, a statistical process, with the *meso* form (*M,P*)/(*P,M*) being twice as likely to occur than either the (*M,M*) or (*P,P*) enantiomers. To the best of our knowledge, all the solid-state structures reported so far include the achiral *meso* form, even when the single crystals were grown from optically pure samples.

We present here a new approach to “Geländer”-type structures to overcome the formation of the *meso* form. The design concept is displayed in Figure 2. If two parallel oligomer chains are interlinked with rigid linkers such as C–C single bonds, a ladder-type structure is obtained if both oligomers have a similar spacing between neighboring connection points (Figure 2a, $b = a$). However, if the periodicity of one oligomer is increased with respect to the other ($b > a$), the two oligomeric chains must compensate for the length mismatch. If rigid subunits are involved, the only way to overcome this discrepancy in length is to wrap the longer oligomer around the shorter one (Figure 2b,c), while the subunits relay the chirality and ensure a continuous helicity. Such a concept tackles both reasons for the formation of the *meso* structure simultaneously: The system can no longer adopt a conformation with a point of inversion, and the helicity is now communicated across the entire structure.

Here we report the first successfully synthesized and fully characterized “Geländer”-type oligomer **1** with a terphenyl backbone and a bannister oligomer consisting of phenyl subunits bridged by *para*-benzyl ether groups (Figures 1 f and 2c). The stiffness and the structural integrity of the *para*-xylene subunit of the longer oligomer allow exclusive formation of the two axially chiral enantiomers as the ground-state conformers. The structure still displays the spirit of Vögtle’s design with a terphenyl backbone, but instead of solely interlinking both biphenyl subunits with independent bridging structures, the entire oligo(*para*-benzyl ether) structure is wrapped around the terphenyl backbone. The result is a structure that resembles a dance ribbon pirouetting around its handling stick.

The synthesis of the “Geländer” oligomer **1** started from commercially available 2-bromo-5-nitroaniline (**3**; Scheme 1).

Side View:



Top View:

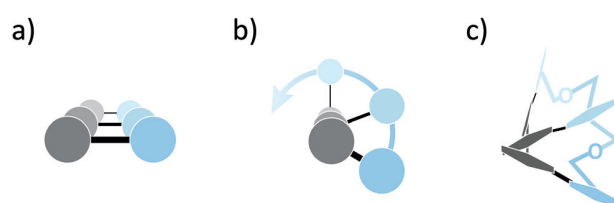
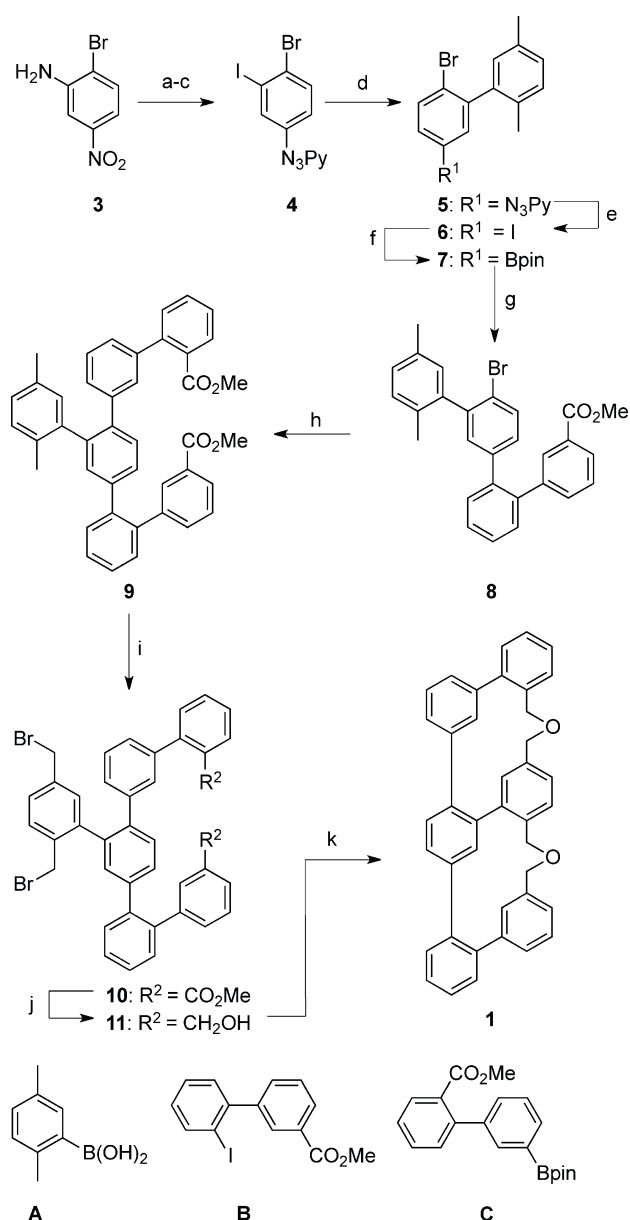


Figure 2. General concept of the new type of “Geländer” oligomer. a) If $a = b$, the resulting structure resembles a ladder. b) If $b > a$, the structure adopts a helical conformation. c) The structure of the new “Geländer” oligomer was designed such that the two adjacent non-backbone phenyl rings (blue) are interlinked in a “meta to ortho” fashion.

The amino group is converted into an iodine substituent via the corresponding diazonium salt. Subsequently, the nitro group is reduced and converted into a triazene, which acts as a masked leaving group. The obtained building block **4** with three different functional groups in positions 1, 3, and 4 is ideally suited as the central synthon for the stepwise attachment of all the required aromatic rings. Under Suzuki–Miyaura cross-coupling conditions, the boronic acid **A** substitutes the iodine to provide intermediate **5**. Treatment of **5** with MeI transforms the triazene into the iodine **6**, which is subsequently converted into the pinacol borane **7** by applying Hosomi–Miyaura borylation conditions. To cross-couple biphenyls **6** and **B** it was necessary to convert **6** into the borane **7**, since all attempts to borylate **B** provided a mixture of regioisomers. The borylated fragment **7** allowed two consecutive Suzuki–Miyaura cross-coupling reactions with **B** and **C** to be carried out to afford intermediates **8** and **9**. Both cross-coupling steps required catalysts optimized for sterically demanding systems.^[6] Intermediate **9** provides the entire required carbon atom skeleton for the target structure **1**, and was isolated in 19% overall yield over 8 steps (longest linear sequence). Benzylic bromination afforded **10** in excellent yield. Subsequent reduction of the ester groups provided **11** quantitatively, which is decorated with the functional groups required for intramolecular bridging by nucleophilic substitution. To our surprise, this final cyclization step turned out to



Scheme 1. Synthesis of target compound **1**. Reaction conditions: a) 1. $\text{BF}_3 \cdot \text{OEt}_2$, ONOtBu , THF, -30°C to RT, 3 h; 2. I_2 , KI, MeCN, RT, 30 min, 85–97%; b) Fe, HCl, EtOH, 0°C , 2 h, 94%; c) 1. $\text{BF}_3 \cdot \text{OEt}_2$, ONOtBu , CH_2Cl_2 , -30°C to -5°C , 15 min; 2. pyrrolidine, K_2CO_3 , RT, 15 min, 95%; d) **A**, $[\text{Pd}(\text{PPh}_3)_2\text{Cl}_2]$, K_2CO_3 , THF/ H_2O 4:1, 60°C , overnight, 88 \rightarrow 99%; e) MeI, 120°C , overnight, 96%; f) $[\text{Pd}(\text{dppf})\text{Cl}_2]$, KOAc, B_2pin_2 , dioxane, 100°C , overnight, 53%; g) **B**, XPhos Pd G2, K_2CO_3 , toluene, 110°C , 1–2 days, 58–84%; h) **C**, SPhos Pd G2, K_2CO_3 , toluene/ H_2O , 110°C , 1–3 days, 50%; i) NBS, DBP, CCl_4 , 75°C , 1 h, 87% to $>99\%$; j) DIBAL-H, CH_2Cl_2 , RT, 30 min, $>99\%$; k) 1. NaH, THF, reflux, 12 h, 30% for the monocyclized intermediate; 2. NaH, $[\text{D}_8]\text{THF}$, reflux, 2–3 days, 28%. **Bpin** = 4,4,5,5-tetramethyl-1,3,2-dioxaborolane, DBP = dibenzoylperoxide, NBS = *N*-bromosuccinimide, N_3Py = diazenylpyrrolidine.

be very challenging, probably because of both the limited stability of the bridging benzylic ether subunits and competing intermolecular reactions. Ultimately, the most efficient method to obtain **1** was to subject **11** to basic reaction

conditions and to stop the reaction at the point when the highest quantity of the monocyclized product was observed in the reaction mixture. Interestingly, only one of the four theoretically possible monocyclized isomers was observed. After this point, the concentration of the monocyclized product decreased, but the desired doubly cyclized compound **1** could only be detected in trace amounts. Consequently, the monocyclized product was isolated and purified before being subjected again to basic conditions to undergo the second cyclization step. This step was performed in $[\text{D}_8]\text{THF}$ at 60°C directly in an NMR tube, and the exclusive formation of the target compound **1** was monitored by ^1H NMR spectroscopy.

Purification of **1** by flash column chromatography (on acidic and passivated silica and Alox) resulted in substantial decomposition of the product. Therefore, crude **1** was subjected directly to HPLC on a chiral stationary phase (Chiralpak IA, eluent *n*-hexane/2-propanol 99:1, 1 mL min^{-1} , $T=25^\circ\text{C}$) to separate the two enantiomers of **1** and afford each enantiomer in about 14% yield ($>99\%$ ee). Once isolated, each enantiomer showed prolonged stability towards air and moisture as well as solubility in most organic solvents. Compound **1** was fully characterized by ^1H and ^{13}C NMR spectroscopy, UV/Vis spectroscopy, high-resolution mass spectrometry (HR-ESI), and single-crystal X-ray diffraction (see the Supporting Information). The ^1H NMR spectrum showed distinct doublets for each of the diastereotopic hydrogen atoms of the bridge, which indicates a slow racemization process on the NMR timescale. Each enantiomer showed only one set of signals and their spectra were identical, thus indicating that the two fractions obtained by HPLC on the chiral stationary phase were indeed enantiomers. Laborious 2D NMR spectroscopy allowed all the observed signals in the ^1H and ^{13}C NMR spectra to be fully assigned. As a result of the high steric constraints and the resulting relaxation times, a suitable ^{13}C NMR spectrum of **1** could be obtained indirectly. The ^{13}C NMR, UV/Vis, and HRMS spectra for both enantiomers were also identical. Further evidence that the isolated fractions were enantiomers was provided by circular dichroism (CD) measurements (Figure 4a). Cotton effects were observed at 240, 220, and 200 nm, with opposite signs for the two enantiomers.

On the basis of the design of the “Geländer” oligomer **1**, we anticipated its conformation to be stiff and thus its helicity to be stable at room temperature. To properly identify the helicity of both enantiomers, we grew single crystals suitable for X-ray analysis from a freshly separated, diluted solution of one of the enantiomers in diethyl ether by slow evaporation within seven days. The solid-state structure provided a surprise: the crystallized sample was the racemate of **1** with two molecules of each enantiomer in the unit cell. Different views of the solid-state structure of **1** are displayed in Figure 3. The solid-state structure corroborates the helical wrapping of the benzyl ether oligomer (blue carbon atoms in Figure 3a and b) in a banister-like manner around the oligophenyl backbone (gray carbon atoms in Figure 3a and b), as postulated in the molecular design. The torsion angles between the two adjacent backbone aromatic rings were found to be 81.5° and 64.3° , which corresponds to a total twist along the entire oligophenylene backbone of 147.3° .

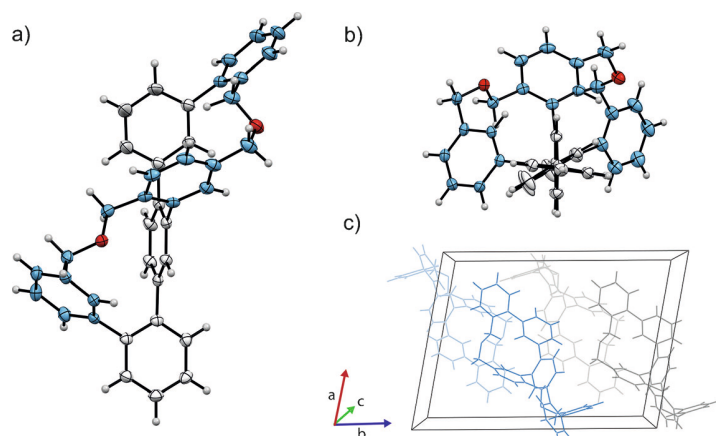


Figure 3. The X-ray structure of racemic **1** from different view points (rotation ellipsoids at 50% probability). a) Side view and b) front view of one enantiomer. c) The unit cell, which contains two molecules of each enantiomer. Color code: bridge: blue, backbone: gray, H: white, O: red (a, b); enantiomers: blue, gray (c).

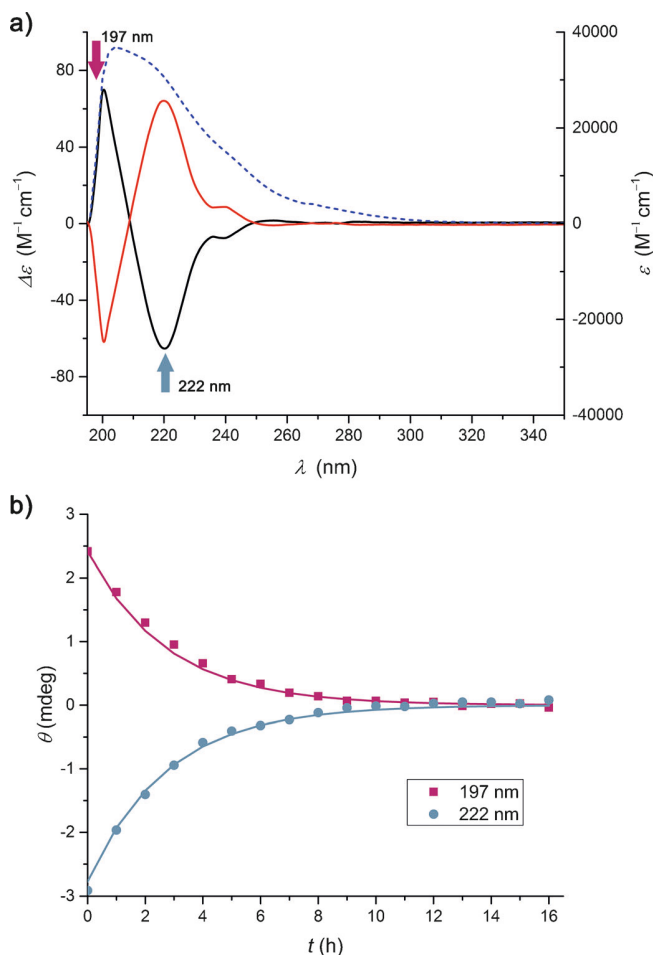


Figure 4. a) UV/Vis spectra (dashed blue line) of racemic **1** and CD traces for the separated enantiomers (black and red lines). The spectra were recorded in *n*-hexanes/2-PrOH (99:1) at 25 °C. Absorption maxima and distinct Cotton effects were observed at 240, 220, and 200 nm. The arrows indicate the wavelengths used to observe the decay of the CD signal over time. b) The decay of the CD signal over time was observed at 222 and 197 nm at 25 °C. The racemic state was reached in approximately 10 h.

As the formation of racemic crystals came as a surprise, we were curious about the racemization process. To investigate the racemization kinetics of **1**, the disappearance of the two most intense CD signals (197 and 222 nm) of a freshly purified enantiomer were recorded as a function of time at 25 °C (Figure 4b). Racemization was almost complete within 10 h. A plot of time (*t*) against $\ln(A)$ (see the Supporting Information) allowed the rate of racemization to be determined as $k_{\text{rac}} = 5.040 \times 10^{-6} \text{ s}^{-1}$ ($k_{\text{rac}}^{222 \text{ nm}} = 5.146 \pm 0.05 \times 10^{-6} \text{ s}^{-1}$, $k_{\text{rac}}^{197 \text{ nm}} = 4.936 \pm 0.05 \times 10^{-6} \text{ s}^{-1}$), which results in half-lives of 3.82 h ($t_{1/2}^{222 \text{ nm}} = 3.74 \text{ h}$, $t_{1/2}^{197 \text{ nm}} = 3.90 \text{ h}$) at 25 °C. The data further allowed the energy barrier for racemization to be determined (see the Supporting Information) as $\Delta G^\ddagger = 97.55 \pm 0.1 \text{ kJ mol}^{-1}$ (23.3 kcal mol⁻¹) at 25 °C. This value is in a similar range as those reported for the most stable “Geländer” oligomers by Vögtle and co-workers. As postulated during the design of the “Geländer” oligomer, the racemization process does

not involve a chiroptically silent, thermodynamically favored intermediate (in other words, no *meso* form). Racemization most likely occurs by rotation around the single bond in the central biphenyl subunit, along with an unwrapping and rewrapping of the benzyl ether oligomer and inversion of helicity.

In summary, a new type of a “Geländer”-type terphenyl oligomer was synthesized, fully characterized, and its racemization behavior studied. Compared to the previously known “Geländer”-type oligomers, the new system interlinks all three terphenyl rings through an oligo(benzyl ether) as a single bridge (instead of two) and thus lacks a point of inversion. As a result, the structure exists exclusively in the form of two stereoisomers, a pair of enantiomers. This structural characteristic leads to a uniform racemization pathway without an achiral intermediate *meso* structure. The high racemization barrier allowed the separation of both enantiomers by HPLC on a chiral stationary phase. These enantiomers subsequently underwent racemization. X-ray diffraction analysis of the racemic single crystals confirmed the helical structure of the “Geländer”-type oligomer.

Received: August 21, 2014

Published online: November 3, 2014

Keywords: atropisomerism · Geländer oligomers · helical structures · hexaphenyls · racemization

- [1] B. Kiupel, C. Niederal, M. Nieger, S. Grimme, F. Vögtle, *Angew. Chem. Int. Ed.* **1998**, *37*, 3031–3034; *Angew. Chem.* **1998**, *110*, 3206–3209.
- [2] For an excellent review, see M. Gingras, *Chem. Soc. Rev.* **2013**, *42*, 968–1006, and references therein.
- [3] “Geländer” is the German word for banister.
- [4] M. Modjowski, S. V. Lindeman, R. Rathore, *Org. Lett.* **2009**, *11*, 4656–4659.
- [5] Representative examples: a) K. Ohkata, R. L. Paquette, L. A. Paquette, *J. Am. Chem. Soc.* **1979**, *101*, 6687–6693; b) K. Müllen, W. Heinz, F. Klärner, W. R. Roth, I. Kindermann, O. Adamczak,

- M. Wette, J. Lex, *Chem. Ber.* **1990**, *123*, 2349–2371; c) J. Rotzler, H. Gsellinger, M. Neuburger, D. Vonlanthen, D. Häussinger, M. Mayor, *Org. Biomol. Chem.* **2011**, *9*, 86; d) J. Rotzler, H. Gsellinger, A. Bihlmeier, M. Gantenbein, D. Vonlanthen, D. Häussinger, W. Klopper, M. Mayor, *Org. Biomol. Chem.* **2012**, *10*, 110–118; e) J. Rotzler, H. Gsellinger, A. Bihlmeier, M. Gantenbein, D. Vonlanthen, D. Häussinger, W. Klopper, M. Mayor, *Org. Biomol. Chem.* **2013**, *11*, 110; f) K. Takaishi, M. Kawamoto, K. Tsubaki, *Org. Lett.* **2010**, *12*, 1832–1835.
- [6] S. L. Buchwald, N. C. Bruno, *The Strom Chemiker Vol. XXVII* **2014**, 1.
-

DOI: 10.1002/ejoc.201403322

Through the Maze: Cross-Coupling Pathways to a Helical Hexaphenyl “Geländer” Molecule

Michel Rickhaus,^[a] Linda Maria Bannwart,^[a] Oliver Unke,^[a] Heiko Gsellinger,^[a]
Daniel Häussinger,^[a] and Marcel Mayor^{*,[a,b]}

Keywords: Helical structures / Cross-coupling / Conformation analysis / Chirality / Regioselectivity

This paper highlights a new concept on how to induce chirality in a hexaphenyl Geländer-type system. Bridging a terphenyl backbone with a considerably longer benzyl ether oligomer enforces a continuous twist of the molecule, while preventing an achiral *meso* form. By highlighting cross-coupling strategies and explored synthetic pathways, this report aims to serve as an Ariadne's thread for the synthesis of precisely functionalized, complex polyaromatic systems. The

synthetic challenges and considerations required to access the designed target are outlined and solutions to each step of the assembly are presented. Encountered isomerizations are discussed as much as synthetic tools to access highly functionalized intermediates with multiorthogonal moieties. A strong focus is made on the employment of Suzuki–Miyaura protocols for the targeted connection of polyaromatic fragments and ultimately the desired oligomeric structure.

Introduction

Polycyclic aromatic compounds (PAC) have caught the attention of material scientists and fundamental researchers since the very beginning of molecular chemistry.^[1] Their unique electronic properties arise from the reduced spacing between their frontier orbitals, and their pronounced chemical stability makes them interesting building blocks for the development of components in electronics, optics, and functional materials.^[2] Furthermore, such compounds offer the opportunity to study fundamental processes such as angular conductivity dependence, molecular motion, or even shed light on the origin of life.^[3] Making PACs chiral allowed increasingly delicate aspects such as circular polarized luminescence (CPL), dynamic processes like racemization and controlled molecular motion to be explored.^[4,5]

Several concepts have been developed to introduce chirality into PACs. Helically twisted acenes^[6] (Figure 1, a) were obtained by the introduction of bulky substituents along the rim of the molecule; helicenes^[7] (Figure 1, b) release the steric strain induced by the hydrogen atoms pointing into the cavity by adopting a spring-like conformation. By inducing defects in a graphene sheet, twisted nano-

sheets were obtained (Figure 1, c).^[8] Chiral naphthalene oligomers (Figure 1, d) show extreme *cisoid* conformations and demonstrate impressive state-of-the-art chiroptical properties.^[9] Geländer oligomers (Figure 1, e)^[10] become chiral due to a second elongated bridging structure forcing the phenyl units of the backbone into an out-of-plane twist. In the Geländer oligomers reported so far, the two bridging motifs were attached in the *ortho*-position of the central phenyl ring. As a consequence of this spatial remoteness, their strain-releasing twist directions are independent and, in most cases, the *meso*-form with twists of opposed chirality is favored. Expanding on the concepts found in the literature, we developed a new approach^[11] (Figure 1, f) to introduce helicity to a polymeric system: Similar to the reported Geländer-oligomers, the structure is based on a terphenyl backbone, but instead of solely bridging neighboring phenyl rings (i.e., two bridges), the backbone is wrapped by a benzyl ether oligomer (only one, continuous bridge). The appealing design feature of this new approach is the absence of an achiral *meso*-form. The central phenyl subunit of the wrapping oligo benzyl ether acts as a rigid joint that relays the helicity from one subunit to the other; as a consequence, the helicity of the system must become continuous. The geometrical molecular design considerations are sketched in Figure 2. A ladder structure consisting of two parallel rails and a finite numbers of cross linkages serves as a model. The model system is, by definition, an achiral, highly symmetrical oligomer or, depending on the length and number of linkages, a monodimensional polymer. Cutting one of the rails into segments (Figure 2, Panel 1) and elongating the sections (blue) by a significant amount (Figure 2, Panel 2b) induces strain after reclosing the system. The system may respond by wrapping the longer rail heli-

[a] Department of Chemistry, University of Basel, St. Johannis-Ring 19, 4056 Basel, Switzerland
E-mail: marcel.mayor@unibas.ch
<http://www.chemie.unibas.ch/~mayor/>

[b] Institute for Nanotechnology (INT), Karlsruhe Institute of Technology (KIT), P. O. Box 3640, 76021 Karlsruhe, Germany

Supporting information for this article is available on the WWW under <http://dx.doi.org/10.1002/ejoc.201403322>.

Pathways to a Helical Hexaphenyl “Geländer” Molecule

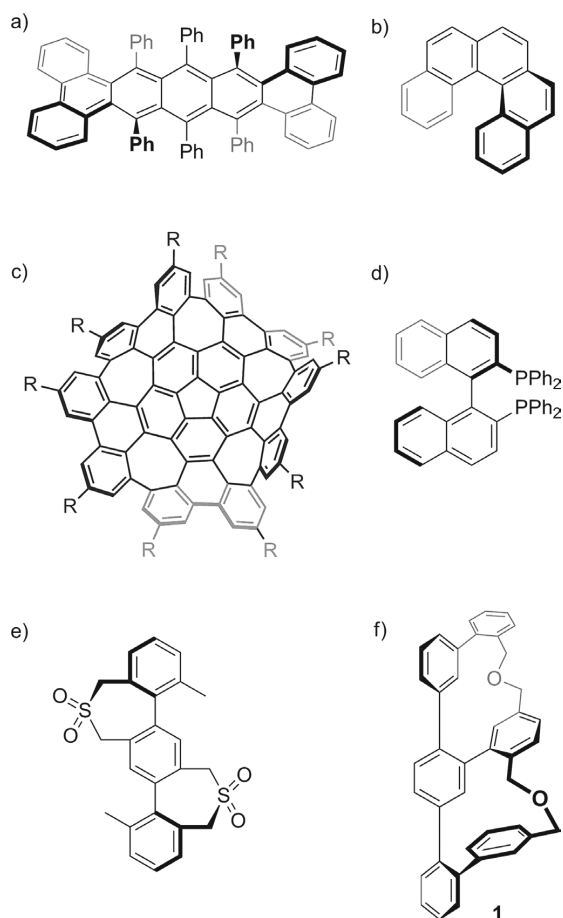


Figure 1. Various realizations of chiral polycyclic aromatic compounds (PACs). (a) Twisted pentacene; (b) [5]-helicene; (c) Scott's nanographene; (d) chiral naphthalene; (e) Vögtle's Geländer oligomer; (f) twisted terphenyl **1** as a new type of Geländer oligomer.

cally around the shorter rail, but if the bridge segments are spaced far apart it also has the option to adopt a *meso*-form, which is the case for most reported Geländer structures. To avoid the *meso*-form preference, a rotatable rigid joint (Figure 2, Panel 2a) is introduced, which guarantees that the helical information is propagated across the junction. Reclosing the system with the rigid joint (Figure 2, Panel 3) induces strain, which the system will try to minimize. The most efficient way to achieve this is to lengthen the spacing between two crosslinks by wrapping them around the principal axis. As a consequence of the length mismatch between both rails, the oligomer (or polymer) becomes helical (Figure 2, Panel 4).

We have recently discussed the conceptual ideas and the physical properties emerging from the Geländer helicity in detail elsewhere;^[11] this full paper focuses mainly on an exploration of the synthetic pathway towards **1**. In particular, the use of Suzuki–Miyaura cross coupling as a synthetic tool with which to assemble complex polycyclic aromatic structures is addressed.^[12] Although a vast number of publications deal with the development and application of undoubtedly very complex aryl-aryl couplings, only a minority of these go beyond the synthesis of (hetero-)biaryls. The target structure presented here provided an excellent opportunity to contribute to the exploration of cross couplings for the construction of complex polyaromatic systems. The target structure requires the precise connection of aryl subunits and, in particular the late stage of the synthesis, of very demanding (both electronically and sterically) systems.

Consequently, we discuss here synthetic strategies that were explored and ultimately allowed the assembly of **1**, the synthesis of the subunits, their convergent assembly to a suitable precursor, and its final cyclization to the target structure **1**, as well as the spectroscopic characterization of key intermediates and their purification by chiral HPLC.

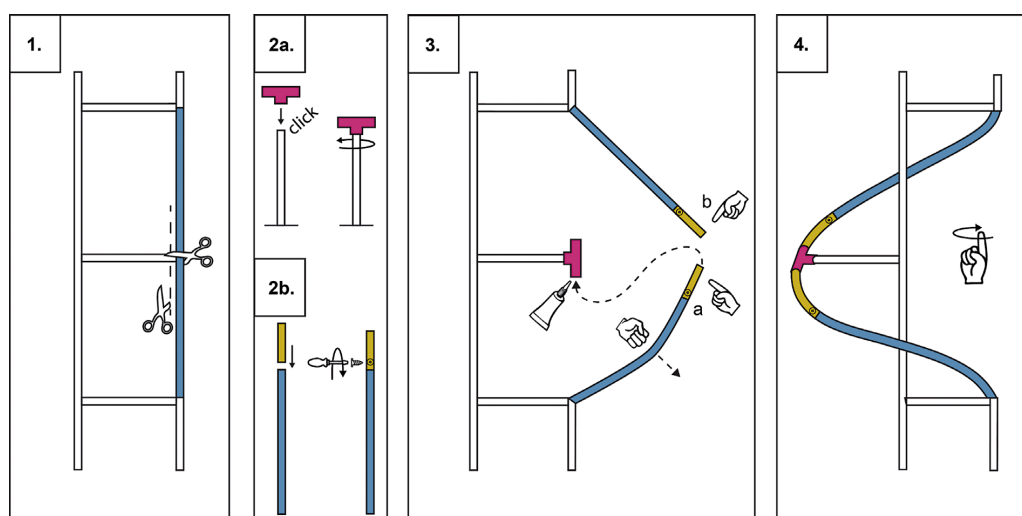


Figure 2. Generalized concept for the introduction of helicity: (1) A ladder-like structure with one of the rails divided. (2a) Introduction of a rotatable joint that relays the twist from one section to the other, and (2b) elongation of the liberated ends. (3) Stepwise reattachment of the significantly elongated sections, which induce strain in the system. (4) The system releases strain by twisting around the original rail and, as a consequence, becomes helical.

FULL PAPER

M. Mayor et al.

Retrosynthetic Analysis

The retrosynthetic analysis of the “Geländer” oligomer **1** is displayed in Figure 3. The lack of symmetry is an important structural feature that avoids the generation of *meso*-forms. As a consequence, the target helical hexaphenyl **1** bears six unique benzyl units: three of the rings feature a single aryl–aryl bond, two benzyls feature two aryl–aryl bonds and the central ring is directly linked to three neighboring aryl subunits. The end capping rings can be grouped into two structurally similar fragments that show reversed substitution patterns (**C** and **D**).

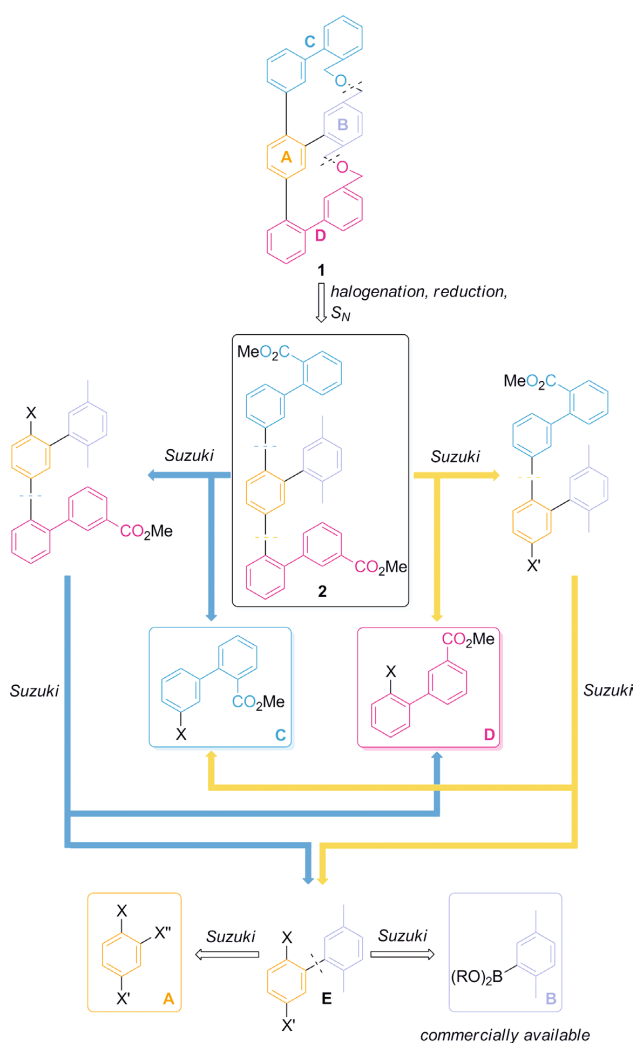


Figure 3. Retrosynthetic analysis for the stepwise assembly of **1**.

The most promising disconnection was the opening of the ether bridges in **1** such that ring **B** (purple ring in Figure 3) supplies the required leaving groups whereas the esters, upon reduction, can provide the necessary oxygen moieties. Esters were particularly interesting because they are generally very susceptible to reductive conditions, even in the presence of benzylic halides. The tolerance of ester

groups to a vast range of reaction conditions further favored their choice as masking group for the benzylic hydroxyl function. A late-stage bromination of the two available benzylic positions of the *para*-xylene subunit would reduce the number of functional groups present over a broad range of the synthesis. Thus, the open precursor **2** becomes the actual key fragment with the entire carbon skeleton correctly connected.

For a convergent synthetic strategy, the use of ring **A** (orange ring in Figure 3) as the central unit interlinking three aryl subunits became the focus of interest. Our plan was to profit from Suzuki–Miyaura-type cross-coupling reactions to form the required aryl–aryl connections, mainly because of the high diversity, versatility, low toxicity, and well-established protocols.^[13] Grouping the four end-capping phenyls into two biphenyl subunits (**C** and **D**) that differ only in their substitution patterns, enabled the transfer of obtained knowledge from one fragment to the other. Both fragments can subsequently be attached by Suzuki–Miyaura coupling to the core fragment **E**, which itself is also accessible by coupling a suitable core **A** with the commercially available boronic acid **B**. The remaining retrosynthetic challenge was to identify the most promising sequence for the stepwise assembly of the aryl subunits. By following a convergent strategy, it was reasonable to interconnect as many rings as possible prior to the attachment to the central core structure (i.e., assembly of the biphenyl groups **C** and **D** prior to attachment rather than attaching one ring at a time). However the exact order of attachment was not straightforward and the optimal synthetic route remained to be deduced experimentally.

The synthetic route that we identified as most likely to succeed was to attach the commercially available boronic acid to the highly substituted core **A**, which already bears all three required halogens, either masked or unmasked. Having accessed the biphenyl **E**, the fragments **C** and **D** (blue and pink, respectively) could be attached subsequently over two complementary pathways: Either by attaching first fragment **C** to **E** and then fragment **D** (olive arrow) or vice versa (dark-blue arrow). Given that there have been few or no preceding reports in this area, the choice of pathway had to be explored empirically. Fortunately, both pathways required the same fragments **C** and **D**. Our strategy was to develop the central building block towards the target structure by attaching boronic derivatives whenever possible.

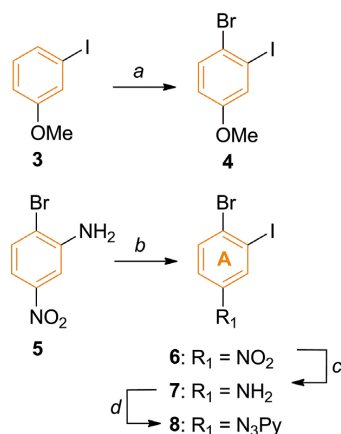
The structure of the central core **A** had to be designed such that it allowed the selective attachment of the three fragments **B–D**. A cornerstone of our synthetic strategy was to make use of the different reactivities of halides in Suzuki–Miyaura cross couplings. Central building blocks with suitable substitution patterns bearing an iodine and a bromine substituent were expected to allow two of the three fragments to be introduced chemoselectively. As third substituent, we planned to profit from a masked leaving group such as a methoxy group, which could later be converted into a triflate that was suitable for cross coupling, or a nitrogen moiety (nitro or triazene) as a precursor of an iodine substituent.

Results and Discussion

Synthesis of Fragments A–D

Fragments A and B

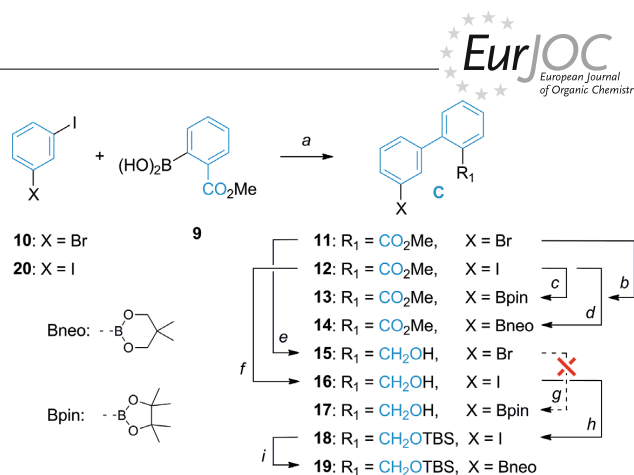
Several potential derivatives as fragment **A** were considered (Scheme 1). Bromination of commercially available 1-iodo-3-methoxybenzene (**3**) by using a reported protocol^[14] with *N*-bromosuccinimide (NBS) yielded **4** in almost quantitative yield. We have recently described the synthesis of **6–8** elsewhere.^[11] In summary, nitro compound **6** was obtained in excellent 97% yield from **5**. In two steps, **6** could be readily converted into the corresponding triazene **8**, giving access to three possible fragments **A** (**4**, **6**, and **8**) that were suitable for subsequent cross coupling with fragment **B**. 2,5-Dimethylphenylboronic acid as potential fragment **B** is commercially available and was not accessed synthetically.



Scheme 1. Reagents and conditions: (a) NBS, MeCN, r.t., 15 h, 96%; (b) BF₃·OEt₂, ONO*t*Bu, THF, –30 °C to r.t., 3 h, then I₂, KI, MeCN, r.t., 30 min, 97%; (c) Fe, HCl, EtOH, 0 °C, 2 h, 94%; (d) BF₃·OEt₂, ONO*t*Bu, CH₂Cl₂, –30 °C to r.t., 15 min, then pyrrolidine, K₂CO₃, r.t., 15 min, 95%; N₃Py = diazenylpyrrolidine.

Fragment C

The two remaining fragments **C** and **D** are both biphenyls, albeit with different substitution patterns. It turned out that the type of substitution pattern had a surprising impact on the chemistry we were able to perform on the fragments. The biphenyl fragment **C** features a borane in the 3-position and either an ester or a benzylic alcohol in the 2'-position. For fragment **D**, the pattern is reversed; the borane is in the 2'-position whereas the ester or benzylic alcohol is located at the 3-position. In particular, the position of the preceding halogen was crucial for the success of the borylation. Starting from 2-methoxycarbonyl phenyl boronic acid (**9** in Scheme 2), Suzuki–Miyaura cross coupling with 1-bromo-3-iodophenyl (**10**) was possible, rendering **11** in 53% after several optimizations (see Table 1 in the Supporting Information).



Scheme 2. Reagents and conditions: (a) Pd(PPh₃)₂Cl₂, K₂CO₃, THF/MeOH (4:1), 60 °C, 15 h, **11**: 53%, **12**: 54%; (b) Pd(dppf)Cl₂, B₂pin₂, KOAc, DMF, 100 °C, 6.5 h, **13**: 5%; (c) Pd(dppf)Cl₂, B₂pin₂, KOAc, DMF, 100 °C, 2 h, >99% (75% for large scale); (d) *i*PrMgCl·LiCl, B(O*t*Pr)₃, neopentyl glycol (NPG), THF, –40 °C to r.t., 19 h, 72%; (e) DIBAL-H, CH₂Cl₂, 0 °C to r.t., 1–2 h, 90%; (f) DIBAL-H, CH₂Cl₂, 0 °C to r.t., 1–2 h, 94%; (g) Pd(dppf)Cl₂, B₂pin₂, KOAc, DMF, 100 °C, 6.5 h, <5%; (h) TBSCl, imidazole, CH₂Cl₂, r.t., 22 h, 86%; (i) *i*PrMgCl·LiCl, B(O*t*Pr)₃, NPG, THF, –40 °C to r.t., 20 h, 45%.

As a starting point, the widely used Pd(PPh₃)₄ was employed as catalyst under an oxygen-free atmosphere in a 1:2 ratio of wet tetrahydrofuran (THF) and methanol, using K₂CO₃ as base and 1.5 equiv. of 1-bromo-3-iodophenyl. Samples were taken after 3 and 24 h, respectively, and analyzed by GC–MS. Generally, it can be stated that Pd(PPh₃)₂Cl₂ showed superior conversions compared with other catalysts employed. Selective cross coupling on the iodine was observed exclusively even at 60 °C, allowing for subsequent attachment of the next fragment (or a boronic moiety) after the cross-coupling step. Both precatalyst XPhos- and SPhos-palladacycle systems described by Buchwald and co-workers,^[15] showed a tendency to also initiate cross coupling on the bromines, which was undesired in this case. This observation, however, pointed to the possibility of employing these highly active systems at a later stage in the synthesis. The choice of solvents played a crucial role in the success of the reaction. A significant decrease in reactivity was observed without the addition of methanol. Interestingly the presence of methanol seems to be important but not the exact ratio, because similar conversions were observed for THF to methanol ratios of both 2:1 and 4:1.

To increase the reactivity of the fragment in a subsequent coupling or *trans*-functionalization reaction, the iodine analogue **12**, together with the benzylic alcohol **16** and the silyl-masked benzylic alcohol **18**, also became a focus of interest. Subjecting 1,3-diiodobenzene (**20**) and the corresponding boronic acid to Suzuki–Miyaura conditions provided **12** in up to 54% yield after optimization. Considering the statistical nature of the reaction, we were pleased with the isolated yield. The only observed side-products were the dicoupled analogue as well as starting material. It is important to note, however, that by adding more than 1 equiv. of boronic acid under suitable conditions [i.e., Pd(PPh₃)₂Cl₂, NaOH, dioxane/water (4:1), 60 °C, 21 h, 88%] it was also possible

FULL PAPER

M. Mayor et al.

to initiate cross coupling on the bromine. The cross coupling was found to be very reliable and robust, even on large scale (>20 g, 54%).

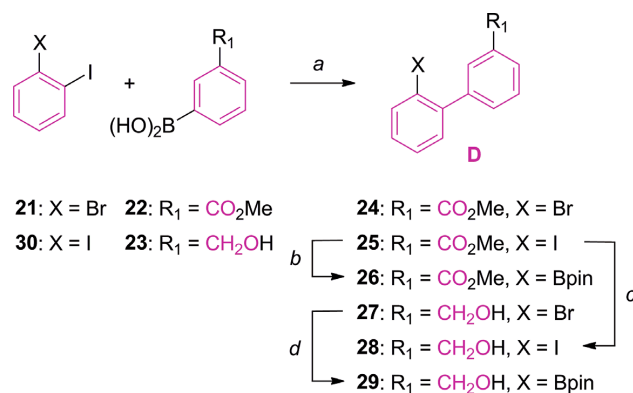
The synthetic strategy relies on a reduction of the methyl esters at a late stage of the synthesis. Compounds **11** and **12** were considered as model compounds with which to investigate the required reaction conditions. Subjecting either **11** or **12** to reductive conditions using diisobutylaluminum hydride (DIBAL-H), the desired benzylic alcohols **15** and **16** were obtained in promising yields of 90 and 94%, respectively, corroborating the potential of these esters as masked benzylic alcohols. In case the reduction should fail on the further advanced (more crowded) precursor, a masked benzylic alcohol might be an alternative building block. Treating the obtained benzylic alcohol **16** with TBSCl under basic conditions provided the TBS-protected alcohol **18** in a pleasing 86% yield.

According to our convergent strategy, borylation of the biphenyl building block was investigated next (Table 2 in the Supporting Information). Reaction conditions were developed starting from reported protocols^[16] with the ester-bearing biphenyls **11** and **12**, the free alcohols **15** and **16**, as well as the TBS-protected alcohol **18** as potential starting materials. Similar to the trends observed for Suzuki–Miyaura couplings, iodines were found to show significantly increased reaction rates towards Hosomi–Miyaura borylation (quantitative conversions for iodines vs. 5% for bromines). The conversion of the iodine worked most reliably on large scale (>14 g) when heating to approximately 112 °C in dioxane overnight (sealed flask). Lithiation of ester **11** by using *s*BuLi, *t*BuLi or lithium diisopropylamide (LDA) as lithium source^[17] resulted in decomposition of the starting material. Another explored possibility to introduce the boronic moiety by metalation was the use of conditions developed by Knochel and co-workers in which the corresponding halide is subjected to Grignard conditions and the formed magnesium intermediate is quenched with a boron source. In our hands the Knochel conditions^[18] turned out to be generally lower yielding compared to the classical Hosomi–Miyaura borylation. Furthermore, upscaling to multigram batches resulted in a substantial drop in yield and the reaction required extended reaction times (72% for small scale, 31% for large scale). For the free alcohol **15**, only low yields were obtained (<5%) with the Knochel system,^[18] because decomposition of the free alcohol **17** was observed under basic conditions even without the presence of a metal source. The TBS-protected alcohol **18** could, however, be successfully borylated (45%).

Synthesis of Fragment D

Building on the knowledge obtained for fragment **C**, we turned our attention to the structurally related fragment **D** (Scheme 3). Starting from 1-bromo-2-iodobenzene (**21**) and [3-(methoxycarbonyl)phenyl]boronic acid (**22**) or [3-(hydroxymethyl)phenyl]boronic acid (**23**), access to **24** and **27** was achieved in good yields. The difference in reactivity

of iodine and bromine towards Suzuki–Miyaura coupling again allowed the iodine to be selectively addressed over the bromine, giving yields of 73% for the ester **24**.



Scheme 3. Reagents and conditions: (a) Pd(PPh₃)₂Cl₂, K₂CO₃, THF/MeOH (4:1), 60 °C, 15 h; **21** + **22** → **24**: 73%; Pd(PPh₃)₂Cl₂; **30** + **22** → **25**: 41%; Pd(PPh₃)₄, Cs₂CO₃, THF/EtOH (4:1), 60 °C, 4 h; **21** + **23** → **27**, 71%; (b) Pd(dppf)Cl₂, B₂pin₂, KOAc, dioxane, 100 °C, 1 h, 57% as regioisomers; (c) DIBAL-H, CH₂Cl₂, 0 °C to r.t., 2 h, >99%; (d) Pd(dppf)Cl₂, B₂pin₂, KOAc, DMF, 100 °C, 1 h, 59% as regioisomers.

In contrast to the observations made for fragment **C**, it was also possible to directly cross couple the free alcohol without prior protection, giving **27** in comparable yield (71%). To benefit from the increased reactivity of iodines over bromines in Hosomi–Miyaura borylations, we also prepared the iodinated analogues **25** and **28**. Statistically subjecting 1,2-diiodobenzene (**30**) and the corresponding boronic acid to Suzuki–Miyaura conditions allowed **25** to be accessed in 41% yield, which is a reasonable yield for a statistical reaction. The only observed side-products were, as in the case for fragment **C**, the dicoupled analogue as well as the starting material. Subjecting **25** to reductive conditions using DIBAL-H again allowed access to the desired benzylic alcohol **28** quantitatively in 2 h.

From the four precursors for the subunit **C** (**24**, **25**, **27**, and **28**), precursors **25** and **27** were initially selected and subjected to Hosomi–Miyaura conditions. Borylation of **27** provided a crude boronic ester derivative in reasonable 59% isolated yield. Interestingly, we were now able to obtain the borylated free hydroxy in good yields, whereas with reversed substitution patterns, the obtained boronic ester **17** was not stable. We found a strong dependence of the isolated yield on the concentration, and significantly lower yields tended to be obtained upon dilution. To our surprise, the isolated boronic ester derivative was not a pure compound, but an inseparable mixture of two regioisomers (Scheme 4). GC–MS, ¹H and ¹³C NMR analyses confirmed the presence of exactly two regioisomers in a 1:1 ratio. 2-D NMR spectroscopy allowed the identification of both compounds as the expected biphenyl **29**, and **31** as the second isomer. Intriguingly, the boronic moiety in **31** is located *para* to the hydroxyl group on the opposite phenyl ring. Whether the formation of that second isomer occurs by deborylation and reborylation of the C–H bond at the 2-posi-

Pathways to a Helical Hexaphenyl “Geländer” Molecule

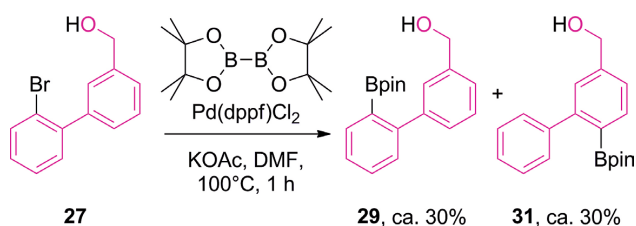
tion or whether the boronic moiety escapes the steric constraint it undoubtedly suffers from and directly isomerizes, is still under investigation. Similar observations have been reported for corannulene and biphenyl using an iridium-catalyzed system.^[19] We wondered whether the observed isomerization was a unique feature of alcohol **27**. Subjecting ester **25** to the same conditions, however, rendered a similar picture (Table 1): The yield was as high as for **27** (isolated yield: 57%) again with a 1:1 ratio of similar regioisomers (entry 1, **26** and **32**). Both regioisomers could be separated by normal-phase HPLC (column: semipreparative Reprisil 100 Si, 5 μ m, 250 \times 16 mm, eluent: CH₂Cl₂, 8 mL/min) and both were fully assigned based on ¹H NMR and 2D NMR spectroscopy. GC–MS showed the same mass and fragmentation pattern for both compounds as expected for regioisomers (see Figure 4). It appears that an ester is equally capable to direct this unexpected rearrangement. However, we never observed the rearrangement when exchanging the positions of the halogen and the ester or alcohol (i.e., for the fragment C homologues), further indicating that steric strain plays an essential role in promoting this unexpected rearrangement. The use of dioxane instead of *N,N*-dimethylformamide (DMF) under otherwise unal-

tered conditions promoted the formation of the rearranged side-product **32** over the expected product **26** (entry 2; 84 and 16%, respectively). It thus appears that the choice of solvent can influence the formation of the regioisomer significantly. Lowering the temperature to 80 °C resulted in formation of the undesired isomer **32** in 71% yield (entry 3), demonstrating that temperature can also influence the extent of the rearrangement.

Table 1. Formation of regioisomers during the Hosomi–Miyaura borylation of **25**.^[a]

Entry	Solvent ^[a]	Δ	26	32
1	DMF	100 °C	51	49
2 ^[c]	dioxane	100 °C	16	84
3	dioxane	80 °C	29	71

[a] Reaction conditions: Pd(dppf)Cl₂, B₂pin₂, KOAc, 15 h. [b] By GC–MS analysis. [c] Significant amount of side-products observed.



Scheme 4. Formation of the two regioisomers **29** and **31** upon borylation of bromobiphenyl **27**, yields were determined by GC–MS analysis.

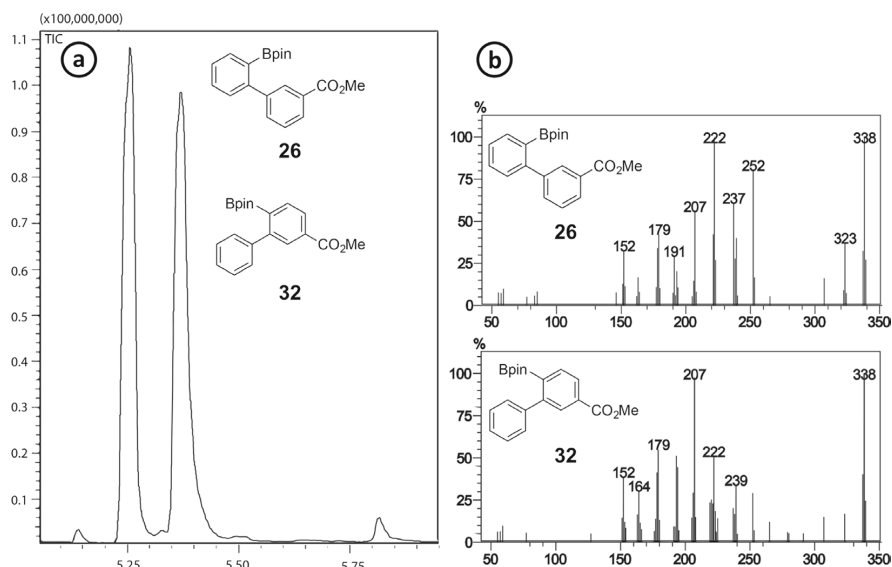


Figure 4. (a) GC–MS trace from the reaction mixture of the borylation of **25** displaying both regioisomers (**26** and **32**), which were formed in a 1:1 ratio. (b) Mass-spectrometric analysis of both GC signals. Both regioisomers give closely related patterns because of their structural similarity.

FULL PAPER

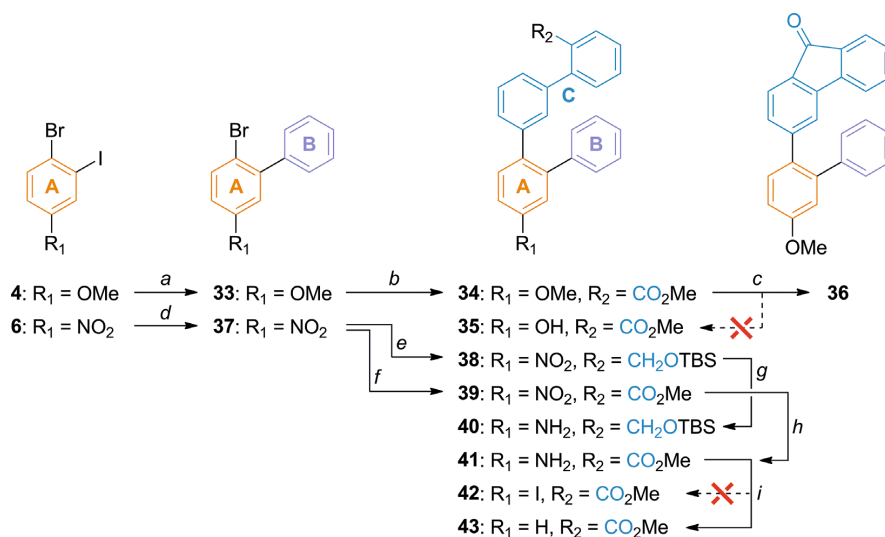
M. Mayor et al.

With all building blocks for a convergent synthesis in hand, our attention moved towards the assembly of the target structure **1**.

Stepwise Connection of the Fragments I: Preliminary Studies with Model Compounds

With all fragments in hand, we aimed to establish a viable sequence for their combination to give the target structure. Fragment **A**, that is **4**, **5** and ultimately **8**, allowed for the envisaged stepwise attachment of the other fragments. At this point we were mainly interested in exploring the synthetic strategy as far as possible. It was therefore of interest to attach a fragment **B** with diminished steric bulk. Coupling of **4** with commercially available phenyl boronic acid gave **33** in excellent 93% yield over 21 h using partially optimized conditions (Scheme 5). A solvent system consisting of dioxane/water (4:1) was found to promote cross coupling on both halides to a significant amount (up to 26% according to GC–MS analysis). Cross coupling **33** with crude **14** under similar conditions to those described before gave tetraphenyl **34** in reasonable 51% yield. To enable the introduction of the last fragment **D**, the hydroxy group needed to be liberated. Typically a strong Lewis acid such as BBr_3 is capable of demethylating the methoxy group.^[20] When subjecting **34** to Lewis-acidic conditions at -78°C , we observed the formation of a single isolable product in 56% yield. 1D ^1H NMR and 2D NMR spectroscopy (namely selective TOCSY), as well as GC–MS analysis allowed the isolated compound to be identified as cyclic ketone **36**, instead of the desired complex quarterphenyl **35** with a liberated phenolic OH group. Apparently, BBr_3 is capable of activating the ester such that cyclization is preferred to the desired methylation. Although Lewis-acid ini-

tiated bond formations are widely used in polyaromatic synthesis (e.g., Scholl-type reactions),^[21] the inability to deprotect the methoxy group forced us to search for alternative routes. The nitro derivative **6** is ideally suited for cross-coupling reactions because of its electronic nature. Indeed, when subjected to the same cross-coupling conditions as applied above for **4**, compound **6** and phenyl boronic acid were converted into **37** in 68% yield. The electron-withdrawing effect of the nitro group has an even larger activating effect on the engagement of the bromine in the *para*-position in cross-coupling reactions. Subsequent coupling of the remaining bromine of the formed biphenyl **37** as a major side-reaction clearly reflected this effect. The increased activity of the bromine leaving group was also promising for the subsequent attachment of fragment **C**. We decided to directly subject the only marginally purified **37** together with **19** to cross-coupling conditions, giving the tetraphenyl building block **38** in excellent 84% yield. Purification of the test system **38** was very challenging and we decided to focus instead on the similar reaction between **37** and **14**, which provided the methyl ester functionalized tetraphenyl building block **39**. To enable the attachment of the remaining fragment **D**, the nitro groups of **38** and **39** had to be transformed into a leaving group. Reductive conditions using SnCl_2 are known to promote the reduction of nitro groups selectively, while leaving ester groups untouched.^[22] Indeed, we were able to reduce the nitro group of both **38** and **39** to the corresponding amines **40** and **41**, albeit in low yields of <27% for the TBS-protected alcohol **40** and <50% for the methyl ester **41**. Reduction using Pd/C and H_2 as an alternative protocol resulted in decomposition of the starting material. Nevertheless, because **41** was accessible in sufficient purity, we attempted to substitute the amine group with an iodine, which would allow the remain-



Scheme 5. Reagents and conditions: (a) phenyl-B(OH)₂, Pd(PPh₃)₂Cl₂, K₂CO₃, toluene/EtOH (4:1), 80 °C, 21 h, 93%; (b) **14**, Pd(PPh₃)₂Cl₂, K₃PO₄, dioxane/water (4:1), 80 °C, 4 h, 51%; (c) BBr_3 , CH_2Cl_2 , -78°C to 0°C , 4 h, 56% of **36**; (d) phenyl-B(OH)₂, Pd(PPh₃)₂Cl₂, K₂CO₃, toluene/EtOH (4:1), 80 °C, 18 h, 68%; (e) **19**, Pd(PPh₃)₂Cl₂, K₃PO₄, dioxane/water (4:1), 80 °C, 5.5 h, 84%; (f) **14**, Pd(PPh₃)₂Cl₂, K₃PO₄, dioxane/water (4:1), 80 °C, 3 h, 81%; (g) SnCl_2 , EtOAc, reflux, 8 h, <27%; (h) SnCl_2 , EtOAc, reflux, 6 h, <50%; (i) 1. $\text{BF}_3 \cdot \text{OEt}_2$, ONOTBu , THF, -30°C to r.t., 3 h; 2. I_2 , KI, MeCN, r.t.

Pathways to a Helical Hexaphenyl ‘Geländer’ Molecule

ing fragment **D** to be attached. By using the established conditions to convert anilines into iodines by forming the corresponding diazonium salt, the ester **41** was subjected to the iodination protocol. Unfortunately, the only observed product was the dehalogenated tetraphenyl **43** and in none of the attempts was the desired iodinated derivative **42** detected.

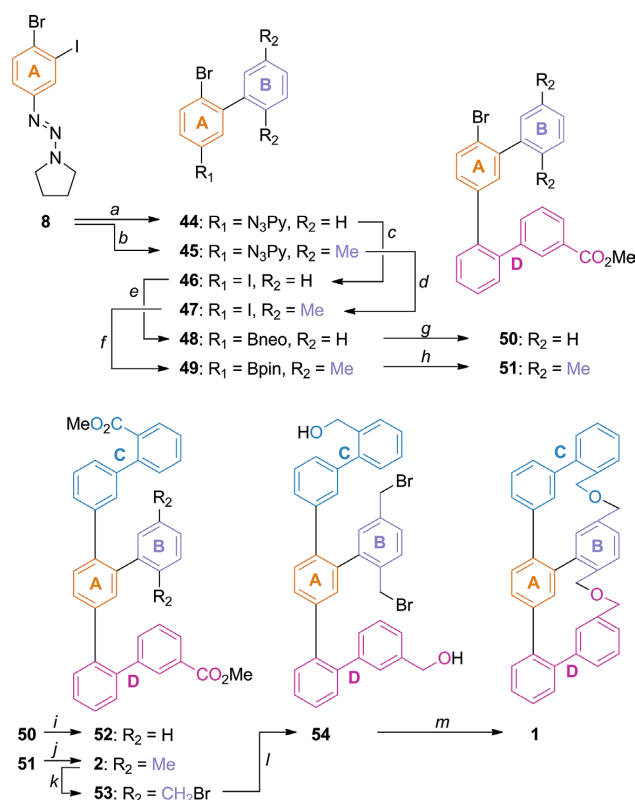
Stepwise Connection of the Fragments II: The End Game

The synthetic routes exploited so far mainly focused on the stepwise attachment of fragments **C** and **D** to **E** following the olive path of the retrosynthetic analysis (Figure 3). Thereby, we faced severe challenges with the attachment of fragment **D**, in particular its troublesome isomerization during borylation. Furthermore, the challenging introduction of a suitable leaving group at the quaterphenyl structure required for the attachment of the fragment **D** raised questions concerning the viability of this route. At this stage we reconsidered our synthetic strategy, building on the insights gained over the course of the various attempts.

The new plan was to profit from the fact that fragment **A** can already feature a masked iodine. Particularly interesting were triazenes, which can be converted into iodines without the need for a reduction/iodination sequence. The iodine was appealing because it would allow for selective borylation in the presence of less reactive bromines. By introducing the boronic ester to the assembled biphenyl system, the troublesome fragment **D** could then be introduced as a halide (iodine), thus potentially preventing the isomerization as well as moving the challenging attachment of the fragment to an earlier point in the synthesis. Thus, the blue path of the retrosynthetic analysis (Figure 3) became more appealing. As fragment **B**, a *para*-xylene derivative was envisaged, which should allow benzylic bromination in a late stage of the synthesis. The conceptual idea was to minimize the number of functional groups present over a large extent of the synthesis. Having all rings in place would allow the investigation and the full characterization of the structure before introducing the required bromines and reducing the ester moieties to benzylic alcohols. As a last step, basic cyclization should then provide the target structure **1**.

Starting from triazene **8**, two different fragments **B** were attached (Scheme 6): Either an unsubstituted phenyl ring, giving **44** as a test system, or 2,5-dimethyl phenyl, which results in **45**. The only difference in reactivity between both fragments might be some steric constrains from the two methyl groups. Both biphenyl fragments **44** and **45** were obtained: 62% for **44**, and excellent yields of up to >99% for **45** under optimized conditions. In both cases, selective substitution of the iodine was observed. Both triazenes **44** and **45** were converted into the corresponding iodines **46** and **47** in very good yields of 83 and 77–96%, respectively, by treatment with MeI at 120 °C overnight.^[23] Subsequent borylation of iodines **46** and **47** was more challenging. The application of Knochels protocol gave access to neopentyl

borane **48** in low yields of 32% for the unsubstituted biphenyl model compound. As this served merely as a test system, the conditions were not improved. As a consequence, however, the palladium-catalyzed Hosomi–Miyaura borylation protocol that we have already established was used for the dimethylated iodobiphenyl **47**, providing pinacol borane **49** in an improved yield of 53%. Given the metastable nature of the intermediate, the obtained borane was typically used directly in the next step.



Scheme 6. Reagents and conditions: (a) phenyl-B(OH)₂, Pd(PPh₃)₂-Cl₂, K₂CO₃, toluene/EtOH (1:1), 80 °C, 23 h, 62%; (b) 2,5-dimethylphenyl-B(OH)₂, Pd(PPh₃)₂-Cl₂, K₂CO₃, THF/H₂O (4:1), 60 °C, 15 h, 88% to >99%; (c) MeI, 120 °C, 15 h, 83%; (d) MeI, 120 °C, 15 h, 77–96%; (e) *i*PrMgCl·LiCl, B(O*i*Pr)₃, NPG, THF, –40 °C to r.t., 19 h, 32%; (f) Pd(dppf)Cl₂, KOAc, B₂pin₂, dioxane, 100 °C, 15 h, 53%; (g) **25**, Pd(PPh₃)₂-Cl₂, K₂CO₃, toluene/EtOH (4:1), 80 °C, 5.5 d, 33%; (h) **25**, XPhos Pd G2, K₂CO₃, toluene, 110 °C, 1–2 d, 58–94%; (i) **14**, Pd(PPh₃)₂-Cl₂, K₃PO₄, dioxane/H₂O (4:1), 80 °C, 4 h, 90%; (j) **13**, SPhos Pd G2, K₂CO₃, toluene/H₂O (20:1), 110 °C, 1–3 d, 50%; (k) NBS, DBP, CCl₄, 75 °C, 1 h, 87% to >99%; (l) DIBAL-H, CH₂Cl₂, r.t., 30 min, >99%; (m) 1. NaH, [D₈]THF, 60 °C, 2–3 d, 28%.

With **48** and **49** in hand, the attachment of fragment **D** became the focus of interest. Suzuki–Miyaura cross coupling of the phenyl-bearing model system **48** with **25** under the conditions optimized for the assembly of the tetraphenyls **38** and **39** gave the desired tetraphenyl **50** in modest 33% yield. Relying on the observations made while screening for optimal Suzuki conditions for the assembly of fragment **C**, we decided to employ a catalyst system that showed a high tendency for cross coupling of sterically challenging

FULL PAPER

M. Mayor et al.

systems.^[24] XPhos Pd G2 was found to be ideal for the successful promotion of the desired cross coupling of **49** with **25**, giving the desired quaterphenyl system **51** in up to 94% yield based on GC–MS analysis. At this stage of the synthesis, the obtained crude material was very challenging to purify and it was best used as obtained in the next step. The cross-coupling reaction was monitored by GC–MS analysis and full conversion was observed within 1–2 days. By placing the borane on the assembled structure rather than on the biphenyl fragment **D**, its troublesome isomerization was prevented entirely. Both quarterphenyls **50** and **51** were suitably functionalized for the attachment of the last fragment **C**.

Whereas slightly modified standard Suzuki–Miyaura conditions were used for the coupling between the sterically less demanding **50** and **14**, the sterically encumbered **51** together with the pinacol borane **C** fragment **13** were subjected to a previously reported, highly active catalyst system [Pd(OAc)₂/SPhos or SPhos Pd G2].^[25] The less hindered model compound **52** was isolated in excellent 90% yield, while the sterically more challenging coupling product **2** was still obtained in a reasonable yield of 50%. Both hexaphenyl systems **52** and **2** were fully characterized by ¹H, ¹³C, as well as 2D NMR spectroscopy, confirming not only the presence of all required rings, but also the desired substitution patterns. DART-MS as well as HRMS (ESI) provided further evidence for the molecular identity of **2**.

With compound **2** in hand, our attention turned to the bromination of its methyl groups. A bromination procedure adapted from a reported protocol was applied.^[26] Treatment of **2** with NBS and dibenzoylperoxide in CCl₄ provided the dibrominated hexaphenyl **53** in up to quantitative yield. The reaction times varied with the batch size, and the course of the reaction had to be closely monitored to avoid over-bromination. All brominated species were structurally and electronically very similar, resulting in comparable retention values in all investigated chromatographic systems; thus, monitoring was best performed by DART-MS. The mono- and tri-brominated species were subsequently removed efficiently by semipreparative HPLC (column: semipreparative Reprosil 100 Si, 5 μm, 250 × 16 mm, eluent: 60:40 hexane/CH₂Cl₂, 8 mL/min). Conventional flash column chromatography (CC) could be used to enrich the dibrominated species **53**, but only after several repeated columns. Interestingly, the ¹H NMR spectrum revealed diastereotopic hydrogen signals for all benzylic positions, indicating that, on the NMR timescale, the structure was already subject to hindered rotation. For the reduction of diester **53**, the protocol established for fragment **C** was applied. Treatment of **53** with DIBAL-H in dichloromethane at room temperature for 30 min provided hexaphenyl diol **54** in almost quantitative yield. The latter diol displayed limited stability and thus subsequent cyclization was best carried out immediately after purification.

During the development of the synthetic strategy, we judged the assembly of the suitably functionalized hexaphenyl system to be the major challenge and assumed that once **54** became available, its double cyclization would be a

straightforward and comparably facile final step. This assumption was based on the observation that, in **54**, the two benzylic alcohols as nucleophiles and the two benzylic bromides as substrates are ideally preorganized for two subsequent intramolecular substitution reactions. Potential polymerization reactions can be avoided by performing both ring-closing reactions under high-dilution conditions. Much to our surprise, the double ring-closing reaction of **54** to **1** turned out to be very challenging. Initial attempts to cyclize **54** to **1** under basic conditions resulted in traces of **1** at best, regardless of full consumption of the starting material. The only promising signs were obtained by DART-MS of the reaction mixture, which revealed at least partial formation of the desired structure. Attempts to isolate **1** failed; instead, substantial loss of mass was observed when exposing the reaction mixture to either silica (acidic or pH-neutral) or aluminum oxide. Closer inspection of the course of the double ring-closing reaction by TLC revealed the rapid formation of a new spot, which was subsequently consumed with the addition of more base. The working hypothesis was that this rapidly formed new spot might be a monocyclized intermediate; indeed, DART-MS analysis of the TLC spot revealed a molecular mass supporting the hypothesis. Given that we failed to cyclize **54** directly to **1**, our desperate final strategy was to isolate the monocyclized derivative of **54** and to investigate its ability to close the second ring. The hope was that cleaner reaction conditions might prevent the formation of side products and thereby favor the second intramolecular ring closure of the intermediate to **1**. By reducing the amount of sodium hydride and carefully monitoring the course of the reaction, selective monocyclization was possible. According to ¹H NMR analysis, a pure monocyclized derivative was isolated and, although we could not identify which, it seemed that exclusively one of the four possible regioisomers was formed. Considering the proximity of the functional subunits, we were confident that we obtained one of the two correctly closed systems, because we reasoned that the designed target structure is the energetically most favored spatial arrangement. Even though the isolation of the monocyclized compound was yield diminishing (30% isolated yield), we hoped that in the monocyclized derivative the remaining functional groups might be even better preorganized, further favoring the second ring closing over competing reaction pathways such as intermolecular substitution reactions. To monitor the course of the second ring closure, the reaction was directly performed in an NMR tube. The tube was charged with the monocyclized regioisomer in deuterated THF, and sodium hydride was added as base. The reaction mixture was heated to 60 °C and the formation of **1** was monitored by ¹H NMR spectroscopy.

Much to our delight, we observed an almost clean transformation of the monocyclized intermediate into a new compound with NMR signals matching the expectations for the desired target structure **1** over a period of 2–3 days (Figure 5). In particular, for each of the eight diastereotopic benzylic hydrogen atoms, an individual signal was observed

(each as a doublet) due to geminal coupling to the second hydrogen at the corresponding benzylic carbon atom. In spite of the clean transformation observed in the NMR spectra, all attempts to isolate the formed species by conventional column chromatography or by normal-phase HPLC failed; in other words, the results further documented the delicate stability properties of the compound at least on these solid phases. Given that the target structure **1** is formed as a racemate, we considered purification by chiral HPLC with the hope of isolating pure enantiomers. Interestingly, both Chiralpak IA and AD-H analytical columns were suitable (eluent: *n*-hexane/2-propanol, 99:1; flow rate 1 mL/min; *T* = 25 °C) to successfully separate **1** into its *M* and *P* enantiomers. The injected sample contained the reaction mixture as obtained directly after filtration and change of solvents. The obtained UV trace of one representative run is displayed in Figure 6, which clearly displays the enantiomeric peaks as major components in the mixture. No significant plateau between the peaks was observed, pointing to a relatively slow racemization process at room temperature on the timescale of a single run (ca. 20 min). The obtained fractions of numerous runs were combined to

yield the target compound **1** in a combined yield of 28% (14% of each enantiomer). Although the yield was somewhat sobering considering the clean transformation monitored by ¹H NMR analysis, we were at this point more than pleased to finally have been able to isolate **1** as pure enantiomers. Interestingly, the purified samples of **1** were reasonably stable; the compounds tolerated air and moisture as well as evaporation of the solvents at elevated temperatures under reduced pressure.

The target structure **1** is a colorless solid that is soluble in common organic solvents (ethers, chlorinated hydrocarbons, aromatics, etc.). It was fully characterized by ¹H and ¹³C NMR spectroscopy and by high-resolution mass spectrometry. 2D NMR experiments enabled the full assignment of all the peaks, confirming the identity of the structure. ¹H NMR spectra were identical for both enantiomers, which clearly demonstrated the diastereotopic benzylic protons (see Figure 5, c). The identity of **1** was finally corroborated without a doubt by X-ray diffraction, which was presented in detail in the preceding communication.^[11] All compounds synthesized over the course of this work were characterized by ¹H and ¹³C NMR spectroscopy and

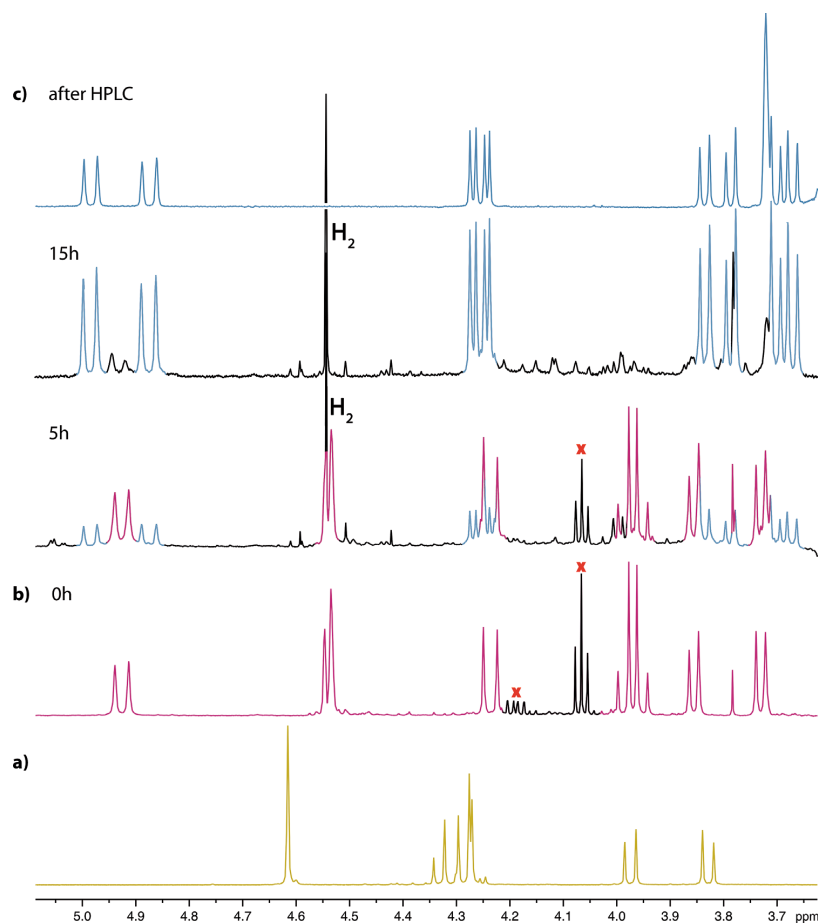


Figure 5. Conversion of the monocyclized intermediate into **1** with NaH in [D₈]THF at 60 °C, monitored by ¹H NMR spectroscopic analysis. (a) Selected ¹H NMR region of the open-chain precursor **54**. The observed benzylic hydrogen atoms are diastereotopic. (b) Monocyclized intermediate at the beginning of the second cyclization. (c) Spectra of the reaction with almost complete conversion into target structure **1**. The topmost spectrum shows the isolated Geländer oligomer **1** after chiral HPLC.

FULL PAPER

M. Mayor et al.

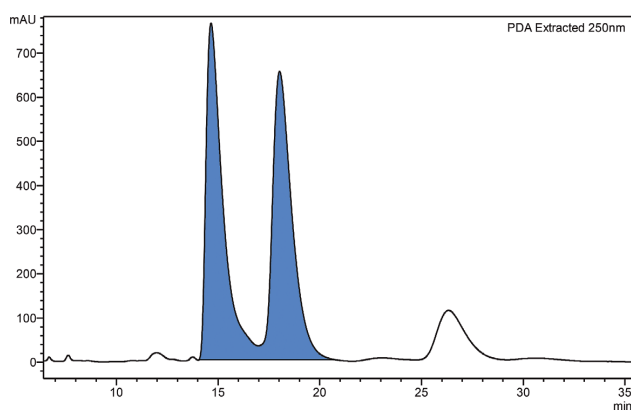


Figure 6. UV trace of a representative chiral HPLC run of the crude reaction mixture after filtration (Chiralpak IA; *n*-hexane/2-propanol (99:1), flow rate 1 mL/min, $T = 25\text{ }^{\circ}\text{C}$). The chart reveals the two enantiomeric peaks (blue) as major compounds. The enantiomeric fractions were collected and combined to give 28% combined yield of the desired target structure **1**.

by mass spectrometry. The intermediates obtained on the synthetic route resulting in the successful assembly of **1** were also characterized by high-resolution ESI mass spectrometry.

Conclusions

We have discussed the synthesis of the new “Geländer” structure **1** as a model compound to demonstrate a new concept to induce helicity in polyaromatic systems. The synthesis of **1** is based on a broad range of Miyaura–Hosomi borylation/Suzuki–Miyaura cross-coupling protocols. In a convergent assembly strategy, suitable precursors were assembled and interlinked to increasingly complex oligophenyl systems to finally yield the suitably functionalized hexaphenyl precursor. The “Geländer” motif was installed by two subsequent intramolecular substitution reactions to build up the elongated benzyl ether oligomer. Whereas careful choice of masking substrates and placement of the boronic moieties allowed the stepwise assembly of the hexaphenyl precursor, persistence was required to close the benzyl ether banister and to isolate the obtained target structure. In spite of numerous obstacles, the “Geländer” oligomer **1** was assembled in an overall yield of 8%, considering only the convergent ten steps interlinking the fragments and installing the “Geländer” motif. Pure enantiomers of **1** were obtained by chiral HPLC.

We now intend to investigate various types of bridges and their influence on the chiroptical properties and racemization behavior.

Experimental Section

General Procedures: All commercially available compounds were purchased and used as received unless explicitly stated otherwise. $[\text{D}_8]\text{THF}$ was purchased from Acros. ^1H NMR spectra were recorded with a Bruker UltraShield 500 MHz Avance III equipped

with a 5 mm BBI probe head with Z-gradients. ^{13}C NMR and all 2D spectra were recorded with a Bruker Ascend 600 MHz Avance III HD equipped with a 1.7 mm TCI cryo probe head. The chemical shifts are reported in parts per million (ppm) relative to tetramethylsilane or a residual solvent peak, and the J values are given in Hz. DART-MS was measured with an IonSense DART-SVP100 (He, $450\text{ }^{\circ}\text{C}$) connected to a Shimadzu LC-2020. GC–MS analysis was performed with a Shimadzu GC–MS-2010 SE equipped with a Zebron 5 MS Inferon column, which allowed temperatures up to $350\text{ }^{\circ}\text{C}$ to be achieved. High-resolution mass spectra (HRMS) were measured as HR-ESI-ToF-MS with a Maxis 4G instrument from Bruker with the addition of NaOAc. For column chromatography, usually silica gel Siliacel p60 ($40\text{--}63\text{ }\mu\text{m}$) from Silicycle was used, and TLC was performed on silica gel 60 F254 glass plates with a thickness of 0.25 mm purchased from Merck. Buffered silica was prepared by using buffer solution pH 7 by Fluka and diluting 1:25 with water. 10 mL of the prepared solution was added to 100 g of silica and allowed to adsorb under mixing overnight. For HPLC, a Shimadzu LC-20AT HPLC was used equipped with a diodearray UV/Vis detector (SPD-M10A VP from Shimadzu, $\lambda = 200\text{--}600\text{ nm}$) equipped with the corresponding column (regular: Reprisil 100, $5\text{ }\mu\text{m}$, $250 \times 16\text{ mm}$; chiral: Chiralpak IA $0.46 \times 25\text{ cm}$; Daicel Chemical Industries Ltd.). All solutions were prepared and measured under air-saturated conditions.

1-Bromo-2-iodo-4-methoxybenzene (**4**) was synthesized from 1-iodo-3-methoxybenzene according to a reported procedure.^[27] The experimental data for the successful route including each intermediate step to access **1** (i.e., **6–8**, **12**, **13**, **25**, **45**, **47**, **49**, **51**, **53**, **54** and **1**) were described previously.^[11]

Methyl 3'-Bromo-[1,1'-biphenyl]-2-carboxylate (11**):** To an oven-dried and argon-flushed Schlenk tube were consecutively added potassium carbonate (2.32 g, 16.6 mmol, 3.00 equiv.), 2-methoxycarbonylphenylboronic acid (**9**; 1.00 g, 5.56 mmol, 1.00 equiv.), $\text{Pd}(\text{PPh}_3)_2\text{Cl}_2$ (82.8 mg, 2 mol-%), and 1-bromo-3-iodobenzene (**63**; 1.42 mL, 11.1 mmol, 2.00 equiv.). Anhydrous THF (20 mL) and anhydrous MeOH (5 mL) were added and the solution was degassed for 15 min before heating to $60\text{ }^{\circ}\text{C}$ and stirring overnight. EtOAc and water were added, the aqueous phase was extracted with EtOAc (2 \times), and the combined organic phases were washed with brine (1 \times). After drying over Na_2SO_4 , the solvent was removed under reduced pressure. Column chromatography (SiO_2 ; EtOAc/cyclohexane, 1:15) gave **11** (859 mg, 2.95 mmol, 53%) as a yellow solid. ^1H NMR (400 MHz, CDCl_3 , $25\text{ }^{\circ}\text{C}$): $\delta = 7.86$ (dd, $^3J_{\text{H,H}} = 7.7$, $^4J_{\text{H,H}} = 1.1$ Hz, 1 H), 7.54 (td, $^3J_{\text{H,H}} = 7.5$, $^4J_{\text{H,H}} = 1.3$ Hz, 1 H), 7.50–7.41 (m, 3 H), 7.34 (dd, $^3J_{\text{H,H}} = 7.6$, $^4J_{\text{H,H}} = 0.7$ Hz, 1 H), 7.29–7.20 (m, 2 H), 3.67 (s, 3 H) ppm. ^{13}C NMR (101 MHz, CDCl_3): $\delta = 168.6$, 143.4, 141.1, 131.5, 131.3, 130.7, 130.6, 130.2, 130.1, 129.5, 127.7, 127.1, 122.1, 52.1 ppm. MS (EI, +): m/z (%) = 292 (48), 291 (12), 290 (49), 261 (52), 259 (53), 181 (20), 180 (100), 152 (48), 151 (18), 76 (22).

Methyl 3'-(5,5-Dimethyl-1,3,2-dioxaborinan-2-yl)-[1,1'-biphenyl]-2-carboxylate (14**):** In an oven-dried and argon-flushed Schlenk tube, isopropylmagnesium chloride lithium chloride complex solution (1.13 mL, 1.47 mmol, 1.10 equiv.) was added to a degassed solution of **12** (451 mg, 1.33 mmol, 1.00 equiv.) in THF (8.5 mL) at $-40\text{ }^{\circ}\text{C}$, followed by stirring for 40 min. After GC–MS analysis revealed full conversion, a solution of triisopropyl borate (380 μL , 1.6 mmol, 1.20 equiv.) in THF (1 mL) was added and the mixture was stirred at $-40\text{ }^{\circ}\text{C}$ for 2 h before warming to room temperature and stirring for an additional 2 h. After adding 2,2-dimethyl-1,3-propanediol (175 mg, 1.67 mmol, 1.25 equiv.), the mixture was stirred for 14 h at room temperature. CH_2Cl_2 and satd. aq. NH_4Cl were added, the

Pathways to a Helical Hexaphenyl “Geländer” Molecule

organic phase was washed with water and brine, the organic layer was dried over Na_2SO_4 , and the solvent was removed under reduced pressure. Column chromatography (SiO_2 ; EtOAc/cyclohexane, 1:20) gave **14** (312 mg, 962 μmol , 72%) as a yellow oil. ^1H NMR (400 MHz, CDCl_3 , 25 °C): δ = 7.84–7.80 (m, 1 H), 7.78 (dd, $^3J_{\text{H,H}} = 5.9$, $^4J_{\text{H,H}} = 2.1$ Hz, 2 H), 7.57–7.45 (m, 1 H), 7.44–7.34 (m, 4 H), 3.77 (s, 4 H), 3.61 (s, 3 H), 1.03 (s, 6 H) ppm. ^{13}C NMR (63 MHz, CDCl_3): δ = 169.5, 143.0, 140.6, 134.0, 132.9, 131.4, 131.4, 131.1, 131.0, 130.8, 129.9, 127.4, 127.2, 72.6, 52.1, 32.1, 22.2 ppm. MS (EI, +): m/z (%) = 325.1 (21), 324.1 (99), 323.1 (44), 294.1 (20), 293.1 (99), 292.1 (26), 208.0 (15), 207.0 (100), 206.1 (27), 181.0 (17), 179.0 (22), 178.0 (25), 177.0 (10), 152.1 (27), 151.1 (12), 69.1 (13), 56.1 (12).

(3'-Bromo-[1,1'-biphenyl]-2-yl)methanol (15): An oven-dried and argon-flushed round-bottomed flask was charged with **11** (408 mg, 1.40 mmol, 1.00 equiv.) and anhydrous CH_2Cl_2 (20 mL) before cooling to 0 °C. DIBAL-H (1 M in hexanes, 4.90 mL, 3.50 equiv.) was slowly added while maintaining the temperature. After stirring for 30 min at 0 °C, the mixture was warmed to room temperature and stirring was continued for an additional 1 h. MeOH (10 mL) was slowly added to the yellow solution (which became dark), followed by *t*BME and aq. HCl (1 M). The organic layer was washed with water and the aqueous layer was extracted three times with *t*BME. The combined organic layers were washed with brine, dried with Na_2SO_4 , concentrated under reduced pressure, and the residual oil was passed through a plug of silica (eluent: EtOAc) to give **15** (332 mg, 1.26 mmol, 90%) as an orange oil. ^1H NMR (400 MHz, CDCl_3 , 25 °C): δ = 7.58–7.53 (m, 2 H), 7.53–7.49 (m, 1 H), 7.41 (td, $^3J_{\text{H,H}} = 7.5$, $^4J_{\text{H,H}} = 1.5$ Hz, 1 H), 7.36 (td, $^3J_{\text{H,H}} = 7.5$, $^4J_{\text{H,H}} = 1.5$ Hz, 1 H), 7.34–7.24 (m, 3 H), 4.61 (d, $^3J_{\text{H,H}} = 5.7$ Hz, 2 H), 1.57 (t, $^3J_{\text{H,H}} = 5.7$ Hz, 1 H) ppm. ^{13}C NMR (101 MHz, CDCl_3): δ = 143.1, 140.2, 138.3, 132.5, 130.7, 130.5, 130.2, 129.0, 128.6, 128.3, 128.2, 122.8, 63.4 ppm. MS (EI, +): m/z (%) = 264 (45), 262 (46), 183 (56), 182 (11), 181 (17), 166 (19), 165 (100), 155 (18), 154 (32), 153 (17), 152 (26), 76 (13).

(3'-Iodo-[1,1'-biphenyl]-2-yl)methanol (16): An oven-dried, argon-flushed Schlenk tube was charged with **12** (369 mg, 1.09 mmol, 1.00 equiv.) and anhydrous CH_2Cl_2 (3 mL) and cooled to 0 °C before adding DIBAL-H (1 M in hexanes, 2.30 mL, 5.91 mmol, 4.20 equiv.) dropwise over 15 min. The mixture was stirred for 30 min at room temperature and cooled to 0 °C before adding more CH_2Cl_2 . The reaction was carefully quenched with brine and the mixture was stirred for an additional 30 min. The solution was neutralized with satd. aq. NH_4Cl , the precipitate was filtered off and discarded, and the filtrate was extracted with CH_2Cl_2 (3 \times). The combined organics were washed with brine and dried over Na_2SO_4 . Removal of the solvent under reduced pressure gave **16** (317.3 mg, 1.02 mmol, 94%) as a colorless solid. ^1H NMR (400 MHz, CDCl_3 , 25 °C): δ = 7.75 (t, $^4J_{\text{H,H}} = 1.8$ Hz, 1 H), 7.71 (ddd, $^3J_{\text{H,H}} = 7.8$, $^4J_{\text{H,H}} = 1.8$, 1.1 Hz, 1 H), 7.58–7.53 (m, 1 H), 7.45–7.31 (m, 3 H), 7.27–7.22 (m, 1 H), 7.16 (t, $^3J_{\text{H,H}} = 7.8$ Hz, 1 H), 4.60 (s, 2 H) ppm; the hydroxy peak is most likely located underneath the broadened water peak at δ = 1.55 ppm. ^{13}C NMR (63 MHz, CDCl_3): δ = 143.0, 140.0, 138.2, 138.1, 136.5, 130.1, 130.1, 128.8, 128.7, 128.4, 128.0, 94.4, 63.2 ppm. MS (EI, +): m/z (%) = 311.1 (11), 310.1 (61), 183.1 (63), 182.1 (11), 181.1 (25), 166.0 (28), 165.1 (100), 164.1 (13), 163.1 (10), 155.2 (46), 154.1 (39), 153.1 (40), 152.1 (49), 151.1 (19), 139.1 (11), 128.1 (12), 127.0 (14), 115.1 (18), 91.2 (11), 82.5 (15), 77.0 (27), 76.1 (23), 75.1 (10), 63.0 (15), 51.0 (14).

***tert*-Butyl{[3'-iodo-(1,1'-biphenyl)-2-yl]methoxy}dimethylsilane (18)**: An argon-flushed round-bottomed flask was charged with **16** (305 mg, 983 μmol , 1.00 equiv.), imidazole (203.5 mg, 2.96 mmol,

3.01 equiv.), and TBSCl (181 mg, 1.18 mmol, 1.20 equiv.) in anhydrous CH_2Cl_2 (3 mL) and the mixture was stirred at room temperature for 7 h, before adding more TBSCl (154.1 mg, 0.983 mmol, 1.0 equiv.) and stirring overnight. The mixture was diluted with CH_2Cl_2 (30 mL) and washed with water (2 \times 20 mL), aq. HCl (1 M, 3 \times 20 mL) and brine (50 mL). The organic layer was dried with Na_2SO_4 and adsorbed on Celite before subjecting to column chromatography (SiO_2 ; EtOAc/cyclohexane, 1:20) to give **18** (358 mg, 844 μmol , 86%) as a colorless oil. ^1H NMR (400 MHz, CDCl_3 , 25 °C): δ = 7.75 (t, $^4J_{\text{H,H}} = 1.7$ Hz, 1 H), 7.69 (dd, $^3J_{\text{H,H}} = 7.9$, $^4J_{\text{H,H}} = 1.7$ Hz, 1 H), 7.55 (dd, $^3J_{\text{H,H}} = 7.7$, $^4J_{\text{H,H}} = 1.5$ Hz, 1 H), 7.38 (td, $^3J_{\text{H,H}} = 7.5$, $^4J_{\text{H,H}} = 1.5$ Hz, 1 H), 7.36–7.29 (m, 2 H), 7.20 (dd, $^3J_{\text{H,H}} = 7.7$, $^4J_{\text{H,H}} = 1.5$ Hz, 1 H), 7.14 (t, $^3J_{\text{H,H}} = 7.9$ Hz, 1 H), 4.56 (s, 2 H), 0.90 (s, 9 H), 0.04 (s, 6 H) ppm. MS (EI, +): m/z (%) = 367.9 (22), 366.9 (100), 336.9 (11), 292.9 (14), 167.1 (13), 166.0 (73), 165.0 (72), 75.0 (62).

***tert*-Butyl{[3'-(5,5-dimethyl-1,3,2-dioxaborinan-2-yl)-(1,1'-biphenyl)-2-yl]methoxy}dimethylsilane (19)**: In an oven-dried and argon-flushed Schlenk tube, isopropylmagnesium chloride lithium chloride complex solution (700 μL , 911 μmol , 1.10 equiv.) was added to a degassed solution of **18** (351 mg, 828 μmol , 1.00 equiv.) in THF (6.5 mL) at –40 °C before stirring for 40 min. After GC–MS analysis revealed full conversion, a solution of triisopropyl borate (230 μL , 994 μmol , 1.20 equiv.) in THF (1 mL) was added. Stirring was continued at –40 °C for 2 h before warming to room temperature and stirring for another 2.5 h. After adding 2,2-dimethyl-1,3-propanediol (109 mg, 1.03 mmol, 1.25 equiv.), the reaction was stirred for 14 h. CH_2Cl_2 and satd. aq. NH_4Cl were added and the organic phase was washed with water and brine. After drying over Na_2SO_4 , the solvent was removed under reduced pressure. Column chromatography (SiO_2 ; EtOAc/cyclohexane, 1:20) gave **19** (243 mg, 604 μmol , 45%) as a brown oil. ^1H NMR (400 MHz, CDCl_3 , 25 °C): δ = 7.77 (tt, $^4J_{\text{H,H}} = 3.2$, 1.2 Hz, 2 H), 7.59–7.54 (m, 1 H), 7.42–7.36 (m, 2 H), 7.36–7.32 (m, 1 H), 7.28 (td, $^3J_{\text{H,H}} = 7.4$, $^4J_{\text{H,H}} = 1.5$ Hz, 1 H), 7.22 (dd, $^3J_{\text{H,H}} = 7.5$, $^4J_{\text{H,H}} = 1.5$ Hz, 1 H), 4.59 (s, 2 H), 3.75 (s, 4 H), 1.02 (s, 6 H), 0.88 (s, 9 H), –0.01 (d, $^4J_{\text{H,H}} = 1.9$ Hz, 6 H) ppm. ^{13}C NMR (63 MHz, CDCl_3): δ = 141.0, 140.2, 138.6, 134.8, 132.7, 131.6, 130.0, 127.8, 127.5, 127.4, 127.0, 72.5, 63.3, 32.1, 26.2, 22.1, 18.6, –5.1 ppm. MS (EI, +): m/z (%) = 354.1 (16), 353.1 (60), 352.2 (15), 225.9 (14), 225.0 (70), 193.0 (51), 192.1 (11), 191.0 (11), 180.0 (16), 179.0 (100), 167.0 (48), 166.1 (18), 165.0 (65), 119.0 (21), 75.0 (36), 73.1 (11), 69.1 (63), 57.1 (13).

Methyl 2'-Bromo-[1,1'-biphenyl]-3-carboxylate (24): To an argon-flushed Schlenk tube was consecutively added potassium carbonate (464 mg, 3.32 mmol, 2.98 equiv.), 3-methoxycarbonylphenylboronic acid (**22**; 201 mg, 1.12 mmol, 1.00 equiv.), $\text{Pd}(\text{PPh}_3)_2\text{Cl}_2$ (16.0 mg, 2 mol-%), and 1-bromo-2-iodobenzene (**21**; 284 μL , 2.19 mmol, 1.96 equiv.). Wet THF (4 mL) and MeOH (1 mL) were added and the solution was degassed for 10 min before heating to 60 °C and stirring overnight. EtOAc and water were added, the aqueous phase was extracted with EtOAc (2 \times) and the combined organic phases were washed with brine (1 \times). After drying over Na_2SO_4 , the solvent was removed under reduced pressure. Column chromatography (SiO_2 ; EtOAc/cyclohexane, 1:15) gave **24** (238 mg, 817 μmol , 73%) as a yellow oil. ^1H NMR (400 MHz, CDCl_3 , 25 °C): δ = 8.10–8.05 (m, 2 H), 7.68 (dd, $^3J_{\text{H,H}} = 8.0$, $^4J_{\text{H,H}} = 1.2$ Hz, 1 H), 7.62 (dt, $^3J_{\text{H,H}} = 7.7$, $^4J_{\text{H,H}} = 1.6$ Hz, 1 H), 7.54–7.48 (m, 1 H), 7.38 (td, $^3J_{\text{H,H}} = 7.4$, $^4J_{\text{H,H}} = 1.2$ Hz, 1 H), 7.33 (dd, $^3J_{\text{H,H}} = 7.6$, $^4J_{\text{H,H}} = 2.0$ Hz, 1 H), 7.26–7.21 (m, 1 H), 3.93 (s, 3 H) ppm. ^{13}C NMR (101 MHz, CDCl_3): δ = 166.9, 141.6, 141.3, 134.0, 133.2, 131.2, 130.5, 130.1, 129.2, 128.8, 128.1, 127.5, 122.5, 52.2 ppm. MS (EI, +): m/z (%) = 293 (14), 292 (95), 291 (15), 290

FULL PAPER

M. Mayor et al.

(96), 262 (13), 261 (97), 260 (13), 259 (98), 153 (13), 152 (100), 151 (18), 76 (28).

Regioisomers 26 and 32: A solution of **25** (202 mg, 597 μmol , 1.00 equiv.), Pd(dppf)Cl₂ (38.7 mg, 47.3 μmol , 8 mol-%), bis-(pinacolato)diboron (166 mg, 653 μmol , 1.10 equiv.), and potassium acetate (175 mg, 1.79 mmol, 3.00 equiv.) in degassed dioxane (4 mL) was prepared in a dry round-bottomed flask under an argon atmosphere and heated to 100 °C. After stirring for 1 h, the solvent was removed under reduced pressure and the residue was purified by column chromatography (SiO₂; EtOAc/cyclohexane, 1:20). The isolated mixture of regioisomers (**26** and **32**, 57%) was purified by HPLC (column: semipreparative Reprosil 100 Si, 5 μm , 250 \times 16 mm, eluent: CH₂Cl₂).

Methyl 2'-(4,4,5,5-Tetramethyl-1,3,2-dioxaborolan-2-yl)-[1,1'-biphenyl]-3-carboxylate (26): ¹H NMR (500 MHz, CDCl₃, 25 °C): δ = 8.00 (td, ⁴J_{H,H} = 1.8, 0.5 Hz, 1 H), 7.95 (ddd, ³J_{H,H} = 7.8, ⁴J_{H,H} = 1.8, 1.2 Hz, 1 H), 7.71 (dd, ³J_{H,H} = 7.7, ⁴J_{H,H} = 1.2 Hz, 1 H), 7.53 (ddd, ³J_{H,H} = 7.8, ⁴J_{H,H} = 1.8, 1.2 Hz, 1 H), 7.43–7.38 (m, 1 H), 7.37 (dd, ³J_{H,H} = 7.7, ⁴J_{H,H} = 0.5 Hz, 1 H), 7.33–7.27 (m, 2 H), 3.85 (s, 3 H), 1.12 (s, 12 H) ppm. ¹³C NMR (125 MHz, CDCl₃): δ = 167.1, 146.7, 143.4, 135, 133.7, 130.6, 130.4, 129.5, 129.2, 128.1, 128, 126.9, 83.7, 24.5 ppm. MS (EI, +): *m/z* (%) = 339.3 (17), 338.3 (81), 337.3 (29), 323.2 (12), 307.2 (11), 252.2 (22), 239.2 (28), 238.2 (14), 237.2 (18), 225.1 (13), 223.2 (18), 222.1 (46), 221.1 (20), 220.2 (24), 219.2 (22), 208.1 (15), 207.1 (100), 206.1 (26), 205.1 (14), 194.1 (41), 193.2 (49), 180.1 (13), 179.1 (55), 178.1 (43), 177.1 (14), 165.2 (13), 164.2 (33), 163.2 (18), 153.2 (14), 152.2 (43), 151.1 (16), 59.1 (12).

Methyl 4-(4,4,5,5-Tetramethyl-1,3,2-dioxaborolan-2-yl)-[1,1'-biphenyl]-3-carboxylate (32): ¹H NMR (600 MHz, CDCl₃, 25 °C): δ = 8.04 (d, ⁴J_{H,H} = 1.7 Hz, 1 H), 7.98 (dd, ³J_{H,H} = 7.7, ⁴J_{H,H} = 1.7 Hz, 1 H), 7.76 (d, ³J_{H,H} = 7.7 Hz, 1 H), 7.43–7.35 (m, 5 H), 3.92 (s, 3 H), 1.21 (s, 12 H) ppm. ¹³C NMR (151 MHz, CDCl₃): δ = 167, 147.5, 142.2, 134.4, 131.3, 129.7, 129.1, 128, 127.3, 127, 84.1, 52.2, 24.6 ppm. MS (EI, +): *m/z* (%) = 339.3 (13), 338.3 (59), 337.3 (15), 323.3 (18), 253.2 (10), 252.2 (46), 239.2 (24), 238.2 (18), 237.2 (39), 223.2 (18), 222.2 (100), 221.1 (27), 207.1 (46), 206.1 (10), 193.2 (16), 191.1 (21), 179.1 (30), 178.1 (25), 163.2 (14), 152.2 (27), 151.2 (11), 59.1 (11).

(2'-Bromo-[1,1'-biphenyl]-3-yl)methanol (27): In an oven-dried and argon-flushed Schlenk tube, 3-(hydroxymethyl)phenylboronic acid (**23**; 400 mg, 2.63 mmol, 1.00 equiv.), 1-bromo-2-iodobenzene (**21**; 410 μL , 3.16 mmol, 1.20 equiv.), Cs₂CO₃ (2.65 g, 8.04 mmol, 3.05 equiv.), and Pd(PPh₃)₄ (60.1 mg, 2 mol-%) were added consecutively and suspended in THF (8 mL) and EtOH (2 mL) before degassing for 15 min. The suspension was then heated to 60 °C for 4 h. The reaction mixture was cooled to room temperature, *t*BME was added, and the suspension was filtered through Celite. The orange solution was washed twice with aq. HCl (1 M), water and brine, dried with Na₂SO₄, before removing the solvent under reduced pressure. The residual oil was passed through a plug of silica (eluent: EtOAc/cyclohexane, 1:2), the solvent was removed under reduced pressure, and the orange oil was purified by column chromatography (SiO₂; EtOAc/cyclohexane, 1:4) to give **27** (492 mg, 1.97 mmol, 71%) as an orange oil. ¹H NMR (400 MHz, CDCl₃, 25 °C): δ = 7.69–7.65 (m, 1 H), 7.47–7.30 (m, 6 H), 7.21 (ddd, ³J_{H,H} = 8.0, 6.9, ⁴J_{H,H} = 2.2 Hz, 1 H), 4.76 (d, ³J_{H,H} = 5.9 Hz, 2 H), 1.72 (t, ³J_{H,H} = 5.9 Hz, 1 H) ppm. ¹³C NMR (101 MHz, CDCl₃): δ = 142.8, 141.8, 141.1, 133.5, 131.7, 129.2, 129.2, 128.6, 128.4, 127.8, 126.6, 123.0, 65.7 ppm. MS (EI, +): *m/z* (%) = 264 (97), 262 (100), 183 (42), 165 (100), 154 (84), 152 (79), 107 (9), 76 (9).

(2'-Iodo-[1,1'-biphenyl]-3-yl)methanol (28): An oven-dried, argon-flushed Schlenk tube was charged with **25** (477 mg, 1.41 mmol, 1.00 equiv.) and anhydrous CH₂Cl₂ (4 mL) and cooled to 0 °C before adding DIBAL-H (1M in hexanes, 5.91 mL, 5.91 mmol, 4.20 equiv.) dropwise over 15 min. The mixture was stirred for 30 min at room temperature before adding more CH₂Cl₂, then the reaction was carefully quenched with brine and the mixture was stirred for an additional 30 min. The solution was neutralized with satd. aq. NH₄Cl, the precipitate was filtered off and discarded, and the filtrate was extracted with CH₂Cl₂ (3 \times). The combined organics were washed with brine and dried with Na₂SO₄. Removal of the solvent under reduced pressure gave **28** (437 mg, 1.41 mmol, >99%) as a brown solid. ¹H NMR (400 MHz, CDCl₃, 25 °C): δ = 7.96 (dd, ³J_{H,H} = 7.9, ⁴J_{H,H} = 1.2 Hz, 1 H), 7.45–7.36 (m, 3 H), 7.34 (t, ⁴J_{H,H} = 1.8 Hz, 1 H), 7.30 (dd, ³J_{H,H} = 7.8, ⁴J_{H,H} = 1.8 Hz, 1 H), 7.28 (d, ³J_{H,H} = 5.2 Hz, 1 H), 7.04 (ddd, ³J_{H,H} = 7.9, 7.3, ⁴J_{H,H} = 1.8 Hz, 1 H), 4.77 (d, ³J_{H,H} = 5.8 Hz, 2 H) ppm; 1.71 (t, ³J_{H,H} = 5.8 Hz, 1 H) ppm. ¹³C NMR (63 MHz, CDCl₃): δ = 146.6, 144.6, 140.8, 139.7, 130.3, 129.1, 128.8, 128.4, 128.4, 128.1, 126.4, 98.7, 65.5 ppm. MS (EI, +): *m/z* (%) = 310.8 (44), 309.9 (97), 183.1 (20), 182.1 (12), 181.1 (24), 166.1 (21), 165.2 (100), 155.1 (40), 154.1 (84), 153.1 (76), 152.2 (97), 151.1 (37), 150.1 (14), 139.1 (10), 128.1 (12), 127.1 (17), 126.1 (14), 115.1 (14), 77.1 (26), 76.0 (17), 75.0 (12), 63.0 (14), 51.0 (14).

Regioisomers 29 and 31: To an oven-dried and argon-flushed Schlenk tube was consecutively added **27** (236 mg, 897 μmol , 1.00 equiv.), potassium acetate (265 mg, 2.70 mmol, 3.01 equiv.), bis(pinacolato)diboron (251 mg, 987 μmol , 1.10 equiv.), PdCl₂(dppf)·CH₂Cl₂ (59.6, 8 mol-%), and anhydrous DMF (5 mL). The mixture was degassed for 5 min and then heated to 100 °C for 1 h (the solution became dark). After cooling to room temperature, *t*BME was added and the mixture was filtered through Celite, then thoroughly washed with water and brine. After drying over Na₂SO₄, the solvent was removed under reduced pressure. Column chromatography (SiO₂; CH₂Cl₂/EtOAc, 20:1) gave a mixture of **29** and **31** (163 mg, 525 μmol , 59%) as a colorless oil. ¹H NMR (400 MHz, CDCl₃, 25 °C): δ = 7.76–7.70 (m, 2 H), 7.48–7.42 (m, 2 H), 7.41–7.30 (m, 12 H), 4.77–4.73 (m, 4 H), 1.68–1.59 (m, 2 H), 1.20 (s, 24 H) ppm. ¹³C NMR (101 MHz, CDCl₃): δ = 148.4, 147.7, 143.9, 143.4, 143.3, 140.7, 135.3, 135.0, 130.6, 129.5, 129.4, 129.0, 128.5, 128.2, 128.1, 127.8, 127.3, 126.8, 125.9, 125.0, 84.2, 65.8, 65.6, 25.0 (2 C) ppm. MS (EI, +): *m/z* (%) = 311 (15), 310 (75), 309 (18), 224 (16), 211 (14), 210 (18), 209 (16), 195 (14), 195 (100), 193 (64), 192 (15), 165 (23).

2-Iodo-5-methoxy-1,1'-biphenyl (33): To an oven-dried and argon-flushed Schlenk tube was consecutively added potassium carbonate (1.19 g, 8.55 mmol, 3.0 equiv.) and phenylboronic acid (348.7 mg, 2.86 mmol, 1.00 equiv.) and vacuum applied for 5 min. Compound **4** (1.00 g, 3.20 mmol, 1.12 equiv. as a solution in 5 mL anhydrous toluene) was added along with anhydrous toluene (23 mL) and anhydrous EtOH (7 mL), and the solution was degassed for 15 min before adding Pd(PPh₃)₂Cl₂ (61.6 mg, 3 mol-%) and heating to 80 °C for 21 h. After cooling to room temperature, EtOAc was added and the brown suspension was filtered. The solution was then adsorbed on Celite and subjected to column chromatography (SiO₂; EtOAc/pentane, 1:100 to 1:20) giving **33** (700 mg, 814 μmol , 93%) as a colorless oil. ¹H NMR (400 MHz, CDCl₃, 25 °C): δ = 7.52 (d, ³J_{H,H} = 8.8 Hz, 1 H), 7.46–7.31 (m, 5 H), 6.87 (d, ⁴J_{H,H} = 3.1 Hz, 1 H), 6.76 (dd, ³J_{H,H} = 8.8, ⁴J_{H,H} = 3.1 Hz, 1 H), 3.78 (s, 3 H) ppm. ¹³C NMR (101 MHz, CDCl₃, 25 °C): δ = 158.9, 143.5, 141.24, 133.8, 129.4, 128.1, 127.8, 116.8, 114.8, 113.2, 55.6 ppm. MS (EI, +): *m/z* (%) = 264.9 (14), 263.9 (99), 262.9 (16), 261.9

Pathways to a Helical Hexaphenyl “Geländer” Molecule

(100), 220.9 (29), 218.9 (30), 168.0 (27), 153.1 (14), 152.0 (25), 140.1 (43), 139.0 (80), 63.0 (14).

Methyl 5'-Methoxy-[1,1':2',1'':3'',1''':4''']-quaterphenyl]-2'''-carboxylate (34): To an oven-dried and argon-flushed Schlenk tube was added potassium phosphate (66.8 mg, 315 μmol , 3.00 equiv.) and vacuum applied for 5 min. Compound **33** (28.1 mg, 107 μmol , 1.00 equiv. as a solution in 0.5 mL dioxane) and **14** (34.0 mg, 105 μmol , 1.00 equiv. as a solution in 0.5 mL dioxane) were added along with dioxane (600 μL) and water (400 μL). The solution was degassed for 15 min before adding $\text{Pd}(\text{PPh}_3)_2\text{Cl}_2$ (2.50 mg, 3 mol-%) and heating to 80 °C for 4 h. After cooling to room temperature, EtOAc and water were added, the organic phase was washed with water (2 \times) and brine (1 \times). After drying over Na_2SO_4 , the solvent was removed under reduced pressure. Column chromatography (SiO_2 ; EtOAc/cyclohexane, 1:4) gave **34** (41.8 mg, 109 μmol , 51%) as a highly viscous, colorless oil. ^1H NMR (400 MHz, CDCl_3 , 25 °C): δ = 7.79–7.75 (m, 1 H), 7.46–7.33 (m, 3 H), 7.25–7.23 (m, 3 H), 7.21–7.17 (m, 3 H), 7.11–7.05 (m, 3 H), 7.02–6.95 (m, 3 H), 3.88 (s, 3 H), 3.63 (s, 3 H) ppm. ^{13}C NMR (151 MHz, CDCl_3): δ = 169.2, 158.9, 142.3, 141.8, 141.7, 141.6, 141.1, 140.9, 140.8, 131.6, 131.1, 130.8, 130.1, 129.9, 129.7, 128.7, 128.0, 127.5, 127.1, 126.6, 126.3, 115.9, 113.1, 55.4, 51.9 ppm. MS (EI, +): m/z (%) = 395.0 (31), 394.1 (100), 362.1 (16), 361.1 (13), 335.1 (15), 334.1 (11), 333.1 (13), 331.1 (11), 319.1 (12), 303.0 (11), 302.0 (17), 291.1 (18), 290.0 (13), 289.0 (27), 151.0 (13), 144.7 (22), 138.1 (14).

2-Bromo-5-nitro-1,1'-biphenyl (37): To an oven-dried and argon-flushed Schlenk tube was consecutively added potassium carbonate (513 mg, 3.67 mmol, 3.00 equiv.), **6** (449 mg, 1.37 mmol, 1.12 equiv.), and phenylboronic acid (149 mg, 1.22 mmol, 1.00 equiv.) before vacuum was applied for 5 min. Anhydrous toluene (10 mL) and anhydrous EtOH (2.5 mL) were added and the solution was degassed for 15 min before adding $\text{Pd}(\text{PPh}_3)_2\text{Cl}_2$ (26.0 mg, 3 mol-%) and heating to 80 °C for 18 h. After cooling to room temperature, EtOAc was added and the brown suspension was filtered. The residual oil was adsorbed on Celite and subjected to column chromatography (SiO_2 ; EtOAc/pentane, 1:20) to give **37** (232 mg, 833 μmol , 68%). ^1H NMR (400 MHz, CDCl_3 , 25 °C): δ = 8.20 (d, $^4J_{\text{H,H}} = 2.7$ Hz, 1 H), 8.06 (dd, $^3J_{\text{H,H}} = 8.8$, $^4J_{\text{H,H}} = 2.7$ Hz, 1 H), 7.86 (d, $^3J_{\text{H,H}} = 8.8$ Hz, 1 H), 7.52–7.44 (m, 3 H), 7.44–7.39 (m, 2 H) ppm. ^{13}C NMR (63 MHz, CDCl_3): δ = 144.3, 139.2, 134.4, 130.4, 129.4, 128.9, 128.6, 126.0, 123.4 ppm. MS (EI, +): m/z (%) = 278.9 (41), 276.9 (41), 153.1 (13), 152.1 (100), 151.1 (28), 150.1 (14), 76.0 (14).

tert-Butyldimethyl[5'-nitro-(1,1':2',1'':3'',1''':4''']-quaterphenyl)-2'''-yl]-methoxy)silane (38): To an oven-dried and argon-flushed Schlenk tube was added potassium phosphate (178 mg, 841 μmol , 3.00 equiv.) and vacuum applied for 5 min. Compound **37** (79.5 mg, 286 μmol , 1.02 equiv. as a solution in 1.8 mL dioxane) and **19** (115 mg, 280 μmol , 1.00 equiv. as a solution in 1 mL dioxane) were added along with dioxane (0.4 mL) and water (0.8 mL). The solution was degassed for 15 min before adding $\text{Pd}(\text{PPh}_3)_2\text{Cl}_2$ (5.9 mg, 3 mol-%) and heating to 80 °C for 5.5 h. After cooling to room temperature, EtOAc and water were added and the organic phase was washed with water (2 \times) and brine (1 \times). After drying over Na_2SO_4 , the solvent was removed under reduced pressure. Column chromatography (SiO_2 ; EtOAc/cyclohexane, 1:50) gave **38** (117 mg, 235 μmol , 84%) as a highly viscous, colorless oil. ^1H NMR (500 MHz, CDCl_3 , 25 °C): δ = 8.34–8.29 (m, 1 H), 8.28–8.23 (m, 1 H), 7.67–7.59 (m, 1 H), 7.55–7.51 (m, 1 H), 7.48–7.40 (m, 1 H), 7.38–7.33 (m, 1 H), 7.30–7.28 (m, 1 H), 7.28–7.25 (m, 4 H), 7.25–7.22 (m, 1 H), 7.20–7.16 (m, 1 H), 7.16–7.13 (m, 1 H), 7.13–7.11 (m, 1 H), 6.91 (dd, $^3J_{\text{H,H}} = 7.6$, $^4J_{\text{H,H}} = 1.4$ Hz, 1 H), 4.49 (s, 2 H),

0.87 (s, 9 H), 0.01 (s, 6 H) ppm. ^{13}C NMR (125 MHz, CDCl_3): δ = 147.1, 141.9, 140.8, 139.8, 139.2, 138.2, 131.5, 130.4, 129.7 (2 C), 129.6 (2 C), 129.4, 128.5, 128.4, 128.3 (2 C), 127.9, 127.8, 127.6, 127.5, 127.0, 126.8, 126.1, 125.5, 122.2, 30.0, 18.4, 0.1 ppm. MS (EI, +): m/z (%) = 439.1 (35), 438.0 (100), 408.0 (12), 364.0 (27), 318.0 (29), 317.1 (19), 315.1 (14), 302.0 (15), 75.0 (59).

Methyl 5'-Nitro-[1,1':2',1'':3'',1''':4''']-quaterphenyl]-2'''-carboxylate (39): To an oven-dried and argon-flushed Schlenk tube was added potassium phosphate (313 mg, 1.47 mmol, 3.20 equiv.) and vacuum applied for 5 min. Compound **37** (131 mg, 470 μmol , 1.02 equiv. as a solution in 3.2 mL dioxane) and **14** (150 mg, 461 μmol , 1.00 equiv. as a solution in 1.0 mL dioxane) were added along with dioxane (2.3 mL) and water (1.6 mL) and the solution was degassed for 15 min before adding $\text{Pd}(\text{PPh}_3)_2\text{Cl}_2$ (10.4 mg, 3 mol-%) and heating to 80 °C for 3 h. After cooling to room temperature, EtOAc and water were added and the organic phase was washed with water (2 \times) and brine (1 \times). After drying over Na_2SO_4 , the solvent was removed under reduced pressure. Column chromatography (SiO_2 ; EtOAc/cyclohexane, 1:8) gave **39** (153 mg, 372 μmol , 81%) as a highly viscous, colorless oil. ^1H NMR (400 MHz, CDCl_3 , 25 °C): δ = 8.32 (d, $^4J_{\text{H,H}} = 2.2$ Hz, 1 H), 8.31–8.21 (m, 1 H), 7.94–7.74 (m, 2 H), 7.71–7.51 (m, 2 H), 7.44 (dddd, $^3J_{\text{H,H}} = 11.0$, 7.4, 5.7, $^4J_{\text{H,H}} = 1.6$ Hz, 2 H), 7.37–7.27 (m, 3 H), 7.25–7.10 (m, 4 H), 7.06–6.92 (m, 1 H), 3.67 (s, 3 H) ppm. MS (EI, +): m/z (%) = 410.1 (25), 409.1 (89), 378.0 (25), 377.0 (61), 376.1 (23), 360.1 (15), 350.1 (32), 349.1 (26), 348.1 (19), 332.1 (18), 331.1 (43), 330.1 (26), 329.1 (14), 313.1 (11), 304.1 (20), 303.1 (52), 302.1 (100), 301.1 (29), 300.1 (39), 289.1 (16), 276.1 (16), 226.0 (10), 165.6 (11), 152.1 (20), 151.1 (47), 150.1 (37), 144.6 (21), 143.7 (10), 138.1 (25).

Methyl 5'-Amino-[1,1':2',1'':3'',1''':4''']-quaterphenyl]-2'''-carboxylate (41): A solution of **39** (41.5 mg, 101 μmol , 1.00 equiv.) and SnCl_2 (98.0 mg, 507 μmol , 5.00 equiv.) in EtOAc (4 mL) was heated to reflux for 6 h. After cooling to room temperature, EtOAc and satd. aq. NaHCO_3 were added, the organic phase was washed with water (1 \times) and brine (1 \times). After drying over Na_2SO_4 , the solvent was removed under reduced pressure. Column chromatography (SiO_2 ; EtOAc/cyclohexane, 1:2) gave **41** (19.4 mg, 51.1 μmol , <50%) as a colorless oil. ^1H NMR (400 MHz, CDCl_3 , 25 °C): δ = 7.78–7.74 (m, 1 H), 7.43 (td, $^3J_{\text{H,H}} = 7.6$, $^4J_{\text{H,H}} = 1.4$ Hz, 1 H), 7.35 (td, $^3J_{\text{H,H}} = 7.6$, $^4J_{\text{H,H}} = 1.4$ Hz, 1 H), 7.30–7.21 (m, 4 H), 7.19–7.15 (m, 3 H), 7.08 (td, $^4J_{\text{H,H}} = 1.8$, 0.6 Hz, 1 H), 7.07–7.02 (m, 2 H), 7.02–6.97 (m, 1 H), 6.78–6.73 (m, 2 H), 3.79 (s, 2 H), 3.63 (s, 3 H) ppm. MS (EI, +): m/z (%) = 380.0 (30), 379.0 (100), 330.0 (10), 319.0 (17), 318.1 (15), 302.0 (11), 158.7 (14), 152.1 (11).

1-[[6-Bromo-(1,1'-biphenyl)-3-yl]diazenyl]pyrrolidine (44): To an oven-dried and argon-flushed Schlenk tube was consecutively added potassium carbonate (733 mg, 5.25 mmol, 3.00 equiv.), **8** (745 mg, 1.96 mmol, 1.12 equiv.), and phenylboronic acid (213 mg, 1.75 mmol, 1.00 equiv.) then vacuum was applied for 5 min. Anhydrous toluene (14 mL) and anhydrous EtOH (14 mL) were added and the solution was degassed for 15 min before adding $\text{Pd}(\text{PPh}_3)_2\text{Cl}_2$ (37.2 mg, 3 mol-%) and heating to 80 °C for 23 h. After cooling to room temperature, EtOAc was added and the brown suspension was filtered and adsorbed on Celite. Column chromatography (SiO_2 ; CH_2Cl_2 /toluene, 1:100) gave **44** (356 mg, 1.08 mmol, 62%) as a brown solid. ^1H NMR (400 MHz, CDCl_3 , 25 °C): δ = 7.58 (d, $^3J_{\text{H,H}} = 8.5$ Hz, 1 H), 7.46–7.34 (m, 5 H), 7.28–7.24 (m, 2 H), 3.77 (s, 4 H), 2.10 (d, $^3J_{\text{H,H}} = 5.7$ Hz, 2 H), 2.00 (d, $^3J_{\text{H,H}} = 5.7$ Hz, 2 H) ppm. MS (EI, +): m/z (%) = 331.0 (4), 329.0 (4), 232.9 (18), 230.9 (18), 153.1 (16), 152.1 (100), 151.1 (16).

2-Bromo-5-iodo-1,1'-biphenyl (46):^[23] In a pressure tube, **44** (345 mg, 1.04 mmol, 1.00 equiv.) was heated to reflux at 120 °C in

FULL PAPER

M. Mayor et al.

MeI (1 mL) overnight. The solvent was removed under reduced pressure and the remaining residue was dissolved in EtOAc. Water was added and the organic phase was washed with NaHCO₃ (2×) and brine (1×). After drying over Na₂SO₄, the solvent was removed under reduced pressure, adsorbed on Celite and subjected to column chromatography (SiO₂; CH₂Cl₂/toluene, 1:100) to give **46** (309 mg, 861 μmol, 83%). ¹H NMR (400 MHz, CDCl₃, 25 °C): δ = 7.66 (d, ⁴J_{H,H} = 2.2 Hz, 1 H), 7.50 (dd, ³J_{H,H} = 8.4, ⁴J_{H,H} = 2.2 Hz, 1 H), 7.46–7.42 (m, 1 H), 7.42–7.35 (m, 5 H) ppm. ¹³C NMR (101 MHz, CDCl₃, 25 °C): δ = 144.9, 140.1, 139.9, 137.8, 134.9, 129.4, 128.3, 128.3, 122.8, 92.5 ppm. MS (EI, +): *m/z* (%) = 359.9 (57), 357.8 (59), 153.1 (13), 152.1 (100), 151.1 (28), 150.1 (16), 126.1 (11), 76.1 (26), 75.1 (13), 74.0 (11), 63.0 (11).

2-(6-Bromo-[1,1'-biphenyl]-3-yl)-5,5-dimethyl-1,3,2-dioxaborinane (48): In an oven-dried and argon-flushed Schlenk tube, isopropylmagnesium chloride lithium chloride complex solution (700 μL, 909 μmol, 1.10 equiv.) was added to a degassed solution of **46** (297 mg, 826 μmol, 1.00 equiv.) in THF (6 mL) at –40 °C before stirring for 3 h. After GC–MS analysis revealed full conversion, a solution of triisopropyl borate (230 μL, 992 μmol, 1.20 equiv.) in THF (1 mL) was added and the mixture was stirred at –40 °C for 1 h and subsequently warmed to room temperature before stirring for another 2 h. After adding 2,2-dimethyl-1,3-propanediol (109 mg, 1.03 mmol, 1.25 equiv.), the reaction was stirred for 13 h. CH₂Cl₂ and saturated aq. NH₄Cl were added and the organic layer was washed with water and brine. After drying over Na₂SO₄, the solvent was removed under reduced pressure. Column chromatography (SiO₂; CH₂Cl₂/toluene, 1:100) gave **48** (90.5 mg, 262 μmol, 32%) as a brown oil. ¹H NMR (400 MHz, CDCl₃, 25 °C): δ = 7.75 (d, ⁴J_{H,H} = 1.6 Hz, 1 H), 7.65 (d, *J* = 8.0 Hz, 1 H), 7.59 (dd, ³J_{H,H} = 8.0, ⁴J_{H,H} = 1.6 Hz, 1 H), 7.43–7.40 (m, 4 H), 7.40–7.33 (m, 1 H), 3.75 (s, 4 H), 1.02 (s, 6 H) ppm. ¹³C NMR (151 MHz, CDCl₃): δ = 142.0, 141.5, 137.0, 134.2, 132.6, 129.7, 128.1, 127.6, 125.8, 72.6, 32.1, 22.1 ppm. MS (EI, +): *m/z* (%) = 346.9 (19), 346.0 (99), 345.0 (43), 344.0 (100), 343.0 (26), 260.9 (13), 259.9 (62), 258.9 (28), 257.9 (62), 256.9 (16), 179.0 (22), 178.0 (34), 177.1 (13), 152.1 (34), 151.1 (14), 56.1 (26), 55.1 (13).

Methyl 4'-Bromo-[1,1':2',1'':3'',1''':4''',1''':3''',1''':4''':5''-quinquephenyl]-3-carboxylate (50): To an oven-dried and argon-flushed Schlenk tube was consecutively added potassium carbonate (547 mg, 547 μmol, 3.04 equiv.), **25** (69.5 mg, 201 μmol, 1.12 equiv.), and **48** (61.0 mg, 180 μmol, 1.00 equiv.) before vacuum was applied for 5 min. Anhydrous toluene (2 mL) and anhydrous EtOH (0.5 mL) were added and the solution was degassed for 15 min before adding Pd(PPh₃)₂Cl₂ (3.7 mg, 3 mol-%) and heating to 80 °C for 5.5 d. After cooling to room temperature, EtOAc was added, the brown suspension was filtered and adsorbed on Celite. Twofold column chromatography (SiO₂; CH₂Cl₂/toluene, 1:100) gave **50** (26.1 mg, 59.5 μmol, 33%) as a colorless solid. ¹H NMR (400 MHz, CDCl₃, 25 °C): δ = 7.95 (tt, ⁴J_{H,H} = 3.3, 1.5 Hz, 2 H), 7.51 (d, ³J_{H,H} = 8.2 Hz, 1 H), 7.45 (d, ⁴J_{H,H} = 1.7 Hz, 4 H), 7.39–7.29 (m, 4 H), 7.29–7.22 (m, 1 H), 7.19–7.13 (m, 2 H), 7.07 (d, ⁴J_{H,H} = 2.3 Hz, 1 H), 6.98 (dd, ³J_{H,H} = 8.2, ⁴J_{H,H} = 2.3 Hz, 1 H), 3.90 (s, 3 H) ppm. MS (EI, +): *m/z* (%) = 444.9 (26), 444.0 (87), 443.0 (28), 441.9 (87), 332.1 (11), 331.1 (36), 305.0 (26), 304.1 (100), 303.1 (73), 302.0 (88), 301.1 (17), 300.1 (26), 289.0 (20), 276.0 (12), 226.0 (12), 152.0 (10), 151.0 (34), 150.1 (27), 144.6 (13), 138.1 (19).

Dimethyl 3''-Phenyl-[1,1':2',1'':4'',1''':3''',1''':4''':5''-quinquephenyl]-2''',3-dicarboxylate (52): To an oven-dried and argon-flushed Schlenk tube was added potassium phosphate (37.9 mg, 179 μmol, 3.00 equiv.) and vacuum applied for 5 min. Compound **50** (26.4 mg,

107 μmol, 1.00 equiv. as a solution in 0.5 mL dioxane) and **14** (19.7 mg, 60.7 μmol, 1.02 equiv. as a solution in 0.5 mL dioxane) were added along with dioxane (0.6 mL) and water (0.4 mL). The solution was degassed for 15 min before adding Pd(PPh₃)₂Cl₂ (1.30 mg, 3 mol-%) and heating to 80 °C for 4 h. After cooling to room temperature, EtOAc and water were added, and the organic phase was washed with water (2×) and brine (1×). After drying over Na₂SO₄, the solvent was removed under reduced pressure. Column chromatography (SiO₂; CH₂Cl₂/toluene, 1:100) gave **52** (30.7 mg, 53.4 μmol, 90%) as a highly viscous, colorless oil. ¹H NMR (400 MHz, CDCl₃, 25 °C): δ = 8.02 (dd, ⁴J_{H,H} = 1.9, 0.9 Hz, 1 H), 7.98–7.93 (m, 1 H), 7.77 (dd, ³J_{H,H} = 7.7, ⁴J_{H,H} = 1.4 Hz, 1 H), 7.58–7.53 (m, 1 H), 7.50–7.39 (m, 4 H), 7.38–7.31 (m, 4 H), 7.19 (tdd, ³J_{H,H} = 8.9, ⁴J_{H,H} = 3.8, 1.6 Hz, 6 H), 7.10–7.06 (m, 3 H), 6.94 (dd, ³J_{H,H} = 7.6, ⁴J_{H,H} = 1.3 Hz, 1 H), 6.92–6.88 (m, 2 H), 3.88 (s, 3 H), 3.62 (s, 3 H) ppm. ¹³C NMR (101 MHz, CDCl₃): δ = 169.1, 167.0, 142.2, 142.0, 141.4, 140.9, 140.8, 140.1, 139.9, 139.6, 138.5, 134.7, 132.4, 131.1, 130.9, 130.8, 130.7, 130.5, 130.5, 130.3, 130.2, 129.9, 129.9, 129.7, 129.0, 128.8, 128.6, 128.2, 128.0, 128.0, 127.9, 127.8, 127.8, 127.4, 127.1, 126.6, 126.4, 52.1, 51.9, 29.7 ppm. MS (EI, +): *m/z* (%) = 576.1 (10), 575.1 (44), 574.1 (100), 511.1 (11), 482.1 (14), 481.1 (12), 454.0 (12), 450.0 (11), 219.3 (12).

Acknowledgments

The authors acknowledge financial support by the Swiss National Science Foundation (SNF).

- [1] For selected examples, see: a) M. Banerjee, R. Shukla, R. Rathore, *J. Am. Chem. Soc.* **2009**, *131*, 1780; b) A. C. Grimdale, K. Leok Chan, R. E. Martin, P. G. Jokisz, A. B. Holmes, *Chem. Rev.* **2009**, *109*, 897–1091; c) L. Vyklicky', S. H. Eichhorn, T. J. Katz, *Chem. Mater.* **2003**, *15*, 3594–3601.
- [2] *Electronic Materials: The Oligomer Approach* (Eds.: K. Müllen, G. Wegner), **2008**.
- [3] For selected examples, see: a) D. Vonlanthen, J. Rotzler, M. Neuburger, M. Mayor, *Eur. J. Org. Chem.* **2010**, 120–133; b) J.-F. Jia, H.-S. Wu, Z. Chen, Y. Mo, *Eur. J. Org. Chem.* **2013**, 611–616; c) S. Nobusue, Y. Mukai, Y. Fukumoto, R. Umeda, K. Tahara, M. Sonoda, Y. Tobe, *Chem. Eur. J.* **2012**, *18*, 12814–12824; d) D. M. Hudgins, C. W. Bauschlicher, L. J. Allamandola, *Astrophys. J.* **2005**, *632*, 316–332.
- [4] For an overview of functional helical structures, see: C. Schmuck, *Angew. Chem. Int. Ed.* **2003**, *42*, 2448–2452; *Angew. Chem.* **2003**, *115*, 2552.
- [5] For selected examples, see: a) J. E. Field, G. Muller, J. P. Riehl, D. Venkataraman, *J. Am. Chem. Soc.* **2003**, *125*, 11808; b) Y. Morisaki, M. Gon, T. Sasamori, N. Tokitoh, Y. Chujo, *J. Am. Chem. Soc.* **2014**, *136*, 3350; c) Y. Yang, R. Correa da Costa, D. M. Smilgies, A. J. Campbell, M. J. Fuchter, *Adv. Mater.* **2013**, *25*, 2624–2628; d) J. Rotzler, H. Gsellinger, A. Bihlmeier, M. Gantenbein, D. Vonlanthen, D. Häussinger, W. Klopfer, M. Mayor, *Org. Biomol. Chem.* **2013**, *11*, 110–118; e) D. Casarini, L. Lunazzi, M. Mancinelli, A. Mazzanti, C. Rosini, *J. Org. Chem.* **2007**, *72*, 7667–7676; f) H. Saito, T. Mori, Y. Origane, T. Wada, Y. Inoue, *Chirality* **2008**, *20*, 278–281; g) T. Kudernac, N. Ruangsupapichat, M. Parschau, B. Macia, N. Katsonis, S. R. Harutyunyan, K. H. Ernst, B. L. Feringa, *Nature* **2011**, *479*, 208; h) N. Koumura, R. W. Zijlstra, R. A. van Delden, N. Harada, B. L. Feringa, *Nature* **1999**, *401*, 152–155; i) C. Scott Hartley, *J. Org. Chem.* **2011**, *76*, 9188–9191.
- [6] R. A. Pascal Jr., *Chem. Rev.* **2006**, *106*, 4809–4819.
- [7] For an overview, see: M. Gingras, *Chem. Soc. Rev.* **2013**, *42*, 968–1095.
- [8] K. Kawasumi, Q. Zhang, Y. Segawa, L. T. Scott, K. Itami, *Nat. Chem.* **2013**, *5*, 739–744.

Pathways to a Helical Hexaphenyl "Geländer" Molecule



- [9] a) K. Tsubaki, H. Tanaka, K. Takaishi, M. Miura, H. Morikawa, T. Furuta, K. Tanaka, K. Fuji, T. Sasamori, N. Tokitoh, T. Kawabata, *J. Org. Chem.* **2006**, *71*, 6579–6587; b) K. Takaiishi, M. Kawamoto, K. Tsubaki, *Org. Lett.* **2010**, *12*, 1832–1835.
- [10] a) B. Kiupel, C. Niederalt, M. Nieger, S. Grimme, F. Vögtle, *Angew. Chem. Int. Ed.* **1998**, *37*, 3031–3034; *Angew. Chem.* **1998**, *110*, 3206; b) M. Modjewski, S. V. Lindeman, R. Rathore, *Org. Lett.* **2009**, *11*, 4656–4659. Geländer is the German word for banister and was introduced by Fritz Vögtle for such axially chiral systems.
- [11] M. Rickhaus, L. M. Bannwart, M. Neuburger, H. Gsellinger, K. Zimmermann, D. Häussinger, M. Mayor, *Angew. Chem. Int. Ed.* **2014**, *10.1002/anie.201408424*.
- [12] a) N. Miyaura, K. Yamada, A. Suzuki, *Tetrahedron Lett.* **1979**, *36*, 3437–3440; b) For a theoretical overview, see: L. Xue, Z. Lin, *Chem. Soc. Rev.* **2010**, *39*, 1692–1705.
- [13] For comprehensive reviews, see: a) N. Miyaura, A. Suzuki, *Chem. Rev.* **1995**, *95*, 2357–2483; b) N. Miyaura, *Top. Curr. Chem.* **2002**, *219*, 11.
- [14] T. Jensen, H. Pedersen, B. Bang-Andersen, R. Madsen, M. Jørgsen, *Angew. Chem.* **2008**, *47*, 888–890.
- [15] S. L. Buchwald, N. C. Bruno, *The Strem Chemiker*, vol. XXVII **2014**, 1.
- [16] a) T. Ishiyama, M. Murata, N. Miyaura, *J. Org. Chem.* **1995**, *60*, 7508–7510; b) for an overview, see: A. J. J. Lennox, G. C. Lloyd-Jones, *Chem. Soc. Rev.* **2014**, *43*, 412–443.
- [17] a) S. O. Lawesson, *Acta Chem. Scand.* **1957**, *11*, 1075–1076; b) W. Li, D. P. Nelson, M. S. Jensen, R. S. Hoerrner, D. Cai, R. D. Larsen, P. J. Reider, *J. Org. Chem.* **2002**, *67*, 5394–5397.
- [18] C. Y. Liu, A. Gavryushin, P. Knochel, *Chem. Asian J.* **2007**, *2*, 1020–1030.
- [19] M. N. Eliseeva, L. T. Scott, *J. Am. Chem. Soc.* **2012**, *134*, 15169–15172.
- [20] J. F. W. McOmie, M. L. Watts, D. E. West, *Tetrahedron* **1968**, *24*, 2289–2292.
- [21] R. Scholl, J. Mansfeld, *Ber. Dtsch. Chem. Ges.* **1910**, *43*, 1734–1746.
- [22] F. D. Bellamy, K. Ou, *Tetrahedron Lett.* **1984**, *25*, 839–842.
- [23] Similar to: J. S. Moore, E. J. Weinstein, Z. Wu, *Tetrahedron Lett.* **1991**, *32*, 2465–2466.
- [24] For an overview, see: R. Martin, S. L. Buchwald, *Acc. Chem. Res.* **2008**, *41*, 1461–1473.
- [25] S. D. Walker, T. E. Barder, J. R. Martinelli, S. L. Buchwald, *Angew. Chem. Int. Ed.* **2004**, *43*, 1871–1876; *Angew. Chem.* **2004**, *116*, 1907.
- [26] Similar to: a) G. A. Holloway, H. M. Hügel, M. A. Rizzacasa, *J. Org. Chem.* **2003**, *68*, 2200–2204; b) S. W. Kang, C. M. Gothard, S. Maitra, Atia-tul-Wahab, J. S. Nowick, *J. Am. Chem. Soc.* **2007**, *129*, 1486–1487.
- [27] T. Jensen, H. Pedersen, B. Bang-Andersen, R. Madsen, M. Jørgsen, *Angew. Chem.* **2008**, *47*, 888–890.

Received: October 9, 2014

Published Online: December 18, 2014

Conformation Analysis | *Hot Paper*
Tuning Helical Chirality in Polycyclic Ladder Systems

 Michel Rickhaus,^[a] Oliver T. Unke,^[a] Rajesh Mannancherry,^[a] Linda M. Bannwart,^[a]
 Markus Neuburger,^[a] Daniel Häussinger,^[a] and Marcel Mayor^{*[a, b, c]}

Abstract: Conceptually and experimentally, a new set of helical model compounds is presented herein that allow correlations between structural features and their expression in the secondary structure to be investigated. A cross-linked oligomer with two strands of mismatching lengths connected in a ladder-type fashion serves as a model system. Compensation for the dimensional mismatch leads to the adoption of a helical arrangement. A strategically placed relay ensures the continuity and uniformity of the helix. Upon exchanging the heteroatomic linkage, the helix responds by increasing or decreasing the torsion of the backbone. Inversion of the relay's substitution pattern causes a distortion of the structure, while maintaining the directionality of

the helix. Based on a short synthetic protocol with a modular precursor, four closely related "Geländer" oligomers (Geländer is the German word for bannister) were accessed and fully characterized. XRD analysis for one representative of each helical arrangement and complementary computational studies for the remaining derivatives allowed the impact of the alterations on the secondary structures to be studied. Isolation of pure enantiomers of all new Geländer oligomers provided insight into the racemization kinetics and estimation of the racemization barrier. In silico simulation of the electronic circular dichroism spectra of the model compounds enabled the helicity of the isolated samples to be assigned.

Introduction

Circular staircases, propellers, and screws are representative examples of helical structures that have fascinated designers, architects, and researchers alike. The formation of these chiral structures on a microscopic scale has been key to relate chirality to structure and structure to function.^[1–10] Among the most prominent examples for such stereocenter-free, chiral molecules are polyaromatic helicenes. Exclusively due to steric interactions, the annulated rings adopt a spring-like configuration that resembles the steps of a helical staircase. Their exceptional optical properties, stability, and versatality, in combination with their structural beauty and simplicity, have made them important model systems for both chemists and physicists. An excellent representation of these fascinating structures can be found in recent reviews celebrating 100 years of helicenes.^[11–13]

Vögtle and co-workers introduced a fundamentally different helical polyaromatic system 17 years ago, which they labeled "Geländer" molecules (Geländer is the German word for bannister).^[14,15] Whereas helicenes and their related structures consist of rings that are arranged perpendicularly to the propagation axis of the helix, Geländer oligomers are axially chiral—in this case, the orientation of the rings is along the propagation axis. The fundamental characteristics are already present in bridged biphenyls: an alkyl linker bridges the phenyl rings, which locks them in a specific conformation (*M* or *P*).^[16–22] Adding a third ring (also conformationally locked by an alkyl bridge) results in Vögtle's terphenylic Geländer-oligomers. The obtained structures show very similar chiroptical properties and conformational stability to those of shorter helicenes. However, due to the symmetry of the molecules, both biphenyl junctions are equivalent and can adopt either *M* or *P* conformations, which results in three possible stereoisomers: *MM* and *PP*, which are enantiomeric, and the achiral *meso* compound (*MP/PM*). If the formation of the bridges is unspecific and independent of the other, the resulting distribution of conformers is statistical (*MM* and *PP* each 25%, *meso* 50%). Indeed, in classical bannister oligomers, 50% of the adopted conformers are achiral, which makes these systems less suited as model compounds for extensive chiroptical studies, especially because their interconversion is dynamic, which results in the degradation of chiroptically pure samples. To date, these delicate studies have required storage and investigations of the samples at sufficiently low temperatures and within narrow time windows.

[a] M. Rickhaus, O. T. Unke, R. Mannancherry, L. M. Bannwart, Dr. M. Neuburger, Dr. D. Häussinger, Prof. Dr. M. Mayor
 Department of Chemistry, University of Basel
 St. Johannis-Ring 19, 4056 Basel (Switzerland)
 E-mail: marcel.mayor@unibas.ch

[b] Prof. Dr. M. Mayor
 Institute for Nanotechnology (INT)
 Karlsruhe Institute of Technology (KIT)
 P.O. Box 3640, 76021 Karlsruhe (Germany)

[c] Prof. Dr. M. Mayor
 Lehn Institute of Functional Materials (LIFM)
 Sun Yat-Sen University
 Guangzhou (P.R. China)

Supporting information for this article is available on the WWW under <http://dx.doi.org/10.1002/chem.201503202>.

We recently addressed this issue by developing a related, ladder-like system,^[23] which could exclusively adopt either *M* or *P* conformations (Figures 1 and 2, green). With Vögtle's systems in mind, the terphenylic backbone is connected to a longer oligomer with individual linkages to each ring of the backbone. The extended oligomer then induces helicity due to spatial constraints. The sense of twist induced by one part of the bridge is communicated across the entire structure with the midsection of the longer oligomer acting as a relay. Accessing the desired structure required the time-consuming development of a synthetic strategy over 12 steps.^[23,24] The purification steps of the target structure were particularly demanding, which resulted in significant deviations in the yield of product

isolated. To our surprise, the yield did not exceed 28% and the fate of the remaining starting material remained ambiguous. The obtained purified structure showed high temperature, air, and moisture stability once isolated. Detailed investigations by 1D and 2D NMR spectroscopy, electronic circular dichroism (ECD) spectroscopy, and XRD analysis demonstrated the viability of the concept. Two enantiomeric helices were found with well-defined stereodynamic behavior, which allowed not only the racemization to be followed by circular dichroism (CD) spectroscopy, but also to determine a racemization barrier of 97.6 kJ mol⁻¹ at 25 °C.

Motivated by these preliminary results, we wondered to what extent the chemical nature of the bridge determined the physical properties of the molecule, such as the structural stability of the helix. From a synthetic point of view, we were still curious about the fate of the remaining material in the final cyclization step. The new focus was set towards chemically altering the bridging structure to investigate its effect on chemical features such as integrity and stability, but also on physicochemical properties, such as the extent of structural twist in the helix and its influence on the racemization barrier. To answer these, and related questions, we devised several strategies to overcome the limitations of the initial diether structure. The linking heteroatom in the bridging structure is ideally suited to precisely alter the extent of twist in the helix; thus, we became interested in exchanging oxygen for the larger sulfur or selenium heteroatom. Consequently, we aimed for a modular approach to incorporate the heteroatom at a late stage of the synthesis procedure.

Herein, we present our new versatile synthetic approach to various polycyclic ladder systems and the study of their properties and stereodynamics. The assembly of a nonspecific tetrabrominated precursor allowed the conclusion of the synthesis with the incorporation of other chalcogens. Replacing oxygen with the significantly larger and softer sulfur and selenium allowed fine-tuning of the helical structures (Figure 2, blue). In addition, variation in the connection of the middle ring gave access to distorted helical structures with different twists in both junctions (Figure 2, purple). The impact of these variations on the structure, especially on the degrees of twist and racemization dynamics, have been studied and are reported in detail.

Results and Discussion

Synthesis of precursor 11

The projected incorporation of a range of heteroatoms required a modular approach. A common denominator of the heteroatoms sulfur and selenium is their occurrence as simple sodium salts (Na₂S and Na₂Se). Contrary to the corresponding sodium oxide, these salts are relatively stable and safe to handle, while showing excellent nucleophilicity. In the context of possible synthetic pathways, the employment of these salts as a source of the heteroatom allows the same precursor to be shared (**11** in Scheme 1). After incorporation of the chalcogen by the nucleophilic displacement of a suitable leaving group,

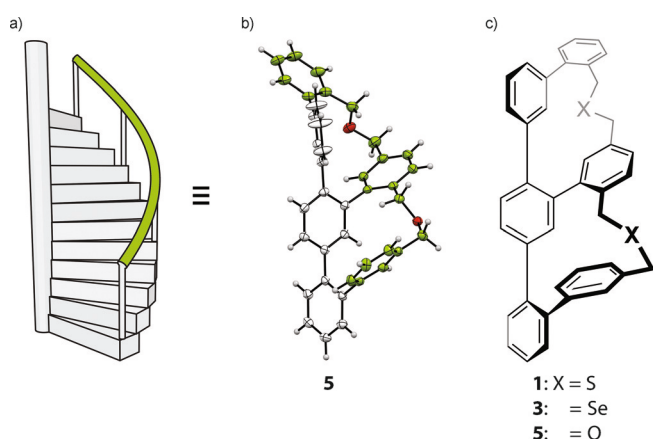


Figure 1. Overview of bannister oligomers. a) Helical staircase with a continuous bannister (green). b) Single-crystal structure of helical oligomer **5**, which exhibits a continuous, bannister-like arrangement. c) Schematic representation of the bannister oligomers **1**, **3**, and **5**, which contain various heteroatoms.

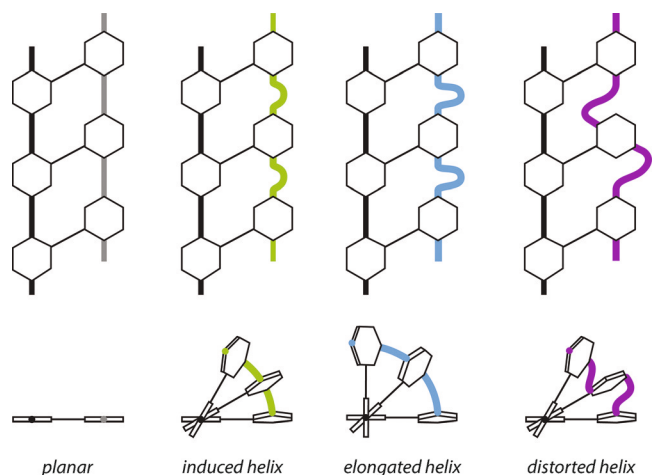
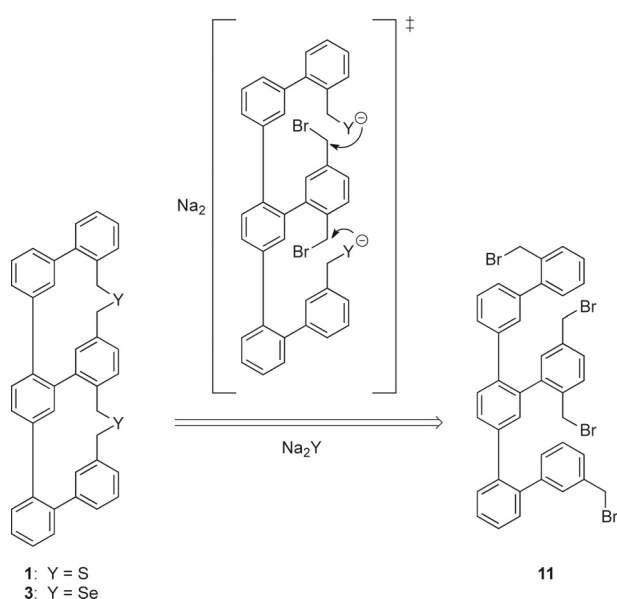


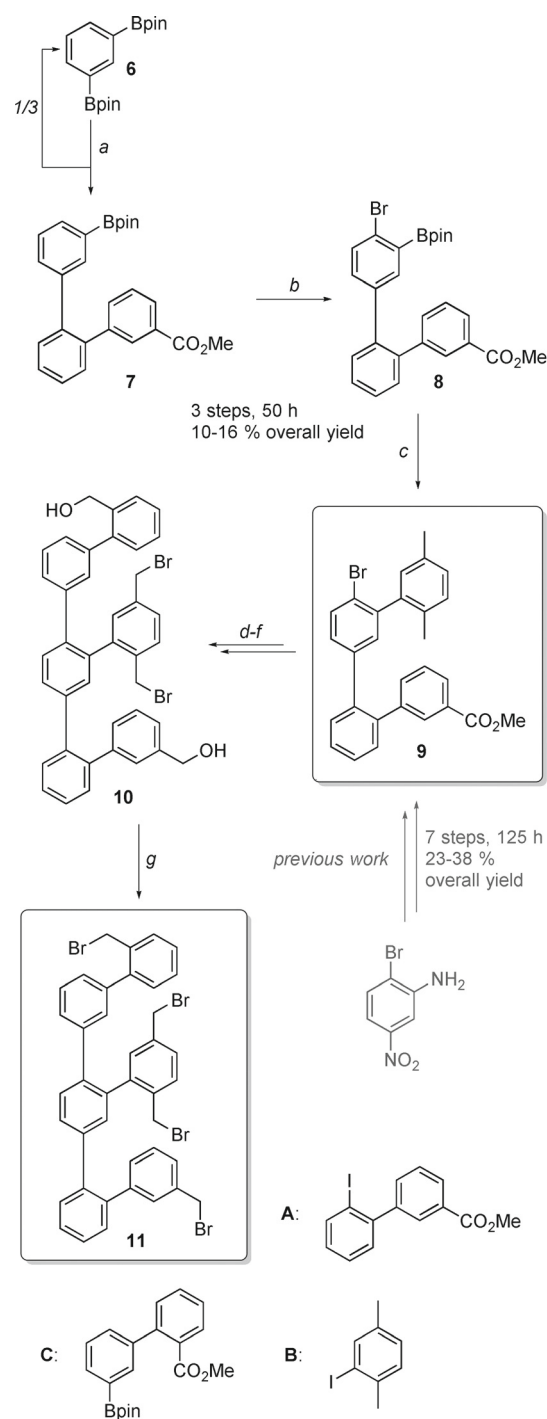
Figure 2. Conceptual representation of a helical ladder structure (left) and the concepts for elongation, and distortion of the original helix (middle and right). Induction of helical chirality is achieved by elongation of the segments on one side of the ladder, while keeping the length on the other (green). Rotation of the longer segment around the shorter leads to a helical arrangement. Elongation of the helix is obtained by increasing the length of both longer segments (blue), whereas inversion of the substitution pattern of the relay leads to discriminated ring sizes (purple) that result in distortion of the helix.



Scheme 1. Modular strategy based on a tetrabromo precursor (**11**) to incorporate the desired heteroatom and subsequently initiate macrocyclization in situ.

the heteroatom remains nucleophilic enough to initiate the desired subsequent macrocyclization without an intermediary workup. Additionally, the use of a versatile leaving group allows the incorporation of other promising linkages (e.g., amines or metals).

In principle, the required tetrabromo precursor is accessible by expanding on the strategy previously described.^[24] However, precursor **11** showed potential for the development of more efficient methodologies. A careful disconnection of the target structure revealed that, in any case, at least three borylations were necessary to minimize the overall amount of required orthogonal functionalities. Borylations are often challenging and can result in fragile intermediates, especially with sterically more evolved structures. A possible starting point would be the symmetric, commercially available, diborylated benzene **6** (Scheme 2), which features two of the three boronic moieties. Statistically attaching fragment **A** then gives the monocoupled intermediate **7**, which features the third boronic moiety for subsequent cross-coupling of the next fragment (**B** in this case). At this stage, we became interested in whether we could use the boronic ester as a directing group to introduce the next handle at the *ortho* position. According to reports in the literature, boronic esters are generally only weakly directing functionalities. Wang and co-workers impressively demonstrated that, under mild Lewis acidic conditions, regioselective halogenations of borylated aromatic systems was possible, and that any other substituents (even methyl groups) would define the location of the halogen.^[25,26] System **7** features three rings suitable for halogenation. However, we reasoned that, under the described conditions, the boronic moiety would define the chemoselectivity in the halogenation step, whereas the adjacent phenyl ring would determine its exact position (*para* over *ortho*). Introducing bromine would



Scheme 2. Synthesis of target precursor **11**: a) **A**, [Pd(PPh₃)₂Cl₂], K₂CO₃, 1,4-dioxane/MeOH 10:1, 60 °C, 2 h, 32%; b) NBS, AuCl₃, DCE, 60 °C, 15 h, 31–49%; c) **B**, [Pd(PPh₃)₂Cl₂], 1,4-dioxane/MeOH 4:1, 60 °C, 15 h, > 99%; d) SPhos Pd G2, K₂CO₃, toluene/H₂O 4:1, reflux, 1–3 d, 50%; e) NBS, DBP, CCl₄, 75 °C, 1 h, 87% to > 99%; f) DIBAL-H, CH₂Cl₂, room temperature, 30 min, > 99%; g) PBr₃, CH₂Cl₂, room temperature, 1 h, 61%; Bpin = 4,4,5,5-tetramethyl-1,3,2-dioxaborolane, DBP = dibenzoylperoxide, NBS = *N*-bromosuccinimide, DCE = dichloroethane, SPhos Pd G2 = chloro(2-dicyclohexylphosphino-2',6'-dimethoxy-1,1'-biphenyl)[2-(2'-amino-1,1'-biphenyl)]palladium(II), DIBAL-H = diisobutylaluminum hydride.

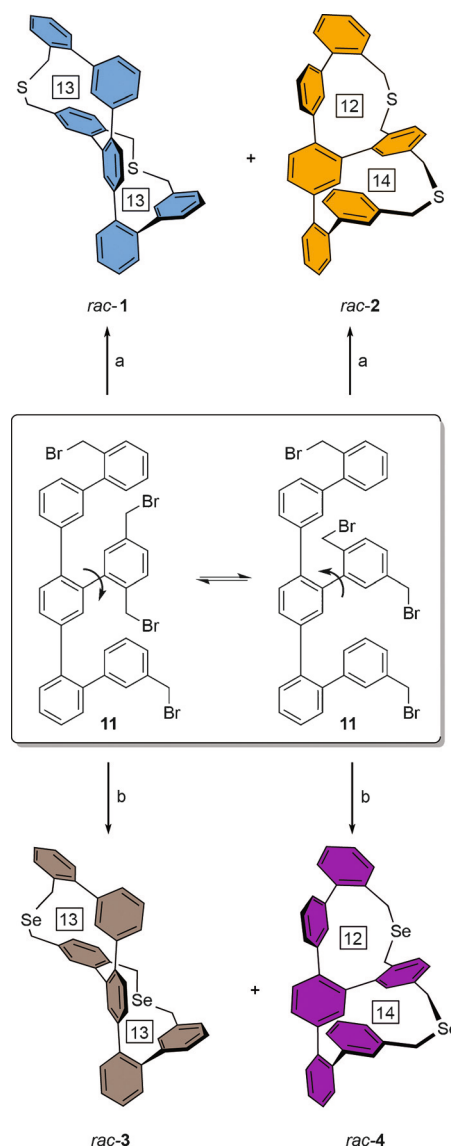
still allow subsequent cross-coupling of the boronic moiety with fragment **B**, which contains the more reactive iodine, leading to intermediate **9**, which is the first fragment, of the

previously described pathway (Scheme 2). We can then follow the route to intermediate **10** by using the remaining bromine as a handle to attach fragment **C** before converting **10** into precursor **11**. Indeed, we found that the statistical cross-coupling of **6** with **A** gave the desired monocoupled intermediate **7**, along with the twofold coupled derivative (60:40 by GC-MS). Although the conversion was excellent for a statistical reaction, purification was usually accompanied by a loss in yield due to the metastability of **7** towards column chromatography. Subsequent bromination at the predicted position proceeded in conversions of typically round 75% (yield: 49%) at the predicted position, as determined by GC-MS. Only minor amounts of the second *ortho* derivative were observed and overbromination was efficiently prevented by the slow addition of solid NBS. Due to the tendency of **8** to undergo deborylation—even more than **7**, possibly resulting from increased steric strain—the subsequent attachment of commercially available **B** was best carried out without extensive purification beforehand. Pleasingly, cross-coupling initiated a complete transition to **9**. Our own, previously published methodology^[24] gave access to **10**, which was efficiently transformed to **11** by Appel-type bromination (61%).

Synthesis and characterization of oligomers 1–4

With **11** in hand, we first turned to sulfur derivative **1**. Much to our delight, macrocyclization was both fast and selective. The direct transformation into the twofold cyclized target structure allowed, for the first time, the formation of the constitutional isomer **2** to be observed as direct consequence of the rotational equilibrium in **11** (Scheme 3). Due to the high similarities of the structures, conventional separation of **1** and **2** was not possible and gave a 1:1 mixture in very satisfying yield (76%; diether **5**: 28%). In oxygen derivative **5**,^[23] the heteroatom was present as a hydroxy group that required deprotonation by a strong base (NaH) before cyclization occurred. We found that the second cyclization would only proceed to a satisfying extent if the structure was purified after the first cyclization. However, only one of the four possible monocyclized intermediates was stable enough to be isolated, resulting in the observed deviations in yield and preventing isolation of the constitutional isomer. In the case presented herein for **1** and **2**, the heteroatoms initiate macrocyclization without the need for an external base directly after incorporation. The isolation of any intermediate becomes obsolete and results in the improved yield of both isomers. From the distribution of constitutional isomers, we conclude that the relay undergoes fast rotation around the central aryl–aryl bond.

Although conventional purifications were unsuitable, the isolation of the four isomers (2 pairs of enantiomers) was possible by HPLC on a chiral stationary phase (Chiralpak IA, 2 mL min⁻¹, 99:1 hexane/*i*PrOH, 18 °C; Figure 3 a–d) directly after a preliminary workup to remove ionic byproducts. Indeed, all four isomers were observed, although two of them (**1b/2b**) did not show baseline separation and required subsequent chromatography (HPLC on a chiral stationary phase). Conveniently, the addition of 1% CH₂Cl₂ allowed us to reasonably resolve the



Scheme 3. Synthesis of target compounds **1–4**: a) Na₂S, EtOH/toluene 1:1, room temperature, 4.5 h, 76% as 4 isomers; b) Na₂Se, EtOH/toluene 3:2, room temperature, 2.5 h, 50% as 4 isomers. The numbers in square boxes correspond to the number of atoms in each macrocycle.

mixed peak. The protocol was reliable enough that upscaling to a semipreparative column was possible, which allowed us to obtain all isomers in amounts suitable for subsequent unambiguous characterization by 1D and 2D NMR spectroscopy and high-resolution ESI-MS (ESI-HRMS). As expected for constitutional isomers, all obtained masses were identical, but required the addition of a sodium source for detection. The well-ordered, helical oligomer pair **1a,b** showed NMR signals that were similar to those obtained for oxygen derivative **5**, and were suitable for full assignment by 2D NMR spectroscopy. Mismatched helix **2**, on the contrary, gave broad signals, especially for the benzylic hydrogen atoms (see page S25 in the Supporting Information) and to lesser degrees also for the aromatic hydrogen atoms of the bridge, that indicated the presence (and interconversion into) of more than one species with

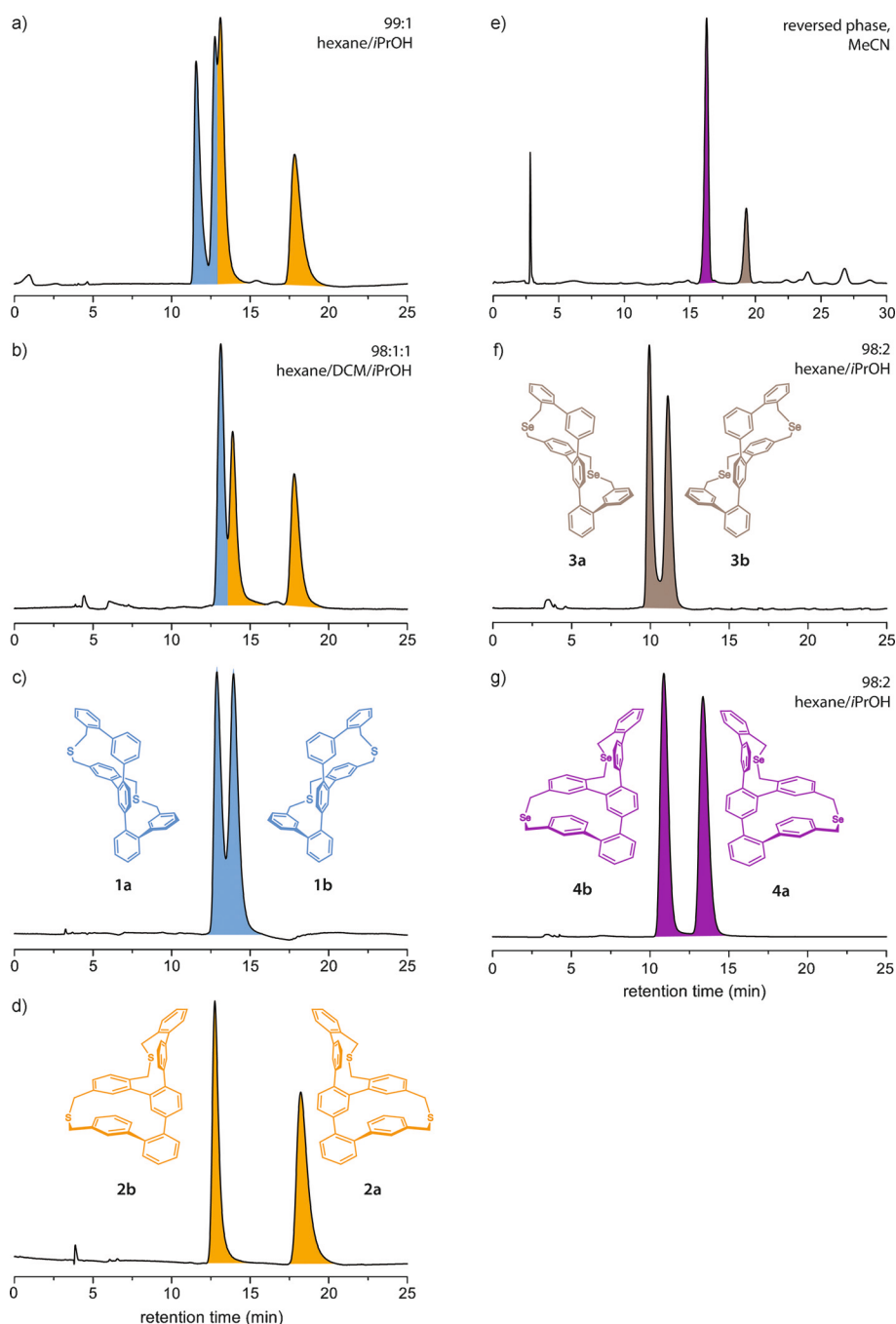


Figure 3. Traces of the HPLC separations on a chiral stationary phase (Chiralpak IA, 18–19 °C, 1–2 mL min⁻¹). a) Separation of **1** and **2** in a mixture of 99:1 hexanes and *i*PrOH. All four isomers (**1a,b** in blue and **2a,b** in orange) can be observed. The middle peak is a mixture of **1b** and **2a**; b) the addition of 1% CH₂Cl₂ allowed the separation of **1b** from **2a**; c) resolution of **1a** and **1b**; d) resolution of **2a** and **2b**; e) reversed-phase separation (Reprosil C18, MeCN, 1 mL min⁻¹) of the obtained reaction mixture of **3** (MeCN, 1 mL min⁻¹) of the obtained reaction mixture of **3** (brown) and **4** (purple); f) chiral resolution of **3a** and **3b** (98:2 hexanes and *i*PrOH); and g) resolution of **4a** and **4b**.

related chirality. It is important to note that broadening of the NMR signals indicates fast structural changes on the NMR timescale and is not very likely to be an indicator of an accelerated racemization process. We suspect that the deformed helix profits from higher degrees of freedom and can adopt multiple conformations of the bridge with similar overall energies. The sharp signals of the aromatic protons of the backbone indicate

that interconversion of the helices is present on a timescale much larger than the one observed by ¹H NMR spectroscopy; this was confirmed by kinetic studies at a later stage. By incrementing the temperature, adoption of all different conformations should be facilitated and result in an averaged structure. Indeed, variable-temperature (VT) NMR spectroscopy of *rac*-**2** in [D₂]tetrachloroethane (TCE) at 105 °C (see page S25 in the Supporting Information) revealed a well-resolved spectrum with sharp, well-defined peaks. This eventually allowed 2D NMR spectra to be recorded and fully assigned; all observed signals confirmed the predicted structure of **2**. Furthermore, for one aromatic hydrogen of **2**, we observed a pronounced high-field shift ($\delta = 5.61$ ppm at 378 K). Most likely, this proton is facing an aromatic ring directly in a reasonably rigid arrangement and is subjected to a high ring current. This signal is comparably well resolved above room temperature with a stable shift, which further supports a slow racemization process on the NMR spectroscopy timescale. A fast inversion would move the hydrogen out of the ring current during the transition from one enantiomer to the other. Once purified, both **1** and **2** were stable towards air and moisture and even reasonably stable towards silica.

Encouraged by the transition of **11** into the sulfur targets **1** and **2**, we aimed to access the selenium-bridged derivative **3** (and potentially **4**), which we expected to show diminished stabilities due to the well-documented ease of oxidation and thermal liability of selenium ethers. For the cyclization of the sulfur oligomers, we used highly nucleophilic Na₂S as the sulfur source; this is comparably stable and can be used without excessive precautions. However, the corresponding selenium salt Na₂Se is much more reactive (towards the desired nucleophilic substitutions and to oxygen and water), toxic, and has to be handled in a glove box. The dropwise addition of

Na₂Se in EtOH/toluene (4:1) to a diluted solution of precursor **11** in EtOH/toluene (1:1) at RT over 2 h resulted in full consumption of the starting material. Due to the instability of the formed products towards conventional chromatography, the reaction was monitored by DART-MS and reversed-phase HPLC (Reprosil C18, MeCN, 1 mL min⁻¹). The two most intense signals in ESI-HRMS were attributed to the desired oligomers **3** and **4**. To our surprise, and in contrast to the sulfur derivatives, the desired oligomers no longer formed in a 1:1 ratio—one of the constitutional isomers was preferably formed (about 4:3 on average; in one case, a ratio of 5:1 was observed). Reversed-phase silica (Reprosil C18, MeCN, 1 mL min⁻¹) proved to be ideal to separate the constitutional isomers **3** and **4** (Figure 3b) in a combined 50% yield.^[25] To identify which peak corresponds to which isomer, 1D and 2D NMR spectroscopy were performed on samples obtained from both peaks. ¹H NMR spectroscopy gave a strong indication as to which isomer was which: For the first eluting peak (purple), the signals were again broad and we quickly suspected it to be an analogous structure to that of **2**, that is, mismatched helix **4**. The spectra obtained for the second peak (brown) were well defined and sharp at room temperature, which made it a likely candidate for uniform analogue **3**. The preliminary assignment was confirmed by 2D NMR spectroscopy, which allowed explicit identification and full characterization of both *rac*-**3** and *rac*-**4**. As with sulfur derivative **2**, compound **4** needed to be heated to 105 °C for deconvolution of the broad signals into an averaged, precise spectrum. The subsequent chiral resolution of *rac*-**3** and *rac*-**4** into the corresponding enantiomers **3a**, **3b**, **4a**, and **4b** under slightly modified conditions (Chiralpak IA, 98:2 hexanes/*i*PrOH, 19 °C) is shown in Figure 3f and g. The peaks were baseline separated in all cases and the protocol readily scaled up.

In contrast to the stable sulfur derivatives **1** and **2**, the mismatched selenium oligomer **4**, in particular, was prone to decompose after several days in an oxygen atmosphere at room temperature. Decomposition of the sample was also observed during extended periods of measuring VT-NMR spectroscopy at elevated temperatures, even under oxygen-free conditions. Although the quality of the obtained spectra allowed full assignment, the sample could not be recovered after the extensive measurements (\approx 1 week).

Uniform and distorted helices

The previously described structure of diether **5**, as elucidated by X-ray crystallography, revealed the expected ladder-like assembly of the six phenyl rings.^[23] A highly uniform helix along the terphenylic backbone was found with an overall torsion of 147° and C–O bonds lengths of 1.43 Å. The torsion was determined by measuring the angle between the bottom and top rings of the backbone. One way to explain the uniformity of the helix is to describe **5** and its new analogues **1** and **3** as a twofold bridged biaryl. The two rings in the middle can be thought of as a single biphenyl with all other structural elements being part of one of the two bridges (top and bottom). Each of the bridges (or better, each ring containing one

heteroatom) features 13 atoms, which are similarly arranged (see numbering in Scheme 3), and hence, both rings prefer a similar spatial arrangement. Indeed, the secondary structure of **5** shows a smooth and continuous helix. In the case of the new model compounds **2** and **4**, the substitution pattern of the relay is reversed and the overall connections of the longer oligomer strand changes from a *meta-ortho-meta-ortho* to a *meta-meta-ortho-ortho* arrangement (see Figure 2, purple). From a similar viewpoint as before, the rings no longer contain an equal amount of atoms (bottom: 14, top: 12; see boxes in Scheme 3) nor do they show the same arrangement. Hence, each of the rings will prefer a different spatial arrangement, which is expected to translate directly into distortion of the helix.

Although NMR spectroscopy results gave indications about some aspects of the adopted structures of **1–4** and their relationship to the oxygen analogue, it was fundamentally important to obtain crystals of the sulfur and selenium analogues. Because we expected the half-times of the enantiopure samples to be in a similar range as that for **5** (approximately 9 h^[23]), the racemic mixtures were directly subjected to crystallization. To our great delight, suitable conditions for two of the four structures (**1** and **4**) were found after extensive screening of solvent mixtures and crystallization conditions. Both crystallized from hexanes by slow evaporation of the solvent. With all other crystallization attempts, we observed exclusive formation of amorphous material. The recorded diffraction data were excellent for **1** and the obtained structure for enantiomer **1a** is shown in Figure 4 (left). Eventually, single crystals suitable for solid-state analysis of one of the distorted, more delicate structures (**4**) were obtained. The extremely small, adhered needles made diffraction analysis demanding, but data of suitable quality to determine the solid-state structure could be recorded with one of the crystals.

The unit cells are racemic for both **1** and **4** and the enantiomers are present in a 2:2 ratio (see page S11 in the Supporting Information). The structures are well ordered with a continuous twist of the longer oligomer around the shorter backbone. Only enantiomers *M* and *P* were observed, with the twist being relayed from one end of the molecule to the other. The unit cell of **4** revealed a very plausible reason for the challenges we faced when growing and measuring crystals. Although crystallization occurred in pure hexanes, residual trace amounts of ethyl acetate (4 molecules per unit cell) from the previous workup were found in the cell. This finding not only clarifies the challenges we faced during attempts to reproduce crystallization, it also explains why the crystals are so small and fragile: the solvent molecules are arranged within the cells such that they form pores throughout the crystal. These pores presumably facilitate migration and their motion is expected to trigger degradation of the crystal upon temperature alterations.

For sulfur derivative **1** (Figure 4, left), the direct analogue of **5**, considerably increased bond lengths (C–S) were found compared with those of **5** (1.82 Å vs. 1.43 Å). As expected, the targeted increase in the bond lengths had an exclusive impact on the degree of twist (from 147 to 178° when compared with **5**),

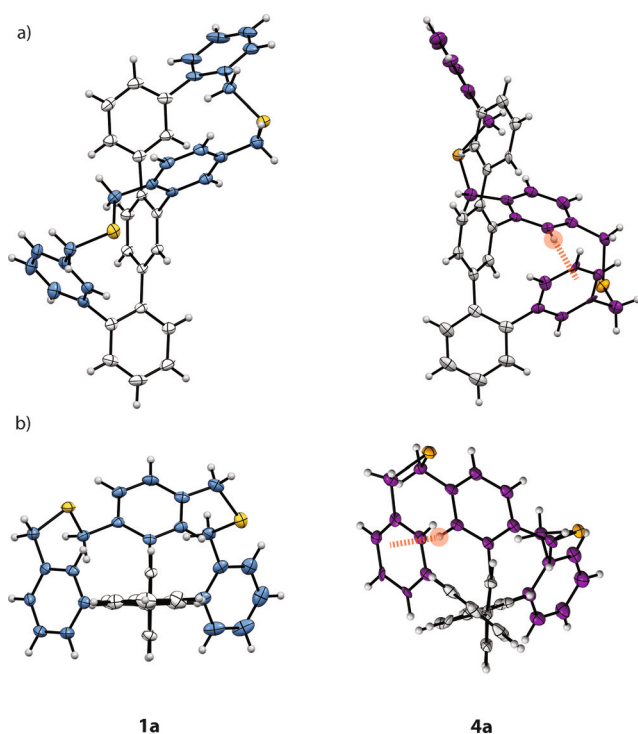


Figure 4. Racemic X-ray structures for **1** and **4** obtained from slow evaporation from solutions in hexanes.^[35] a) Side and b) front views of **1a** and **4a**. Color code: bridge=blue or purple, backbone=gray, hydrogen atoms=white, sulfur atoms=yellow, selenium atoms=orange. The red circle and dashed line highlight the aromatic proton pointing into the neighboring aromatic ring. Ellipsoids are drawn at the 50% probability level.

while maintaining all other aspects of the initial structure, such as linearity of the backbone and continuity of the helix. In contrast, selenium-containing oligomer **4** (Figure 4, right) shows increased C–Het bond lengths of 1.98 Å on average (1.43 and 1.82 Å for **5** and **1**, respectively), in accordance with the nonlinear change in the size of the heteronuclei. The change in the substitution pattern in the midsection of the wrapping selenoether caused significant changes to the secondary structure. The helix was still continuous with the helicity being transmitted from end to end. However, the overall torsion not only decreased to 121° (more than 20° less than that for **5**), the top and bottom rings of the backbone now deviated about 10° from the relaxed molecular axis. This bending of the backbone is most likely to be related to changes in ring size (12 and 14 atoms instead of 13 each) and reflects the importance of the original design concept to obtain a stable, continuous helix. A closer look at the individual atoms revealed a rationalization for the high shift of one of the aromatic hydrogen atoms. Only that particular hydrogen points directly into an aromatic ring with a distance of approximately 2.6 Å (Figure 4, highlighted in red). As already discussed during the interpretation of the NMR spectra above, it is therefore strongly affected by the ring current of the neighboring aromatic ring, resulting in a strong upfield shift to $\delta = 5.61$ ppm at 378 K.

It is important to note that, despite considerable efforts, so far we have not been able to grow suitable crystals from mixtures of *rac*-**2** or *rac*-**3**. Possible reasons include the structures

being subjected to fast conformational changes with related chirality and the apparent strong dependence of crystal growth factors such as trace amounts of cosolvents.

CD spectra and racemization barriers of 1–4

HPLC on a chiral stationary phase allowed the separation of the formed isomers of *rac*-**1–4** (4 for sulfur and 4 for selenium, consisting of 2 constitutional isomers that each consist of a pair of enantiomers). In other words, for each oligomer, the corresponding *M* and *P* helices were isolated in high enantiomeric purities (> 95% ee). Because enantiomers show complementary ECD spectra,^[27] we recorded ECD and UV/Vis spectra for each isomer, **1a**, **1b**, **2a**, **2b**, **3a**, **3b**, **4a**, and **4b** (Figure 5), in 99:1 hexanes/*i*PrOH (for **1** and **2**) and 98:2 hexanes/*i*PrOH (**3** and **4**) immediately after separation under air-saturated conditions at 10 °C. The reduction of temperature was important to prevent racemization over the timescale of the measurements. Indeed, complementary Cotton effects were observed in each case (**1a,b**: $\lambda = 244, 224,$ and 205 nm; **2a,b**: $\lambda = 278, 270, 232,$ and 206 nm; **3a,b**: $\lambda = 288, 254, 232,$ and 206 nm; **4a,b**: $\lambda = 280, 241, 225,$ and 206 nm). The recording of the corresponding UV/Vis spectra allowed us to determine the concentrations of samples to normalize the spectra. ECD spectroscopy is routinely used to determine structural similarities between systems. Although it is very challenging to deduce a specific arrangement in space based on ECD alone, it is often the case that structural similarities lead to characteristic bands. Once the arrangement is known, it is possible to identify the same arrangement in another, remotely similar system, as represented by the importance of ECD spectroscopy in protein characterization and dynamics.^[28] Similarities between the spectra of uniform and distorted helices were found. For example, compounds **2** and **4** each show a strong band at $\lambda \approx 280$ nm. The same band is, although still present, diminished in the case of **1** and **3**. Similar observations were made for most other bands, which indicated similar secondary structures of **1** and **3** (and consequently, also **2** and **4**). It is therefore likely that the arrangement in space we have deduced for **1** and **4** by XRD analysis can be transferred to **3** and **2**.

Both samples **1** and **4** crystallized with racemic unit cells, and thus, solid-state analysis did not allow us to determine the absolute configuration. The arrangement of the chromophores in space can, in some cases, be determined directly from the obtained ECD spectra, but this requires well-resolved exciton coupling bands, which is not the case for any of the systems presented herein. However, the strong, distinct Cotton bands in the ECD spectra offered an opportunity to determine the absolute conformation *in silico*, especially because we could profit from the single-crystal structures as starting points for the calculations. Also, the mainly carbon-based scaffold of the structures simplified the calculations significantly. To take the softer heteroatoms into account, calculations were performed with the B3LYP/6-31G** basis set, which has already demonstrated its accuracy for systems that involve heteroatoms.^[29] Structure optimizations and subsequent time-dependent calculations (TD-B3LYP/6-31G**, 150 states) with 75 triplet and 75

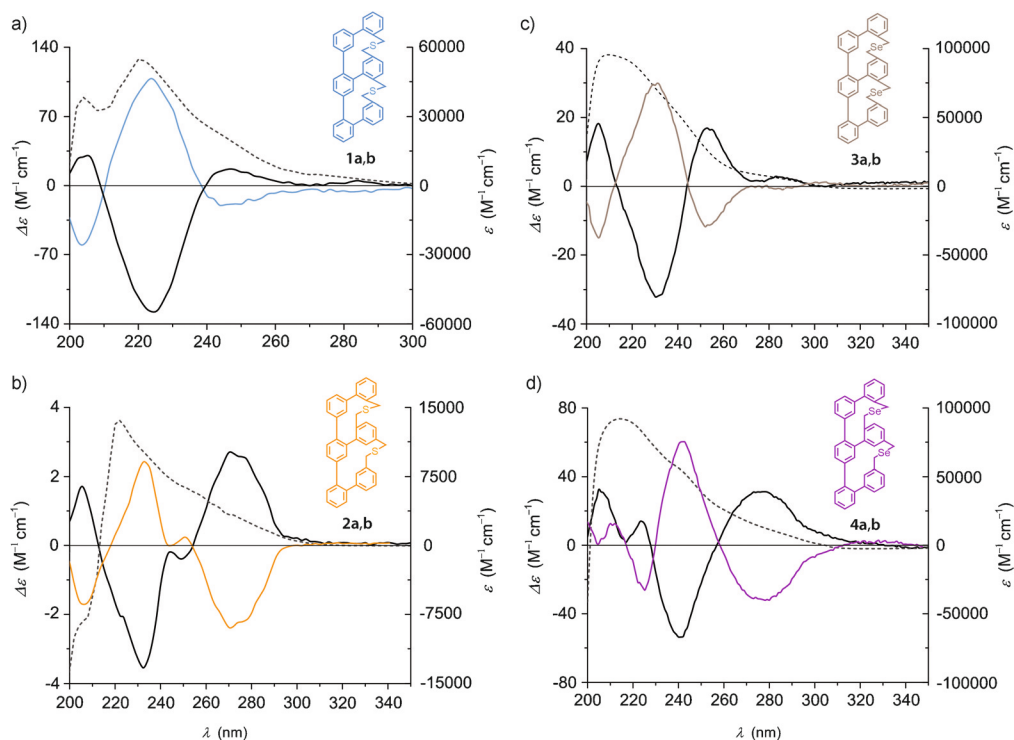


Figure 5. UV/Vis (dashed) and CD plots (full) for the sulfur oligomers a) **1a,b** and b) **2a,b** in 99:1 hexanes/*i*PrOH at 10 °C, and the selenium oligomers c) **3a,b** and d) **4a,b** in 98:2 hexanes/*i*PrOH at 10 and 5 °C, respectively.

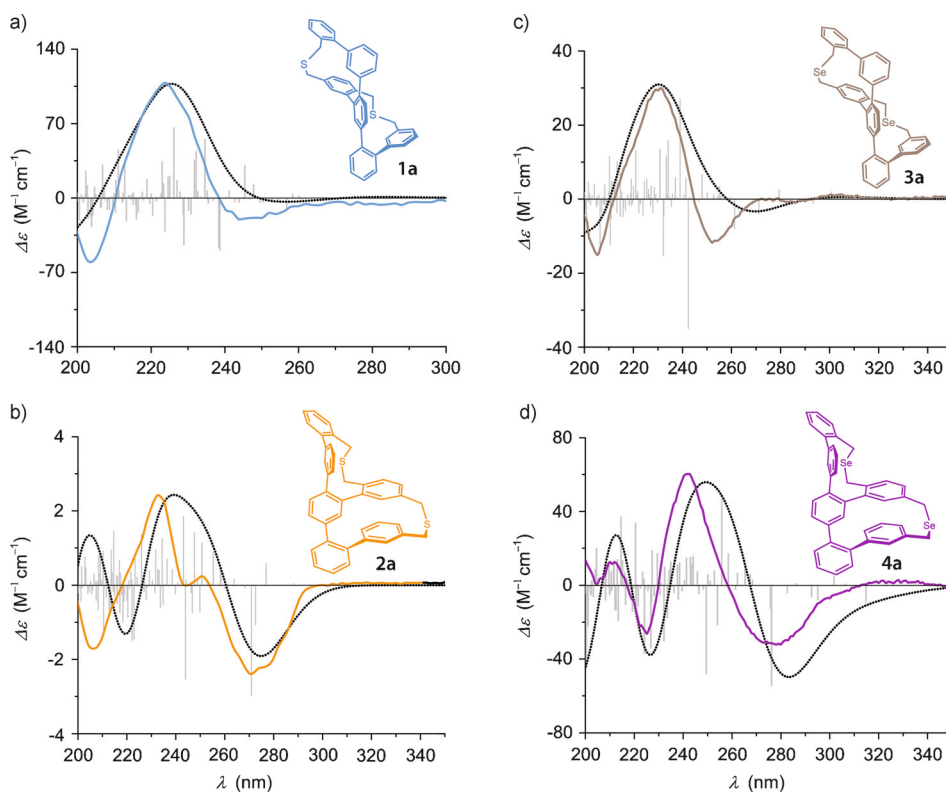


Figure 6. Experimental and calculated ECD spectra of **1a** (a), **2a** (b), **3a** (c), and **4a** (d) by using the TD-B3LYP/6-31G** functional with 75 triplet and 75 singlet excitations; total: 150 states; width 0.4 eV. The calculated spectra are based on the conformer with minimal energy. Colored: experimental spectra, black: calculated spectra, bars: calculated transitions.

singlet excitations were performed, and the obtained signs of the Cotton bands were compared with experimental spectra (Figure 6). Despite the rather rudimentary approach, good enough agreement between predicted and recorded ECD spectra was observed in all cases, which enabled the assignment of **1 a–4 a** and **1 b–4 b** to the *P* and *M* helices, respectively.

Based on this assignment of the absolute configurations, the recorded HPLC traces were re-evaluated. For the uniform cases (**1** and **3**), the *P* helices elute before their enantiomeric counterpart, whereas in the case of the distorted helices **2** and **4** the order is reversed. We thus conclude that the secondary structure of the constitutional isomers is considerably different such that the interaction with the chiral stationary phase leads to inversion of the elution order.

Dynamics of the helices 1–4

ECD spectroscopy not only allows chiral phenomena to be investigated, but also enables the observation of racemization and enantiomerization processes.^[30–33] We were interested to compare the racemization barriers with the already known ether analogue **5**. Of particular interest was the impact of the elongated bridges (**1** and **3**) and the mismatched ring sizes in **2** and **4** on the racemization process. A racemic sample of each derivative **1–4** ($\approx 0.2 \text{ mg mL}^{-1}$) in the eluent was prepared. An aliquot (300 μL) of the solution was injected and the enantiomers separated by HPLC on a chiral stationary phase (Chiralpak IA, 4 mL min⁻¹, 99:1 hexanes/*i*PrOH, 18 °C for **1** and **2**; 1 mL min⁻¹, 98:2 hexanes/*i*PrOH, 19 °C for **3** and **4**). A sample of the *P* conformer (**1 a–4 a**) was collected after elution and immediately subjected to ECD spectroscopy. Over a set amount of time, 50 points were recorded at the most intense Cotton band (**1 a**: $\lambda = 222 \text{ nm}$, **2 a**: $\lambda = 230 \text{ nm}$, **3 a**: $\lambda = 230 \text{ nm}$, **4 a**: $\lambda = 241 \text{ nm}$) at 25 °C until complete disappearance of the CD signal revealed that the racemate was reached.^[34]

Figure 7 shows the exponential decay for both **1 a–4 a**. Because the racemization process is not mediated by another molecule, the kinetics are expected to be of first order. If valid, linearization of the data by plotting time versus $\ln A$ gives direct access to the rate constant of racemization, k_{rac} and eventually to the racemization barrier, $\Delta G^{\ddagger}_{\text{rac}}$ at 25 °C (see also page S39 of the Supporting Information). The data was linear (and hence, first order) and resulted in excellent fits in all cases. The obtained values are summarized in Table 1.

It was particularly interesting to see changes in the values of $\Delta G^{\ddagger}_{\text{rac}}$ for the well-ordered helices **1** and **3**. Thioether **1** gives a racemization barrier that is very similar to that of (oxygen)-ether-bridged oligomer **5** ($\Delta\Delta G^{\ddagger}_{\text{rac}} = 0.4 \text{ kJ mol}^{-1}$). Apparently, the length of the bond (1.43 vs. 1.82 Å for **5** and **1**, respectively), which translates directly into an increased twist (147 vs. 178°), as obtained by XRD analysis, has almost no impact on the rate of racemization. We thus rationalize that the larger and softer sulfur atoms allow adaptation of a greater variety of angles, which compensates for the increased twist. Similar to **5**, the transition from *M* to *P* conformers (and vice versa) is smooth without any observable intermediate on the timescale

Table 1. Measured racemization barriers at 25 °C for **1 a–4 a** from the corresponding linear fits, including the value for diether **5** (*P* helices). The corresponding bond lengths and torsion angles of the backbone are given for comparison.

Helix	Compd.	Linkage	C–Het [Å]	Torsion angle [°]	$\Delta G^{\ddagger}_{\text{rac}}$ [kJ mol ⁻¹]
uniform	5	O	1.43	147	97.6 ± 0.1
	1 a	S	1.82	178	97.2 ± 0.1
	3 a	Se	1.98 ^[a]	159 ^[a]	90.4 ± 0.1
distorted	2 a	S	1.86 ^[a]	126 ^[a]	96.0 ± 0.1
	4 a	Se	1.98	121	96.2 ± 0.1

[a] Computed values.

of the experiments. Selenium analogue **3** is the key structure to deduce which of the opposing trends will dominate. Exchanging oxygen for sulfur and selenium means a continuous increase in the atomic radius and further elongated bonds (and thus, presumably an even higher overall torsion). On the other hand, the larger and softer atom results in an even less defined angle at the heteroatom, which is expected to further reduce the racemization barrier. If a further increased value of $\Delta G^{\ddagger}_{\text{rac}}$ is found, the increased torsion helps to stabilize the helix, whereas a reduced racemization barrier might indicate that the softer nucleus allows the interconversion to proceed more readily. For both **5** and **1**, the observed racemization is well behaved and undergoes a direct interconversion. Strikingly, the obtained barrier is significantly decreased ($\Delta\Delta G^{\ddagger}_{\text{rac}} \approx 7 \text{ kJ mol}^{-1}$) and clearly deviates from the other two model compounds. Because it was not possible to obtain a crystal structure for selenium derivative **3**, we relied on the B3LYP-optimized in silico geometry (Figure 8) used to calculate the CD spectra. We based the structure on the solid-state structure of **1** and exchanged sulfur for selenium. The obtained structure revealed significantly reduced torsion angles relative to **1** (159° instead of 178°). However, the average C–Se bond length (1.98 Å) found was identical to that of the distorted seleno-diemer **4**. Because the calculated CD spectra is in very good agreement with the experimental data, we have strong reason to assume that the calculated structure is accurate. We surmise that the further elongation of the C–Het bond no longer increases the overall torsion. Contrary to sulfur helix **3**, for which elongation leads to an increase in torsion angle and that, in turn, compensates for the enhanced flexibility of the heteroatom, these trends are no longer counteracting and are very likely to be the reason for the significantly reduced racemization barrier.

We next turned our attention to the two mismatched helices. As outlined before, both **2** and **4** show broad NMR signals for protons of the bridge, which indicates the presence of multiple, rapidly interchanging conformers. However, we do not consider them to be racemization processes, but rather fast, small conformation changes of the bridge because the protons on the backbone are well defined and sharp. That the racemization processes are generally much slower than the NMR timescale is clearly supported by the successful separation of the enantiomers by chiral HPLC. Again, the clear doublet in the

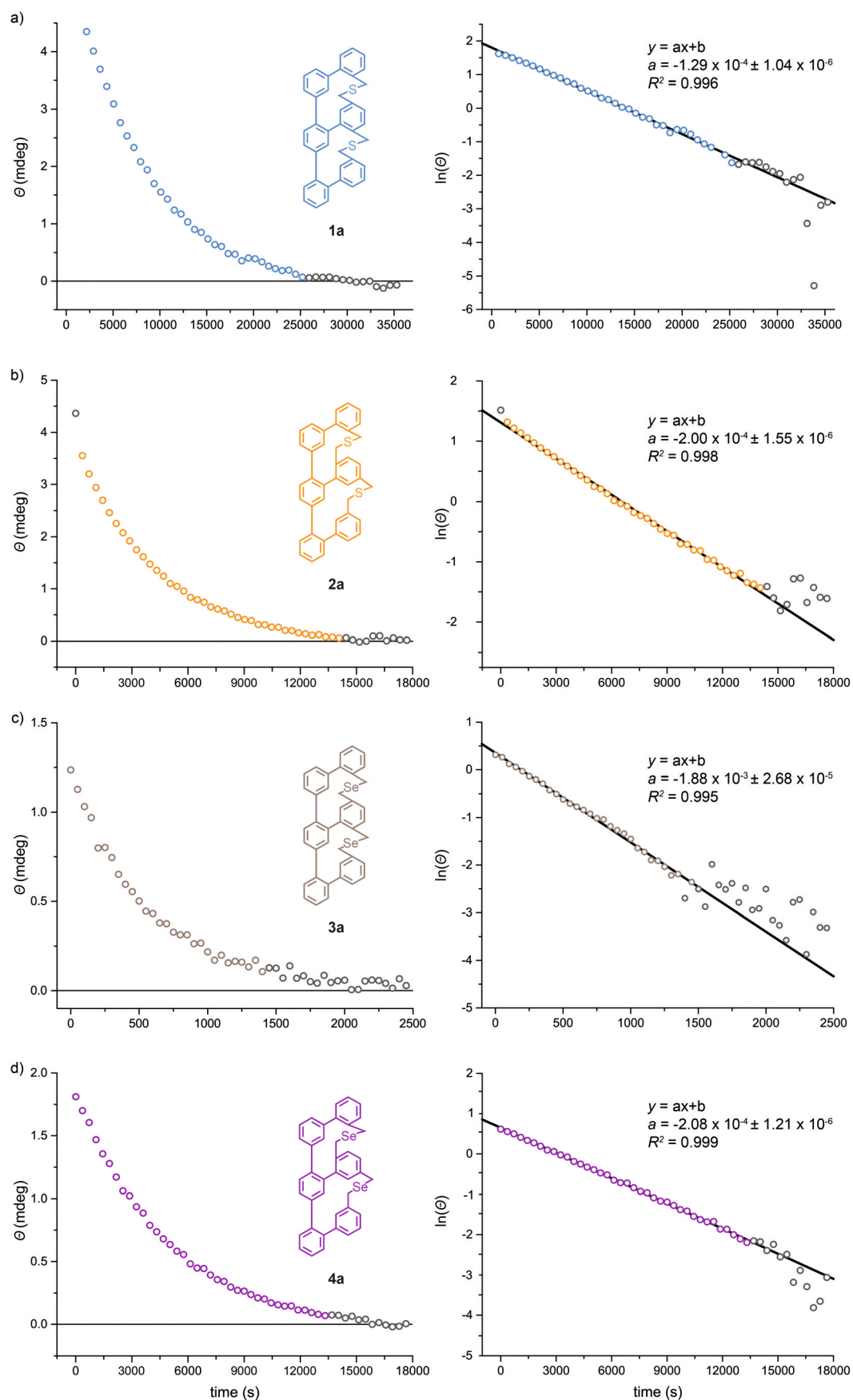


Figure 7. Decay of the CD signals for the oligomers **1a** (a), **2a** (b), **3a** (c), and **4a** (d). After isolation of one corresponding enantiomer, the loss of CD signal was observed at ΔA_{\max} at 25 °C over time. Linear fitting of $\ln A$ versus time allowed the rate constant of racemization, k_{rac} , to be accessed, and thus, the racemization barrier, $\Delta G^{\ddagger}_{\text{rac}}$ at 25 °C to be calculated.

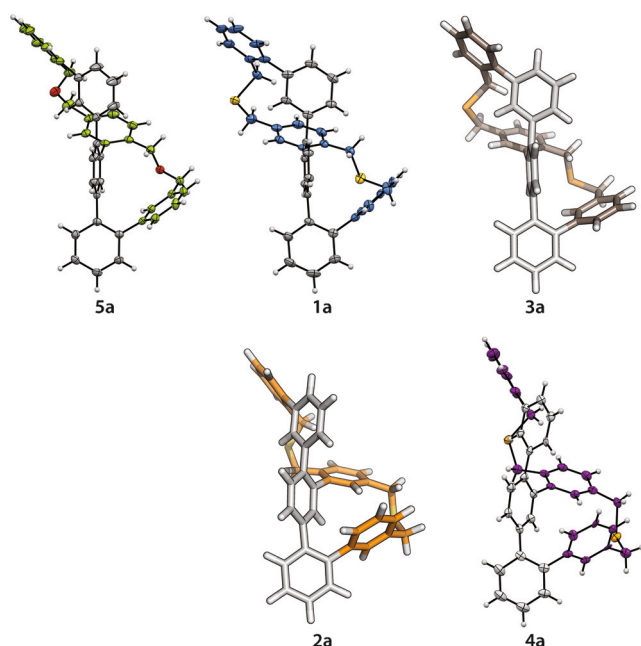


Figure 8. Solid-state structures obtained by XRD analysis (**5a**, **1a**, **4a**) and calculated structures (**2a** and **3a**) obtained by using the Gaussian 09^[36] program and B3LYP/6-31G** functional. The top row depicts the matched helices with a smooth helical wrapping of the longer oligomer. The lower row shows the mismatched, distorted helices. In all cases, continuous wrapping of the longer oligomer was determined (or predicted), which gave only one pair of enantiomers (*M* and *P*) each.

HPLC trace and the resulting complementary CD spectra strongly suggest that only two types of long-lived helices are present. Furthermore, heating the samples resulted in averaged, well-defined spectra, which indicated that the barrier for these small conformation changes was low. It is thus not surprising that the observed CD decays and subsequent plot of $\ln A$ versus time showed excellent linear behavior and very well defined values of $\Delta G_{\text{rac}}^{\ddagger}$ (96.0 ± 0.1 mol⁻¹ for **2** and 96.2 ± 0.1 kJ mol⁻¹ for **4**). Neither the uniformity of the helix nor the enlarged ring size has a significant impact on the racemization barrier because the measured values are only marginally lower than that of the uniform helices ($\Delta\Delta G_{\text{rac}}^{\ddagger} \approx 1$ kJ mol⁻¹). Furthermore, the mismatched helices do not follow the trend set by the matched derivatives upon exchange of the heteroatom. The torsion angle (**2**: calculated: 126°; **4**: measured: 121°) changes only marginally, whereas the barrier increases by $\Delta\Delta G_{\text{rac}}^{\ddagger} = 0.1$ kJ mol⁻¹, which is smaller than the accuracy of the method. Based on these findings, we conclude that either the racemization process of these distorted oligomers does not rely on the size or nature of the incorporated heteroatom or there are two competing features at work, which compensate each other perfectly in the two model compounds. Because of similarity to the model compounds **1**, **3**, and **5**, we currently favor the second hypothesis.

Conclusion

New types of chiral ladder systems that showed induced, elongated, or distorted helicity were assembled by an efficient synthetic route. The studies demonstrated conceptually and ex-

perimentally that elongation of the bridge mainly altered the degree of twist, whereas changes in ring size led to distortion of the helix. More accurately, modulation of the overall torsion with alteration of the heteroatoms and distortion of the helices by a targeted change in the substitution pattern of the relay were demonstrated. Access to the new derivatives was possible due to a short synthetic route, which included minimal amounts of borylations, precise regioselective halogenation mediated by a neighboring boronic ester, and Appel-type substitution of two benzylic hydroxy groups to a versatile, modular precursor. This precursor allowed for two consecutive macrocyclizations and the successful integration of either two sulfur or selenium atoms in a single synthetic step. The flexibility of the precursor gave access to two further (constitutional) isomers with an inverted substitution pattern on the relay. A total of eight structures—for each type of heteroatom, two structural isomers existed as enantiomeric pairs—were accessed in high yields and separated into the individual isomers by a multitude of chromatographic protocols (both achiral and chiral). Extensive NMR spectroscopy and HRMS studies allowed the unambiguous identification of each structure, whereas ECD spectroscopy of the purified isomers allowed confirmation of similar secondary structures and identification of the enantiomeric pairs. In silico ECD calculations allowed us to assign the absolute stereochemistry of the enantiomers and project the arrangement of the helices in space. The structural arrangements of two of the four structural isomers were confirmed by XRD analysis, which revealed alteration of the secondary structure upon changing the substitution pattern (uniform and distorted helix). Elongation of the heteroatomic bonds increased the torsion angle in the case of the sulfur system, whereas decreased torsion angles were observed for the selenoether. Two dynamic processes were investigated: the flexibility of the bridge by VT-NMR spectroscopy for the distorted helices and the racemization processes of all four model compounds by ECD decay spectroscopy. VT-NMR spectroscopy demonstrated that the bridge of the distorted helix derivatives is indeed flexible and can undergo small structural changes on the NMR spectroscopy timescale, as indicated by broad signals at 25 °C that coalesce at elevated temperatures. The proton signals of the backbone are sharp at room temperature, which is consistent with a racemization process on a larger timeframe. The observation of decay of the most prominent Cotton band by ECD led to precise values for the racemization barrier and allowed the racemization to be related to the spatial arrangement of the structures. Two main trends were found: the length of the heteroatomic bonds (increased torsion) and the size of the heteronucleus (softer nuclei with less defined bond angles) compensate for each other in the case of sulfur. The seleno ether containing larger heteroatoms showed a highly reduced racemization barrier in the case of the uniform helix due to a reduced torsion angle and a softer nucleus. In both cases, neither of the distorted helices responded to changes in the heteroatom. The prevention of an achiral *meso* form, the continuity of the induced helices, and the observed uniform racemization pathways made the study of these fascinating structures possible.

The prospect of introducing a variety of linkages is an important step towards stable Geländer-type helices. Because ring size plays a crucial role in the stereodynamics and spatial arrangement of the oligomer, a more constrained helix with decreased ring sizes becomes desirable. In particular, sulfur is an ideal entry point to access all carbon-based, tighter derivatives. A further option towards long-term stable helices is the elongation of the helix, leading to longer ladders with increased overall torsion angles. These studies are currently ongoing and will be reported in due course.

Acknowledgements

We acknowledge financial support by the Swiss National Science Foundation (SNF).

Keywords: atropisomerism · chirality · conformation analysis · helical structures · oligomers

- [1] J. L. Alonso-Gómez, P. Rivera-Fuentes, N. Harada, N. Berova, F. Diederich, *Angew. Chem. Int. Ed.* **2009**, *48*, 5545–5548; *Angew. Chem.* **2009**, *121*, 5653–5656.
- [2] W. Nakanishi, T. Matsuno, J. Ichikawa, H. Isobe, *Angew. Chem. Int. Ed.* **2011**, *50*, 6048–6051; *Angew. Chem.* **2011**, *123*, 6172–6175.
- [3] K. S. Hayes, M. Nagumo, J. F. Blount, K. Mislow, *J. Am. Chem. Soc.* **1980**, *102*, 2773–2776.
- [4] G. S. Kottas, L. I. Clarke, D. Horinek, J. Michl, *Chem. Rev.* **2005**, *105*, 1281–1376.
- [5] Y. Wang, A. D. Stretton, M. C. McConnell, P. A. Wood, S. Parsons, J. B. Henry, A. R. Mount, T. H. Galow, *J. Am. Chem. Soc.* **2007**, *129*, 13193–13200.
- [6] H. Ito, T. Abe, K. Saigo, *Angew. Chem. Int. Ed.* **2011**, *50*, 7144–7147; *Angew. Chem.* **2011**, *123*, 7282–7285.
- [7] S. Nobusue, Y. Mukai, Y. Fukumoto, R. Umeda, K. Tahara, M. Sonoda, Y. Tobe, *Chem. Eur. J.* **2012**, *18*, 12814–12824.
- [8] R. A. Pascal, *Chem. Rev.* **2006**, *106*, 4809–4819.
- [9] C. S. Hartley, *J. Org. Chem.* **2011**, *76*, 9188–9191.
- [10] T. Kudernac, N. Ruangsupapichat, M. Parschau, B. Maciá, N. Katsonis, S. R. Harutyunyan, K.-H. Ernst, B. L. Feringa, *Nature* **2011**, *479*, 208–211.
- [11] M. Gingras, *Chem. Soc. Rev.* **2013**, *42*, 968–1006.
- [12] M. Gingras, G. Félix, R. Peresutti, *Chem. Soc. Rev.* **2013**, *42*, 1007–1050.
- [13] M. Gingras, *Chem. Soc. Rev.* **2013**, *42*, 1051–1095.
- [14] B. Kiupel, C. Niederal, M. Nieger, S. Grimme, F. Vögtle, *Angew. Chem. Int. Ed.* **1998**, *37*, 3031–3034; *Angew. Chem.* **1998**, *110*, 3206–3209.
- [15] M. Modjewski, S. V. Lindeman, R. Rathore, *Org. Lett.* **2009**, *11*, 4656–4659.
- [16] K. Ohkata, R. L. Paquette, L. A. Paquette, *J. Am. Chem. Soc.* **1979**, *101*, 6687–6693.
- [17] K. Müllen, W. Heinz, F.-G. Klärner, W. R. Roth, I. Kindermann, O. Adamczak, M. Wette, J. Lex, *Chem. Ber.* **1990**, *123*, 2349–2371.
- [18] L. Venkataraman, J. E. Klare, C. Nuckolls, M. S. Hybertsen, M. L. Steigerwald, *Nature* **2006**, *442*, 904–907.
- [19] D. Vonlanthen, A. Mishchenko, M. Elbing, M. Neuburger, T. Wandlowski, M. Mayor, *Angew. Chem. Int. Ed.* **2009**, *48*, 8886–8890; *Angew. Chem.* **2009**, *121*, 9048–9052.
- [20] J. Rotzler, H. Gsellinger, A. Bihlmeier, M. Gantenbein, D. Vonlanthen, D. Häussinger, W. Klopfer, M. Mayor, *Org. Biomol. Chem.* **2012**, *10*, 110–118.
- [21] D. P. Iwaniuk, K. W. Bentley, C. Wolf, *Chirality* **2012**, *24*, 584–589.
- [22] S. Menning, M. Krämer, B. A. Coombs, F. Rominger, A. Beeby, A. Drew, U. H. F. Bunz, *J. Am. Chem. Soc.* **2013**, *135*, 2160–2163.
- [23] M. Rickhaus, L. M. Bannwart, M. Neuburger, H. Gsellinger, K. Zimmermann, D. Häussinger, M. Mayor, *Angew. Chem. Int. Ed.* **2014**, *53*, 14587–14591; *Angew. Chem.* **2014**, *126*, 14816–14820.
- [24] M. Rickhaus, L. M. Bannwart, O. Unke, H. Gsellinger, D. Häussinger, M. Mayor, *Eur. J. Org. Chem.* **2015**, *2015*, 786–801.
- [25] About 25% of the remaining yield was attributed to structures containing three selenium atoms, most likely to systems containing one selenium and one diselenium bridge, as indicated by ESI-HRMS: F. Mo, J. M. Yan, D. Qiu, F. Li, Y. Zhang, J. Wang, *Angew. Chem. Int. Ed.* **2010**, *49*, 2028–2032; *Angew. Chem.* **2010**, *122*, 2072–2076.
- [26] D. Qiu, F. Mo, Z. Zheng, Y. Zhang, J. Wang, *Org. Lett.* **2010**, *12*, 5474–5477.
- [27] For an excellent tutorial, see: N. Berova, L. D. Bari, G. Pescitelli, *Chem. Soc. Rev.* **2007**, *36*, 914–931.
- [28] For a comprehensive introduction, see: G. Pescitelli, L. D. Bari, N. Berova, *Chem. Soc. Rev.* **2011**, *40*, 4603–4625.
- [29] G. S. Heverly-Coulson, R. J. Boyd, *J. Phys. Chem. A* **2011**, *115*, 4827–4831.
- [30] P. Osswald, F. Würthner, *J. Am. Chem. Soc.* **2007**, *129*, 14319–14326.
- [31] H. Saito, T. Mori, Y. Origane, T. Wada, Y. Inoue, *Chirality* **2008**, *20*, 278–281.
- [32] L. Lunazzi, M. Mancinelli, A. Mazzanti, M. Pierini, *J. Org. Chem.* **2010**, *75*, 5927–5933.
- [33] S. Ando, E. Ohta, A. Kosaka, D. Hashizume, H. Koshino, T. Fukushima, T. Aida, *J. Am. Chem. Soc.* **2012**, *134*, 11084–11087.
- [34] Measuring **3a** in 99:1 hexanes/*i*PrOH gave an identical spectrum. For convenience and reproducibility, the respective eluent of the HPLC run was chosen for the CD measurements.
- [35] CCDC 1405407 (1) and 1405272 (4) contain the supplementary crystallographic data for this paper. These data are provided free of charge by The Cambridge Crystallographic Data Centre.
- [36] Gaussian 09, Revision C.01, M. J. Frisch, G. W. Trucks, H. B. Schlegel, G. E. Scuseria, M. A. Robb, J. R. Cheeseman, G. Scalmani, V. Barone, B. Menonucci, G. A. Petersson, H. Nakatsuji, M. Caricato, X. Li, H. P. Hratchian, A. F. Izmaylov, J. Bloino, G. Zheng, J. L. Sonnenberg, M. Hada, M. Ehara, K. Toyota, R. Fukuda, J. Hasegawa, M. Ishida, T. Nakajima, Y. Honda, O. Kitao, H. Nakai, T. Vreven, J. A. Montgomery, Jr., J. E. Peralta, F. Ogliaro, M. Bearpark, J. J. Heyd, E. Brothers, K. N. Kudin, V. N. Staroverov, R. Kobayashi, J. Normand, K. Raghavachari, A. Rendell, J. C. Burant, S. S. Iyengar, J. Tomasi, M. Cossi, N. Rega, J. M. Millam, M. Klene, J. E. Knox, J. B. Cross, V. Bakken, C. Adamo, J. Jaramillo, R. Gomperts, R. E. Stratmann, O. Yazyev, A. J. Austin, R. Cammi, C. Pomelli, J. W. Ochterski, R. L. Martin, K. Morokuma, V. G. Zakrzewski, G. A. Voth, P. Salvador, J. J. Dannenberg, S. Dapprich, A. D. Daniels, Ö. Farkas, J. B. Foresman, J. V. Ortiz, J. Cio-slowski, D. J. Fox, Gaussian, Inc., Wallingford CT, **2009**.

Received: August 13, 2015

Published online on November 5, 2015



PCCP

PAPER



Cite this: *Phys. Chem. Chem. Phys.*,
2015, 17, 11165

Activation enthalpies and entropies of the atropisomerization of substituted butyl-bridged biphenyls

Angela Bihlmeier,^{*a} Jürgen Rotzler,^b Michel Rickhaus,^b Marcel Mayor^{*bc} and Wim Klopper^{*ac}

A combined quantum chemical and experimental study of the atropisomerization energies of di-*para*-substituted butyl-bridged biphenyl cyclophanes is presented. We studied the influence of electron donor and electron acceptor substituents on the height of the enantiomerization barrier and examined the enthalpic and entropic contributions. The reaction pathway with minimum and transition state structures was established using density functional theory calculations. The Gibbs free activation energies derived from this pathway correspond well to the ones determined by temperature dependent high performance liquid chromatography (HPLC) measurements. Surprisingly, large discrepancies were found for the contributions of enthalpy and entropy. Thermodynamic data derived from circular dichroism (CD) measurements support the quantum chemical calculations for the distribution of enthalpy and entropy, contrary to the HPLC measurements. Rationalizations for this are given.

Received 22nd December 2014,
Accepted 16th February 2015

DOI: 10.1039/c4cp06009a

www.rsc.org/pccp

1 Introduction

Chiral biarylic structures are highly interesting from a number of viewpoints. The torsion angle between the planes of the two phenyl rings can readily be adjusted synthetically which allowed to study the degree of π overlap in the two phenyl rings and the resulting extent of delocalization over both π systems. This has been used as a key to unlock the secrets of angular dependence on conjugation and ultimately conductance.^{1–3} Further, substitution allows the introduction of axial chirality in the system, making biphenyls an important structural motif for the development of efficient catalysts for asymmetric synthesis.^{4–7} Crucial for the application is a high conformational stability, that is, a sufficiently high barrier for the rotation about the phenyl–phenyl bond.⁸ Many experimental studies have been conducted in the past to determine the rotation barriers of various types of biphenyls, see for example ref. 9–12, and thorough quantum chemical calculations have been carried out, ranging from highly correlated methods¹³ to the extensive study of different density functionals.¹⁴ Among a vast number of potential candidate structures that have been

investigated theoretically and/or experimentally, alkyl-bridged biphenyls have a long-standing tradition as model systems. Their relatively slow racemization, synthetic modifiability and overall stability allowed the extensive study of electronic and optical properties as well as their racemization behaviour.^{3,15–20}

For the propyl-bridged biphenyl cyclophanes, we have previously studied the influence of substituents in *para* position (electron donors and electron acceptors) on the enantiomerization barrier.²⁰ We found rather small effects on the Gibbs free activation energy ΔG^\ddagger but based on the geometry of the transition state we suggested that the functionalization of the propyl bridge provides the possibility to increase the activation barrier. Compared to the propyl-bridged push–pull cyclophane, the corresponding butyl-bridged compound **1i** (Fig. 1) showed a much higher enantiomerization barrier.¹⁸ Hence we expected that these systems are even more susceptible to synthetic modifications that lead to increased conformational stability.

In the present work, we aim at understanding the mechanism of the enantiomerization reaction of the butyl-bridged biphenyl cyclophanes **1a–1l** (Fig. 1) and at identifying the factors that govern the height of the activation barrier. The influence of different types of substituents in *para* position on ΔG^\ddagger and a comparison with the results of the propyl-bridged compounds are also of interest. Our investigations are described in the following and comprise density functional theory (DFT) calculations and high performance liquid chromatography (HPLC) measurements, as well as circular dichroism (CD) measurements on a selected compound.

^a Institute of Physical Chemistry, Karlsruhe Institute of Technology (KIT), Kaiserstr. 12, 76131 Karlsruhe, Germany. E-mail: angela.bihlmeier@kit.edu

^b Department of Chemistry, University of Basel, St. Johannis-Ring 19, 4056 Basel, Switzerland. E-mail: marcel.mayor@unibas.ch

^c Institute of Nanotechnology, Karlsruhe Institute of Technology (KIT), P. O. Box 3640, 76021 Karlsruhe, Germany. E-mail: klopper@kit.edu

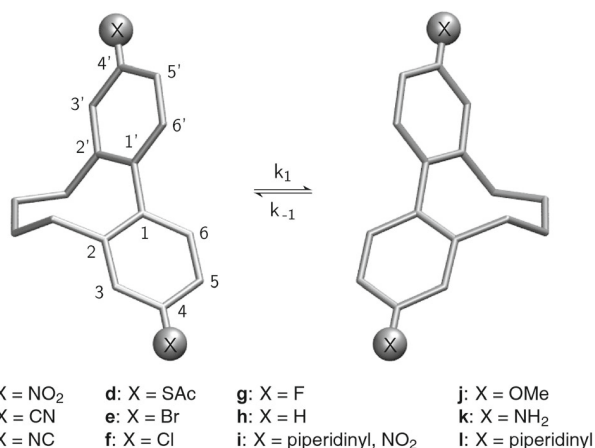


Fig. 1 Studied butyl-bridged biphenyl cyclophanes **1a–1l**. For clarity, the hydrogen atoms are omitted.

II Methods

A. Computational studies

All quantum chemical calculations in this work have been carried out using the TURBOMOLE program package.²¹ The geometries of the relevant species in the atropisomerization reaction path of **1a–1l** were optimized within the framework of DFT. Following our earlier work on propyl-bridged biphenyl cyclophanes,²⁰ both the TPSS²² and B3LYP²³ functionals were used in combination with the def2-TZVP basis set²⁴ employing tight convergence criteria and fine quadrature grids (m5).²⁵ In case of the TPSS functional the efficient resolution of the identity approximation for the evaluation of two-electron Coulomb integrals was used. The nature of the obtained stationary points was confirmed through calculation of the vibrational frequencies, and in case of transition states the imaginary frequency was ensured to correspond to the desired reaction coordinate.

Thermodynamic data (ΔH^\ddagger , ΔS^\ddagger , ΔG^\ddagger) were computed for a standard pressure of 0.1 MPa and a temperature of 298.15 K. For the evaluation of the partition functions the vibrational frequencies were scaled²⁶ by a factor of 0.9914 for TPSS and 0.9614 for B3LYP, respectively.

For X = SAc, OMe, NH₂ and piperidinyl, the rotation about the bond between the phenyl ring and the substituent as well as rotations within the substituent allow for several conformers with similar energy and often relatively low barrier heights. In these cases, we assumed that the substituents can rotate freely and that the respective rotation potentials stay similar for all species along the reaction path. Hence, we have only considered the energetically most favoured conformer for the computation of thermodynamic data, exploiting the error cancellation which occurs when taking energy differences.

B. Syntheses

Compounds **1a** and **1l** were synthesized according to the procedures used for the corresponding propyl-bridged derivatives and starting from the already available diamino derivative **1k**.²⁷ The protocols feature an oxidation using a potassium

iodide-*tert*-butyl hydroperoxide catalytic system²⁸ and an azacycloalkylation with 1,5-dibromopentane in an aqueous sodium-dodecylsulfate solution and sodium hydrogen carbonate as a base, respectively.²⁷ Dicyano substituted derivative **1b**,¹⁹ *S*-acetyl substituted derivative **1d** (ref. 3) and dimethoxy substituted derivative **1j** (ref. 19) were available in our group from molecular electronics investigations. Compound **1b** was synthesized by hetero cross-coupling of potassium cyanide and the ditriflate substituted derivative using a Pd⁰ catalyst (Pd₂(dba)₃) and Xanthphos as a ligand. Compound **1d** was obtained by nucleophilic aromatic substitution of dibromobiphenyl **1e** with sodium thiomethanolate to afford the free thiol which was *in situ* transprotected with acetyl chloride.

C. Dynamic HPLC

The free energies ΔG^\ddagger for the atropisomerization of the synthesized compounds were determined by temperature dependent HPLC measurements. Solutions of **1a**, **1b**, **1d**, **1j** and **1l** of approximately 1 mg mL⁻¹ in *i*PrOH were prepared. 3 μ L of these solutions were injected into a chiral Chiralpak AD-H column (0.46 \times 25 cm; Daicel Chemical Industries Ltd) at the defined temperature (CTO-10AS VP oven from Shimadzu). The atropisomers were eluted with a mixture of *n*-hexane/*i*PrOH = 97 : 3 for **1a**, **1b**, **1j** and **1l** and *n*-hexane/*i*PrOH = 95 : 5 for **1d** at a flow rate of 0.5 mL min⁻¹ (SCL-10A VP HPLC from Shimadzu). To guarantee an efficient mixing of both solvents the eluent was prepared as a 94 : 6 or 90 : 10 mixture from *n*-hexane and *n*-hexane/*i*PrOH = 1 : 1. For detection of the chromatogram a UV/Vis detector (SPD-M10A VP from Shimadzu) operating at the absorption maxima of the compound under investigation was used (λ_{max} = 254 nm). The column was preconditioned for 2 hours under the conditions used for the dynamic HPLC experiments before a set of temperature dependent measurements was performed. After each run the column was equilibrated for half an hour. The studies were performed at temperatures between 15 °C and 35 °C in 5 °C steps. Two different samples of each compound were measured twice in the whole temperature range. The forward reaction rate constants were evaluated with the unified equation²⁹ valid for first order processes by direct integration of the elution profiles using the software DCXplorer.³⁰ The Gibbs free activation energy was calculated by estimation of the activation enthalpy ΔH^\ddagger from the slope of an Eyring plot and the activation entropy ΔS^\ddagger from the intercept. For **1i**, previously published thermodynamic data of Rotzler *et al.* were taken.¹⁸

D. CD spectroscopic studies

The Gibbs free activation energies can also be accessed by separation of the atropisomers and then measuring the decay of circular dichroism (CD) directly in solution. Such kinetic CD measurements have been used previously to investigate the racemization processes in helices,³¹ propellers,³² oligomers,³³ and structures showing planar³⁴ or axial chirality,^{35,36} to name just a few examples.

A solution of **1j** of approximately 1 mg mL⁻¹ in a mixture of *n*-hexane/*i*PrOH = 98 : 2 was prepared. 3 μ L of the solution were injected into a Chiralpak IA column (0.46 \times 25 cm; Daicel Chemical

Industries Ltd) at 16 °C (CTO-20AC oven from Shimadzu). The atropisomers were eluted with a mixture of *n*-hexane/*i*PrOH = 98:2 at a flow rate of 1 mL min⁻¹ (LC-20AT HPLC from Shimadzu). For detection of the chromatogram a diodearray UV/Vis detector (SPD-M10A VP from Shimadzu) was used. The column was preconditioned overnight and kept under a flow of 0.1 mL min⁻¹ between measurements. Before each run the column was equilibrated for 30 min. After passing the UV/Vis detector the corresponding enantiomer was directly collected into a cuvette (Hellma 10 mm QS 1400 μL) containing 300 μL of the eluent mixture and immediately subjected to CD measurement. CD measurements were performed on a Chirascan CD Spectrometer while controlling the temperature with a Series 800 Thermoelectric Cooler (Alpha Omega Instruments Inc.). CD decay was measured at Δε_{max} (λ = 246 nm) with a bandwidth of 1 nm, a measuring time of 2 s per point, appropriately timed intervals between each data point measured (5 °C = 1200 s, 10 °C = 600 s, 15 °C = 300 s, 20 °C = 150 s, 25 °C = 90 s, 30 °C = 60 s, 35 °C = 30 s and 40 °C = 20 s, respectively) and a set of 50 repetitions for each temperature. Three eluted samples were measured for each temperature. The forward rate constants were obtained by plotting the logarithm of the CD decay against time. The thermodynamic data were deduced from an Eyring plot similar to the dynamic HPLC measurements.

III Results and discussion

A. DFT results: reaction path, transition state structures and activation energy for atropisomerization

The atropisomerization mechanism of the various butyl-bridged biphenyl cyclophanes was studied in detail using quantum chemical calculations. We considered all symmetrically substituted biphenyls, that is, all compounds listed in Fig. 1 except for the push-pull system **1i**. In the following, we describe our established reaction path, the relevant structures within this path and the calculation of the thermodynamic data.

Our attempts to locate the transition state for the atropisomerization process started with a *C_s* symmetric structure for X = H, similar to the transition state we found for the smaller propyl-bridged compound, see Fig. 2. However, in case of the butyl-bridged system, this structure represents not a first order but a second order saddle point with two imaginary frequencies. These are combinations of the rotation about the phenyl-phenyl bond and the rotation about the central CH₂-CH₂ bond in the butyl bridge, which both occur at the same time. Distortions of this geometry finally yielded two transition state structures where either the rotation about the phenyl-phenyl bond or the rotation about the central bond in the butyl bridge takes place first.

The complete reaction profile is illustrated in Fig. 3, together with the optimized geometries of the relevant species in the reaction path. We found that the flexibility of the butyl bridge allows for two conformational isomers A and B. The energetically more stable conformer A exhibits *C₂* symmetry and is connected to B *via* a *C₂* symmetric transition state, TS1. The isomerization

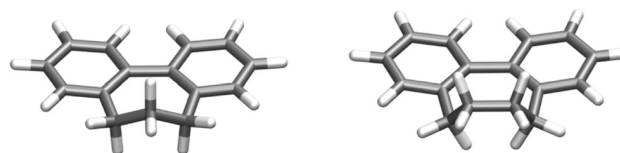


Fig. 2 *C_s* symmetric first order saddle point for the propyl-bridged biphenyl (X = H) and *C_s* symmetric second order saddle point for the butyl-bridged biphenyl (X = H).

reaction eventually takes place between conformer B and its enantiomer. The corresponding transition state TS2 can adapt two chiral structures (TS2-a and TS2-b) and involves both the rotation of the phenyl rings as well as the rotation of the central CH₂ units in the butyl bridge. The shown reaction profile is also valid for the other investigated compounds (X ≠ H) which revealed very similar stationary points.

Several structural parameters are affected along the reaction coordinate going from A to TS2. With respect to the activation barrier of isomerization, the torsion angle between the phenyl rings and the length of the central phenyl-phenyl bond are of particular interest. While for A, B and TS1 the torsion angle amounts to about 60°, it is reduced to 15° in TS2. The bond between the two phenyl rings is elongated from 149 pm (A, B, TS1) to about 153 pm (TS2).

In order to compute thermodynamic data for the isomerization process, it is important to understand how the various species in the reaction path contribute to the reaction rate. Here it is helpful to have a closer look at the relative energies of A, B, TS1 and TS2 (we use zero-point vibrational energy corrected electronic energies at the TPSS level, see also Fig. 3). Using conformer A as the reference, conformer B is about 14 kJ mol⁻¹ higher in energy. The relative energy of TS1 amounts to 31 kJ mol⁻¹ while the one for TS2 is roughly 90 kJ mol⁻¹.

According to these values, we proceed as follows:

- The barrier for atropisomerization (TS2) is about three times higher than the barrier for the interconversion of the reactants (TS1). Thus, the reaction rate for atropisomerization is not affected by the transition state between the conformers A and B.

- The contribution of several reactant conformers to the reaction rate is usually accounted for by weighting with a Boltzmann factor. In our case, the contribution of conformer B is very small and we therefore neglect it.

- The chiral structures for TS2 contribute to the reaction rate with a factor of 2. We account for this by an additional contribution of *R* ln 2 to the activation entropy.

Hence, only the electronic energies and partition functions of conformer A and transition state TS2 are needed for the computation of the activation barrier. The obtained results are summarized in Table 1 where we give the Gibbs free activation energies as well as the enthalpic and entropic contributions.

The Gibbs free activation energies Δ*G*_{theo}[‡] range between 84–93 kJ mol⁻¹ for the TPSS functional and 94–102 kJ mol⁻¹ for the B3LYP functional. Similar trends are observed regarding the dependence of the barrier height on the different substituents.

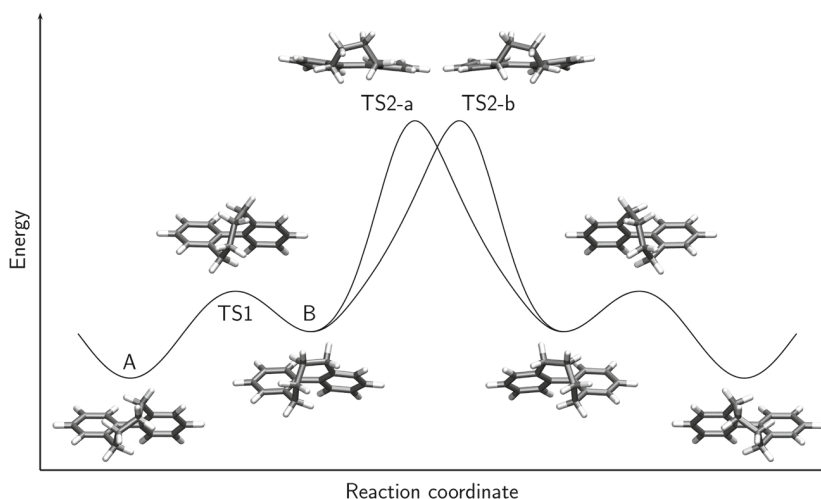


Fig. 3 Scheme of the calculated atropisomerization mechanism.

Table 1 Calculated Gibbs free activation energies $\Delta G_{\text{theo}}^{\ddagger}$ for the rotation of the butyl-bridged biphenyls. The contributions of the enthalpy ($\Delta H_{\text{theo}}^{\ddagger}$) and entropy ($\Delta S_{\text{theo}}^{\ddagger}$) are also given. Values for $\Delta G_{\text{theo}}^{\ddagger}$ and $\Delta H_{\text{theo}}^{\ddagger}$ are given in kJ mol^{-1} , values for $\Delta S_{\text{theo}}^{\ddagger}$ are given in $\text{J mol}^{-1} \text{K}^{-1}$

Compound	X	$\Delta G_{\text{TPSS}}^{\ddagger}$	$\Delta H_{\text{TPSS}}^{\ddagger}$	$\Delta S_{\text{TPSS}}^{\ddagger}$	$\Delta G_{\text{B3LYP}}^{\ddagger}$	$\Delta H_{\text{B3LYP}}^{\ddagger}$	$\Delta S_{\text{B3LYP}}^{\ddagger}$
1a	NO ₂	92.8	90.4	-7.9	101.9	99.9	-6.7
1b	CN	91.0	88.7	-7.6	100.5	98.7	-6.1
1c	NC	90.8	88.6	-7.5	100.1	98.3	-6.0
1d	SAc	93.1	90.4	-9.0	101.7	100.4	-4.0
1e	Br	91.0	88.7	-8.0	100.3	98.3	-6.5
1f	Cl	90.9	88.7	-7.6	100.1	98.3	-6.1
1g	F	92.9	90.8	-7.2	102.0	100.3	-5.8
1h	H	92.6	90.5	-7.1	101.8	100.1	-5.6
1j	OMe	88.6	86.2	-7.7	97.8	95.9	-6.3
1k	NH ₂	86.7	84.3	-8.1	96.3	94.3	-6.5
1l	pip	84.0	82.5	-5.3	94.5	93.2	-4.4

We find that the size of $\Delta G_{\text{theo}}^{\ddagger}$ is almost exclusively determined by the enthalpic contribution, $\Delta H_{\text{theo}}^{\ddagger}$ (>97%). $\Delta S_{\text{theo}}^{\ddagger}$ is negative but of very small magnitude for all compounds. Overall, both functionals give similar results, the values for B3LYP are just slightly shifted towards larger energies compared to TPSS.

B. HPLC results: rate constants and thermodynamic data

In previous studies of Rotzler *et al.*, dynamic HPLC has proven to be an ideal method to estimate the rotation barrier about the central C–C bond of push–pull cyclophane **1i**.¹⁸ Hence, temperature dependent HPLC measurements were performed in order to evaluate the racemization process also of compounds other than **1i**. For **1a**, **1b**, **1d**, **1j** and **1l**, the chromatography was successfully accomplished on a coated chiral amylose derived Chiralpak AD-H column eluting with iPrOH–*n*-hexane mixtures. For all compounds, temperature dependent plateau formation was observed ranging from nearly separated peaks (**1b** and **1d** at 15 °C) to peak profiles close to coalescence (**1l** at 35 °C), see Fig. 4. The separation of less polar derivatives like halogen substituted butyl-bridged biphenyls was attempted but failed, even when tried on a variety of differently coated columns.

The rate constants of atropisomerization were directly calculated using the software DCXplorer. The program is based on the unified equation derived by Trapp from the theoretical plate model.^{29,37} Within this model the column is divided into small plates where each plate is considered as a chemical reactor (Fig. 5) in which three basic steps are performed: (1) establishment of the distribution equilibrium of A and B between the mobile and the stationary phase, (2) reversible first-order enantiomerization of A and B in both phases, and (3) shifting of the mobile phase to the next theoretical plate. The statistical description of the theoretical plate model led to the development of the stochastic model³⁸ which allows much faster simulation of elution profiles. However, it is not possible to differentiate between the rate constants in the mobile and stationary phase from a single elution profile of a dynamic chromatographic experiment. Only apparent rate constants k_1^{app} which are weighted means of the reaction rate constants of the mobile and stationary phase, k_1^{mob} and k_1^{stat} , are obtained. The unified equation allows the determination of the apparent forward rate constant from the retention times of the two enantiomers, the peak widths at half-height, the height of the plateau, and the number of theoretical plates.²⁹

The obtained rate constants using DCXplorer are summarized in Table 2 for all investigated compounds and a series of five different temperatures. Note that each rate constant represents the averaged value of four repeated measurements. Using these values, the Gibbs free energy of atropisomerization was calculated according to the Eyring equation

$$k_1 = \frac{k_B T}{h} \exp\left\{-\frac{\Delta G^{\ddagger}}{RT}\right\} = \frac{k_B T}{h} \exp\left\{-\frac{\Delta H^{\ddagger}}{RT} + \frac{\Delta S^{\ddagger}}{R}\right\} \quad (1)$$

by plotting $R \ln\left(\frac{k_1 h}{k_B T}\right)$ against $1/T$ (R is the gas constant, h Planck's constant, and k_B Boltzmann's constant). The enthalpy ΔH^{\ddagger} is obtained from the slope and the entropy ΔS^{\ddagger} from the intercept of a linear regression analysis. The resulting thermodynamic data for the investigated biphenyl compounds are

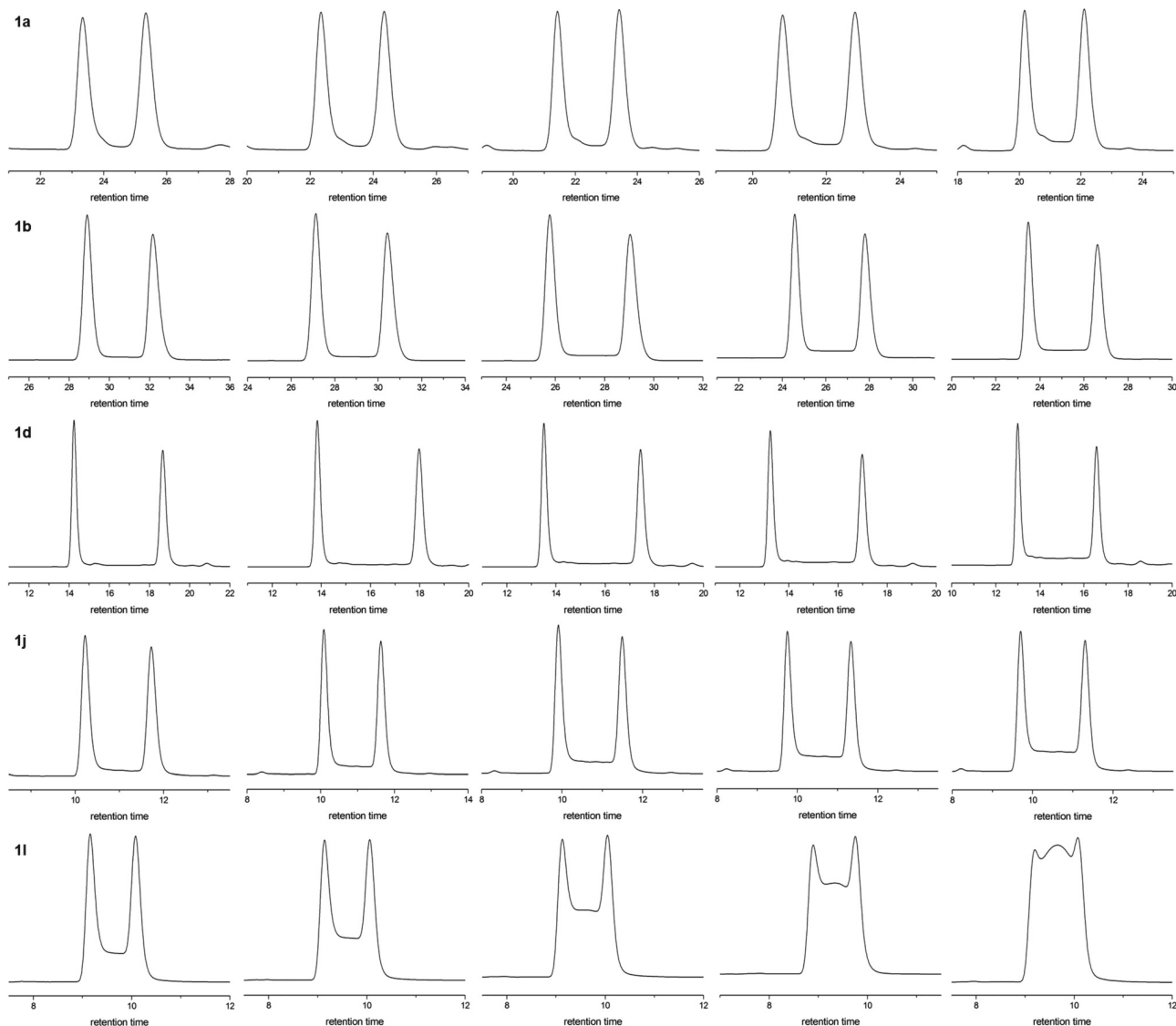


Fig. 4 Elution profiles of compounds **1a**, **1b**, **1d**, **1j** and **1l** on an amylose derived Chiralpak AD-H column between 15 °C and 35 °C in 5 °C steps (left to right).

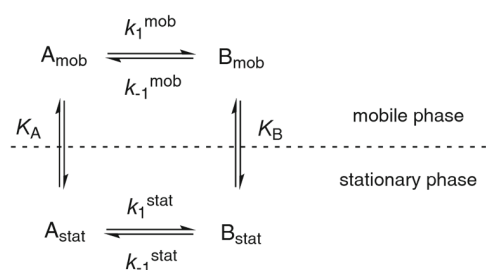


Fig. 5 Equilibrium in a chromatographic theoretical plate. A is the first eluted compound, B the second eluted compound, k_1 and k_{-1} represent the forward and backward reaction rate constants in the mobile phase (mob) and stationary phase (stat), and K denotes the distribution constant.²⁹ Reprinted from Trapp.

summarized in Table 3 (the values for the push-pull system **1l** were taken from the previous work of Rotzler *et al.*¹⁸). Statistical errors were obtained by assuming an error in the temperature

of 1 K and an error in the rate constant of 5% (same procedure as described in the electronic supplementary material to ref. 20, pages 12–13).

We find that the experimentally determined Gibbs free activation energies (at 298.15 K) range from 89 to 97 kJ mol⁻¹. $\Delta H_{\text{HPLC}}^\ddagger$ roughly amounts to 50 kJ mol⁻¹ while the activation entropy $\Delta S_{\text{HPLC}}^\ddagger$ takes large negative values of about -150 J mol⁻¹ K⁻¹. This means that the activation enthalpy and the activation entropy virtually contribute to the same extent to $\Delta G_{\text{HPLC}}^\ddagger$ (50% each).

C. Discussion and comparison of quantum chemical and experimental HPLC data

The computationally determined Gibbs free activation energies $\Delta G_{\text{theo}}^\ddagger$ for the atropisomerization of substituted butyl-bridged biphenyls range between 84–93 kJ mol⁻¹ for TPSS and 94–102 kJ mol⁻¹ for B3LYP (see Table 1). When we compare these values with the inversion barriers of the propyl-bridged

Table 2 Rate constants k_1^{app} of the enantiomerization process between 15 °C and 35 °C as calculated with the DCXplorer software. All values are given in s^{-1}

Compound	X	308 K	303 K	298 K	293 K	288 K
1a	NO ₂	1.448×10^{-4}	9.85×10^{-5}	8.27×10^{-5}	6.06×10^{-5}	2.61×10^{-5}
1b	CN	1.658×10^{-4}	1.194×10^{-4}	9.00×10^{-5}	5.74×10^{-5}	3.86×10^{-5}
1d	SAc	3.621×10^{-4}	2.677×10^{-4}	1.898×10^{-4}	1.326×10^{-4}	8.93×10^{-5}
1j	OMe	8.038×10^{-4}	6.041×10^{-4}	4.417×10^{-4}	3.083×10^{-4}	2.217×10^{-4}
1l	pip	2.254×10^{-3}	1.810×10^{-3}	1.297×10^{-3}	9.080×10^{-4}	6.887×10^{-4}

Table 3 Thermodynamic data of the experimentally investigated butyl-bridged biphenyls for 298 K. The values are calculated from the kinetic data obtained by temperature dependent HPLC measurements

Compound	X	$\Delta G_{\text{HPLC}}^{\ddagger}/\text{kJ mol}^{-1}$	$\Delta H_{\text{HPLC}}^{\ddagger}/\text{kJ mol}^{-1}$	$\Delta S_{\text{HPLC}}^{\ddagger}/\text{J mol}^{-1} \text{K}^{-1}$
1a	NO ₂	96.6 ± 0.1	55.5 ± 4.5	-138 ± 15
1b	CN	96.2 ± 0.1	51.4 ± 4.3	-150 ± 14
1d	SAc	94.3 ± 0.1	49.2 ± 4.1	-151 ± 14
1i^a	push-pull	90.3 ± 0.2	54.7 ± 6.1	-120 ± 21
1j	OMe	92.2 ± 0.1	45.5 ± 3.9	-157 ± 13
1l	pip	89.5 ± 0.1	42.7 ± 3.8	-157 ± 13

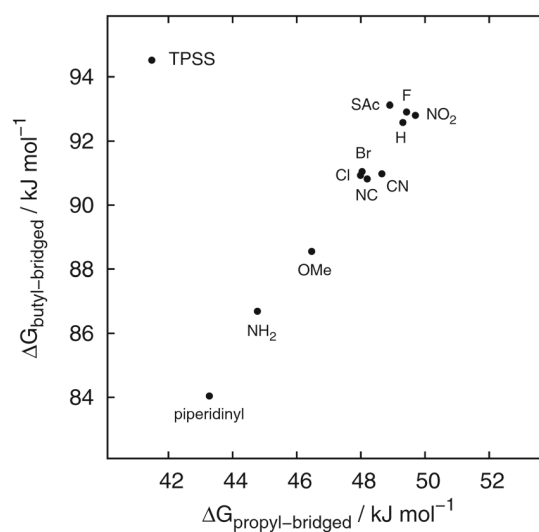
^a From 4 rate constants of ref. 18.

biphenyls ($43\text{--}50 \text{ kJ mol}^{-1}$ for TPSS and $46\text{--}52 \text{ kJ mol}^{-1}$ for B3LYP, see ref. 20) and the unbridged biphenyl ($<10 \text{ kJ mol}^{-1}$), we notice a distinct increase of the atropisomerization energy. In order to understand the reasons for the entirely different barrier heights we first analyze the contributions of the activation enthalpy $\Delta H_{\text{theo}}^{\ddagger}$ and the activation entropy $\Delta S_{\text{theo}}^{\ddagger}$ to $\Delta G_{\text{theo}}^{\ddagger}$. According to Table 1, the main contribution for the butyl-bridged systems comes from $\Delta H_{\text{theo}}^{\ddagger}$ while $\Delta S_{\text{theo}}^{\ddagger}$ plays only a minor role. The same holds for the smaller biphenyls where we found the entropic contribution to be negligible.²⁰ This is insofar not surprising as we consider a unimolecular reaction and changes in the entropy only arise from small changes in the rotational and vibrational partition functions and/or multiple reactant conformers and transition state structures. The increase of the atropisomerization barrier $\Delta G_{\text{theo}}^{\ddagger}$ in the series unbridged-propyl-bridged-butyl-bridged is thus mainly due to an increase in $\Delta H_{\text{theo}}^{\ddagger}$.

The different barrier heights can be explained with the degree of unfavourable structural distortions in the respective transition states. For the propyl-bridged system, the phenyl rings are coplanar in the transition state as for the unbridged biphenyl. Due to the space requirements of the bridge they are however not perfectly linear but slightly bent towards the unbridged side. In the butyl-bridged system, the phenyl rings are distorted from being coplanar in the transition state (the coplanar structure represents a second order saddle point, see above). Additionally, the phenyl rings themselves are puckered and the bonds towards the butyl bridge are slightly out of plane. As can be seen in Fig. 3, the hydrogen atoms of the *ortho* CH₂ groups in the butyl bridge pass each other in the transition state. The distance between them is very small (about 184 pm) and even shorter than for the propyl-bridged biphenyls (about 228 pm, see also Fig. 2). We therefore suggest that structural modifications at this position of the butyl bridge provide the possibility to further increase the atropisomerization barrier.

The size of $\Delta G_{\text{theo}}^{\ddagger}$ is also dependent on the substituents in *para* position. However this effect is small compared to the

influence of the alkyl bridge. For the electron donor substituted compounds **1j**, **1k** and **1l** lower $\Delta G_{\text{theo}}^{\ddagger}$ values than for the acceptor substituted systems are observed. In case of electron donor substituents the electron density at the phenyl-phenyl bond is increased leading to a slightly shorter bond distance than in case of electron acceptor substituents. This is due to the small torsion angle between the phenyl rings in the transition state (about 15°) which enables a larger extent of communication between the two individual π systems. For large torsion angles, as for example in TS1 (about 60°), no influence of the substituents is observed. A comparison between the computed activation barriers for the propyl- and butyl-bridged biphenyls is shown in Fig. 6 for the TPSS functional. We find a linear correlation ($R^2 = 0.97$) with a slope of 1.38 meaning that the effect of the substituents is of the same type and of similar size

**Fig. 6** Comparison of computed rotation barriers for the propyl-bridged and butyl-bridged systems. The values for the propyl-bridged systems were taken from ref. 20.

in both systems. For B3LYP, an analogous plot is obtained, with the values being shifted towards higher energies.

The Gibbs free activation energies for the butyl-bridged biphenyls determined with temperature dependent HPLC experiments range from 89 to 97 kJ mol⁻¹ (Table 3). These values are approximately twice as large as for the propyl-bridged systems which we have previously studied with NMR coalescence measurements, and for which inversion barriers of 44 to 55 kJ mol⁻¹ were obtained.²⁰ To gain more insight, we had a look at the contributions of the activation enthalpy and the activation entropy to $\Delta G_{\text{HPLC}}^\ddagger$. We find that $\Delta H_{\text{HPLC}}^\ddagger$ and $\Delta S_{\text{HPLC}}^\ddagger$ seem to contribute nearly equally to $\Delta G_{\text{HPLC}}^\ddagger$ for the butyl-bridged systems. This is significantly different from the propyl-bridged systems where the activation barrier is mainly determined by the enthalpic part. Moreover, the comparison between the propyl-bridged and butyl-bridged biphenyls shows that the experimental values for ΔH^\ddagger are very similar. If correct, this implies that the larger Gibbs free activation energy for the butyl-bridged systems is almost exclusively caused by changes in the entropy.

The size of $\Delta G_{\text{HPLC}}^\ddagger$ varies with the substituents in *para* position of the phenyl rings. For the donor substituted compounds **1j** and **1l** as well as for the push-pull system **1i**, lower $\Delta G_{\text{HPLC}}^\ddagger$ values than for the acceptor substituted systems are observed. This can also be seen in Fig. 7, where we have plotted the $\Delta G_{\text{HPLC}}^\ddagger$ values for the butyl-bridged system against the values for the smaller propyl-bridged system from our earlier work.²⁰ Again, we obtain a linear correlation with respect to the bridge length ($R^2 = 0.95$) with a slope of 0.81. Thus, the influence of the substituents is of similar type for both biphenyl systems.

The computed and experimental ΔG^\ddagger values for the butyl-bridged biphenyls investigated in this work are of similar size and about twice as large as for the propyl-bridged biphenyls. In both cases, similar trends for the dependence of the barrier

height on the substitution with electron donors or electron acceptors in *para* position are obtained. This is in compliance with our previous studies for the propyl-bridged systems where an equally good agreement for computed and experimental Gibbs free activation energies has been found.

The contributions of the activation enthalpy ΔH^\ddagger and the activation entropy ΔS^\ddagger however, show large discrepancies between the computationally and experimentally determined values. While the calculated values $\Delta S_{\text{theo}}^\ddagger$ are in the range of $-10 \text{ J mol}^{-1} \text{ K}^{-1}$, the extrapolation of the experimental data yields values of about $-150 \text{ J mol}^{-1} \text{ K}^{-1}$. Consequently, $\Delta H_{\text{theo}}^\ddagger$ appears to be much larger than $\Delta H_{\text{HPLC}}^\ddagger$. How can this remarkable difference be explained?

We started by critically assessing several approximations we made for the quantum chemical calculation of the thermodynamic data. We used rigid rotor and harmonic oscillator approximations for the evaluation of the partition functions, while neglecting the contribution of conformer B and any solvation effects. For the given reaction all of these approximations seem justified and should not introduce errors of the given magnitude – especially as we benefit from error cancellations when evaluating the difference between the minimum energy structure and the transition state. In particular, the electronic contribution which mainly constitutes the value of ΔH^\ddagger is expected to be described reasonably well by density functional theory calculations. From our previous work on propyl-bridged biphenyls, which were investigated with NMR coalescence measurements, we furthermore conclude that solvent effects contribute only marginally.

We therefore reason that the experimental determination of the enthalpy and entropy contributions using HPLC is susceptible to errors while the Gibbs free activation energy can be obtained with much higher accuracy. Several arguments support this reasoning. First, the obtained experimental values for $\Delta S_{\text{HPLC}}^\ddagger$ are in the order of an entropy decrease typically found for a bond formation. Similar values have been observed by Bringmann *et al.*³⁹ for the atropisomerization of biaryl lactones but only for the cases where the reaction indeed involves a bond formation (chemically induced atropisomerization instead of physical rotation). Such a process can definitely be ruled out for the systems investigated in this work. Second, the experimentally obtained $\Delta H_{\text{HPLC}}^\ddagger$ values are of the same size as the values obtained for the smaller propyl-bridged system. This implies that the larger Gibbs free activation energy is exclusively caused by entropy loss in the transition state. The previously discussed additional structural distortions in the transition state of the butyl-bridged system contradict this statement. Third, it has been shown that the method used for modelling the elution profiles (here as implemented in the DCXplorer software) can lead to large discrepancies in the contributions of ΔH^\ddagger and ΔS^\ddagger while the value of ΔG^\ddagger stays the same.⁴⁰ We expect that this is even more pronounced when the HPLC measurements are conducted in a very small temperature range. The extrapolation based on the Eyring equation will then only give reliable results for ΔG^\ddagger while the determination of ΔH^\ddagger and ΔS^\ddagger may suffer from large errors.

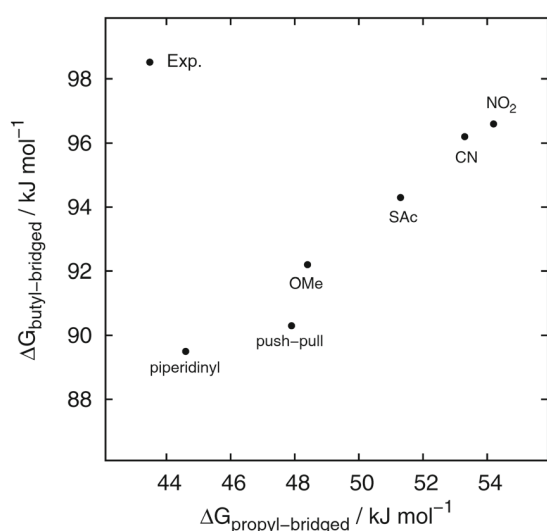


Fig. 7 Comparison of experimental rotation barriers for the propyl-bridged and butyl-bridged systems. The values for the propyl-bridged systems were taken from ref. 20.

D. CD results and discussion

In order to better understand the above-mentioned discrepancies, we searched for a different experimental method to determine the forward rate constant and consequently the thermodynamic data. We found that a straightforward way would be to measure the decay of the CD signal of an isolated enantiomer, which delivers the rate constant in solution directly. This method is challenging however, as it requires the separation of the enantiomers right before each measurement. From the set of compounds investigated with HPLC, the dimethoxy derivative **1j** is most convenient for subsequent CD measurements: the separation is good at low temperatures and the retention times are reasonably short (see Fig. 4). We therefore decided to choose **1j** for a series of CD measurements in an extended temperature range compared to the HPLC measurements.

For eight different temperatures (about 5, 10, 15, 20, 25, 30, 35, and 40 °C), three independent measurements of the CD signal $C(t)$ as a function of time t were performed. Each measurement was evaluated by plotting $\ln(C(t)/C(0))$ against time, yielding a value for the rate constant k together with its standard deviation σ_k derived from a linear-regression approach (note that the slope of the straight line yields $-2k$). Since the (nearly constant) temperature was recorded during each measurement, we also determined the average temperature T together with its standard deviation σ_T . Using these values, we computed the quantities $x = 1/T$ and $y = R \ln\left(\frac{hk}{k_B T}\right)$ with corresponding standard deviations σ_x and σ_y . Each set of three x and y values was further used to determine the weighted averages \bar{x} , \bar{y} , $\sigma_{\bar{x}}$, and $\sigma_{\bar{y}}$ (using σ_x and σ_y to assign the weights). We finally obtained ΔH^\ddagger and ΔS^\ddagger from an Eyring plot of \bar{y} against \bar{x} by means of fitting a straight-line model to data with errors in both coordinates using the program fitexy of ref. 41. Mean values for ΔH^\ddagger and ΔS^\ddagger and their standard deviations were computed from 2500 fits in which the data were randomly distributed according to $\sigma_{\bar{x}}$ and $\sigma_{\bar{y}}$. Fig. 8 shows data points of 200 of these fits, together with the $8 \times 3 = 24$ original measurements. The final results for **1j** (with one standard deviation as error bar) obtained from the above evaluation are:

$$\Delta G_{\text{CD}}^\ddagger = 95.1 \pm 0.1 \text{ kJ mol}^{-1}$$

$$\Delta H_{\text{CD}}^\ddagger = 88.0 \pm 1.9 \text{ kJ mol}^{-1}$$

$$\Delta S_{\text{CD}}^\ddagger = -24 \pm 7 \text{ J mol}^{-1} \text{ K}^{-1}$$

The value for the Gibbs free activation energy compares nicely with the values from the HPLC experiment (92.2 kJ mol^{-1}) and the quantum chemical calculations (88.6 kJ mol^{-1} for TPSS and 97.8 kJ mol^{-1} for B3LYP). The main contribution to $\Delta G_{\text{CD}}^\ddagger$ is given through $\Delta H_{\text{CD}}^\ddagger$ (more than 92%) while $\Delta S_{\text{CD}}^\ddagger$ is rather small. This result supports the outcome from the quantum chemical calculations and corroborates our reasoning regarding the HPLC results for ΔH^\ddagger and ΔS^\ddagger .

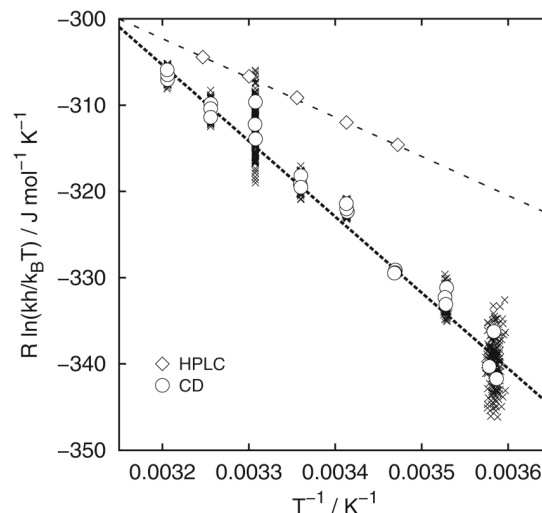


Fig. 8 Eyring plot of the kinetic data obtained via CD spectroscopic measurements (○) for compound **1j**. Concerning the randomly generated data points (×), see text for further details. For comparison, the kinetic data obtained via HPLC measurements (◇) for compound **1j** are also included.

IV Summary and conclusions

In summary, we presented a systematic study of the atropisomerization process of *para*-substituted butyl-bridged biphenyls. The reaction pathway including minimum and transition state structures was established using density functional theory calculations. Gibbs free activation energies computed for this pathway mutually agree with experimental values obtained via temperature dependent HPLC measurements. Comparison with the previously studied propyl-bridged biphenyls revealed that increasing the bridge length has a larger effect on the inversion barrier than the different substituents in *para* position. Based on the structure of the transition state we predict a further increase of the barrier height upon modifications of the butyl bridge.

Large discrepancies between computationally and experimentally determined contributions of the activation enthalpy ΔH^\ddagger and entropy ΔS^\ddagger were found. The careful analysis of the data and their acquisition led us to the conclusion that both the modelling of the elution profiles in order to obtain rate constants as well as the extrapolation procedure used for the Eyring plot may lead to large errors in the enthalpic and entropic contributions while the error for the Gibbs free activation energy remains small. This reasoning is supported by detailed, solution based dynamic CD measurements. Dynamic HPLC therefore represents a valuable tool to access ΔG^\ddagger , however we recommend to be cautious when determining values of ΔH^\ddagger and ΔS^\ddagger .

Acknowledgements

We are grateful to the Bundesministerium für Bildung und Forschung (BMBF) through the Helmholtz Research Programme “Science and Technology of Nanosystems”.

References

- 1 J. Wang, G. Cooper, D. Tulumello and A. P. Hitchcock, *J. Phys. Chem. A*, 2005, **109**, 10886.
- 2 L. Venkataraman, J. E. Klare, C. Nuckolls, M. S. Hybertsen and M. L. Steigerwald, *Nature*, 2006, **442**, 904.
- 3 D. Vonlanthen, A. Mishchenko, M. Elbing, M. Neuburger, T. Wandlowski and M. Mayor, *Angew. Chem., Int. Ed.*, 2009, **48**, 8886.
- 4 K. Mikami, T. Korenaga, M. Terada, T. Ohkuma, T. Pham and R. Noyori, *Angew. Chem., Int. Ed.*, 1999, **38**, 495.
- 5 S. Lee, M. Jørgensen and J. F. Hartwig, *Org. Lett.*, 2001, **3**, 2729.
- 6 E. R. Strieter, D. G. Blackmond and S. L. Buchwald, *J. Am. Chem. Soc.*, 2003, **125**, 13978.
- 7 G. Haberhauer, C. Tepper, C. Wölper and D. Bläser, *Eur. J. Org. Chem.*, 2013, 2325.
- 8 G. Bringmann, A. J. Price Mortimer, P. A. Keller, M. J. Gresser, J. Garner and M. Breuning, *Angew. Chem., Int. Ed.*, 2005, **44**, 5384.
- 9 F. Ceccacci, G. Mancini, P. Mencarelli and C. Villani, *Tetrahedron: Asymmetry*, 2003, **14**, 3117.
- 10 D. Casarini, L. Lunazzi, M. Mancinelli, A. Mazzanti and C. Rosini, *J. Org. Chem.*, 2007, **72**, 7667.
- 11 R. Ruzziconi, S. Spizzichino, A. Mazzanti, L. Lunazzi and M. Schlosser, *Org. Biomol. Chem.*, 2010, **8**, 4463.
- 12 L. Lunazzi, M. Mancinelli, A. Mazzanti, S. Lepri, R. Ruzziconi and M. Schlosser, *Org. Biomol. Chem.*, 2012, **10**, 1847.
- 13 M. P. Johansson and J. Olsen, *J. Chem. Theory Comput.*, 2008, **4**, 1460.
- 14 E. Masson, *Org. Biomol. Chem.*, 2013, **11**, 2859.
- 15 M. Oki, H. Iwamura and G. Yamamoto, *Bull. Chem. Soc. Jpn.*, 1971, **44**, 262.
- 16 K. Ohkata, R. L. Paquette and L. A. Paquette, *J. Am. Chem. Soc.*, 1979, **101**, 6687.
- 17 R. B. Bates, F. A. Camou, V. Kane, P. K. Mishra, K. Suvannachut and J. J. White, *J. Org. Chem.*, 1989, **54**, 311.
- 18 J. Rotzler, H. Gsellinger, M. Neuburger, D. Vonlanthen, D. Häussinger and M. Mayor, *Org. Biomol. Chem.*, 2011, **9**, 86.
- 19 D. Vonlanthen, A. Rudnev, A. Mishchenko, A. Käslin, J. Rotzler, M. Neuburger, T. Wandlowski and M. Mayor, *Chem. – Eur. J.*, 2011, **17**, 7236.
- 20 J. Rotzler, H. Gsellinger, A. Bihlmeier, M. Gantenbein, D. Vonlanthen, D. Häussinger, W. Klopffer and M. Mayor, *Org. Biomol. Chem.*, 2013, **11**, 110.
- 21 *Turbomole Version 6.3*, Program Package for ab initio Electronic Structure Calculations, a development of University of Karlsruhe and Forschungszentrum Karlsruhe GmbH 1989–2007, Turbomole GmbH, 2007, <http://www.turbomole.com>.
- 22 J. Tao, J. P. Perdew, V. N. Staroverov and G. E. Scuseria, *Phys. Rev. Lett.*, 2003, **91**, 146401.
- 23 A. D. Becke, *J. Chem. Phys.*, 1993, **98**, 5648.
- 24 F. Weigend and R. Ahlrichs, *Phys. Chem. Chem. Phys.*, 2005, **7**, 3297.
- 25 O. Treutler and R. Ahlrichs, *J. Chem. Phys.*, 1995, **102**, 346.
- 26 A. P. Scott and L. Radom, *J. Phys. Chem.*, 1996, **100**, 16502.
- 27 J. Rotzler, D. Vonlanthen, A. Barsella, A. Boeglin, A. Fort and M. Mayor, *Eur. J. Org. Chem.*, 2010, 1096.
- 28 K. R. Reddy, C. U. Maheswari, M. Venkateshwar and M. L. Kantam, *Adv. Synth. Catal.*, 2009, **351**, 93.
- 29 O. Trapp, *Anal. Chem.*, 2006, **78**, 189.
- 30 O. Trapp, *J. Chromatogr. B: Anal. Technol. Biomed. Life Sci.*, 2008, **875**, 42.
- 31 M. Watanabe, H. Suzuki, Y. Tanaka, T. Ishida, T. Oshikawa and A. Tori-i, *J. Org. Chem.*, 2004, **69**, 7794.
- 32 T. Benincori, A. Marchesi, T. Pilati, A. Ponti, S. Rizzo and F. Sannicolò, *Chem. – Eur. J.*, 2009, **15**, 94.
- 33 S. Ando, E. Ohta, A. Kosaka, D. Hashizume, H. Koshino, T. Fukushima and T. Aida, *J. Am. Chem. Soc.*, 2012, **134**, 11084.
- 34 H. Saito, T. Mori, Y. Origane, T. Wada and Y. Inoue, *Chirality*, 2008, **20**, 278.
- 35 P. Osswald and F. Würthner, *J. Am. Chem. Soc.*, 2007, **129**, 14319.
- 36 L. Lunazzi, M. Mancinelli, A. Mazzanti and M. Pierini, *J. Org. Chem.*, 2010, **75**, 5927.
- 37 O. Trapp, *Chirality*, 2006, **18**, 489.
- 38 J. Veciana and M. I. Crespo, *Angew. Chem., Int. Ed. Engl.*, 1991, **30**, 74.
- 39 G. Bringmann, M. Heubes, M. Breuning, L. Göbel, M. Ochse, B. Schöner and O. Schupp, *J. Org. Chem.*, 2000, **65**, 722.
- 40 G. Uray, S. Jahangir and W. M. Fabian, *J. Chromatogr. A*, 2010, **1217**, 1017.
- 41 W. H. Press, S. A. Teukolsky, W. T. Vetterling and B. P. Flannery, *Numerical Recipes in Fortran 77, The Art of Scientific Computing*, Cambridge University Press, Cambridge, 2nd edn, 2001.

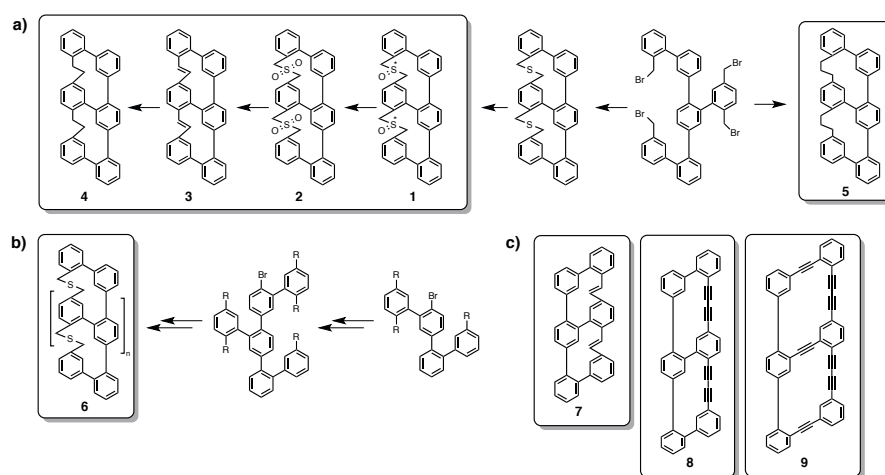
Conclusion and Outlook

As demonstrated with this thesis, it is possible to induce helical chirality by using a ladder-type arrangement. The deliberate mismatch in length is compensated by rotation of the longer rail around the shorter, giving rise to a helical bannister structure. Due to a relay located at the intersections of the longer oligomer, the sense of twist is communicated across the entire structure, giving exclusively enantiomeric helices (*M/P*).

A realization of the concept was demonstrated using a hexaphenylic oligomer. The shorter rail consists of a terphenylic rod, while the longer oligomer contains three phenyl rings that are bridged by two benzylic ethers. The rails are interlinked by aryl-aryl bonds. After an elaborate synthesis, the structure was elucidated by conventional analysis including

X-Ray diffraction analysis of a single racemic crystal confirming the uniform helical configuration and revealing an end-to-end twist of 147°. Upon exchanging the heteroatom (O to S) torsions up to 178°

were achieved. HPLC using a chiral stationary phase allowed to separate the enantiomers and confirm their identity by Circular Dichroism measurements. Calculations based on the single crystal structures allowed to assign the absolute stereoconfiguration. Subsequently the racemization dynamics of the pure enantiomers was studied by Circular Dichroism decay measurements. The racemization barrier was determined to be in the range of other bannister systems (about 97 kJ mol⁻¹ at 25°C) which could be influenced by the nature of the heteroatom (O, S or Se) or the configuration of the relay. Racemization proceeded without any observable intermediates (chiral or achiral).



Future prospects. **a)** Upon sulfur oxidation a subset of structures can be achieved: (1) Sulfoxides with additional stereocenters, (2) sulfones providing additional steric bulk on the bridge, that can be extruded with heat and base (3) leading to a tighter, all carbon derivative. (4) Hydrogenation yields a more flexible alkyl derivative. The tetrabromo precursor allows also the direct access to the all-carbon analogue (5) with identical ring sizes as published. **b)** Using existing building blocks, elongation is possible (6) – either discretely or by using polymerization techniques. **c)** (7) - (9) Possible structures showing extended conjugation as potential emitters of circular polarized light.

Indeed, no conformation except the expected helices was found in any of the studied model systems.

Accessing a total of five derivatives allowed to identify key features. I) The adopted helices are uniform and the only configuration the system adopts, even upon heating. II) Racemization is surprisingly fast with half lives of about 3-4 h at 25°C. III) The relay is important but its exact configuration is not, as the racemization barrier for the distorted helix is only marginally lower than its undistorted counterpart. IV) Sulfur is appealing as heteroatom due to its high reactivity in the macrocyclization and the stability of the analogue. V) Due to the insulating nature of the heteroalkyl linkages, the optical properties remain modest, besides strong Cotton effects.

With the obtained knowledge the project is now at an exciting stage. Three prospects are appealing. On the one

hand to improve the configurational stability of the helices to make them suitable in

material applications (chiral polymers for instance). Strategies and structures are presented in (a).

Especially sulfur is an ideal chemical platform to allow extrusion or incorporation of

additional stereocenters. Secondly, to obtain higher oligomers (b) with more stable helices and potentially useful material properties. A third prospect is to improve the optical properties by incorporation of conducting elements such as acetylenes, ideally to connect the π -systems of all rings to form an extended delocalized system (c). Such structures would be very appealing as emitters of circular polarized light (circular polarized luminescence). Other possible uses involve, but are not limited to, surface functionalization and investigation using scanning tunneling microscopy (STM).



Supporting Information

© Wiley-VCH 2014

69451 Weinheim, Germany

Inducing Axial Chirality in a “Geländer” Oligomer by Length Mismatch of the Oligomer Strands**

*Michel Rickhaus, Linda Maria Bannwart, Markus Neuburger, Heiko Gsellinger, Kaspar Zimmermann, Daniel Häussinger, and Marcel Mayor**

anie_201408424_sm_miscellaneous_information.pdf

Supporting Information

Table of Contents

Synthetic Procedures of structures (B)-(C), (4)-(11) and (1)	2
Crystal data for (1)	12
¹ H-, ¹³ C-NMR (CDCl ₃ , 400/101 MHz, 25 °C) of 4-bromo-3-iodoaniline	13
¹ H-, ¹³ C-NMR (CDCl ₃ , 400/101 MHz, 25 °C) and HR-ESI spectra of compound (4)	15
¹ H-, ¹³ C-NMR (CDCl ₃ , 400/101 MHz, 25 °C) and HR-ESI spectra of compound (5)	17
¹ H-, ¹³ C-NMR (CDCl ₃ , 400/101 MHz, 25 °C) and HR-ESI spectra of compound (6)	19
¹ H-, ¹³ C-NMR (CDCl ₃ , 400/101 MHz, 25 °C) and HR-ESI spectra of compound (7)	21
¹ H-, ¹³ C-NMR, HMBC (CDCl ₃ , 600/150 MHz, 25 °C) and HR-ESI spectra of compound (9)	23
¹ H-NMR, HMBC, HMQC (CDCl ₃ , 600/150 MHz, 25 °C) and HR-ESI spectra of compound (10)	26
¹ H-, ¹³ C-NMR, HMBC, HMQC (CDCl ₃ , 600/150 MHz, 25 °C) and HR-ESI spectra of compound (11)	29
¹ H-NMR (CDCl ₃ , 600 MHz, 25 °C) of enantiomer A of compound (1)	33
¹ H-NMR (CDCl ₃ , 600 MHz, 25 °C) of enantiomer B of compound (1)	33
¹ H-, ¹³ C-NMR, COSY, NOESY, HMBC, HMQC (CDCl ₃ , 600/150 MHz, 25 °C) and HR-ESI spectra of enantiomer A of compound (1) with full assignment	34
Measured CD decay at 222 nm of one enantiomer of (1) and linear regression of ln(θ) against t	41
Measured CD decay at 197 nm of one enantiomer of (1) and linear regression of ln(θ) against t	41
Determination of the rotation barrier of compound (1) at 222 nm	42
Δε and ε values of compound (1)	43

Synthetic Procedures of structures (B)-(C), (4)-(11) and (1)

General Procedures: All commercially available compounds were purchased and used as received unless explicitly stated otherwise. THF- d_8 was purchased from Acros. ^1H NMR was recorded on a Bruker UltraShield 500MHz Avance III equipped with a 5 mm BBI probe head with Z-gradients. ^{13}C NMR and all 2D Spectra were recorded on a Bruker Ascend 600 MHz Avance III HD equipped with a 1.7 mm TCI cryo probe head. The chemical shifts are reported in parts per million (ppm) relative to tetramethylsilane or a residual solvent peak, and the J values are given in Hz. In the case of the enantiomerically pure **1**, only ca. 50 μg (100 nmol) of compound were available which was not sufficient material to obtain a one-dimensional $^{13}\text{C}\{^1\text{H}\}$ -NMR spectrum. We recorded, therefore, the much more sensitive HMBC experiment, first with low and later on with high resolution and determined all carbon resonances unambiguously. The high resolution experiment was acquired with 2048 data points in the indirect dimension, 16 scans per increment and a sweep width of 40 ppm. This resulted in an acquisition time in the carbon dimension of 169.8 ms and a resolution of 2.9 Hz / point. The total experiment time was 14 hours and 42 min. Correlation peaks to the benzylic carbons were outside the chemical shift window in carbon and appear therefore as peaks in the spectrum (twofold alias). These correlations have been marked in the spectrum with an asterisk. DART-MS was measured on a IonSense DART-SVP100 (He, 450 °C) connected to a Shimadzu LC-2020. GC-MS was performed on a Shimadzu GCMS-2020 SE equipped with a Zebron 5 MS Inferno column which allowed to achieve temperatures up to 350 °C. High-resolution mass spectra (HRMS) were measured as HR-ESI-ToF-MS with a Maxis 4G instrument from Bruker with the addition of NaOAc. For column chromatography, usually silica gel Siliacel[®] p60 (40–63 μm) from Silicycle was used, and TLC was performed on silica gel 60 F254 glass plates with a thickness of 0.25 mm purchased from Merck. Buffered silica was prepared by using buffer solution pH=7 by Fluka and diluting 1:25 with water. 10 mL of the prepared solution were added to 100 g of silica and allowed to adsorb under mixing overnight. For HPLC a Shimadzu LC-20AT HPLC was used equipped with a diodearray UV/Vis detector (SPD-M10A VP from Shimadzu, λ = 200 - 600 nm) equipped with the corresponding column (regular: Reprosil 100, 5 μm , 250 x 16 mm; chiral: chiralpak IA 0.46 x 25 cm; Daicel Chemical Industries Ltd.). CD measurements were performed on a Chirascan CD Spectrometer in *n*-hexane/*i*PrOH = 98:2 at room temperature in 1 cm quartz glass cuvettes directly after the chiral HPLC. All solutions were prepared and measured under air saturated conditions.

Methyl 2'-iodo-[1,1'-biphenyl]-3-carboxylate (B): To an argon flushed Schlenk tube was consecutively added potassium carbonate (19.2 g, 137 mmol, 3.00 equiv.), 3-methoxycarbonylphenylboronic acid (8.25 g, 45.8 mmol, 1.00 equiv.), and 1-bromo-2-iodobenzene (9.00 mL, 68.7 mmol, 1.50 equiv.). Wet THF (160 mL) and MeOH (40 mL) were added and the solution degassed for 15 min before adding Pd(PPh₃)₂Cl₂ (917 mg, 2 mol %) and heating to 60 °C overnight. EtOAc and water were added, the aqueous phase extracted with EtOAc (2 x) and the combined organic phases washed with brine (1x). After drying over Na₂SO₄ the solvent was removed under reduced pressure. Column chromatography (SiO₂, 1:20 EtOAc/cyclohexane) yielded **B** as a yellow oil (6.38 g, 19.9 mmol, 41%). ¹H NMR (400 MHz, CDCl₃, 25 °C): δ = 8.08 (dt, ³J_{H,H} = 7.5, ⁴J_{H,H} = 1.6 Hz, 1H), 8.03 (td, ⁴J_{H,H} = 1.8, 0.6 Hz, 1H), 7.97 (dd, ³J_{H,H} = 8.0, ⁴J_{H,H} = 1.2 Hz, 1H), 7.56 (dt, ³J_{H,H} = 7.7, ⁴J_{H,H} = 1.6 Hz, 1H), 7.50 (td, ³J_{H,H} = 7.6, ⁴J_{H,H} = 0.6 Hz, 1H), 7.41 (td, ³J_{H,H} = 7.5, ⁴J_{H,H} = 1.2 Hz, 1H), 7.31 (dd, ³J_{H,H} = 7.6, ⁴J_{H,H} = 1.8 Hz, 1H), 7.06 (ddd, ³J_{H,H} = 8.0, 7.3, ⁴J_{H,H} = 1.8 Hz, 1H), 3.93 (s, 3H) ppm; ¹³C NMR (101 MHz, CDCl₃) δ = 167.0, 145.7, 144.5, 139.8, 134.0, 130.6, 130.2 (2 C), 129.4, 129.0, 128.4, 128.3, 98.5, 52.4 ppm; MS (EI, +): *m/z* (%) = 63.1 (20), 75.1 (16), 76.1 (49), 90.1 (14), 126.2 (12), 150.2 (19), 151.2 (38), 152.2 (100), 153.3 (20), 279.1 (13), 307.1 (66), 338.2 (87), 339.2 (12).

Methyl 3'-(4,4,5,5-tetramethyl-1,3,2-dioxaborolan-2-yl)-[1,1'-biphenyl]-2-carboxylate (C): To an oven dried and argon flushed Schlenk tube was consecutively added potassium carbonate (16.3 g, 116 mmol, 3.00 equiv.), 2-methoxycarbonylphenylboronic acid (7.00 g, 38.9 mmol, 1.00 equiv.), and 1,2-diiodobenzene (7.94 mL, 58.2 mmol, 1.50 equiv.). Dry THF (120 mL) and dry MeOH (30 mL) were added and the solution degassed for 15 min before adding Pd(PPh₃)₂Cl₂ (555 mg, 2 mol %) and heating to 60 °C for 15 h. EtOAc and water were added, the aqueous phase extracted with EtOAc (2 x) and the combined organic phases washed with brine (1x). After drying over Na₂SO₄ the solvent was removed under reduced pressure. Column chromatography (SiO₂, 1:20 EtOAc/Cy) yielded methyl 2'-iodo-[1,1'-biphenyl]-3-carboxylate as an orange oil (7.18 g, 21.2 mmol, 54%). ¹H NMR (400 MHz, CDCl₃, 25 °C): δ = 7.85 (ddd, ³J_{H,H} = 7.7, ⁴J_{H,H} = 1.4, 0.5 Hz, 1 H), 7.72 – 7.66 (m, 2 H), 7.53 (td, ³J_{H,H} = 7.5, ⁴J_{H,H} = 1.5 Hz, 1 H), 7.43 (td, ³J_{H,H} = 7.6, ⁴J_{H,H} = 1.3 Hz, 1 H), 7.33 (ddd, ³J_{H,H} = 7.7, ⁴J_{H,H} = 1.3, 0.5 Hz, 1 H), 7.29 – 7.24 (m, 1 H), 7.12 (dd, ³J_{H,H} = 8.4, 7.7 Hz, 1 H), 3.67 (s, 3 H) ppm; ¹³C NMR (63 MHz, CDCl₃) δ = 168.7, 143.6, 141.1, 137.3, 136.3, 131.6, 130.8, 130.7, 130.2, 129.8, 127.9, 127.9, 94.0, 52.2 ppm; MS (EI, +): *m/z* (%) = 338 (100) M⁺, 307 (65), 152 (36), 151 (10), 76 (12); HRMS (ESI, +): *m/z* calcd. for C₁₄H₁₁I₁NaO₂ [M+Na]⁺ 360.9696; found: 360.9701.

To an oven dried, argon flushed Schlenk tube was added methyl 2'-iodo-[1,1'-biphenyl]-3-carboxylate (7.04 g, 20.8 mmol, 1.00 equiv.), along with bis(pinacolato)diboron (5.82 g, 22.9 mmol, 1.10 equiv.) and potassium acetate (3.00 equiv.) before subjecting the flask to vacuum for 15 min. Dry dioxane (100 mL) was added and the solution degassed by passing argon through before adding Pd(dppf)Cl₂ (1.36 g, 1.67 mmol, 8 mol %) while continuing degassing. The flask was then heated to 115 °C overnight. After cooling to room temperature, more dioxane was added and the suspension filtered over Celite before removing the solvent under reduced pressure. The residue was dissolved in *t*BME, water was added and the resulting suspension again filtered over Celite before washing the organic phase with water (3x). The separated organic layer was dried over Na₂SO₄ and the solvent removed under reduced pressure. The residual oil was subjected to column chromatography (SiO₂, EtOAc/cyclohexane 1:8) yielding **C** as a colourless solid on standing (5.35 g, 15.8 mmol, 76%). ¹H NMR (400 MHz, CDCl₃, 25 °C): δ = 7.85 – 7.77 (m, 3 H), 7.52 (ddd, ³J_{H,H} = 7.8, 7.1, ⁴J_{H,H} = 1.4 Hz, 1 H), 7.42 – 7.37 (m, 4 H), 3.62 (s, 3 H), 1.35 (s, 12 H) ppm, ¹³C NMR (101 MHz, CDCl₃) δ = 142.5, 134.5, 133.6, 131.2, 131.2, 130.9, 130.7, 129.8, 127.3, 127.1, 83.8, 51.9, 24.9, MS (EI, +): *m/z* (%) = 146.0 (12), 151.0 (11), 152.0 (30), 153.0 (11), 178.0 (32), 179.0 (30), 180.0 (13), 181.0 (15), 195.0 (26), 206.0 (26), 207.0 (100), 208.0 (15), 220.0 (15), 237.0 (17), 238.0 (12), 263.0 (31), 277.0 (47), 278.0 (52), 279.0 (22), 337.1 (17), 338.1 (65), 339.0 (14).

1-((4-Bromo-3-iodophenyl)diazanyl)pyrrolidine (4): 4-Bromo-3-iodoaniline was synthesized from 2-bromo-5-nitroaniline (**3**) similar to a literature known procedure for 4-bromo-1-iodo-2-nitrobenzene followed by a Bechamp reduction.^[1] To a dry argon flushed two-necked flask was added BF₃·OEt₂ (64.0 mL, 496 mmol, 4.20 equiv.) and the flask cooled to –30 °C. A solution of 2-bromo-5-nitroaniline (**3**) (25.6 g, 118 mmol, 1.00 equiv.) in dry THF (500 mL) was added via cannula. After complete addition, a solution of *tert*-butyl nitrite (51.7 mL, 389 mmol, 3.30 equiv.) in THF (400 mL) was added via cannula. The mixture was warmed to 0 °C and cold ether (600 mL) was added. The mixture was stirred for 10 min at 0 °C and the formed white precipitate was filtered off. The solid was added in portions to a cooled solution of iodine (21.4 g, 84.1 mmol, 0.71 equiv.) and potassium iodide (27.7 g, 167 mmol, 1.42 equiv.) in MeCN (470 mL). The mixture was warmed to room temperature and stirred for 30 min. Saturated aq. Na₂S₂O₃ (300 mL) was added. The aqueous layer was extracted with DCM and the combined organic layers washed with saturated aq. Na₂S₂O₃ and brine. The combined organic layers were dried over Na₂SO₄ and the solvent removed

^[1] K. Flatt, Y. Yao, F. Maya, J. M. Tour, *J. Org. Chem.* **2004**, *69*, 1752–1755.

under reduced pressure to yield 4-bromo-3-iodo-nitrobenzene (37.8 g, 115 mmol, 98 %). ^1H NMR (400 MHz, CDCl_3 , 25 °C): δ = 8.68 (d, $^4J_{\text{H,H}}$ = 2.6 Hz, 1 H), 8.06 (dd, $^3J_{\text{H,H}}$ = 8.8, $^4J_{\text{H,H}}$ = 2.6 Hz, 1 H), 7.80 (d, $^3J_{\text{H,H}}$ = 8.7 Hz, 1 H) ppm. All other spectroscopic data are in accordance to those previously published.^[2]

A sulfonation flask was equipped with a mechanical stirrer and charged with a suspension of 4-bromo-3-iodo-nitrobenzene (37.2 g, 113 mmol, 1.00 equiv.) and iron (64.9 g, 113 mol, 100 equiv.) in EtOH (400 mL). The mixture was cooled to 0 °C and concentrated HCl (37%, 17.3 mL, 564 mmol, 5.0 equiv.) was added. After complete addition the mixture was allowed to warm to room temperature and stirred for 2.5 h with careful monitoring of the reaction. Upon completion, Celite was added and the suspension stirred for an additional 10 min. Afterwards the mixture was filtered over a pad of Celite and the solvent removed under reduced pressure. EtOAc and water were added and the aqueous layer extracted with EtOAc. The organic layer was washed with saturated aq. NaHCO_3 (2x) and brine (1x). After drying over Na_2SO_4 the solvent was removed under reduced pressure to yield 4-bromo-3-iodoaniline (27.6 g, 92.7 mmol, 82 %). ^1H NMR (250 MHz, CDCl_3 , 25 °C): δ = 7.32 (d, $^3J_{\text{H,H}}$ = 8.6 Hz, 1 H), 7.20 (d, $^4J_{\text{H,H}}$ = 2.7 Hz, 1 H), 6.52 (dd, $^3J_{\text{H,H}}$ = 8.6, $^4J_{\text{H,H}}$ = 2.7 Hz, 1 H), 3.67 (s, 2 H) ppm; ^{13}C NMR (101 MHz, CDCl_3 , 25 °C) δ = 146.5, 132.8, 126.3, 117.3, 116.7, 101.6 ppm; MS (ESI, +): m/z (%) = 299.0 (75), 297.0 (74) $[\text{M}]^+$, 172.0 (35), 170.1 (36), 145.1 (21), 143.1 (23), 127.0 (41), 91.1 (78), 90.1 (61), 74.1 (11), 65.1 (23), 64.1 (56), 63.1 (100), 62.1 (44), 61.1 (23), 52.1 (26), 50.1 (12); HRMS (ESI, +): m/z calcd. for $\text{C}_6\text{H}_6\text{BrIN}$ $[\text{M}+\text{H}]^+$ 297.8723; found: 297.8727.

To a dry, argon flushed three-necked flask was added $\text{BF}_3 \cdot \text{OEt}_2$ (50.7 mL, 392 mmol, 4.20 equiv.) and cooled down to -30 °C. 4-Bromo-3-iodoaniline (27.8 g, 93.3 mmol, 1.00 equiv.) in dry THF (290 mL) was added drop wise through a dropping funnel to the reaction mixture. After complete addition *tert*-butylnitrite (90%, 46.0 mL, 345 mmol, 3.70 equiv.) in dry THF (290 mL) was added drop wise. The mixture was allowed to warm to -5 °C before adding cold Et_2O (360 mL). The mixture was stirred for an additional 10 min and the residual precipitate was filtered off. The solid diazonium salt was washed with cold ether and added in portions to a solution of K_2CO_3 (65.1 g, 467 mmol, 5.00 equiv.) and pyrrolidine (15.5 mL, 187 mmol, 2.00 equiv.) in MeCN (290 mL) and H_2O (290 mL). The mixture was stirred for 10 minutes before diluting with DCM. The layers were separated and the aqueous layer was extracted with DCM (3x). The combined organic layers were dried over Na_2SO_4 and the solvents removed under reduced pressure yielding triazene **4** (33.8 g, 88.9 mmol, 95 %) as an orange-brown solid which was sufficiently pure to be

² G. A. Olah, Q. Wang, G. Sandford, G. K. Prakash, *J. Org. Chem.* **1993**, *58*, 3194 - 3195

employed in the next reaction step. For analytical purposes, a small sample was purified by recrystallization from pentane yielding orange crystals. ^1H NMR (400 MHz, CDCl_3 , 25 °C): δ = 7.92 (d, $^4J_{\text{H,H}}$ = 2.4 Hz, 1 H), 7.52 (d, $^3J_{\text{H,H}}$ = 8.5 Hz, 1 H), 7.24 (dd, $^3J_{\text{H,H}}$ = 8.6, $^4J_{\text{H,H}}$ = 2.4 Hz, 1 H), 3.91 (s, br, 4 H), 3.63 (s, br, 2 H), 2.16 – 1.87 (m, 4 H) ppm; ^{13}C NMR (101 MHz, CDCl_3 , 25 °C) δ = 151.1, 132.5, 131.6, 124.8, 121.9, 101.1, 23.8 ppm; HRMS (ESI, +): m/z calcd. for $\text{C}_{10}\text{H}_{12}\text{BrIN}_3$ $[\text{M}]^+$ 379.9254; found: 379.92546.

1-((6-bromo-2',5'-dimethyl-[1,1'-biphenyl]-3-yl)diazenyl)pyrrolidine (5): To an argon flushed Schlenk tube was added 2,5-dimethylphenylboronic acid (14.7 g, 97.8 mmol, 1.10 equiv.), triazene **4** (33.8 g, 88.9 mmol, 1.00 equiv.) and K_2CO_3 (37.3 g, 267 mmol, 3.00 equiv.) before subjecting the tube to vacuum for 15 minutes. The tube was reflushed with argon, toluene (360 mL) and water (100 mL) were added and the system degassed by passing argon through for 15 minutes. $\text{Pd}(\text{PPh}_3)_2\text{Cl}_2$ (2.52 g, 3.56 mmol, 4 mol%) was added and degassing continued for an additional 10 minutes before sealing the tube and heating to 60 °C overnight. More toluene was added, the layers were separated, the organic layer dried over Na_2SO_4 , and the solvent removed under reduced pressure. The crude residue was directly subjected to column chromatography (SiO_2 , 1:8 EtOAc/cyclohexane) yielding **5** (31.9 g, 88.9 mmol, >99%) as an off white solid. ^1H NMR (400 MHz, CDCl_3 , 25 °C): δ = 7.57 (d, $^3J_{\text{H,H}}$ = 8.4 Hz, 1 H), 7.31 – 7.27 (m, 1 H), 7.26 (d, $^4J_{\text{H,H}}$ = 2.3 Hz, 1 H), 7.15 (d, J = 7.7 Hz, 1 H), 7.10 (dd, $^3J_{\text{H,H}}$ = 7.8, $^4J_{\text{H,H}}$ = 1.9 Hz, 1 H), 6.97 (d, $^4J_{\text{H,H}}$ = 1.8 Hz, 1 H), 3.77 (s, br, 4 H), 2.34 (s, 3 H), 2.10 (s, 3 H), 2.06 – 1.98 (m, 4 H) ppm; ^{13}C NMR (101 MHz, CDCl_3 , 25 °C): δ = 150.7, 143.3, 141.5, 135.0, 133.1, 132.8, 130.1, 129.8, 128.7, 122.7, 121.0, 119.6, 24.0, 21.2, 19.6 ppm; MS (ESI, +): m/z (%) = 361.1 (11), 360.1 (74), 359.1 (11), 358.1 (79) $[\text{M}]^+$; HRMS (ESI, +): m/z calcd. for $\text{C}_{18}\text{H}_{21}\text{BrN}_3$ $[\text{M}]^+$ 358.0913; found: 358.0915.

2-Bromo-5-iodo-2',5'-dimethyl-1,1'-biphenyl (6): To a pressure vessel was added **5** (14.4 g, 40.2 mmol, 1.00 equiv.) and dissolved in MeI (14.4 mL, 229 mmol, 5.70 equiv.) before sealing the vessel and heating to 130 °C overnight. After cooling to room temperature, DCM was added and the solvents removed by distillation. DCM was added to the black residue followed by washing with $\text{Na}_2\text{S}_2\text{O}_3$ and brine. After drying over Na_2SO_4 and removing the solvent under reduced pressure the residue was subjected to a plug of silica (eluent: cyclohexane) yielding **6** as an off white oil (11.9 g, 30.7 mmol, 77%). ^1H NMR (400 MHz, CDCl_3 , 25 °C): δ = 7.56 (d, $^4J_{\text{H,H}}$ = 2.2, 1 H), 7.51 (dd, $^3J_{\text{H,H}}$ = 8.4, $^4J_{\text{H,H}}$ =

2.2, 1 H), 7.36 (d, $J=8.4$, 1 H), 7.17 – 7.09 (m, 2 H), 6.90 (t, $^4J_{H,H} = 1.2$, 1 H), 2.34 (s, 3H), 2.06 (s, 3H) ppm; ^{13}C NMR (101 MHz, CDCl_3) $\delta = 145.2, 139.8, 139.7, 137.7, 135.3, 134.3, 132.9, 130.0, 129.8, 129.2, 123.9, 92.3, 21.1, 19.5$ ppm; MS (EI, +): m/z (%) = 63.1 (14), 75.1 (10), 76.1 (31), 88.1 (13), 89.1 (56), 90.0 (17), 152.1 (16), 163.1 (10), 164.1 (11), 165.1 (100), 166.1 (15), 178.1 (30), 179.1 (24), 180.1 (87), 181.1 (13), 386.0 (59), 387.9 (60); HRMS (EI, +): m/z calcd. for $\text{C}_{14}\text{H}_{12}\text{BrI}$ $[\text{M}]^+$ 385.9152; found: 385.9167.

Dimethyl 3''-(2,5-dimethylphenyl)-[1,1':2',1'':4'',1''':3''',1''''-quinquephenyl]-2''',3-dicarboxylate (9): To an oven dried, argon flushed Schlenk tube was added potassium acetate (4.34 g, 44.2 mmol, 3.00 equiv.) bis(pinacolato)diboron (4.11 g, 16.2 mmol, 1-10 equiv.) and **6** (5.70, 14.7 mmol, 1.00 equiv.) before subjecting the tube to vacuum for 15 min. After refilling with argon, dry dioxane (100 mL) was added and degassed by a stream of argon over 15 minutes. $\text{Pd}(\text{dppf})\text{Cl}_2$ (962 mg, 1.18 mmol, 8 mol-%) was added and degassing continued for another 5 min before heating to 110 °C overnight. After cooling to room temperature, dioxane was added and the suspension filtered over Celite before removing the solvent under reduced pressure. *t*BME and water were added and the resulting suspension filtered again over Celite. The organic layer was washed with brine, dried and the solvent removed under reduced pressure. Column chromatography (buffered SiO_2 , 1:4 EtOAc/cyclohexane) yielded **7** (3.00 g, 7.75 mmol, 53 %) as an orange oil which was directly used without further purification. An analytical sample was further purified by twofold column chromatography (buffered SiO_2 , EtOAc/cyclohexane 1:8 and 1:20). ^1H NMR (400 MHz, CDCl_3 , 25 °C): $\delta = 7.66 - 7.61$ (m, 3 H), 7.15 – 7.04 (m, 2 H), 6.94 – 6.90 (m, 1 H), 2.32 (s, Hz, 3 H), 2.05 (s, 3 H), 1.32 (s, 12 H); ^{13}C NMR (101 MHz, CDCl_3) $\delta = 142.5, 141.0, 137.3, 134.9, 134.9, 133.0, 132.0, 130.0, 129.7, 128.7, 127.8, 127.5, 84.2, 25.0, 21.1, 19.5$ ppm; MS (EI, +): m/z (%) = 55.1 (17), 57.1 (21), 59.1 (38), 83.1 (18), 85.1 (28), 101.1 (28), 165.1 (53), 166.1 (22), 178.1 (22), 179.1 (29), 180.1 (15), 190.1 (12), 191.1 (45), 192.1 (33), 193.1 (13), 205.1 (14), 206.1 (31), 207.1 (64), 208.1 (12), 221.1 (23), 285.1 (16), 286.1 (58), 287.1 (63), 288.0 (60), 289.1 (49), 300.1 (25), 301.1 (13), 302.1 (25), 371.1 (25), 372.1 (11), 373.1 (24), 385.2 (25), 386.2 (100), 387.2 (45), 388.2 (94), 389.2 (20).

Crude **7** (8.89 g, 23.0 mmol, 1.10 equiv.) was added to an argon flushed round bottom flask along with **B** (7.06 g, 20.9 mmol, 1.00 equiv.), K_2CO_3 (17.5 g, 125 mmol, 6.00 equiv.), and XPhos Pd G2 (329 mg, 418 μmol , 2 mol-%) before subjecting the flask to vacuum for 15 min. After refiling with argon, toluene (300 mL) and water (3 mL) were added

and the system degassed by passing argon through for 15 minutes. After heating to 100 °C, the reaction was monitored until full conversion was achieved (typically 1-2 d). After cooling to room temperature, the solvent was removed under reduced pressure and the crude residue directly subjected to column chromatography (SiO₂, 1:40 EtOAc/cyclohexane) yielding **8** as an amorphous solid (7.04 g, 14.9 mmol, 72 %) which was sufficiently pure to be used in the next step. An analytical sample was purified by GPC (recycling, column: PSS SDV 500 Å, 5 µm, 20 x 600 mm, eluent: chloroform, 7 cycles). ¹H NMR (400 MHz, CDCl₃, 25 °C): δ = 7.94 – 7.89 (m, 2 H), 7.53 (d, ³J_{H,H} = 8.2 Hz, 1 H), 7.47 – 7.41 (m, 4 H), 7.34 – 7.25 (m, 2 H), 7.05 (q, ⁴J_{H,H} = 2.1 Hz, 3 H), 6.88 (d, ⁴J_{H,H} = 2.2 Hz, 1 H), 6.67 – 6.64 (m, 1 H), 3.87 (s, 3 H), 2.28 (s, 3 H), 1.87 (s, 3 H) ppm; ¹³C NMR (101 MHz, CDCl₃) δ = 166.8, 142.4, 141.6, 140.6, 140.3, 139.5, 139.3, 134.8, 134.5, 132.7, 132.6, 132.3, 130.9, 130.6, 130.4, 130.2, 129.9, 129.8, 129.5, 128.5, 128.1, 128.0, 128.0, 127.8, 122.2, 52.1, 20.9, 19.1 ppm; MS (EI, +): *m/z* (%) = 59.0 (14), 138.1 (12), 143.7 (10), 144.6 (23), 150.1 (23), 151.0 (34), 152.0 (11), 156.6 (11), 157.6 (40), 157.7 (48), 165.1 (17), 239.1 (13), 289.1 (16), 302.1 (26), 303.1 (16), 313.1 (25), 314.1 (21), 315.2 (70), 316.2 (81), 317.1 (37), 329.1 (33), 330.2 (26), 331.2 (79), 332.2 (44), 333.2 (11), 359.2 (73), 360.2 (27), 438.1 (17), 440.1 (18), 470.1 (100), 471.2 (31), 472.1 (99), 473.2 (30); HRMS (ESI, +): *m/z* calcd. for C₂₈H₂₃BrNaO₂ [M+Na]⁺ 493.0770; found: 493.0774.

Crude **8** (844 mg, 2.50 mmol, 1.05 equiv.) was added to an argon flushed round bottom flask along with **C** (1.60 g, 2.38 mmol, 1.00 equiv.), and K₂CO₃ (995 mg, 7.14 mmol, 3.00 equiv.), before subjecting the flask to vacuum for 15 min. After refilling with argon, toluene (10 mL) and water (0.5 mL) were added and the system degassed by passing argon through for 15 minutes. Pd(OAc)₂ (10.7 mg, 47.5 µmol, 2 mol%) and SPhos (46.7 mg, 95.0 µmol, 4 mol-%) were added under continued degassing. After heating to 100 °C the reaction was monitored until full conversion (typically 1-2 d) was achieved typically with further addition of base, catalyst and ligand if no conversion was observed within 1 d. After cooling to room temperature, the solvent was removed under reduced pressure and the crude residue directly subjected to column chromatography (SiO₂, 1:100 EtOAc/cyclohexane) and subsequent GPC (recycling, column: PSS SDV 500 Å, 5 µm, 20 x 600 mm, eluent: chloroform) yielding **9** after 6 cycles as a colourless, amorphous solid (712 mg, 1.18 mmol, 50 %). ¹H NMR (400 MHz, CDCl₃, 25 °C): δ = 7.98 (dt, ⁴J_{H,H} = 1.8, 1.0 Hz, 1 H), 7.93 (ddd, ³J_{H,H} = 6.1, ⁴J_{H,H} = 2.7, 1.7 Hz, 1 H), 7.77 – 7.73 (m, 1 H), 7.57 – 7.53 (m, 1 H), 7.50 – 7.27 (m, 8 H), 7.16 (td, ³J_{H,H} = 7.5, ⁴J_{H,H} = 0.7 Hz, 1 H), 7.09 (ddd, ³J_{H,H} = 9.1, ⁴J_{H,H} = 1.8, 1.0 Hz, 2 H), 7.05 – 7.01 (m, 1 H), 6.97 – 6.94 (m, 2 H), 6.88 (d, ³J_{H,H} = 7.8 Hz, 1 H), 6.84 – 6.80 (m, 1 H), 6.65 (d, ⁴J_{H,H} = 1.8 Hz, 1 H), 3.86 (s, 3 H), 3.61 (s, 3 H), 2.22 (s, 3 H), 1.62 (s, 3 H)

ppm; ^{13}C NMR (101 MHz, CDCl_3) δ = 167.1, 157.5, 142.4, 142.2, 141.2, 141.1, 140.7, 140.3, 140.2, 140.0, 139.8, 139.1, 134.91, 134.9, 132.84, 132.81, 131.5, 131.2, 131.12, 131.1, 130.9, 130.71, 130.71, 130.3, 129.82, 129.77, 129.76, 129.71, 128.97, 128.6, 128.18, 128.18, 127.97, 127.9, 127.85, 127.4, 127.2, 126.8, 52.3, 52.1, 21, 19.4 ppm; MS (EI, +): m/z (%) = 59.0 (10), 218.8 (19), 225.2 (19), 226.0 (21), 269.1 (27), 510.1 (20), 511.1 (11), 523.0 (19), 538.1 (15), 539.1 (11), 602.1 (100), 603.1 (46), 604.1 (11); HRMS (ESI, +): m/z calcd. for $\text{C}_{42}\text{H}_{34}\text{NaO}_4$ $[\text{M}]^+$ 625.2349; found: 625.2354.

Dimethyl 3''-(2,5-bis(bromomethyl)phenyl)-[1,1':2',1'':4'',1''':3''',1''''-quinquephenyl]-2''''',3-dicarboxylate (10**)**^[3]: To an argon flushed round bottom flask was added **9** (500 mg, 830 μmol , 1.00 equiv.), NBS (360 mg, 2.00 mmol, 2.41 equiv.), and dibenzoyl peroxide (105 mg, 420 μmol , 0.507 equiv.), along with degassed CCl_4 (5 mL). The solution was heated to 60 °C for 1 h while monitoring the course of the reaction by DART-MS. As soon as full conversion was reached, the reaction was cooled to room temperature, diluted with DCM and quenched with sat. aq. $\text{Na}_2\text{S}_2\text{O}_3$. The aqueous layer was back extracted with DCM (3x). After drying the combined layers over Na_2SO_4 and removing the solvents under reduced pressure, the residual solid was subjected to semi-preparative HPLC (column: semi preparative repositil 100 Si, 5 μm , 250 x 16 mm; eluent: hexane/DCM 60:40) yielding **10** as a colourless solid (416 mg, 547 μmol , 66 %). ^1H NMR (400 MHz, CDCl_3 , 25 °C): δ = 7.95 (td, $^4J_{\text{H,H}}$ = 1.6, 0.8 Hz, 1 H), 7.91 (dt, $^3J_{\text{H,H}}$ = 6.8, $^4J_{\text{H,H}}$ = 2.2 Hz, 1 H), 7.71 (dd, $^3J_{\text{H,H}}$ = 7.9, $^4J_{\text{H,H}}$ = 1.3 Hz, 1 H), 7.51 – 7.47 (m, 1 H), 7.42 – 7.34 (m, 5 H), 7.32 – 7.21 (m, 5 H), 7.22 – 7.14 (m, 1 H), 7.14 – 7.05 (m, 1 H), 7.02 – 6.97 (m, 4 H), 6.85 (dd, $^3J_{\text{H,H}}$ = 7.8, $^4J_{\text{H,H}}$ = 1.1 Hz, 1 H), 6.78 (d, $^4J_{\text{H,H}}$ = 1.9 Hz, 1 H), 4.28 (s, 2 H), 3.88 (d, $^2J_{\text{H,H}}$ = 10.5 Hz, 1 H), 3.82 (s, 3H), 3.78 (d, $^2J_{\text{H,H}}$ = 10.5 Hz, 1 H) 3.58 (s, 3 H) ppm; ^{13}C NMR (151 MHz, CDCl_3) δ = 31.0;32.5; 52.0; 52.2; 126.9; 127.2; 127.5; 127.9; 128.0; 128.17; 128.2; 128.3 (2C); 129.7 (3C); 130.1; 130.6 (2C); 130.9 (2C); 130.93 (2C); 131.3 (2C); 132.1; 132.6; 134.7; 135.5; 136.0; 137.3; 137.7; 139.0; 139.5; 139.6; 139.8; 140.3; 140.9; 141.3; 141.9; 142.0; 166.9; 168.7 ppm; DART-MS (450 °C, +): m/z (%) = 1382.5 (10), 1381.5 (15), 1380.4 (21), 734.6 (11), 734.6 (13), 706.5 (23), 701.1 (42), 700.1 (100), 699.2 (30), 698.2 (98), 537.1 (11), 377.2 (19), 376.1 (73), 359.2 (24), 349.2 (14), 348.1 (52), 341.1 (11), 183.8 (32); HRMS (ESI, +): m/z calcd. for $\text{C}_{42}\text{H}_{32}\text{Br}_2\text{NaO}_4$ 781.0560 $[\text{M}+\text{Na}]^+$; found: 781.0574.

^[3] Similar to: a) G. A. Holloway, H. M. Hügel, M. A. Rizzacasa, *J. Org. Chem.*, **2003**, *68*, 2200–2204. b) S. W. Kang, C. M. Gothard, S. Maitra, Atia-tul-Wahab, J. S. Nowick, *J. Am. Chem. Soc.* **2007**, *129*, 1486–1487.

(3''-(2,5-Bis(bromomethyl)phenyl)-[1,1':2',1'':4'',1''':3''',1''''-quinquephenyl]-2''',3-diyl)dimethanol (11): To a dry and argon flushed round bottom flask was added **10** (428 mg, 563 μmol , 1.00 equiv.) along with dry DCM (10 mL) before adding DIBAL-H (1 M solution in hexane, 2.25 mL, 2.25 mmol, 4.00 equiv.) and stirring at room temperature for 15 min. The solution was diluted with more DCM before subsequently slowly adding water (90 μL), aq. NaOH (15%, 90 μL) and water (225 μL) before stirring for 30 min. The residual suspension was filtered and concentrated under reduced pressure yielding **11** (396 mg, 563 μmol , >99%) as a colourless solid. ^1H NMR (600 MHz, CDCl_3 , 25 $^\circ\text{C}$): δ = 7.55 – 7.52 (m, 1 H), 7.49 – 7.43 (m, 5 H), 7.39 (dd, $^3J_{\text{H,H}} = 7.9$, $^4J_{\text{H,H}} = 1.9$ Hz, 1 H), 7.33 (ddd, $^3J_{\text{H,H}} = 7.5$, $^4J_{\text{H,H}} = 5.0$, 2.3 Hz, 3H), 7.31 – 7.23 (m, 4 H), 7.22 – 7.18 (m, 3 H), 7.16 (dt, $^3J_{\text{H,H}} = 7.6$, $^4J_{\text{H,H}} = 1.5$ Hz, 1 H), 7.07 – 7.01 (m, 2 H), 6.98 (dd, $^3J_{\text{H,H}} = 7.5$, $^4J_{\text{H,H}} = 1.4$ Hz, 1 H), 6.83 (d, $^4J_{\text{H,H}} = 1.9$ Hz, 1 H), 4.61 (s, 2 H), 4.33 (d, $^2J_{\text{H,H}} = 10.3$ Hz, 1H), 4.28 (d, $^2J_{\text{H,H}} = 13.1$ Hz, 1 H), 4.28 (s, 2 H), 3.98 (d, $^2J_{\text{H,H}} = 10.5$ Hz, 1 H), 3.83 (d, $^2J_{\text{H,H}} = 10.5$ Hz, 1 H) ppm; ^{13}C NMR (101 MHz, CDCl_3) δ = 142.0, 141.6, 141.1, 141.0, 140.9, 140.7, 140.4, 140.4, 139.8, 139.2, 138.1, 137.8, 137.2, 135.6, 133.0, 132.5, 131.3, 130.8 (2 C), 130.7, 130.5, 130.2, 129.8, 129.5, 129.1, 128.7, 128.5, 128.4, 128.4, 128.4, 128.0, 127.9, 127.9, 127.8, 127.7, 125.5, 65.4, 63.0, 32.8, 31.5 ppm; DART-MS (450 $^\circ\text{C}$, +): m/z (%) = 525.1 (15), 587.0 (19), 589.1 (31), 605.0 (11), 640.3 (18), 642.1 (34), 643.1 (11), 644.2 (18), 667.0 (14), 669.0 (29), 670.0 (11), 671.1 (15), 703.9 (14), 720.1 (55), 721.0 (16), 722.1 (100), 723.1 (36), 724.0 (51), 725.2 (18), 799.9 (11), 801.8 (11), 904.4 (14); HRMS (ESI, +): m/z calcd. for $\text{C}_{40}\text{H}_{32}\text{Br}_2\text{NaO}_2$ 725.0661 $[\text{M}+\text{Na}]^+$; found: 725.0673.

Twisted Hexaphenyl 1

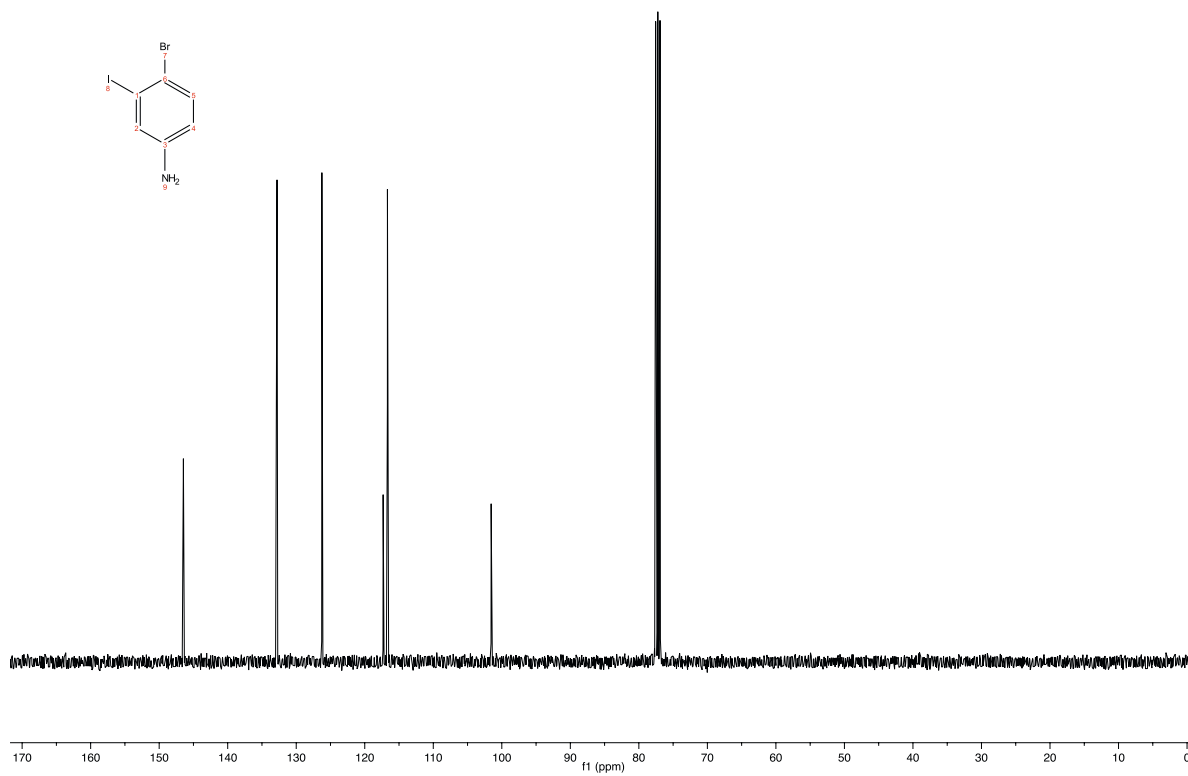
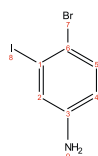
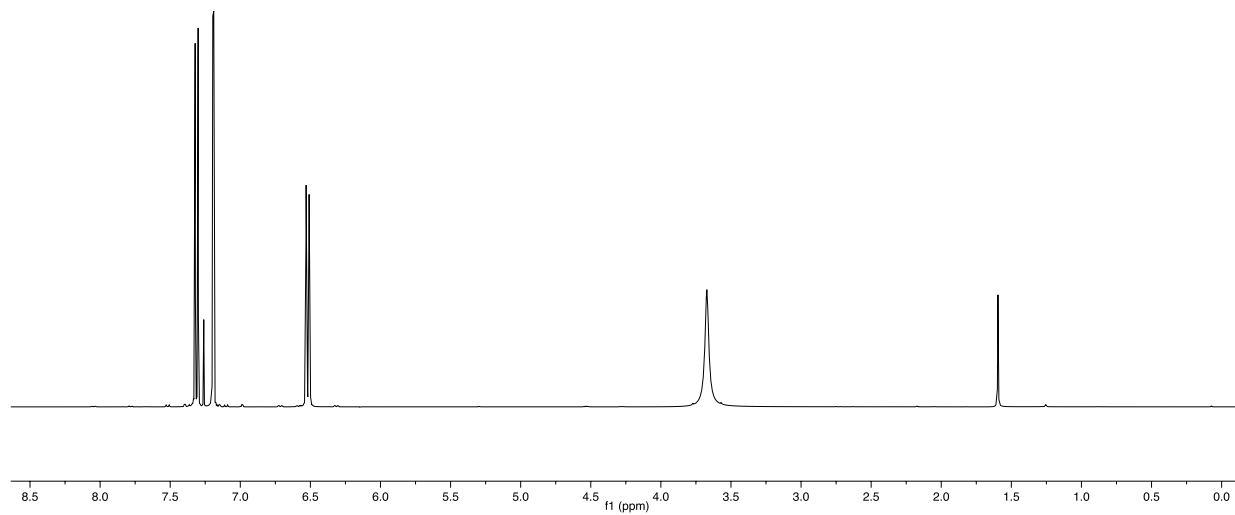
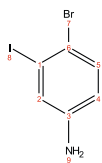
An oven dried, argon flushed Schlenk tube was charged with **11** (13.9 mg, 19.7 μmol), NaH (60% in mineral oil; 1.9 mg, 47 μmol), and dry THF (20 mL) before heating at reflux for 12 h. After dilution with THF (20 mL), the suspension was filtered and the solvent was removed under reduced pressure. Column chromatography on buffered (pH \approx 7) silica gel (cyclohexane/ethyl acetate, 4:1) afforded the monocyclized intermediate (4.8 mg, 39%). The monocyclized intermediate was dissolved in THF- d_8 (0.75 mL) in a dry and argon flushed NMR tube before adding NaH (60% in mineral oil, 1.7 mg, 43 μmol), sealing the tube and heating at reflux for 2 - 3 d. Once a full conversion was observed by ^1H NMR spectroscopy, the mixture was filtered and the solvent removed under reduced pressure. Separation by

chiral HPLC (analytical Chiralpak® IA column, eluent *n*-hexane/2-propanol (99:1), flow rate 1 mL min⁻¹, *T* = 25 °C) directly afforded the pure desired product **1** (501 μg, 14 %) as enantiomers as colourless solids. ¹H NMR (500 MHz, THF-*d*₈): δ = 7.66 (q, ⁴*J*_{H,H} = 1.8 Hz, 2H), 7.57 (dd, ⁴*J*_{H,H} = 1.8, 0.5 Hz, 1H), 7.50 (dd, ³*J*_{H,H} = 7.6, ⁴*J*_{H,H} = 1.5 Hz, 1H), 7.44 – 7.36 (m, 4H), 7.34 – 7.28 (m, 2H), 7.28 – 7.23 (m, 2H), 7.21 (t, ³*J*_{H,H} = 7.5 Hz, 1H), 7.14 – 7.07 (m, 5H), 7.03 (d, ³*J*_{H,H} = 7.5 Hz, 1H), 6.97 (dd, ³*J*_{H,H} = 7.8, 1.9 Hz, 1H), 6.91 (ddd, ³*J*_{H,H} = 7.6, ⁴*J*_{H,H} = 1.8, 1.2 Hz, 1H), 6.80 (ddd, ³*J*_{H,H} = 7.6, ⁴*J*_{H,H} = 1.8, 1.2 Hz, 1H), 4.98 (d, ²*J*_{H,H} = 12.6 Hz, 1H), 4.87 (d, ²*J*_{H,H} = 13.7 Hz, 1H), 4.26 (dd, ²*J*_{H,H} = 13.1, ⁴*J*_{H,H} = 5.2 Hz, 2H), 3.81 (dd, ²*J*_{H,H} = 24.5, ³*J*_{H,H} = 8.8 Hz, 2H), 3.69 (dd, ²*J*_{H,H} = 15.7, ³*J*_{H,H} = 8.8 Hz, 2H) ppm; ¹³C NMR (125 MHz, THF-*d*₈) δ = 143.4, 142.9, 142.6, 142.3, 141.55, 141.42, 141.36, 141, 140.8, 138.8, 138.7, 138.3, 136.42, 136.36, 132.6, 132.5, 132.48, 132.4, 131.3, 130.9, 130.4, 130.2, 129.6, 129.4, 128.7, 128.6, 128.4, 128.3, 128.2, 128.17, 128.16, 128, 127.95, 127.86, 126.3, 72.9, 72.5, 68.5, 68.3 ppm; DART-MS (450 °C, +): *m/z* (%) = 100.0 (63), 141.0 (37), 223.9 (67), 224.8 (7), 240.9 (38), 493.0 (6), 494.8 (15), 496.1 (5), 507.1 (40), 508.0 (15), 525.2 (65), 526.2 (23), 527.1 (5), 542.1 (13), 543.0 (14), 560.2 (100), 561.2 (42), 562.2 (10), 566.1 (13), 567.2 (6), 578.4 (8), 601.2 (35), 602.1 (15), 616.2 (8), 725.3 (8), 742.3 (22), 743.2 (11), 1102.4 (29), 1103.5 (24), 1103.6 (16); HRMS (ESI), calc. for C₄₀H₃₀O₂Na 565.2131 [M+Na]⁺, found 565.2138.

Crystal data for (1)

Formula $C_{40}H_{30}O_2$, $M = 542.68$ m/z, $F(000) = 1144$, colourless block, size $0.040 \cdot 0.140 \cdot 0.210$ mm³, monoclinic, space group $P 2_1/c$, $Z = 4$, $a = 14.2231(10)$ Å, $b = 10.7708(8)$ Å, $c = 19.3984(15)$ Å, $\alpha = 90^\circ$, $\beta = 100.579(3)^\circ$, $\gamma = 90^\circ$, $V = 2921.2(4)$ Å³, $D_{\text{calc.}} = 1.234$ Mg m⁻³. The crystal was measured on a Bruker Kappa Apex2 diffractometer at 123 °K using graphite-monochromated Cu K_α -radiation with $\lambda = 1.54178$ Å, $\Theta_{\text{max}} = 68.272^\circ$. Minimal/maximal transmission 0.92/0.98, $\mu = 0.578$ mm⁻¹. The Apex2 suite has been used for datacollection and integration. From a total of 20135 reflections, 5250 were independent (merging $r = 0.037$). From these, 4861 were considered as observed ($I > 2.0\sigma(I)$) and were used to refine 379 parameters. The structure was solved by using the program Superflip. Least-squares refinement against F was carried out on all non-hydrogen atoms using the program CRYSTALS. $R = 0.0385$ (observed data), $wR = 0.0488$ (all data), $GOF = 1.1229$. Minimal/maximal residual electron density = $-0.19/0.20$ e Å⁻³. Chebychev polynomial weights were used to complete the refinement. Plots were produced using CAMERON. Crystallographic data (excluding structure factors) for **1** in this paper have been deposited with the Cambridge Crystallographic Data Center, the deposition number is CCDC 995567. Copies of the data can be obtained, free of charge, on application to the CCDC, 12 Union Road, Cambridge CB2 1EZ, UK [fax: +44-1223-336033 or e-mail: deposit@ccdc.cam.ac.uk].

^1H -, ^{13}C -NMR (CDCl_3 , 400/101 MHz, 25 °C) of 4-bromo-3-iodoaniline



Mass Spectrum SmartFormula Report

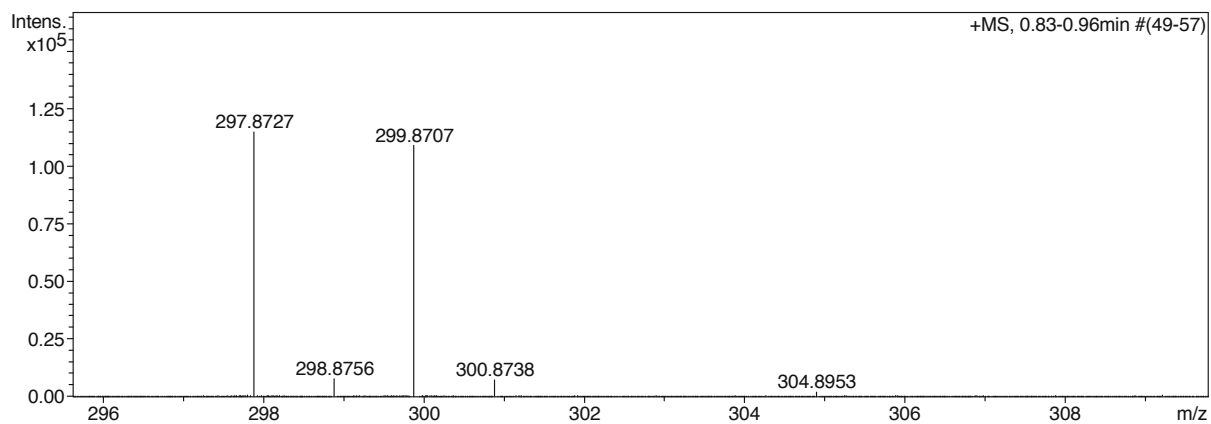
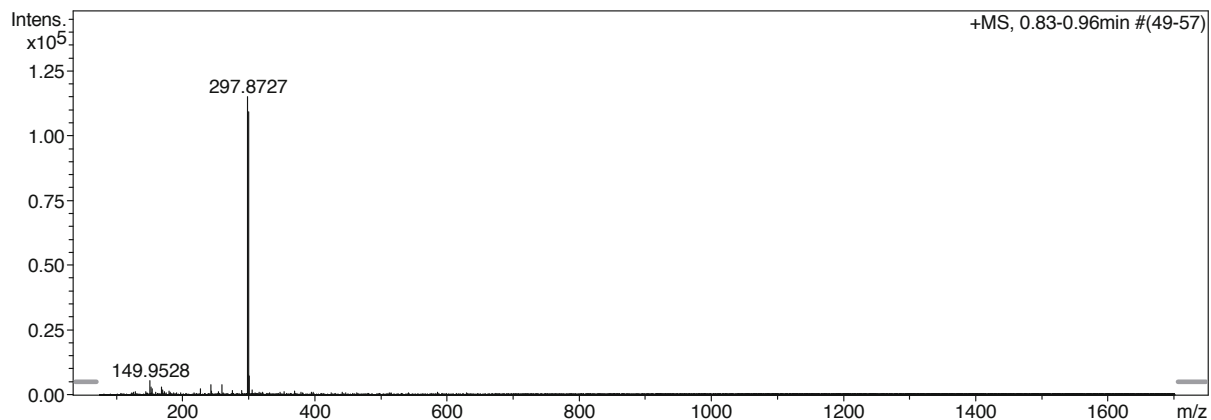
Analysis Info

Analysis Name N:\new acq data\ri705 002.d
 Method hn Direct_Infusion_pos mode_75-1700 mid 4eV.m
 Sample Name Michel Rickhaus, Ri705
 Comment Ri705, ca. 5 ug/ml MeCN, hinter MeCN/HCOOH

Acquisition Date 06.10.2014 16:59:30
 Operator hn
 Instrument / Ser# maXis 4G 21243

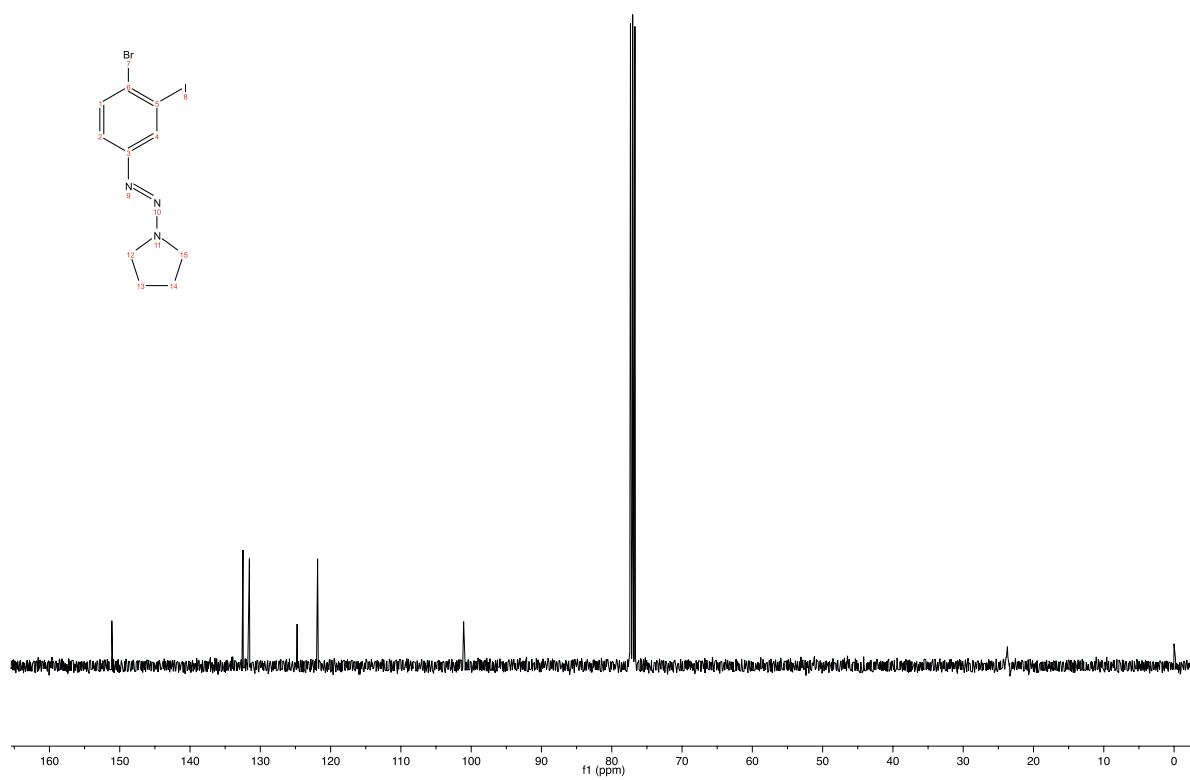
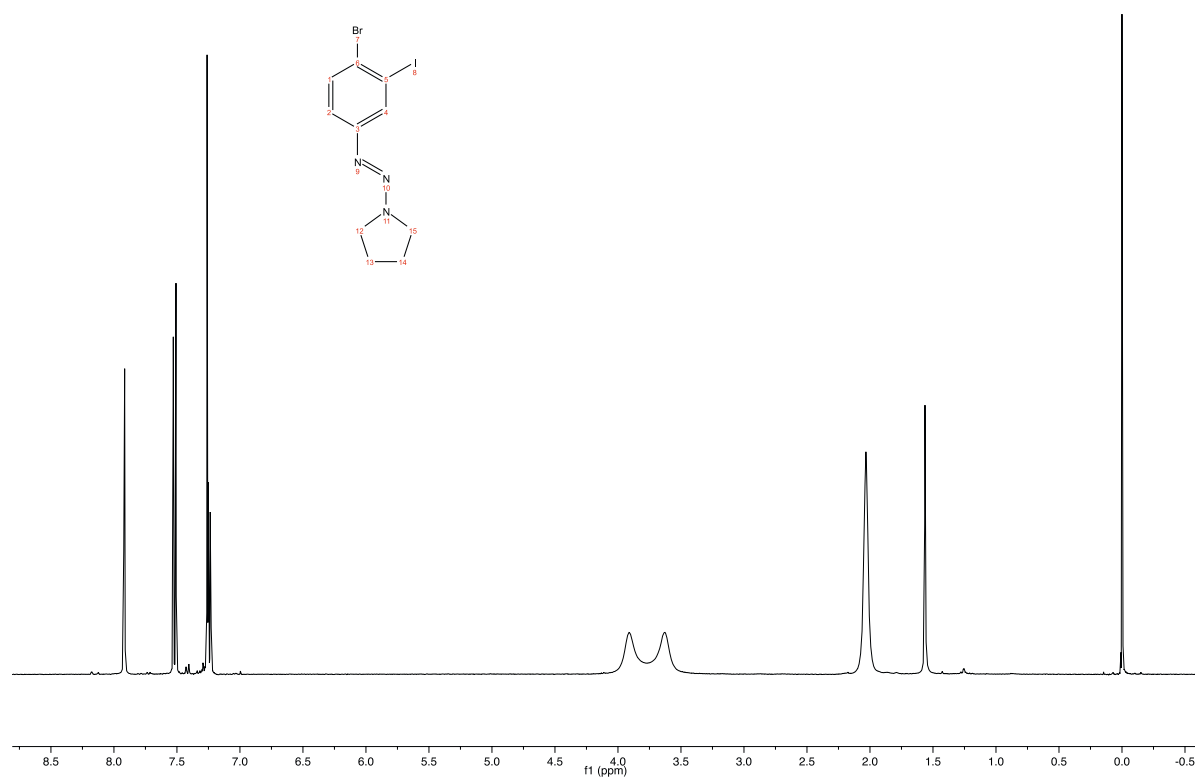
Acquisition Parameter

Source Type	ESI	Ion Polarity	Positive	Set Nebulizer	0.4 Bar
Focus	Not active	Set Capillary	3600 V	Set Dry Heater	180 °C
Scan Begin	75 m/z	Set End Plate Offset	-500 V	Set Dry Gas	4.0 l/min
Scan End	1700 m/z	Set Collision Cell RF	500.0 Vpp	Set Ion Energy (MS only)	4.0 eV



Meas. m/z	#	Formula	Score	m/z	err [mDa]	err [ppm]	mSigma	rdb	e ⁻ Conf	N-Rule	z
297.8727	1	C 6 H 6 Br I N	100.00	297.8723	-0.5	-1.5	12.5	3.5	even	ok	1+

^1H -, ^{13}C -NMR (CDCl_3 , 400/101 MHz, 25 °C) and HR-ESI spectra of compound (4)



Mass Spectrum SmartFormula Report

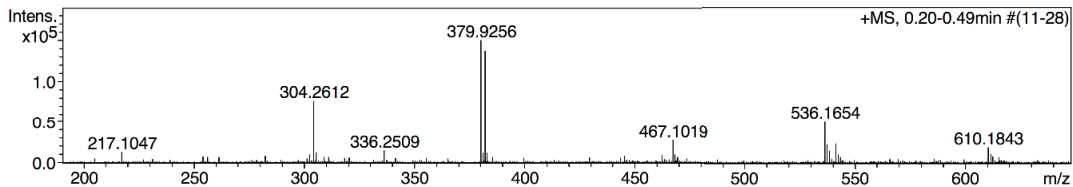
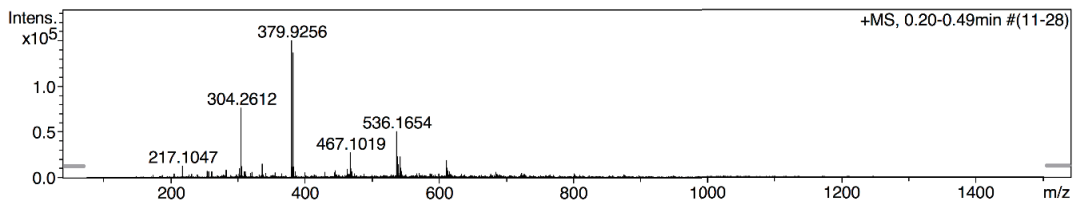
Analysis Info

Analysis Name N:\new acq data\ri655 001.d
 Method hn Direct_Infusion_pos mode_75-1500 mid 4eV.m
 Sample Name Michel Rickhaus, Ri655
 Comment Ri655, ca. 7 ug / ml MeCN

Acquisition Date 11.03.2014 11:22:01
 Operator hn
 Instrument / Ser# maXis 4G 21243

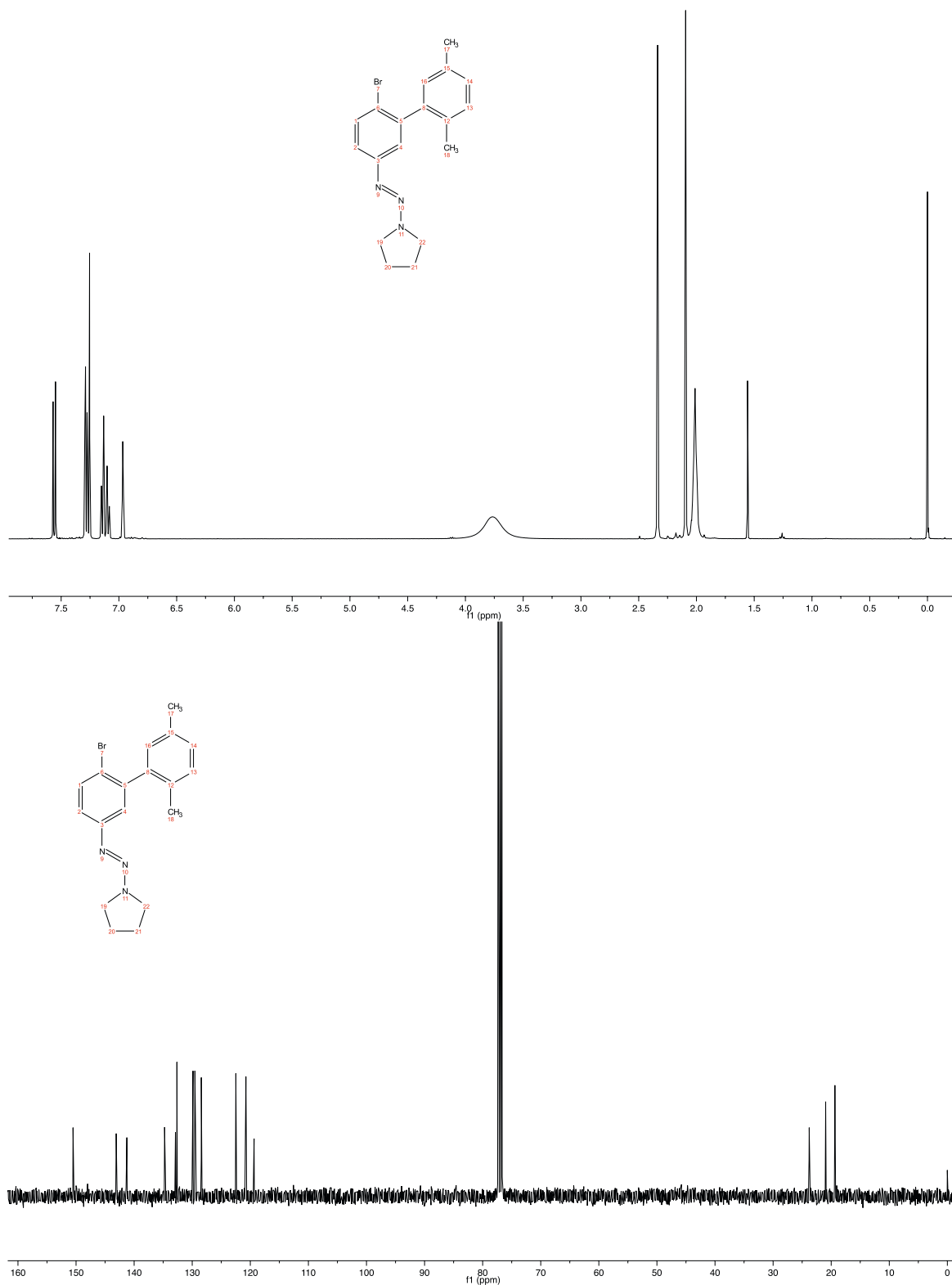
Acquisition Parameter

Source Type	ESI	Ion Polarity	Positive	Set Nebulizer	0.4 Bar
Focus	Not active	Set Capillary	4500 V	Set Dry Heater	180 °C
Scan Begin	75 m/z	Set End Plate Offset	-500 V	Set Dry Gas	4.0 l/min
Scan End	1500 m/z	Set Collision Cell RF	500.0 Vpp	Set Divert Valve	Waste



Meas. m/z	#	Formula	Score	m/z	err [mDa]	err [ppm]	mSigma	rdb	e ⁻	Conf	N-Rule	z
379.9256	1	C 10 H 12 Br I N 3	100.00	379.9254	-0.2	-0.5	40.7	5.5	even		ok	1+

^1H -, ^{13}C -NMR (CDCl_3 , 400/101 MHz, 25 °C) and HR-ESI spectra of compound (5)



Mass Spectrum SmartFormula Report

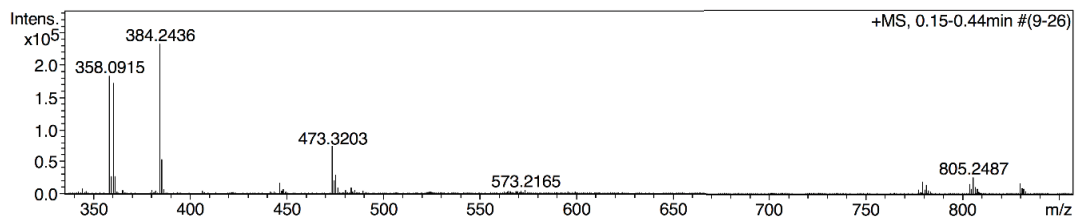
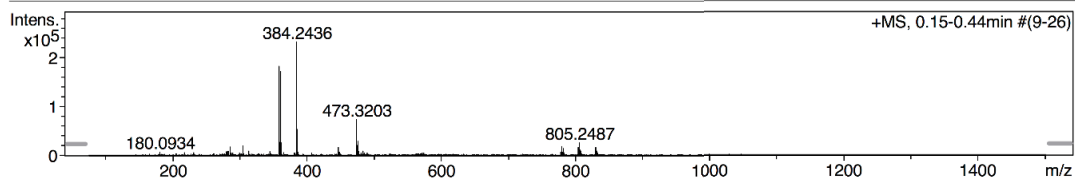
Analysis Info

Analysis Name N:\new acq data\ri656 001.d
 Method hn Direct_Infusion_pos mode_75-1500 mid 4eV.m
 Sample Name Michel Rickhaus, Ri656
 Comment Ri656, ca 5 ug/ml MeCN

Acquisition Date 12.03.2014 11:01:31
 Operator hn
 Instrument / Ser# maXis 4G 21243

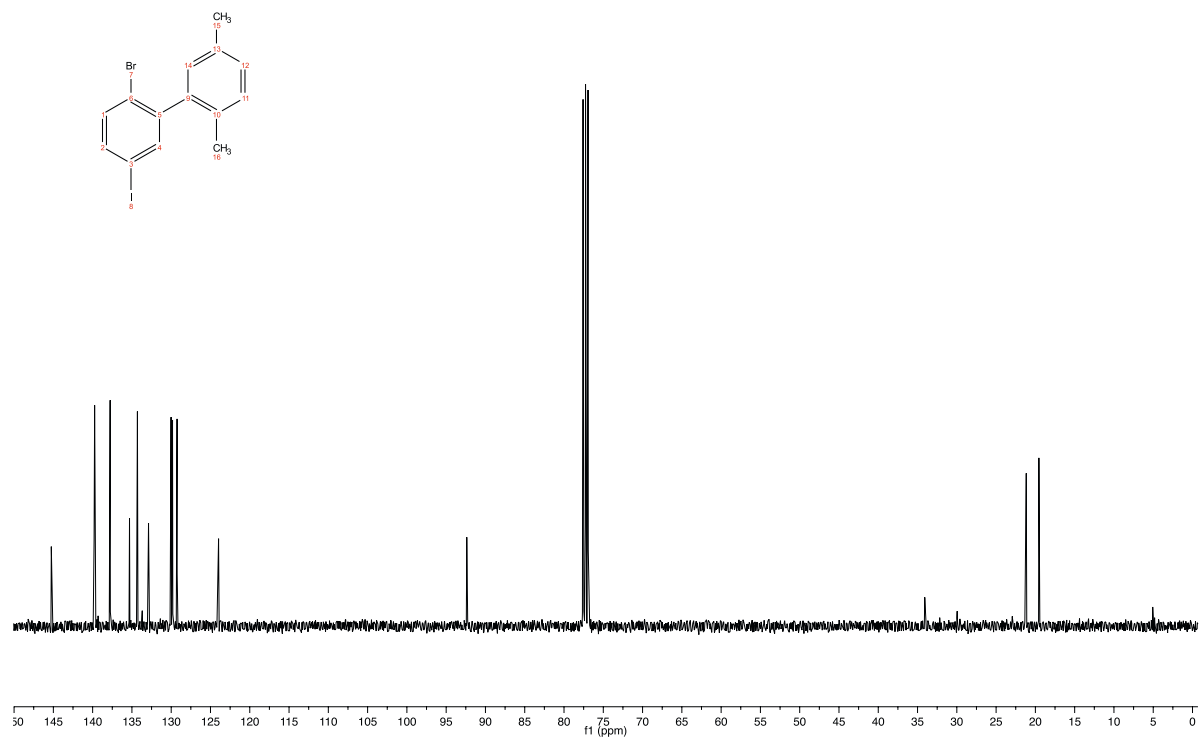
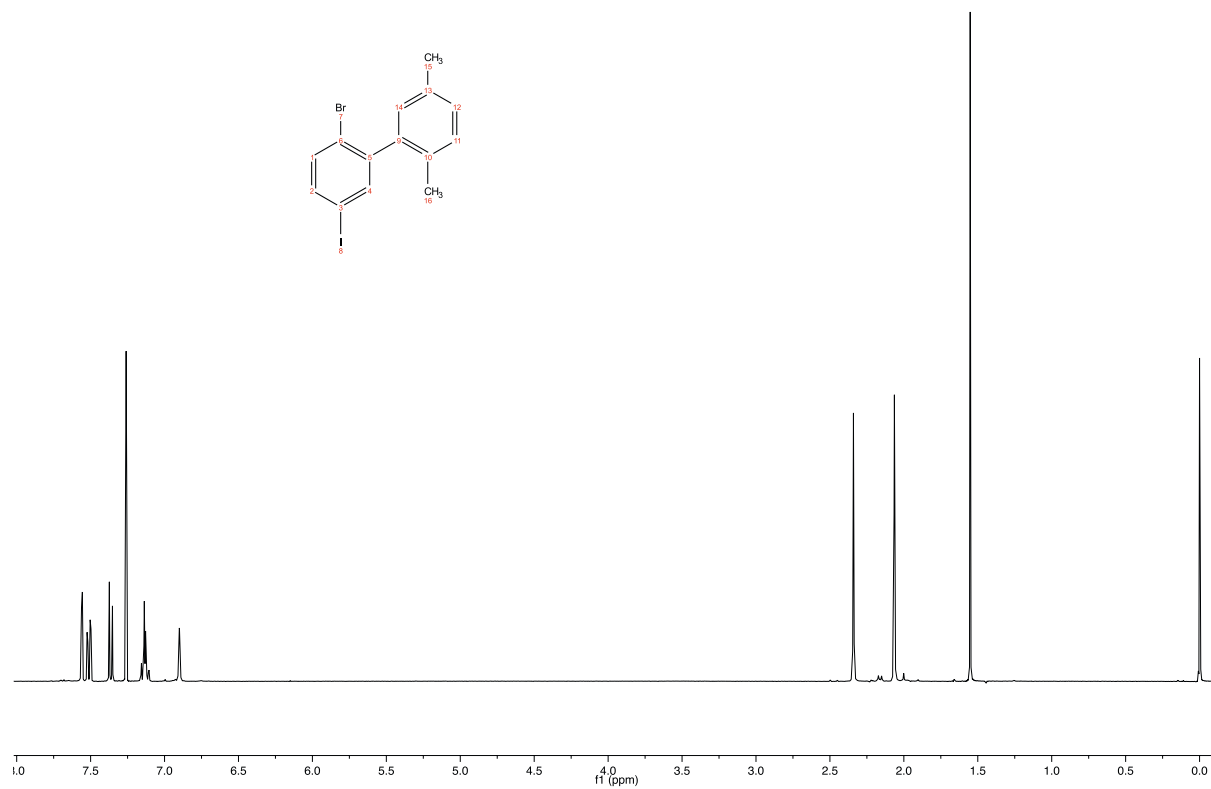
Acquisition Parameter

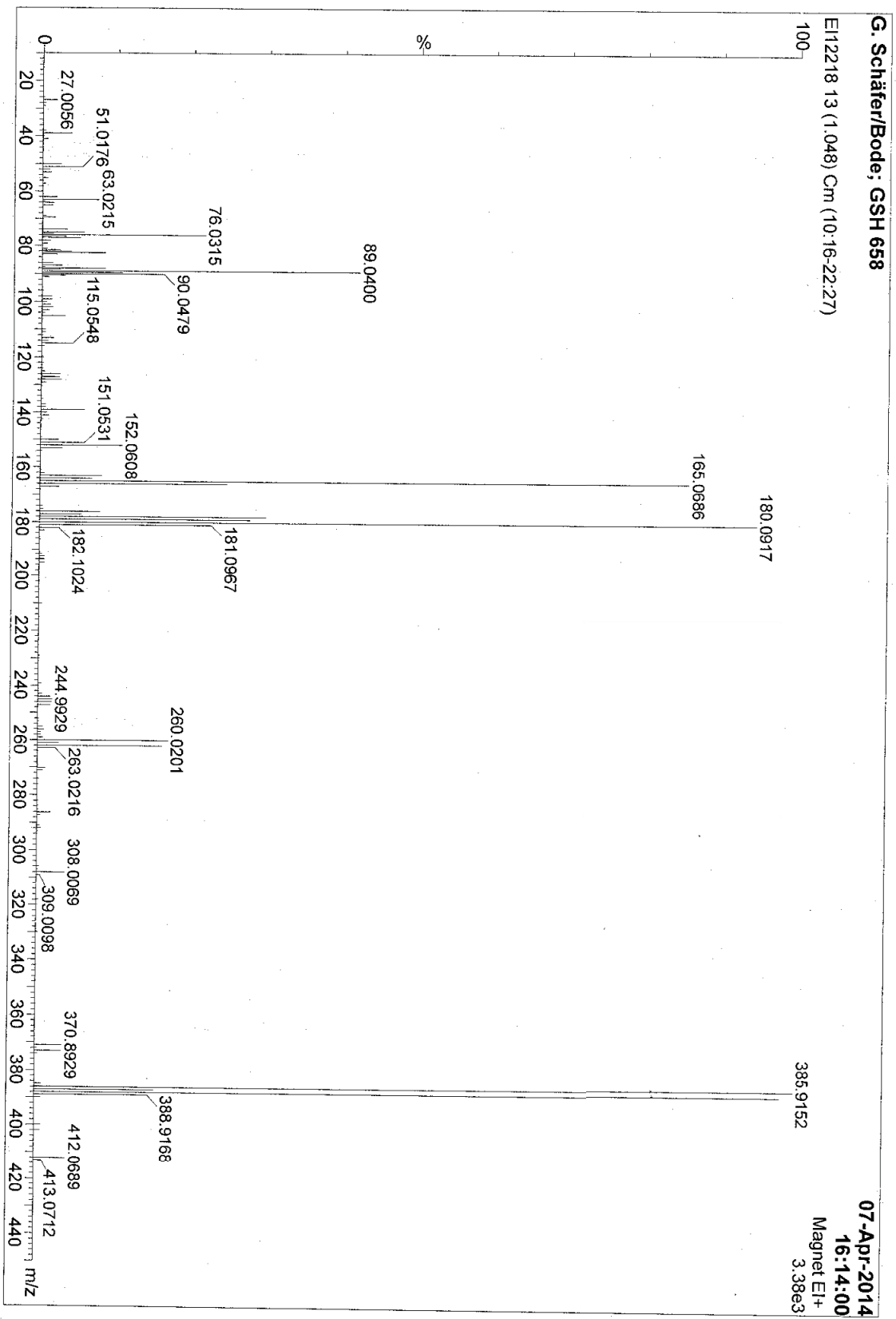
Source Type ESI Ion Polarity Positive Set Nebulizer 0.4 Bar
 Focus Not active Set Capillary 4500 V Set Dry Heater 180 °C
 Scan Begin 75 m/z Set End Plate Offset -500 V Set Dry Gas 4.0 l/min
 Scan End 1500 m/z Set Collision Cell RF 500.0 Vpp Set Divert Valve Waste



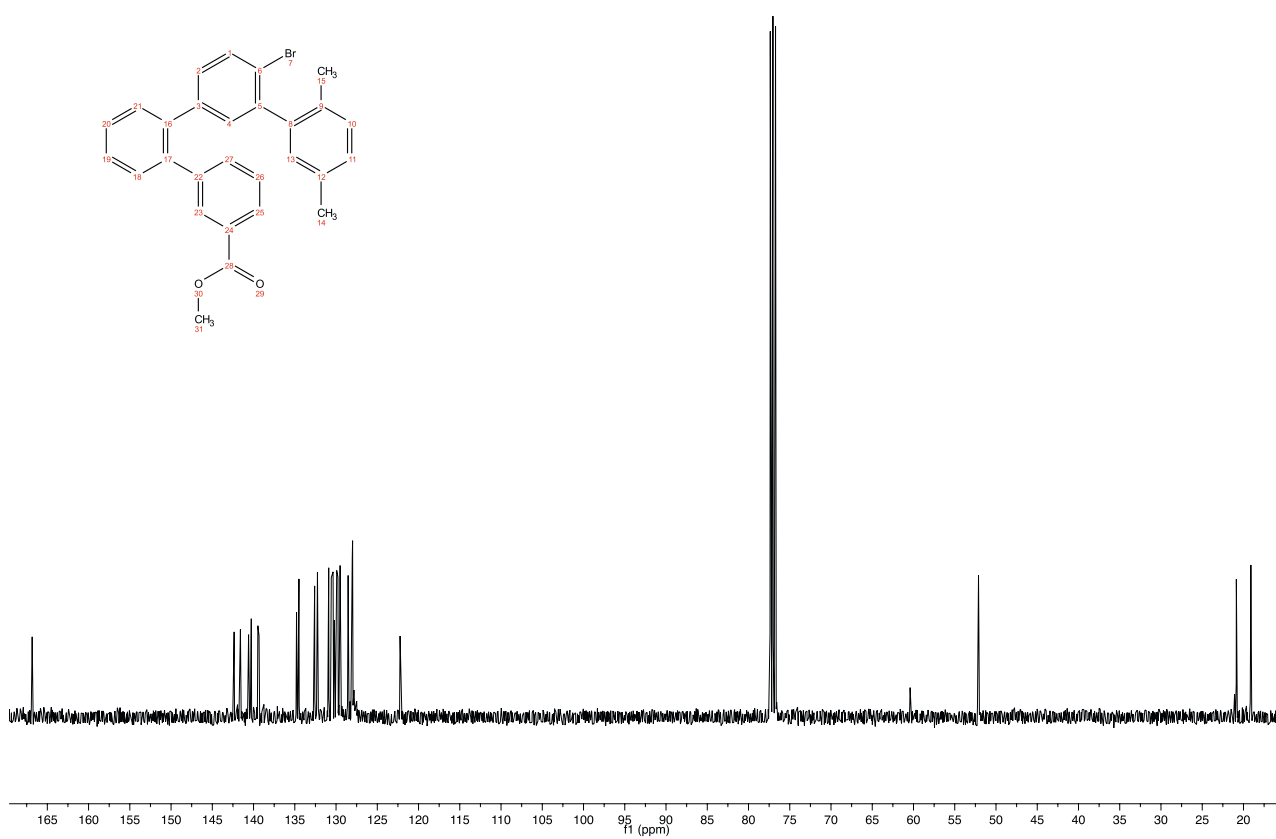
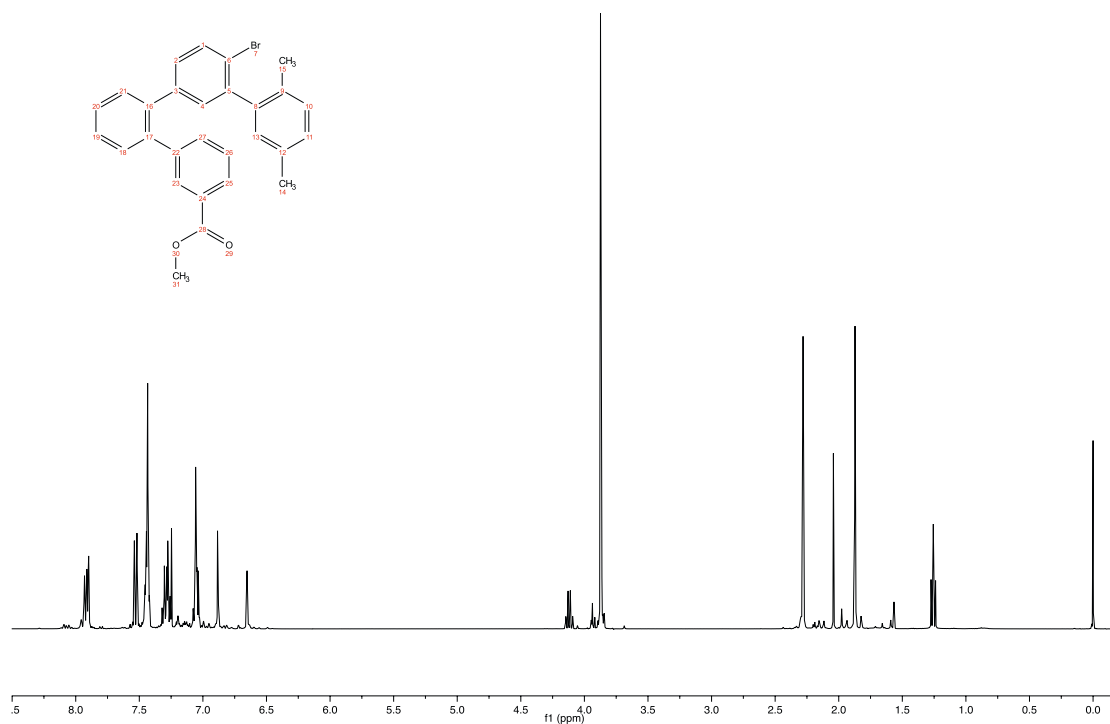
Meas. m/z	#	Formula	Score	m/z	err [mDa]	err [ppm]	mSigma	rdb	e ⁻ Conf	N-Rule	z
358.0915	1	C 18 H 21 Br N 3	100.00	358.0913	-0.2	-0.5	45.7	9.5	even	ok	1+

^1H -, ^{13}C -NMR (CDCl_3 , 400/101 MHz, 25 °C) and HR-EI spectra of compound (6)





^1H -, ^{13}C -NMR (CDCl_3 , 400/101 MHz, 25 °C) and HR-ESI spectra of compound (7)



Mass Spectrum SmartFormula Report

Analysis Info

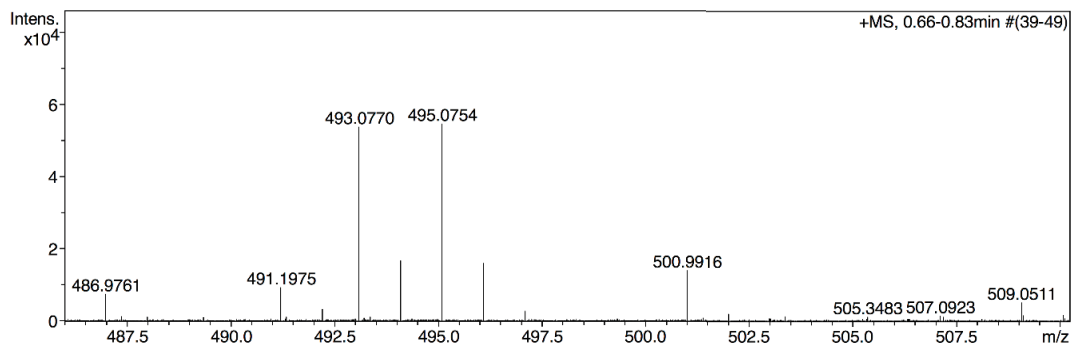
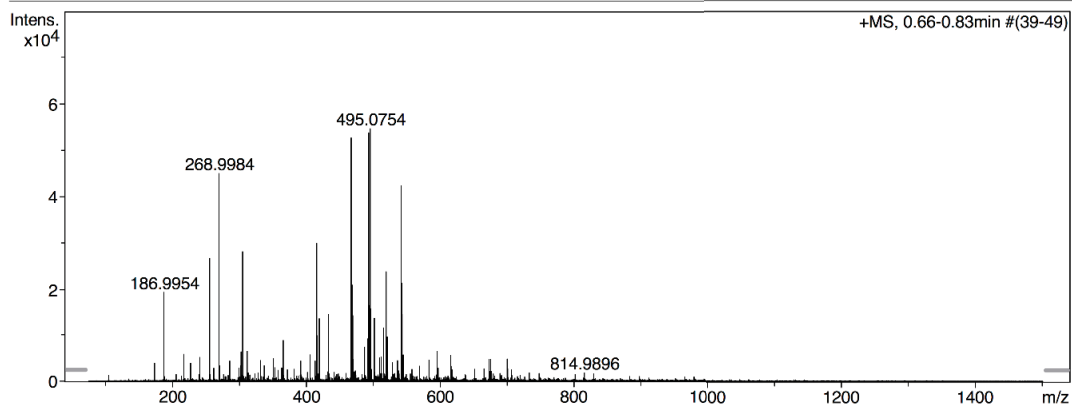
Analysis Name N:\new acq data\ri661 001.d
 Method hn Direct_Infusion_pos mode_75-1500 mid 7eV.m
 Sample Name Michel Rickhaus, Ri661
 Comment Ri661, ca 5 ug/ml MeCN, via Spritze, hinter MeOH/NaOAc

Acquisition Date 25.04.2014 17:07:33

Operator hn
 Instrument / Ser# maXis 4G 21243

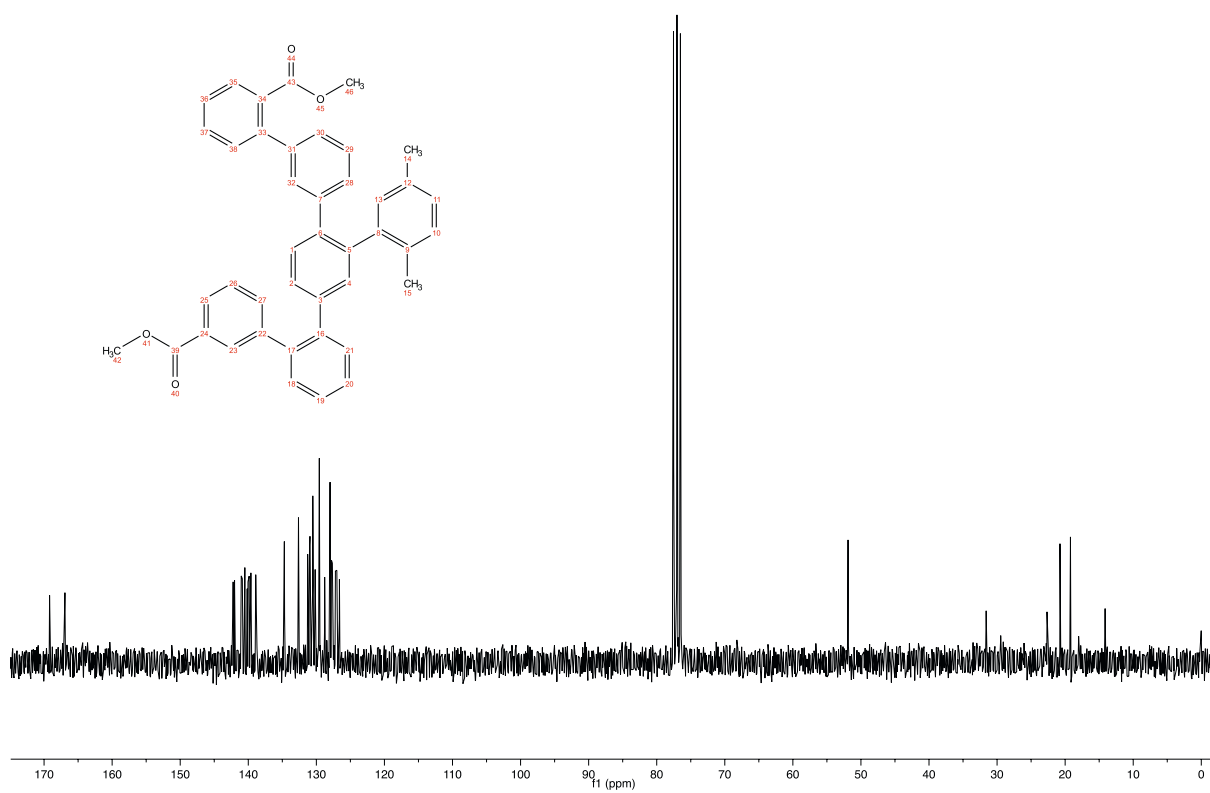
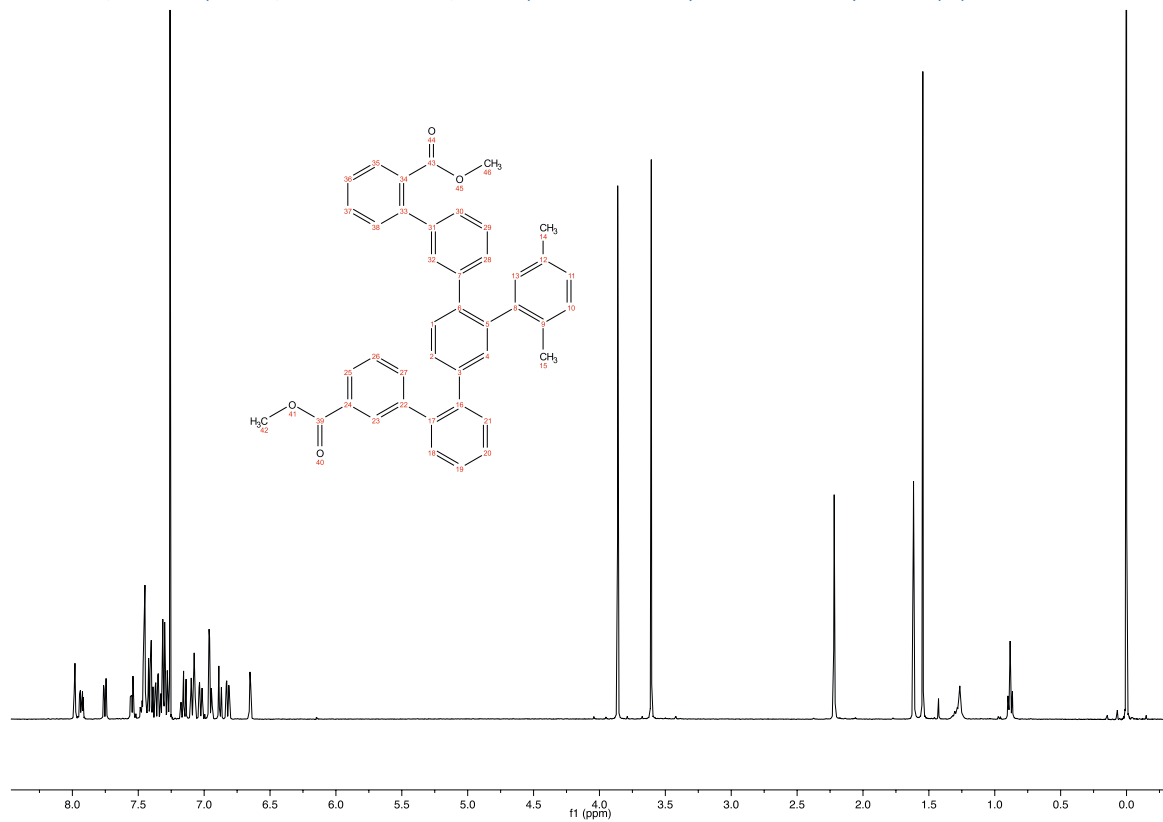
Acquisition Parameter

Source Type	ESI	Ion Polarity	Positive	Set Nebulizer	0.4 Bar
Focus	Not active	Set Capillary	3600 V	Set Dry Heater	180 °C
Scan Begin	75 m/z	Set End Plate Offset	-500 V	Set Dry Gas	4.0 l/min
Scan End	1500 m/z	Set Collision Cell RF	500.0 Vpp	Set Ion Energy (MS only)	7.0 eV

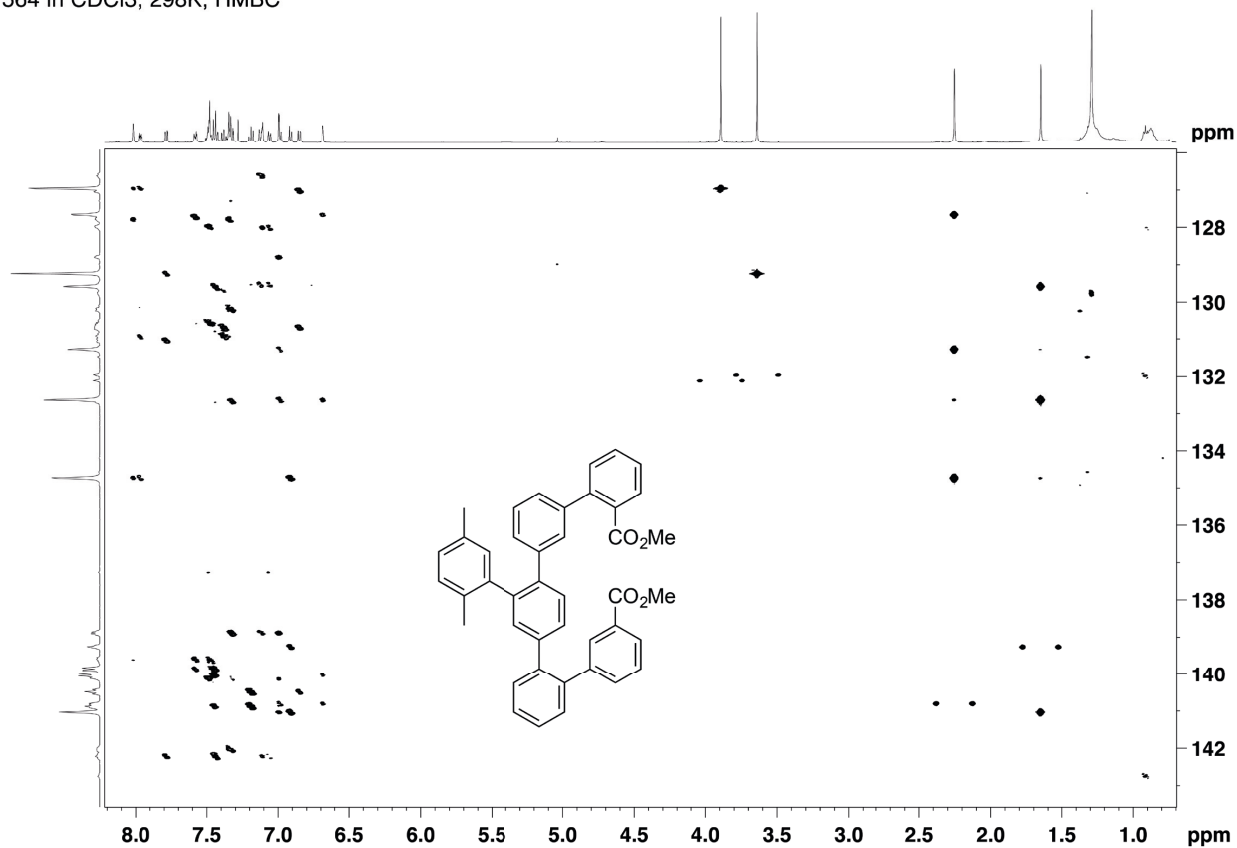


Meas. m/z	#	Formula	Score	m/z	err [mDa]	err [ppm]	mSigma	rdb	e ⁻	Conf	N-Rule	z
493.0770	1	C 28 H 23 Br Na O 2	100.00	493.0774	0.4	0.8	3.8	16.5	even		ok	1+

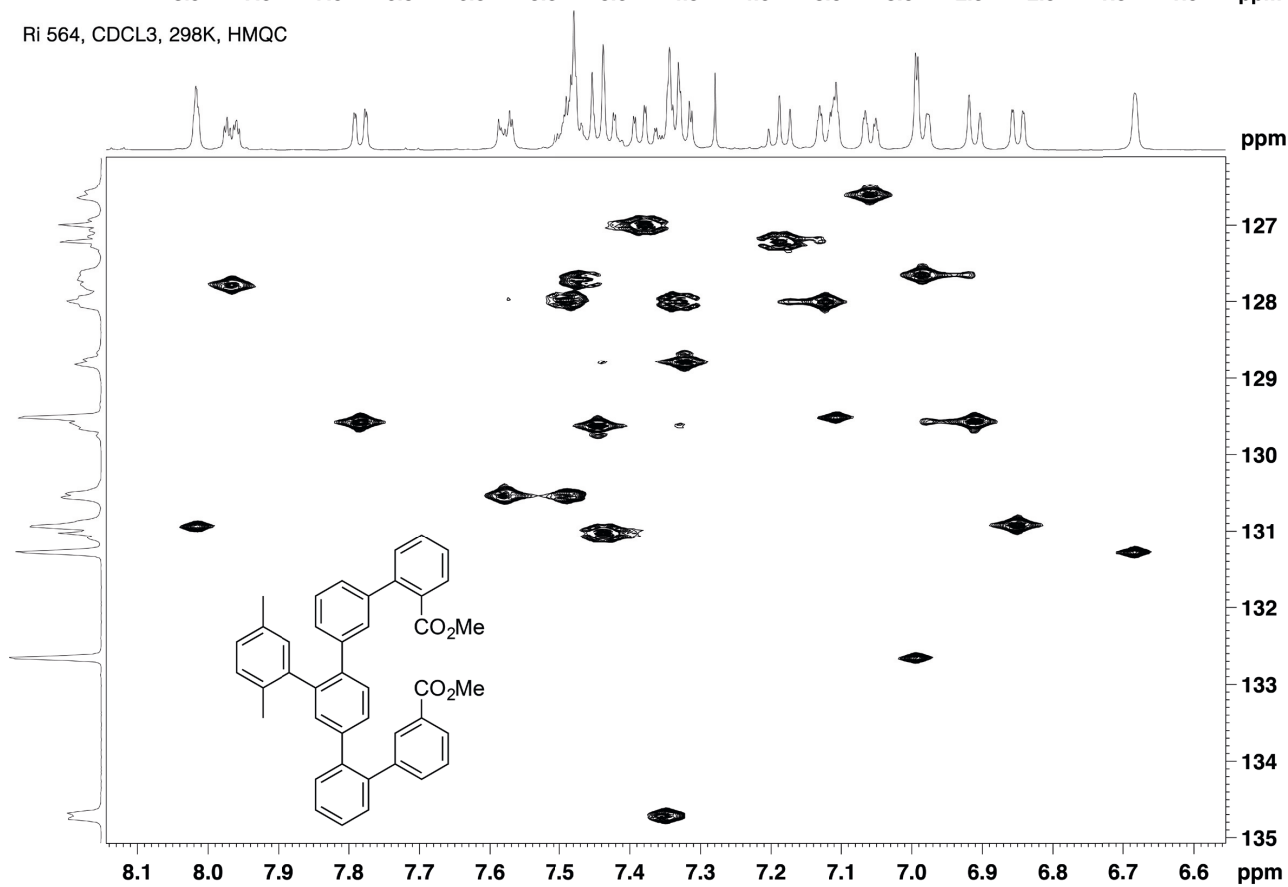
^1H -, ^{13}C -NMR, HMBC (CDCl_3 , 600/150 MHz, 25 °C) and HR-ESI spectra of compound (9)



Ri 564 in CDCl₃, 298K, HMBC



Ri 564, CDCl₃, 298K, HMQC



Mass Spectrum SmartFormula Report

Analysis Info

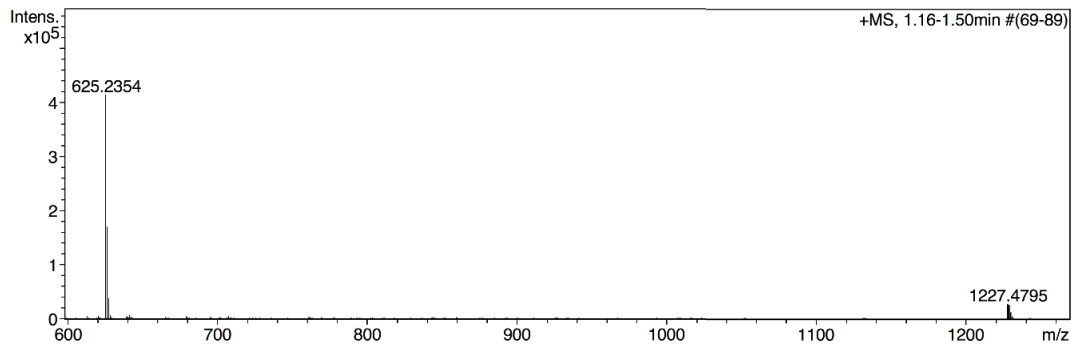
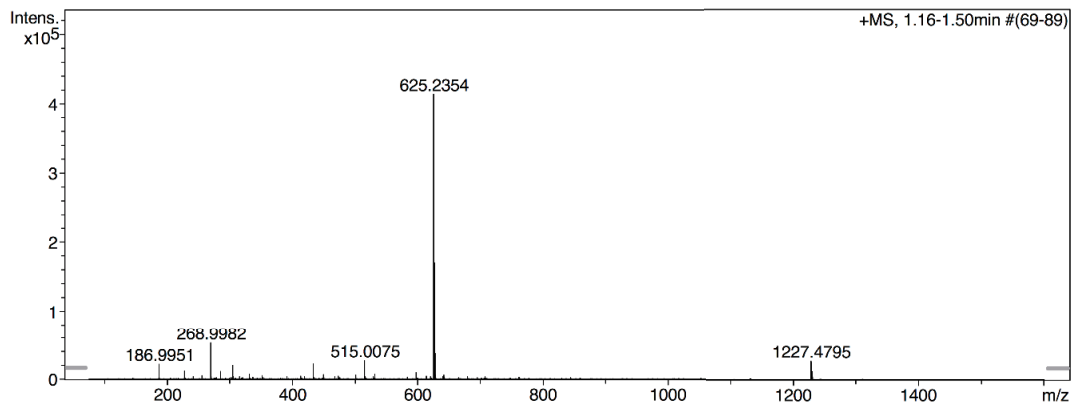
Analysis Name N:\new acq data\Ri665 001.d
 Method hn Direct_Infusion_pos mode_75-1600 mid 4eV.m
 Sample Name Michel Rickhaus, Ri665
 Comment Ri665, ca. 5 ug/ml MeCN, via Spritze hinter MeOH/NaOAc

Acquisition Date 08.07.2014 14:13:09

Operator hn
 Instrument / Ser# maXis 4G 21243

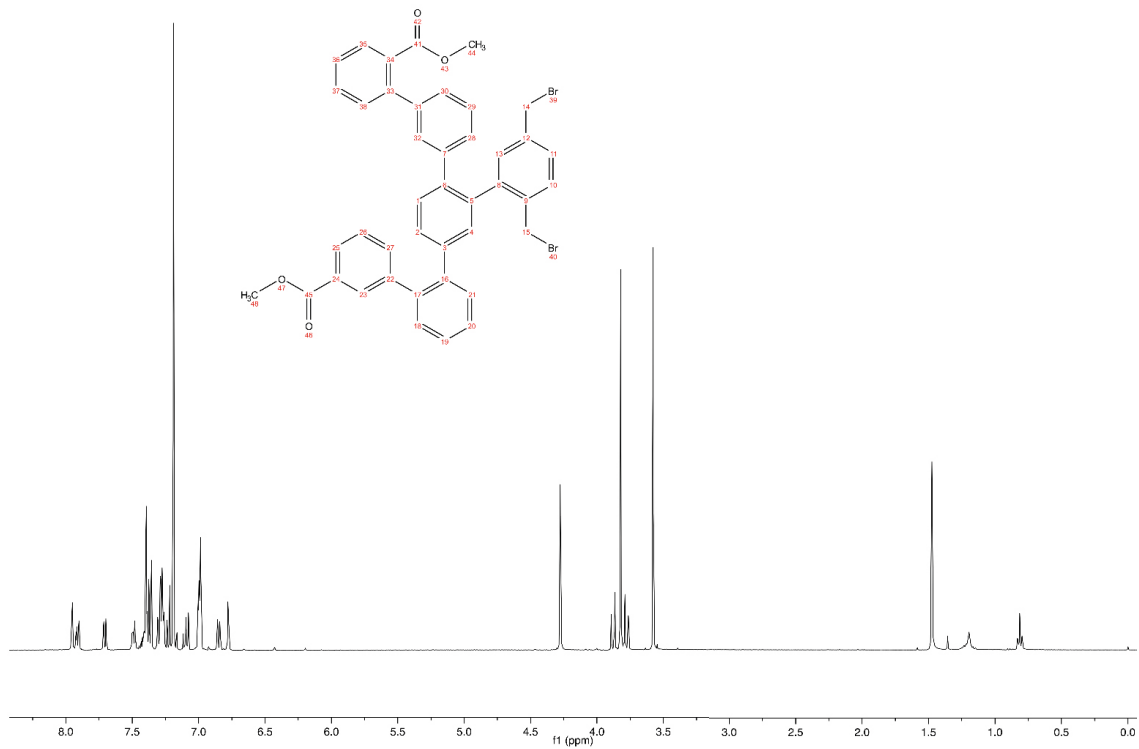
Acquisition Parameter

Source Type	ESI	Ion Polarity	Positive	Set Nebulizer	0.4 Bar
Focus	Not active	Set Capillary	3600 V	Set Dry Heater	180 °C
Scan Begin	75 m/z	Set End Plate Offset	-500 V	Set Dry Gas	4.0 l/min
Scan End	1600 m/z	Set Collision Cell RF	500.0 Vpp	Set Ion Energy (MS only)	4.0 eV

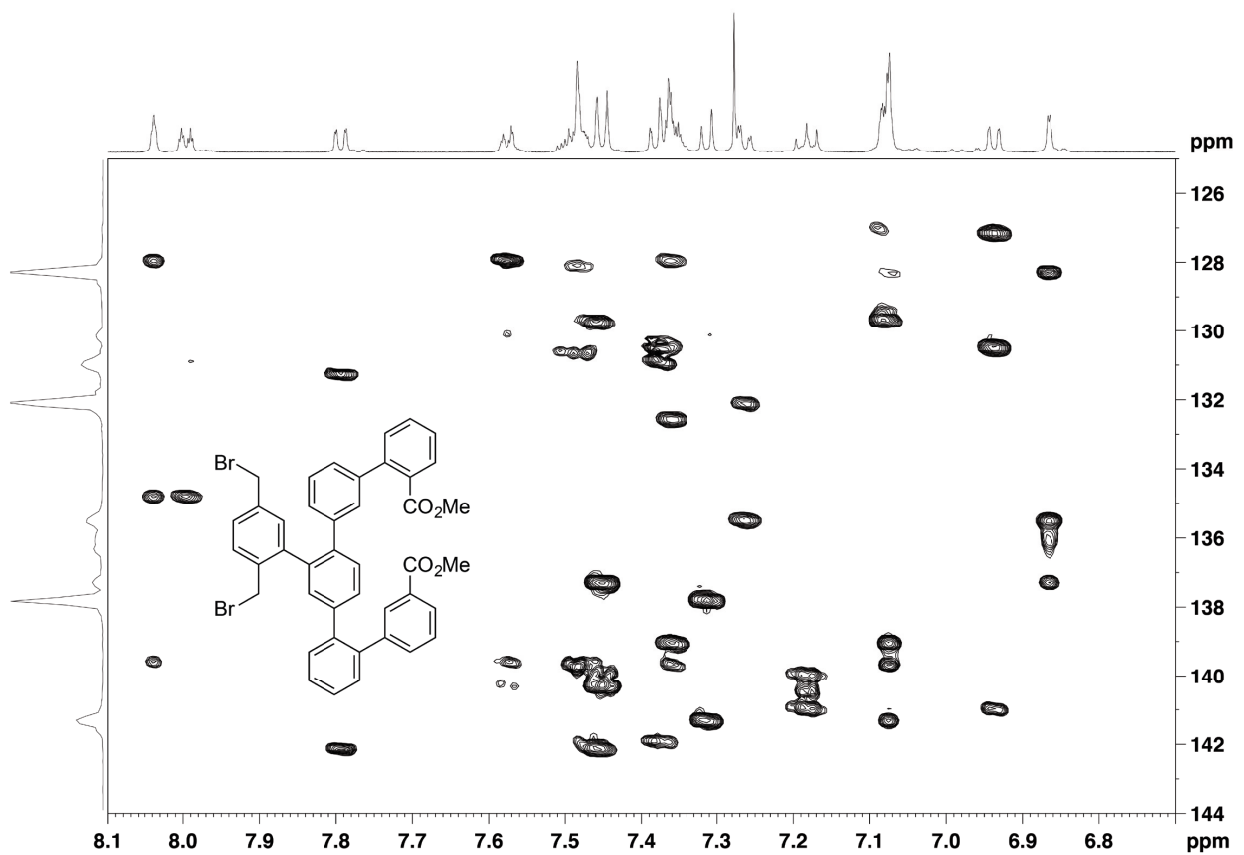


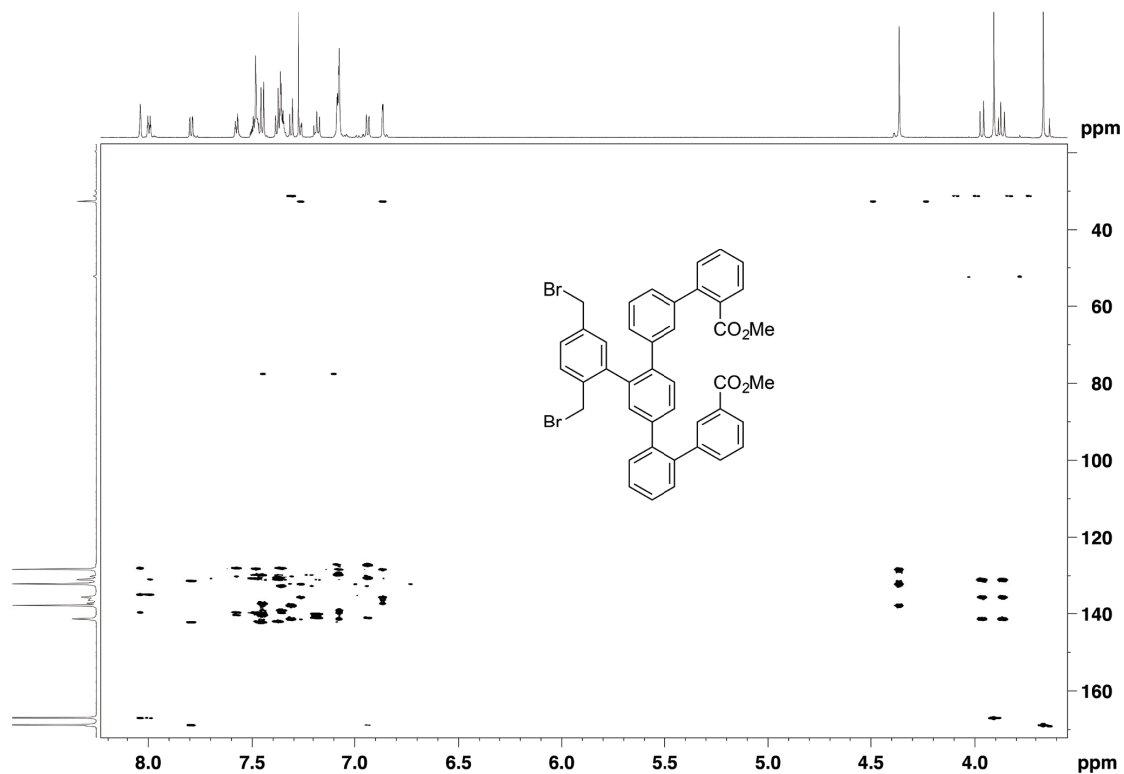
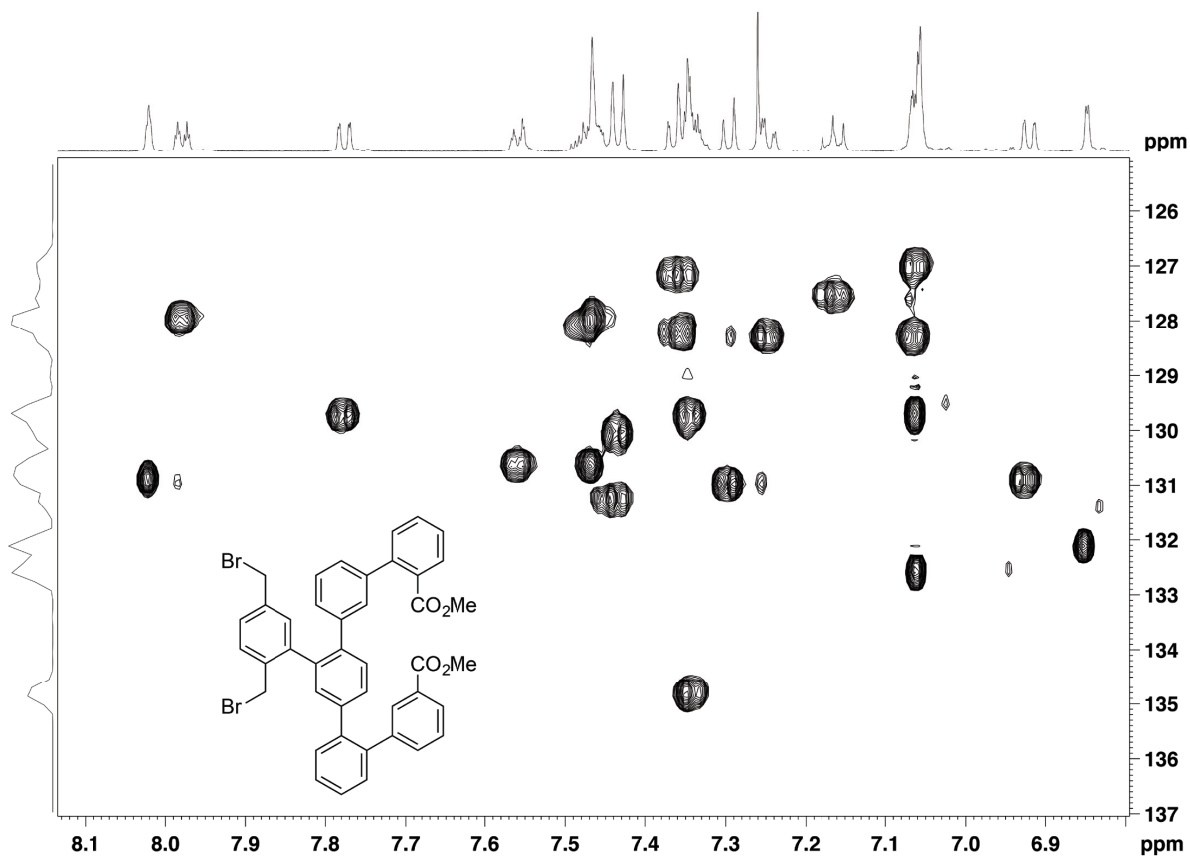
Meas. m/z	#	Formula	Score	m/z	err [mDa]	err [ppm]	mSigma	rdb	e ⁻ Conf	N-Rule	z
625.2354	1	C 42 H 34 Na O 4	100.00	625.2349	-0.5	-0.8	26.0	25.5	even	ok	1+
1227.4795	1	C 84 H 68 Na O 8	100.00	1227.4806	1.1	0.9	11.2	50.5	even	ok	

$^1\text{H-NMR}$, HMBC, HMQC (CDCl_3 , 600/150 MHz, 25 °C) and HR-ESI spectra of compound (10)



Ri-675 in CDCl_3 , 298K, HMBC



Ri-675 in CDCl₃, 298K, HMBCRi-675 in CDCl₃, 298K, HMQC

Mass Spectrum SmartFormula Report

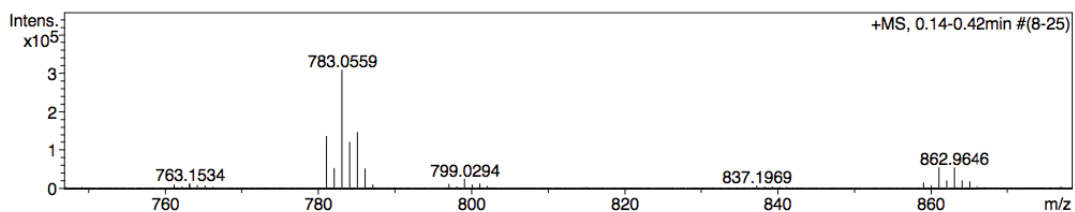
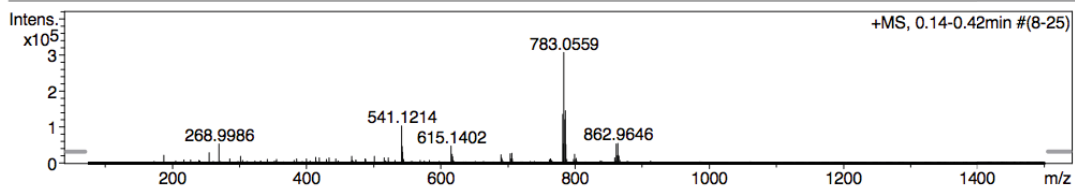
Analysis Info

Analysis Name N:\new acq data\Ri639 002.d
 Method hn Direct_Infusion_pos mode_75-1500 mid.m
 Sample Name Michel Rickhaus, Ri639
 Comment Ri639, 3.8 ug/ml MeCN ?

Acquisition Date 18.02.2014 09:34:23
 Operator hn
 Instrument / Ser# maXis 4G 21243

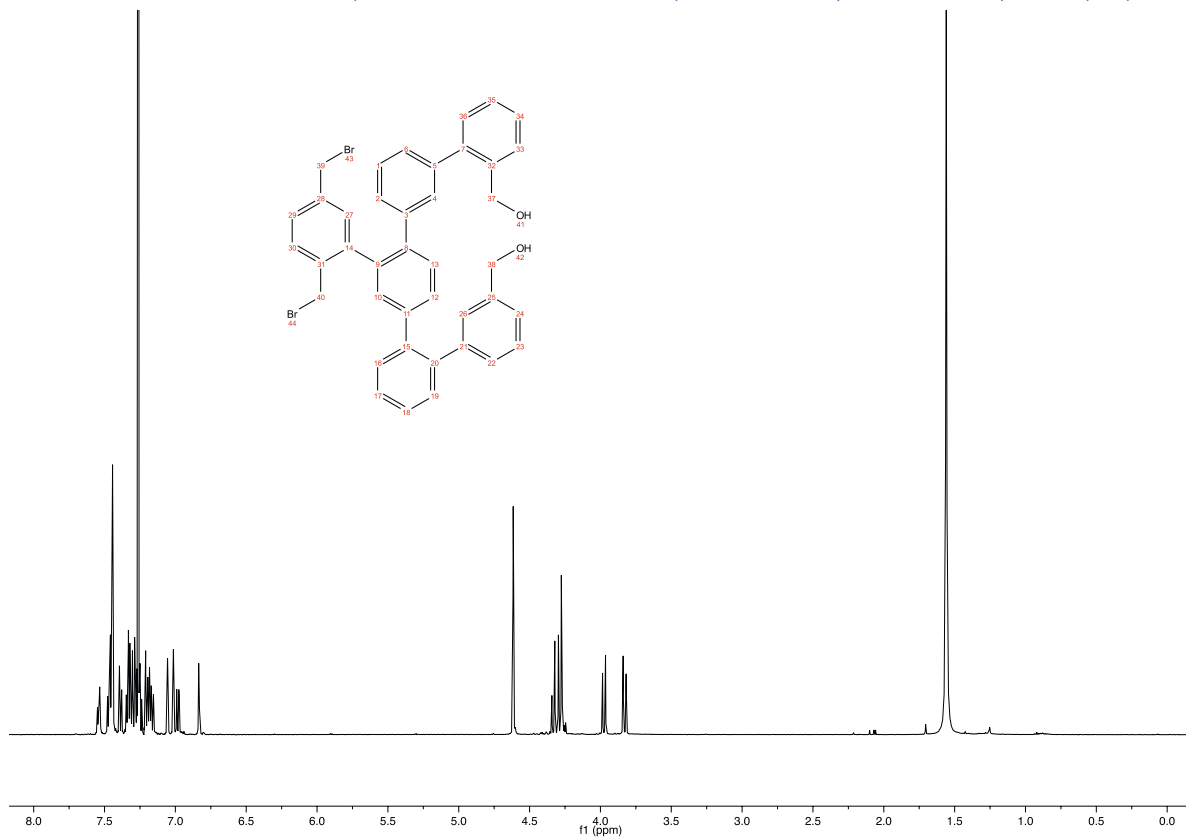
Acquisition Parameter

Source Type	ESI	Ion Polarity	Positive	Set Nebulizer	0.4 Bar
Focus	Not active	Set Capillary	4500 V	Set Dry Heater	180 °C
Scan Begin	75 m/z	Set End Plate Offset	-500 V	Set Dry Gas	4.0 l/min
Scan End	1500 m/z	Set Collision Cell RF	500.0 Vpp	Set Divert Valve	Waste

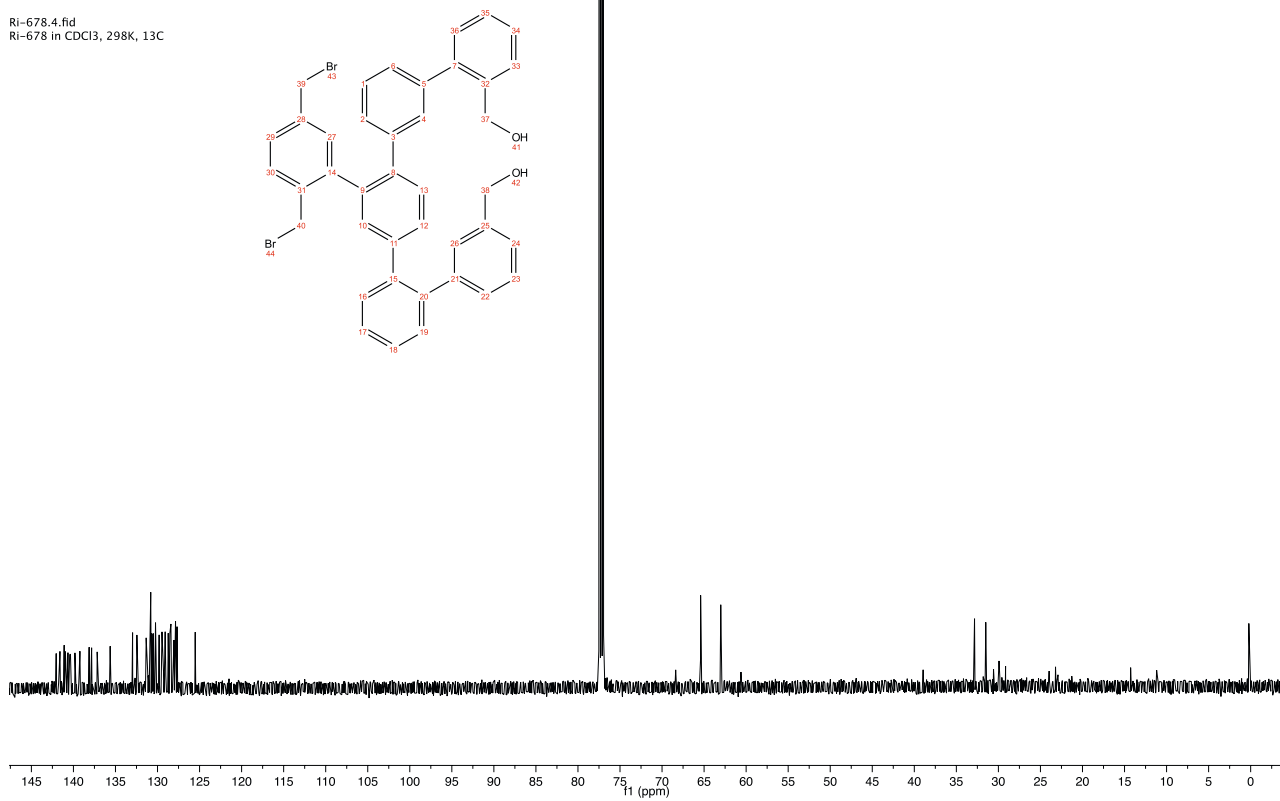


Meas. m/z	#	Formula	Score	m/z	err [mDa]	err [ppm]	mSigma	rdb	e ⁻ Conf	N-Rule	z
781.0574	1	C 42 H 32 Br 2 Na O 4	100.00	781.0560	-1.4	-1.9	50.3	25.5	even	ok	1+

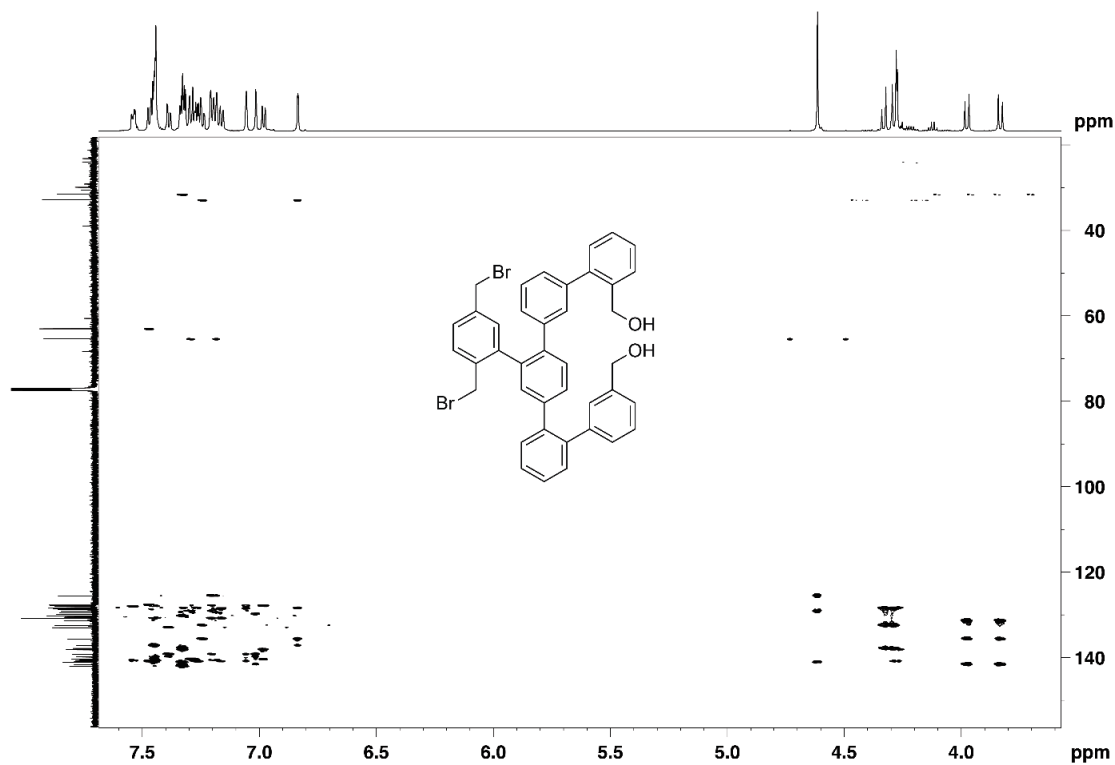
^1H -, ^{13}C -NMR, HMBC, HMQC (CDCl_3 , 600/150 MHz, 25 °C) and HR-ESI spectra of compound (**11**)



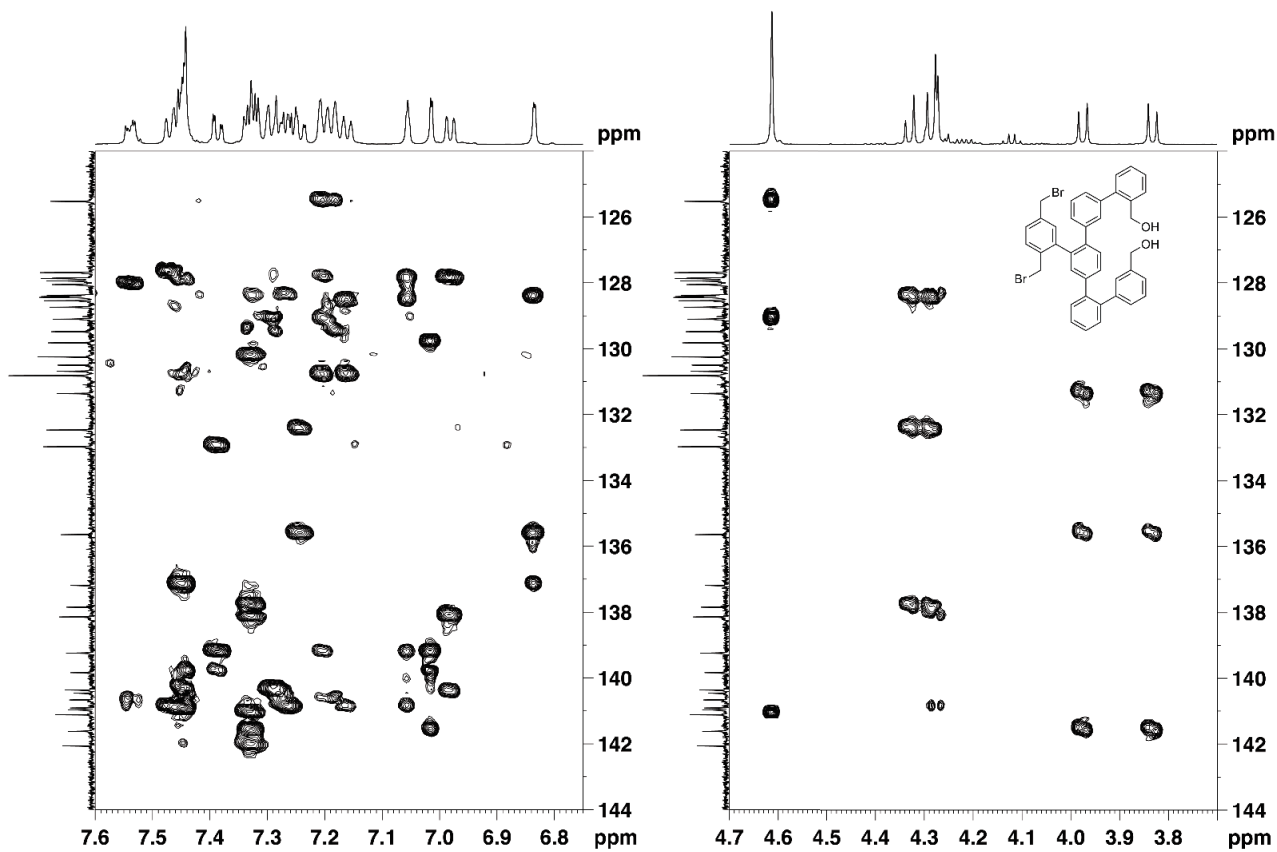
R1-678.4.fid
R1-678 in CDCl_3 , 298K, 13C

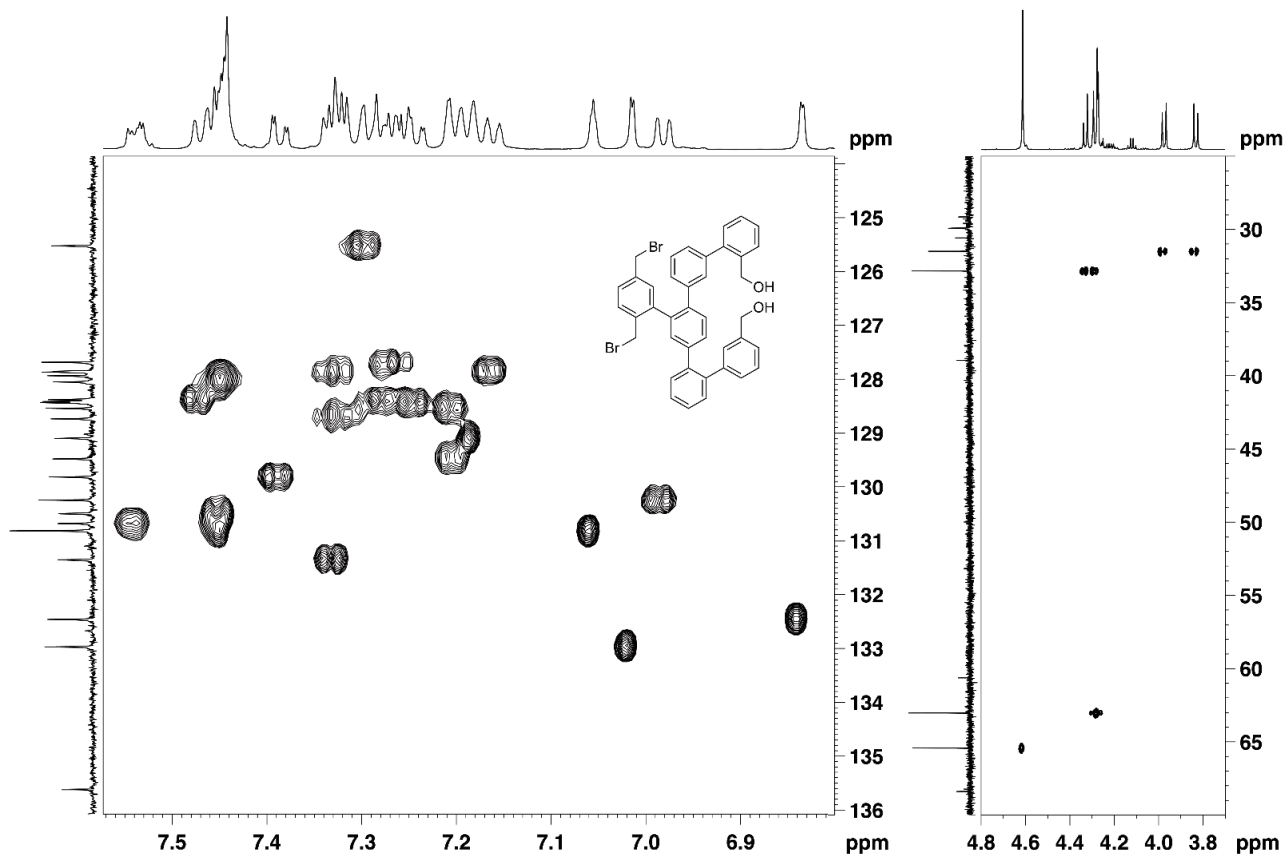


Ri-678 in CDCl₃, 298K, HMBC



Ri-678 in CDCl₃, 298K, HMBC



Ri-678 in CDCl₃, 298K, HMQC

Mass Spectrum SmartFormula Report

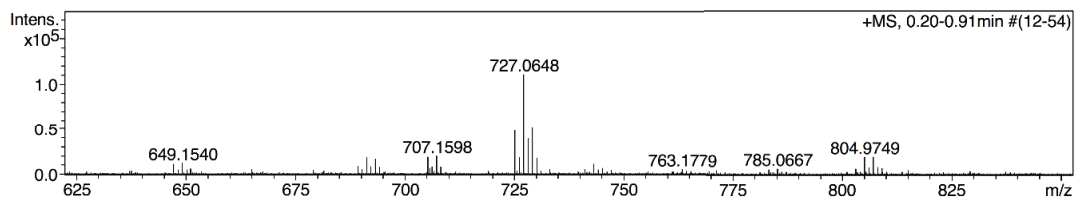
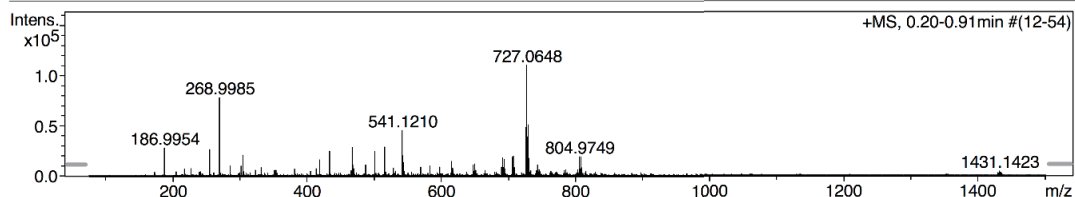
Analysis Info

Analysis Name N:\new acq data\Ri647 002.d
 Method hn Direct_Infusion_pos mode_75-1500 mid.m
 Sample Name Michel Rickhaus, Ri647
 Comment Ri647, 3 ug/ml MeCN ?

Acquisition Date 18.02.2014 09:01:56
 Operator hn
 Instrument / Ser# maXis 4G 21243

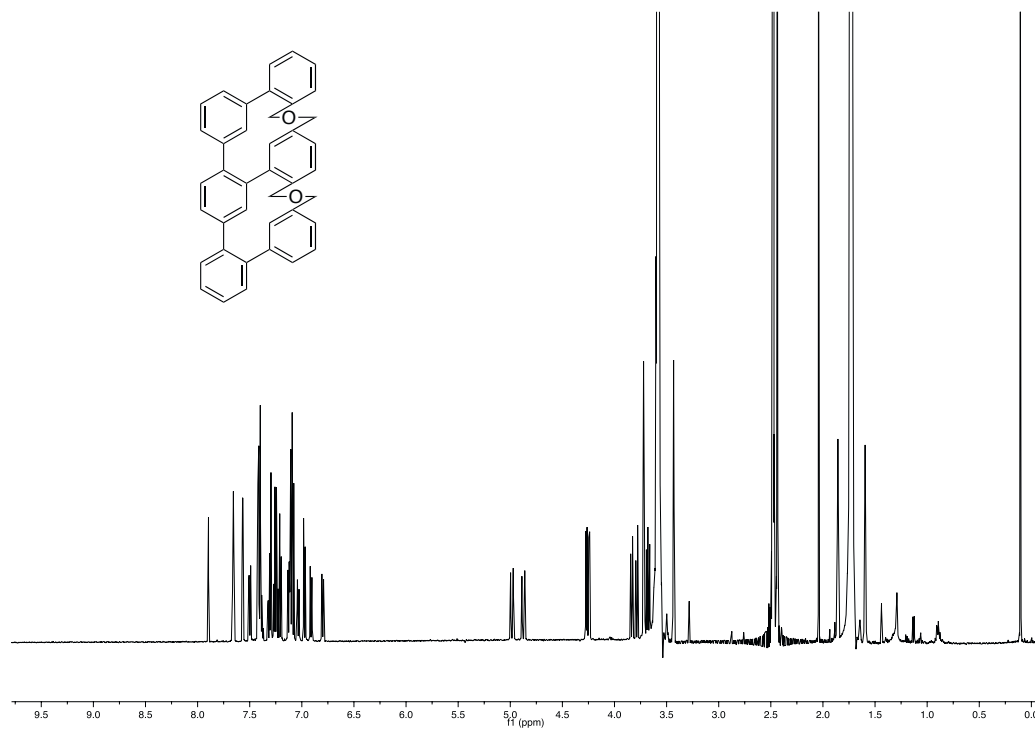
Acquisition Parameter

Source Type	ESI	Ion Polarity	Positive	Set Nebulizer	0.4 Bar
Focus	Not active	Set Capillary	4500 V	Set Dry Heater	180 °C
Scan Begin	75 m/z	Set End Plate Offset	-500 V	Set Dry Gas	4.0 l/min
Scan End	1500 m/z	Set Collision Cell RF	500.0 Vpp	Set Divert Valve	Waste

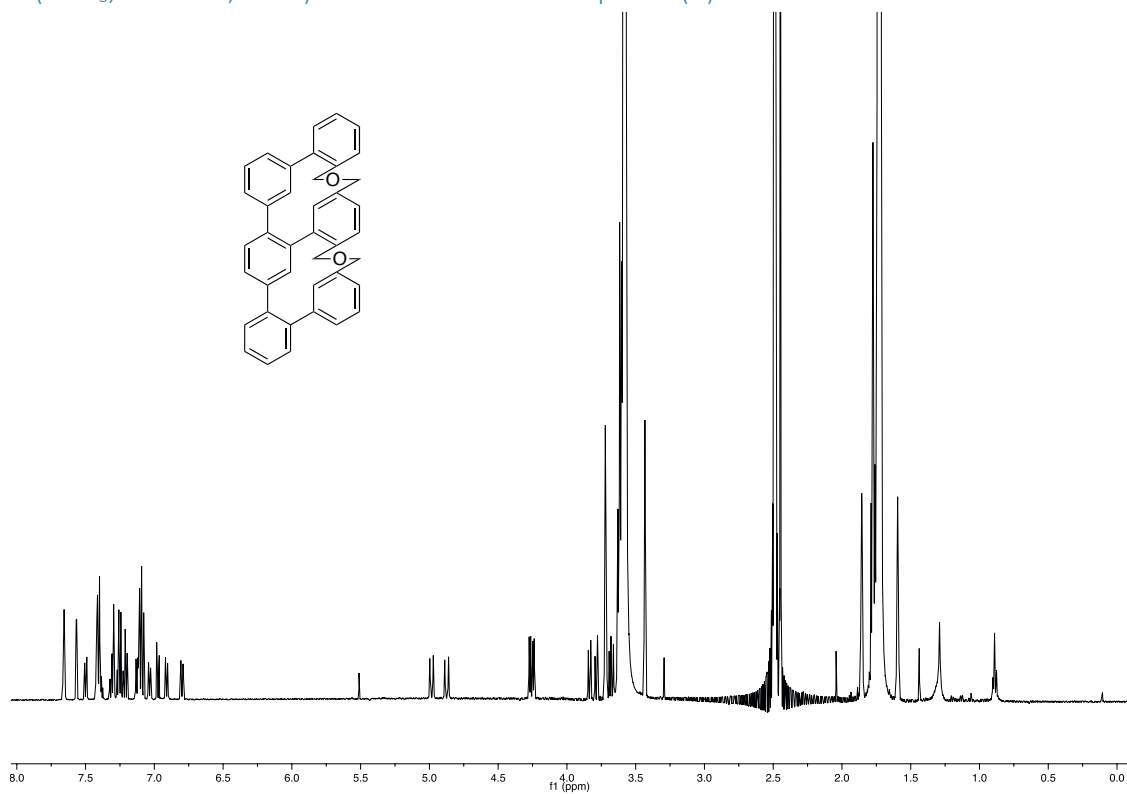


Meas. m/z	#	Formula	Score	m/z	err [mDa]	err [ppm]	mSigma	rdb	e ⁻ Conf	N-Rule	z
725.0663	1	C 40 H 32 Br 2 Na O 2	100.00	725.0661	-0.2	-0.3	53.9	23.5	even	ok	1+

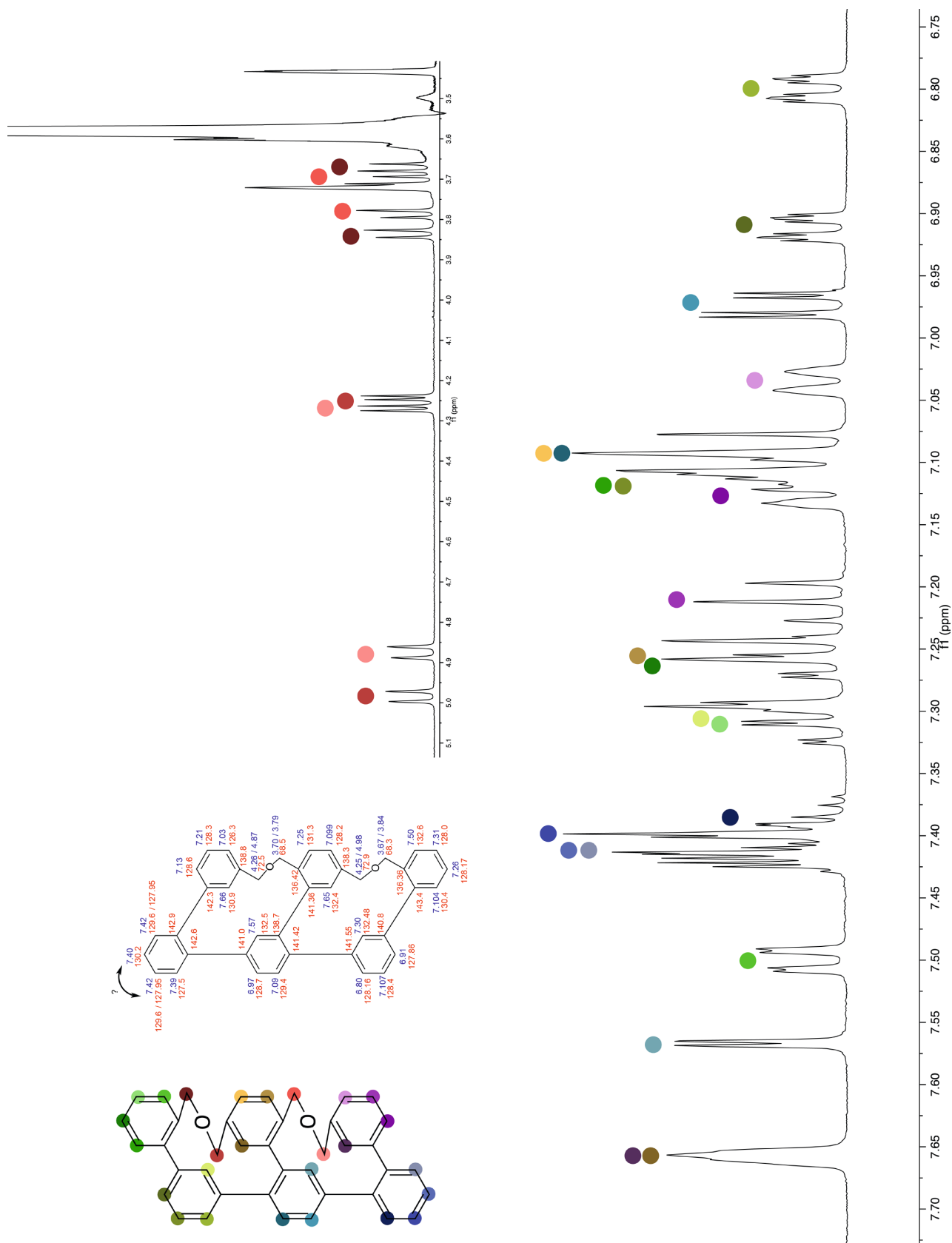
$^1\text{H-NMR}$ (CDCl_3 , 600 MHz, 25 °C) of enantiomer A of compound (1)



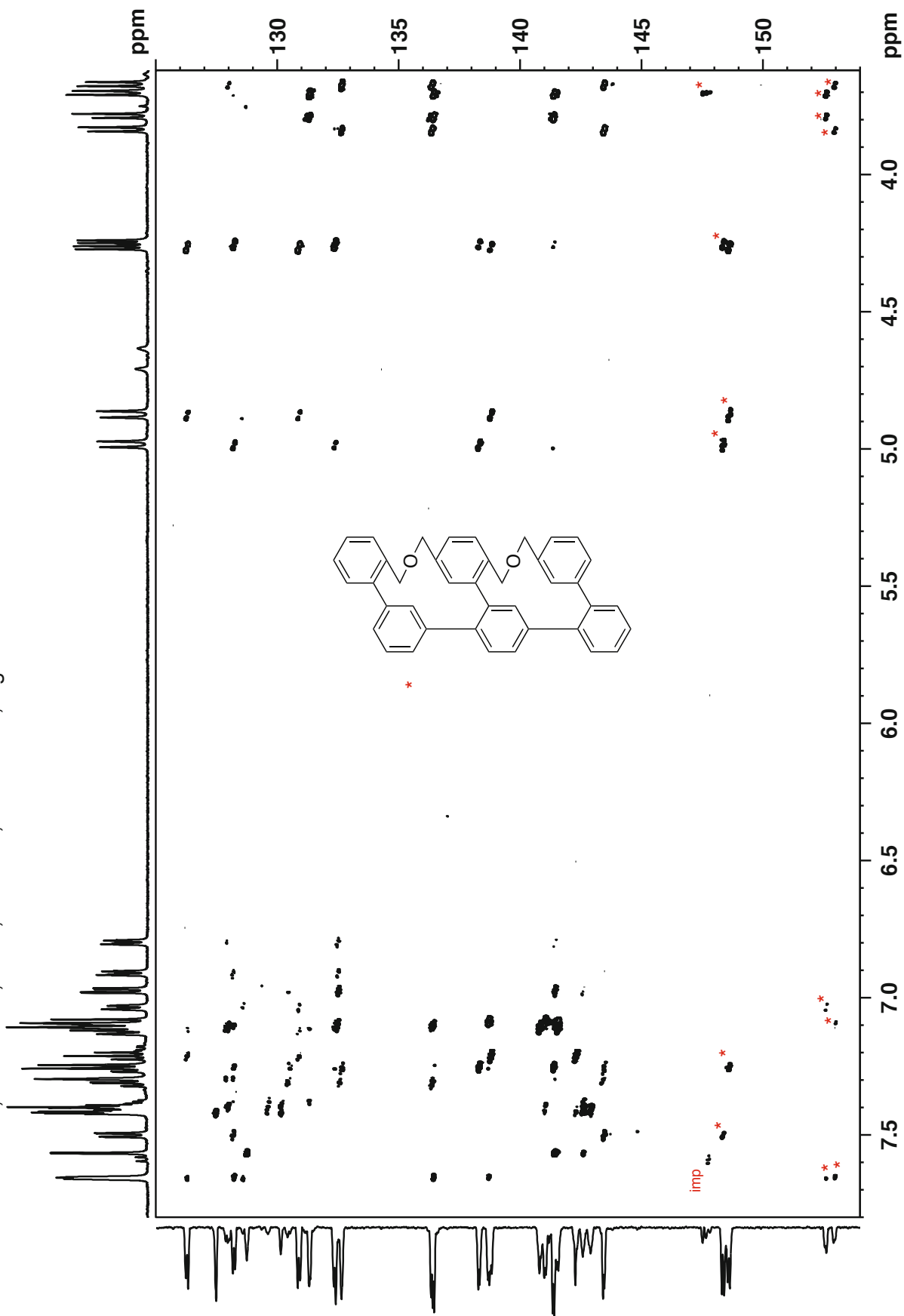
$^1\text{H-NMR}$ (CDCl_3 , 600 MHz, 25 °C) of enantiomer B of compound (1)



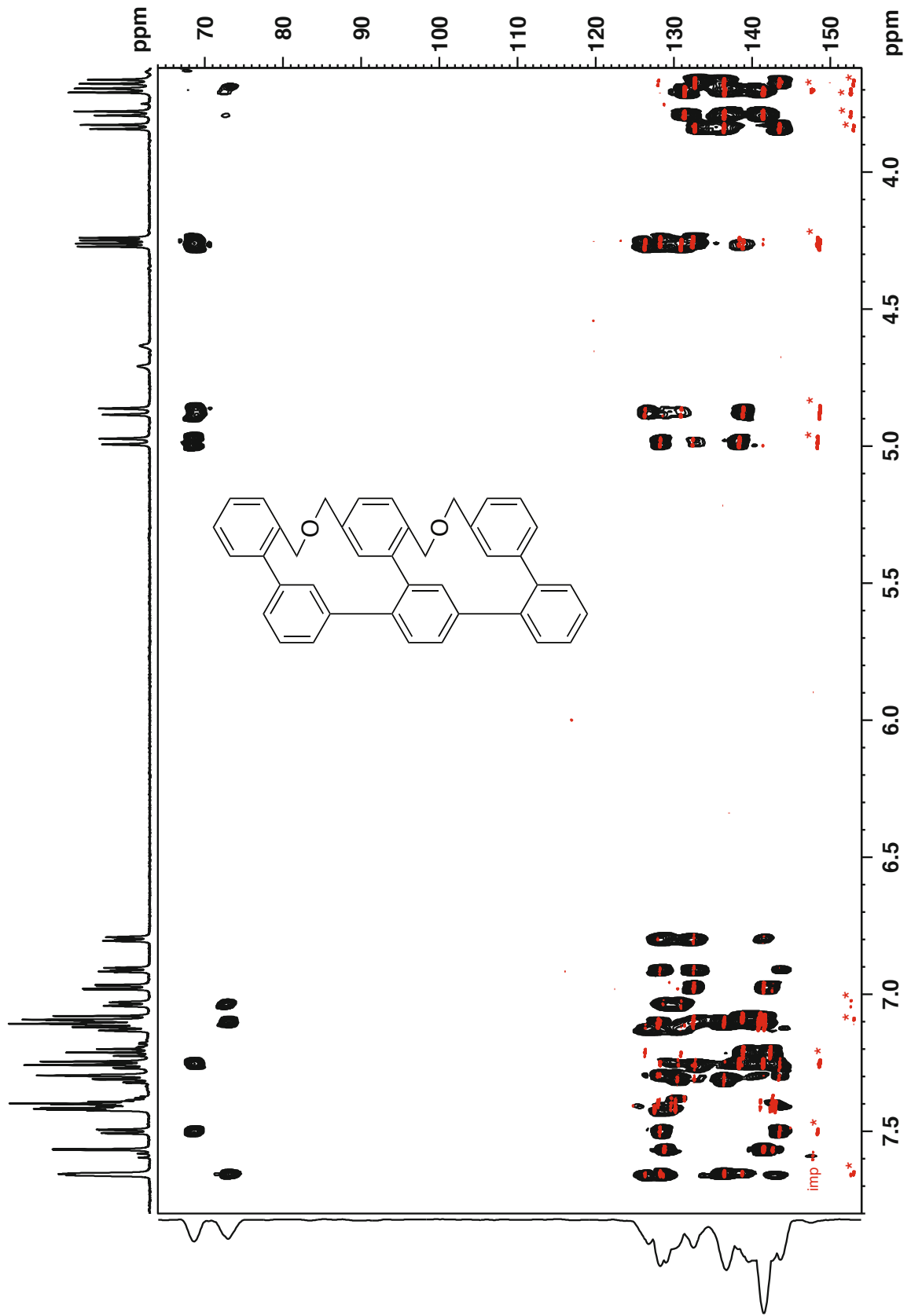
¹H-, ¹³C-NMR, COSY, NOESY, HMBC, HMQC (THF-d₈, 600/151 MHz, 25 °C) and HR-ESI spectra of enantiomer A of compound (1) with full assignment



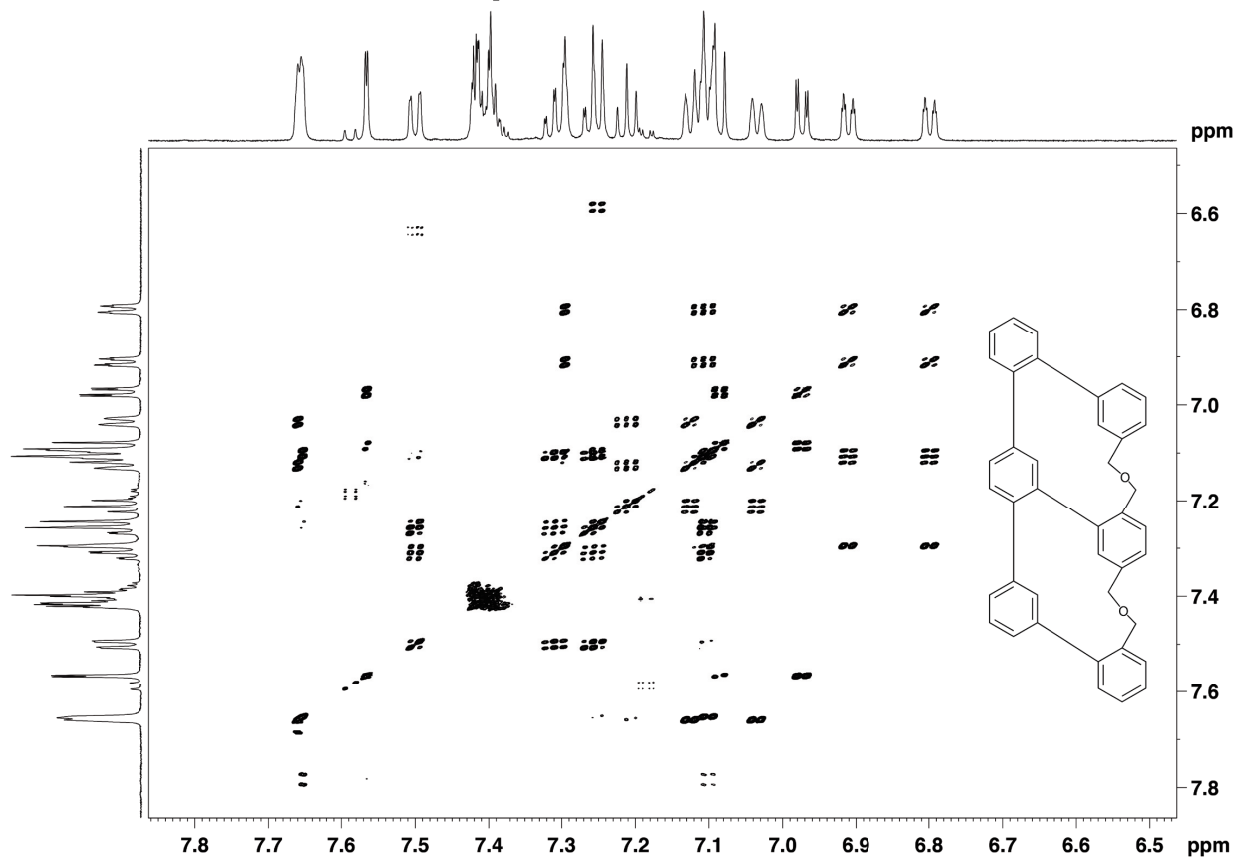
Ri-642-E1, in THF-d8, 298K, 600MHz, HMBC TCl, high resolution



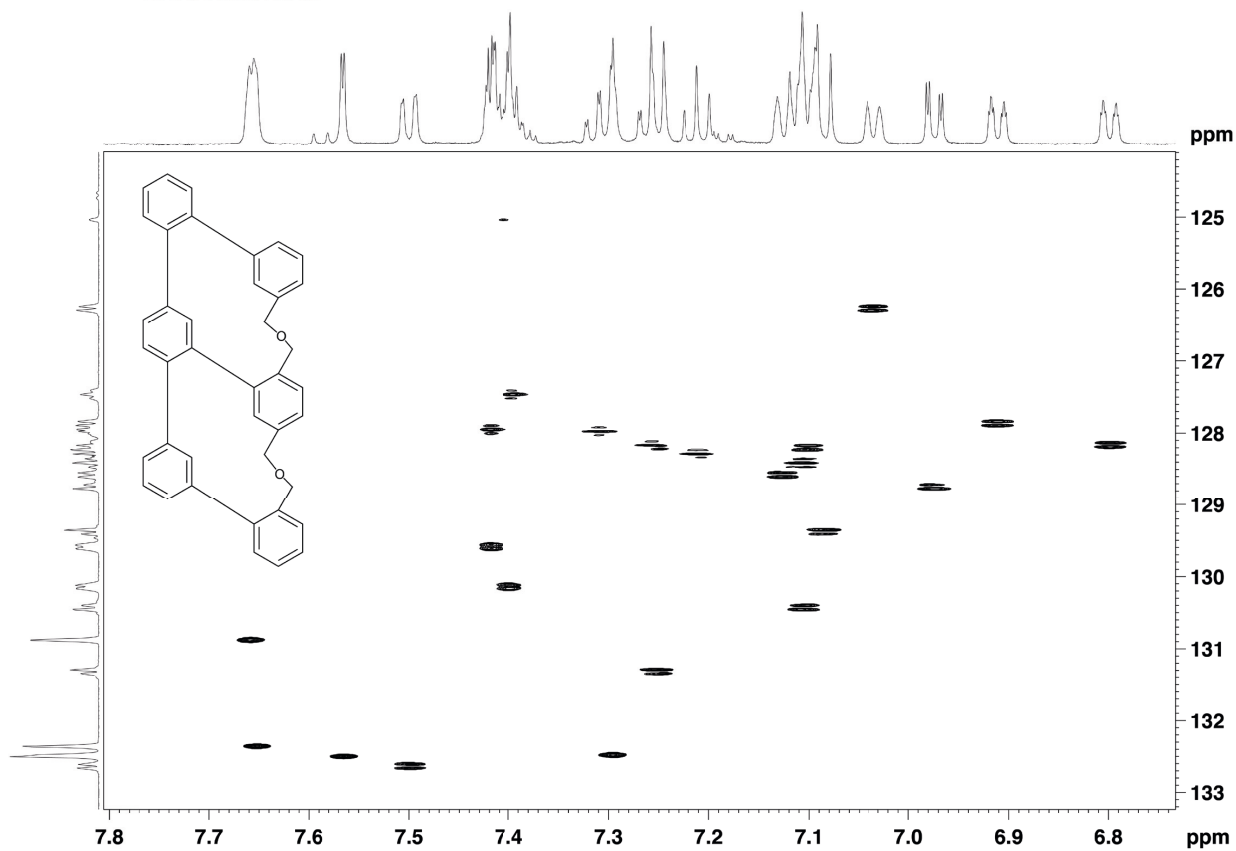
Ri-642-E1, in THF-d8, 298K, 600MHz, HMBC TCI



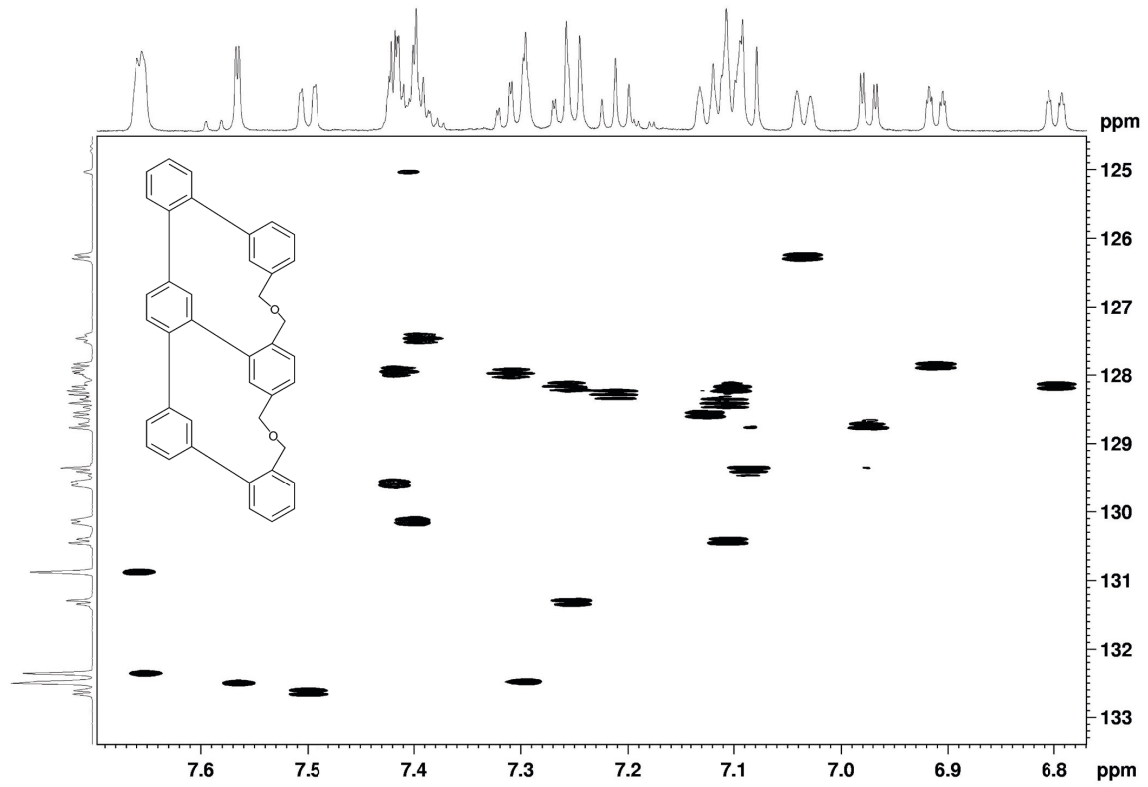
Ri-642-E1, in THF-d8, 298K, 600MHz, TCI, cosy



Ri 642 E1, THF-d8, 298K, 600M, HMQC



Ri 642 E1, THF-d8, 298K, 600M, HSQC



S

Mass Spectrum SmartFormula Report

Analysis Info

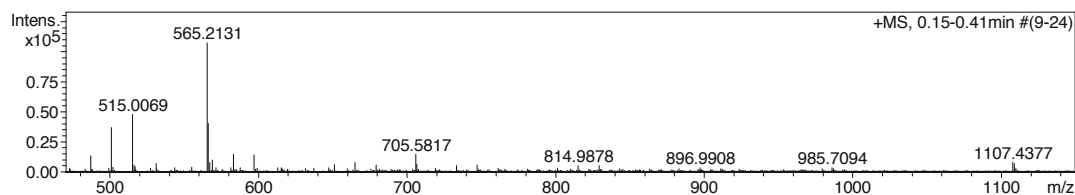
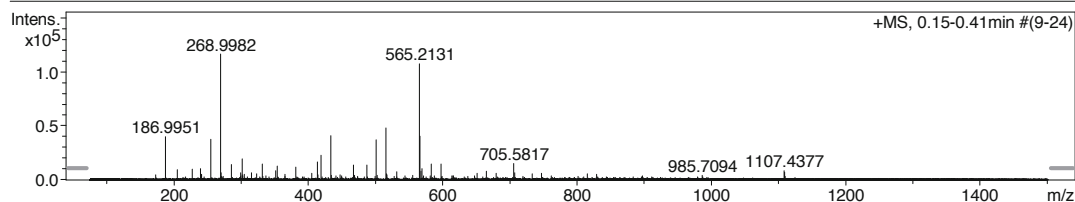
Analysis Name N:\new acq data\Ri642 001.d
 Method hn Direct_Infusion_pos mode_75-1500 mid.m
 Sample Name Michel Rickhaus, Ri642
 Comment Ri642, 2 ug/ml MeCN, hinter MeOH/NaOAc

Acquisition Date 18.02.2014 11:18:58

Operator hn
 Instrument / Ser# maXis 4G 21243

Acquisition Parameter

Source Type	ESI	Ion Polarity	Positive	Set Nebulizer	0.4 Bar
Focus	Not active	Set Capillary	4500 V	Set Dry Heater	180 °C
Scan Begin	75 m/z	Set End Plate Offset	-500 V	Set Dry Gas	4.0 l/min
Scan End	1500 m/z	Set Collision Cell RF	500.0 Vpp	Set Divert Valve	Waste



Meas. m/z	#	Formula	Score	m/z	err [mDa]	err [ppm]	mSigma	rdb	e ⁻ Conf	N-Rule	z
565.2131	1	C 40 H 30 Na O 2	100.00	565.2138	0.7	1.2	31.9	25.5	even	ok	1+
1107.4377	1	C 80 H 60 Na O 4	100.00	1107.4384	0.7	0.6	13.0	50.5	even	ok	

Generic Display Report

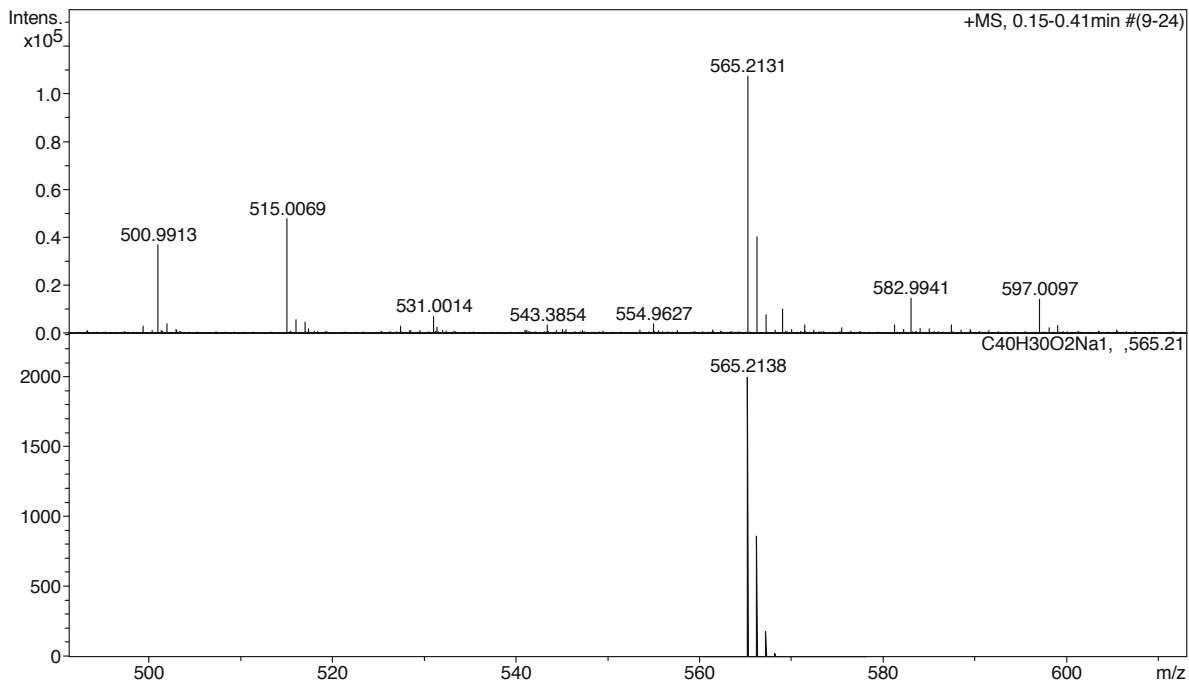
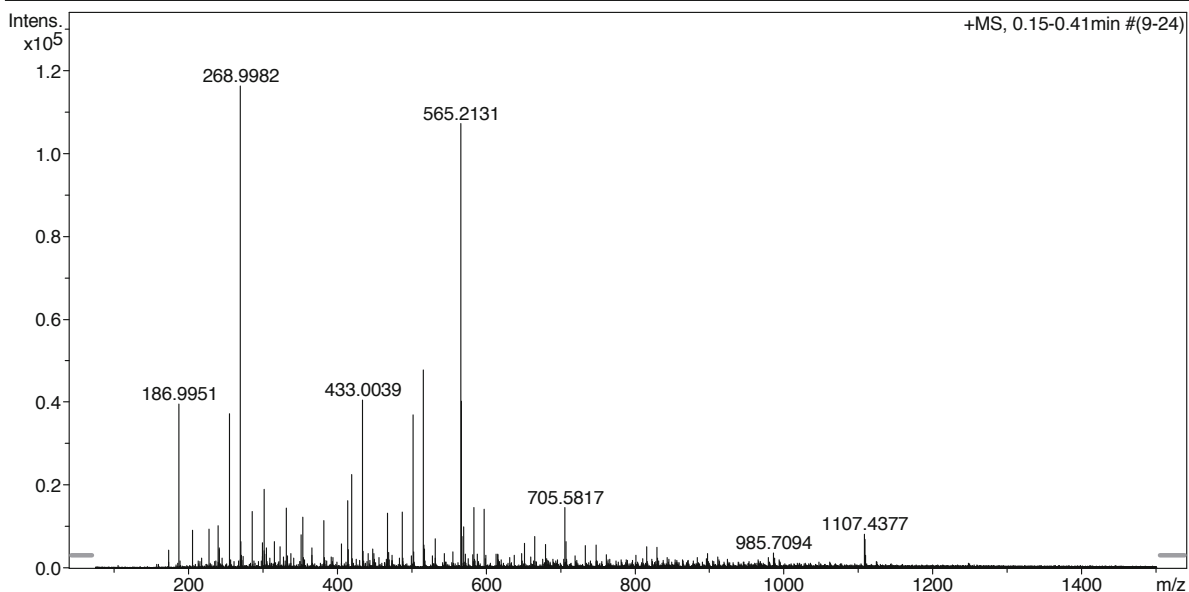
Analysis Info

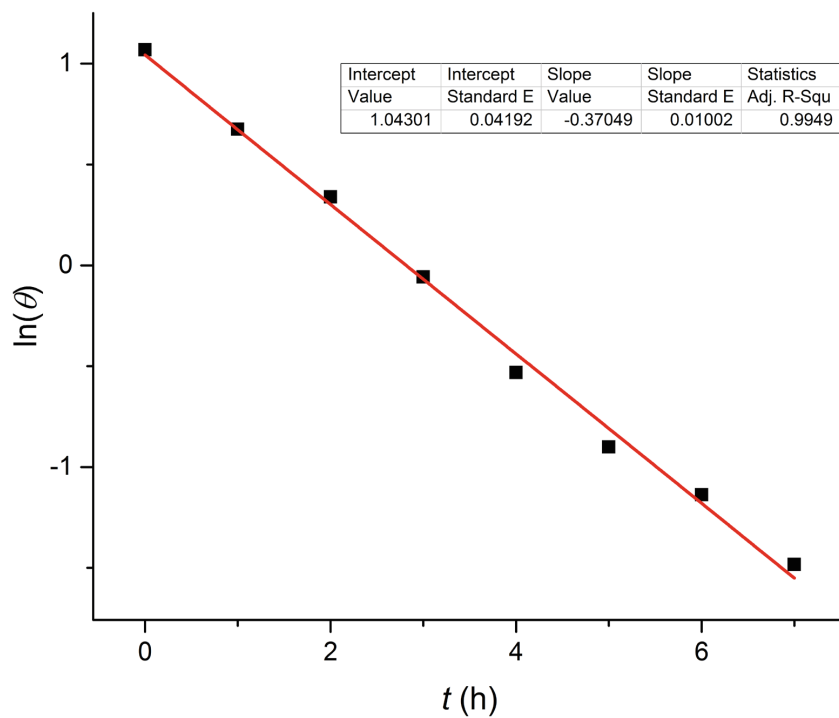
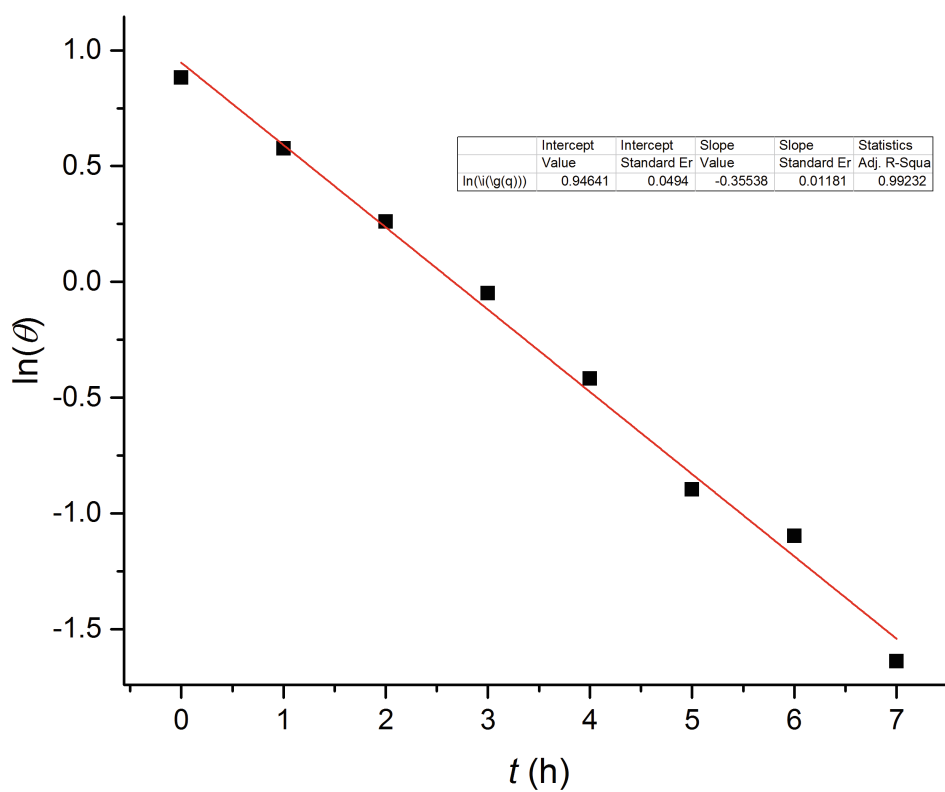
Analysis Name N:\new acq data\ri642 001.d
 Method hn Direct_Infusion_pos mode_75-1500 mid.m
 Sample Name Michel Rickhaus, Ri642
 Comment Ri642, 2 ug/ml MeCN, hinter MeOH/NaOAc

Acquisition Date 18.02.2014 11:18:58
 Operator hn
 Instrument / Ser# maXis 4G 21243

Acquisition Parameter

Source Type	ESI	Ion Polarity	Positive	Set Nebulizer	0.4 Bar
Focus	Not active	Set Capillary	4500 V	Set Dry Heater	180 °C
Scan Begin	75 m/z	Set End Plate Offset	-500 V	Set Dry Gas	4.0 l/min
Scan End	1500 m/z	Set Collision Cell RF	500.0 Vpp	Set Divert Valve	Waste



Measured CD decay at 222 nm of one enantiomer of (1) and linear regression of $\ln(\theta)$ against t Measured CD decay at 197 nm of one enantiomer of (1) and linear regression of $\ln(\theta)$ against t 

Determination of the rotation barrier of compound (1) at 222 nm

The rate of racemization between *M* and *P* enantiomer can be described as a first order process with

$$\ln \frac{[A]_t - [A]_{eq}}{[A]_0 - [A]_{eq}} = (k_1 + k_{-1})t \quad (1)$$

with $[A]_0$ being the concentration at $t = 0$, $[A]_t$ the concentration at the observed time t and $[A]_{eq}$ the concentration at the equilibrium and, k_1 and k_{-1} the rate constants for the forward and backward process.

Equation 1 can be expressed as

$$\ln \frac{\Delta A_t}{\Delta A_0} = -2k_1 t \sim \ln \Delta A_t \quad (2)$$

since $k_1 = k_{-1}$ and the linear relationship between the CD signal and the initial concentration. ΔA_0 and ΔA_t are the difference in absorption at $t = 0$ or t , respectively.

Plotting t against $\ln \Delta A_t$ gives access to k_1 directly from the slope. The obtained k_1 can then be used to calculate the free Gibbs energy of racemization ΔG^\ddagger by the rearranged Eyring equation:

$$\Delta G^\ddagger(T) = -RT \ln \left(\frac{hk_1}{k_B T} \right) = 97.5 \frac{\text{kJ}}{\text{mol}} \quad (3)$$

Where k_1 is the obtained kinetic rate constant ($k_1 = 5.14568 \times 10^{-6} \text{ s}^{-1}$), k_B the Boltzmann constant ($k_B = 1.380662 \times 10^{-23} \text{ J K}^{-1}$), h Planck's constant ($h = 6.626176 \times 10^{-34} \text{ J s}$), R the universal gas constant ($R = 8.31446 \times 10^{-3} \text{ kJ K}^{-1} \text{ mol}^{-1}$), and T the temperature (298.15 °K).

$\Delta\epsilon$ and ϵ values of compound (1)

λ [nm]	$\Delta\epsilon$ for enantiomer A [M ⁻¹ cm ⁻¹]	$\Delta\epsilon$ for enantiomer B [M ⁻¹ cm ⁻¹]	ϵ for racemate [M ⁻¹ cm ⁻¹]
350	0.5183	-0.5095	49.6732
348	0.4573	-0.5453	111.7648
346	0.4997	-0.6114	111.7648
344	0.5771	-0.5043	111.7648
342	0.4640	-0.6046	49.6732
340	0.5198	-0.5785	49.6732
338	0.5339	-0.5897	136.6014
336	0.4856	-0.6789	111.7648
334	0.5696	-0.7086	136.6014
332	0.3852	-0.7731	136.6014
330	0.4663	-0.7400	136.6014
328	0.4603	-0.6221	161.4380
326	0.5443	-0.6564	223.5295
324	0.4388	-0.6982	161.4380
322	0.4901	-0.6921	186.2746
320	0.3986	-0.6827	186.2746
318	0.4878	-0.7105	273.2027
316	0.4469	-0.6350	298.0394
314	0.4127	-0.7565	322.8760
312	0.3882	-0.6352	347.7126
310	0.4432	-0.6926	372.5492
308	0.4744	-0.6776	397.3858
306	0.5324	-0.6611	509.1506
304	0.3978	-0.5438	558.8238
302	0.4707	-0.7331	695.4252
300	0.4536	-0.6096	745.0984
298	0.3726	-0.6429	881.6998
296	0.5466	-0.6773	1018.3011
294	0.4938	-0.6328	1154.9025
292	0.6001	-0.5990	1279.0856
290	0.5704	-0.6010	1440.5236
288	0.6172	-0.6563	1626.7982
286	0.8254	-0.6614	1813.0728
284	0.8254	-0.7057	2086.2755
282	0.8924	-0.6441	2297.3867
280	0.6834	-0.4216	2533.3346
278	0.1688	-0.0642	2744.4458
276	-0.0341	0.2641	3042.4851
274	0.2826	-0.0327	3278.4330
272	0.3696	-0.0704	3514.3808
270	0.2781	-0.0684	3812.4201
268	0.1599	0.1367	4110.4595
266	0.2945	-0.1227	4135.2961
264	0.6492	-0.2563	4420.9172

λ [nm]	$\Delta\epsilon$ for enantiomer A [M ⁻¹ cm ⁻¹]	$\Delta\epsilon$ for enantiomer B [M ⁻¹ cm ⁻¹]	ϵ for racemate [M ⁻¹ cm ⁻¹]
262	0.7660	-0.4921	4855.5579
260	0.9370	-0.6048	5302.6169
258	1.3386	-0.8819	5861.4407
256	1.5096	-1.0126	6469.9378
254	1.4352	-0.9363	7301.9643
252	1.2270	-0.6209	8171.2458
250	0.7050	0.0575	9264.0568
248	-0.3101	1.1612	10406.5410
246	-1.8889	2.8089	11611.1167
244	-0.9934	4.9400	12778.4375
242	-0.0086	7.0782	13920.9217
240	-0.5659	8.6313	15038.5693
238	-0.5047	8.5021	16131.3803
236	-0.9308	8.3424	17298.7011
234	-0.6685	10.0731	18602.6233
232	-12.4923	14.2081	20092.8201
230	-18.9721	20.2790	21744.4549
228	-08.9773	29.9199	23445.7629
226	-01.1793	41.9012	25258.8357
224	-03.1204	52.9409	27171.2549
222	-02.3531	61.2677	28959.4911
220	-05.2993	64.1538	30648.3808
218	-01.5807	61.3199	32026.8128
216	-02.5628	52.4251	33231.3886
214	-09.7120	40.4031	34175.1799
212	-04.3132	26.2233	34845.7684
210	-0.5818	11.4507	35466.6838
208	9.0024	-0.7453	36037.9259
206	26.0612	-00.1554	36571.9130
204	42.3066	-05.5014	36795.4426
202	59.8076	-00.4774	35814.3963
200	68.7126	-09.9030	30536.6160
198	29.7386	-00.3408	14492.1638
196	2.8333	-0.1119	1316.3405

Eur. J. Org. Chem. **2015** · © WILEY-VCH Verlag GmbH & Co. KGaA, 69451 Weinheim, 2015 · ISSN 1099–0690

SUPPORTING INFORMATION



DOI: 10.1002/ejoc.201403322

Title: Through the Maze: Cross-Coupling Pathways to a Helical Hexaphenyl “Geländer” Molecule

Author(s): Michel Rickhaus, Linda Maria Bannwart, Oliver Unke, Heiko Gsellinger, Daniel Häussinger, Marcel Mayor*

!

Supporting Information

Table of Contents

Table 1: Screening for optimal Suzuki conditions to access 11 and 12	2
Table 2: Screening for borylation conditions of 11 , 12 , 15 and 18	2
¹ H-, ¹³ C-NMR (CDCl ₃ , 400/101 MHz, 25 °C) of methyl 3'-bromo-[1,1'-biphenyl]-2-carboxylate (11).....	4
¹ H-, ¹³ C-NMR (CDCl ₃ , 400/63 MHz, 25 °C) of methyl 3'-(5,5-dimethyl-1,3,2-dioxaborinan-2-yl)-[1,1'-biphenyl]-2-carboxylate (14).....	5
¹ H-, ¹³ C-NMR (CDCl ₃ , 400/101 MHz, 25 °C) of (3'-bromo-[1,1'-biphenyl]-2-yl)methanol (15).....	6
¹ H-, ¹³ C-NMR (CDCl ₃ , 400/63 MHz, 25 °C) of (3'-Iodo-[1,1'-biphenyl]-2-yl)methanol (16).....	7
¹ H-NMR (CDCl ₃ , 400 MHz, 25 °C) of <i>tert</i> -butyl((3'-iodo-[1,1'-biphenyl]-2-yl) methoxy) dimethylsilane (18).....	8
¹ H-, ¹³ C-NMR (CDCl ₃ , 400/63 MHz, 25 °C) of <i>tert</i> -butyl((3'-(5,5-dimethyl-1,3,2-dioxaborinan-2-yl)-[1,1'-biphenyl]-2-yl)methoxy)dimethylsilane (19).....	9
¹ H-, ¹³ C-NMR (CDCl ₃ , 400/101 MHz, 25 °C) of methyl 2'-bromo-[1,1'-biphenyl]-3-carboxylate (24).....	10
¹ H-, ¹³ C-NMR (CDCl ₃ , 400/101 MHz, 25 °C) of methyl 2'-iodo-[1,1'-biphenyl]-3-carboxylate (25).....	11
¹ H-NMR, HMBC, HMQC and COSY (CDCl ₃ , 500/125 MHz, 25 °C) of methyl 2'-(4,4,5,5-tetramethyl-1,3,2-dioxaborolan-2-yl)-[1,1'-biphenyl]-3-carboxylate (26).....	12
¹ H-, ¹³ C-NMR (CDCl ₃ , 400/101 MHz, 25 °C) of (2'-bromo-[1,1'-biphenyl]-3-yl)methanol (27).....	14
¹ H-, ¹³ C-NMR (CDCl ₃ , 400/63 MHz, 25 °C) of (2'-Iodo-[1,1'-biphenyl]-3-yl) methanol (28).....	15
¹ H-, ¹³ C-NMR (CDCl ₃ , 400/101 MHz, 25 °C) of regioisomers (29) and (31).....	16
¹ H-, ¹³ C-NMR (CDCl ₃ , 400/101 MHz, 25 °C) of 1-bromo-2-iodo-4-methoxybenzene (33).....	20
¹ H-, HMQC (CDCl ₃ , 400/151 MHz, 25 °C) of methyl 5'-methoxy-[1,1':2',1'':3'',1'''-quaterphenyl]-2'''-carboxylate (34).....	21
¹ H-, ¹³ C-NMR, HMBC, HSQC, COSY, NOESY, TOCSY (CD ₂ Cl ₂ , 600/151 MHz, 25 °C) of 3-(5-methoxy-[1,1'-biphenyl]-2-yl)-9H-fluoren-9-one (36).....	22
¹ H-, ¹³ C-NMR, (CDCl ₃ , 400/63 MHz, 25 °C) of 2-bromo-5-nitro-1,1'-biphenyl (37).....	28
¹ H-, HMQC, (CDCl ₃ , 500/125 MHz, 25 °C) of <i>tert</i> -butyldimethyl((5'-nitro-[1,1':2',1'':3'',1'''-quaterphenyl]-2'''-yl)methoxy)silane (38).....	29
¹ H-NMR, (CDCl ₃ , 400 MHz, 25 °C) of methyl 5'-nitro-[1,1':2',1'':3'',1'''-quaterphenyl]-2'''-carboxylate (39).....	30
¹ H-NMR, (CDCl ₃ , 400 MHz, 25 °C) of methyl 5'-amino-[1,1':2',1'':3'',1'''-quaterphenyl]-2'''-carboxylate (41).....	31
¹ H-NMR, (CDCl ₃ , 400 MHz, 25 °C) of 1-((6-Bromo-[1,1'-biphenyl]-3-yl) diazenyl)pyrrolidine (44).....	31
¹ H-, ¹³ C-NMR, (CDCl ₃ , 400/101 MHz, 25 °C) of 2-bromo-5-iodo-1,1'-biphenyl (46):.....	32
¹ H-, ¹³ C-NMR, (CDCl ₃ , 400/151 MHz, 25 °C) of 2-(6-bromo-[1,1'-biphenyl]-3-yl)-5,5-dimethyl-1,3,2-dioxaborinane (48).....	33
¹ H-, NOESY, TOCSY (CDCl ₃ , 600 MHz, 25 °C) and HR-ESI of methyl 4''-bromo-[1,1':2',1'':3'',1'''-quaterphenyl]-3-carboxylate (50).....	34
¹ H-, ¹³ C-NMR (CDCl ₃ , 400/101 MHz, 25 °C) of dimethyl 3''-phenyl-[1,1':2',1'':4'',1''':3''',1''''-quinquephenyl]-2''''',3-dicarboxylate (52).....	37

Table 1: Screening for optimal Suzuki conditions to access 11 and 12

entry	coupling	cat	Base	solvent ⁽¹⁾	time	Δ	conv. (yield) ⁽⁵⁾
1	10 + 9 → 11	Pd(PPh ₃) ₄	K ₂ CO ₃	THF/MeOH 2:1	3 h/24 h (15 h)	60 °C	47/51 (49)
2 ⁽⁴⁾	10 + 9 → 11	XPhos Pd G2	K ₂ CO ₃	THF/MeOH 2:1	3 h/24 h	60 °C	24
3 ⁽⁴⁾	10 + 9 → 11	SPhos Pd G2	K ₂ CO ₃	THF/MeOH 2:1	3 h/24 h	60 °C	22
4 ⁽⁴⁾	10 + 9 → 11	Pd(dppf)Cl ₂	K ₂ CO ₃	THF/MeOH 2:1	3 h/24 h	60 °C	56
5	10 + 9 → 11	Pd(PPh ₃) ₂ Cl ₂	K ₂ CO ₃	THF/MeOH 2:1	3 h/24 h	60 °C	63
6 ⁽²⁾	10 + 9 → 11	Pd(PPh ₃) ₂ Cl ₂	K ₂ CO ₃	THF/MeOH 2:1	3 h/24 h	40 °C	63
7 ⁽²⁾	10 + 9 → 11	Pd(PPh ₃) ₂ Cl ₂	K ₂ CO ₃	THF/MeOH 2:1	3 h/24 h	60 °C	
8	10 + 9 → 11	Pd(PPh ₃) ₂ Cl ₂	KF	THF/MeOH 2:1	3 h/24 h (40 h)	60 °C	63 (51)
9	10 + 9 → 11	Pd(PPh ₃) ₂ Cl ₂	K ₂ CO ₃	THF	3 h/24 h	60 °C	24/54
10	10 + 9 → 11	Pd(PPh ₃) ₂ Cl ₂	K ₂ CO ₃	THF/MeOH 4:1	3 h/24 h	60 °C	63
11	10 + 9 → 11	Pd(PPh ₃) ₂ Cl ₂	K ₂ CO ₃	dioxane/H ₂ O 4:1	3 h/24 h	100 °C	52/57
12	20 + 9 → 12	Pd(PPh ₃) ₂ Cl ₂	K ₂ CO ₃	dioxane/H ₂ O 4:1	(20 h)	100 °C	(19)
13 ⁽⁴⁾	20 + 9 → 12	Pd(PPh ₃) ₂ Cl ₂	K ₂ CO ₃	dioxane/H ₂ O 4:1	3 h/24 h	100 °C	64
14 ⁽²⁾	20 + 9 → 12	Pd(PPh ₃) ₂ Cl ₂	K ₂ CO ₃	THF/MeOH 4:1	(16 h)	60 °C	(29)
15 ⁽³⁾	20 + 9 → 12	Pd(PPh ₃) ₂ Cl ₂	K ₂ CO ₃	THF/MeOH 4:1	(15 h)	60 °C	(54)

⁽¹⁾ 2 equivalents of 1,3-dihalobenzene; ⁽²⁾ 1 equivalent of 1,3-dihalobenzene; ⁽³⁾ 1.5 equivalents of 1,3-dihalobenzene; ⁽⁴⁾ side-products observed;

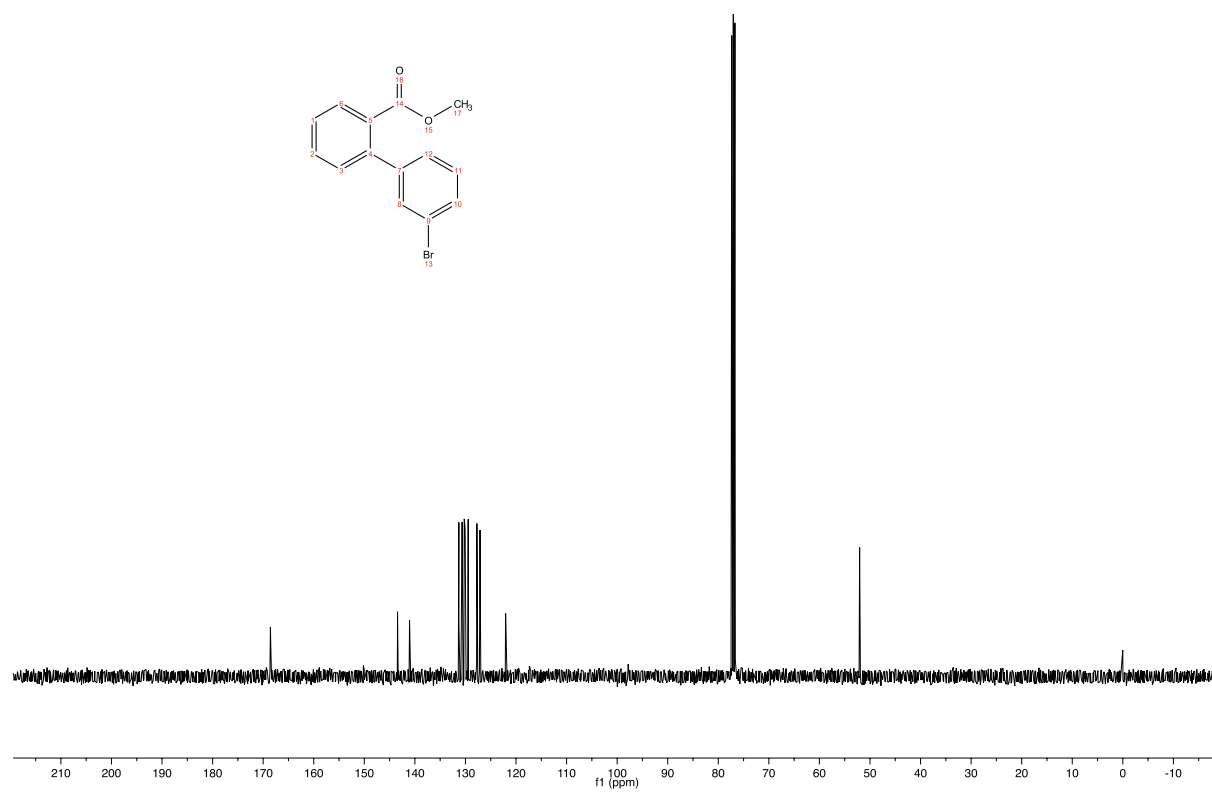
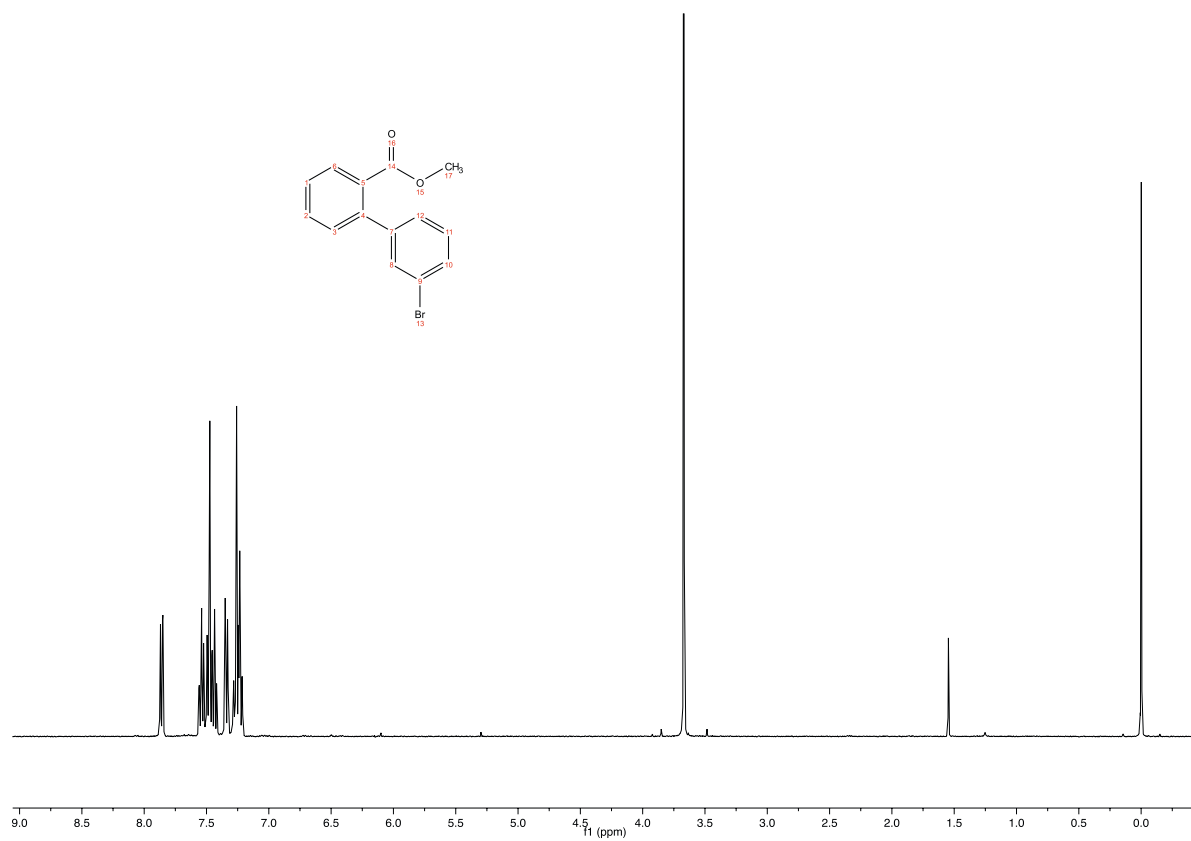
⁽⁵⁾ Conversion calculated with respect to 2-bromo-iodophenyl. If no change in conversion was observed from 3 h to 24 h, only one number is given.

Table 2: Screening for borylation conditions of 11, 12, 15 and 18

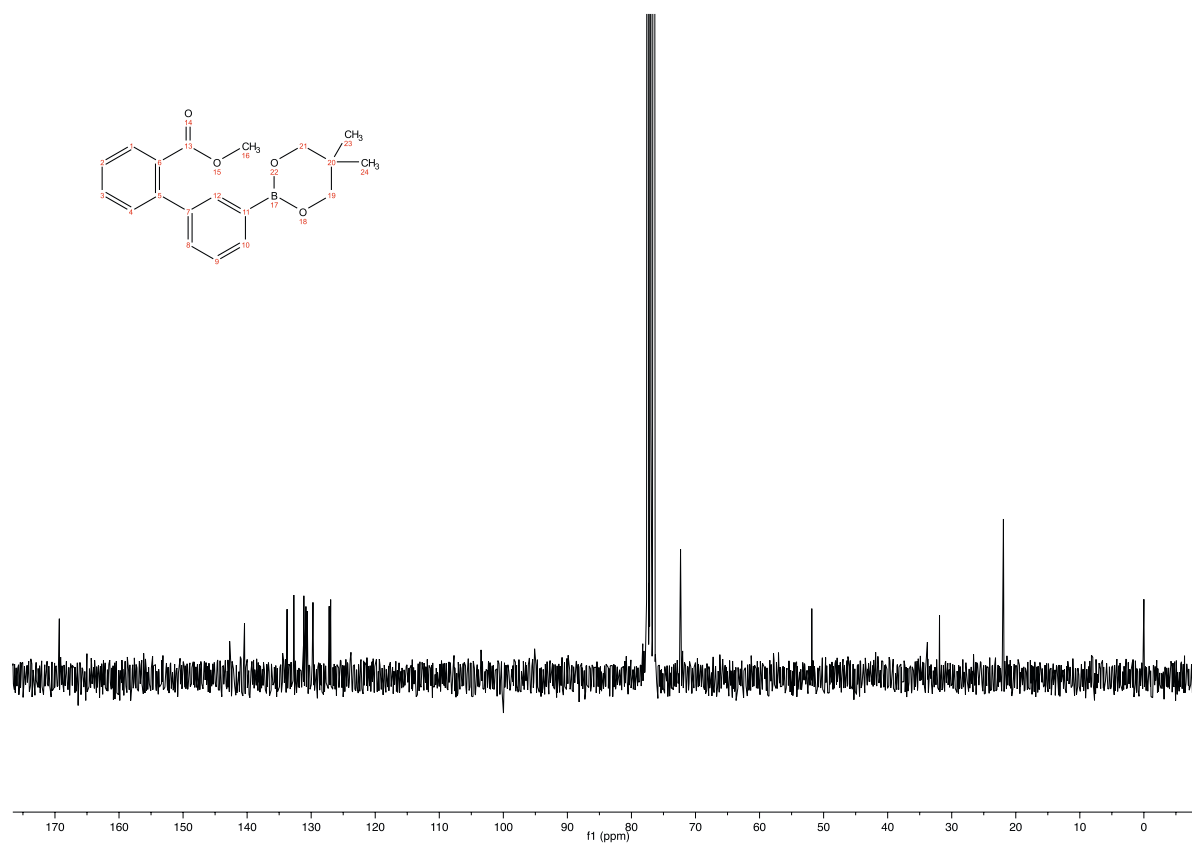
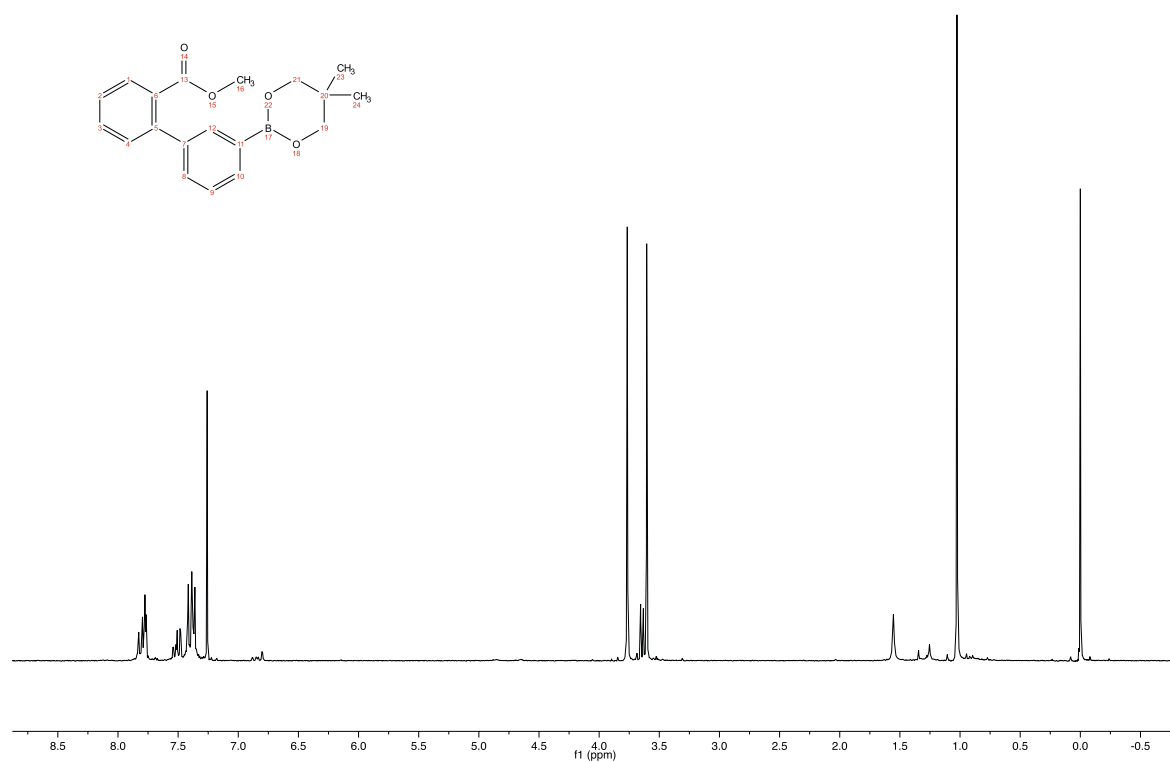
entry	starting material	product	Conditions ⁽¹⁾	time	conv. ⁽²⁾
1	11	13	A	6.5 h	5%
2	11	13	B	6.5 h	- ⁽⁴⁾
3	12	13	A	2 h	>99%
4	12	13	A ⁽⁵⁾	15 h	>99%/76% ⁽⁶⁾
5	12	14	C	15 h	72 ⁽³⁾ /31% ^(3,6)
6	15	17	A	6.5 h	<5% ⁽⁴⁾
7	18	19	C	6.5 h	45%

⁽¹⁾ A: Pd(dppf)Cl₂, B₂pin₂, KOAc, DMF, 100 °C; B: Conditions explored include sBuLi, tBuLi and LDA; C: *i*PrMgCl·LiCl, B(O*i*Pr)₃, neopentyl glycol, THF, -40 °C to room temperature; ⁽²⁾ determined by GC-MS; ⁽³⁾ isolated yield; ⁽⁴⁾ decomposition observed; ⁽⁵⁾ dioxane instead of DMF; ⁽⁶⁾ large scale.

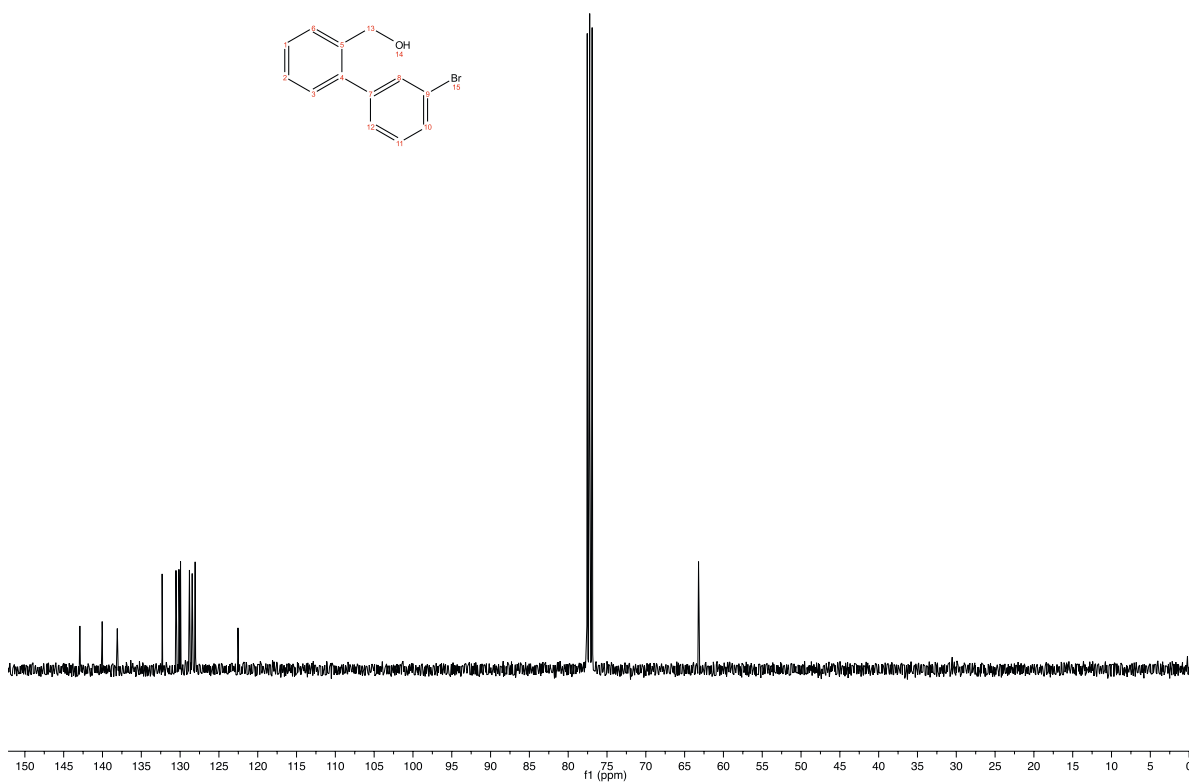
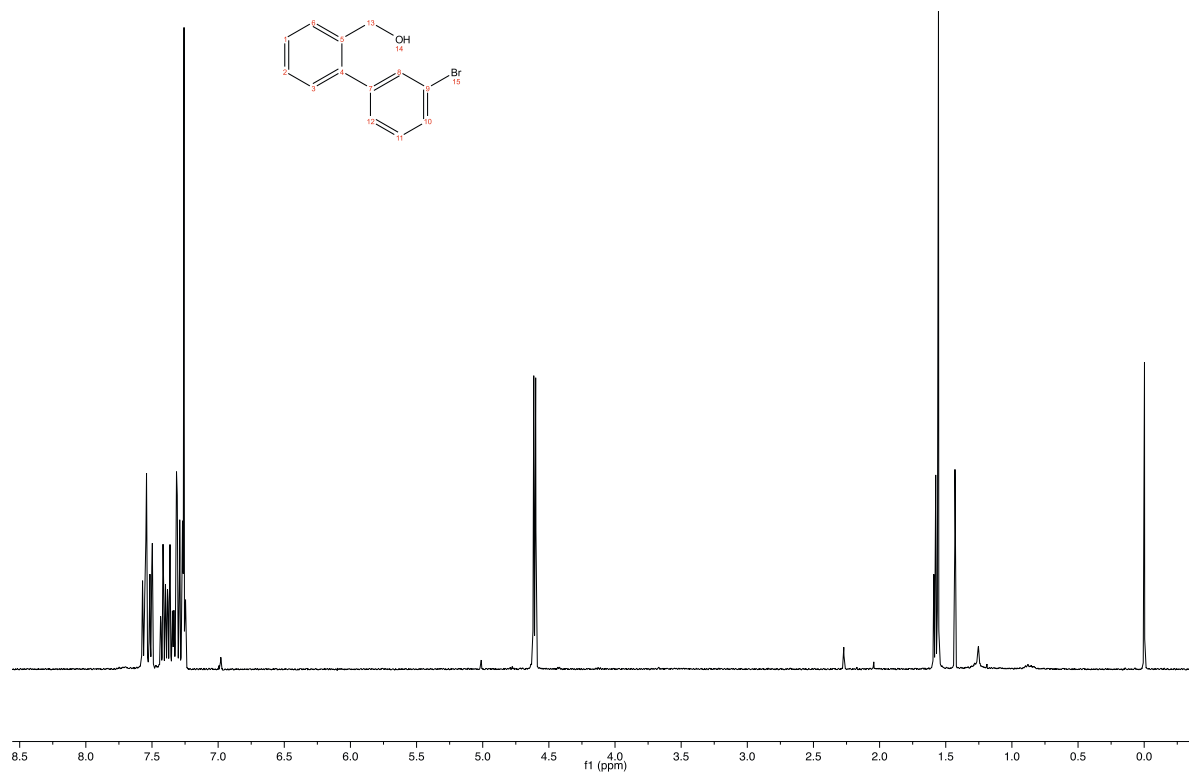
^1H -, ^{13}C -NMR (CDCl_3 , 400/101 MHz, 25 °C) of methyl 3'-bromo-[1,1'-biphenyl]-2-carboxylate (**11**)



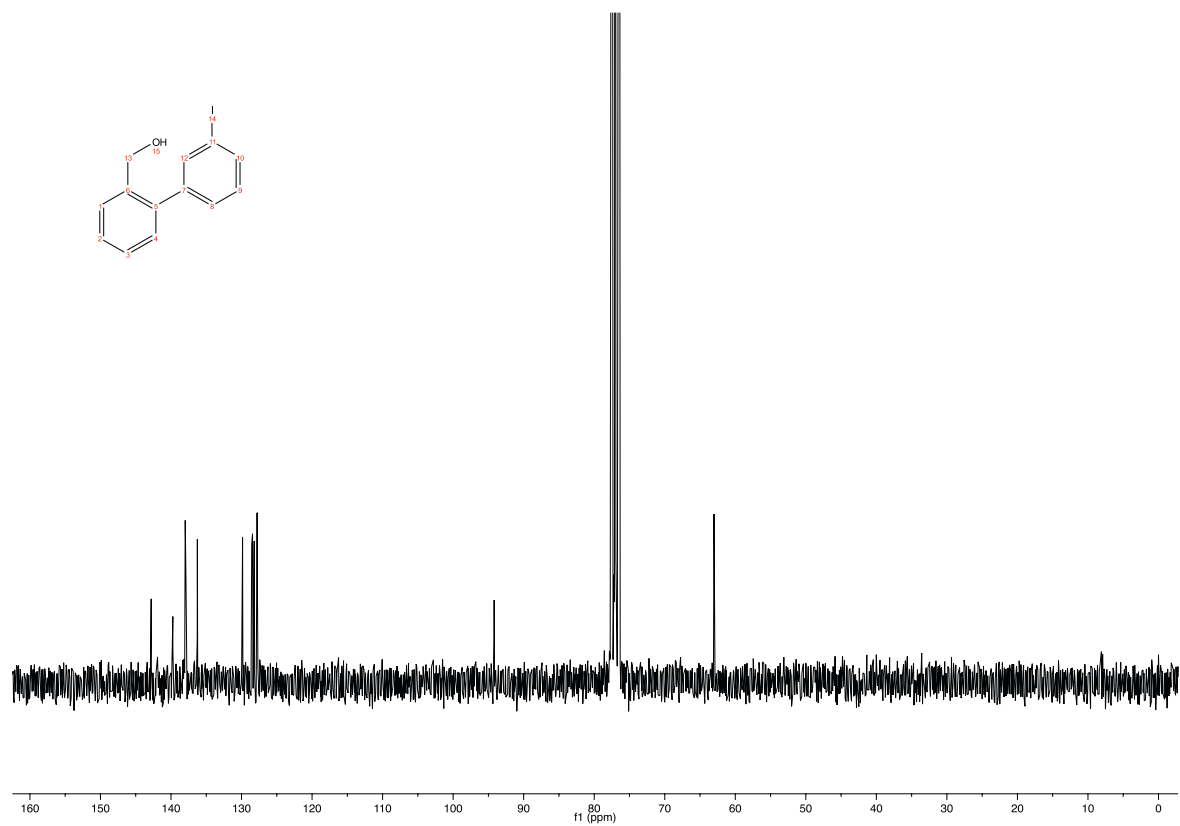
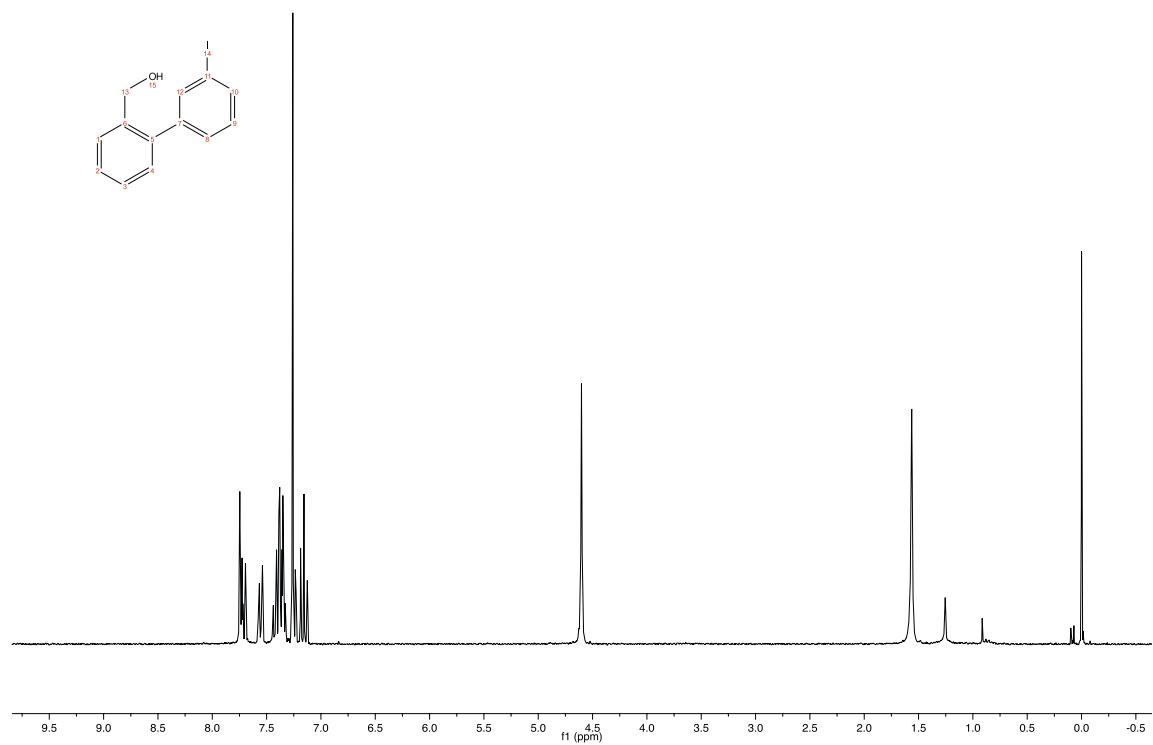
^1H -, ^{13}C -NMR (CDCl_3 , 400/63 MHz, 25 °C) of methyl 3'-(5,5-dimethyl-1,3,2-dioxaborinan-2-yl)-[1,1'-biphenyl]-2-carboxylate (**14**)



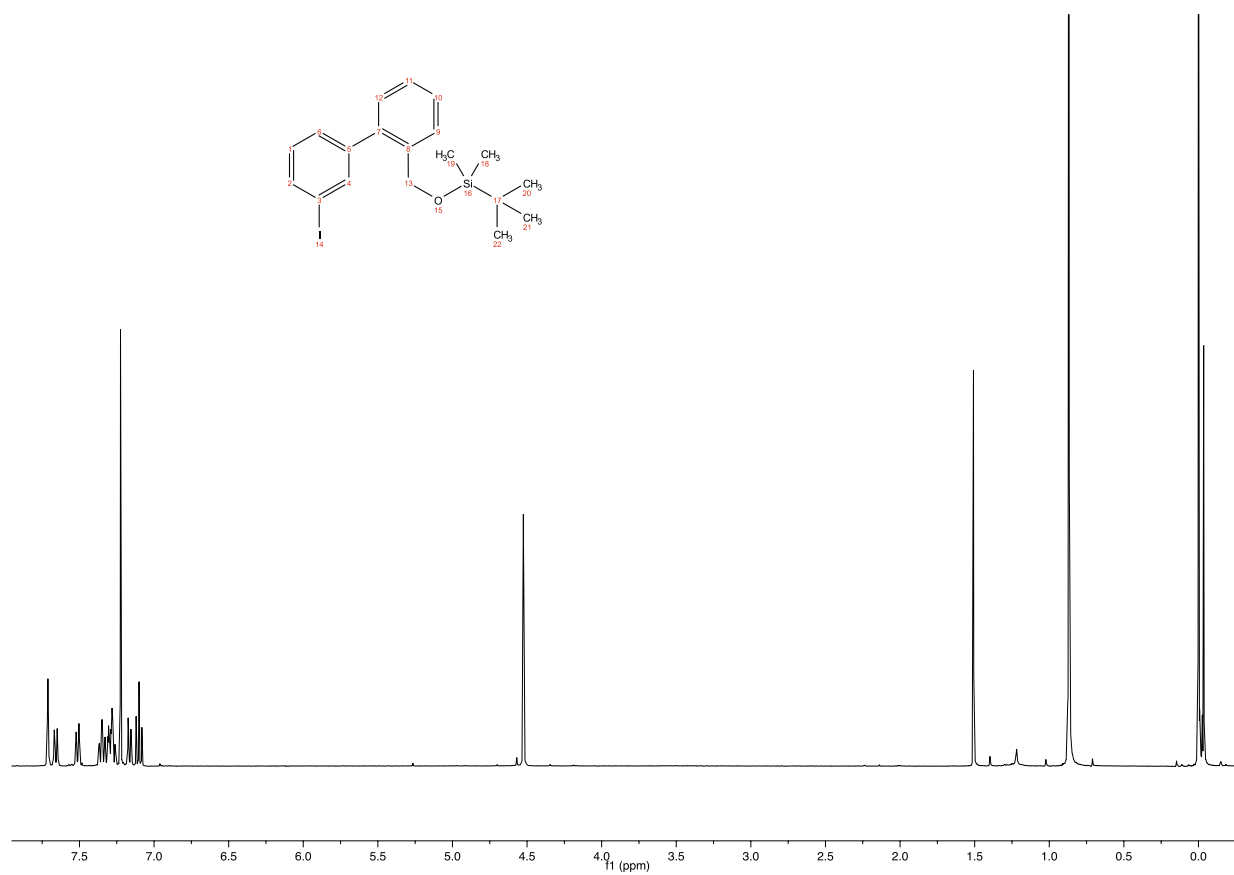
^1H -, ^{13}C -NMR (CDCl_3 , 400/101 MHz, 25 °C) of (3'-bromo-[1,1'-biphenyl]-2-yl)methanol (**15**)



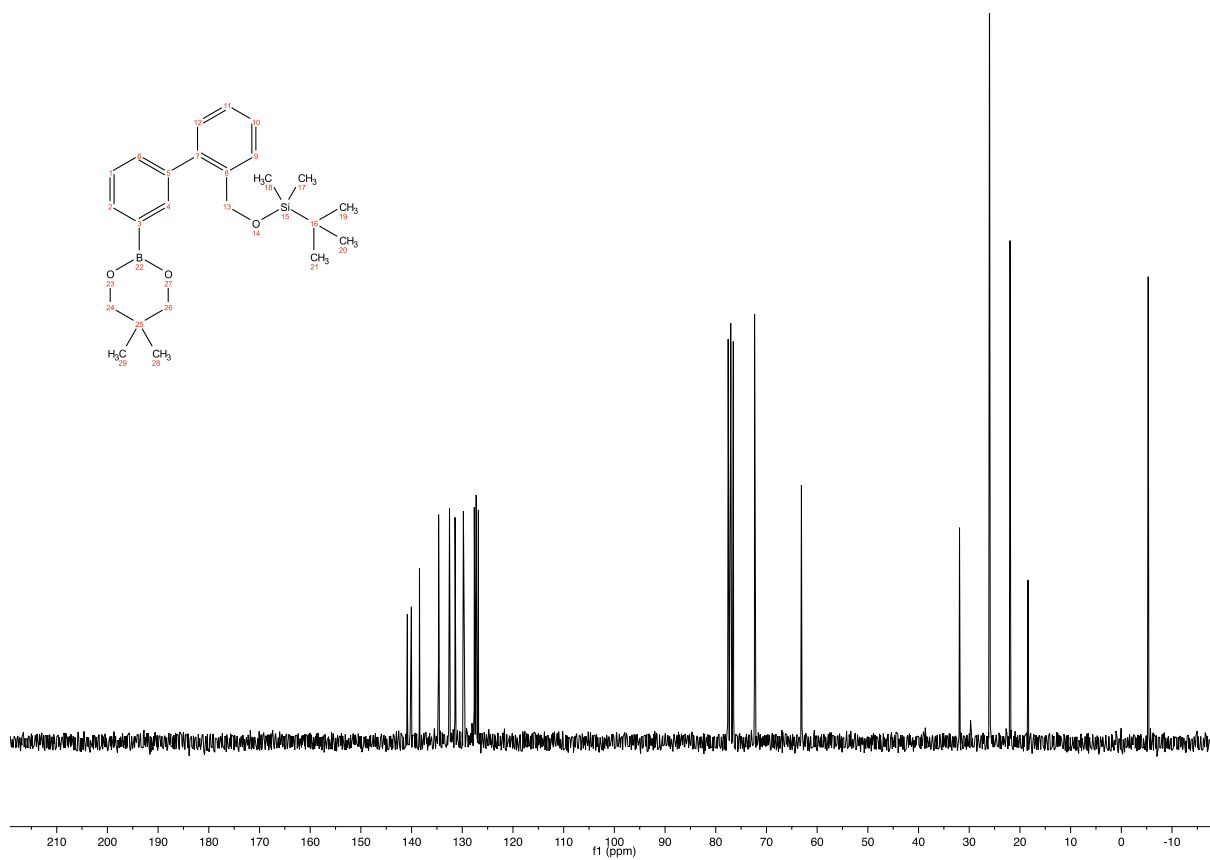
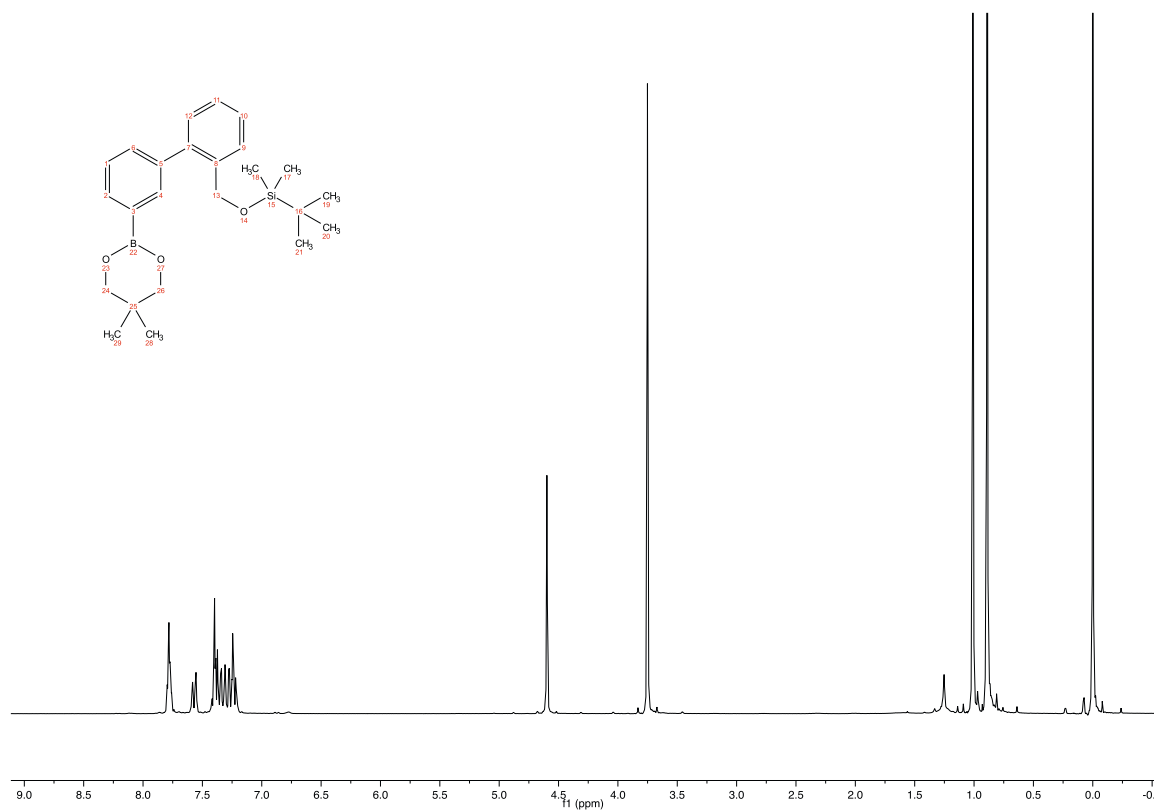
^1H -, ^{13}C -NMR (CDCl_3 , 400/63 MHz, 25 °C) of (3'-Iodo-[1,1'-biphenyl]-2-yl)methanol (**16**)



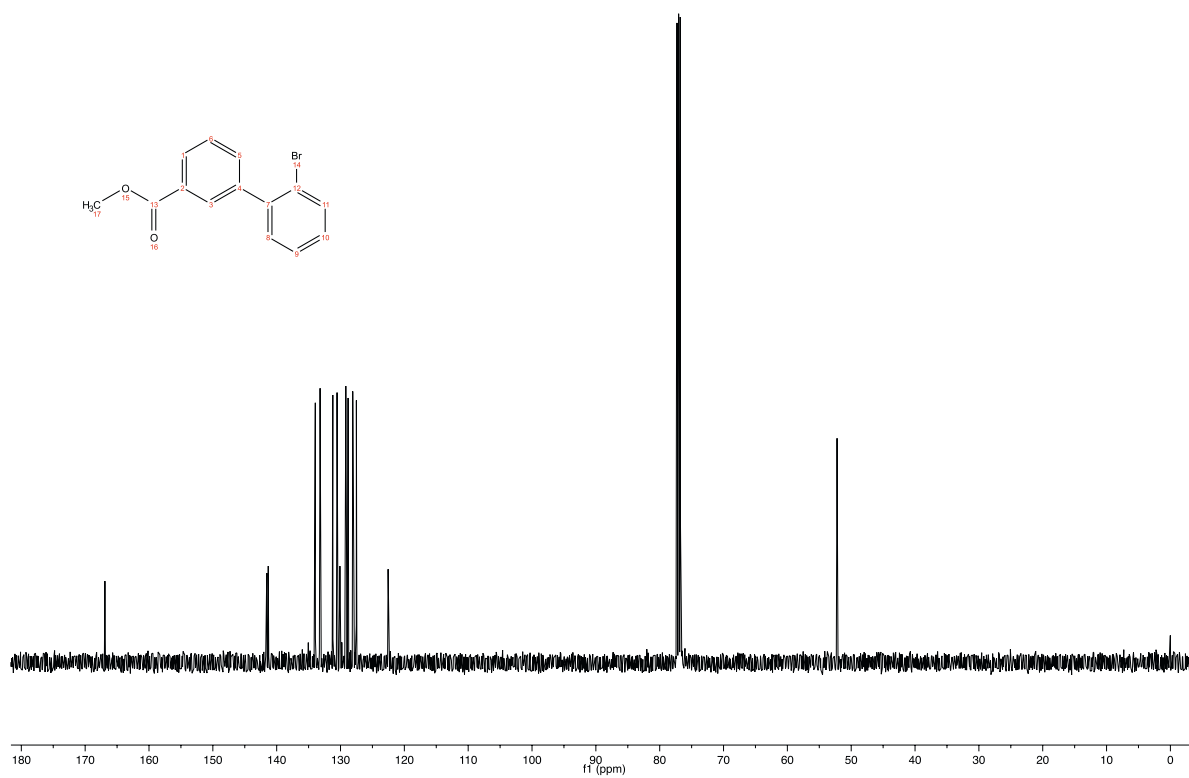
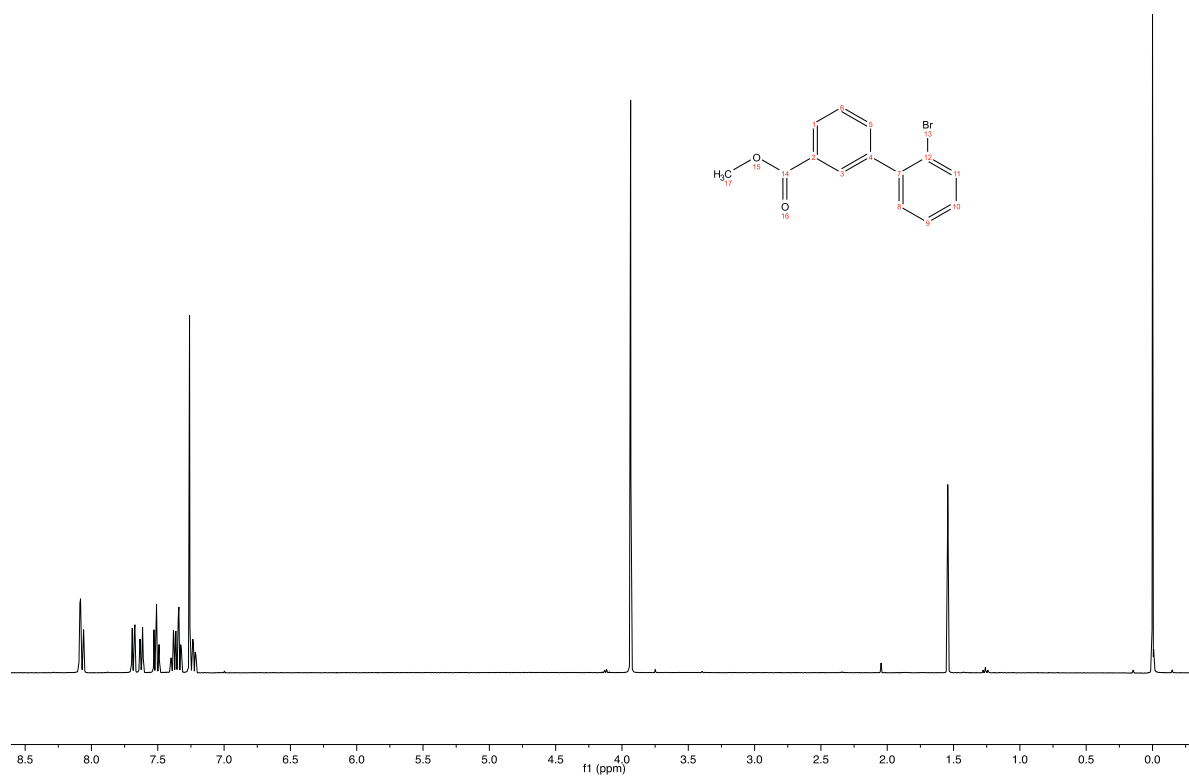
$^1\text{H-NMR}$ (CDCl_3 , 400 MHz, 25 °C) of *tert*-butyl((3'-iodo-[1,1'-biphenyl]-2-yl) methoxy) dimethylsilane (**18**)



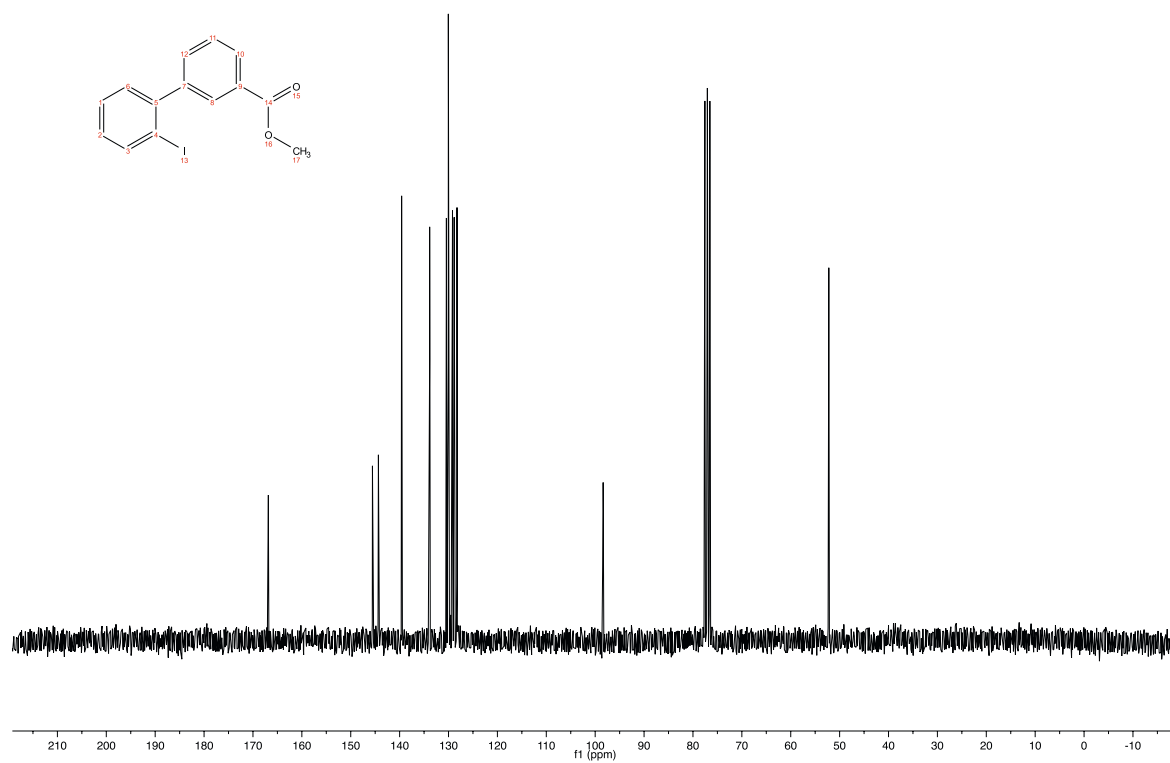
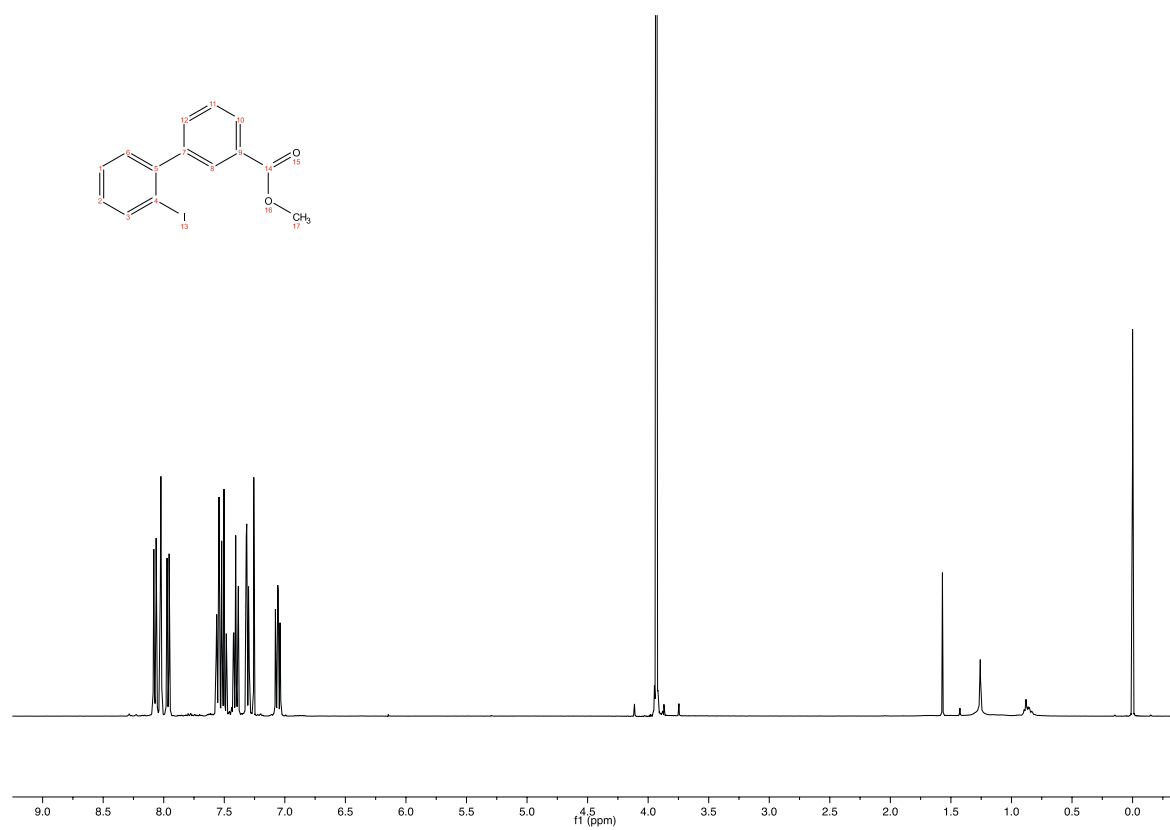
^1H -, ^{13}C -NMR (CDCl_3 , 400/63 MHz, 25 °C) of *tert*-butyl((3'-(5,5-dimethyl-1,3,2-dioxaborinan-2-yl)-[1,1'-biphenyl]-2-yl)methoxy)dimethylsilane (**19**)



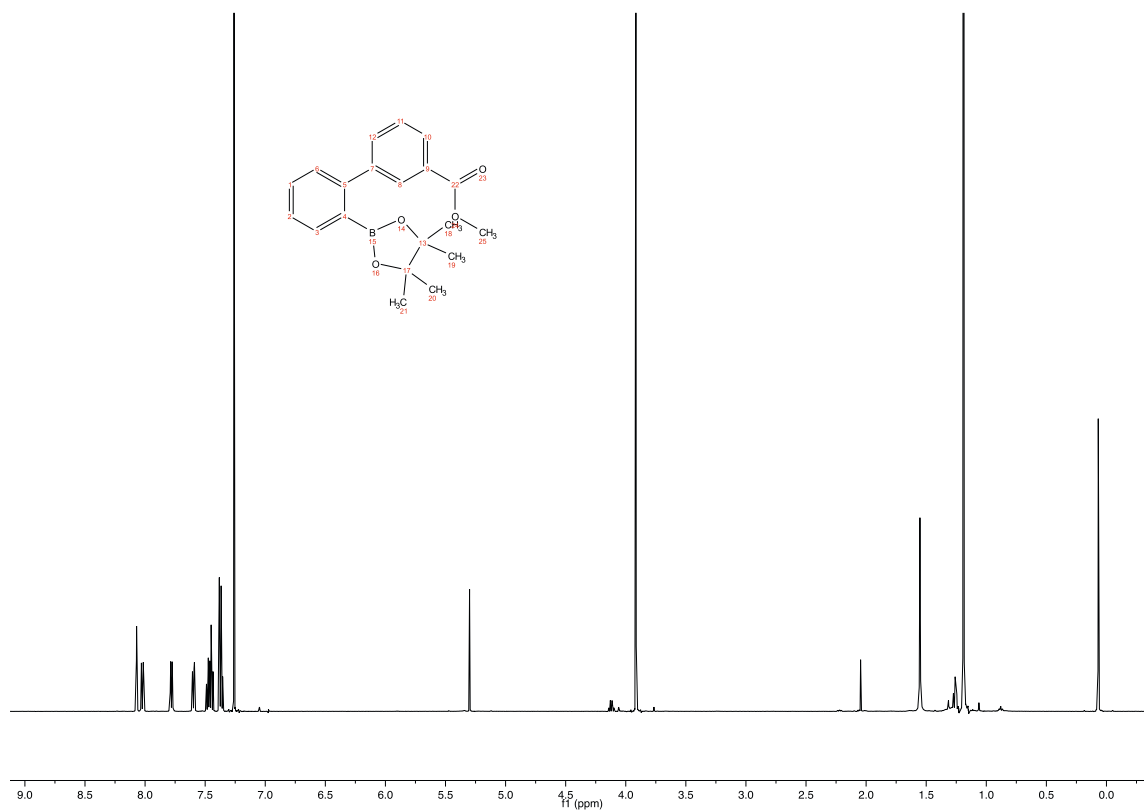
^1H -, ^{13}C -NMR (CDCl_3 , 400/101 MHz, 25 °C) of methyl 2'-bromo-[1,1'-biphenyl]-3-carboxylate (**24**)



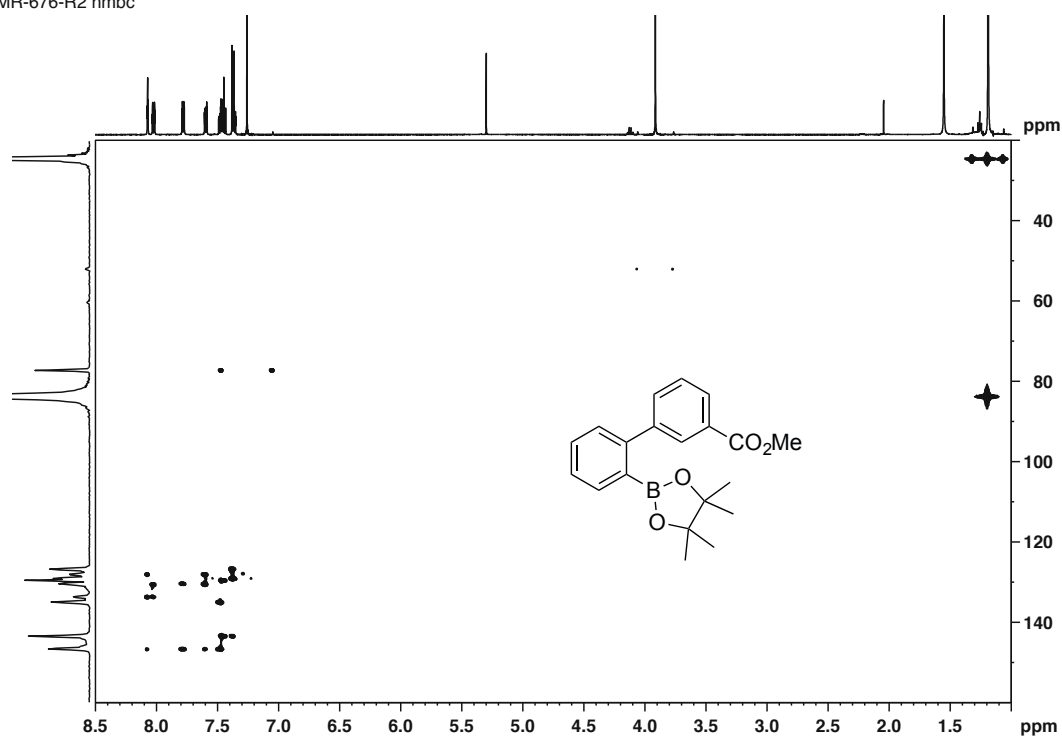
^1H , ^{13}C -NMR (CDCl_3 , 400/101 MHz, 25 °C) of methyl 2'-iodo-[1,1'-biphenyl]-3-carboxylate (**25**)

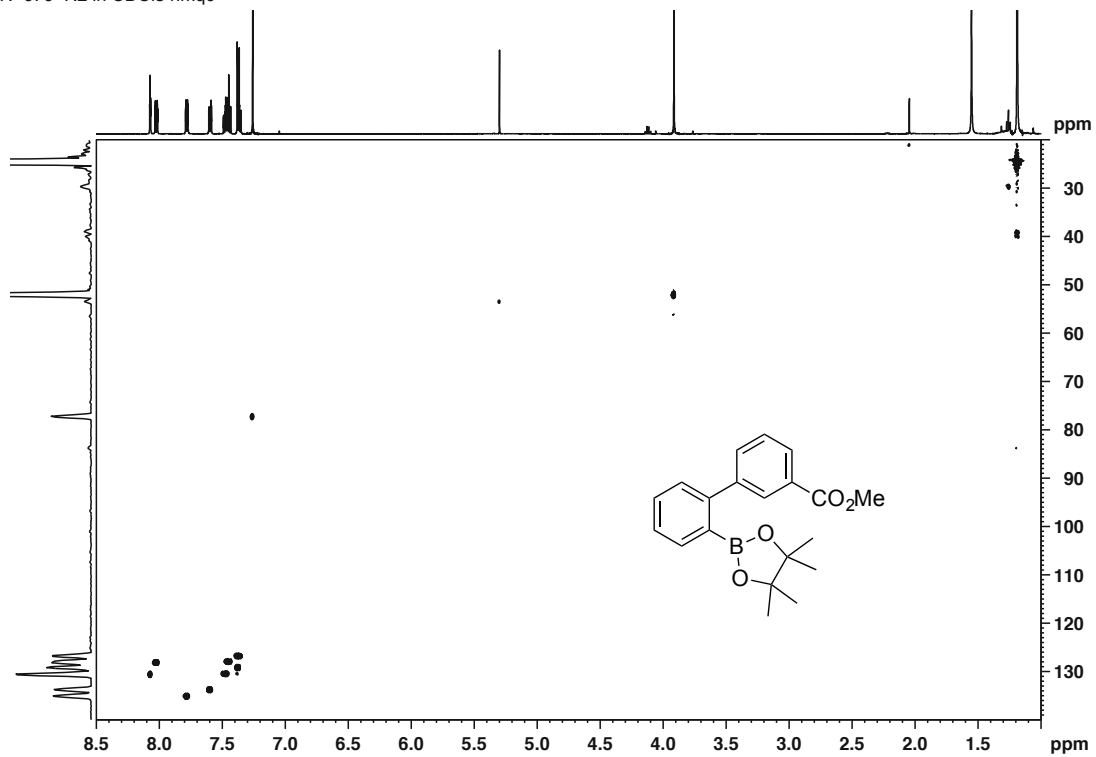
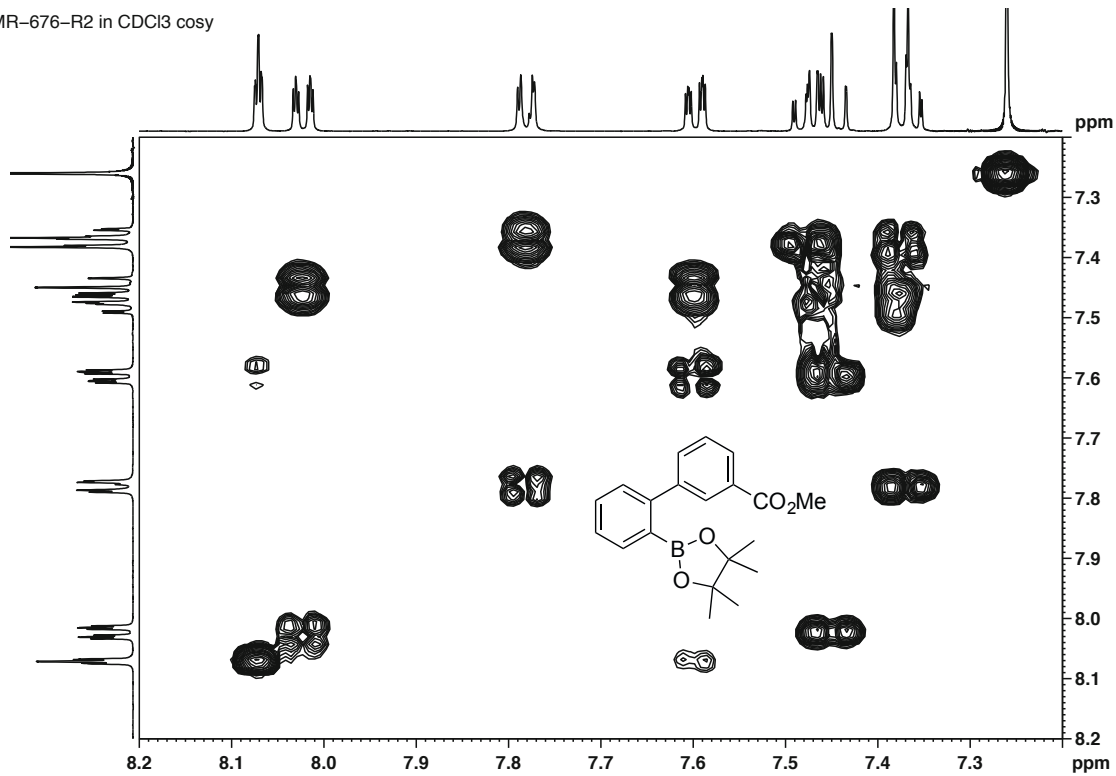


$^1\text{H-NMR}$, HMBC, HMQC and COSY (CDCl_3 , 500/125 MHz, 25 °C) of methyl 2'-(4,4,5,5-tetramethyl-1,3,2-dioxaborolan-2-yl)-[1,1'-biphenyl]-3-carboxylate (**26**)

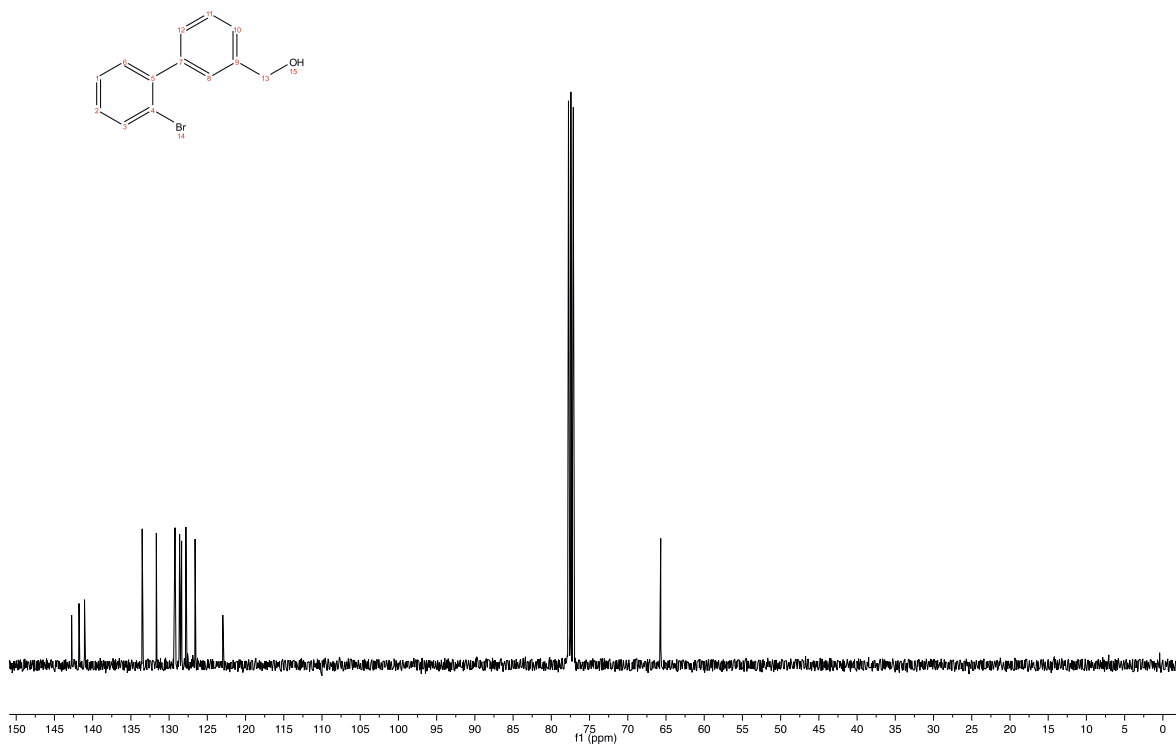
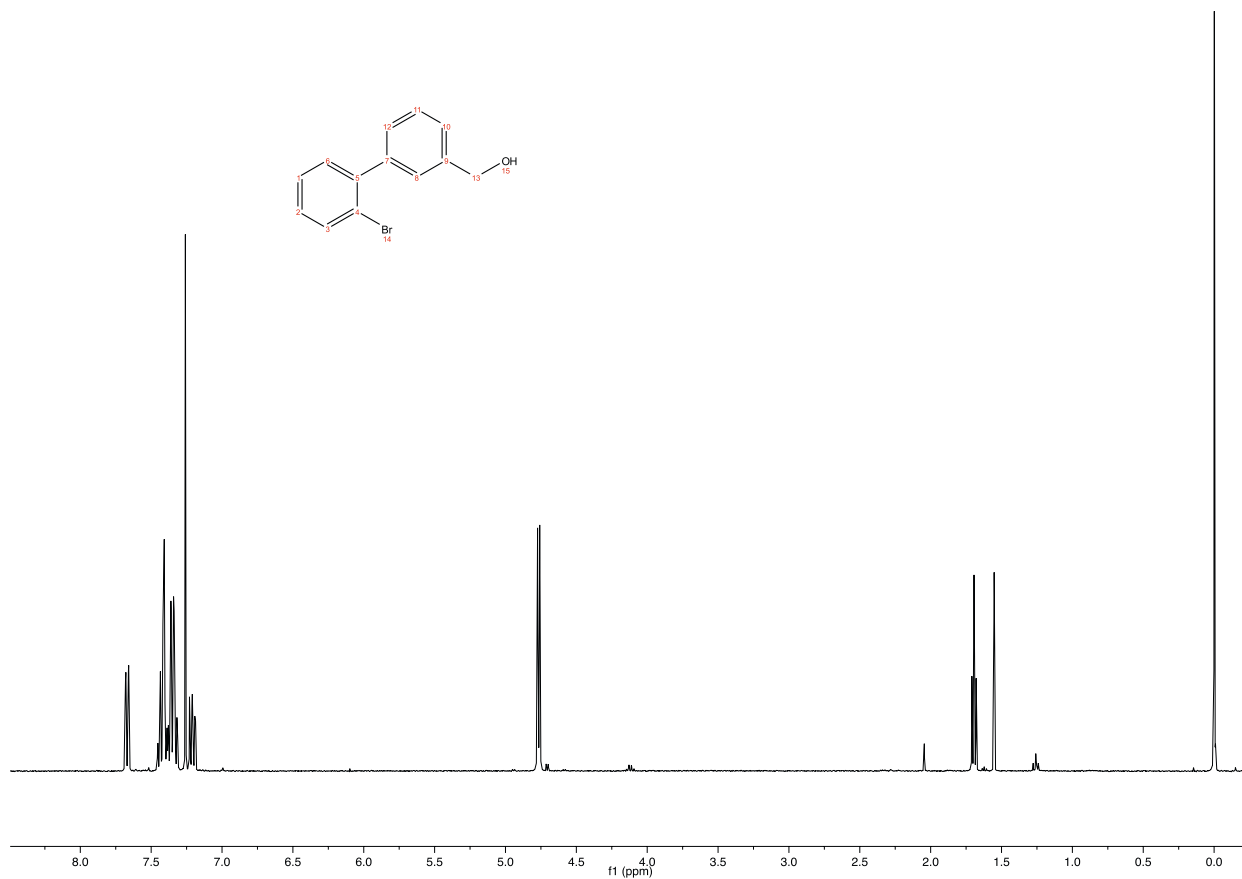


MR-676-R2 hmbc

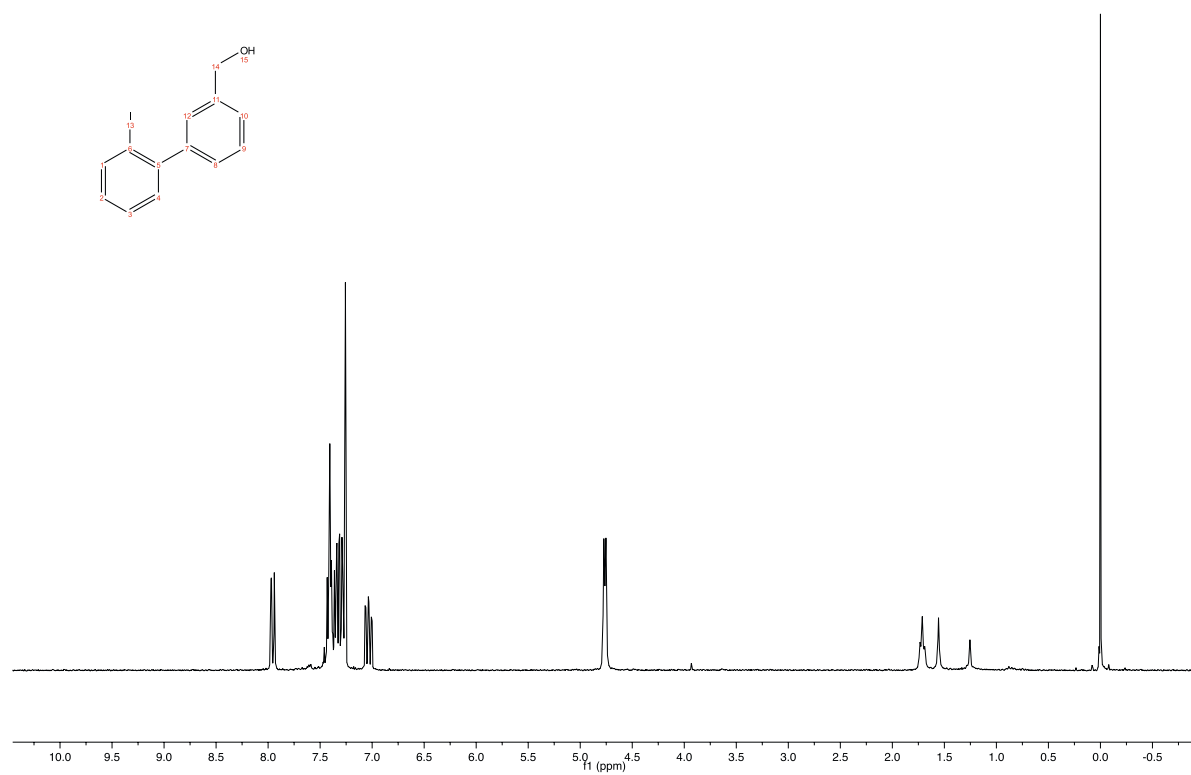
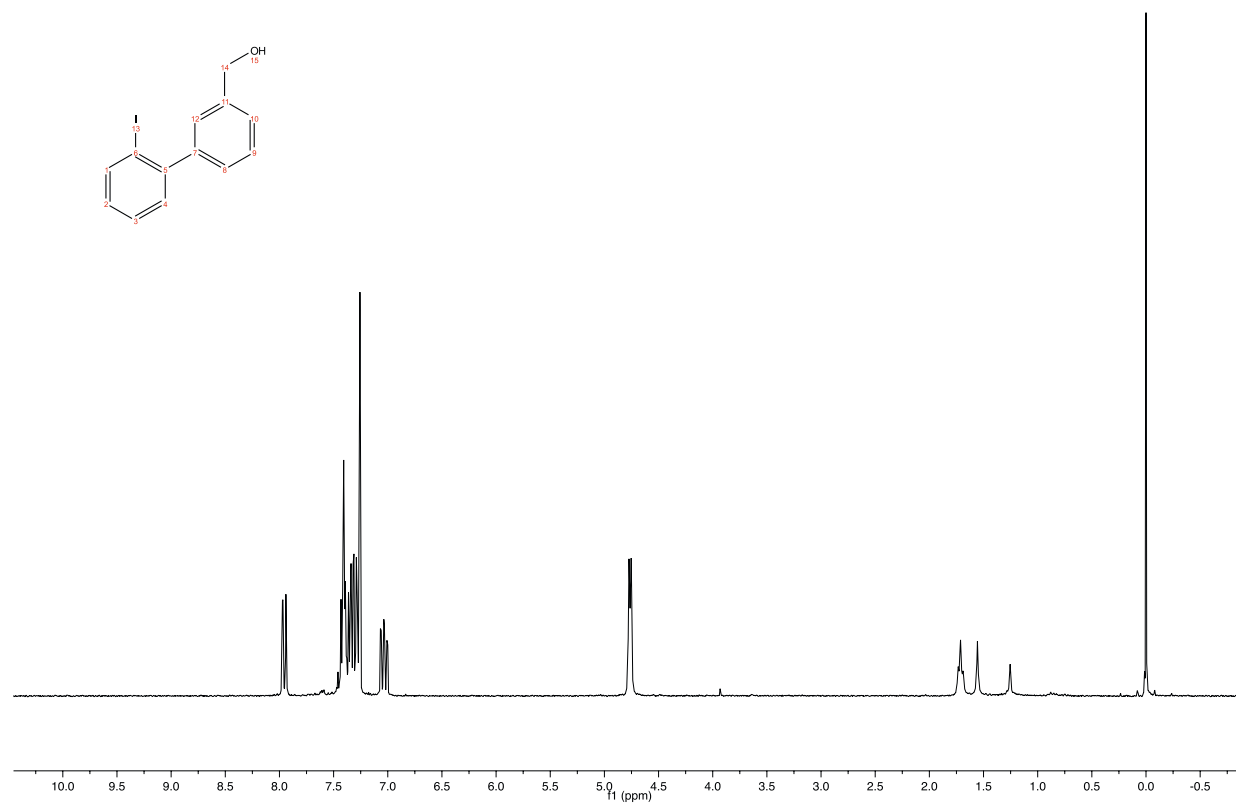


MR-676-R2 in CDCl₃ hmqcMR-676-R2 in CDCl₃ cosy

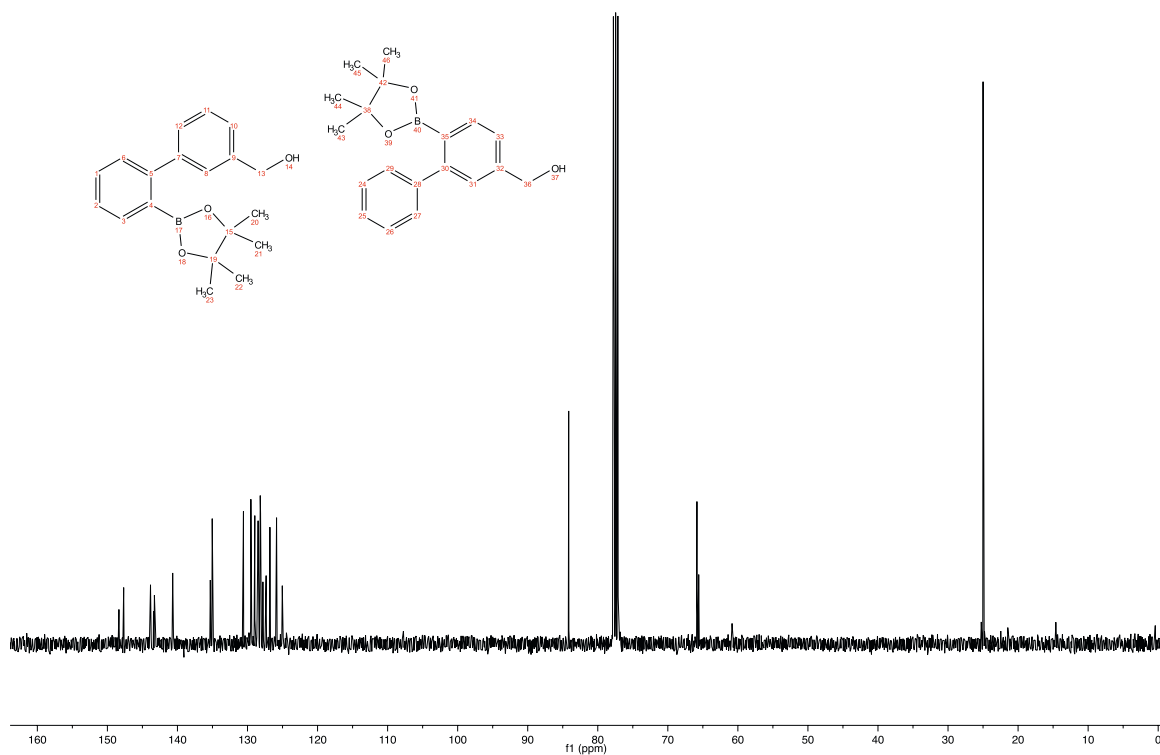
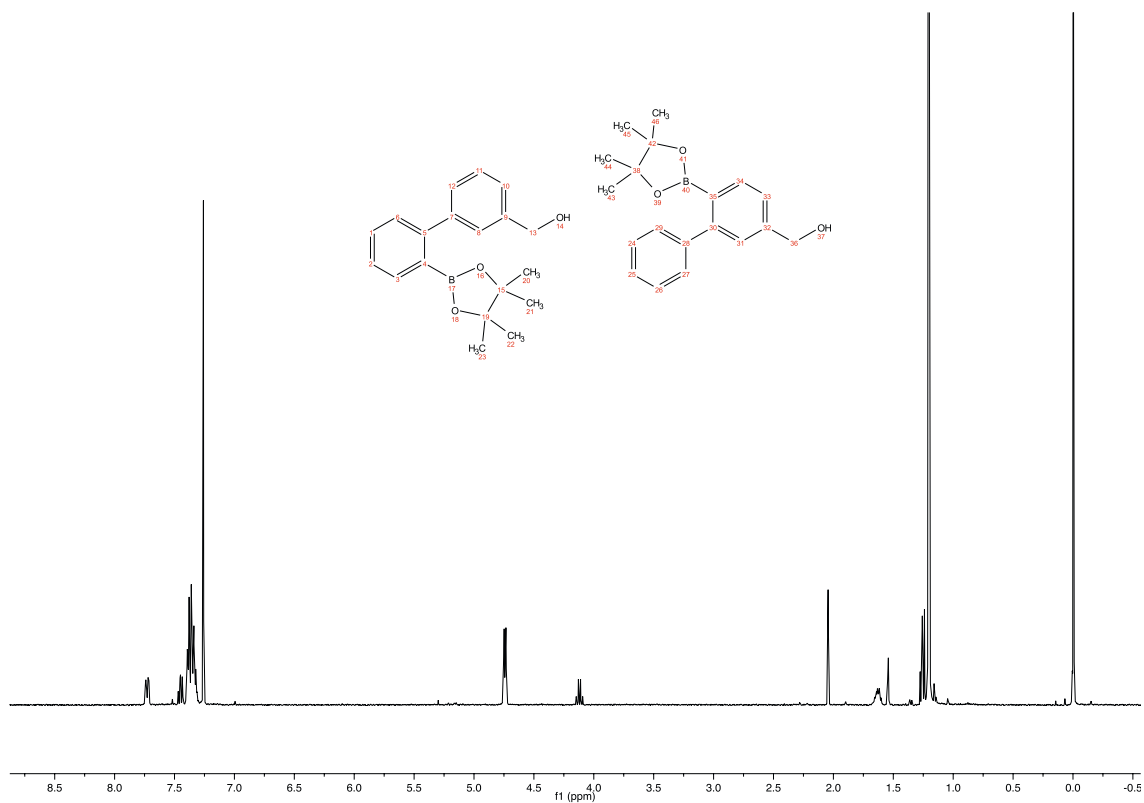
^1H -, ^{13}C -NMR (CDCl_3 , 400/101 MHz, 25 °C) of (2'-bromo-[1,1'-biphenyl]-3-yl)methanol (**27**)



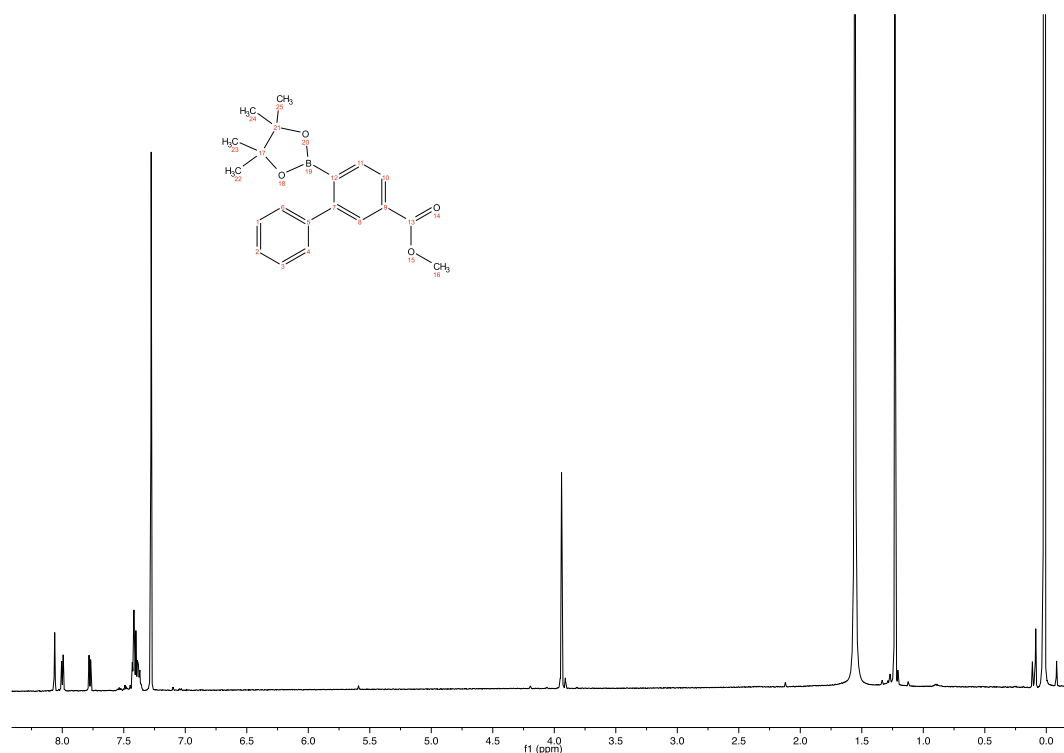
^1H -, ^{13}C -NMR (CDCl_3 , 400/63 MHz, 25 °C) of (2'-Iodo-[1,1'-biphenyl]-3-yl) methanol (**28**)



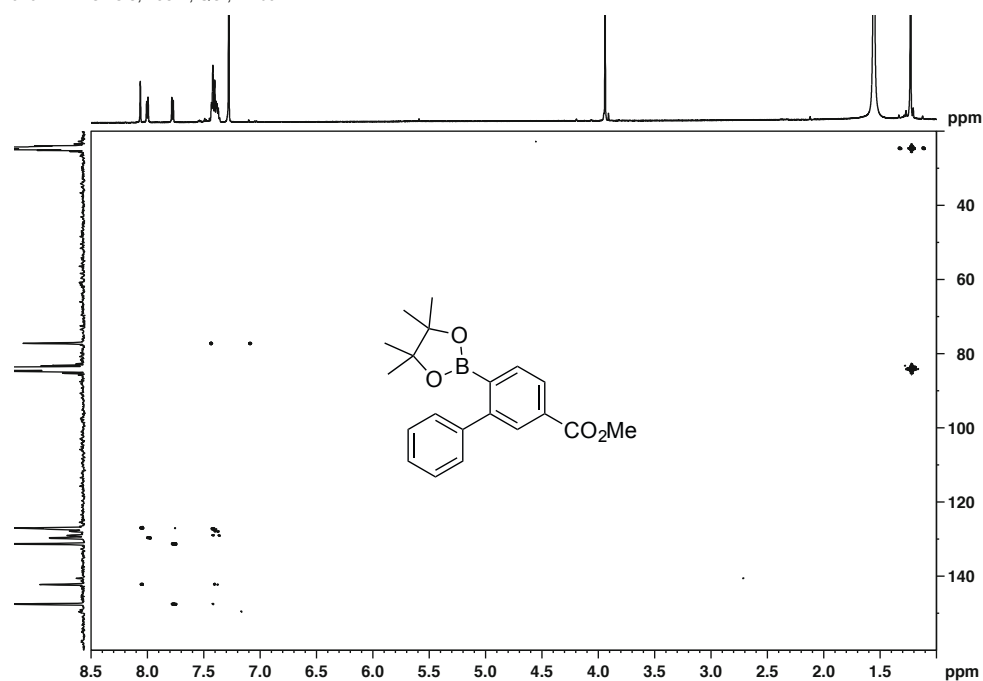
^1H -, ^{13}C -NMR (CDCl_3 , 400/101 MHz, 25 °C) of regioisomers (29) and (31)

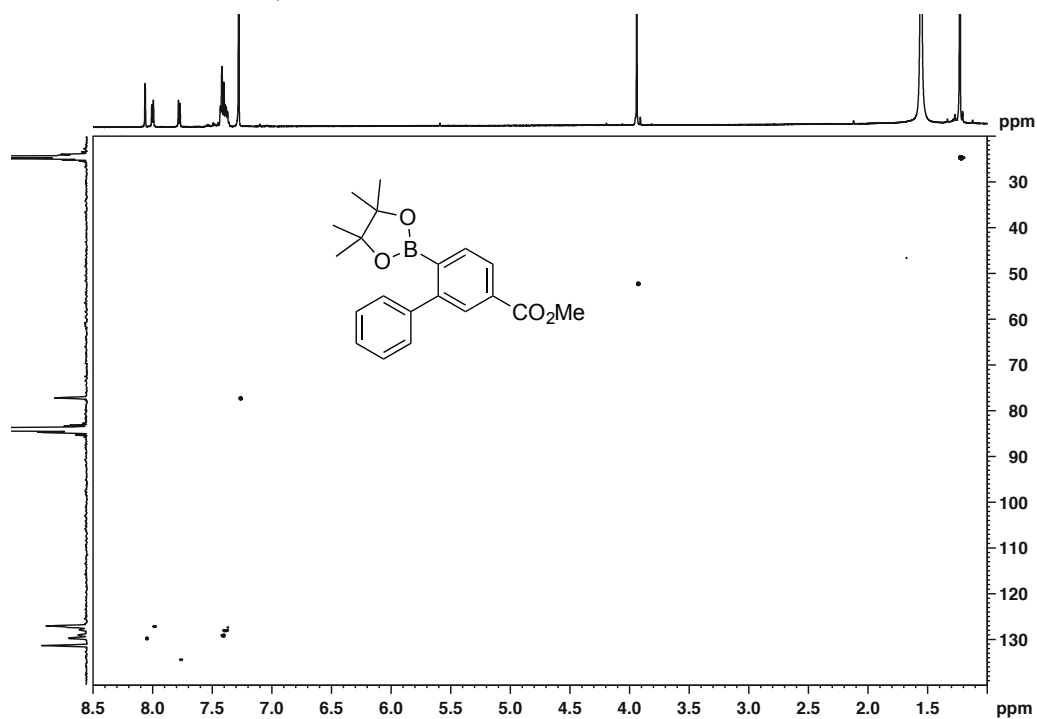
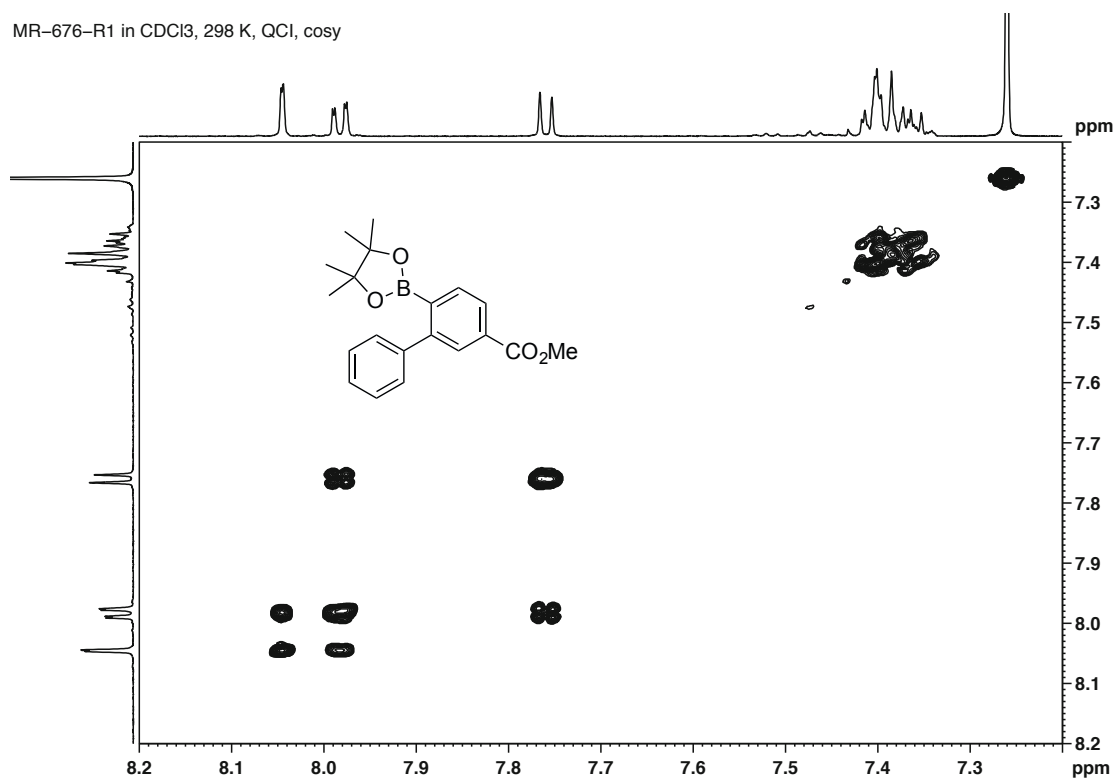


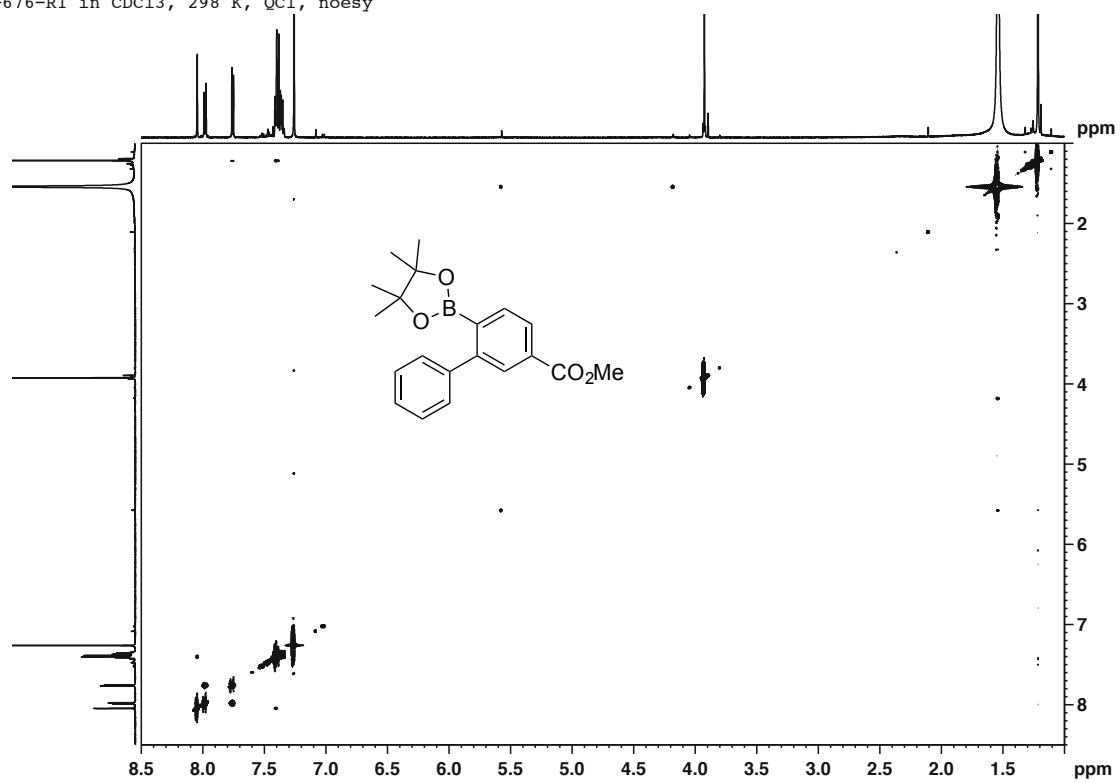
$^1\text{H-NMR}$, HMBC, HMQC and COSY and NOESY (CDCl_3 , 600/151 MHz, 25 °C) of methyl 4-(4,4,5,5-tetramethyl-1,3,2-dioxaborolan-2-yl)-[1,1'-biphenyl]-3-carboxylate (**32**)



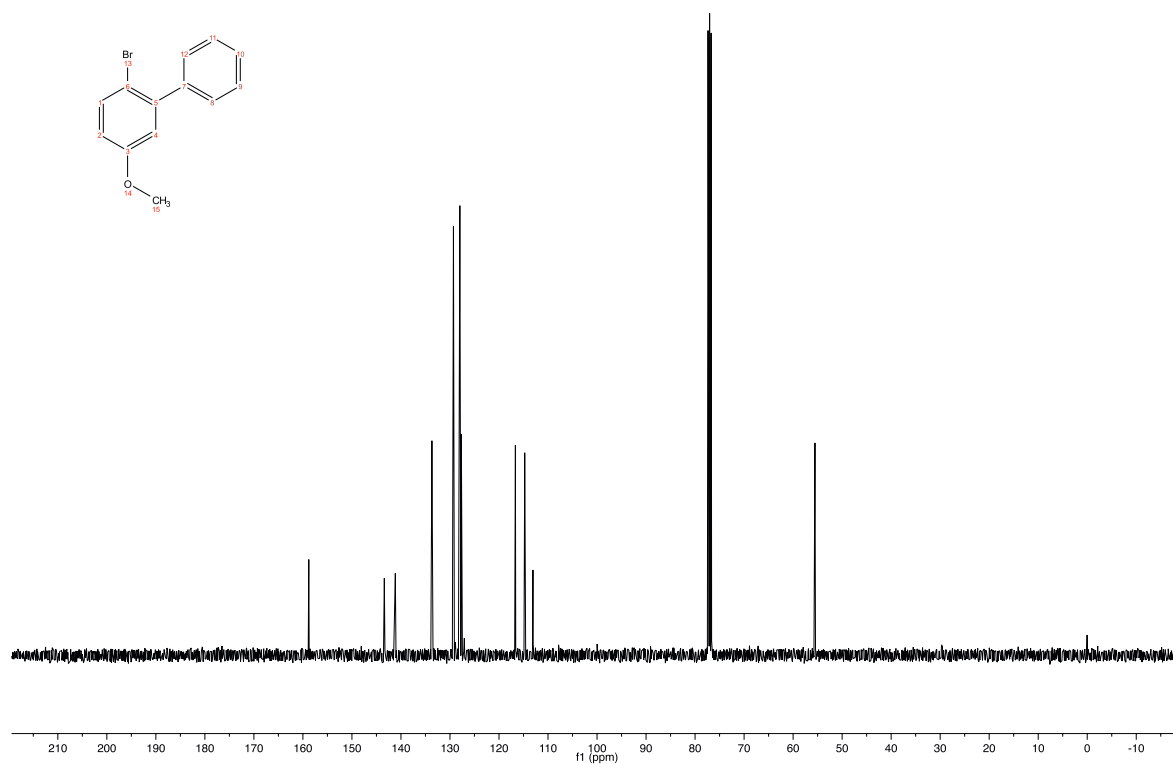
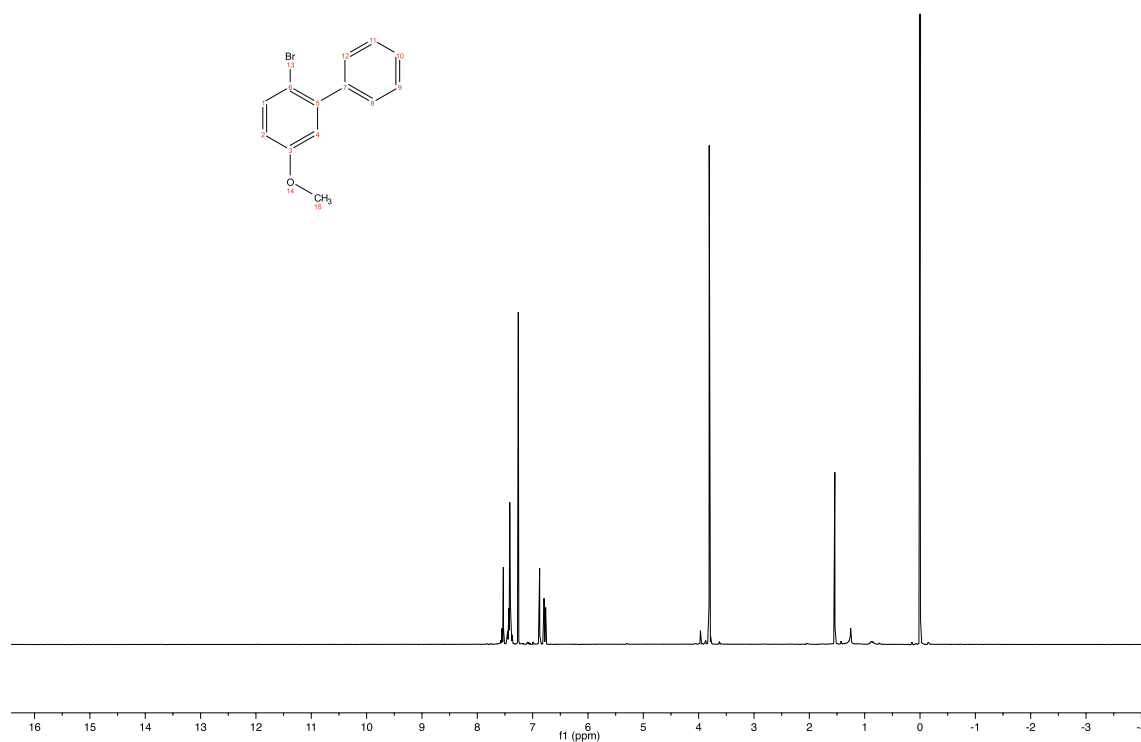
MR-676-R1 in CDCl_3 , 298 K, QCI, hmbc



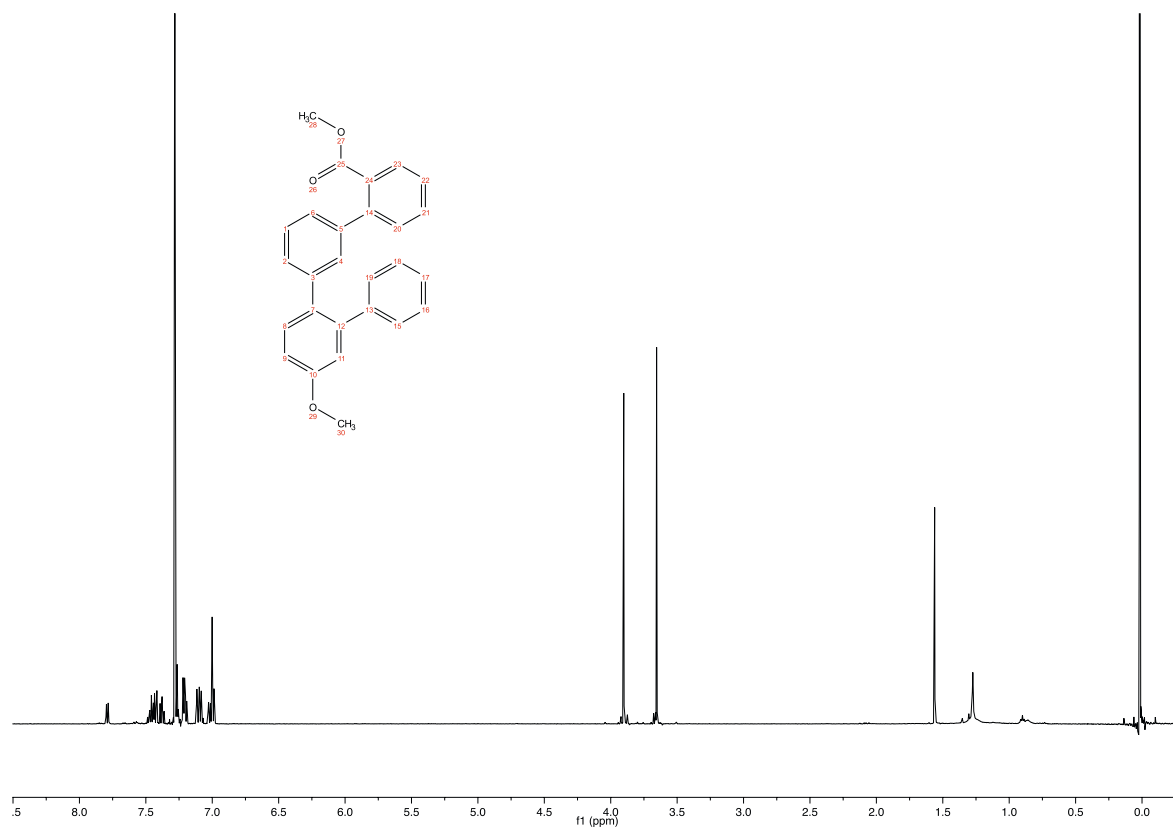
MR-676-R1 in CDCl₃, 298 K, QCI, hmqcMR-676-R1 in CDCl₃, 298 K, QCI, cosy

MR-676-R1 in CDCl₃, 298 K, QCI, noesy

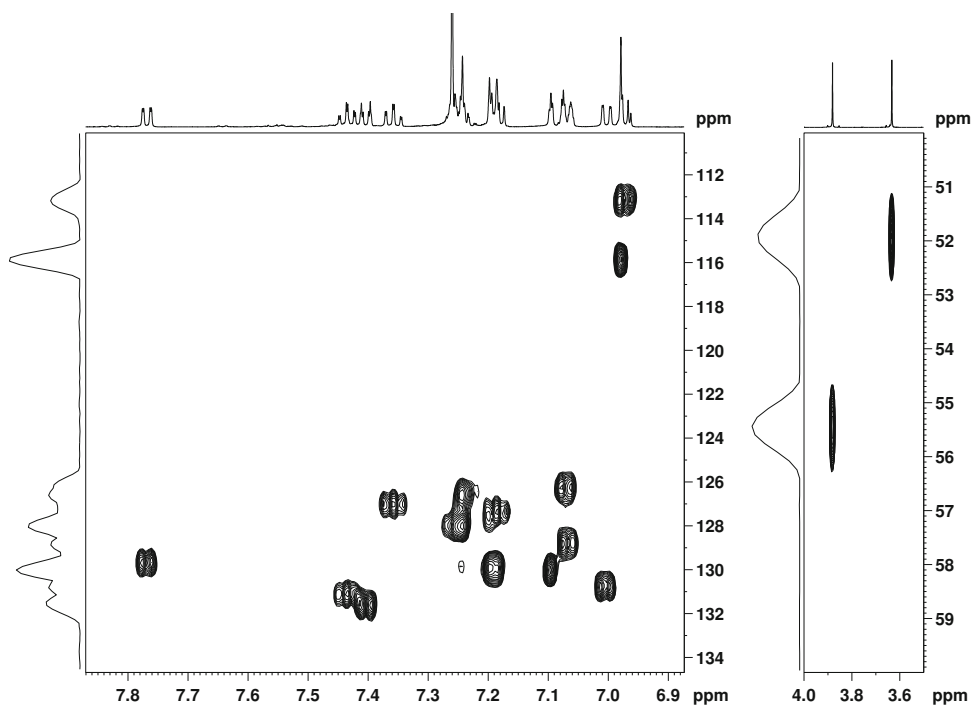
^1H -, ^{13}C -NMR (CDCl_3 , 400/101 MHz, 25 °C) of 1-bromo-2-iodo-4-methoxybenzene (**33**)



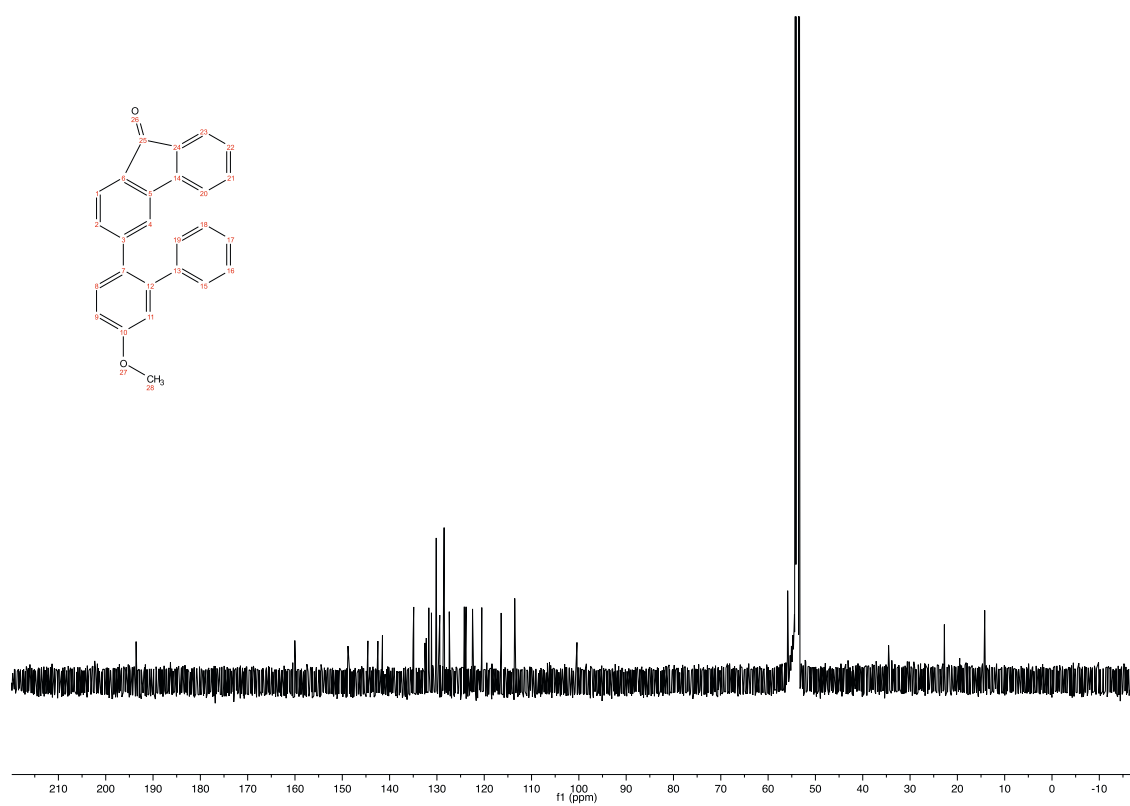
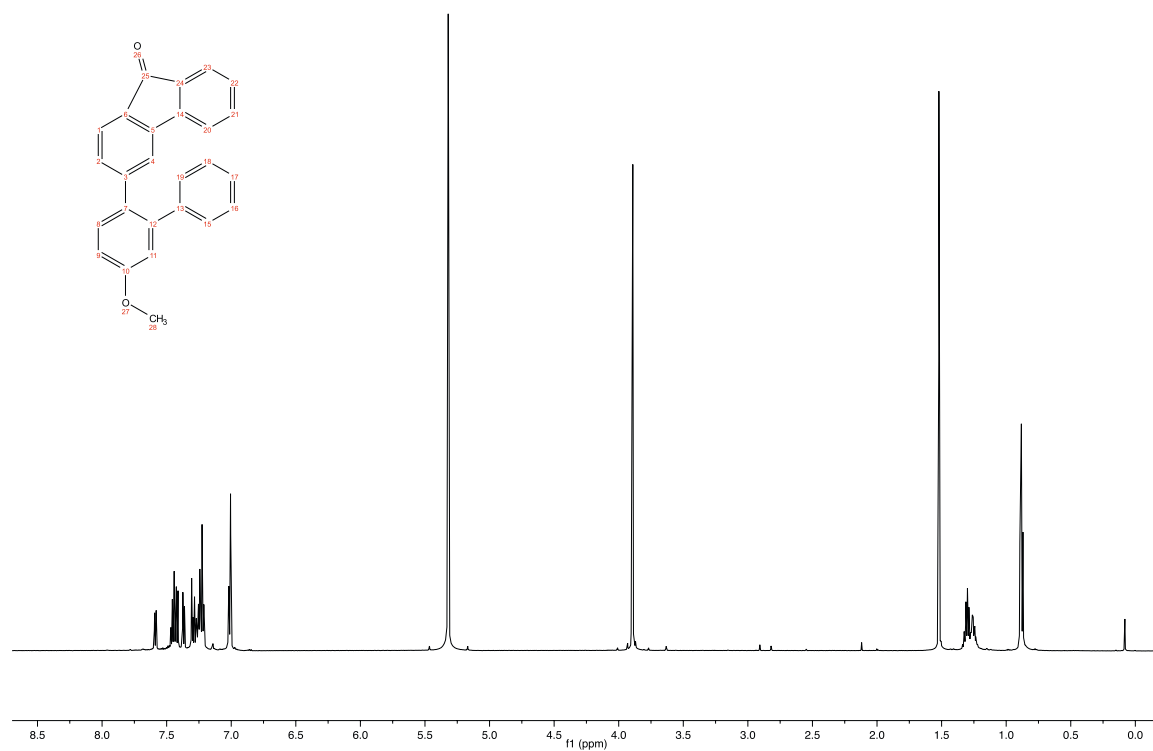
^1H -, HMQC (CDCl_3 , 400/151 MHz, 25 °C) of methyl 5'-methoxy-[1,1':2',1'':3'',1'''-quaterphenyl]-2'''-carboxylate (**34**)

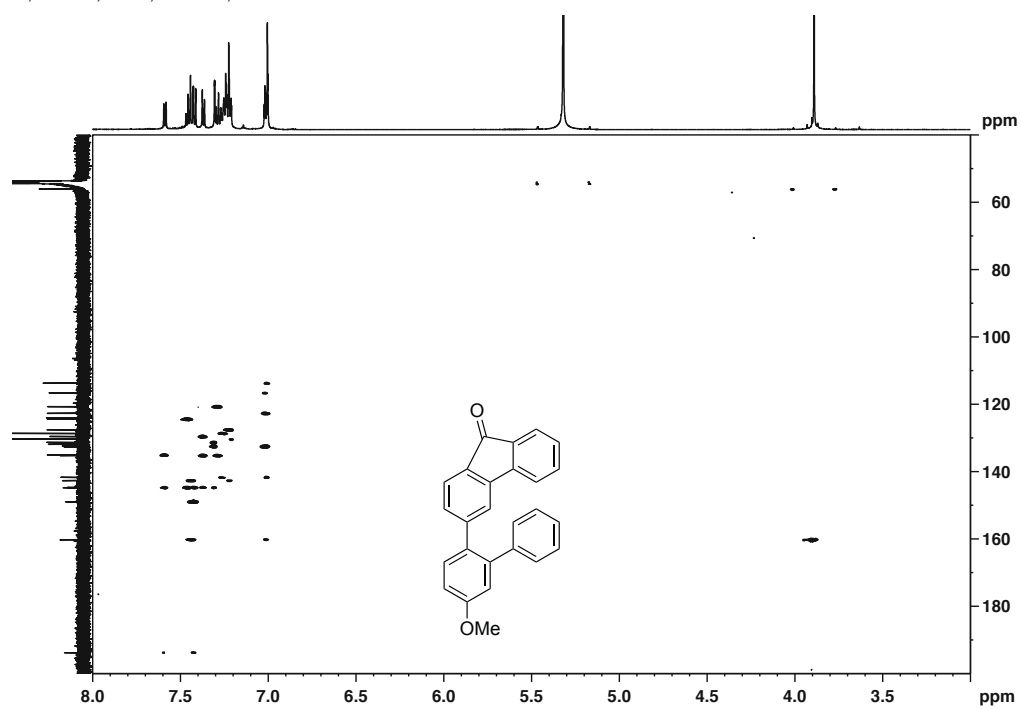
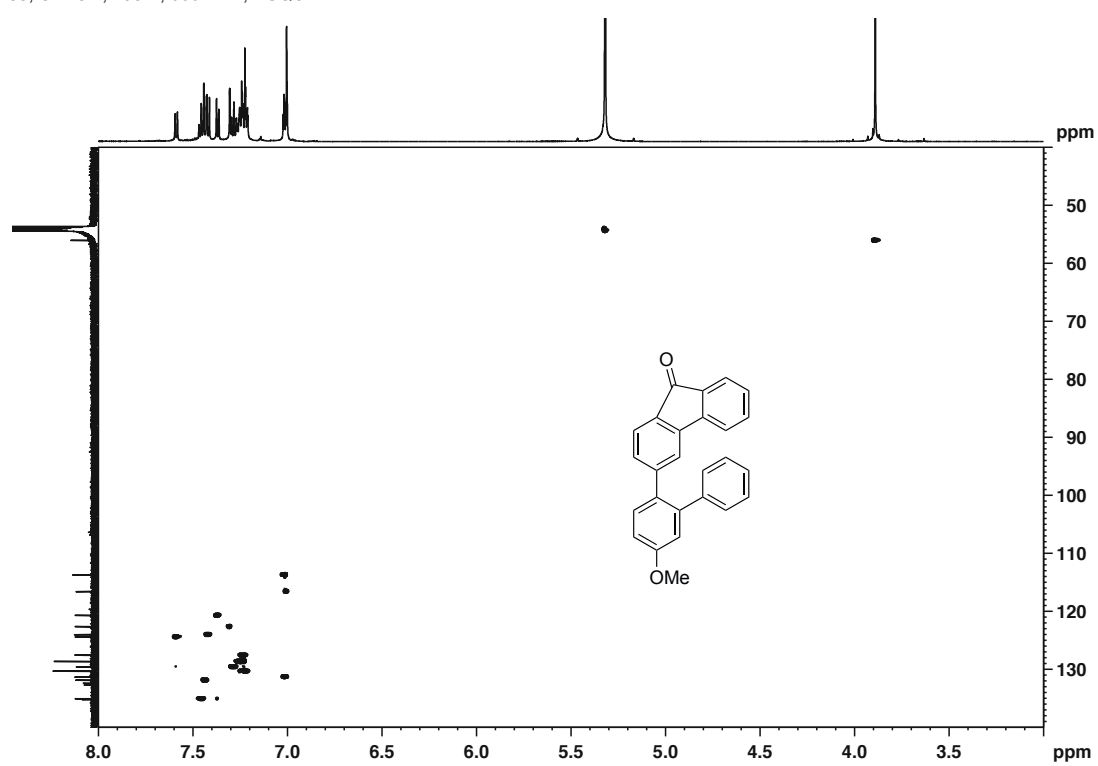


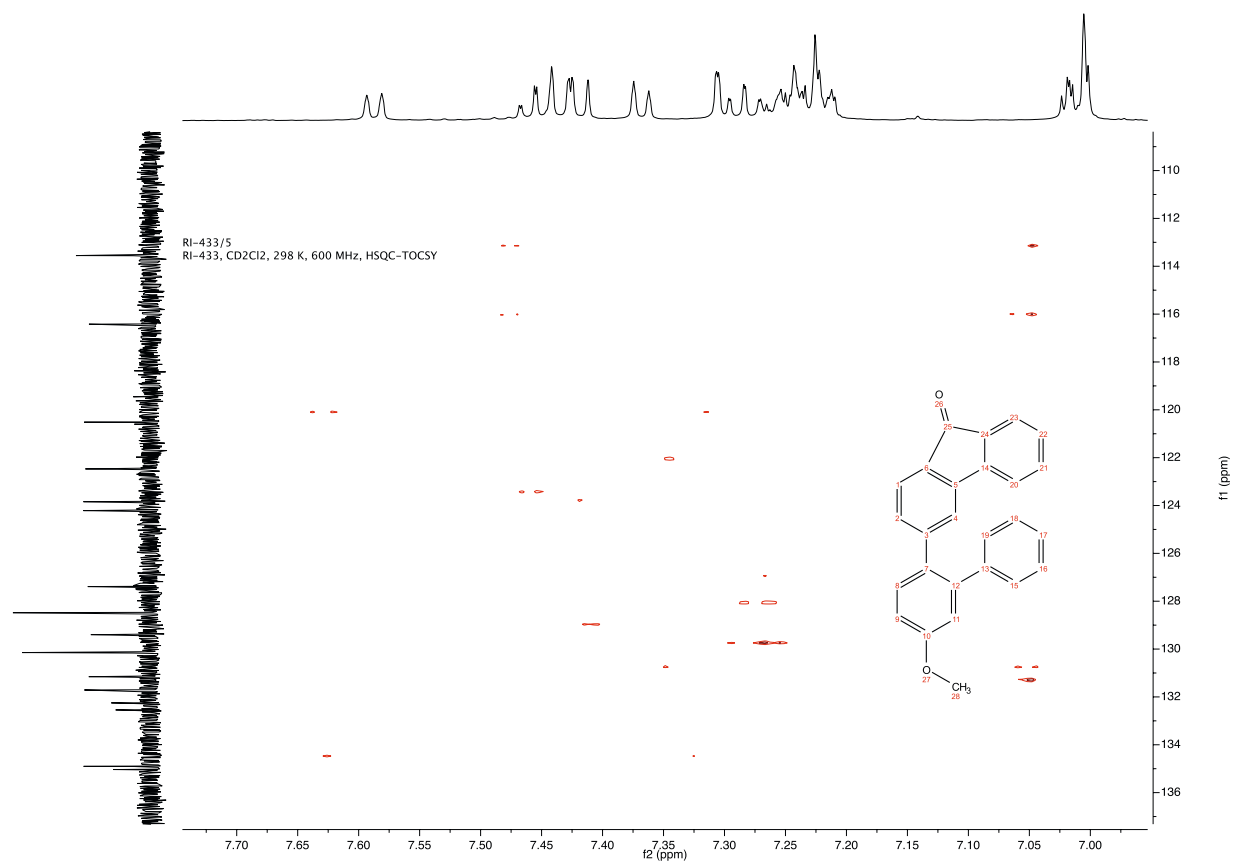
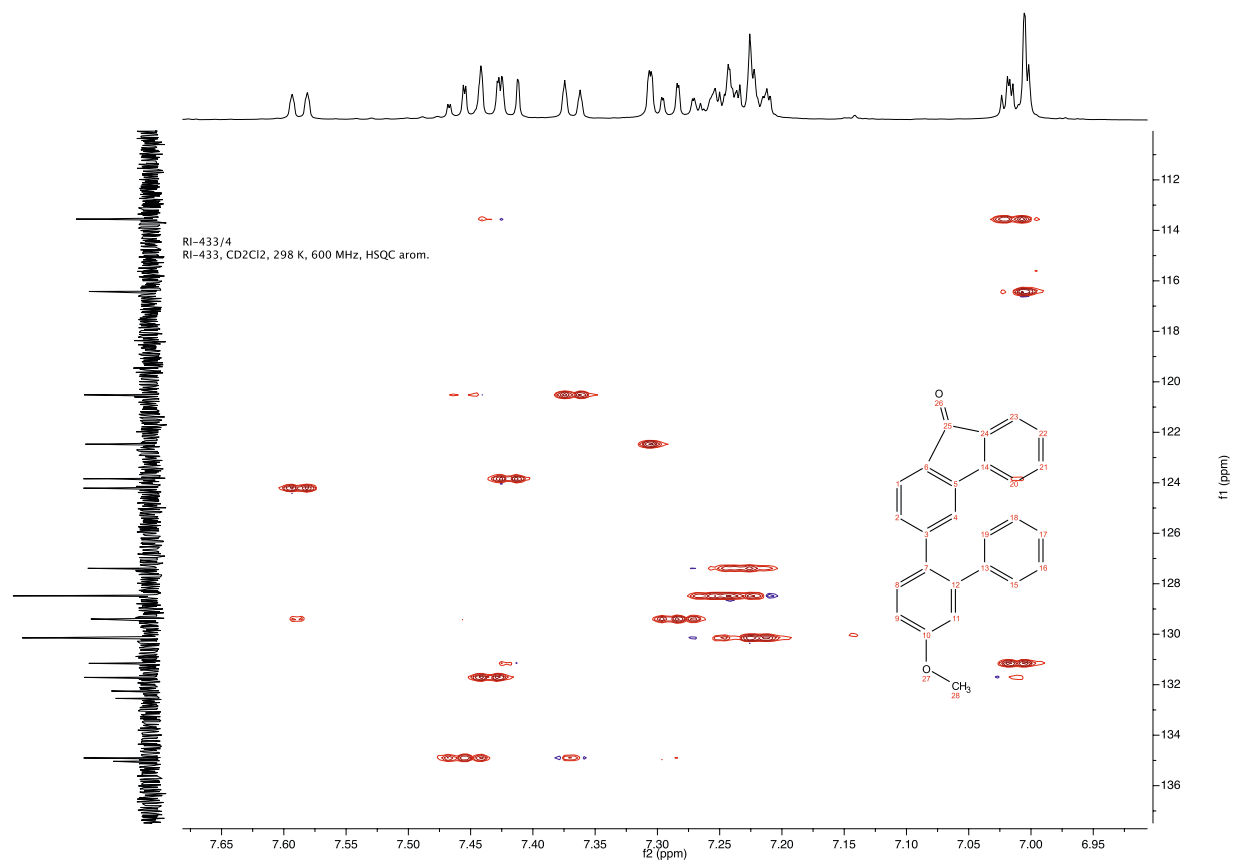
Ri-431 in CDCl_3 , 298K, HMQC

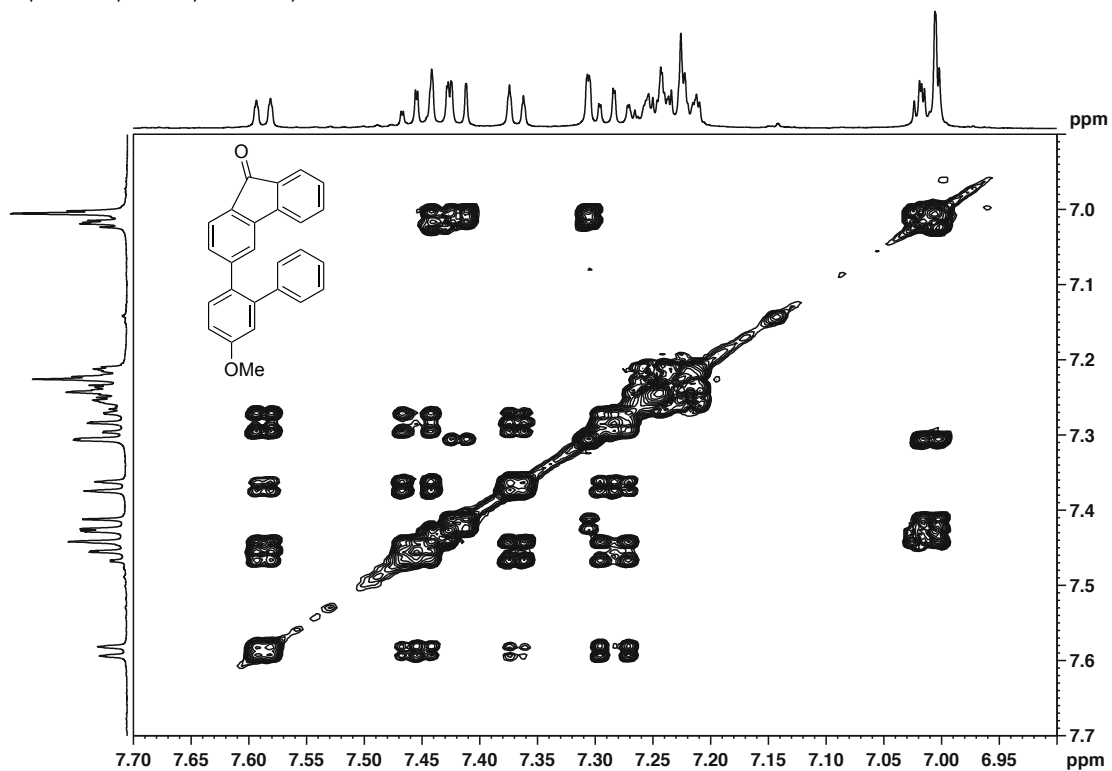
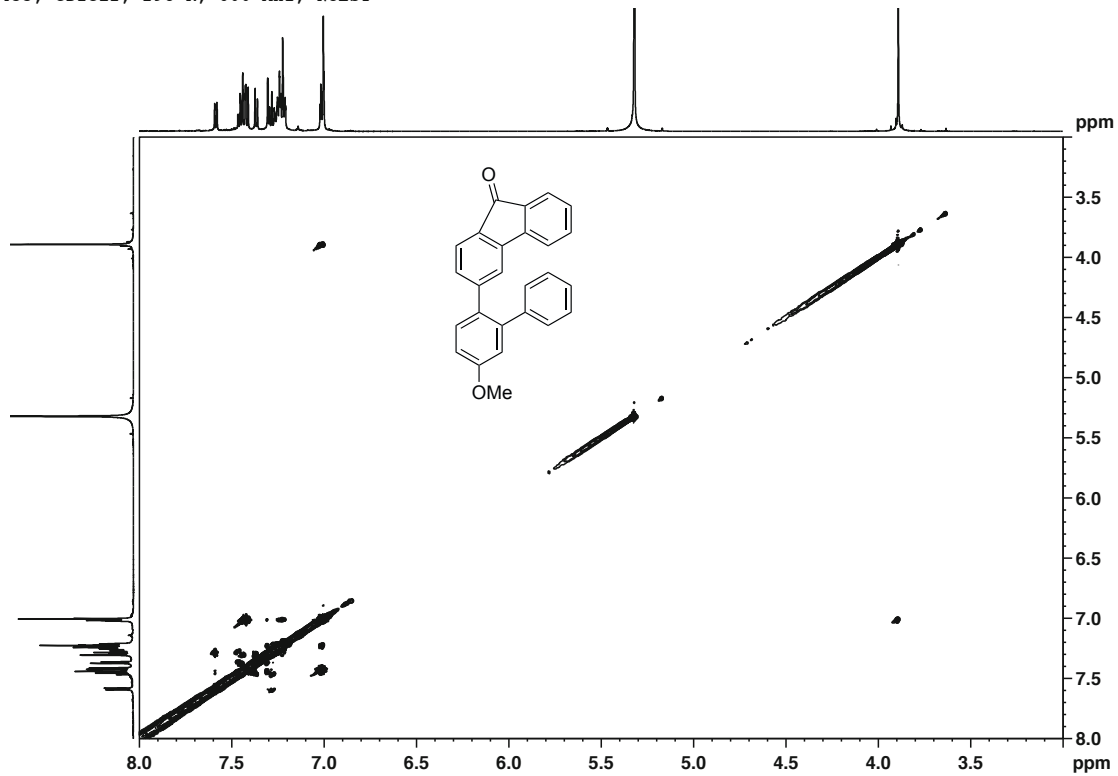


^1H -, ^{13}C -NMR, HMBC, HSQC, COSY, NOESY, TOCSY (CD_2Cl_2 , 600/151 MHz, 25 °C) of 3-(5-methoxy-[1,1'-biphenyl]-2-yl)-9H-fluoren-9-one (**36**)

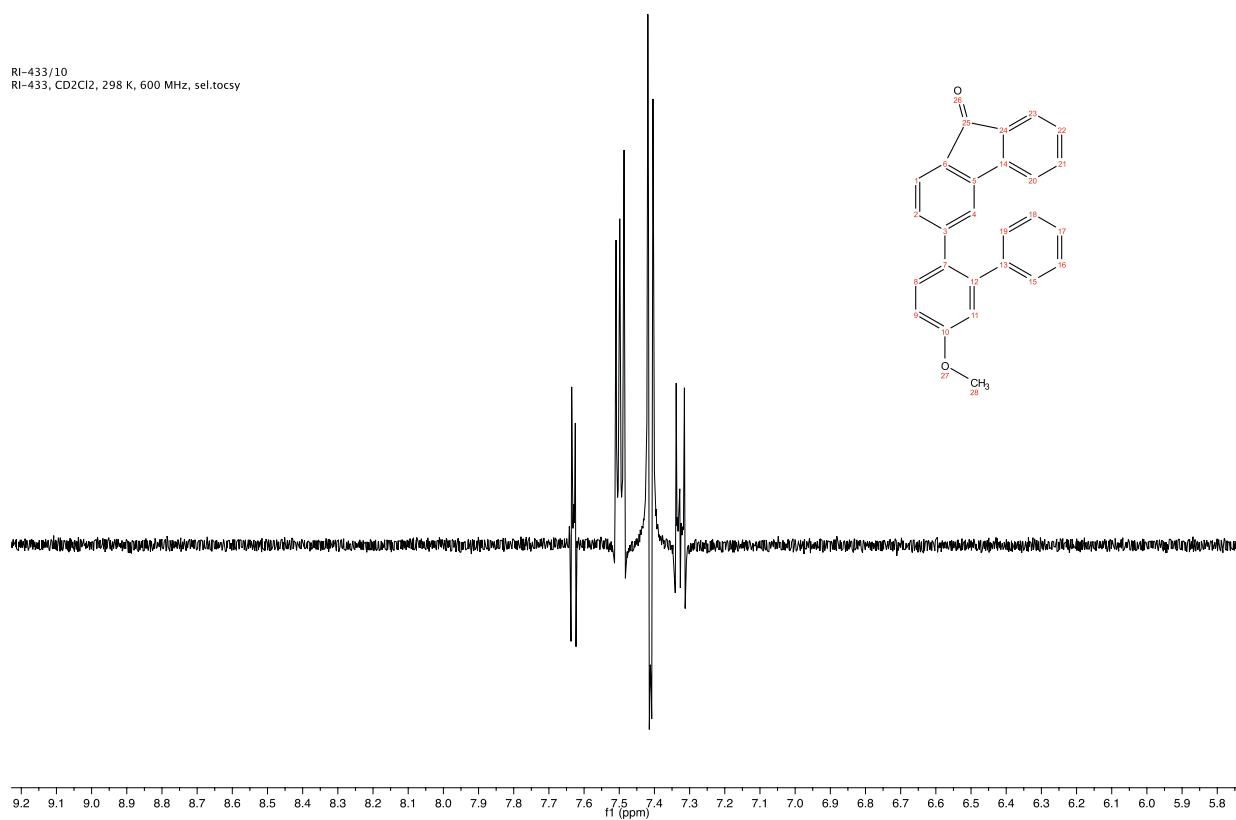


RI-433, CD₂Cl₂, 298 K, 600 MHz, HMBCRI-433, CD₂Cl₂, 298 K, 600 MHz, HSQC

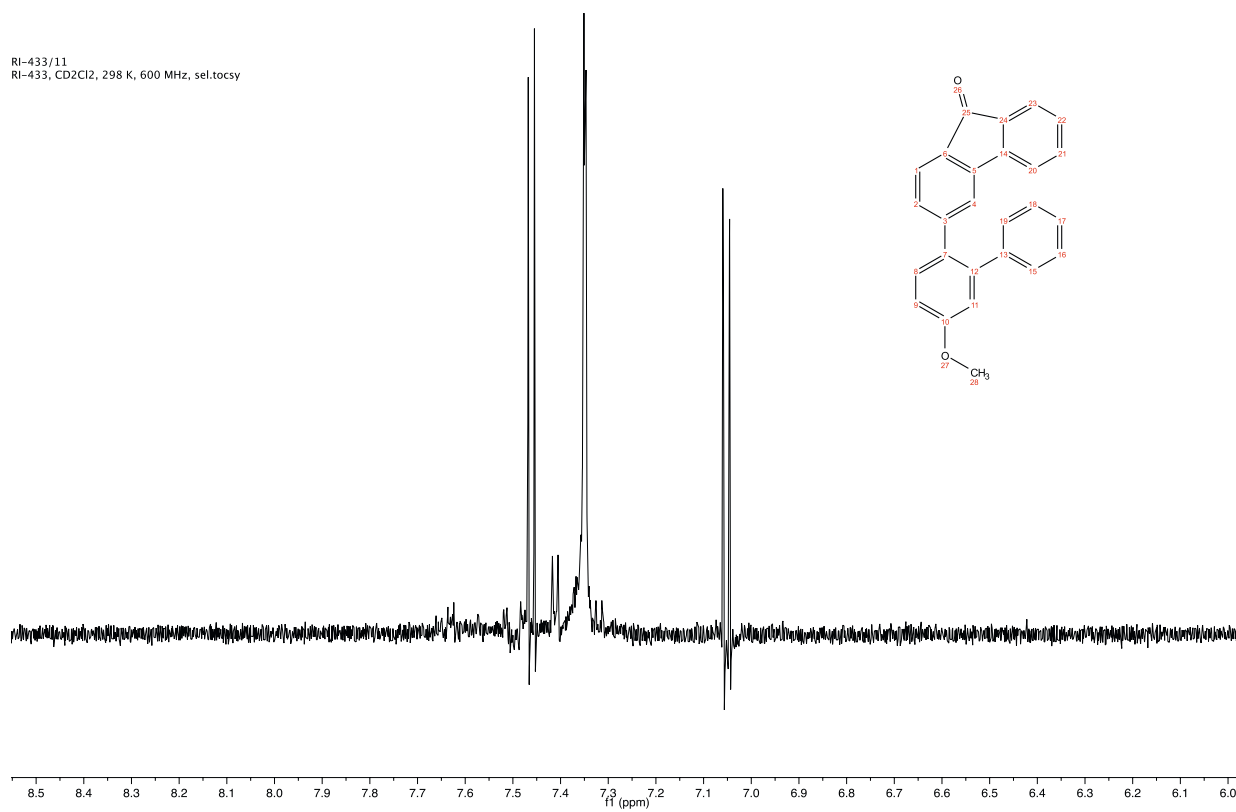


RI-433, CD₂Cl₂, 298 K, 600 MHz, COSYRI-433, CD₂Cl₂, 298 K, 600 MHz, NOESY

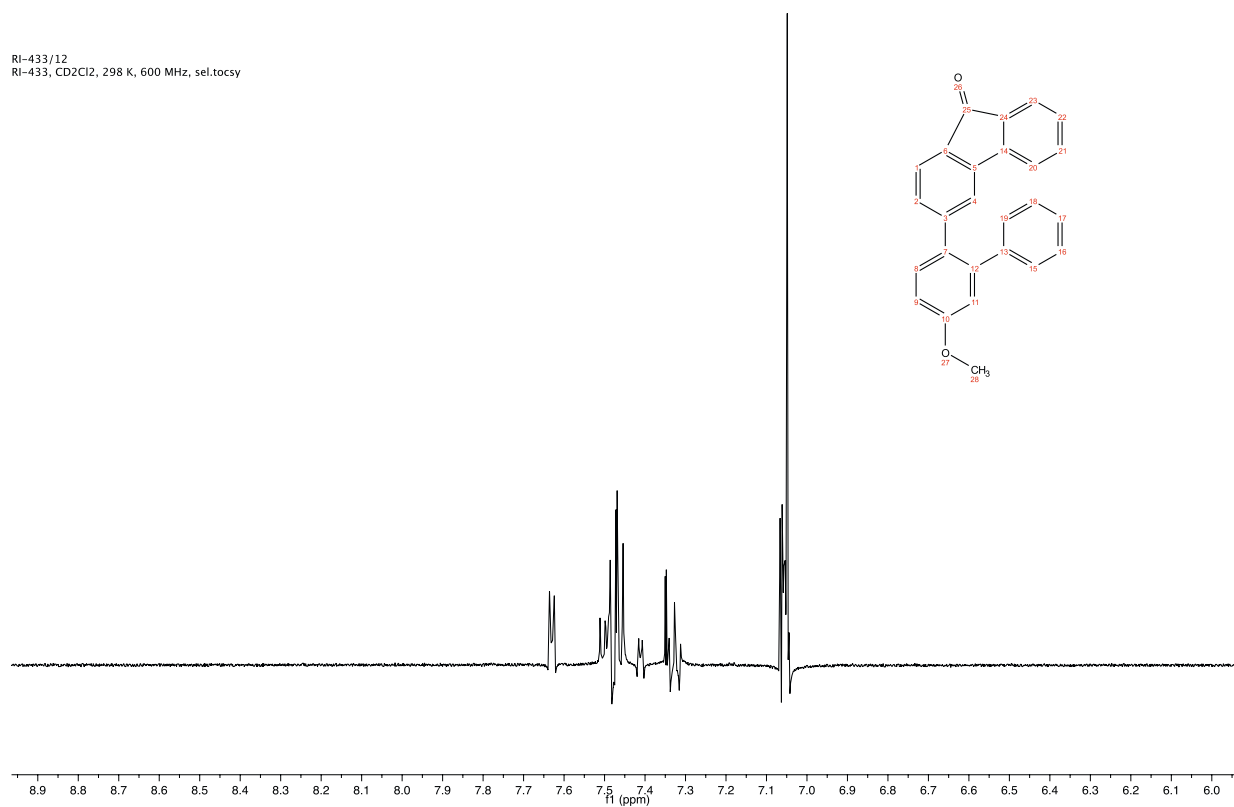
RI-433/10
RI-433, CD₂Cl₂, 298 K, 600 MHz, sel.tocsy



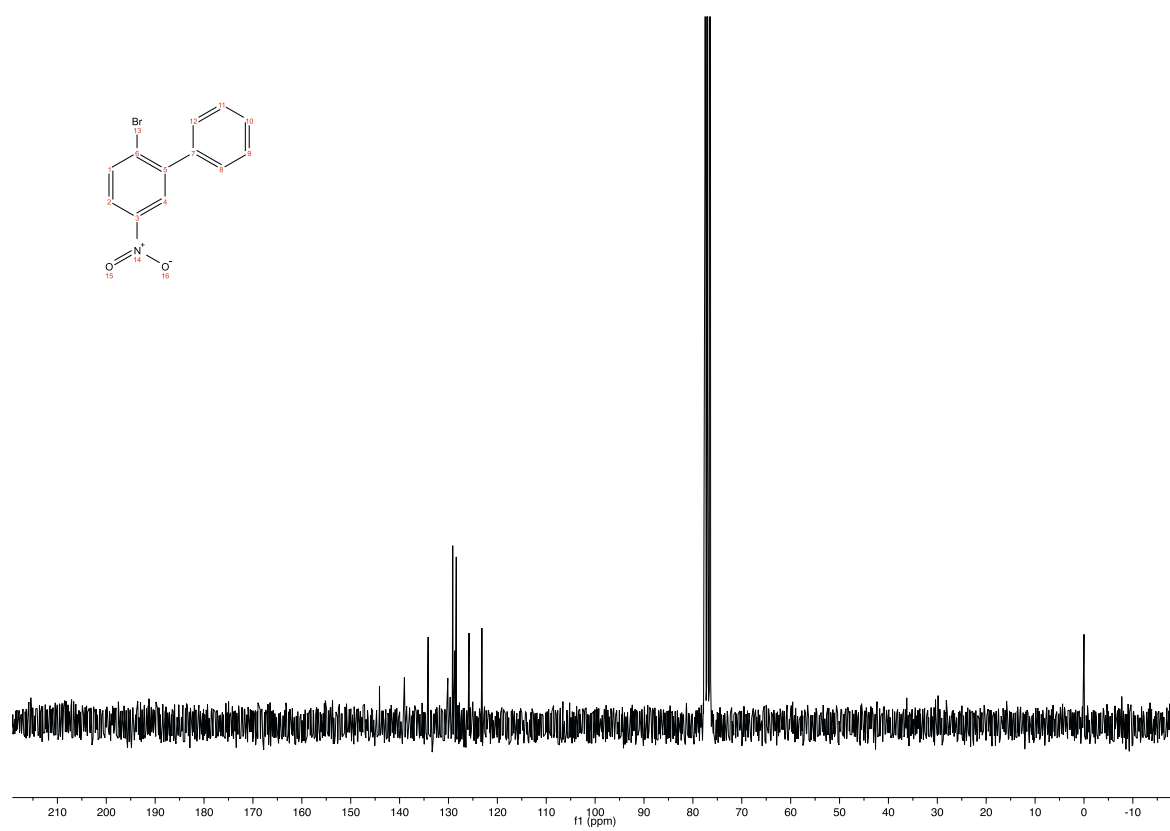
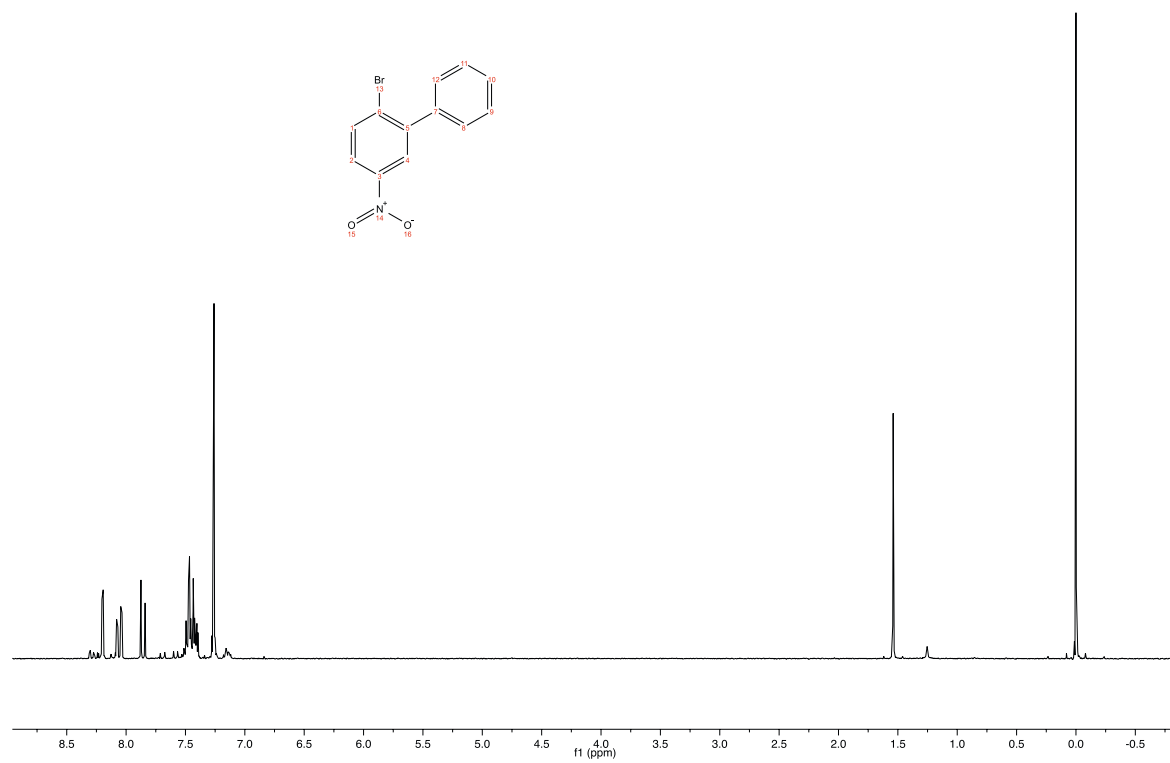
RI-433/11
RI-433, CD₂Cl₂, 298 K, 600 MHz, sel.tocsy



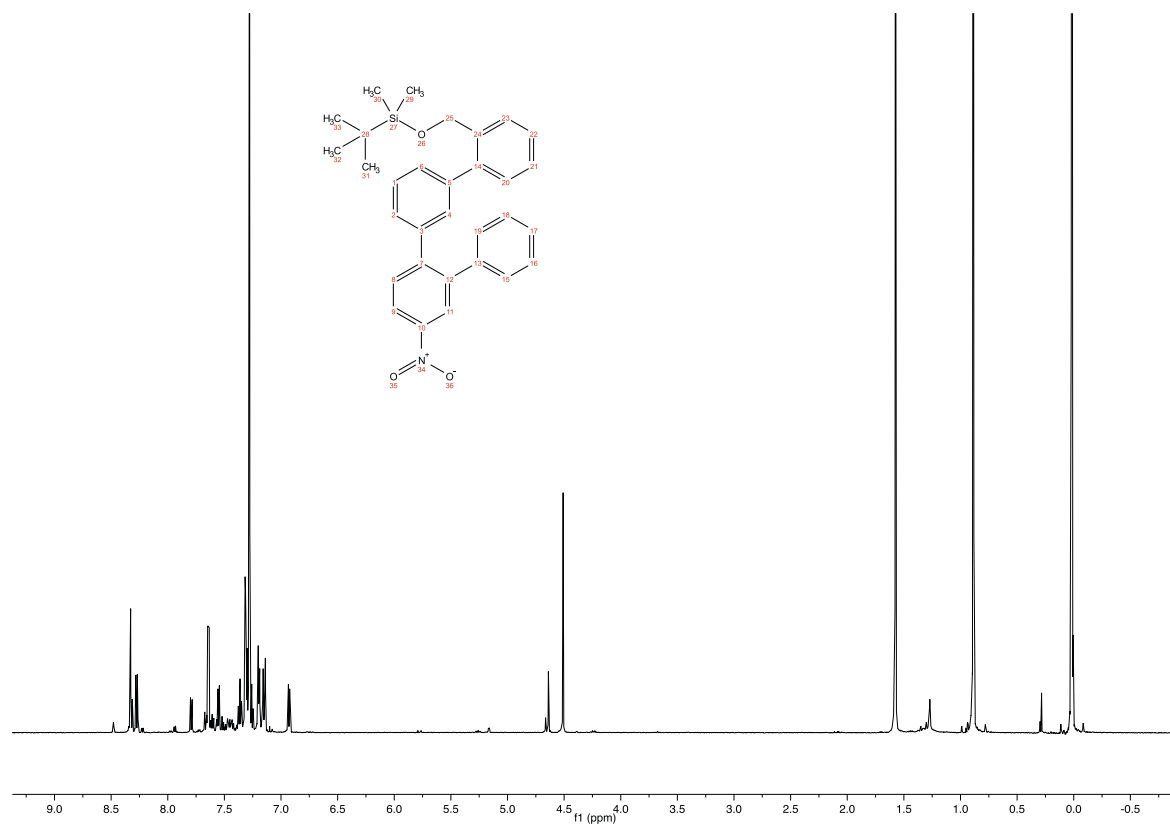
RI-433/12
RI-433, CD₂Cl₂, 298 K, 600 MHz, sel.tocsy



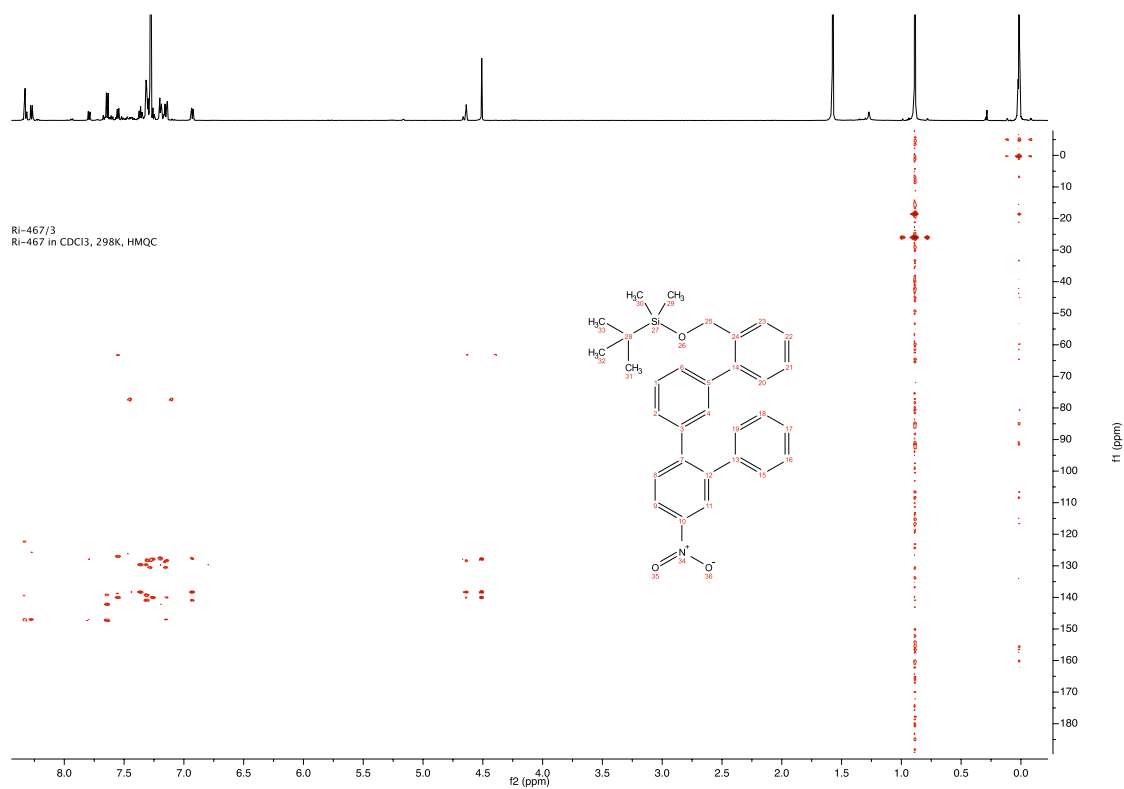
^1H -, ^{13}C -NMR, (CDCl_3 , 400/63 MHz, 25 °C) of 2-bromo-5-nitro-1,1'-biphenyl (**37**)



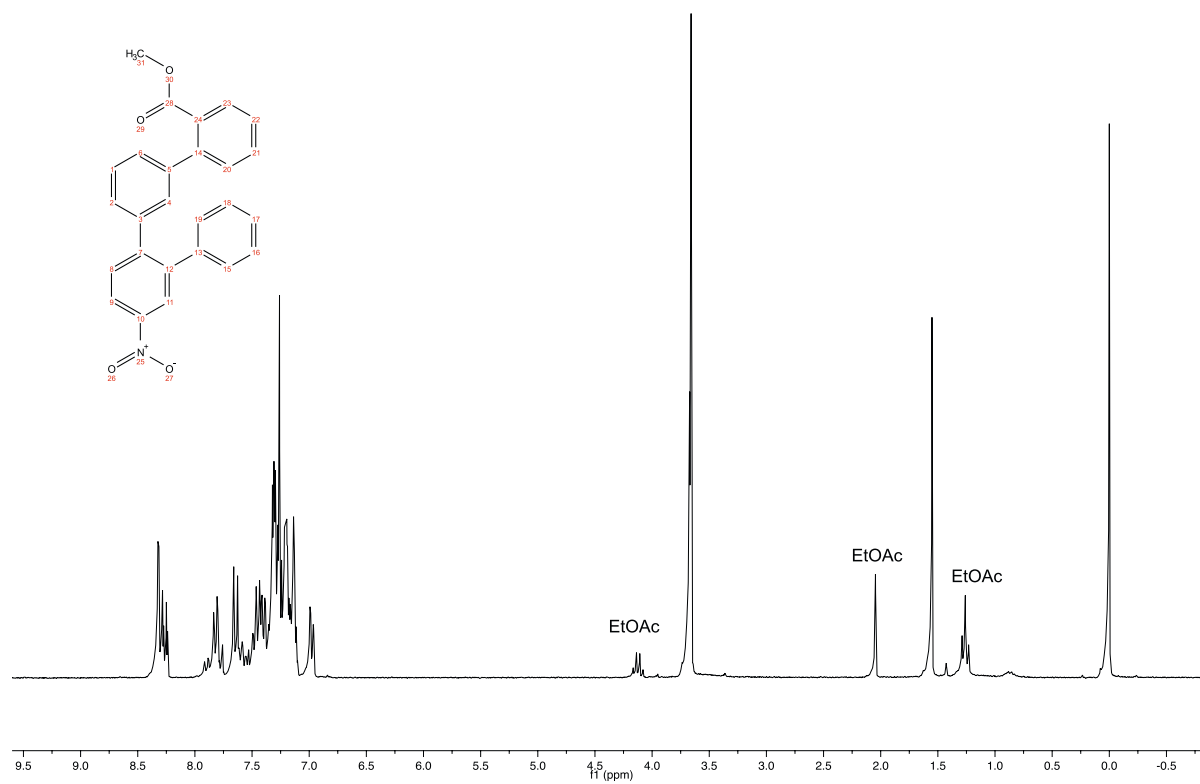
^1H -, HMQC, (CDCl_3 , 500/125 MHz, 25 °C) of *tert*-butyldimethyl((5'-nitro-[1,1':2',1'':3'',1'''-quaterphenyl]-2'''-yl)methoxy)silane (**38**)



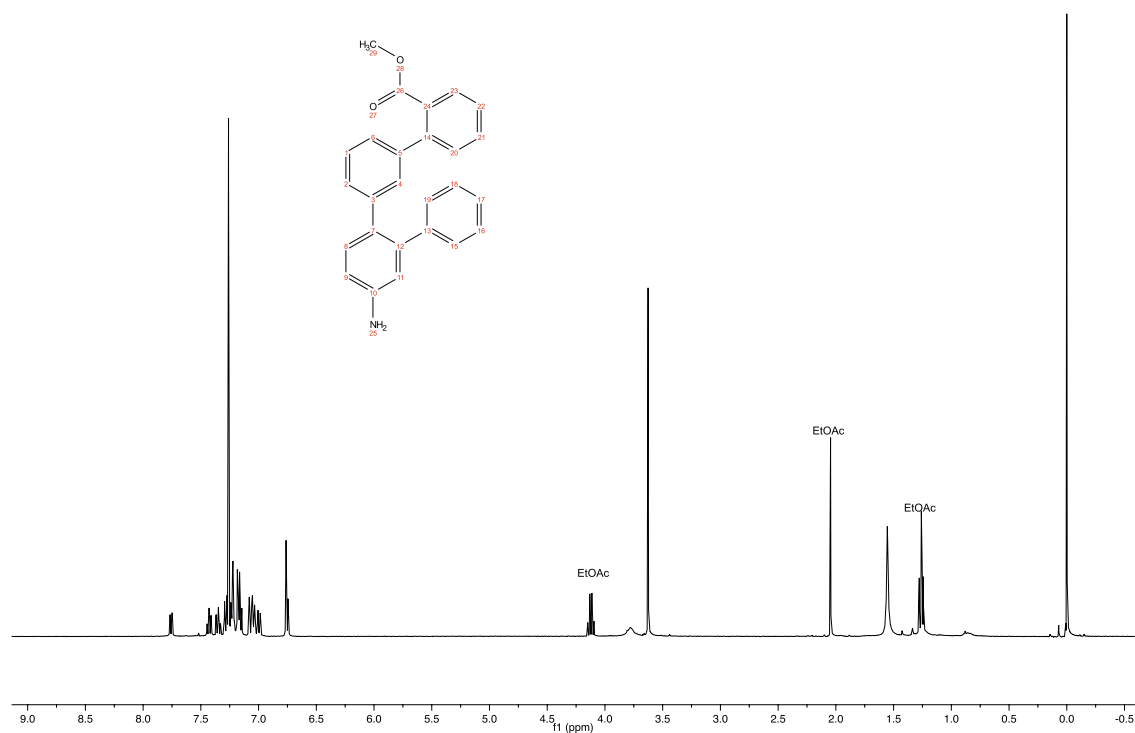
check



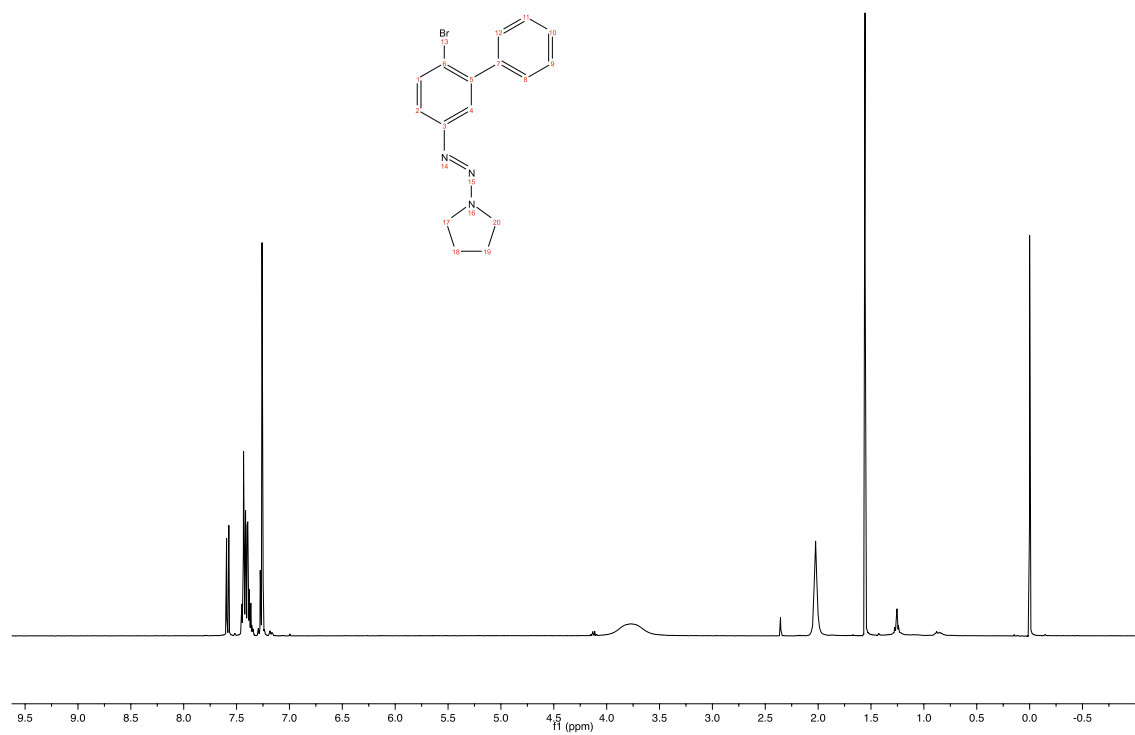
$^1\text{H-NMR}$, (CDCl_3 , 400 MHz, 25 °C) of methyl 5'-nitro-[1,1':2',1'':3'',1'''-quaterphenyl]-2'''-carboxylate (**39**)



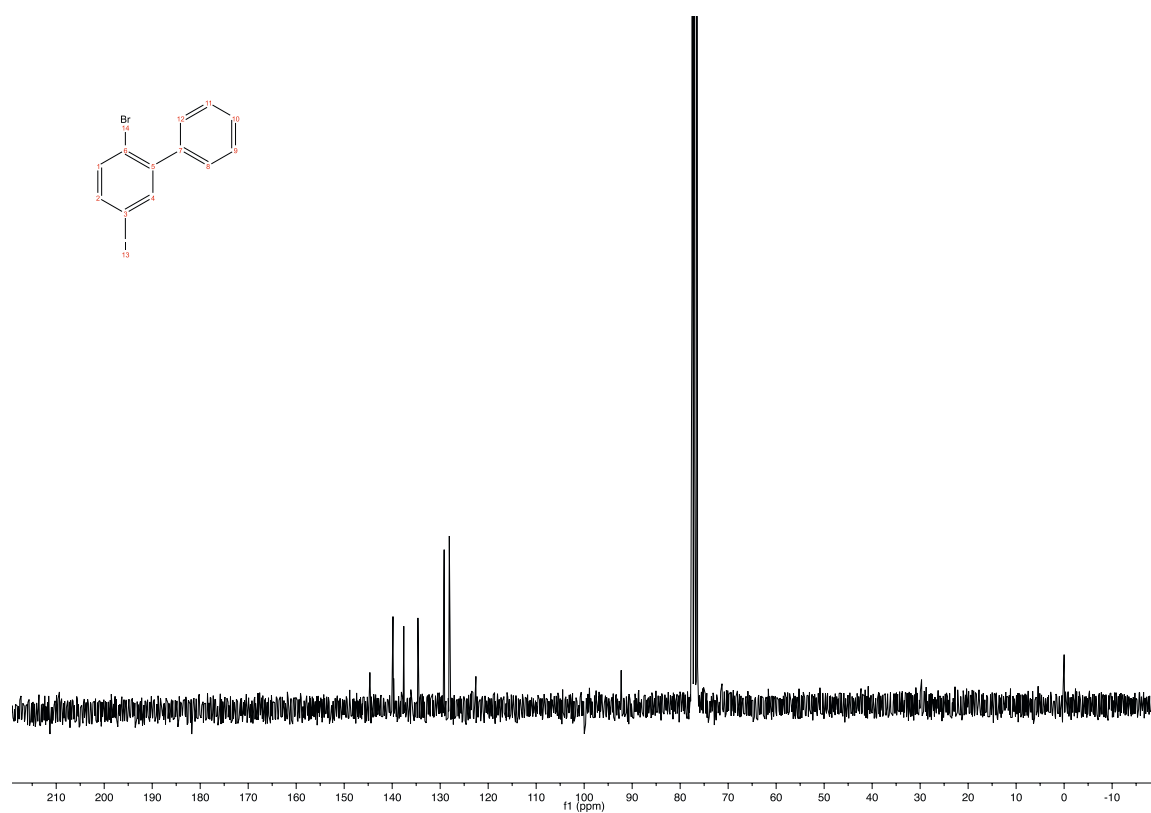
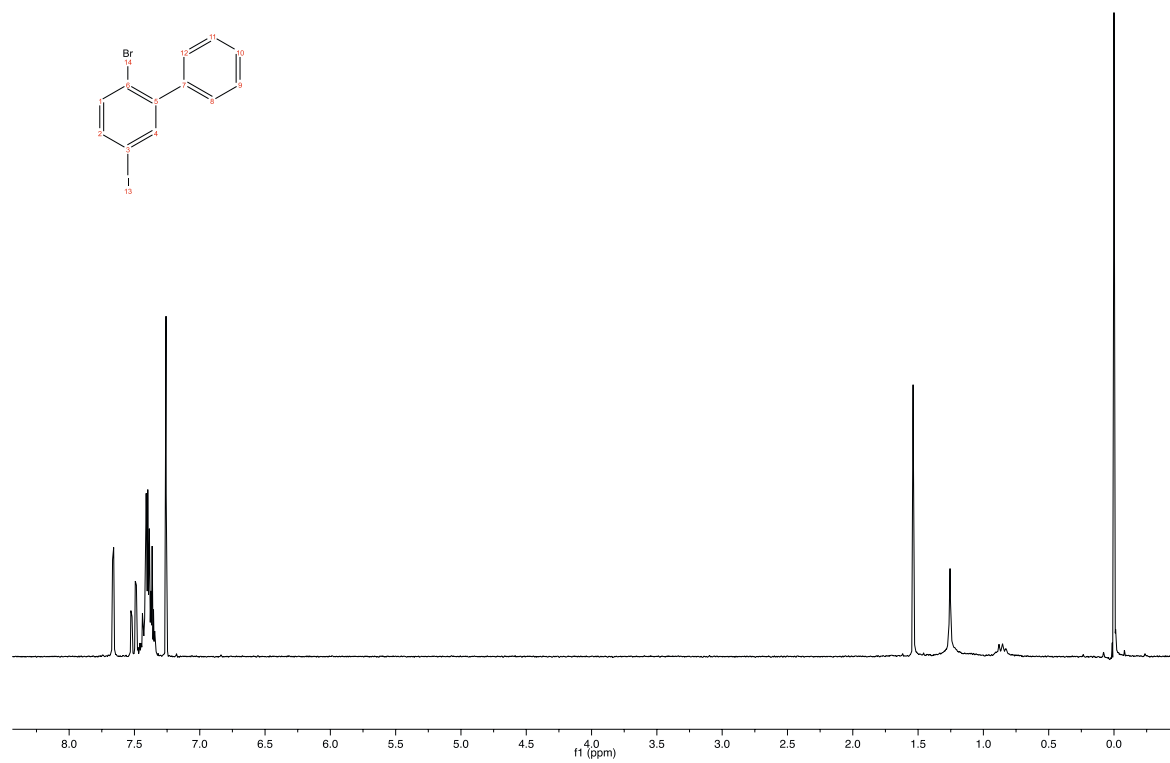
$^1\text{H-NMR}$, (CDCl_3 , 400 MHz, 25 °C) of methyl 5'-amino-[1,1':2,1'':3'',1''':4''':5''':6''']-quaterphenyl-2'''-carboxylate (**41**)



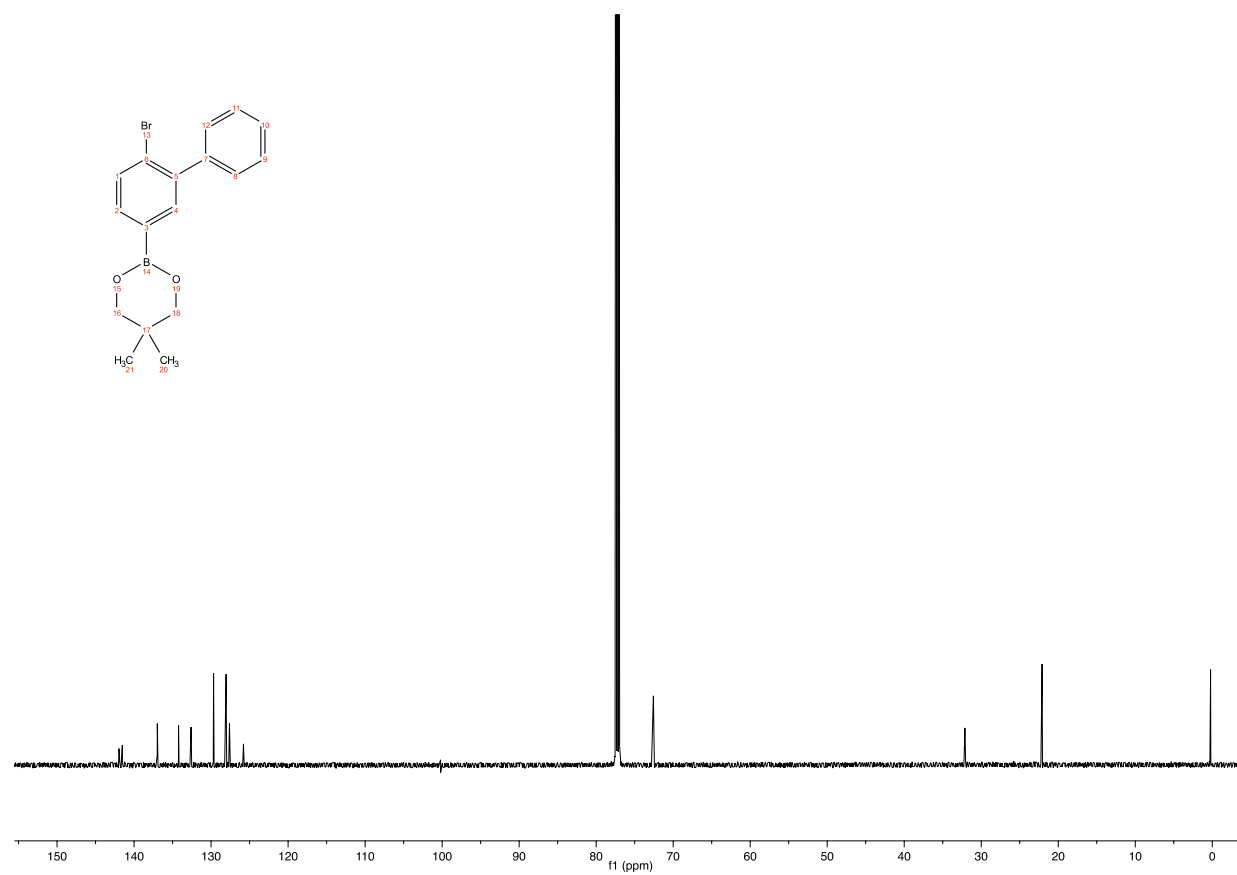
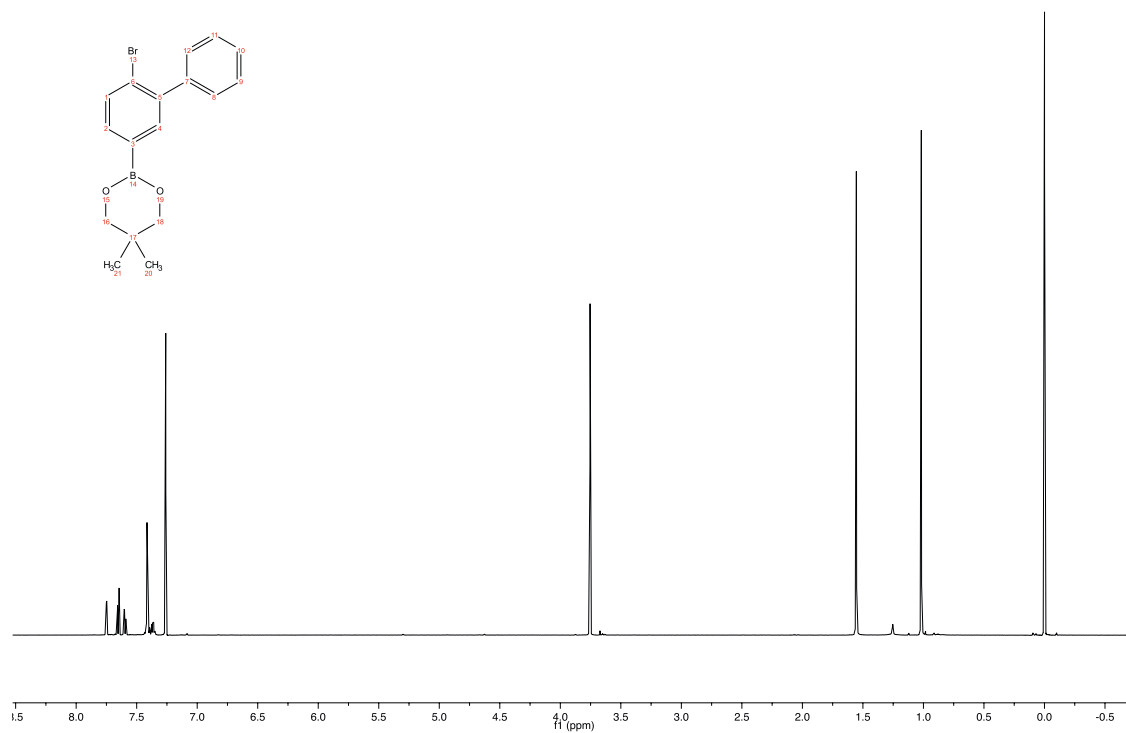
$^1\text{H-NMR}$, (CDCl_3 , 400 MHz, 25 °C) of 1-((6-Bromo-[1,1'-biphenyl]-3-yl) diazenyl)pyrrolidine (**44**)



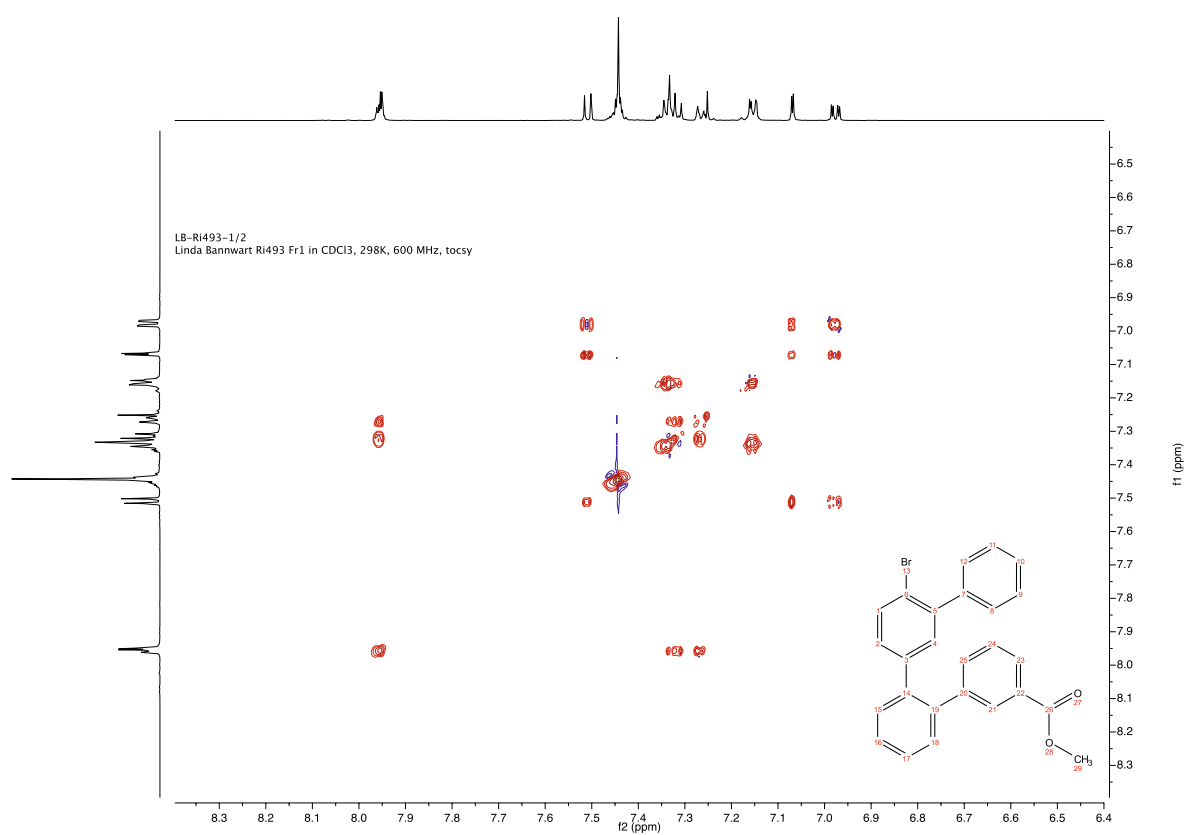
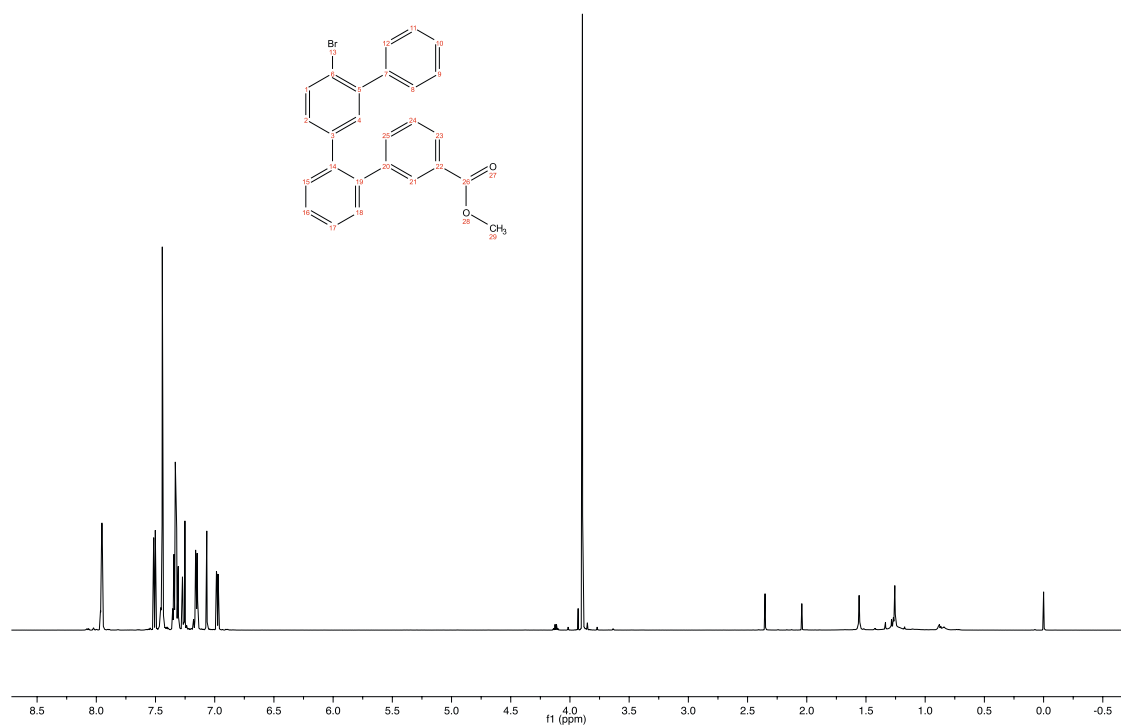
^1H -, ^{13}C -NMR, (CDCl_3 , 400/101 MHz, 25 °C) of 2-bromo-5-iodo-1,1'-biphenyl (**46**):



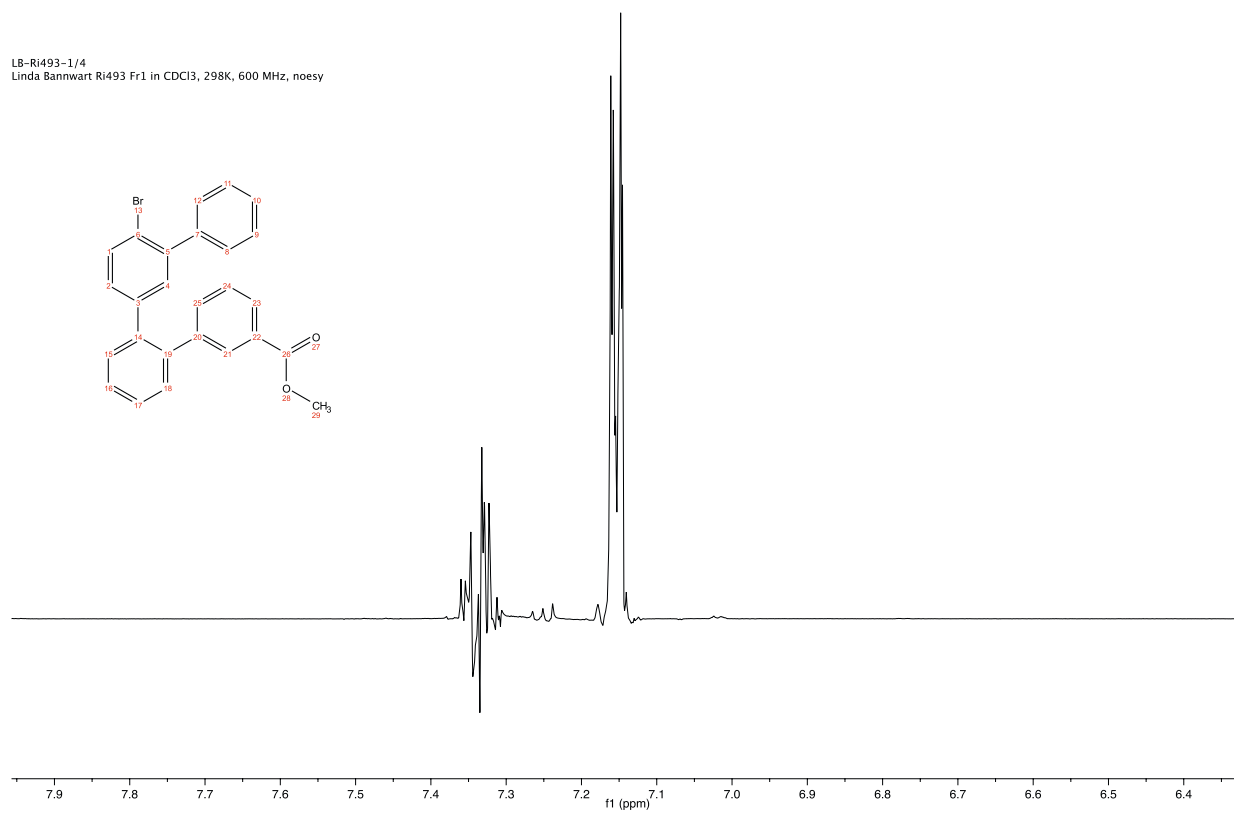
^1H -, ^{13}C -NMR, (CDCl_3 , 400/151 MHz, 25 °C) of 2-(6-bromo-[1,1'-biphenyl]-3-yl)-5,5-dimethyl-1,3,2-dioxaborinane (**48**)



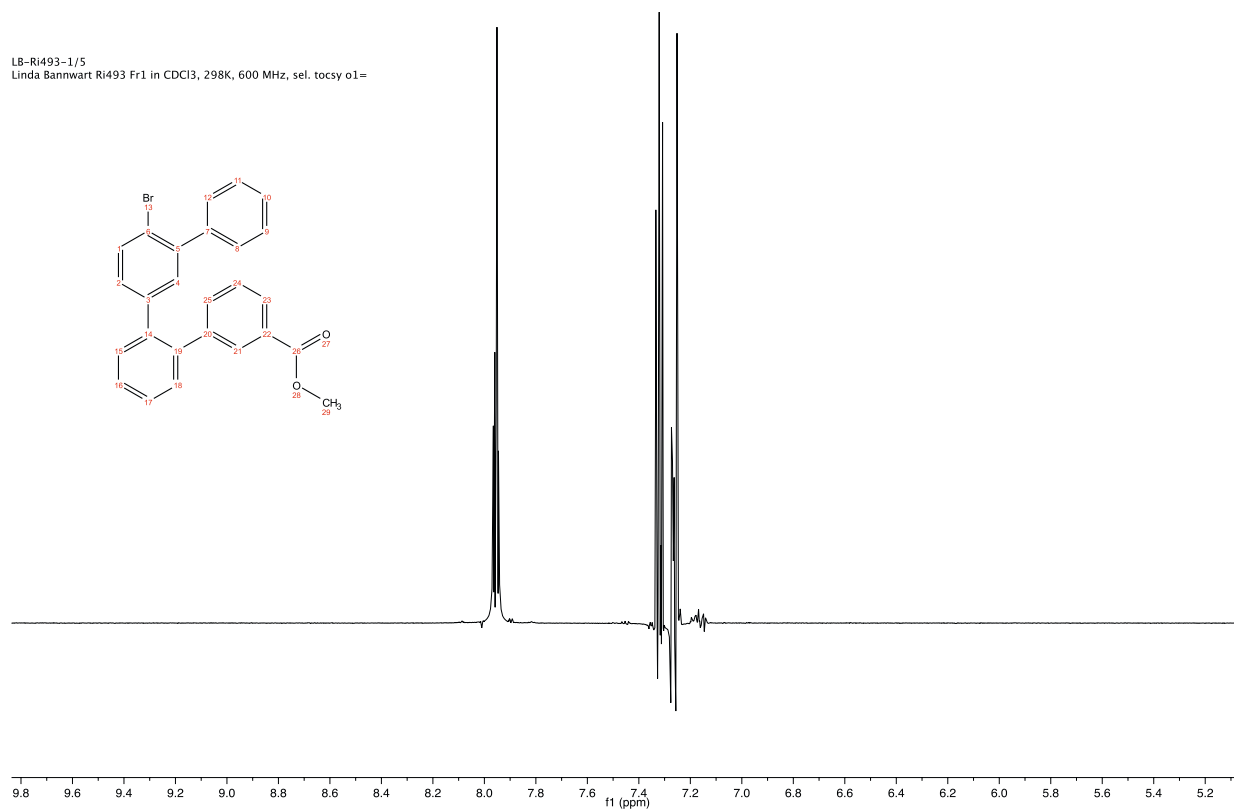
^1H -, NOESY, TOCSY (CDCl_3 , 600 MHz, 25 °C) and HR-ESI of methyl 4''-bromo-[1,1':2',1'':3'',1'''-quaterphenyl]-3-carboxylate (**50**)



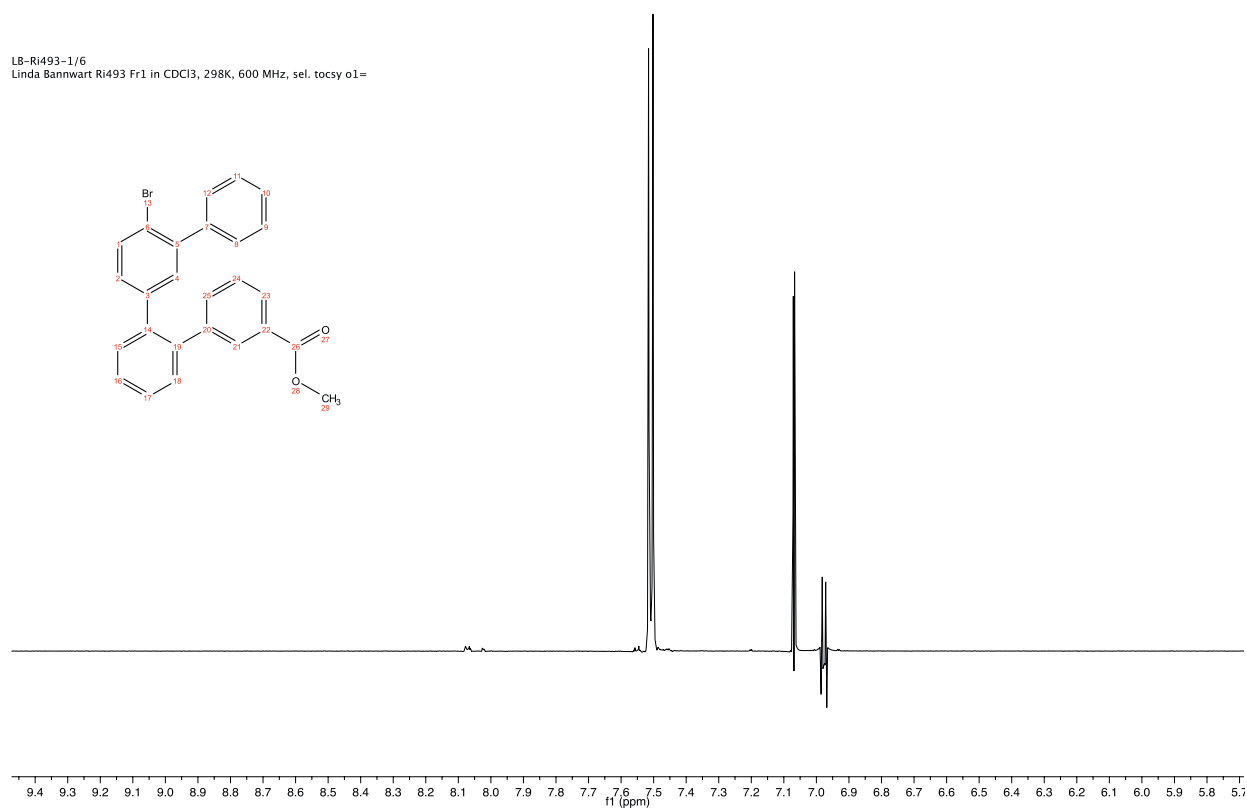
LB-Ri493-1/4
Linda Bannwart Ri493 Fr1 in CDCl₃, 298K, 600 MHz, noesy



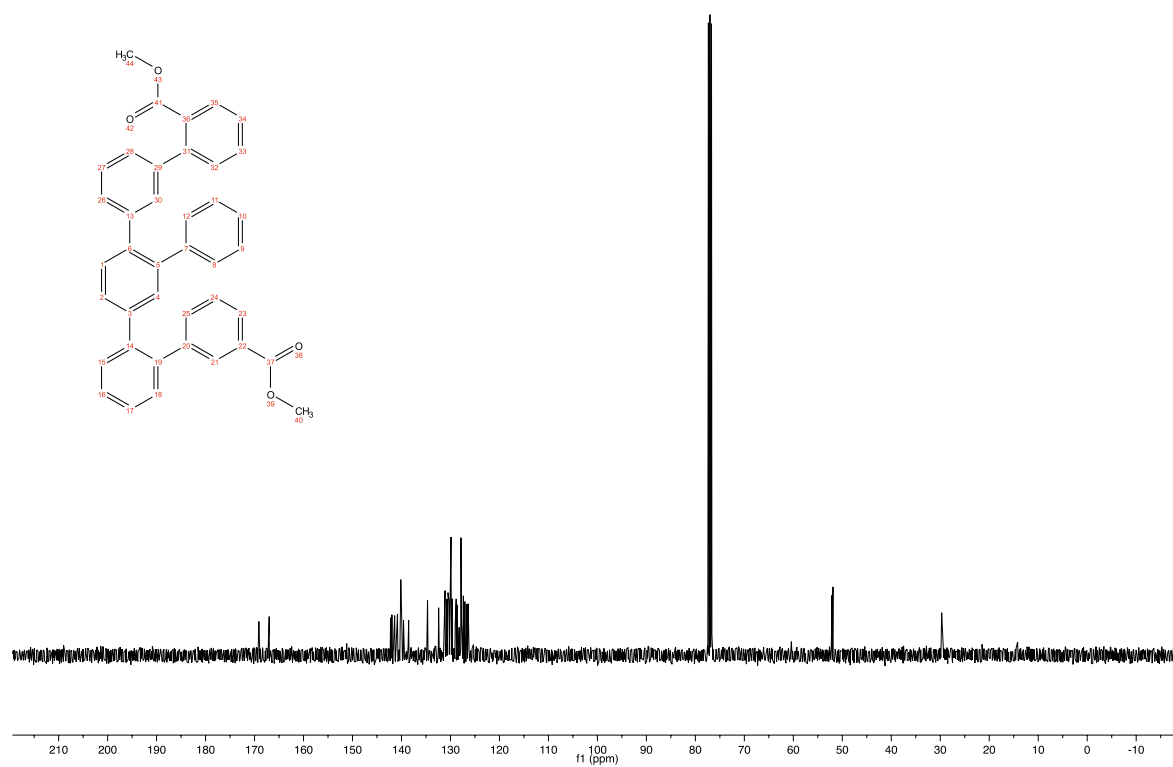
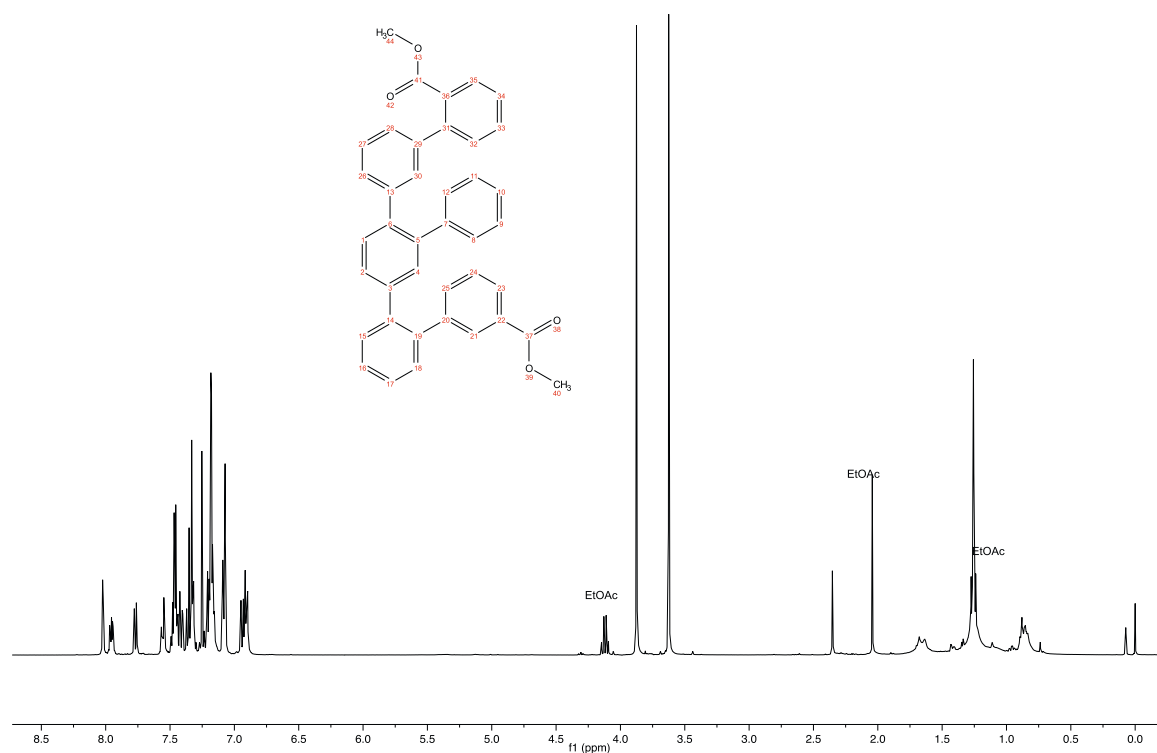
LB-Ri493-1/5
Linda Bannwart Ri493 Fr1 in CDCl₃, 298K, 600 MHz, sel. tocsy o1=



LB-Ri493-1/6
Linda Bannwart Ri493 Fr1 in CDCl₃, 298K, 600 MHz, sel. tocsy o1=



^1H -, ^{13}C -NMR (CDCl_3 , 400/101 MHz, 25 °C) of dimethyl 3''-phenyl-[1,1':2',1'':4'',1''':3''',1''''-quinquephenyl]-2''',3-dicarboxylate (**52**)



CHEMISTRY

A EUROPEAN JOURNAL

Tuning Helical Chirality in Polycyclic Ladder Systems

Supporting Information

*Michel Rickhaus, Oliver T. Unke, Rajesh Mannancherry, Linda M. Bannwart, Markus Neuburger, Daniel Häussinger, and Marcel Mayor**

[*] M. Rickhaus, O. T. Unke, R. Mannancherry, L. M. Bannwart, Dr. M. Neuburger, Dr. D. Häussinger, Prof. Dr. M. Mayor

Department of Chemistry

University of Basel

St. Johannis-Ring 19

4056 Basel, Switzerland

E-mail: marcel.mayor@unibas.ch

Prof. Dr. M. Mayor

Institute for Nanotechnology (INT)

Karlsruhe Institute of Technology (KIT)

P. O. Box 3640

76021 Karlsruhe, Germany

Lehn Institute of Functional Materials (LIFM)

Sun Yat-Sen University

Guangzhou, China

Accepted August, 2015

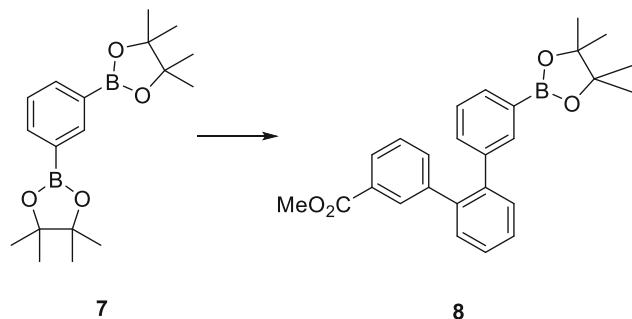
Supporting Information

Table of Contents

Synthetic Procedures of structures (7) – (9), (11), (1)-(4)	2
Crystal data for (1)	9
Crystal data for (4)	10
Unit cell for (1)	11
Unit cell for (4)	11
¹ H-, ¹³ C-NMR (CDCl ₃ , 400/101 MHz, 25 °C) and HR-ESI-MS spectra of 7	12
¹ H-, ¹³ C-NMR (CDCl ₃ , 500/101 MHz, 25 °C) and HR-ESI-MS spectra of 8	14
¹ H-, ¹³ C-NMR (CDCl ₃ , 400/101 MHz, 25 °C) and HR-MALDI-MS spectra of 11	16
¹ H-, hmbc, hmqc (CDCl ₃ , 600/125 MHz, 25 °C) and HR-ESI-MS spectra of 1	18
¹ H-, hmbc, hmqc, VT (C ₂ Cl ₄ D ₂ , 600/125 MHz, 105 °C) and HR-ESI-MS spectra of 2	22
¹ H-, hmbc, hmqc, (CDCl ₃ , 600/125 MHz, 25 °C) and HR-ESI-MS spectra of 3	27
¹ H-, hmbc, hmqc, VT (C ₂ Cl ₄ D ₂ , 600/125 MHz, 105 °C) and HR-ESI-MS spectra of 4	31

Synthetic Procedures of structures (7) – (9), (11), (1)-(4)

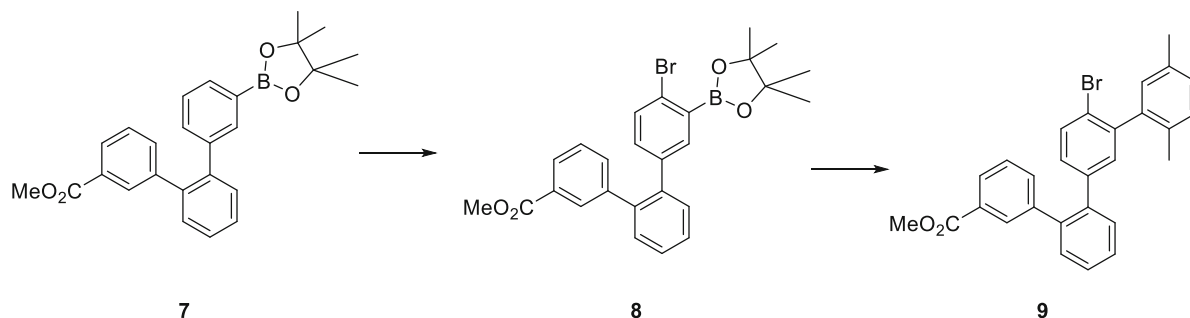
General Procedures: All commercially available compounds were purchased and used as received unless explicitly stated otherwise. ^1H NMR was recorded on a Bruker UltraShield 500MHz Avance III equipped with a 5 mm BBI probe head with Z-gradients. All 2D NMR-Spectra were recorded on Bruker 600 MHz Avance III instruments equipped with either a 5 mm BBI probe for experiments at 378 K, a 5 mm BBFO or a 1.7 mm TCI cryo probe head. The chemical shifts are reported in parts per million (ppm) relative to tetramethylsilane or a residual solvent peak. Temperature calibration was performed with a glycerol sample. Complete assignment of compounds **1** to **5** was possible using HSQC or HMQC, COSY, NOESY, TOCSY and HMBC experiments. In all cases only small amounts of the compounds were available which were not sufficient to obtain meaningful one-dimensional $^{13}\text{C}\{^1\text{H}\}$ -NMR spectrum. We recorded, therefore, the much more sensitive HMBC experiments, first with low and later on with high resolution (acquisition time in the carbon dimension of 169.8 ms and a resolution of 2.9 Hz / point) and determined all carbon resonances unambiguously. The total experiment times for the HMBC experiments varied between 6.5 and 79 hours. DART-MS was measured on a IonSense DART-SVP100 (He, 450 °C) connected to a Shimadzu LC-2020. GC-MS was performed on a Shimadzu GCMS-2020 SE equipped with a Zebron 5 MS Inferno column which allowed to achieve temperatures up to 350 °C. High-resolution ESI mass spectra (HR-ESI-MS) were measured as HR-ESI-ToF-MS with a Maxis 4G instrument from Bruker with the addition of NaOAc. High-resolution MALDI mass spectra (HR-MALDI-MS) were measured as HR-MALDI-ToF-MS with a SOLARIX instrument from Bruker. For column chromatography, usually silica gel Siliaflash® p60 (40–63 μm) from Silicycle was used, and TLC was performed on silica gel 60 F254 glass plates with a thickness of 0.25 mm purchased from Merck. Bulk reversed phase chromatography was performed with C18 coated silica gel (60A, 17 % Carbon, 0.69 mmol/g loading) by Silicycle. For HPLC a Shimadzu LC-20AT HPLC was used equipped with a diodearray UV/Vis detector (SPD-M10A VP from Shimadzu, $\lambda = 200 - 600 \text{ nm}$) equipped with the corresponding column (regular: Reprosil 100, 5 μm , 250 x 16 mm; reversed; Reprosil 100 C18, 5 μm , 250 x 16 mm; chiral: chiralpak IA 0.46 x 25 cm; Daicel Chemical Industries Ltd.; GPC: 2 x Repro-Gel GPC 500, 5 μm , 20 x 600 mm). CD measurements were performed on a Chirascan CD Spectrometer in *n*-hexane/*i*PrOH = 98:2 at room temperature in 1 cm quartz glass cuvettes directly after the chiral HPLC. All solutions were prepared and measured under air saturated conditions. Calculations were performed using Gaussian G09 version C.01.

Methyl 3''-(4,4,5,5-tetramethyl-1,3,2-dioxaborolan-2-yl)-[1,1':2',1''-terphenyl]-3-carboxylate (**7**)

To an argon flushed Schlenk tube was added **6** (1.04 g, 3.16 mmol, 1.30 equiv.), along with **A** (820 mg, 2.43 mmol, 1.00 equiv.) and K_3CO_3 (1.01 g, 7.29 mmol, 3.00 equiv.) before subjecting the flask to vacuum for 15 minutes. After reflushing with argon, 1,4-dioxane (15 mL) and MeOH (1.5 mL) and $Pd(PPh_3)_2Cl_2$ (34.5 mg, 2 mol %) were added and the resulting suspension degassed by passing argon through followed by heating to 60 °C for 2h. After cooling to room temperature, the suspension was diluted with DCM and the solids removed by filtration and removal of the solvents under reduced pressure. The residue was directly subjected to flash column chromatography (SiO_2 , cyclohexane/EtOAc 1:20) yielding **7** as colorless solid (320 mg, 772 μ mol, 32 %) in sufficient purity. If desired, subsequent further purification by recycling gel permeation chromatography (GPC) can be performed ($CHCl_3$, ~20 cycles).

1H NMR (400 MHz, $CDCl_3$): δ = 7.98 (td, $^4J_{H,H}$ = 1.6, 0.8 Hz, 1 H), 7.86 (ddd, $^3J_{H,H}$ = 6.7, $^4J_{H,H}$ = 2.4, 1.7 Hz, 1 H), 7.73 (ddd, $^4J_{H,H}$ = 1.9, 1.2, 0.6 Hz, 1 H), 7.63 (dt, $^3J_{H,H}$ = 7.3, $^4J_{H,H}$ = 1.3 Hz, 1 H), 7.50 – 7.47 (m, 1 H), 7.44 – 7.41 (m, 3 H), 7.19 – 7.16 (m, 2 H), 7.12 (ddd, $^3J_{H,H}$ = 7.9, 7.2, $^4J_{H,H}$ = 0.6 Hz, 1 H), 7.05 (ddd, $^3J_{H,H}$ = 7.7, $^4J_{H,H}$ = 2.0, 1.4 Hz, 1 H), 3.88 (s, 3 H), 1.32 (s, 12 H) ppm. ^{13}C NMR (101 MHz, $CDCl_3$) δ = 167.3, 142.1, 140.7, 140.5, 139.7, 136.3, 135.0, 133.2, 133.1, 131.0, 130.9, 130.6, 130.2, 128.0, 127.9, 127.9, 127.7, 127.3, 84.0 (2 C), 52.2, 25.1 (4 C). The quaternary aromatic carbon next to the boronic ester could not be resolved. MS (EI, +): m/z (%) = 415.1 (28), 414.1 (M^+ , 100), 413.1 (25), 339.1 (27), 328.1 (28), 315.1 (10), 313.1 (19), 297.1 (27), 284.0 (18), 283.0 (84), 282.0 (22), 270.1 (11), 269.1 (13), 256.1 (10), 255.0 (41), 254.0 (46), 253.0 (21), 252.0 (10), 237.0 (24), 229.0 (11), 228.0 (25), 227.0 (12), 226.0 (16). HRMS (ESI), calc. for $C_{26}H_{28}BO_4$ 415.2080 [$M+H$] $^+$, found 415.2077; calc. for $C_{26}H_{28}BNaO_4$ 437.1899 [$M+Na$] $^+$, found 437.1903.

Methyl 4''-bromo-3''-(4,4,5,5-tetramethyl-1,3,2-dioxaborolan-2-yl)-[1,1':2',1''-terphenyl]-3-carboxylate (**8**)¹ and methyl 4''-bromo-2''',5'''-dimethyl-[1,1':2',1''':3'',1''''-quaterphenyl]-3-carboxylate (**9**)



An oven dried, argon flushed Schlenk tube was charged with **7** (230 mg, 555 μmol , 1.00 equiv.). Dry dichloroethane (20 mL) was added and the solution heated to 60 $^{\circ}\text{C}$. NBS (130 mg, 722 μmol , 1.30 equiv.) was added in portions to the reaction mixture and the solution left stirring overnight. DCM and water were added and the organic layer extracted with water (3 x) and dried over Na_2SO_4 before removing the solvents under reduced pressure yielding **8** in sufficient purity (typically 30-49 %). Due to limited stability the crude product (**8**) was best directly used in the next step. An analytical sample was purified by reversed phase HPLC (semi-preparative Reprisil 100 C18, eluent: MeCN, flow rate: 4 mL min^{-1} , $T = 25^{\circ}\text{C}$).

To an argon flushed Schlenk tube was consecutively added crude **8** (246 mg, 499 μmol , 1.00 equiv.), 2-iodo-1,4-dimethylbenzene (**B**, 107 μL , 749 μmol , 1.50 equiv.), and K_2CO_3 (207 mg, 1.50 mmol, 3.00 equiv.). Wet 1,4-dioxane (8 mL) and MeOH (2 mL) were added and the solution degassed by a stream of argon for 15 min while adding $\text{Pd}(\text{PPh}_3)_2\text{Cl}_2$ (14 mg, 4 mol %) and heating to 60 $^{\circ}\text{C}$ overnight. DCM was added and the solids removed by filtration. The solvent was removed under reduced pressure before subjecting the residue to flash column chromatography (SiO_2 , 1:20 EtOAc/cyclohexane) yielding **9** as a pale yellow oil (105 mg, 223 μmol , 40 % over two steps).

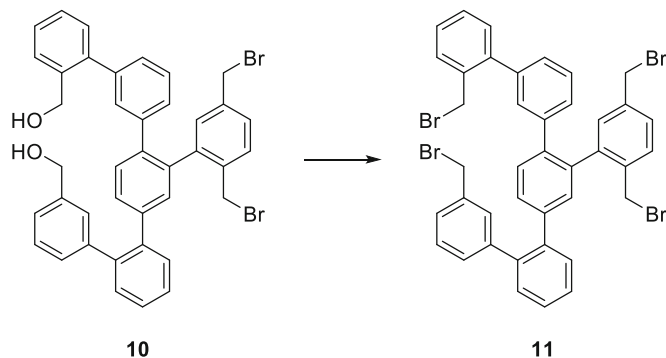
8: $^1\text{H NMR}$ (500 MHz, CDCl_3): $\delta = 7.98$ (td, $^4J_{\text{H,H}} = 1.8$, $^4J_{\text{H,H}} = 0.6$ Hz, 1 H), 7.89 (ddd, $^3J_{\text{H,H}} = 7.7$, $^4J_{\text{H,H}} = 1.7$, $^4J_{\text{H,H}} = 1.2$ Hz, 1 H), 7.46 (d, $^4J_{\text{H,H}} = 2.4$ Hz, 1 H), 7.45 – 7.41 (m, 4 H), 7.31 (d, $^3J_{\text{H,H}} = 8.2$ Hz, 1 H), 7.22 (td, $^3J_{\text{H,H}} = 7.7$, $^4J_{\text{H,H}} = 0.6$ Hz, 1 H), 7.14 (ddd, $^3J_{\text{H,H}} = 7.7$, $^4J_{\text{H,H}} = 1.9$, $^4J_{\text{H,H}} = 1.2$ Hz, 1 H), 6.88 (dd, $^3J_{\text{H,H}} = 8.3$, $^4J_{\text{H,H}} = 2.4$ Hz, 1 H), 3.90 (s, 3 H), 1.33 (s, 12 H) ppm. $^{13}\text{C NMR}$ (101 MHz, CDCl_3) $\delta = 167.2$, 141.8, 139.7, 139.5, 139.3, 138.0, 134.9, 133.5, 132.3, 130.9, 130.8, 130.6, 130.4, 128.2, 128.1, 128.1, 128.1, 126.7, 84.5 (2 C), 52.3, 24.9 (4 C) ppm. The quaternary aromatic carbon next to the boronic ester could not be resolved. DART-MS (450 $^{\circ}\text{C}$, +): m/z (%) = 495.0 (11), 494.0 (42), 493.0 (20), 492.0 (M^+ , 40), 362.9 (29), 361.9 (13), 360.9 (29), 340.0 (24), 339.0 (100), 338.1 (24), 255.0 (12), 254.0 (35), 253.0 (33), 252.0 (21), 226.0 (17). HRMS (ESI), calc. for $\text{C}_{26}\text{H}_{30}\text{BBrNO}_4$ 510.1450 [M] $^+$, found 510.1452; calc. for $\text{C}_{26}\text{H}_{26}\text{BBrNaO}_4$ 515.1004 [$\text{M}+\text{Na}$] $^+$, found 515.1009.

9: All spectra match those previously reported.²

¹ D. Qiu, F. Mo, Z. Zheng, Y. Zhang and J. Wang, *Org. Lett.* **2010**, *12*, 5474–5477.

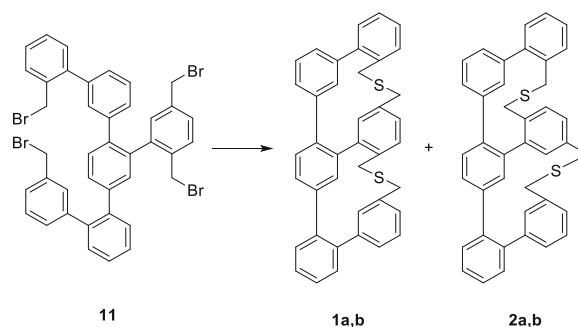
² M. Rickhaus, L. M. Bannwart, M. Neuburger, H. Gsellinger, K. Zimmermann, D. Häussinger and M. Mayor, *Angew. Chem. Int. Ed.* **2014**, *53*, 14587–14591.

3''-(2,5-bis(bromomethyl)phenyl)-2'''',3-bis(bromomethyl)-1,1':2',1'':4'',1''':3''',1''''-quinquephenyl (**11**)



The precursor for **11** was accessed from **9** as described in literature.² The precursor was then suited to undergo the *Appel* transformation as described here. An argon flushed, oven dried Schlenk tube was charged with **10** (150 mg, 259 μmol , 1.00 equiv.) and dry DCM (10 mL) before adding PBr_3 (54.6 μL , 570 μmol , 2.20 equiv.) at room temperature and stirring for 1 h. The solvent was removed under reduced pressure and the residue adsorbed on Celite before directly subjecting to flash column chromatography (SiO_2 , cyclohexane/EtOAc 1:50) to yield the desired product **11** as a colorless solid (130 mg, 157 μmol , 61 %).

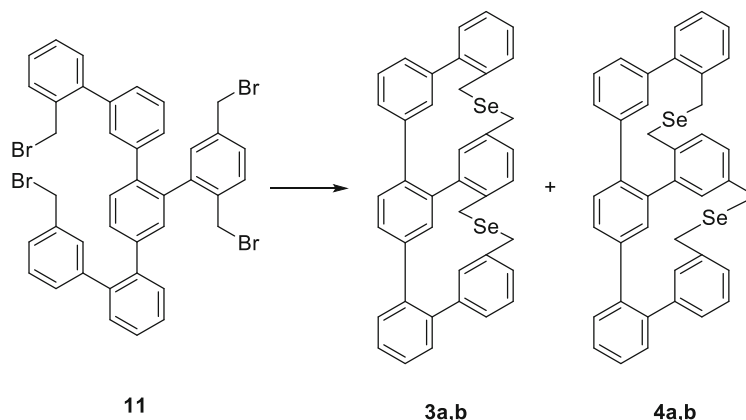
^1H NMR (400 MHz, CDCl_3): δ = 7.57 – 7.54 (m, 1 H), 7.49 – 7.42 (m, 5 H), 7.37 (d, $^4J_{\text{H,H}} = 1.9$ Hz, 1 H), 7.36 – 7.34 (m, 1 H), 7.34 – 7.31 (m, 3 H), 7.31 – 7.28 (m, 2 H), 7.27 – 7.19 (m, 5 H), 7.11 (td, $^4J_{\text{H,H}} = 1.8, 1.8, 0.6$ Hz, 1 H), 7.05 (dd, $^4J_{\text{H,H}} = 1.9, 0.4$ Hz, 1 H), 6.97 (dd, $^3J_{\text{H,H}} = 7.4, ^4J_{\text{H,H}} = 1.6$ Hz, 1 H), 6.89 (d, $^4J_{\text{H,H}} = 1.9$ Hz, 1H), 4.43 (q, $^2J_{\text{H,H}} = 10.2, ^4J_{\text{H,H}} = 10.2$, Hz, 2 H), 4.33 (q, $^2J_{\text{H,H}} = 10.2, ^4J_{\text{H,H}} = 10.2$ Hz, 2 H), 4.14 (d, $^4J_{\text{H,H}} = 1.1$ Hz, 2H), 4.05 (d, $^2J_{\text{H,H}} = 10.4$ Hz, 1 H), 3.88 (d, $^2J_{\text{H,H}} = 10.4$ Hz, 1 H) ppm. ^{13}C NMR (101 MHz, CDCl_3) δ = 142.0, 141.7, 141.3, 140.4, 140.1, 139.8, 139.7, 139.6, 138.9, 137.6 (2 C), 137.1, 135.4, 134.9, 132.6, 132.1, 131.1, 131.0, 130.5, 130.5, 130.5, 130.4, 130.3, 130.2, 129.9, 129.5, 128.7, 128.5, 128.3, 128.2, 128.1, 127.8, 127.8, 127.8, 127.3, 127.2, 33.5, 32.5, 32.3, 31.2 ppm. DART-MS (500 $^\circ\text{C}$, +): m/z (%) = 852.0 (20), 850.9 (21), 849.9 (66), 848.9 (26), 847.7 ($\text{M}+\text{NH}_4^+$, 100), 847.4 (14), 845.9 (64), 843.9 (17), 770.1 (32), 769.0 (18), 767.9 (71), 766.9 (16), 766.0 (58), 764.0 (17), 686.1 (11), 589.0 (16), 587.3 (15). HRMS (MALDI, +), calc. for $\text{C}_{40}\text{H}_{30}\text{Br}_4$ 825.9076 $[\text{M}+\text{Na}]^+$, found 825.9080, calc. for $\text{C}_{40}\text{H}_{30}\text{NaBr}_4$ 848.8973 $[\text{M}+\text{Na}]^+$, found 848.8975.

Twisted Hexaphenyls **1** and **2**

An oven dried, argon flushed Schlenk tube was charged with Na₂S (60 % as plates, 19.7 mg, 151 μmol, 5.53 equiv.) and a mixture of EtOH/toluene (12 mL each). The resulting suspension was degassed under a stream of argon before slowly adding a degassed solution of **11** (22.7 mg, 27.0 μmol, 1.00 equiv.) in toluene (10 mL) over 3h at room temperature. Stirring was continued at room temperature for an additional 1.5 h. The resulting suspension was directly subjected to a plug of silica (cyclohexanes/EtOAc 8:1) yielding the constitutional isomers **1** and **2** (11.9 mg, 21.0 mmol, 76 %) as colorless powders. Separation of the enriched fractions by HPLC on a chiral stationary phase (semi-preparative Chiralpak® IA column, eluent: *n*-hexane/2-propanol (99:1), flow rate: 1 mL min⁻¹, T = 18 °C) afforded sufficient amounts of enantiopure **1a**, **1b**, **2a** and **2b** for all subsequent measurements.

1a,b: ¹H NMR (600 MHz, TCE-d₂): δ = 7.71 (s, 1 H), 7.51 (s, 1 H), 7.48 (dd, ³J_{H,H} = 6.5, ⁴J_{H,H} = 3.1 Hz, 1 H), 7.45 – 7.41 (m, 4 H), 7.35 (d, ⁴J_{H,H} = 1.8 Hz, 1 H), 7.26 (dd, ³J_{H,H} = 9.1, ³J_{H,H} = 7.6 Hz, 2 H), 7.23 – 7.20 (m, 2 H), 7.17 – 7.13 (m, 3 H), 7.12 – 7.07 (m, 4 H), 6.93 (dq, ³J_{H,H} = 7.7, ⁴J_{H,H} = 2.4, ⁴J_{H,H} = 1.9, 2 H), 6.90 (dt, ³J_{H,H} = 7.7, ⁴J_{H,H} = 1.4 Hz, 1 H), 3.77 (d, ²J_{H,H} = 14.4 Hz, 1 H), 3.69 (d, ²J_{H,H} = 14.4 Hz, 1 H), 3.65 (s, 2 H), 3.47 (d, ²J_{H,H} = 10.5 Hz, 1 H), 3.27 (d, ²J_{H,H} = 11.9 Hz, 1 H), 2.86 (d, ²J_{H,H} = 10.5 Hz, 1 H), 2.75 (d, ²J_{H,H} = 11.9 Hz, 1 H) ppm. ¹³C NMR (125 MHz, CDCl₃) δ = 140.73, 140.71, 140.62, 140.25, 139.81, 139.62, 139.48, 139.25, 138.93, 137.00, 135.85, 135.10, 133.26, 133.14, 130.45, 129.88, 129.68, 129.51, 129.33, 129.17, 128.47, 128.24, 128.22, 127.72, 127.45, 127.17, 127.12, 127.08, 126.88, 126.82, 126.73, 126.49, 126.43, 126.38, 126.13, 126.00, 39.90, 35.89, 30.96, 30.50 ppm. DART-MS (500 °C, +): *m/z* (%) = 1743.8 (10), 1741.7 (12), 1480.7 (16), 1168.2 (16), 1167.3 (30), 1166.3 (28), 1150.0 (11), 775.3 (13), 774.3 (13), 594.1 (14), 593.2 (30), 592.1 (M+NH₄⁺, 100), 577.2 (11), 576.1 (23), 575.1 (M+H⁺, 41), 543.1 (11), 542.3 (30), 541.2 (82), 508.0 (11), 507.1 (19). HRMS (ESI), calc. for C₄₀H₃₀NaS₂ 597.1681 [M+Na]⁺, found 597.1670, calc. for C₄₀H₃₀KS₂ 613.1421 [M+Na]⁺, found 613.1411.

2a,b: ¹H NMR (600 MHz, TCE-d₂): δ = 7.83 (d, ⁴J_{H,H} = 2.1 Hz, 1 H), 7.66 (dd, ³J_{H,H} = 7.6, ⁴J_{H,H} = 1.4 Hz, 1 H), 7.53 – 7.47 (m, 2 H), 7.45 – 7.41 (m, 4 H), 7.41 – 7.38 (m, 1 H), 7.36 (d, ³J_{H,H} = 7.6 Hz, 1 H), 7.34 – 7.28 (m, 4 H), 7.26 (s, 1 H), 7.20 (ddd, ³J_{H,H} = 7.6, ⁴J_{H,H} = 4.4, ⁴J_{H,H} = 2.8 Hz, 2 H), 7.08 (dd, ³J_{H,H} = 8.0, ⁴J_{H,H} = 2.0 Hz, 1 H), 7.05 (d, ³J_{H,H} = 7.8 Hz, 1 H), 6.77 (d, ³J_{H,H} = 7.7 Hz, 1 H), 6.75 (d, ⁴J_{H,H} = 1.9 Hz, 1 H), 5.64 (s, 1 H), 4.23 (d, ²J_{H,H} = 13.7 Hz, 1 H), 3.87 (d, ²J_{H,H} = 15.5 Hz, 1 H), 3.79 (d, ²J_{H,H} = 13.7 Hz, 1 H), 3.76 (d, ²J_{H,H} = 13.9 Hz, 1 H), 3.70 (d, ²J_{H,H} = 13.9 Hz, 1 H), 3.67 (d, ²J_{H,H} = 13.8 Hz, 1 H), 3.62 (d, ²J_{H,H} = 15.5 Hz, 1 H), 3.25 (d, ²J_{H,H} = 13.8 Hz, 1 H) ppm. ¹³C NMR (125 MHz, CDCl₃) δ = 142.85, 142.38, 141.79, 140.20, 139.94, 139.93, 139.54, 139.45, 138.80, 138.12, 137.82, 137.56, 136.33, 136.10, 133.56, 131.62, 130.26, 130.00, 129.73, 129.70, 129.01, 128.82, 128.78, 128.35, 128.03, 127.13, 127.12, 127.12, 127.09, 126.99, 126.78, 126.71, 126.67, 126.50, 126.50, 126.04, 36.10, 34.73, 34.39, 32.30 ppm. DART-MS (500 °C, +): *m/z* (%) = 1744.8 (17), 1743.9 (20), 1742.8 (52), 1741.7 (68), 1740.5 (51), 1725.6 (14), 1723.6 (16), 1690.9 (10), 1168.7 (49), 1167.3 (100), 1166.1 (24), 1150.3 (19), 1132.5 (19), 1116.4 (9), 1115.3 (12), 594.1 (11), 593.3 (19), 592.2 (M+NH₄⁺, 54), 575.0 (M+H⁺, 20), 573.4 (9), 543.1 (11), 542.2 (39), 541.2 (95), 507.2 (11). HRMS (ESI), calc. for C₄₀H₃₀NaS₂ 597.1681 [M+Na]⁺, found 597.1676, calc. for C₄₀H₃₀KS₂ 613.1421 [M+Na]⁺, found 613.1415.

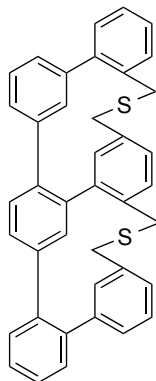
Twisted Hexaphenyls **3** and **4**

In a glove box an oven dried round bottom flask was charged with **11** (99.7 mg, 120 μmol , 1.00 equiv.) and a mixture of dry toluene and dry EtOH (50 mL each). A dropping funnel was charged with a solution of Na_2Se (71.6 mg, 264 μmol , 2.20 equiv.) in EtOH (40 mL) and toluene (10 mL). Drop-wise addition was initiated at room temperature and maintained over 2 h. Once the addition was complete, the resulting hazy solution was stirred for an additional 30 min. before removing the solvent under reduced pressure and directly subjecting the mixture to reversed phase chromatography (bulk C18 coated silica, eluent: MeCN) yielding the constitutional isomers **3** and **4** (combined yield: 40.4 mg, 60.4 μmol , 50 %) as colorless powders. Separation of the enriched fractions by HPLC on a chiral stationary phase (semi-preparative Chiralpak® IA column, eluent: *n*-hexane/2-propanol (98:2), flow rate: 1 mL min^{-1} , $T = 19^\circ\text{C}$) afforded sufficient amounts of enantiopure **3a**, **3b**, **4a** and **4b** for all subsequent measurements.

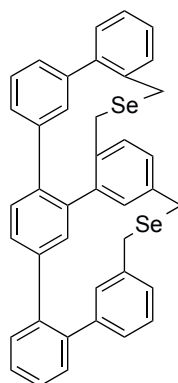
3a,b: ^1H NMR (600 MHz, CDCl_3): $\delta = 7.57$ (d, $^4J_{\text{H,H}} = 1.9$ Hz, 1 H), 7.53 – 7.50 (m, 1 H), 7.43 (q, $^4J_{\text{H,H}} = 2.5$, $^4J_{\text{H,H}} = 2.5$, $^4J_{\text{H,H}} = 2.1$ Hz, 3 H), 7.40 (dd, $^3J_{\text{H,H}} = 7.7$, $^4J_{\text{H,H}} = 1.5$ Hz, 1 H), 7.28 (d, $^4J_{\text{H,H}} = 1.9$ Hz, 1 H), 7.25 – 7.19 (m, 7 H), 7.18 (dd, $^3J_{\text{H,H}} = 7.6$, $^4J_{\text{H,H}} = 1.5$ Hz, 1 H), 7.14 (dt, $^3J_{\text{H,H}} = 7.6$, $^4J_{\text{H,H}} = 1.5$, 1 H), 7.11 (td, $^3J_{\text{H,H}} = 8.5$, $^3J_{\text{H,H}} = 7.6$, $^4J_{\text{H,H}} = 1.6$ Hz, 2 H), 7.02 (dt, $^3J_{\text{H,H}} = 7.6$, $^4J_{\text{H,H}} = 1.5$, 1 H), 6.96 (dt, $^3J_{\text{H,H}} = 7.7$, $^4J_{\text{H,H}} = 1.4$, 2 H), 6.86 (dd, $^3J_{\text{H,H}} = 7.7$, $^4J_{\text{H,H}} = 2.0$ Hz, 1 H), 3.79 (d, $^2J_{\text{H,H}} = 12.8$ Hz, 1 H), 3.76 – 3.71 (m, 2 H), 3.70 (s, 2 H), 3.44 (d, $^2J_{\text{H,H}} = 11.6$ Hz, 1 H), 2.88 (d, $^2J_{\text{H,H}} = 9.8$ Hz, 1 H), 2.77 (d, $^2J_{\text{H,H}} = 11.6$ Hz, 1 H). ^{13}C NMR (125 MHz, CDCl_3) $\delta = 141.46$, 141.24, 141.10, 140.84, 140.74, 140.72, 140.16, 140.15, 139.95, 138.23, 137.85, 136.53, 135.07, 134.84, 131.66, 131.10, 130.93, 130.48, 130.11, 129.69, 129.61, 129.57, 129.56, 128.65, 128.45, 128.44, 128.36, 128.02, 127.94, 127.87, 127.80, 127.69, 127.52, 127.44, 127.37, 126.78, 28.76, 28.40, 24.21, 23.63 ppm. DART-MS (500 $^\circ\text{C}$, +): m/z (%) = 1438.1 (13), 1437.0 (11), 1435.9 (12), 1434.9 (13), 1433.9 (25), 1431.3 (13), 1359.5 (11), 1357.2 (11), 1356.2 (23), 1355.2 (23), 1354.2 (28), 1353.3 (19), 1352.2 (12), 1350.2 (12), 1347.9 (12), 870.1 (15), 868.0 (15), 840.9 (11), 770.1 (16), 768.7 (15), 767.9 (45), 766.8 (23), 765.8 (58), 764.8 (17), 764.0 (81), 762.7 (37), 761.5 (24), 759.3 (22), 758.1 (10), 748.9 (16), 746.7 (35), 745.1 (13), 691.0 (12), 690.2 (31), 689.2 (35), 688.1 ($\text{M}+\text{NH}_4^+$, 98), 687.0 (23), 686.1 (100), 685.0 (25), 684.0 (56), 682.9 (10), 682.0 (18), 680.9 (19), 673.2 (10), 672.1 (32), 671.0 (37), 670.0 (M^+ , 17), 669.0 (41), 668.0 (24), 667.0 (32), 666.0 (16), 624.0 (13), 590.1 (19), 589.0 (60), 588.0 (11), 587.2 (21), 585.1 (12), 538.1 (11), 508.9 (19), 508.1 (11), 507.1 (44). HRMS (ESI), calc. for $\text{C}_{40}\text{H}_{30}\text{NaSe}_2$ 693.0578 [$\text{M}+\text{Na}$] $^+$, found 693.0577.

4a,b: ^1H NMR (600 MHz, TCE-d_2): $\delta = 7.84$ (d, $^4J_{\text{H,H}} = 1.8$ Hz, 1 H), 7.69 – 7.65 (m, 1 H), 7.54 (dd, $^3J_{\text{H,H}} = 7.8$, $^4J_{\text{H,H}} = 1.9$ Hz, 1 H), 7.50 (ddd, $^3J_{\text{H,H}} = 7.5$, 6.6, $^4J_{\text{H,H}} = 2.2$ Hz, 1 H), 7.46 – 7.41 (m, 4 H), 7.37 (s, 1 H), 7.35 – 7.29 (m, 4 H), 7.27 (td, $^3J_{\text{H,H}} = 7.4$, $^4J_{\text{H,H}} = 1.5$ Hz, 1 H), 7.22 (dd, $^3J_{\text{H,H}} = 7.6$, $^4J_{\text{H,H}} = 1.5$ Hz, 1 H), 7.19 (dt, $^3J_{\text{H,H}} = 7.7$, $^4J_{\text{H,H}} = 1.4$ Hz, 1 H), 7.16 (t, $^3J_{\text{H,H}} = 7.7$ Hz, 1 H), 7.04 (d, $^3J_{\text{H,H}} = 7.8$ Hz, 1 H), 7.00 (dd, $^3J_{\text{H,H}} = 8.0$, $^4J_{\text{H,H}} = 2.0$ Hz, 1 H), 5.61 (d, $^4J_{\text{H,H}} = 2.0$ Hz, 1 H), 4.15 (d, $^2J_{\text{H,H}} =$

12.1 Hz, 1 H), 4.03 (d, $^2J_{\text{H,H}} = 13.8$ Hz, 1 H), 3.91 (t, $^2J_{\text{H,H}} = 12.1$ Hz, 2 H), 3.80 (d, $^2J_{\text{H,H}} = 12.3$ Hz, 1 H), 3.74 (dd, $^2J_{\text{H,H}} = 13.8$, 12.1 Hz, 2 H), 3.30 (d, $^2J_{\text{H,H}} = 12.3$ Hz, 1 H) ppm. ^{13}C NMR (125 MHz, TCE- d_2) $\delta = 143.03, 142.26, 141.71, 140.37, 140.10, 139.53, 139.33, 139.04, 138.54, 138.34, 137.87, 137.83, 137.82, 136.31, 132.90, 132.04, 130.01, 129.69, 129.44, 129.10, 128.93, 128.61, 128.53, 128.22, 128.06, 127.79, 127.52, 127.16, 127.10, 127.08, 127.00, 126.78, 126.74, 126.51, 126.50, 120.91, 28.08, 26.51, 25.70, 25.03$ ppm. DART-MS (500 °C, +): m/z (%) = 1925.3 (13), 1360.4 (14), 1359.2 (25), 1357.2 (37), 1356.2 (37), 1355.0 (40), 1354.2 (31), 1353.4 (24), 1352.2 (22), 1351.3 (24), 1350.2 (12), 870.1 (15), 868.0 (12), 769.0 (13), 768.0 (27), 766.9 (41), 766.0 (68), 765.1 (34), 764.1 (78), 762.8 (15), 761.8 (26), 759.8 (21), 750.0 (14), 749.2 (11), 748.3 (11), 700.2 (11), 690.0 (21), 689.1 (29), 688.0 (M+NH $_4^+$, 83), 686.9 (13), 686.2 (100), 685.1 (56), 683.8 (19), 681.8 (19), 672.0 (18), 671.0 (24), 669.9 (M $^+$, 30), 668.9 (21), 668.1 (21), 667.4 (14), 666.1 (19), 606.3 (14), 591.0 (16), 590.1 (21), 589.1 (96), 588.0 (12), 586.9 (64), 585.1 (24), 507.8 (19). HRMS (ESI), calc. for C $_{40}$ H $_{30}$ NaSe $_2$ 693.0578 [M+Na] $^+$, found 693.0582.

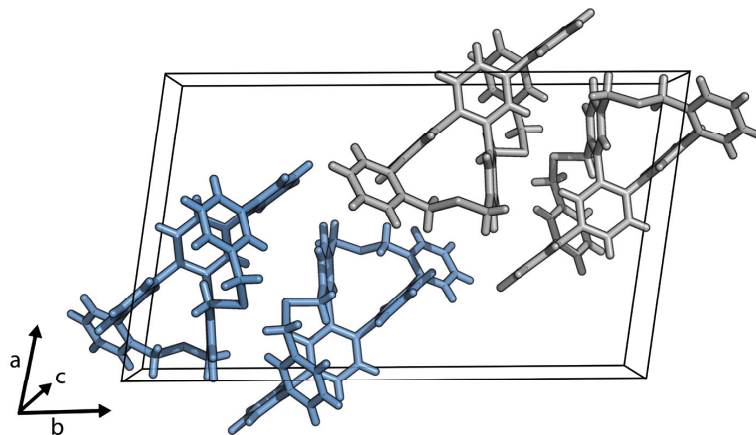
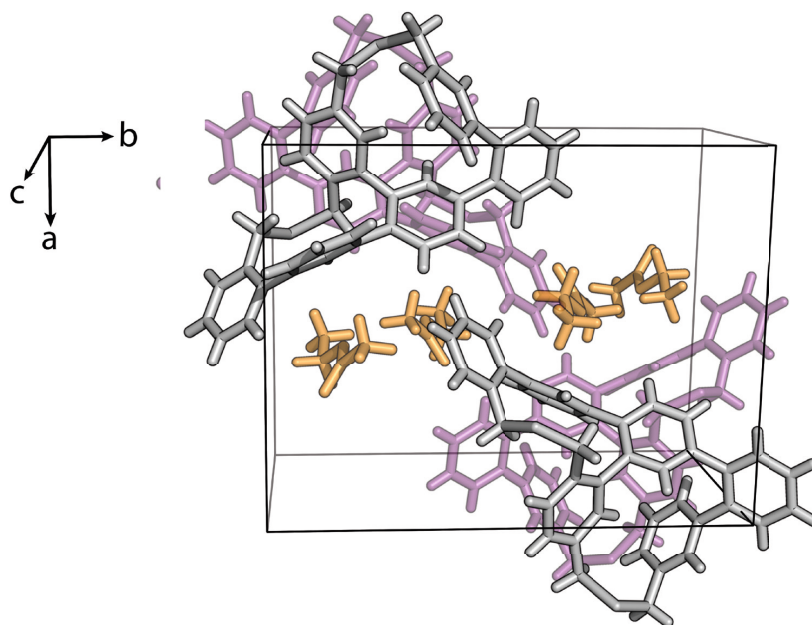
Crystal data for (1)**1a,b**

Crystal data for **1**: formula $C_{40}H_{30}S_2$, $M = 574.81$, $F(000) = 1208$, colourless needle, size $0.030 \cdot 0.050 \cdot 0.190$ mm³, monoclinic, space group $P 2_1/n$, $Z = 4$, $a = 15.055(2)$ Å, $b = 8.0219(13)$ Å, $c = 25.489(4)$ Å, $\alpha = 90^\circ$, $\beta = 98.350(10)^\circ$, $\gamma = 90^\circ$, $V = 3045.7(8)$ Å³, $D_{\text{calc.}} = 1.253$ Mg · m⁻³. The crystal was measured on a Bruker Kappa Apex2 diffractometer at 123K using graphite-monochromated Cu $K\alpha$ -radiation with $\lambda = 1.54178$ Å, $\Theta_{\text{max}} = 68.930^\circ$. Minimal/maximal transmission 0.91/0.95, $\mu = 1.780$ mm⁻¹. The Apex2 suite has been used for datacollection and integration. From a total of 17569 reflections, 5426 were independent (merging $r = 0.057$). From these, 3726 were considered as observed ($I > 2.0\sigma(I)$) and were used to refine 379 parameters. The structure was solved by using the program Superflip. Least-squares refinement against F was carried out on all non-hydrogen atoms using the program CRYSTALS. $R = 0.0392$ (observed data), $wR = 0.0714$ (all data), $GOF = 1.0907$. Minimal/maximal residual electron density = $-0.34/0.28$ e Å⁻³. Chebychev polynomial weights were used to complete the refinement. Plots were produced using CAMERON. Crystallographic data (excluding structure factors) for the structure **1** in this paper have been deposited with the Cambridge Crystallographic Data Center, the deposition number is CCDC 1405407. Copies of the data can be obtained, free of charge, on application to the CCDC, 12 Union Road, Cambridge CB2 1EZ, UK [fax: +44-1223-336033 or e-mail: deposit@ccdc.cam.ac.uk].

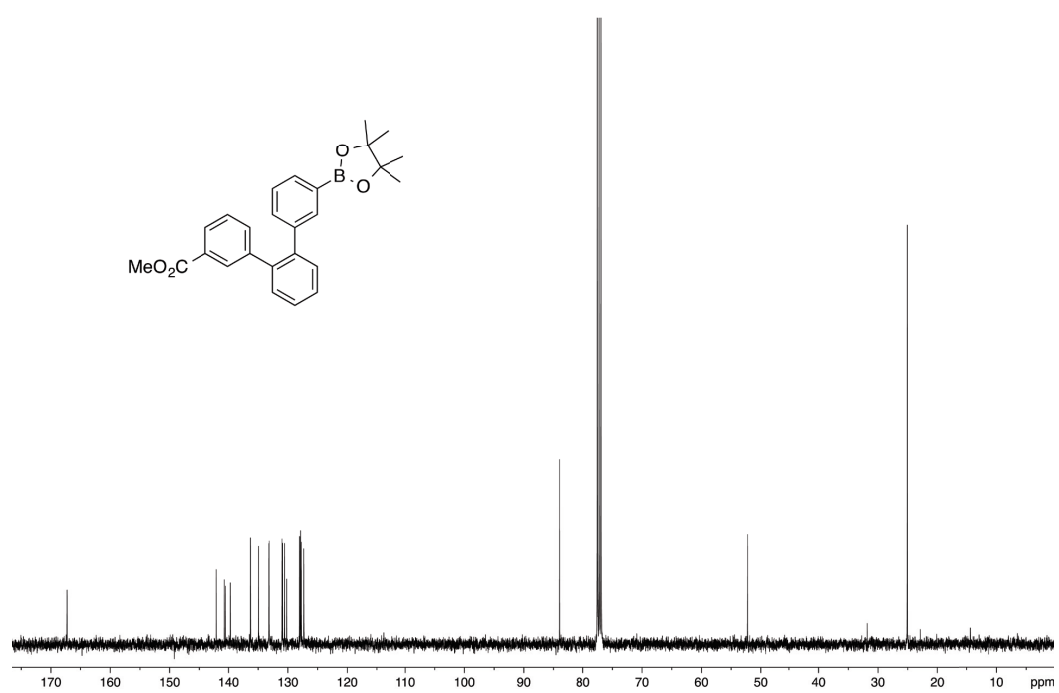
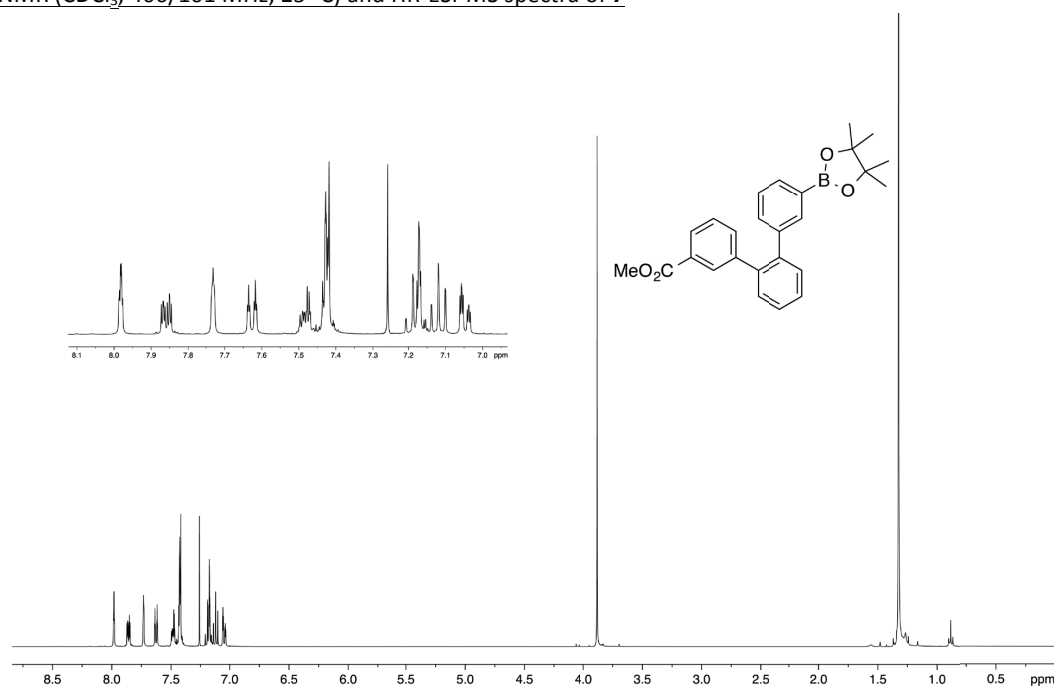
Crystal data for (4)**4a,b**

Important note: The crystals of this compound were extremely difficult to measure. As they were growing as very fine needles in heaps, the isolation of one single needle was difficult. The scattering power was good enough for a successful structure determination, but the aims in completeness and maximum diffraction angle could not be reached. During refinement restraints for the displacement parameters had to be used as anisotropic displacement parameters were not stable otherwise. Nevertheless, and especially when looking at the difficult starting conditions of this structure determination, the refinement can be regarded as successful.

Crystal data for **4**: formula $C_{44}H_{38}O_2Se_2$, $M = 756.70$, $F(000) = 1544$, colourless needle, size $0.010 \cdot 0.030 \cdot 0.150$ mm³, monoclinic, space group $P 21/c$, $Z = 4$, $a = 14.252(3)$ Å, $b = 17.804(4)$ Å, $c = 13.933(3)$ Å, $\alpha = 90^\circ$, $\beta = 99.177(16)^\circ$, $\gamma = 90^\circ$, $V = 3490.4(8)$ Å³, $D_{calc.} = 1.440$ Mg · m⁻³. The crystal was measured on a Bruker Kappa Apex2 diffractometer at 123K using graphite-monochromated Cu K α -radiation with $\lambda = 1.54180$ Å, $\Theta_{max} = 55.356^\circ$. Minimal/maximal transmission 0.92/0.97, $\mu = 2.932$ mm⁻¹. The Apex2 suite has been used for datacollection and integration. From a total of 12115 reflections, 4209 were independent (merging $r = 0.142$). From these, 4181 were considered as observed ($I > 2.0\sigma(I)$) and were used to refine 433 parameters. The structure was solved by using the program Superflip. Least-squares refinement against F_{sqd} was carried out on all non-hydrogen atoms using the program CRYSTALS. $R = 0.0719$ (observed data), $wR = 0.1799$ (all data), $GOF = 1.0306$. Minimal/maximal residual electron density = $-1.65/1.61$ e Å⁻³. Chebychev polynomial weights were used to complete the refinement. Plots were produced using CAMERON. Crystallographic data (excluding structure factors) for the structure **4** in this paper have been deposited with the Cambridge Crystallographic Data Center, the deposition number is CCDC 1405272. Copies of the data can be obtained, free of charge, on application to the CCDC, 12 Union Road, Cambridge CB2 1EZ, UK [fax: +44-1223-336033 or e-mail: deposit@ccdc.cam.ac.uk].

Unit cell for (1)Unit cell for (4)

^1H -, ^{13}C -NMR (CDCl_3 , 400/101 MHz, 25 °C) and HR-ESI-MS spectra of **7**



Mass Spectrum SmartFormula Report

Analysis Info

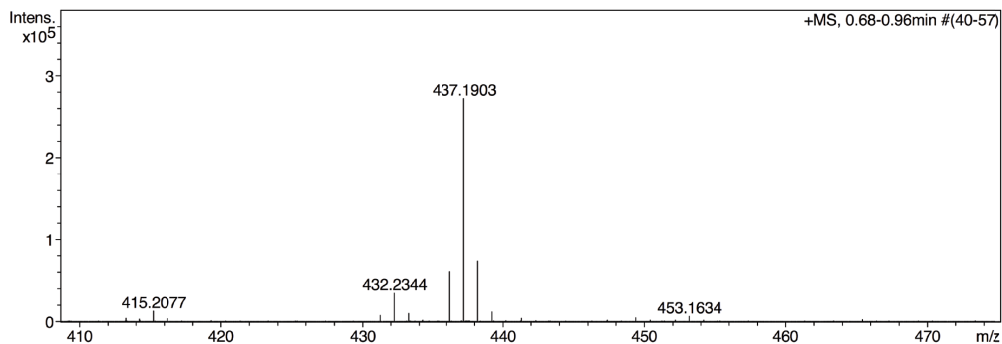
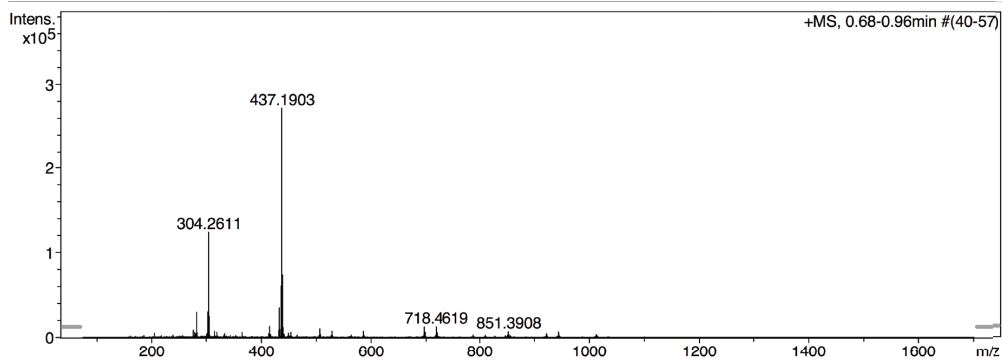
Analysis Name N:\new acq data\Ri745 001.d
 Method hn Direct_Infusion_pos mode_75-1700 mid 4eV.m
 Sample Name Michel Rickhaus, Ri745
 Comment Ri745, ca. 5 ug/ml MeCN

Acquisition Date 06.02.2015 10:21:18

 Operator hn
 Instrument / Ser# maXis 4G 21243

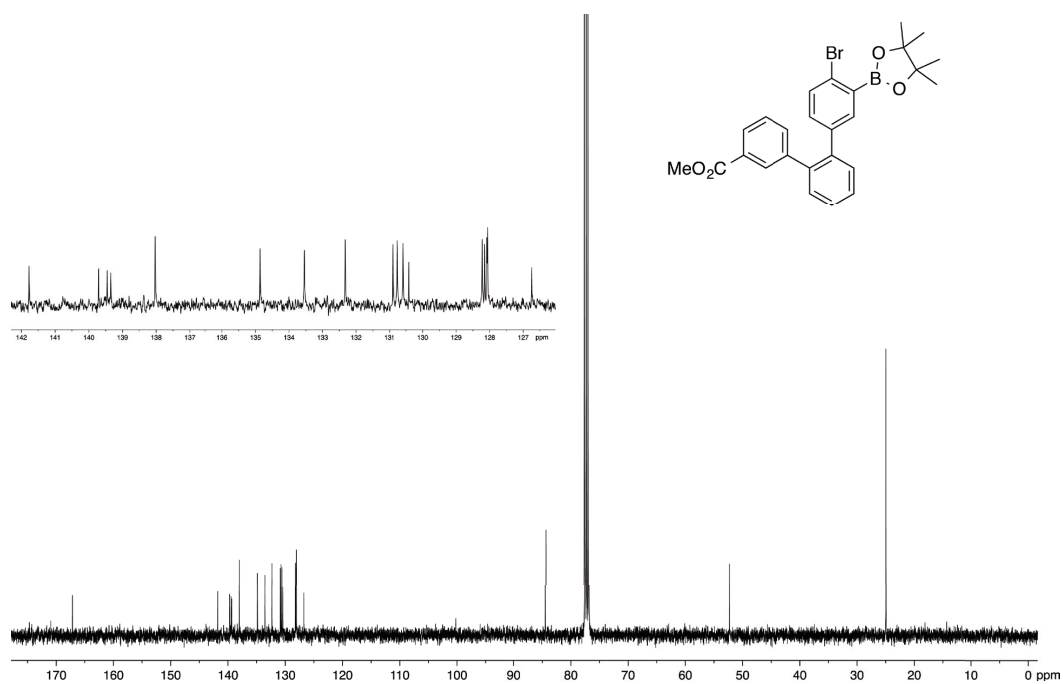
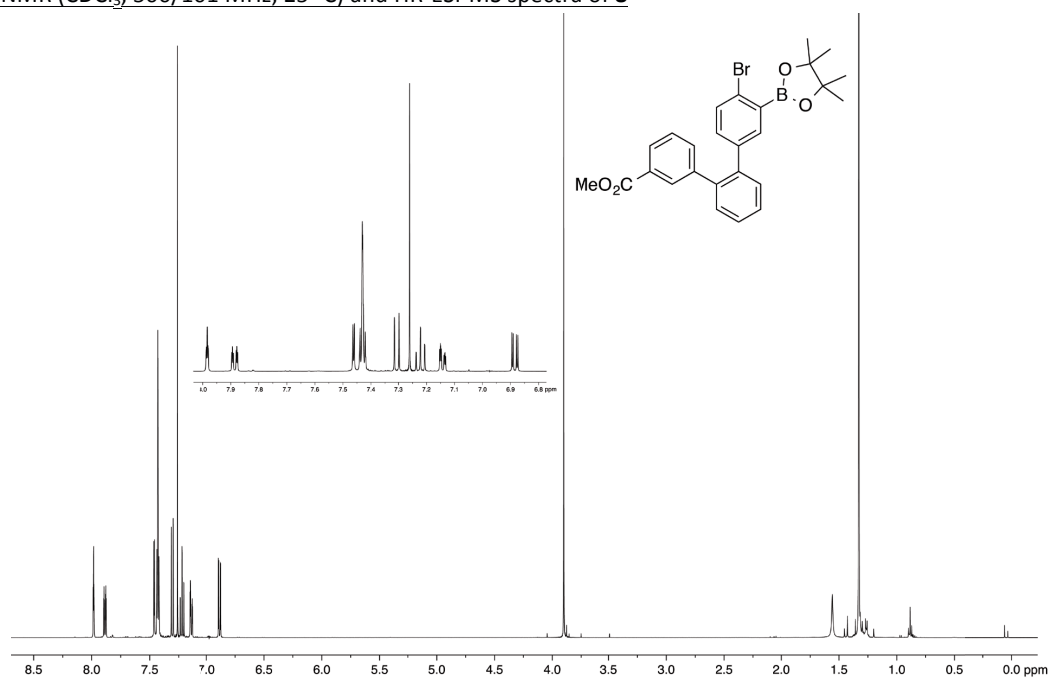
Acquisition Parameter

Source Type	ESI	Ion Polarity	Positive	Set Nebulizer	0.4 Bar
Focus	Not active	Set Capillary	3600 V	Set Dry Heater	180 °C
Scan Begin	75 m/z	Set End Plate Offset	-500 V	Set Dry Gas	4.0 l/min
Scan End	1700 m/z	Set Collision Cell RF	500.0 Vpp	Set Ion Energy (MS only)	4.0 eV



Meas. m/z	#	Formula	Score	m/z	err [mDa]	err [ppm]	mSigma	rdb	e ⁻ Conf	N-Rule	z
415.2077	1	C 26 H 28 B O 4	100.00	415.2080	-0.2	-0.4	8.7	13.5	even	ok	1+
432.2344	1	C 26 H 31 B N O 4	100.00	432.2345	0.2	0.4	5.0	12.5	even	ok	
437.1903	1	C 26 H 27 B Na O 4	100.00	437.1899	-0.4	-0.8	4.9	13.5	even	ok	
453.1634	1	C 26 H 27 B K O 4	100.00	453.1639	-0.0	-0.0	13.1	13.5	even	ok	
851.3908	1	C 52 H 54 B 2 Na O 8	100.00	851.3913	0.5	0.6	8.5	26.5	even	ok	

^1H -, ^{13}C -NMR (CDCl_3 , 500/101 MHz, 25 °C) and HR-ESI-MS spectra of **8**



Mass Spectrum SmartFormula Report

Analysis Info

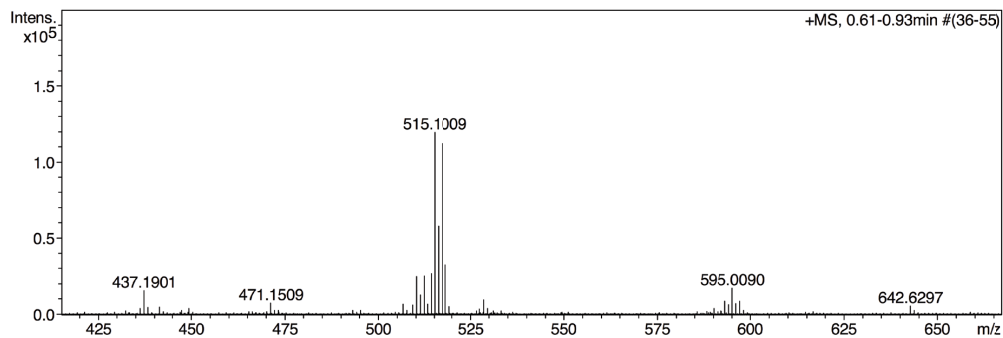
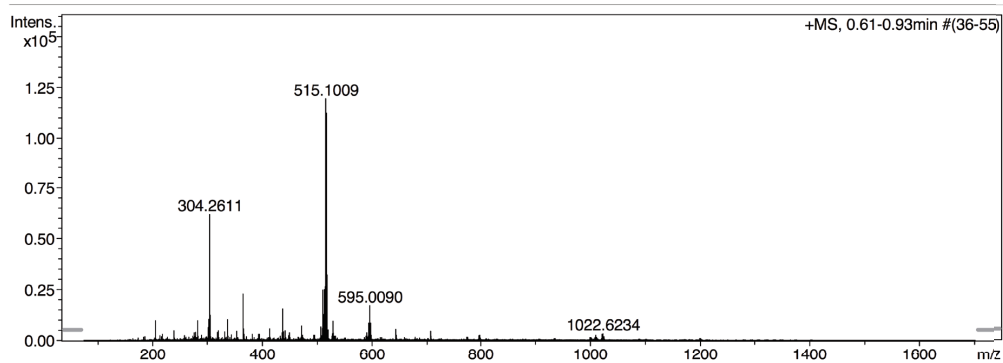
Analysis Name N:\new acq data\ri752 001.d
 Method hn Direct_Infusion_pos mode_75-1700 mid 4eV.m
 Sample Name Michel Rickhaus, Ri752
 Comment Ri752, ca 4 ug/ml MeCN

Acquisition Date 11.02.2015 15:32:05

 Operator hn
 Instrument / Ser# maXis 4G 21243

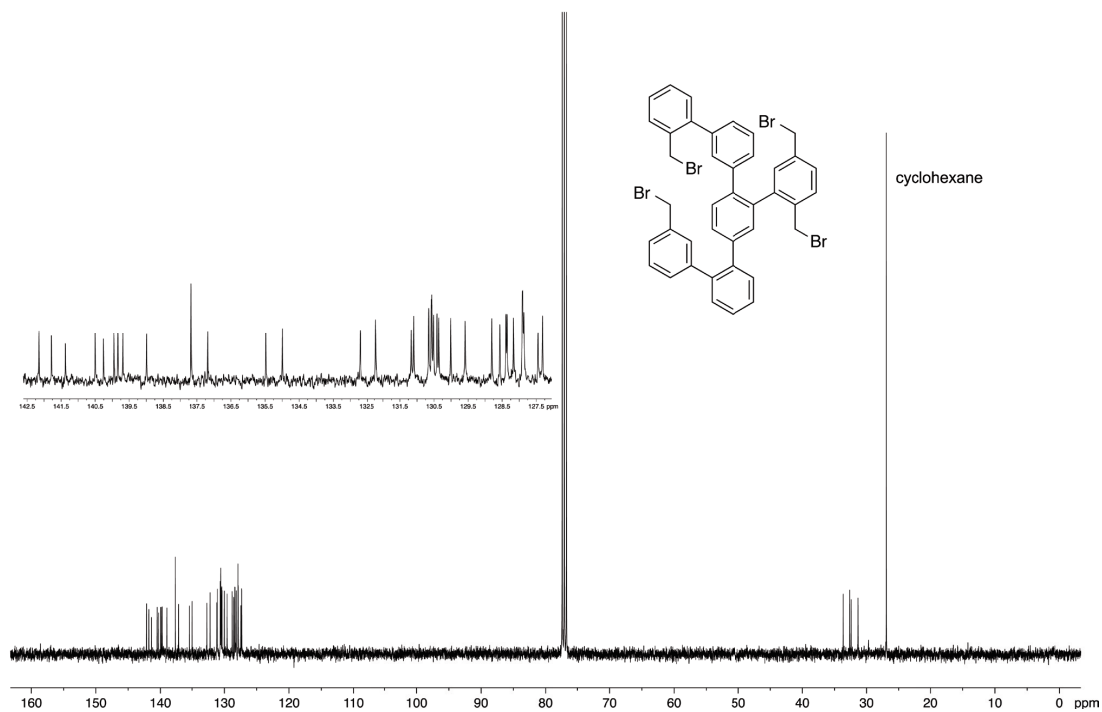
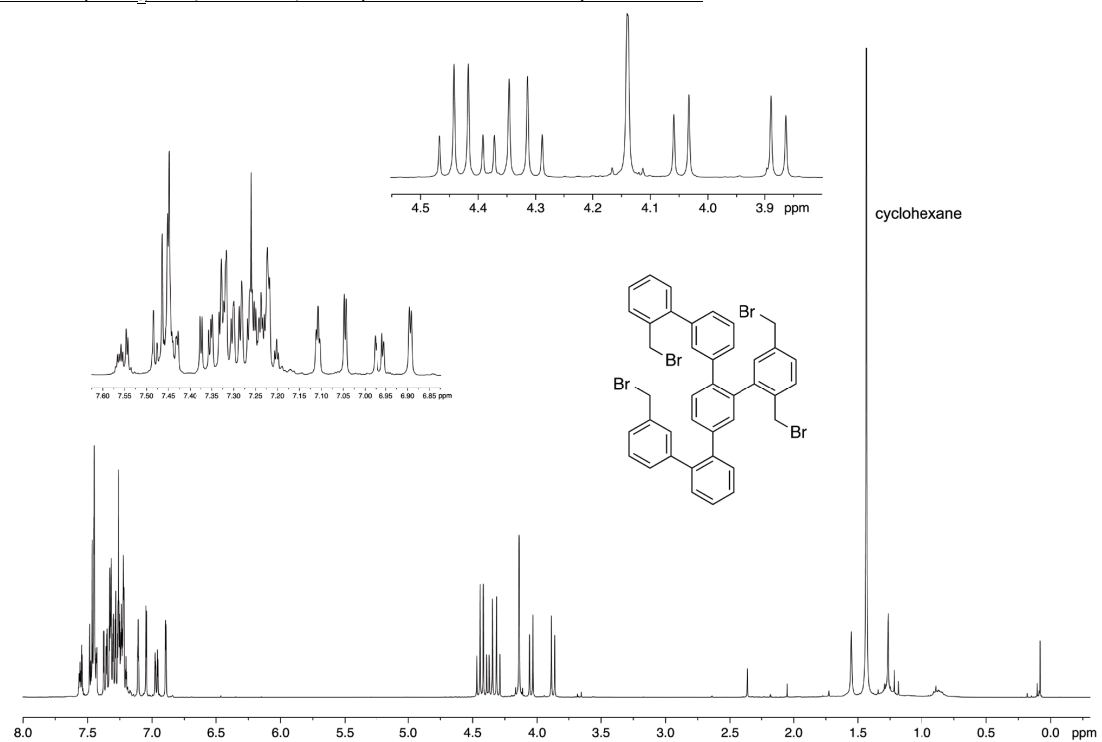
Acquisition Parameter

Source Type	ESI	Ion Polarity	Positive	Set Nebulizer	0.4 Bar
Focus	Not active	Set Capillary	3600 V	Set Dry Heater	180 °C
Scan Begin	75 m/z	Set End Plate Offset	-500 V	Set Dry Gas	4.0 l/min
Scan End	1700 m/z	Set Collision Cell RF	500.0 Vpp	Set Ion Energy (MS only)	4.0 eV



Meas. m/z	#	Formula	Score	m/z	err [mDa]	err [ppm]	mSigma	rdb	e ⁻ Conf	N-Rule	z
510.1452	1	C 26 H 30 B Br N O 4	100.00	510.1450	-0.1	-0.2	9.8	12.5	even	ok	1+
515.1009	1	C 26 H 26 B Br Na O 4	100.00	515.1004	-0.5	-0.9	25.6	13.5	even	ok	

^1H -, ^{13}C -NMR (CDCl_3 , 400/101 MHz, 25 °C) and HR-MALDI-MS spectra of **11**

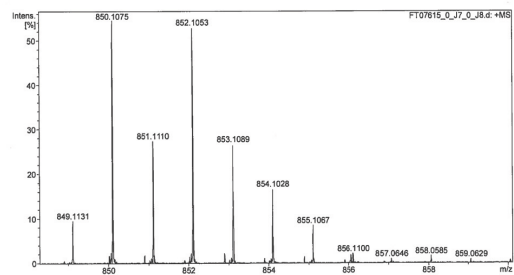
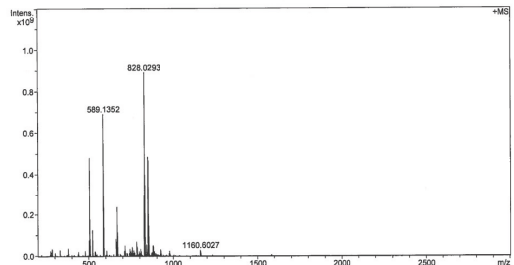


FT07615 Patrick Hilpert/Wennemers - RI 689 - DCTB



Acquisition Parameter
 Method: Medium_mass_MALDI_VIII
 File Name: D:\data\ESI-MALDI Daten\FT07615_0_J7_0_18.d
 Source: Dual (MALDI/ESI) Polarity: Positive
 Broadband Low Mass: 202.1 m/z Laser Shot Frequency: 0.002 sec
 Broadband High Mass: 3000.0 m/z Laser Power: 20.0 W
 No. of Cell Fills: 1 No. of Laser Shots: 100
 Apodization: Sine-Bell Flight Time to Acq. Cell: 0.001 sec

Acquisition Date: 10.06.2015 14:51:08
 Operator: Rolf Häfjiger
 Nebulizer Gas: 1.3 bar
 Drying Gas Flow Rate: 3.1 L/min
 Capillary: 4500.0 V
 Drying Gas: 200.0 °C
 Temperature

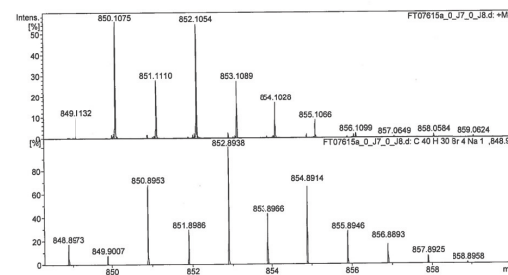
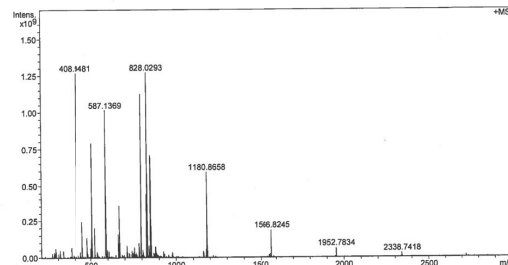


FT07615a Patrick Hilpert/Wennemers - RI 689 - DCTB



Acquisition Parameter
 Method: Medium_mass_MALDI_VIII
 File Name: D:\data\ESI-MALDI Daten\FT07615a_0_J7_0_18.d
 Source: Dual (MALDI/ESI) Polarity: Positive
 Broadband Low Mass: 202.1 m/z Laser Shot Frequency: 0.002 sec
 Broadband High Mass: 3000.0 m/z Laser Power: 20.0 W
 No. of Cell Fills: 1 No. of Laser Shots: 100
 Apodization: Sine-Bell Flight Time to Acq. Cell: 0.001 sec

Acquisition Date: 10.06.2015 14:52:05
 Operator: Rolf Häfjiger
 Nebulizer Gas: 1.3 bar
 Drying Gas Flow Rate: 3.1 L/min
 Capillary: 4500.0 V
 Drying Gas: 200.0 °C
 Temperature



FT07615a Patrick Hilpert/Wennemers - RI 689 - DCTB



Evaluation Spectra / Validation Formula:

#	Formula	m/z	Mass. m/z	z	mSigma	N-Rule	err [mDa]	err [ppm]
1	C ₄₀ H ₃₀ Br ₄	825.9076	825.9080	1+	40.7	ok	-0.5	-0.6
1	C ₄₀ H ₃₀ Br ₄ Na	848.8973	848.8975		45.6	ok	-0.2	-0.3

FT07615a Patrick Hilpert/Wennemers - RI 689 - DCTB



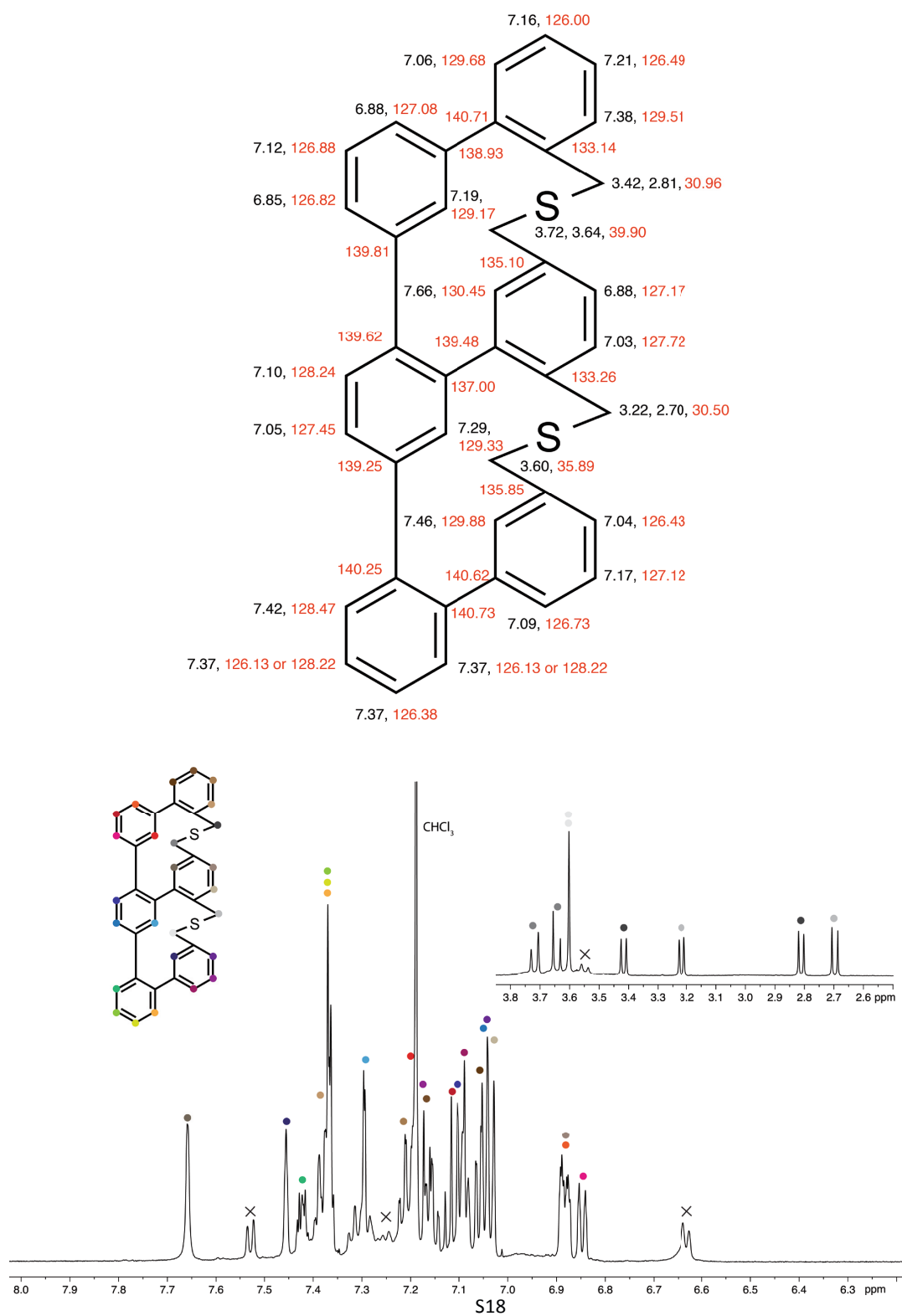
#	m/z	Res.	S/N	I %	FWHM
9	855.8946	75301	27.8	0.0114	
10	856.8953	75388	20.5	0.0114	
11	856.9056	75390	0.1	0.0114	
12	857.8925	75476	7.2	0.0114	
13	858.8958	75565	1.5	0.0114	
14	859.8992	75653	0.2	0.0114	

Calibration Info:

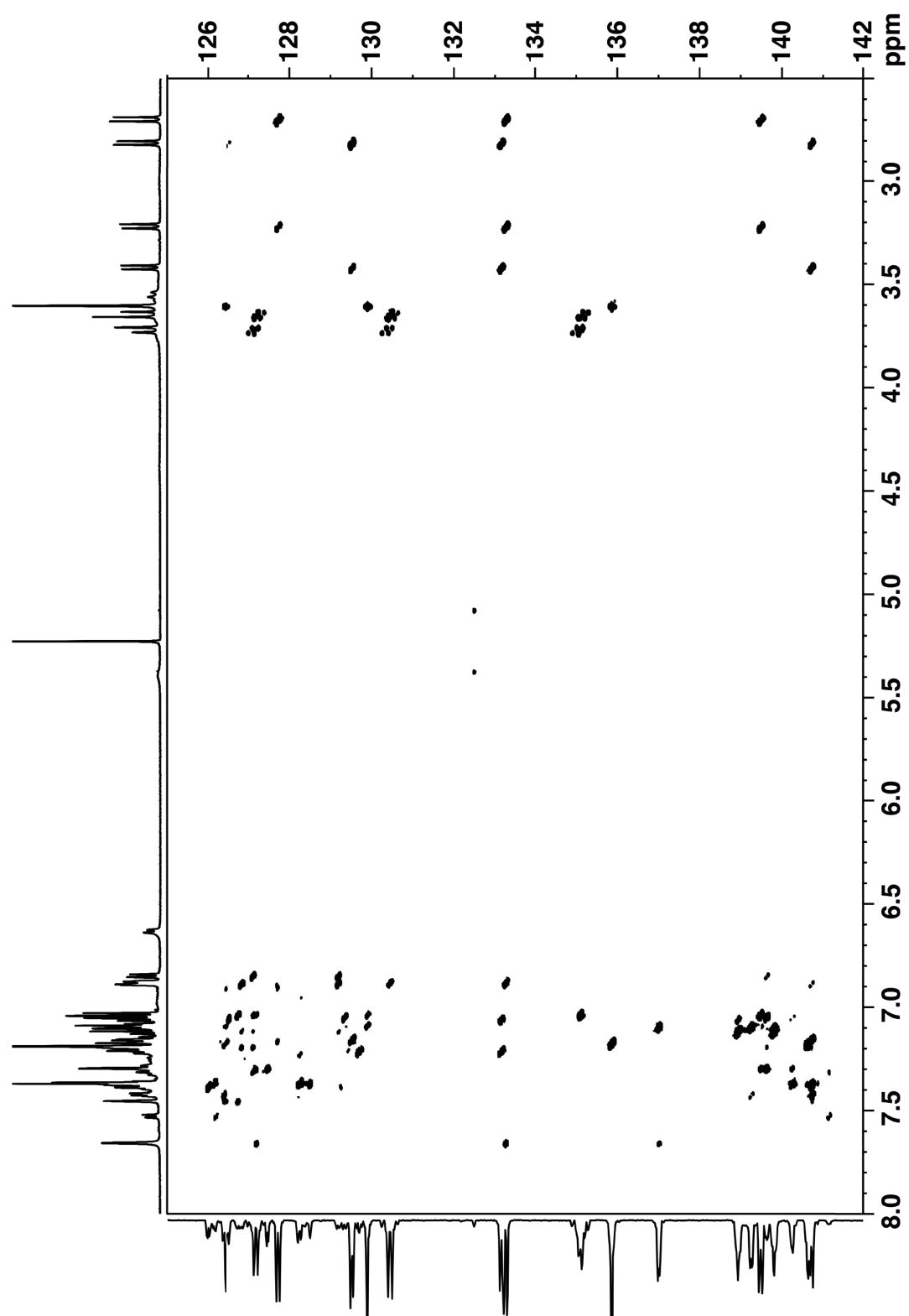
Internal calibration
 Date: 10.06.2015 14:58:00
 Polarity: Positive
 Calibration spectrum: +MS_Scan
 Reference mass list: ESI: Na-PPHA
 Calibration mode: Quadratic

Mass List:

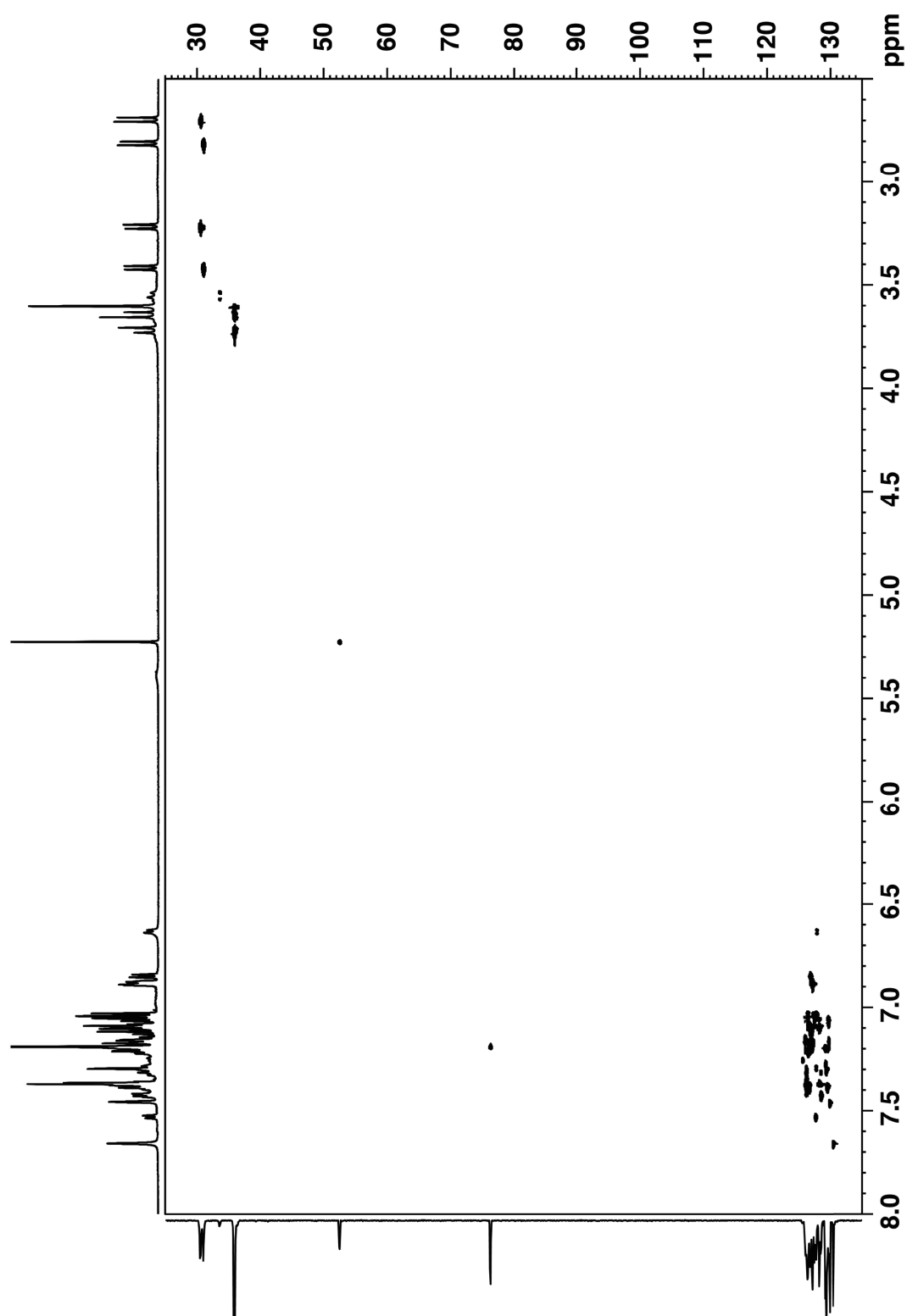
#	m/z	Res.	S/N	I %	FWHM
1	408.9491	148530	3810.4	99.7	0.0029
2	449.9746	133299	718.3	19.6	0.0034
3	477.3646	125166	394.5	11.0	0.0038
4	504.5139	122314	351.2	10.1	0.0041
5	505.0295	120308	2196.4	62.9	0.0042
6	507.2107	121318	452.4	13.0	0.0042
7	507.5526	119622	798.7	22.9	0.0042
8	509.2263	117933	332.8	8.6	0.0043
9	523.3241	117283	549.7	16.0	0.0045
10	587.1369	106071	2570.2	79.9	0.0065
11	588.1402	107769	1121.4	34.8	0.0065
12	589.1548	103843	2558.9	79.3	0.0057
13	590.1381	106699	1100.4	34.1	0.0055
14	663.4537	83471	376.7	12.7	0.0071
15	667.0531	82938	443.4	14.9	0.0072
16	669.0811	82330	842.2	28.3	0.0072
17	670.0639	89526	346.2	11.7	0.0067
18	671.0290	80215	394.8	13.3	0.0074
19	784.9069	79098	2136.8	88.8	0.0102
20	785.9104	78949	322.6	13.5	0.0102
21	828.0314	75331	799.1	34.8	0.0110
22	827.0347	75135	381.6	16.6	0.0110
23	828.0293	75941	2285.3	100.0	0.0109
24	829.0327	75607	1107.1	48.5	0.0110
25	830.0271	76989	2181.4	85.5	0.0109
26	830.0395	123181	278.0	12.2	0.0067
27	831.0306	76959	1058.0	46.3	0.0110
28	832.0248	80297	876.0	29.6	0.0104
29	832.0383	104300	227.7	10.0	0.0080
30	833.0284	77099	331.1	14.7	0.0109
31	848.1097	73839	443.5	19.5	0.0115
32	849.1132	73955	228.2	10.1	0.0116
33	850.1075	74315	1265.8	50.3	0.0114
34	851.1110	73417	635.5	27.9	0.0116
35	852.1054	78138	1248.7	54.7	0.0112
36	853.1089	73870	627.8	27.5	0.0115
37	854.1028	80624	388.6	17.1	0.0108
38	1180.8658	53167	1088.8	46.7	0.0222
39	1181.8692	53336	247.7	10.7	0.0222
40	1566.8245	40068	294.0	14.9	0.0391

^1H -, hmbc, hmqc (CDCl_3 , 600/125 MHz, 25 °C) and HR-ESI-MS spectra of **1**

1 in CDCl₃ 13C-1H-HMBC



1 in CDCl₃ 13C-1H-HMQC



S20

Mass Spectrum SmartFormula Report

Analysis Info

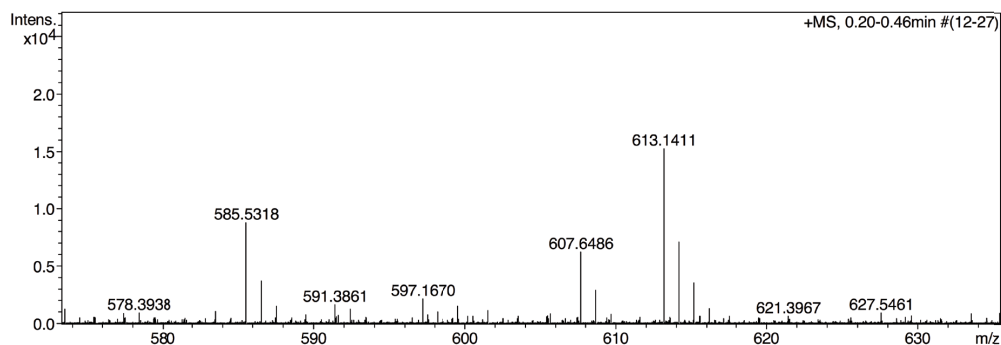
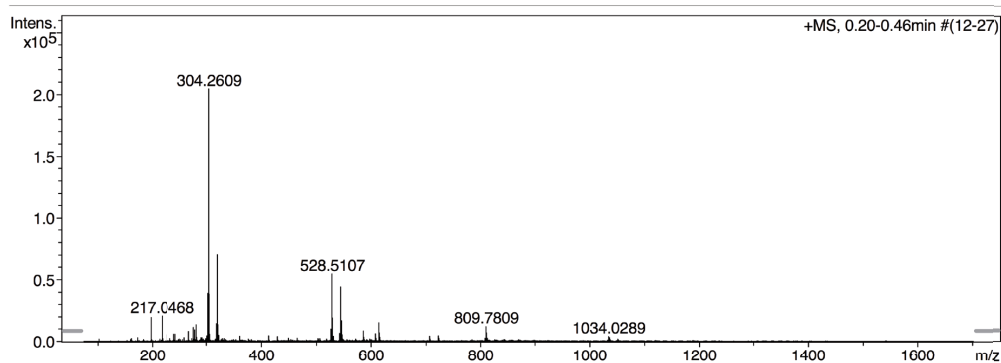
Analysis Name N:\new acq data\ri692 003.d
 Method hn Direct_Infusion_pos mode_75-1700 mid 4eV.m
 Sample Name Michel Rickhaus, Ri692
 Comment Ri692, ca. 10 ug/ml MeCN, hinter MeOH/KCl

Acquisition Date 20.08.2014 16:23:55

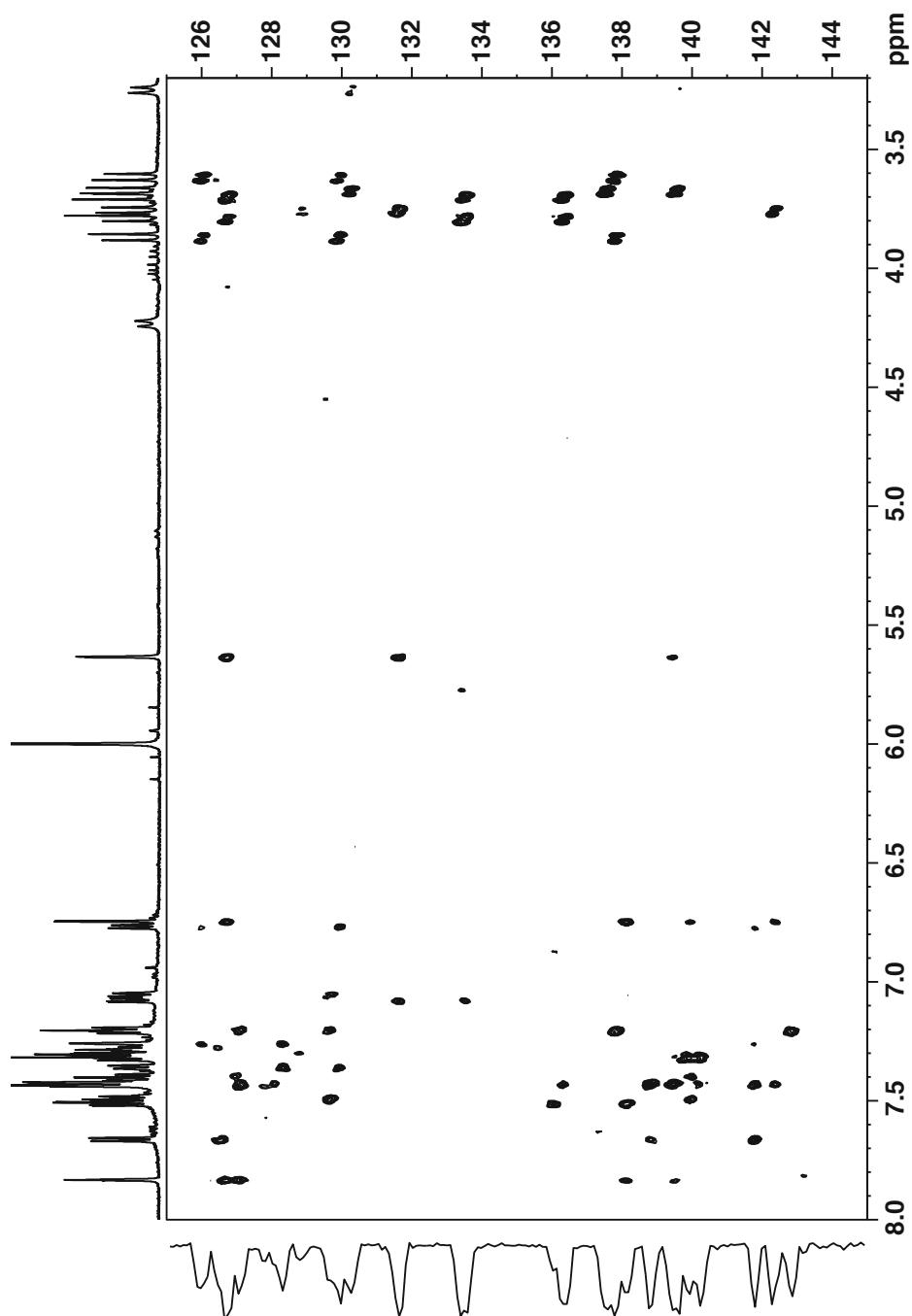
Operator hn
 Instrument / Ser# maXis 4G 21243

Acquisition Parameter

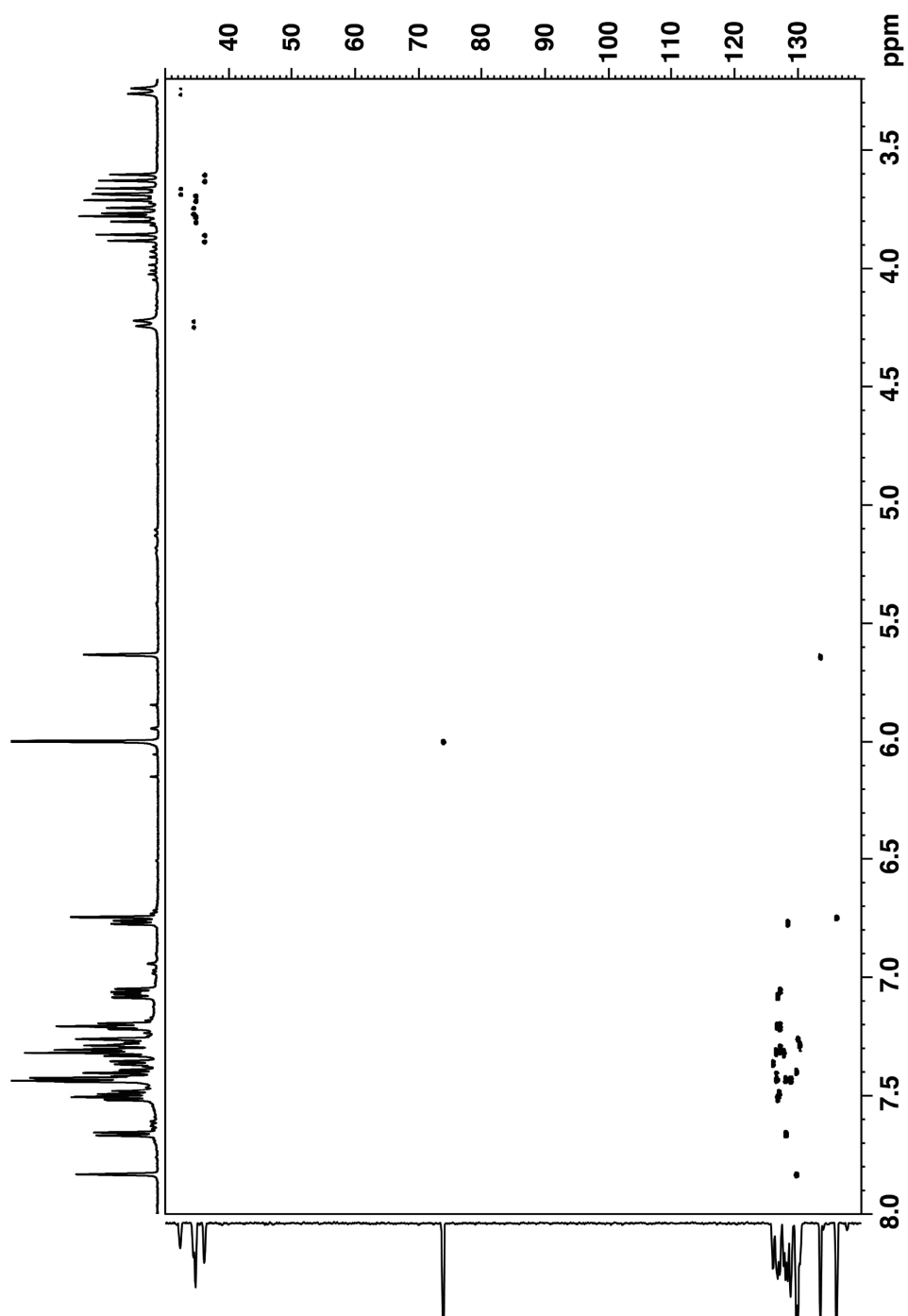
Source Type	ESI	Ion Polarity	Positive	Set Nebulizer	0.4 Bar
Focus	Not active	Set Capillary	3600 V	Set Dry Heater	180 °C
Scan Begin	75 m/z	Set End Plate Offset	-500 V	Set Dry Gas	4.0 l/min
Scan End	1700 m/z	Set Collision Cell RF	500.0 Vpp	Set Ion Energy (MS only)	4.0 eV



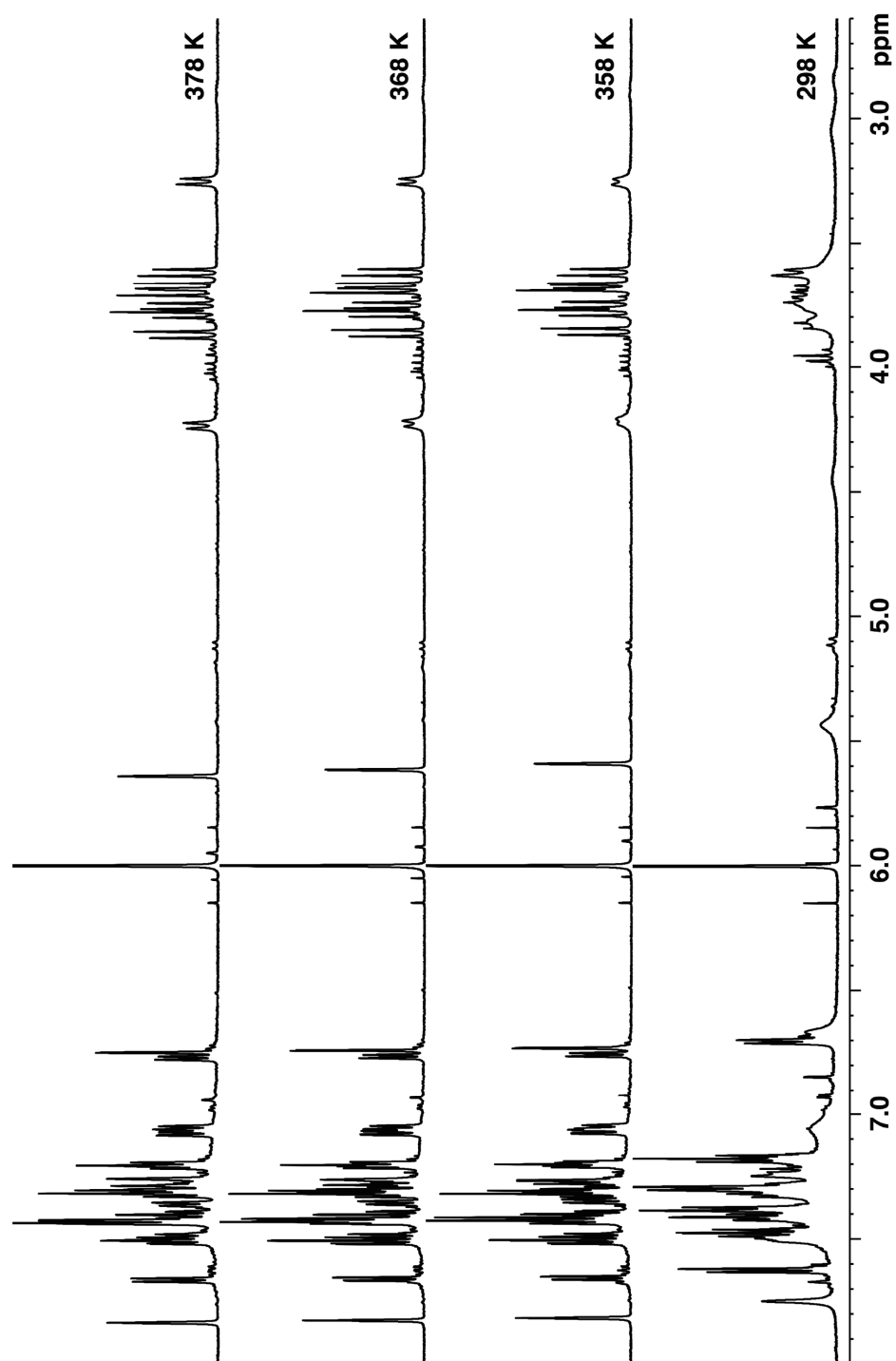
Meas. m/z	#	Formula	Score	m/z	err [mDa]	err [ppm]	mSigma	rdb	e ⁻ Conf	N-Rule	z
597.1670	1	C 40 H 30 Na S 2	100.00	597.1681	1.1	1.9	110.0	25.5	even	ok	1+
613.1411	1	C 40 H 30 K S 2	100.00	613.1421	0.9	1.5	15.5	25.5	even	ok	

2 in C₂Cl₄D₂ 13C-1H-HMBC

2 in C2Cl4D2 13C-1H-HSQC



2 in C₂Cl₄D₂ VT-1H-NMR



Mass Spectrum SmartFormula Report

Analysis Info

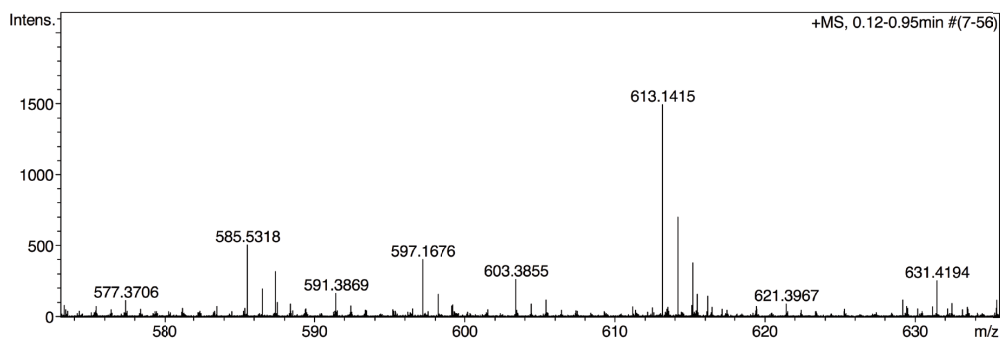
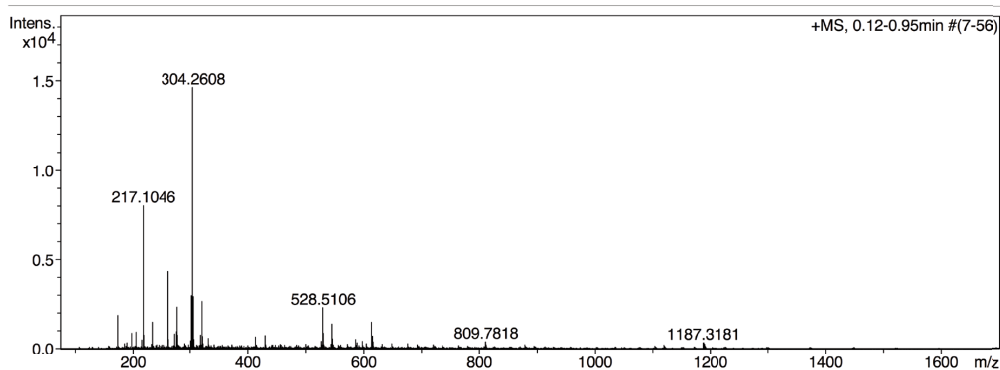
Analysis Name N:\new acq data\Ri692E3_4 002.d
 Method hn Direct_Infusion_pos mode_75-1700 mid 4eV.m
 Sample Name Michel Rickhaus, Ri692E3/4
 Comment Ri692E3/4, ca 6 ug/ml MeCN

Acquisition Date 02.09.2014 11:43:59

Operator hn
 Instrument / Ser# maXis 4G 21243

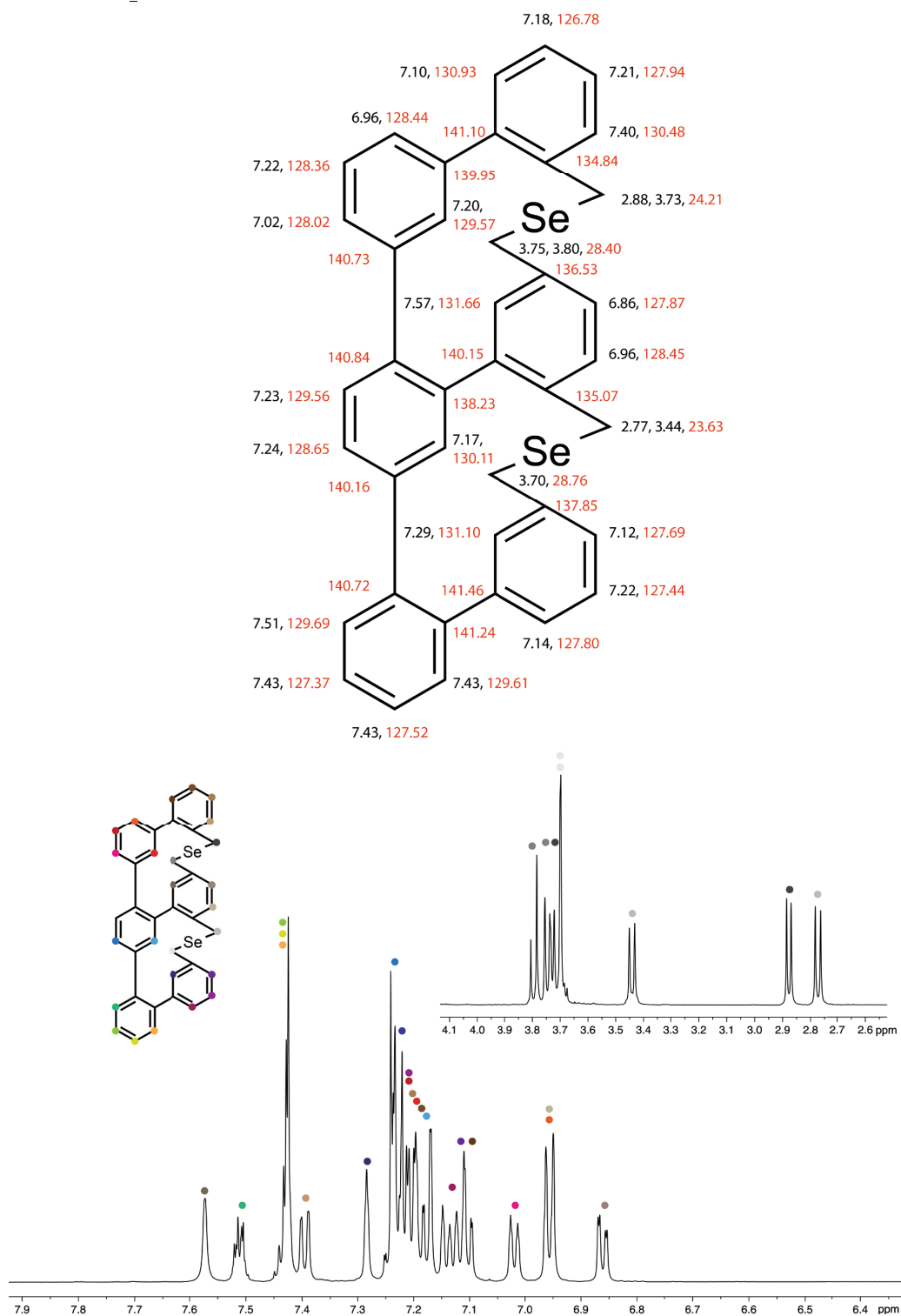
Acquisition Parameter

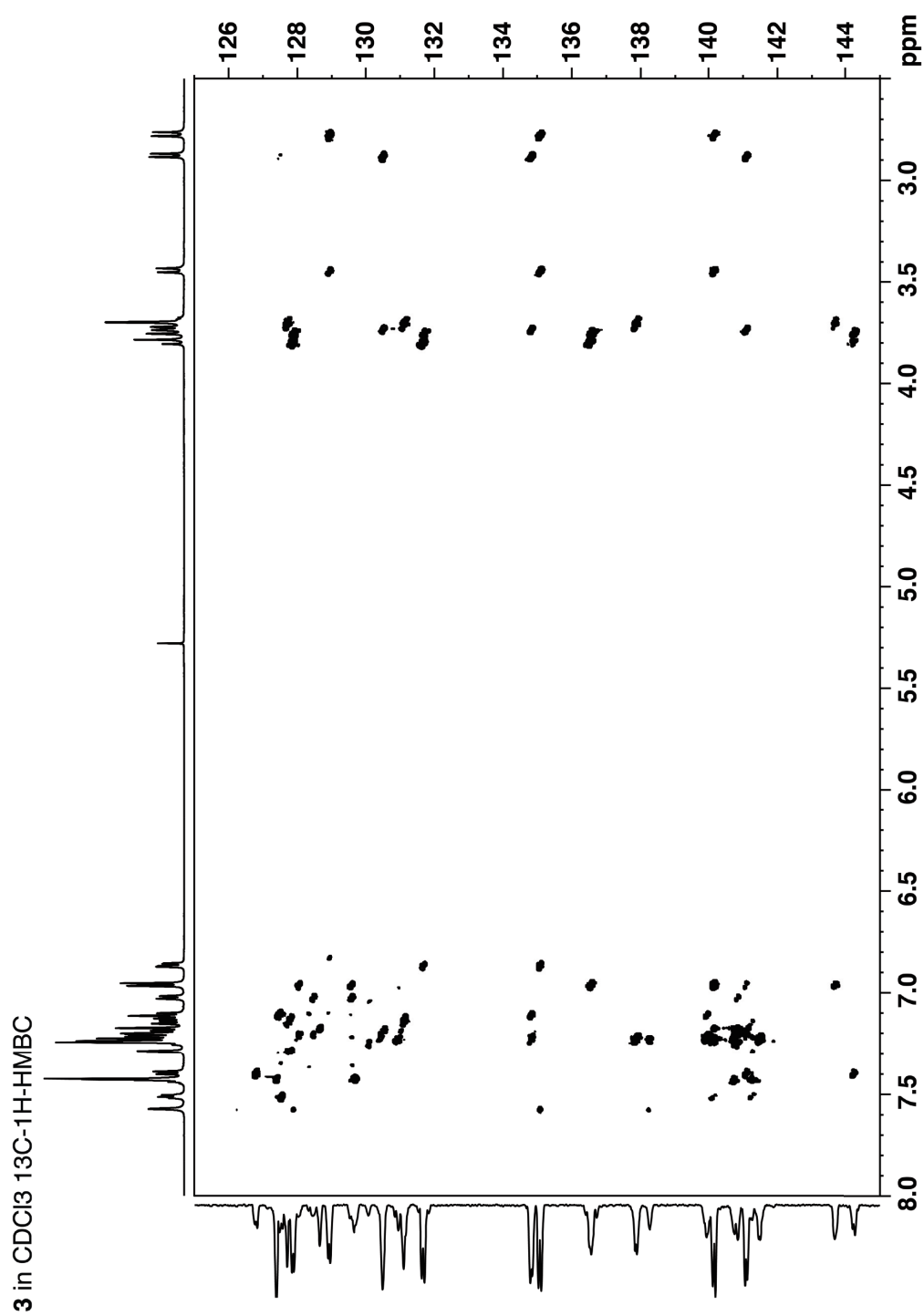
Source Type	ESI	Ion Polarity	Positive	Set Nebulizer	0.4 Bar
Focus	Not active	Set Capillary	3600 V	Set Dry Heater	180 °C
Scan Begin	75 m/z	Set End Plate Offset	-500 V	Set Dry Gas	4.0 l/min
Scan End	1700 m/z	Set Collision Cell RF	500.0 Vpp	Set Ion Energy (MS only)	4.0 eV

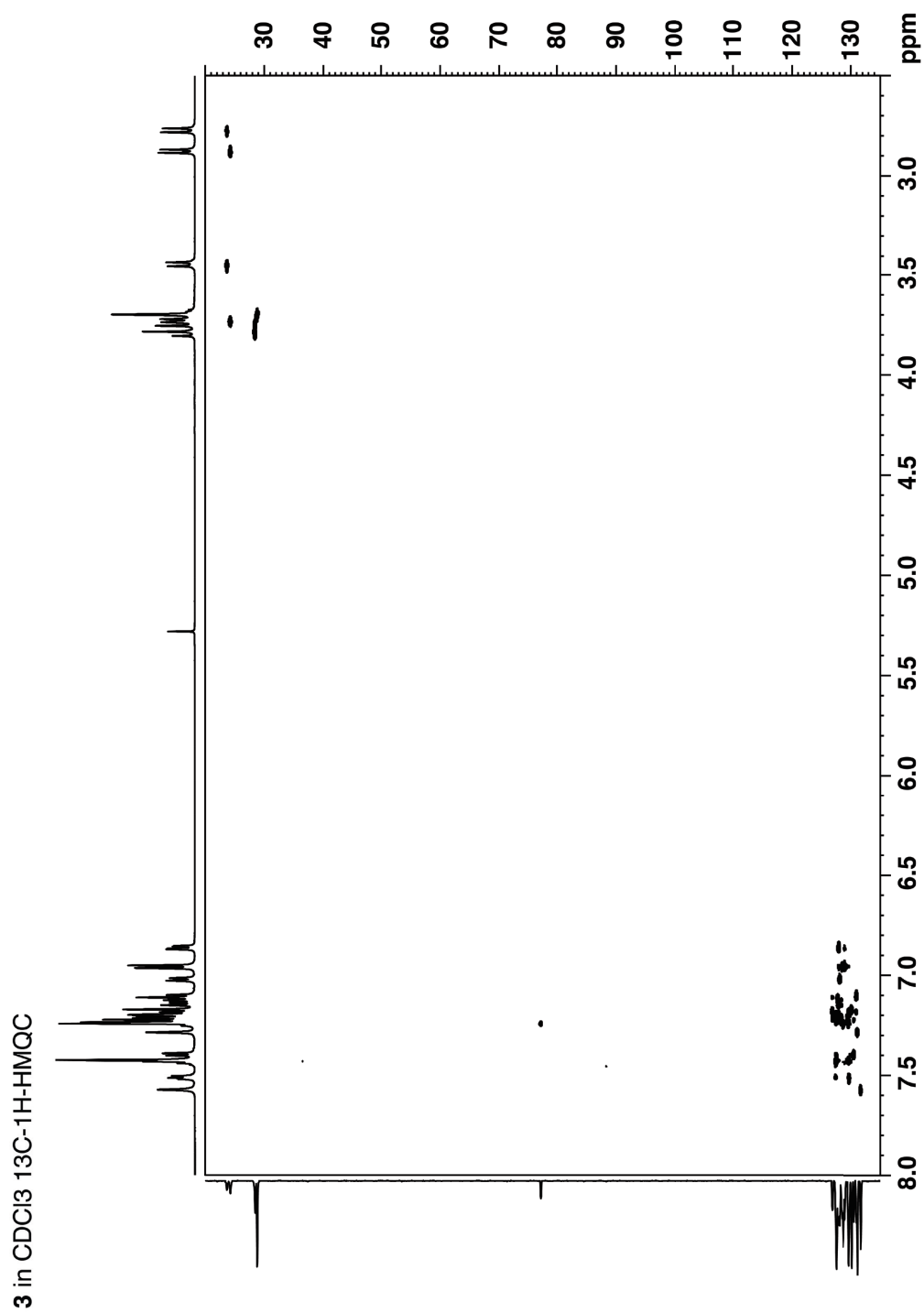


Meas. m/z	#	Formula	Score	m/z	err [mDa]	err [ppm]	mSigma	rdb	e ⁻ Conf	N-Rule	z
597.1676	1	C 40 H 30 Na S 2	100.00	597.1681	0.5	0.8	28.5	25.5	even	ok	1+
613.1415	1	C 40 H 30 K S 2	100.00	613.1421	0.5	0.9	11.8	25.5	even	ok	

^1H -, hmbc, hmqc, (CDCl_3 , 600/125 MHz, 25 °C) and HR-ESI-MS spectra of **3**







Mass Spectrum SmartFormula Report

Analysis Info

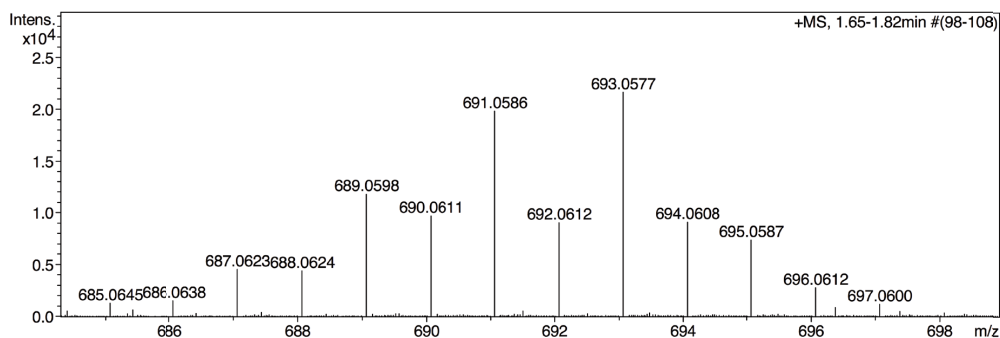
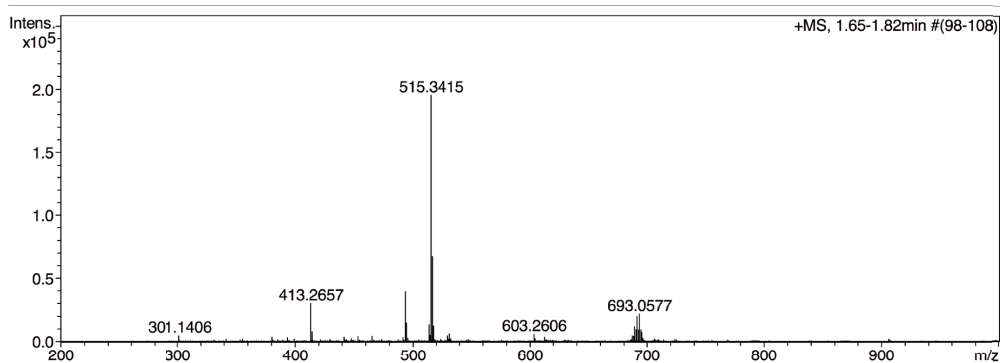
Analysis Name N:\new acq data\Ri767 II_2 003.d
 Method hn Direct_Infusion_pos mode_sensitive S_Drayss.m
 Sample Name Michel Rickhaus Ri767 II_2
 Comment Ri767 II_2, > 5 ug / ml MeCN

Acquisition Date 25.03.2015 11:18:26

Operator hn
 Instrument / Ser# maXis 4G 21243

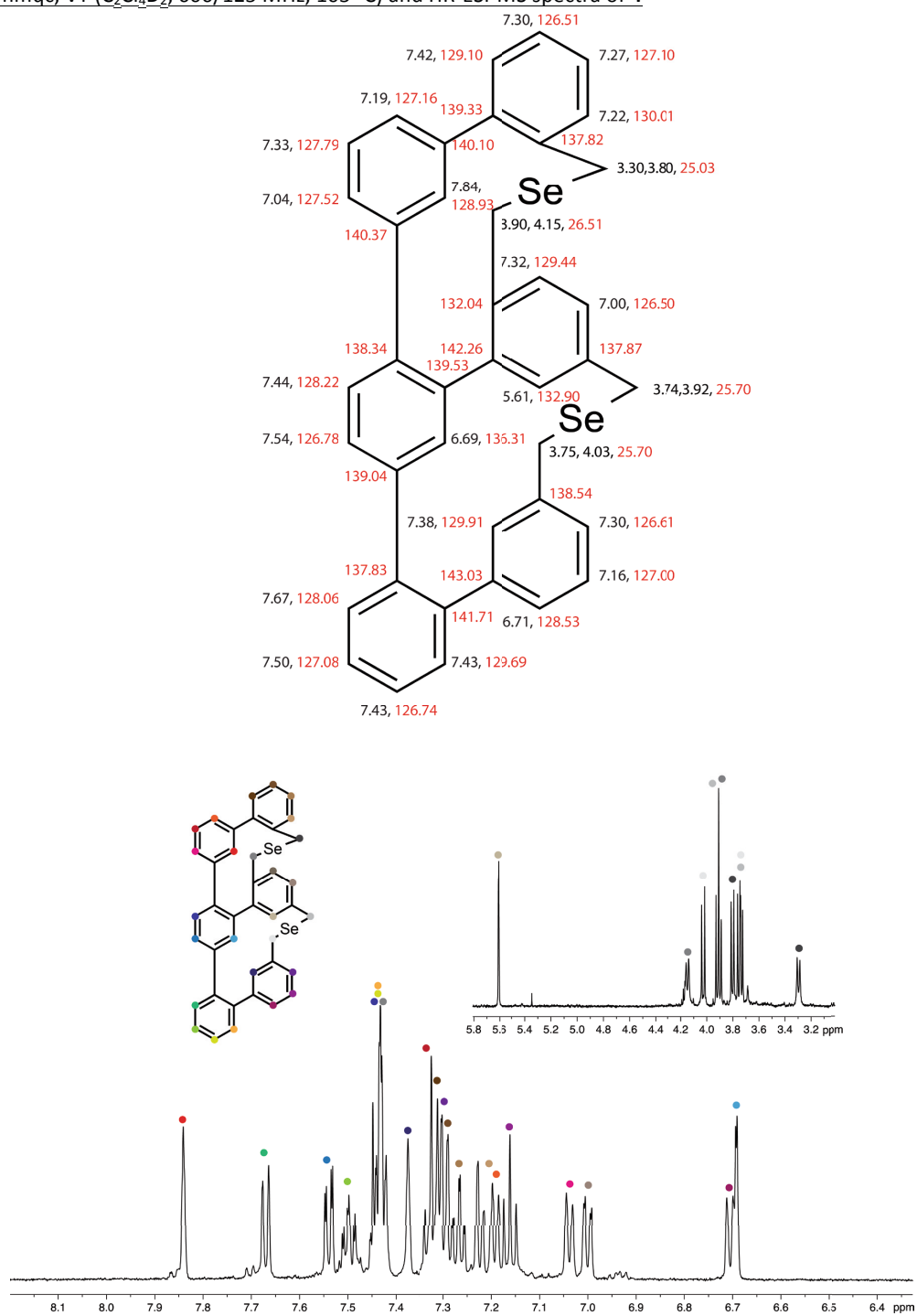
Acquisition Parameter

Source Type	ESI	Ion Polarity	Positive	Set Nebulizer	0.4 Bar
Focus	Not active	Set Capillary	4500 V	Set Dry Heater	180 °C
Scan Begin	75 m/z	Set End Plate Offset	-500 V	Set Dry Gas	4.0 l/min
Scan End	1600 m/z	Set Collision Cell RF	800.0 Vpp	Set Ion Energy (MS only)	10.0 eV



Meas. m/z	#	Formula	Score	m/z	err [mDa]	err [ppm]	mSigma	rdb	e ⁻ Conf	N-Rule	z
693.0577	1	C 40 H 30 Na Se 2	100.00	693.0578	0.1	0.2	10.2	25.5	even	ok	1+

^1H -, hmbc, hmqc, VT ($\text{C}_2\text{Cl}_4\text{D}_2$, 600/125 MHz, 105 °C) and HR-ESI-MS spectra of **4**



Personal Data

Name Michel Rickhaus
 Marital Status Married, no children
 Nationality Swiss, born 02.11.1985 in Belp BE

Education and Professional Career

08/2011 – 10/2015 University of Basel, Switzerland
PhD Summa Cum Laude in Chemistry,
Addressing Chirality by Polycyclic Aromatic Compounds without Stereocenters.
 Grade: 6.0/6.0
 Thesis advisor: *Prof. Dr. Marcel Mayor.*
 Results published in very high impact, peer-reviewed scientific journals.
 Presented (talks and posters) at 21 scientific meetings and conferences in Europe.

10/2010 – 04/2011 University of Basel, Switzerland
M.Sc. with Honors in Chemistry,
Emission with a Twist - Towards a New Geländer-Type Oligomer.
 Grade 6.0/6.0,
 Thesis advisor: *Prof. Dr. Marcel Mayor.*

02/2010 – 07/2010 Boston College, Chestnut Hill, USA
Scholarship,
Investigation of the Potassium Induced Anionic Cyclodehydrogenation in 1,1-Binaphthyl.
 Advisor: *Prof. Dr. Lawrence T. Scott.*
 Results published in a high impact, peer-reviewed scientific journal and presented at a conference for reaction mechanisms at the University of Massachusetts, USA.

2006 – 2009 University of Basel, Switzerland
B.Sc. in Chemistry, grade 5.3/6.0.

2002 – 2005 Gymnasium Laufen BL, Switzerland
Matura with focus on biology/chemistry, grade 5.1/6.0.

Honors and Awards

05/2015 **Chemistry Travel Award** of the SCNAT, SCS and SSFEC.

03/2015 **Fellowship of the Camille and Henry Dreyfuss Foundation,** Scholarship (1/y for Chemistry) of the Camille and Henry Dreyfuss Foundation, issued for excellent research.

03/2015 Travel-Stipend of the **Freiwillige Akademische Gsellschaft (FAG) Basel.**
 Travel-Stipend of the **Josef und Olga Tomcsik Stiftung.**

01/2015 **YSCS Snow Symposium,** Switzerland, Best Oral Presentations.
 01/2014

09/2014 **Status Workshop Functional Nanomaterials,** Germany, Best Oral Presentation.

09/2013 **SCS Fall Meeting,** Switzerland, Runner Up Poster Price.

01/2013 **YSCS Snow Symposium,** Switzerland, Best Poster.

11/2012 **Schwizerhüsli-Preis,** Award for the best Master-Thesis of the Faculty of Natural Sciences, awarded all 4 years. Awarded by the Fraternity Schwizerhüsli Basiliensis, Basel.

02/2010 Scholarship of the **Mobility Office of the University of Basel.**

01/2010 Scholarship of the **Werenfels Fonds der Freiwilligen Akademischen Gesellschaft,** Basel.

Important Publications

- 2016 **Chem. Soc. Rev.**, 2016, 45, 1542–1556.
Strain-Induced Helical Chirality in Polyaromatic Systems
M. Rickhaus, M. Mayor, and M. Juriček.
Chimia, 2016, Accepted, (Invited Paper).
Determining Inversion Barriers in Atropisomers – A Tutorial for Organic Chemists
M. Rickhaus, L. Jundt, and M. Mayor
Angew. Chem. Int. Ed., 2016, 55, 2920–2923.
Stereoselective Arene-Forming Aldol Condensation: Synthesis of Configurationally Stable Oligo-1,2-naphthylenes
 D. Lotter, M. Neuburger, M. Rickhaus, D. Häussinger, C. Sparr.
Angew. Chem. Int. Ed., 2016, 55, 1183–1186.
Cethrene: A Helically Chiral Biradicaloid Isomer of Heptazethrene
 P. Ravat, T. Šolomek, M. Rickhaus, D. Häussinger, M. Neuburger, M. Baumgarten, and M. Juriček.
- 2015 **Chem. Eur. J.**, 2015, 21, 18156–18167 (Hot Paper).
Tuning Helical Chirality in Polycyclic Ladder Systems
M. Rickhaus, O. T. Unke, R. Mannancherry, L. M. Bannwart, M. Neuburger, D. Häussinger, and M. Mayor.
Phys. Chem. Chem. Phys., 2015, 17, 11165–11173.
Activation Enthalpies and Entropies of the Atropisomerization of Substituted Butyl-Bridged Biphenyls,
 A. Bihlmeier, J. Rotzler, M. Rickhaus, M. Mayor, W. Klopfer.
Eur. J. Org. Chem., 2015, 4, 786–801.
Through the Maze: Cross-Coupling Pathways to a Helical Hexaphenyl “Geländer” Molecule,
M. Rickhaus, L. M. Bannwart, O. Unke, H. Gsellinger, D. Häussinger, M. Mayor.
- 2014 **Angew. Chem. Int. Ed.**, 2014, 53, 52, 14587–14591, (Very Important Paper).
Inducing Axial Chirality in a “Geländer” Oligomer by Length Mismatch of the Oligomer Strands,
M. Rickhaus, L. M. Bannwart, M. Neuburger, H. Gsellinger, K. Zimmermann, D. Häussinger, M. Mayor.
- 2010 **J. Org. Chem.**, 2010, 75, 21, 7358–7364.
An Oxidation Induced by Potassium Metal. Studies on the Anionic Cyclodehydrogenation of 1,1'-Binaphthyl to Perylene,
M. Rickhaus, A. P. Belanger, H. A. Wegner, L. T. Scott.

Selected Oral Presentations

- 07/2015 *Molecular Dance Ribbons – Inducing Helicity by Length Mismatch*,
 ISNA16, Madrid, Spain
- 01/2015 *Inducing Helicity in Polyaromatic Systems: Stairs and Bannisters*,
 YSCS Snow Symposium, Saas Fee, Switzerland.
- 09/2014 *Inducing Helicity in Polyaromatic Systems: Stairs and Bannisters*,
 Status-Workshop of the Competence Network *Functional Nanomaterials*, Bad Herrenalp, Germany.
- 09/2014 *Dart-MS, Benefits for the Synthetic Chemist* (Invited Talk),
 Applica, Basel, Switzerland.
- 09/2014 *Inducing Helicity in Polyaromatic Systems: Stairs and Bannisters*,
 Regio-Symposium, Sornetan, Switzerland.
- 01/2014 *Stars and Stripes – Emission with a Twist*,
 PCC Research Seminar (Invited Talk), University of Basel, Basel.
- 03/2013 *Twisting Light - The Dialectic of the Left-handed Yogurt*,
 Award Lecture for the Schwizerhüsli Price, University of Basel, Switzerland.

